NASA CR-159831

EDR 10119

EXPERIMENTAL DETERMINATION OF UNSTEADY BLADE ELEMENT AERODYNAMICS IN CASCADES

TORSION MODE CASCADE FINAL REPORT

VOLUME I

By
R.E. Riffel and M.D. Rothrock

DETROIT DIESEL ALLISON
DIVISION OF GENERAL MOTORS CORPORATION
INDIANAPOLIS, INDIANA 46206

Prepared For

NATIONAL AERONAUTICS AND SPACE ADMINISTRATION

JUNE 1980

NASA LEWIS RESEARCH CENTER

CONTRACT: NAS3-20055

EXPERIMENTAL DETERMINATION OF UNSTEADY BLADE ELEMENT AERODYNAMICS IN CASCADES

TORSION MODE CASCADE FINAL REPORT
VOLUME I

By
R. E. Riffel and M. D. Rothrock

DETROIT DIESEL ALLISON
DIVISION OF GENERAL MOTORS CORPORATION
INDIANAPOLIS, INDIANA 46206

Prepared For
NATIONAL AERONAUTICS AND SPACE ADMINISTRATION

JUNE 1980

NASA LEWIS RESEARCH CENTER
CONTRACT: NAS3-20055

TABLE OF CONTENTS

LIST OF ILLUSTRATIONS

LIST OF TABLES

I. SUMMARY

Three separate two-dimensional cascade experiments of five harmonically oscillating airfoils were designed to investigate the time-steady and time-unsteady aerodynamics associated with supersonic torsional mode flutter. The first or baseline cascade experiment was designed to model a near-tip section from a rotor which was known to have experienced this type of flutter. The second cascade evaluated the aerodynamics of the baseline airfoil profile but with a reduction in cascade solidity. The third cascade experiment was conducted at the reduced solidity level, but the airfoil was reset to a more open setting angle. This report contains the documentation of the data obtained during the testing, and the correlation of the time-unsteady data with an appropriate state-of-the-art analysis. Also included is a description of the aerodynamic and mechanical design of the research hardware as well as a description of the facilities.

The torsional cascade airfoil was modeled from the 86.7% span section of the second stage of the five-stage TF41-A100 LP-IP compressor rig. The cascades were tested at static pressure ratios between 1.05 and 1.45:1. These pressure ratios approximated the blade element operating conditions of the rotor along a constant speed line, which penetrated the torsional flutter boundary. The cascade inlet Mach number was 1.315.

In order to achieve the realistically-high reduced frequency level of 0.44, and to maximize the airfoil torsional amplitude, unique airfoils were fabricated from graphite/epoxy composite material, with hollow steel trunnions attached at the 50% chord location. Torsional excitation forces were imparted to hollow torsion rods via computer-controlled electromagnetic drivers. These torsion rods were attached to both of the airfoil's trunnions to ensure a two-dimensional mode shape.

Each test program involved three distinct phases during which the center airfoil was replaced with a particular instrumented airfoil. The first or steady-state aerodynamics phase utilized a static pressure tap airfoil. This was followed by the time variant aerodynamic testing with Kulite dynamic pressure transducers mounted on the center airfoil. During this test phase approximately six interblade phase angles were investigated for each steady state operating condition. The third and final phase involved studying the regions of flow separation on the airfoil surface using an airfoil instrumented with surface-mounted heated film gages.

This report completes the experimental test program for the NASA I torsion cascade as described under Task I of Contract NAS3-20055. The results of this program are summarized in the following:

- o Developed high reduced-frequency torsional-mode drive system
- o Provided fundamental quantitative time variant data at realistic reduced frequency levels for three torsional mode cascades

- Examined effect of cascade loading on unsteady aerodynamic data
- Provided cascade stability plots over a range of back pressures
- Determined large-amplitude shock motion not required for cascade instability
- Correctly modeled TF41-A100 LP2 rotor flutter test results with respect to loading effects and interblade phase angle
- Verified usage of DDA's in-house supersonic flutter analysis at low back pressures
- Identified requirement for moderately loaded cascade analysis to predict TF41-A100 type flutter
- Examined effects of cascade solidity and setting angle on unsteady aerodynamic data

II. INTRODUCTION

The advent of the high speed turbofan engine led to the discovery of a new type of blading instability--supersonic unstalled flutter. This instability is a self-excited vibration of the airfoils, which are operating in a uniform supersonic relative inlet flow field with unstalled passage flow, and is typically in the torsional mode of oscillation. To avoid this instability during the design phase it becomes necessary to calculate the time-variant pressure distributions on harmonically oscillating airfoils. The designer can use this information combined with structural damping to accurately predict the flutter boundaries. The generally used calculation procedure assumes an inviscid supersonic flow with a subsonic axial component through a differential radial height fan stage. This differential fan stage is then developed into a two-dimensional rectilinear cascade of zero thickness flat plates executing small harmonic oscillations.

DDA has pioneered the concept of investigating fundamental blade instability mechanisms through the use of computer-controlled, time-variant, supersonic, rectilinear cascades to obtain time unsteady pressure data. These data have provided a reference for correlation studies using appropriate state-of-the-art analyses, and have pointed out necessary refinements to the analyses. This program has made use of the aforementioned experience to extend the level of reduced frequency to the realistic test value of 0.44.

III. HARDWARE DESCRIPTION

CASCADE AIRFOIL DESIGN

The torsional mode airfoil was modeled from a multiple circular arc (MCA) blade element located at 86.7% span on the second rotor of the DDA TF41-A100 LP-IP compressor rig. The reference blade element was modified geometrically to account for the lack of radius change and area (streamline) convergence in the two-dimensional cascade. The geometric modification is performed under the restriction specified in the following equation:

$$\frac{(\tan\beta_1 + \tan\beta_2)}{2}_{\text{rotor}} = \frac{(\tan\beta_1 + \tan\beta_2)}{2}_{\text{cascade}} \qquad (1)$$

where β_1 and β_2 are respectively the inlet and exit air angles. The cascade air angles are determined iteratively through the use of the continuity equation, and the axial and tangential momentum equations. These angles define the cascade velocity triangles and in turn the airfoil section profile to be used for cascade testing. The following design parameters are maintained between the rotor blade element and the cascade airfoil profile.

- o Solidity
- o Maximum thickness location
- o Thickness-to-chord ratio
- o Leading and trailing edge radius-to-chord ratio
- o Incidence
- o Deviation
- o Starting margin

Table I compares the resulting cascade and blade element section data. The cascade airfoil has a 7.62 cm (3.00 in.) chord and 7.62 cm (3.00 in.) span. The profile is indicated schematically in Figure 1.

Test data was used to construct the TF41-A100 second stage rotor characteristics shown in Figure 2. The flutter boundary is indicated by the shaded region on this compressor map. Interstage data from the rig testing was used to select the cascade operating conditions in terms of inlet Mach number and static pressure ratio. The requirement for the torsion cascade harmonic oscillation was such that its reduced frequency value (k) be approximately equal to that exhibited by the A100 second rotor. The rotor test reduced frequency level was 0.52 during flutter. An additional requirement of the drive system was that it be capable of producing a two-dimensional torsional motion while forcing the airfoil at the specified frequency and interblade phase angle. A composite graphite/epoxy material was selected for airfoil fabrication to meet these requirements. The material features included low inertia, high modulus

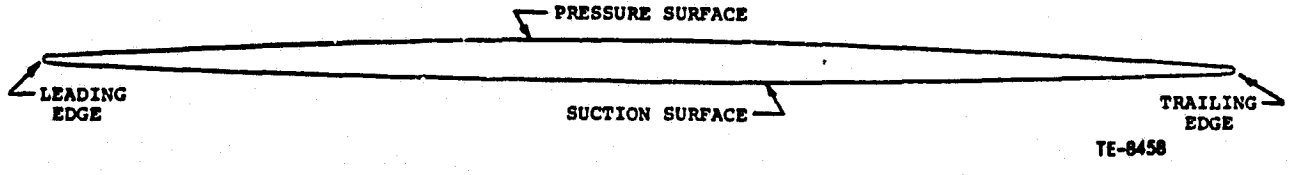

Figure 1. NASA I torsion airfoil profile schematic.

Table I.
Design data comparison between TF41-A-100 second rotor streamline element #28 and cascade airfoil.

Velocity Diagram Data

	Rotor	Cascade
Inlet Mach	1.213	1.214
Exit Mach	0.905	0.905
Inlet Air Angle, rad	1.13 (64.95°)	1.13 (64.51°)
Exit Air Angle, rad	1.10 (62.81°)	1.10 (63.28°)
Diffusion Factor	0.300	0.299
$\Delta P_s/Q$	0.240	0.241
Turning, rad	0.04 (2.14°)	0.02 (1.23°)

Blading Design Data

	Rotor	Cascade
Inlet Metal Angle, rad	1.06 (60.69°)	1.06 (60.46°)
Exit Metal Angle, rad	1.07 (61.29°)	1.08 (61.76°)
Inflection Angle, rad	1.09 (62.32°)	1.09 (62.70°)
Net Camber, rad	-0.01 (-0.60°)	-0.02 (-1.30°)
Forward Camber, rad	-0.03 (-1.63°)	-0.04 (-2.24°)
Rear Camber, rad	0.02 (+1.03°)	0.02 (0.94°)
Meanline Incidence, rad	0.07 (4.26°)	0.07 (4.05°)
Suction Surface Incidence, rad	0.03 (1.60°)	0.03 (1.57°)
Meanline Deviation, rad	0.03 (1.52°)	0.03 (1.52°)
Setting Angle, rad	1.07 (61.57°)	1.07 (61.55°)
Solidity	1.17	1.170
Chord, cm	9.90 (3.898 in.)	7.62 (3.00 in.)
Thickness/Chord	0.034	0.034
LER/Chord	0.0026	0.0026
TER/Chord	0.0026	0.0026
T Max Location	0.50	0.50
Inflection Location	0.769	0.769
Minimum A/A* (Starting Margin)	1.033	1.030

to density (E/ρ) ratio, and also the capability to imbed the appropriate aerodynamic instrumentation into the surface during fabrication.

The airfoils were fabricated from Hercules 3501-AS-5 pre-impregnated graphite tape wrapped with an outer layer of Kevlar cloth, and injected with an epoxy resin under pressure into a booking mold. The graphite fiber orientation was controlled to meet the torsional stress requirements while maintaining a low density and a high modulus of elasticity. A "flat-plate" airfoil was fabricated and bench tested to evaluate fiber orientation. The fiber orientations used for fabrication were alternating layers of 0 rad, $\pi/2$ rad and $\pm \pi/4$ rad (0°, 90°, and $\pm$ 45°) to the torsional axis of the airfoil.

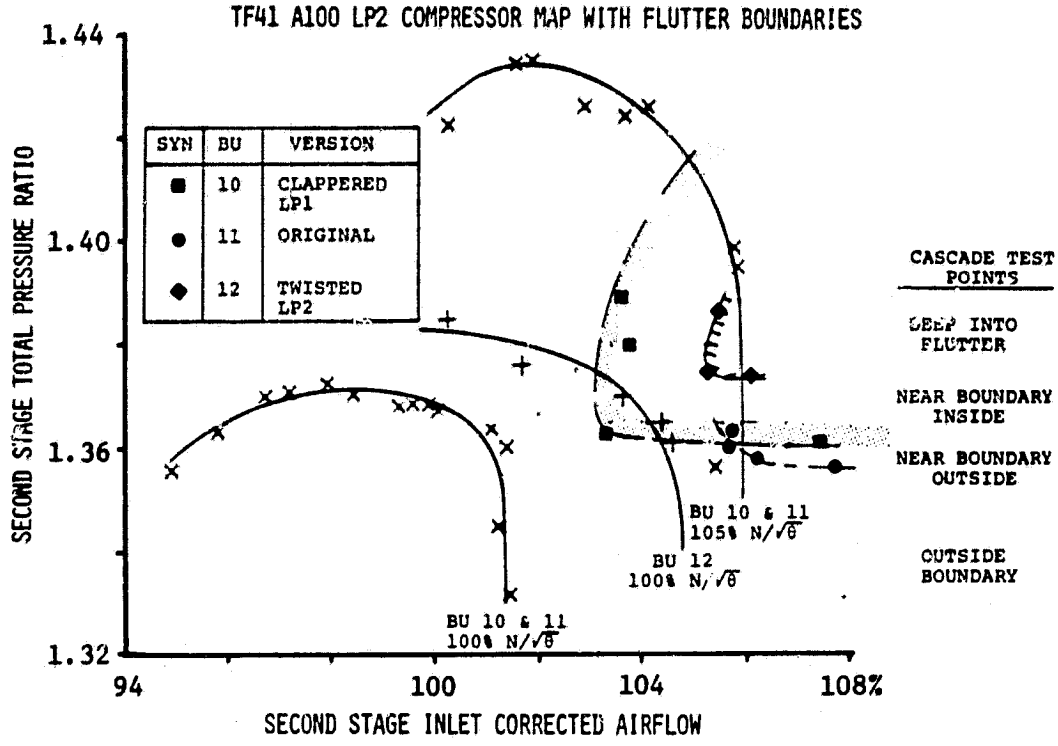

Figure 2. TF41-A-100 second rotor compressor map with flutter boundaries.

Hollow steel (AMS 5643) trunnions were attached to the composite airfoils at mid-chord. Figure 3 is a photograph showing the hollow trunnions and a composite airfoil blank. Graphite chips and an epoxy fill were used in the trunnion caps to provide strength at the airfoil-trunnion interface. The splines located on the trunnion were used for mounting and to produce positive torsional displacement.

In order to maintain the composite material properties and airfoil surface contour, the use of nonconventional instrumentation techniques were employed during airfoil fabrication. Twenty 0.041 cm (0.016 in.) diameter hypodermic tubes with 0.010 cm (0.004 in.) wall thickness were imbedded in the steady-state airfoil by relieving the laminate during layup. Wiring harnesses to accommodate twelve dynamic pressure transducers and ten heated film gages were also embedded into their respective airfoils during fabrication. The ends of the lead wires were exposed during installation of the respective sensor by local spot-facing of the airfoil surface.

TORSION MODE DRIVE SYSTEM DESIGN

The frequency of oscillation desired for equal values of reduced frequency between the cascade and the rotor was 836 Hz. A torsion drive system utilizing a torsion rod was designed, fabricated and bench checked. This drive system is illustrated in Figure 4. The driving arm assembly and hollow torsion rods were match-machined to individual airfoil trunnions to minimize run-out.

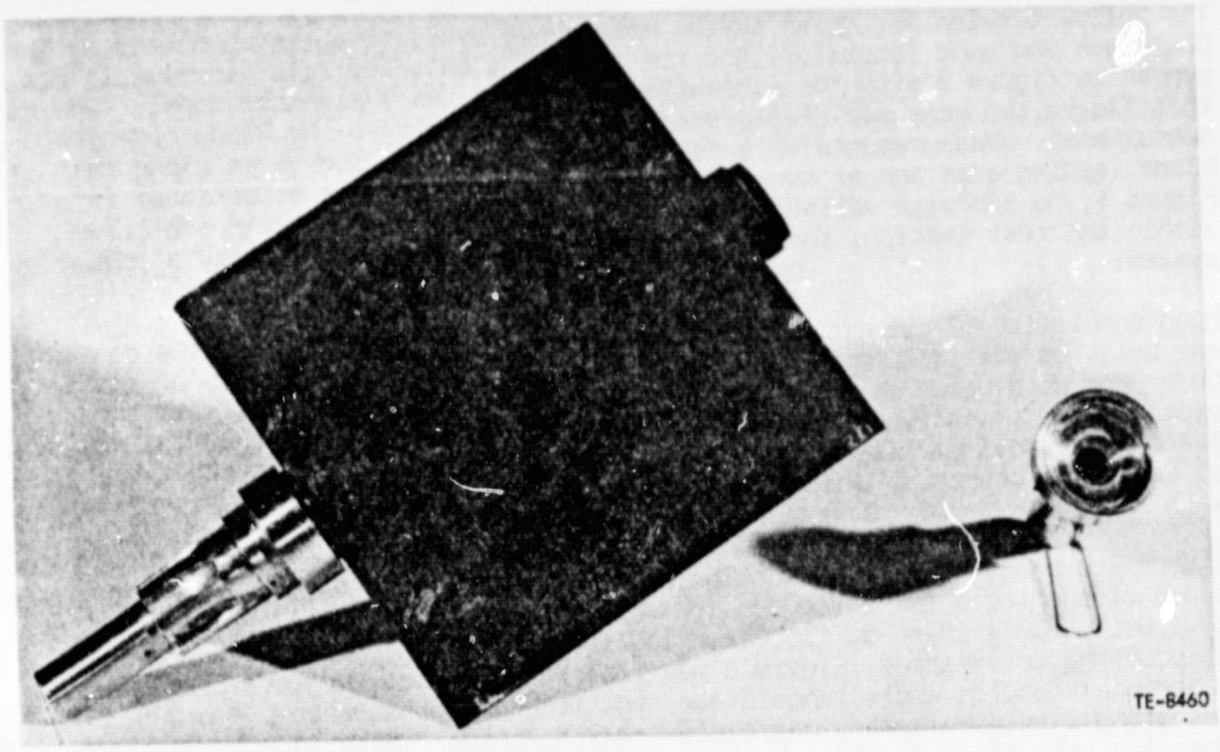

Figure 3. NASA I torsion graphite epoxy airfoil blank with hollow steel trunnions.

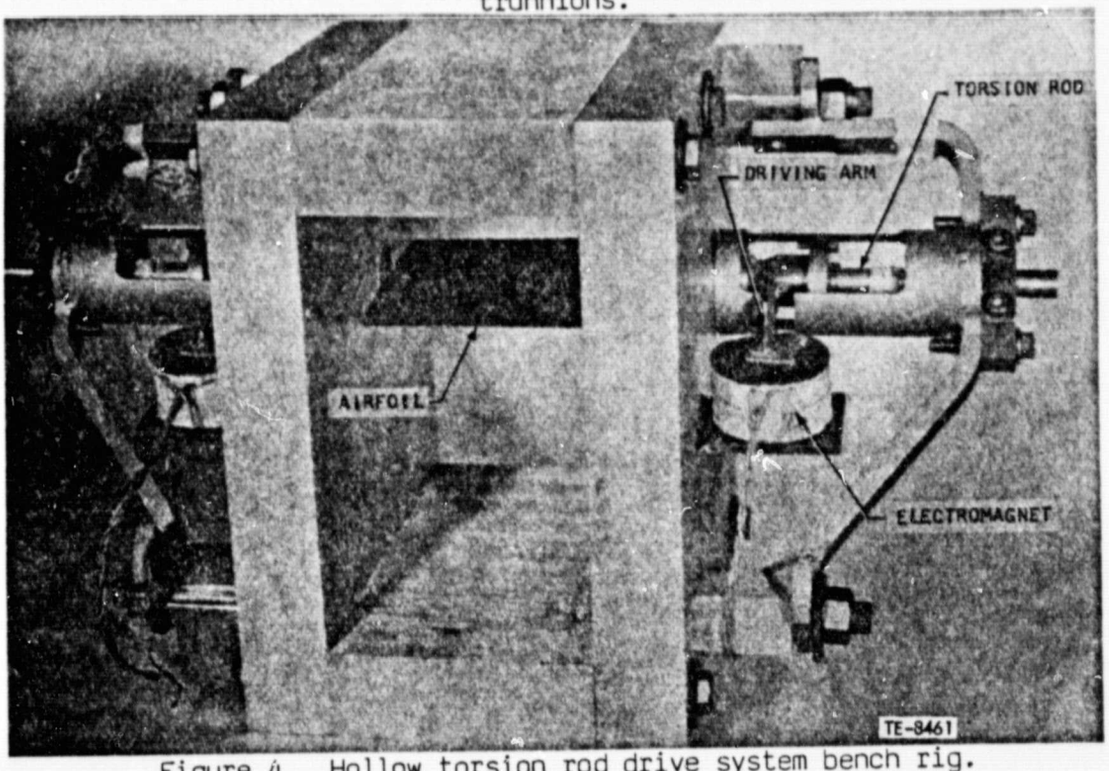

Figure 4. Hollow torsion rod drive system bench rig.

The hollow torsion bar drive system mode shape evaluation was conducted in the DDA blade and vane laboratory and the resulting data for first torsion is presented in Figure 5 with the schematic describing the analytical model. In this figure the measured displacements are normalized to the blade mid-span measurement. Measurements were taken at five spanwise locations along the blade leading edge and at each of the driving hammers. As illustrated in Figure 5, no spanwise variation in amplitude was observed on the airfoil within the test section, thereby preserving the two-dimensionality of the system.

Upon completion of the torsional drive system blade investigation the cascade was built up with 750 Hz blade driver hardware. Acceptable levels of amplitude were attainable at a no load condition for all the airfoils with the exception of the instrumented airfoil. Its amplitude was lower than the minimum system torsional amplitude based on previous testing. Utilizing this torsional amplitude criteria, a maximum resonant frequency of 720 Hz was attainable with the instrumented airfoil.

A separate analytical investigation was carried out to determine the significance of running a lower reduced frequency on the calculated cascade stability. Using DDA's in-house flutter calculation, and the torsion cascade operational characteristics, Figure 6 was constructed. For two levels of interblade phase angles and a range of reduced frequencies between 0.2 and 0.55 the resulting imaginary moment coefficient was defined. These results indicate that the calculated cascade stability is relatively unaffected by the lower (0.44) reduced frequency.

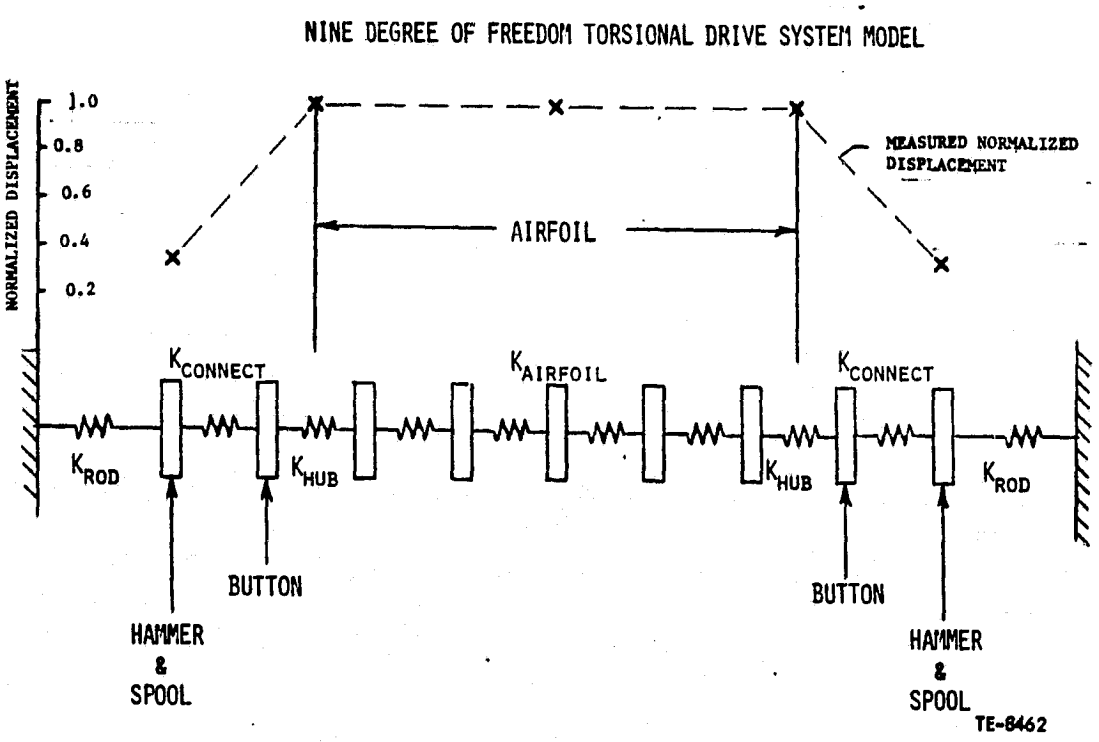

Figure 5. Torsion airfoil analytical model with measured mode shape data.

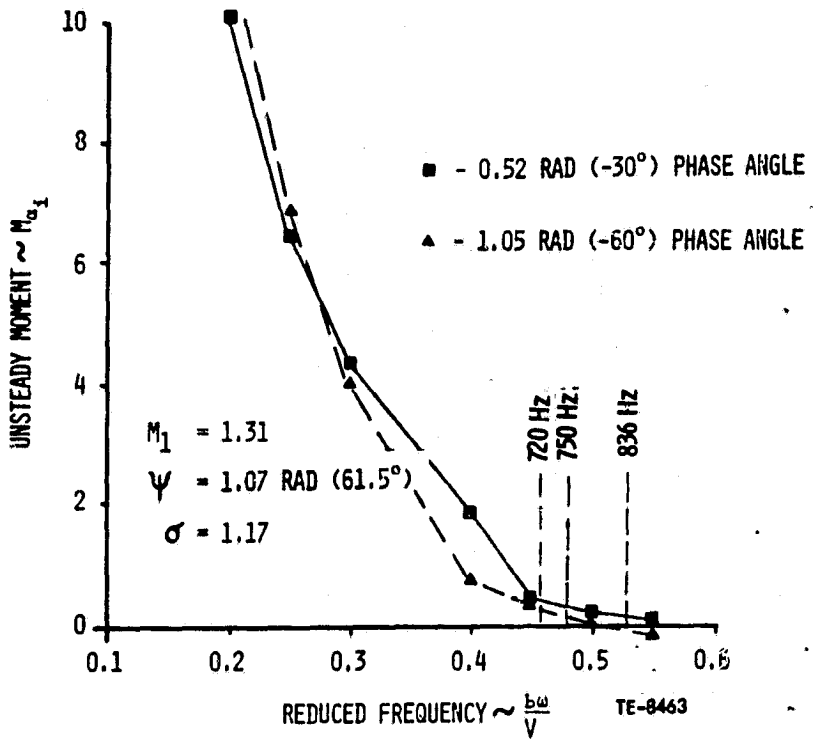

Figure 6. Unsteady flow analysis results showing effect of reduced frequency on stability.

REDUCED SOLIDITY CASCADE HARDWARE MODIFICATIONS

The torsion mode cascade solidity level was changed by fabricating a new set of plexiglas windows with a 10% increase in the spacing between the airfoil trunnions. This increased spacing results in a reduction in the cascade solidity to a level of 1.06. The setting angle change at this reduced solidity level was accomplished by a simple open reset to 1.02 rad (58.5^{o}) from the baseline value of 1.07 rad (61.5^{o}). The magnitude and direction of these geometry changes were influenced by a combination of cascade aerodynamics and hardware limitations.

IV. TEST FACILITY

The DDA rectilinear cascade facility shown in Figure 7 was conceived and built as a research tool to evaluate the aerodynamic characteristics of compressor and turbine blade sections. The facility is a continuous flow, nonreturn, pressure-vacuum type wind tunnel with the test section evacuated by means of two primary steam ejectors. Up to 4.54 kg/s (10 lbm/sec) of filtered, dried, and temperature-controlled air can be supplied.

Major features of the rectilinear cascade facility include:

- o Continuous operation for extended time periods
- o Mechanized test section for rotating a cascade of airfoils with the tunnel in operation
- o Schlieren optical system for visual observation and photography of the cascade in operation
- o Endwall and sidewall boundary layer control systems
- o Sophisticated instrumentation system centered on laboratory-size digital computers

The cascade facility was designed to permit testing of existing and advanced technology airfoil designs through a wide range of Mach numbers, setting angles, incidence angles, and pressure ratios. General specifications of the cascade facility are listed in Table II.

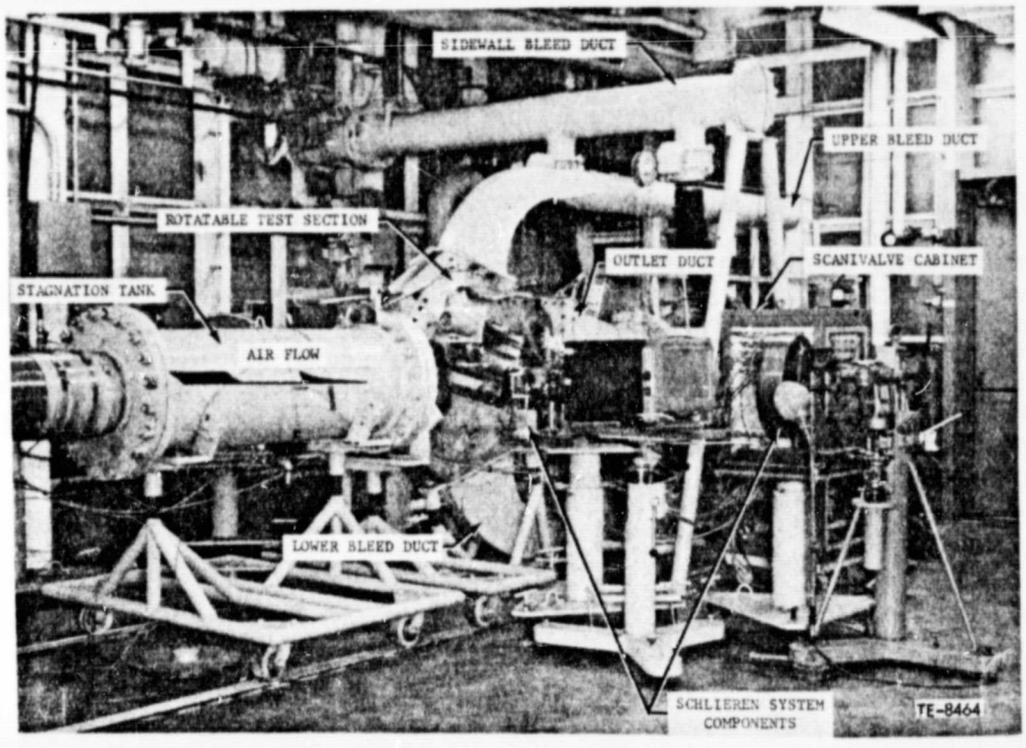

Figure 7. DDA rectilinear cascade facility.

Table II.
Wind tunnel specifications.

Test Section Inlet Mach Number - Subsonic, Mach 1.2 - 5.0
Test Section Size - 7.62 cm side x 20.32 cm high
Instrumentation: 48 temperatures
192 pressures
On-line computer w/32 K memory
On-line computer w/16 K memory (dynamic operation)
Teleprinter
CRT display terminal
80 column line printer (350 to 1100 lines per minute)
High speed punch
High speed punched tape reader
X-Y digital plotter
X-Y analog plotter
Magnetic disc with 1.2×10^6 word capacity
40.64 cm schlieren optical system
Three axis conical probe (magnitude and direction of the flow velocity vector)
16 channel analog to digital conversion system
2 channel laser velocimeter
Operation - Continuous forced or indraft inlet-steam ejector at exit
Flow rate - 4.54 kg/s air max (forced air inlet)
Steam ejector flow rate - 4.41 to 8.82 kg/s
- 1.51 kg/s for sidewall bleed system
Max inlet pressure - 689.5 kPa abs @ 4.54 kg/s (forced air inlet)
Exhaust pressure - 41.4 kPa abs @ 4.54 kg/s (forced air inlet)
20.7 kPa abs @ 2.77 kg/s (forced air inlet)
Test Section Reynolds No. - 0.15×10^6 to 0.21×10^6/cm @ M 1.5
Test Section Temperature - Ambient to $366.7^{\circ}K$
Sidewall Bleed System - Suction pressure 13.8 kPa abs with 0.32 kg/s air flow

The single-pass schlieren optical system, shown schematically in Figure 8, was used for documentation and evaluation of both steady-state and dynamic-flow behavior. This system used a mercury vapor light-source, plane and parabolic mirrors, and a knife edge or tricolor filter, permitting visual observation and/or photography of the test section. The colored schlieren results in improved visual flow analysis in that it increases the ability to distinguish between the flow field and the test model as well as between different flow regimes.

The wind tunnel boundary layer control system had the capability of removing the boundary layers on the tunnel sidewalls and endwalls prior to the flow entering the cascade test section. The supersonic nozzle boundary layers were removed utilizing an upper and lower bleed system as shown in Figure 9. To

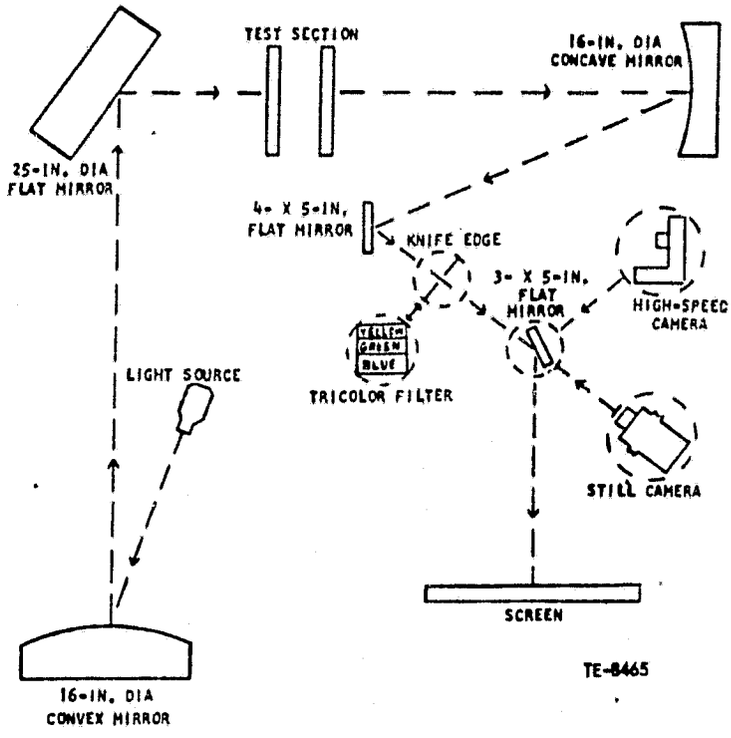

Figure 8. DDA cascade facility single pass Schlieren schematic.

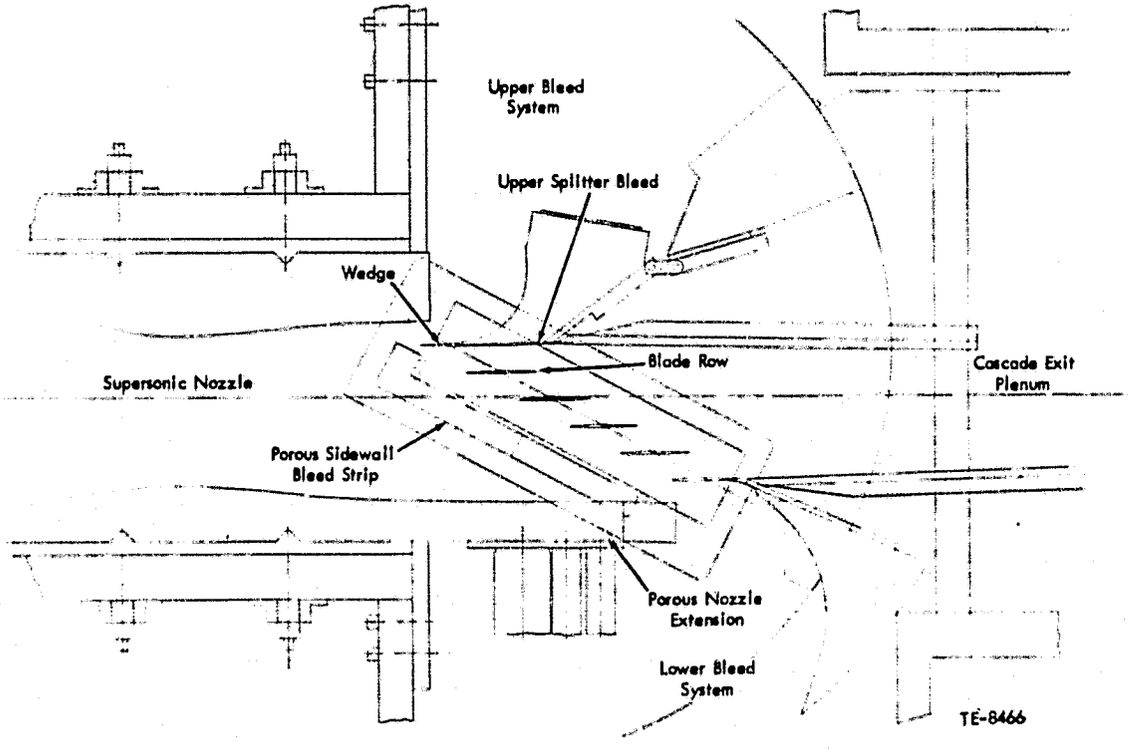

Figure 9. Schematic of cascade facility with NASA I torsion cascade installed.

obtain the desired two-dimensional cascade configuration and to control sidewall boundary layer-cascade interactions, a sidewall boundary layer control system was also employed. This was accomplished with a porous bleed strip containing five discrete regions. This technique is preferred since it is not optically restrictive and schlieren photographs of the cascade can be obtained.

The NASA torsion cascade, including the boundary layer control system, is shown in Figure 10. The cascade was equipped with adjustable upper and lower exit tailboards, which were porous with a 50% open area. These tailboards were open to the exit plenum pressure level. The setting of the upper tailboard in conjunction with the application of atmospheric bleed in the upper splitter aft cavity was critical in setting the exit periodicity. The object was to produce an endwall which simulates the streamline of an infinite cascade at the operating pressure ratio.

The wind tunnel facility is equipped with a sophisticated instrumentation system centered around laboratory-size digital computers to provide rapid on-line data acquisition and reduction. The computers and associated peripheral equipment are shown in Figure 11. The computers have core memory capacities of 16,000 and 32,000 words with a 16-bit word length. Memory cycle time is 0.98 sec. Peripheral equipment includes a CRT terminal, an 80-column line printer (350 to 1100 lines per minute), high-speed punch, high-speed punched-tape reader, X-Y digital plotter, magnetic disk storage unit with 2.5×10^6 word capacity, and 16-channel-100KHz analog to digital converter.

The computer was used for control of instrumentation during both steady-state and dynamic testing, data acquisition, and data reduction. During steady-state operation, the computer controls a digital voltmeter, an electronic scanner, a Scanivalve stepping motor, an indexer for positioning the conical probe, and the computer peripheral equipment. Pressure measurements were obtained by using a Scanivalve system incorporating four 48-port, rotary valves (Scanivalves) which provided a total pressure measurement capacity of 192 pressures. Other necessary wind tunnel data measured by the computer included the test section angular position (used to define the cascade inlet Mach number and flow direction) and the conical probe position (angular, horizontal, and vertical). The computer also performed two functions which can be easily accomplished by an on-line data acquisition system. The first seven ports on each of the four Scanivalves were used for three reference calibration pressures. Each time the computer initiated a set of pressure readings, the calibration pressures were measured, providing direct on-line calibration of the Scanivalve pressure transducers. Secondly, the wind tunnel total pressure and total temperature were monitored during data acquisition of each test point. If the pressure or temperature varied outside a preset tolerance, the computer automatically presented the out-of-limit reading(s) and waited for instructions.

The computer also reduced the cascade test data on-line. As the data was acquired, the computer analyzed it to determine not only the test operating conditions, but also the complete performance characteristics of the cascade.

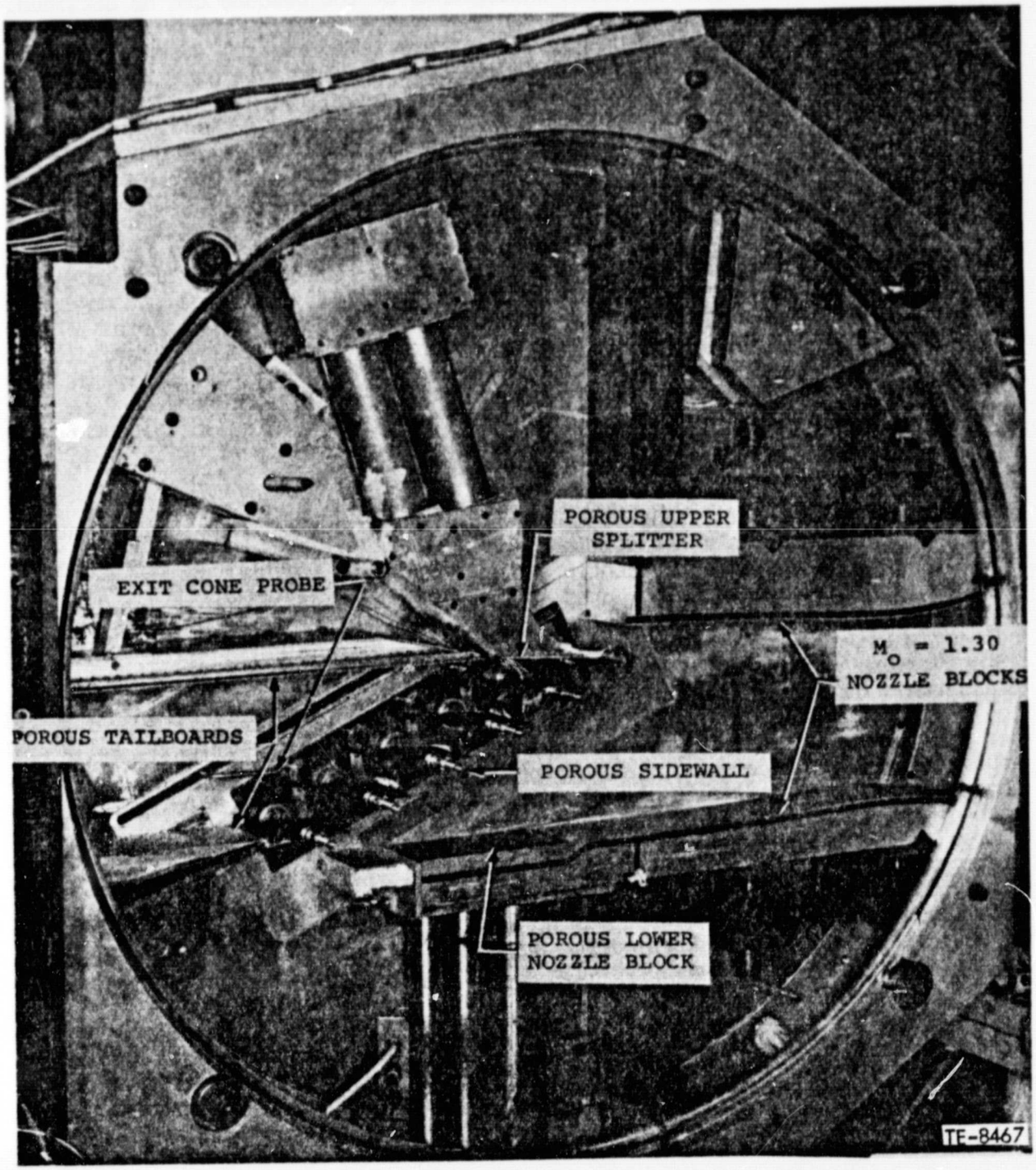

Figure 10. NASA I torsion baseline cascade installed in rectilinear cascade facility.

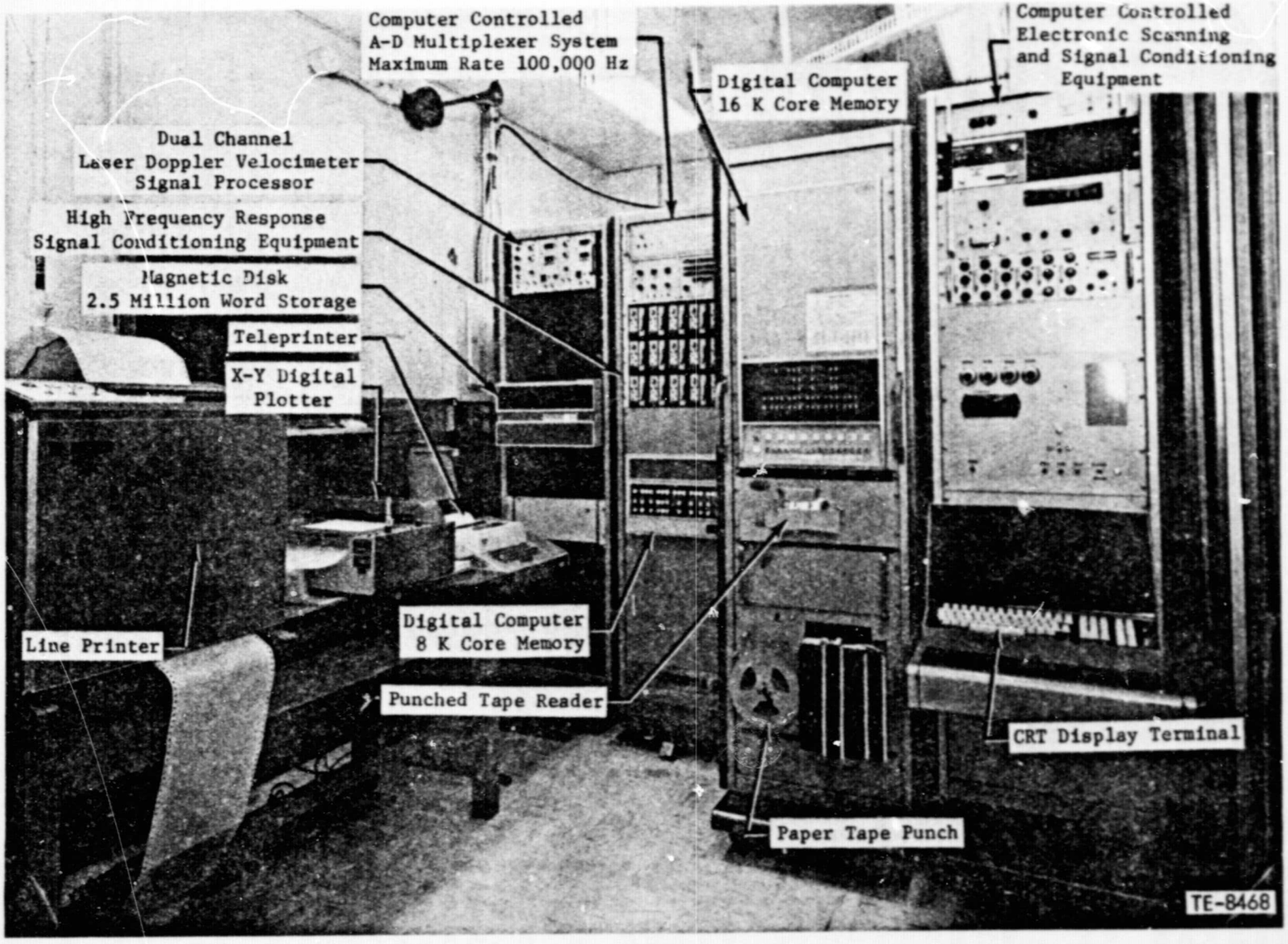

Figure 11. DDA rectilinear cascade facility data acquisition center.

For the dynamic or time-dependent studies, the computer and associated peripheral equipment was used to:

- o Control cascade excitation to produce desired unsteady phenomena
- o Digitize the resulting analog signals at a rate of 100,000 points per second for 16 channels of information
- o Store these data on removable magnetic disks
- o Control dual channel storage oscilloscopes for an analog signal record
- o Control high speed motion picture camera for schlieren movies of the unsteady phenomena

The experimental data obtained was analyzed on-line to evaluate the unsteady operation while the cascade was being tested.

Dynamic testing to investigate and correctly simulate time-dependent cascade aerodynamic phenomena relevant to flutter requires the airfoil cascade to harmonically oscillate in a predetermined mode at known frequencies. DDA has developed and successfully demonstrated a unique computer controlled electromagnetic driver system to oscillate an airfoil cascade at specified frequency and interblade phase angle values. This system uses a 16K digital computer to repetitively generate five one-half square wave signals, one for each airfoil in the cascade. The frequency of these square waves and their phase relationships are arbitrarily specified input quantities to the 16K computer. These signals are transmitted through a main 32K experiment control computer to individual power supplies and then to the electromagnet drivers. Blade amplitude of oscillation is regulated through the power supply. This method is adequate if the resonant frequency of each airfoil in the cascade is identically equal, however, minor frequency differences can introduce changes in the phase relation between the driving force and the blade motion. These frequency differences result in significant blade-to-blade phase variations between the driving signal and the resulting strain gage signal.

The airfoil driving force is the sum of the electromagnetically induced force and the aerodynamic force induced on the airfoil by other airfoils vibrating in the cascade. These aerodynamic forces vary throughout the cascade. For example, the aerodynamic loading of the first (upstream) airfoil in the cascade induced by the motion of other airfoils is certainly different than the aerodynamic loading of the third (center) airfoil in the cascade. These differences in loading are a function of the reduced frequency, interblade phase angle and other flutter parameters. The summation of the electromagnetic force and the aerodynamically induced force results in a force vector which is different for each airfoil, resulting in phase and amplitude differences along the cascade.

Variations in phase angle along the cascade require that certain adjustments be made blade-to-blade to obtain a constant interblade phase angle, i.e. constant phase relation between blade strain gage motion signals. In order to expedite the testing, and provide for more positive control, the cascade blade driving routine was modified to incorporate provisions for variable blade-to-blade phase angle and duty cycle. With these revisions it was possible to vary independently the driving signal to the electromagnetic driver for each airfoil, allowing compensation for variations in driving force/blade motion phase due to frequency differences.

V. INSTRUMENTATION AND CALIBRATION

The instrumentation for this unsteady blade element cascade aerodynamics program was of prime concern. To make the proposed experiments meaningful, it was necessary to accurately measure in detail both time-steady and time-unsteady cascade flow parameters. In general, the instrumentation was selected to:

- o Establish the airfoil surface steady pressure distributions
- o Establish the airfoil surface unsteady pressure distributions
- o Define regions of flow separation
- o Define the steady and unsteady shock wave patterns
- o Define the steady cascade inlet and exit aerodynamics

This instrumentation is divided into the following two functional areas, with some overlap.

- o Steady-state aerodynamic instrumentation
- o Unsteady aerodynamic instrumentation

All instrumentation was designed and distributed in such a manner as to obtain meaningful data and minimize aerodynamic interference. Detailed calibrations were performed on the instrumentation to assure the attainment of exact quantitative data.

STEADY-STATE AERODYNAMIC INSTRUMENTATION

The objective of the steady-state testing was to quantitatively determine the details of the cascade steady flow field. The instrumentation was selected to accurately determine the cascade inlet and exit pressure, flow angle, and Mach number distributions as well as the blade surface static pressure distributions. The steady-state instrumentation was concerned with three basic flow regions: cascade inlet, cascade exit, and airfoil surface. A discussion of each region follows.

In the DDA rectilinear cascade facility, the cascade inlet flow field was established by means of a sharp-edged wedge positioned upstream of the cascade at the exit of the calibrated 1.3 Mach nozzle. The inlet flow direction was determined by the orientation of this wedge with respect to the nozzle exit flow field. The wedge boundary layer profile has been established experimentally and was accounted for in defining the inlet flow direction. Changes of the inlet flow field are made by rotating the cascade with respect to the fixed nozzle blocks. The inlet Mach number was established by expansion (Prandtl-Meyer) of the nozzle flow about the wedge. The 1.31 cascade inlet Mach number was calculated based on the degree of expansion. Using this procedure, the inlet flow field was defined employing the following instrumentation techniques.

The cascade inlet total temperature and total pressure were defined, based on measurements in the facility low velocity stagnation tank. The inlet flow angle was determined by the orientation of the wedge with respect to the nozzle flow, with the wedge boundary layer profile taken into account. The inlet Mach number was calculated based on the degree of expansion of the flow. The inlet static pressure was based on the isentropic flow relations. Cascade sidewall static pressure taps were located immediately upstream of the leading

edge of each airfoil in the cascade and were used to verify the cascade inlet flow field and to quantitatively aid in establishing the cascade steady-state periodicity.

The cascade exit flow field properties were measured by means of a five-port conical probe similar to the one shown in Figure 12. The probe was calibrated over a range of Mach numbers between 0.35 and 1.80 at various incidence angles between ± 0.26 rad ($\pm 15^{o}$). The probe was mounted on a computer-controlled, three-axis traversing mechanism which was capable of traversing the complete cascade exit flow field. The sensing element of the probe was located approximately one chord length downstream of the cascade exit. The tangential passage length was divided into 5% increments with discrete data taken at each increment over two complete passages downstream of airfoils #2 and #3 (instrumented airfoil). The calibrated probe performance permits the determination of flow parameters via measured pressures on the probe. A series of exit sidewall static pressure taps were located such as to define the exit static pressure distributions across a minimum of two passages and were also located at the trailing edge position of each blade passage to help establish exit periodicity.

The blade surface static pressure distribution was determined during the cascade steady-state testing phase with an airfoil instrumented with 20 surface static pressure taps - ten per surface -- as seen in Figure 13. The chordwise locations are also presented in Figure 13. Twelve of these static taps, six per surface, were at identical locations to those of the Kulite dynamic pressure transducers. Measurements obtained from this airfoil were used to determine the airfoil steady surface pressure distributions, thereby aiding in defining shock location and flow separation regions. Schlieren flow visualization was also used in defining the shock locations and separation zones.

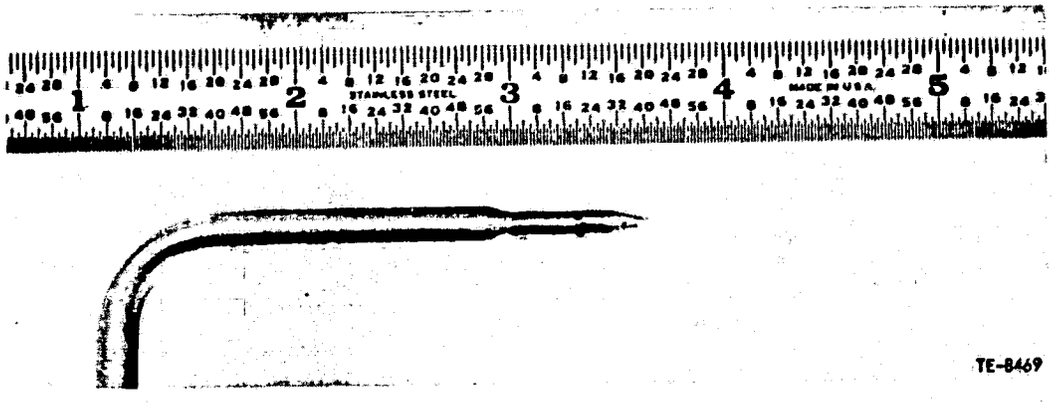

Figure 12. Five port cone probe.

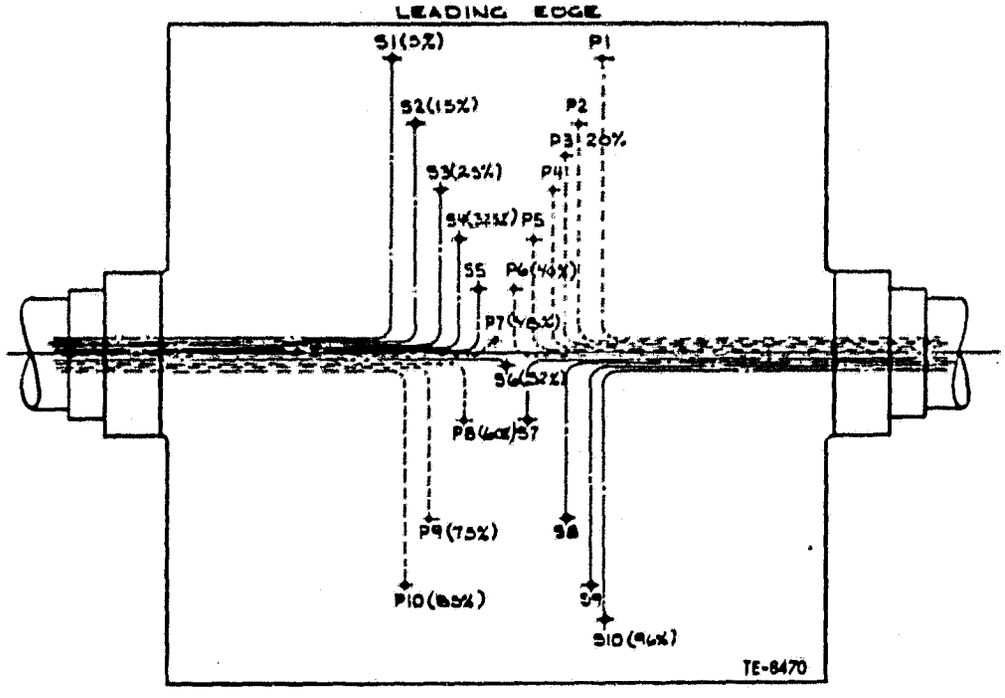

Figure 13. NASA I torsion static tap airfoil schematic.

In summary, the blade surface static pressure tap data was used to:

- Indicate pressure gradients leading to boundary layer separation
- Indicate location of shock waves
- Provide accurate blade surface Mach number distributions.

TIME VARIANT AERODYNAMIC INSTRUMENTATION

To achieve the program goal of producing fundamental experimental data to offer guidance in the development of analytical models for flutter prediction, detailed data needed to be acquired and analyzed to establish the relationships existing between the airfoil motion and that of the surrounding air. The time-unsteady blade surface pressure distributions were of particular interest as they represented the physical driving force of the flutter phenomena. In addition to the unsteady pressure and blade motion measurements, instrumentation was also provided to detect such gross aerodynamic instabilities as boundary layer separation. In the following discussion, provisions for making the necessary unsteady aerodynamic measurements are outlined.

Kulite Semiconductor Products type XTL-1-190-25 thin-line design transducers were used to make the dynamic pressure measurements. Experience in the use of this type of transducer has been gained in DOA stationary and rotating cascade facilities. These high-response pressure transducers were flush mounted on the test airfoil at six chordwise locations staggered across the center 50% of the span on each surface of the airfoil. The distribution of the transducers is shown schematically in Figure 14. A thin, pliable coating over the transducer diaphragm was used to preserve the airfoil surface contour and minimize the aerodynamic disturbances.

To obtain quantitative data from the dynamic pressure measurements, it was necessary to provide not only a static calibration for the pressure transducers, but also a dynamic calibration. Both the static and dynamic calibrations were conducted with the transducers installed on the airfoil. The dynamic calibration reflects such transducer system characteristics as viscous or mechanical damping caused by the method and manner in which the transducer is affixed to the airfoil.

This calibration was made using a dynamic pressure generator which is capable of varying the frequency and amplitude of the input pressure signal. This device is basically a siren-tuned oscillator employing a 120-hole rotor wheel upstream of a similar 120-hole stator plate. The pressure signal amplitude is controlled by the air pressure level supplied to the rotor inlet. The signal frequency is simply controlled by the rotor angular speed. An axisymmetric contraction horn attached to the stator exhaust serves to focus the pressure signal to the smaller test section. In the calibration procedure, the input signal was monitored for amplitude and frequency with a piezoelectric reference

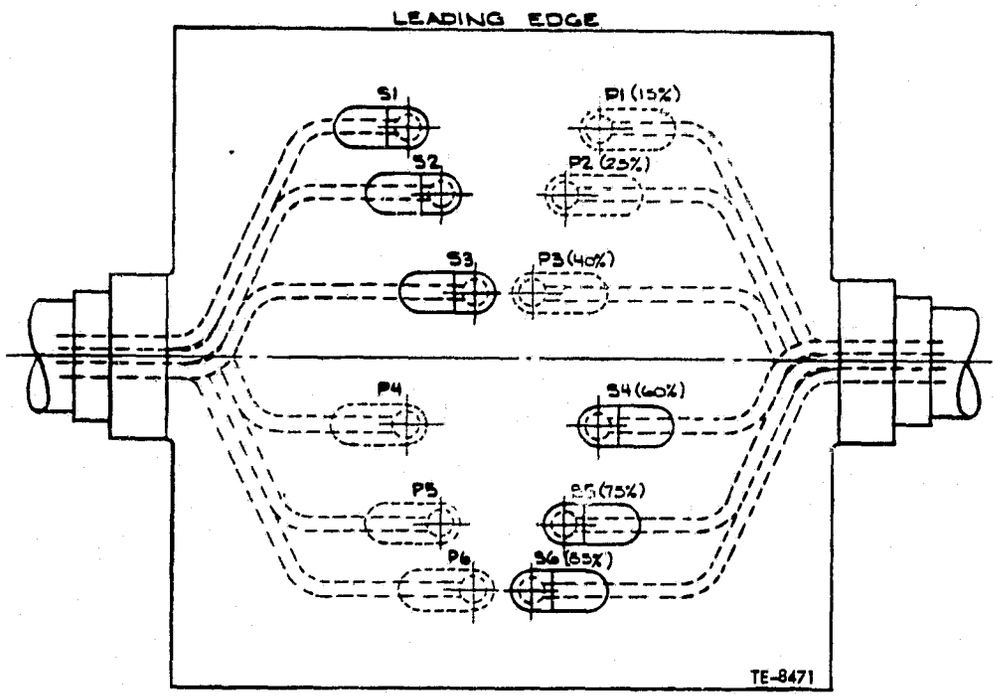

Figure 14. NASA I torsion Kulite dynamic pressure instrumented airfoil schematic.

transducer. This high frequency transducer was dynamically calibrated by the manufacturer over a range of known pressure step inputs. In addition, the transducer was calibrated at DDA for lower pressure ranges using a pistonphone acoustic generator. The output signal from the instrumented test blade was monitored and analyzed for signal strength and frequency content. Figure 15 presents the frequency response data for two Kulites coated with RTV and flush mounted on an airfoil. The transducer mounting techniques and RTV coating procedure is identical to that used in the NASA torsional cascade. The amplitude ratios were calculated over a frequency range of 400 to 1000 Hz. The mean RMS amplitude ratio of the Kulite output to the reference output was approximately 0.95 in the test frequency range, and was independent of signal frequency. As a result of this calibration, it was concluded that the effects of frequency and signal amplitude on the sensitivity of the RTV-covered Kulites was negligible, being well within the limits of experimental accuracy. Thus additional testing of the NASA torsional airfoil was deemed unnecessary.

In addition to the dynamic pressure calibration just described, it was also necessary to account for the acceleration sensitivity of the installed transducers. The published perpendicular acceleration sensitivity of a Kulite XTL-1-190-25 transducer with an uncovered diaphragm is 0.0005 %FS/g. However, from prior experimental programs, an increased acceleration sensitivity of the Kulites has been identified as being created by the RTV coating used to preserve airfoil contour. Prior to the actual acceleration calibration, the signal conditioners and associated electronics were calibrated at the same frequency level at which the test was conducted. The instrumented airfoil was then installed in the torsion rod bench fixture, and a set of sensitivities relating torsional amplitude to strain gage signal level was obtained for the

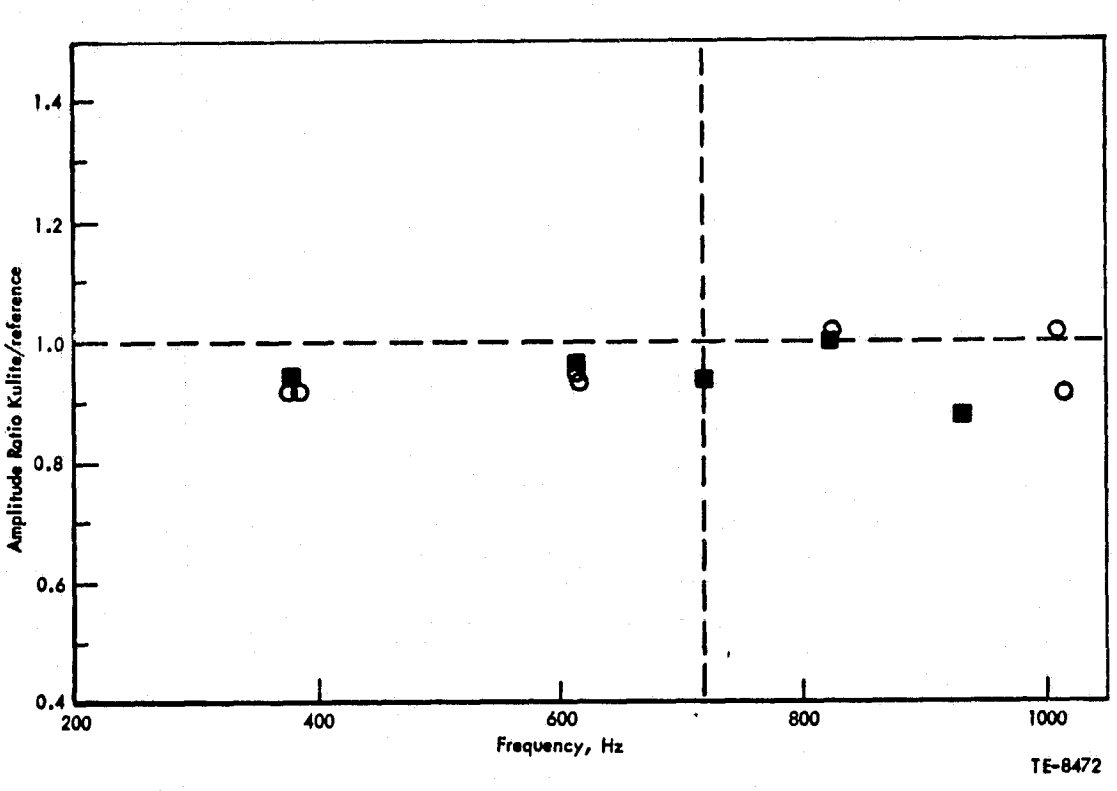

Figure 15. Frequency response data for Kulites coated with RTV.

torsion rod strain gages. The airfoil and bench rig were then installed in a controlled pressure chamber for the transducer calibrations. The Kulites were first calibrated for static pressure over a range of pressures between 2.0 and 10.0 psia, which is typical of their static operating conditions. The pressure in the vacuum chamber was controlled at a prescribed level using a Mensor quartz manometer-controller. The resulting Kulite static pressure sensitivities are presented in Table III.

Table III.
NASA I instrumented airfoil Kulite transducer static calibration sensitivity.

Kulite transducer	Number	Location percent chord	Sensitivity mv/kPa(mv/psi)
Pressure surface	1	15	0.782 (5.393)
	2	25	0.828 (5.711)
	3	40	0.672 (4.630)
	4	60	0.786 (5.416)
	5	75	0.633 (4.365)
	6	85	0.777 (5.360)
Suction surface	1	15	0.619 (4.268)
	2	25	0.726 (5.348)
	3	40	0.675 (4.654)
	4	60	0.641 (4.421)
	5	75	0.838 (5.776)
	6	85	0.663 (4.570)

Upon completion of the Kulite static calibration, the torsion rod bench rig was tuned to the same frequency level as the blade experiences in cascade operation. This was done to ensure that the transducers were calibrated at the same level of frequency and airfoil mode shape as it experiences in the cascade. The vacuum signals are directly relatable to acceleration effects of the RTV/diaphragm or any strain related phenomena resulting from airfoil/transducer deformation. The Kulite signals were analyzed over a range of airfoil torsional amplitudes corresponding to those expected to be encountered in testing. By knowing the torsional amplitude during a particular test, that portion of the total pressure signal due to acceleration/deformation can be removed directly by simple vector subtraction.

As described in the Test Procedure, the time-dependent aerodynamic data was referenced to airfoil torsional motion as determined from strain gage measurements. Blade-to-blade motion was also determined in this manner. Multiple use of strain gages provided for strain gage redundancy and the ability to check out the driver system operation. Misalignment or binding of the driver systems could be observed by checking the phase shift across the tunnel from one driver to another. The strain gages were dynamically calibrated for blade motion using the following technique. The bench rig was assembled with a given blade, and its associated torsion rod pair was instrumented with strain gages. This system was then tuned to the desired torsional natural frequency. The computer was used to digitize and analyze the strain gage signals, printing out the peak voltage produced at each gage by the blade oscillations. The blade amplitude at the leading edge was then determined using a

vernier height-gage. The linear displacements at the leading edge were converted to degrees of rotation and plotted against voltage to yield the gage factors for each strain gage.

Regions of flow separation were identified using surface-type heated film gages in conjunction with flow visualization techniques. Ten film gages were surface mounted at the locations shown in Figure 16. These gages were placed near midspan in a staggered configuration to prevent aerodynamic interference with one another. The chordwise locations for these gages correspond to the chordwise locations of the first five Kulite pressure transducers. Film gage calibration was accomplished by installing the static tap instrumented airfoil in a low speed wind tunnel and mapping out the chordwise progression of the separation zone with increased incidence. This was accomplished by injecting alcohol back through the static pressure taps and observing its flow direction. Once this mapping procedure was finished the heated film airfoil was installed in the tunnel and the procedure repeated. The resulting ac and dc voltage levels of the heated film gage were then recorded. For this type of instrumentation the voltage level is an indicator of the level of wall shear stress. The dc component is related to the mean level of wall shear stress and the fluctuating component is related to the fluctuations in the shear stress level. By assuming that a fully developed turbulent boundary layer exists, the following emperical relationship can be developed for the wall shear stress intensity parameter:

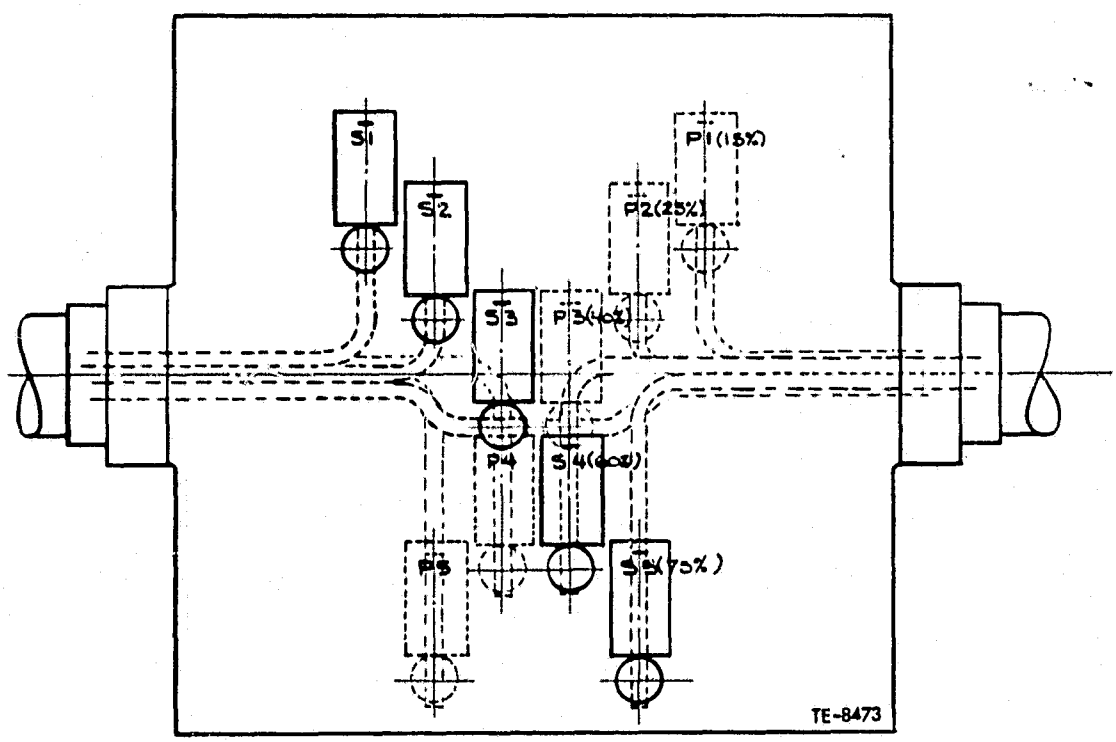

Figure 16. NASA I torsion heated film gage airfoil schematic.

$$\frac{\sqrt{\overline{\tau_w}^2}}{\tau_w} \qquad \frac{6.0E^2\ E'^2}{(E^2 - E_o^2)E}$$

where $\frac{\sqrt{\overline{\tau_w}^2}}{\tau_w}$ = shear stress intensity parameter, E = dc voltage, E' = ac voltage, and E_o = zero flow voltage. Figure 17 is a typical plot showing the shear intensity level as a function of airfoil incidence angle. The sharp increase in shear intensity near 0.07 rad (4^o) is an indicator of flow separation.

Flow visualization was used to aid in the evaluation of the unsteady aerodynamic data obtained throughout the test. Time-dependent schlieren flow visualization of the unsteady aerodynamic cascade phenomena was obtained with a high-speed movie camera.

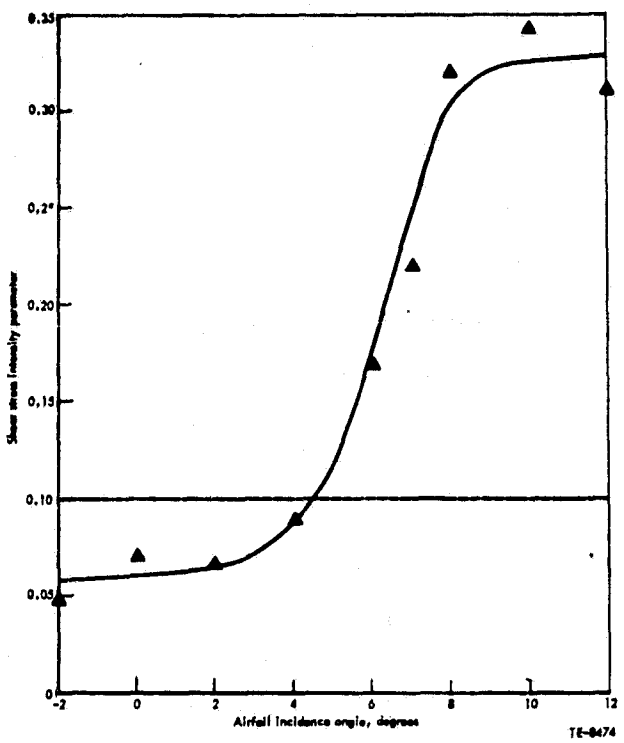

Figure 17. Typical heated film gage calibration curve.

VI. EXPERIMENTAL TEST PROCEDURE

All three of the torsional mode cascades evaluated followed the same overall experimental test procedure. The three cascade configurations are tabulated below.

Cascade Configuration	Solidity	Setting Angle
Baseline	1.17	1.07 rad (61.5^{o})
Reduced solidity-nominal setting	1.06	1.07 rad (61.5^{o})
Reduced solidity-open setting	1.06	1.02 rad (58.5^{o})

The cascade test procedures were designed to obtain valid two-dimensional steady and time-variant data and were based on the invaluable experience acquired by DDA in approximately seven years of time-unsteady experiments and ten years of steady flow supersonic cascade investigations. Three phases of test effort were performed for each cascade:

- o Steady state cascade investigation
- o Unsteady cascade investigation
- o Flow separation study

The nominal solidity-nominal setting angle cascade was first tested, being evaluated in each of three distinct phases. When it was completed the reduced solidity hardware was installed and the testing was repeated for the two levels of cascade setting angle.

STEADY STATE CASCADE INVESTIGATION

The objectives of the steady cascade testing were to establish a periodic steady-state cascade flow field and to obtain a complete definition of the cascade steady-state performance and the blade surface pressure distributions. The airfoil cascade was installed in the DDA supersonic cascade facility with the airfoils in a fixed stationary mode. The center airfoil in the cascade was instrumented with 20 static pressure taps, 10 per surface, as defined in the instrumentation plans.

Cascade periodicity was established, based on the leading edge sidewall static pressure tap measurements, the cone probe exit survey over the center two airfoil passages, and the schlieren flow visualization of the cascade operation. With the periodicity established, the steady performance of the cascade was measured at the specified steady operating points. The baseline cascade was tested at the four steady operating points as outlined as follows:

	Cascade static pressure ratio	Cascade exit Mach number
Far away from flutter boundary	1.04	1.25
Near flutter boundary - outside	1.20	1.14
Near flutter boundary - inside	1.35	1.05
Deep into flutter region	1.45	.99

It was felt that these cascade static pressure ratios best met the test objectives of describing the A100 operating characteristics through flutter, and provide a realistic distribution of cascade exit Mach number.

Because of its lower pressure ratio capability, as caused by the reduced solidity level, the reduced solidity cascade was evaluated at the "near flutter boundary-inside" condition along with the "far away from flutter boundary" condition. This was true for both cascade setting angle levels. The steady cascade investigation served to establish the cascade operation and to obtain the steady-state aerodynamic data without the complication of the airfoils being able to respond.

TIME VARIANT CASCADE INVESTIGATION

Upon completion of the steady cascade investigation for each task, the static tap instrumented airfoil (the center airfoil in the cascade) was replaced with the one instrumented with 12 flush-mounted Kulite pressure transducers. The airfoil cascade drive systems were then made operational, and the unsteady cascade investigation initiated.

At each of the steady operating points, the cascade periodicity was reestablished. Six interblade phase angle values were investigated for each steady point. For each of the unsteady data points, the motion of each airfoil in the cascade was measured, and once an interblade phase was established, the pressure signals were recorded on tape along with the reference strain gage signal. These taped pressure signals were analyzed as detailed in Data Reduction/Correlation section.

During the time variant investigation, only four of the five cascade airfoil drivers were operational. The fifth or last cascade airfoil was fixed because of its proximity to the lower tailboard. Earlier testing, over a range of cascade pressure ratios, had verified that the fifth airfoil motion had no effect on the middle airfoil's unsteady flow field.

FLOW SEPARATION INVESTIGATION

The flow separation study followed the completion of the steady and unsteady cascade investigation for each torsional mode cascade configuration. This involved replacing the center airfoil in the cascade with the previously described instrumented heated film gage airfoil. The four other airfoils in the cascade were untouched.

With the airfoils in a stationary mode, steady operating conditions were established at the two unsteady operating points for each cascade wherein the aerodynamic work per cycle had a maximum and a minimum value, determined from the previously described unsteady cascade data. At these operating points the heated-film gage signals and strain gage signals were recorded and qualitatively analyzed to determine any relationships between the boundary layer behavior and the blade motion.

VII. DATA REDUCTION/CORRELATION

Described herein are summaries of the data reduction procedures and data presentation for both the steady and the unsteady data. A brief discussion of the theoretical technique used for correlation purposes is also included.

STEADY-STATE AERODYNAMIC DATA

The steady state data reduction procedures which are incorporated in the DDA wind tunnel on-line instrumentation system were used to analyze data from the torsional mode compressor cascades. The supersonic wind tunnel on-line instrumentation system yields thirteen pages of computer print-out describing the cascade steady performance for each test condition. Identification of the first stage print out is shown in Figure 18. On this page of the print-out following the title lines, four entries appear which describe the test point operating conditions; cascade inlet Mach number, cascade ideal static pressure ratio, the cascade blade behind which the conical probe data was taken, and the conical probe axial location behind the blade row.

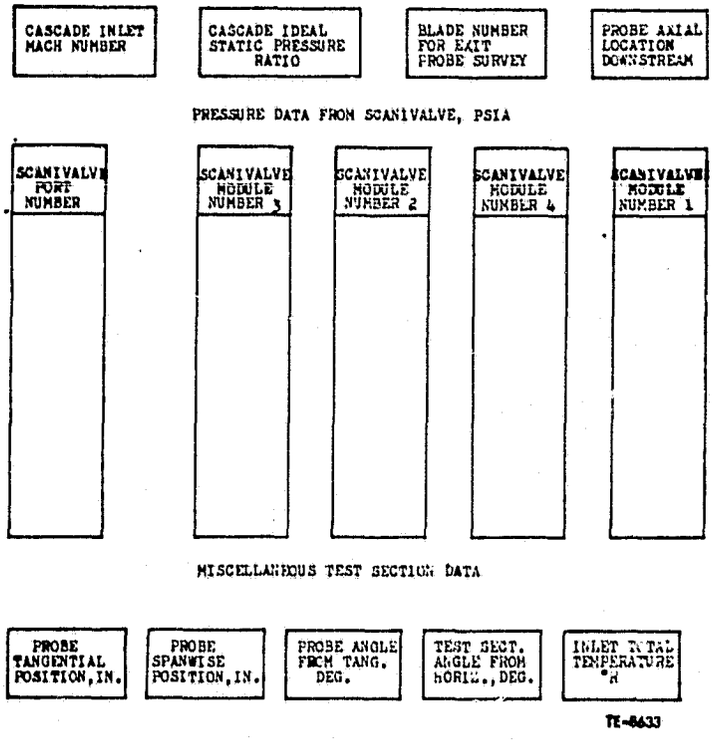

Figure 18. Computer print-out identification--Scanivalve pressure data.

The second entry on the first page of print-out presents a listing of the pressures measured on the four Scanivalves. The first seven ports of each Scanivalve are used for reference calibration pressures with alternate ports thereafter connected to a vacuum source to eliminate transducer hysteresis and minimize pneumatic settling time. From these pressures, the cascade performance is determined.

The last entry on the first page of the print-out presents miscellaneous test section data including the conical probe position in the exit flow field, test section angular position, and the wind tunnel total temperature.

The first entry on the second page of the print-out presents the nozzle exit flow field properties.

The second entry on the second page is the wedge and blade inlet flow parameters determined from the sidewall static pressure taps located in the sidewall ahead of the wedge and each blade.

The last entry on the second page describes the flow properties across the sharp leading edge wedge which is used to expand or compress the nozzle exit flow to establish the cascade inlet Mach number and flow direction.

The first entry on the third page of the print-out consists of two lines describing the cascade physical design parameters.

The last entry on the third page describes the cascade inlet flow field conditions. Identification of the cascade inlet parameters is presented in Figure 19.

The entry on the fourth page of the computer print-out as identified in Figure 20 is the cascade ideal performance based on sidewall static pressures. Included is a listing of the pressures presented on the first page of the print-out for the sidewall static pressure taps. From these pressures, a mean

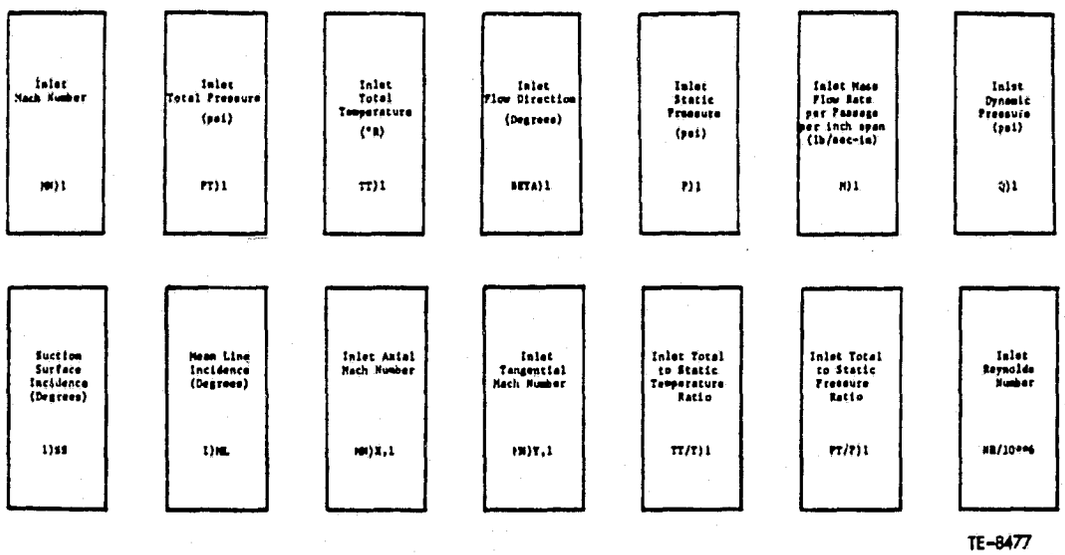

Figure 19. Computer print-out identification - cascade inlet conditions.

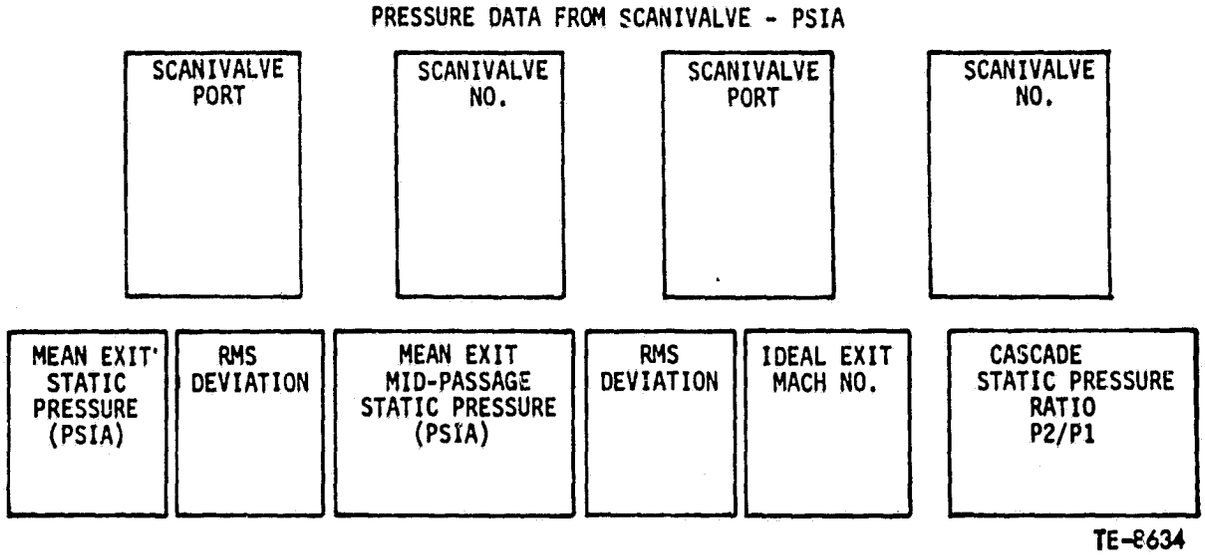

Figure 20. Computer print-out identification - cascade ideal performance.

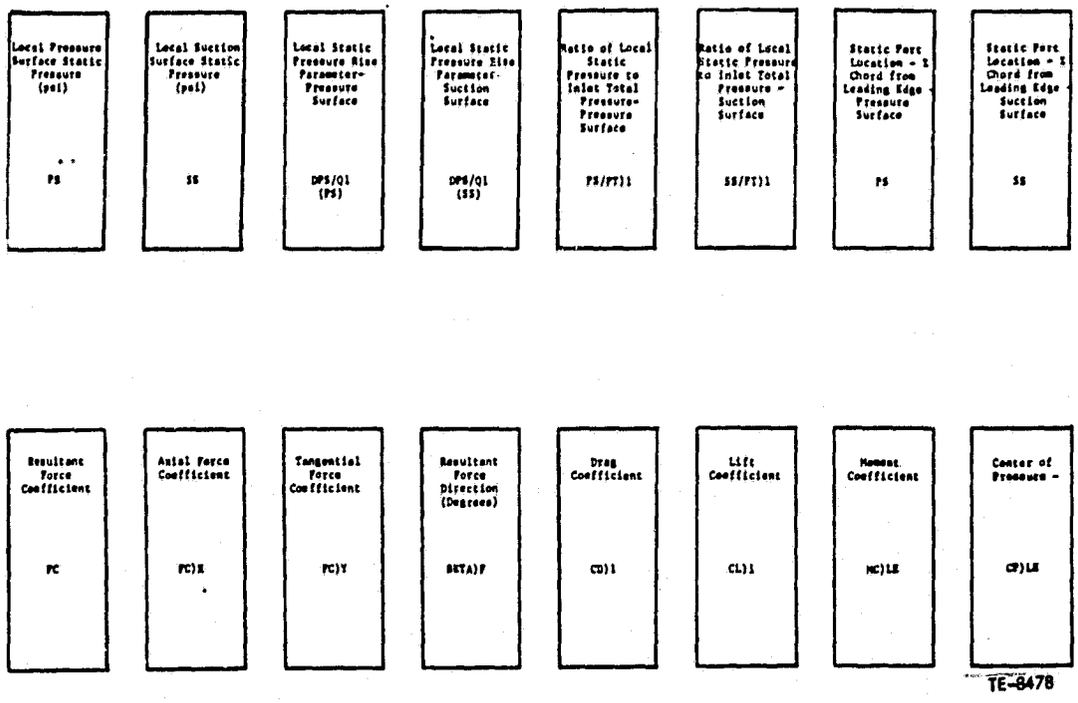

Figure 21. Computer print-out identification - instrumented blade parameters.

exit static pressure and RMS deviation are calculated along with the same parameters for the trailing edge static pressure taps. The cascade ideal exit Mach number and ideal static pressure ratio are determined from the mean exit static pressure.

The fifth page of the computer print-out describes the instrumented blade parameters. The first entry presents the static pressure disbribution on the cascade blade surface along with associated columns describing local performance characteristics and static tap locations in terms of percent chord. Figure 21 provides identification of the entries on the fifth page.

The local cascade exit performance is determined by utilizing a conical probe to measure Mach number, flow angle, and total pressure at twenty discrete points across one passage of the cascade. The probe is positioned at the center of cascade passage number 2 and measurements taken in five percent steps to the center of passage number 4 (data obtained behind blade number 3). The sixth through eleventh pages of the computer print-out present the local exit performance characteristics of the cascade. Figure 22 provides the identification for the parameters presented on these pages.

The cascade exit flow field properties are determined by mass-averaging and mixing to uniform flow the local exit parameters. Identification of the exit flow field parameters on the twelth page of the computer print-out is presented in Figure 23.

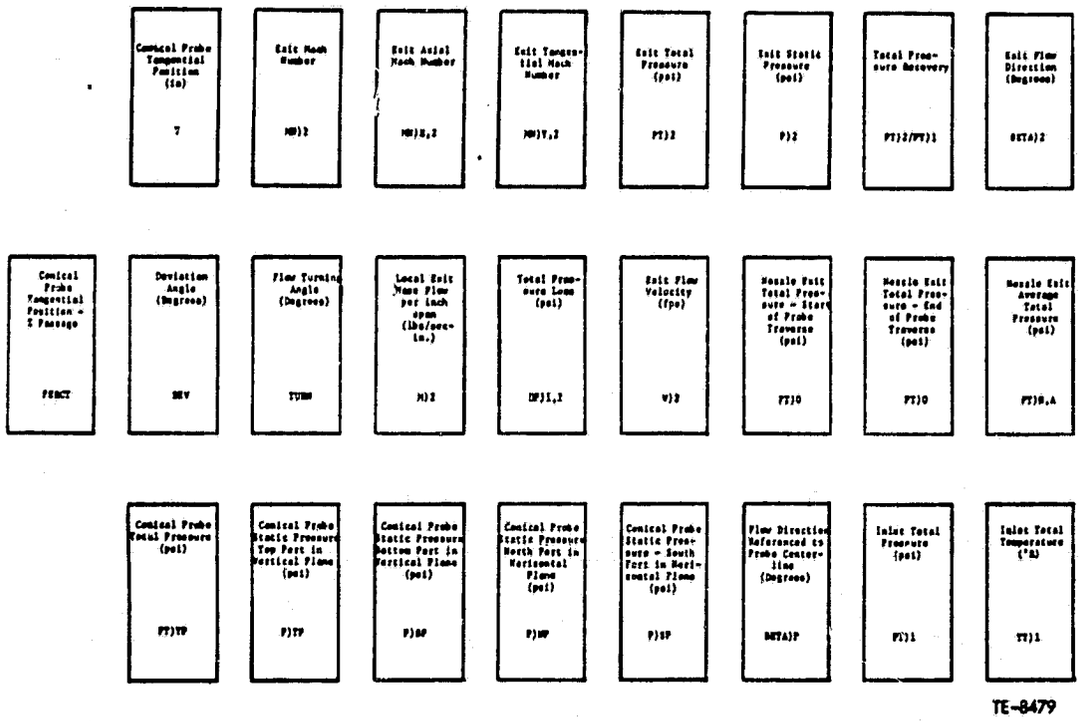

Figure 22. Computer print-out identification - local cascade exit performance.

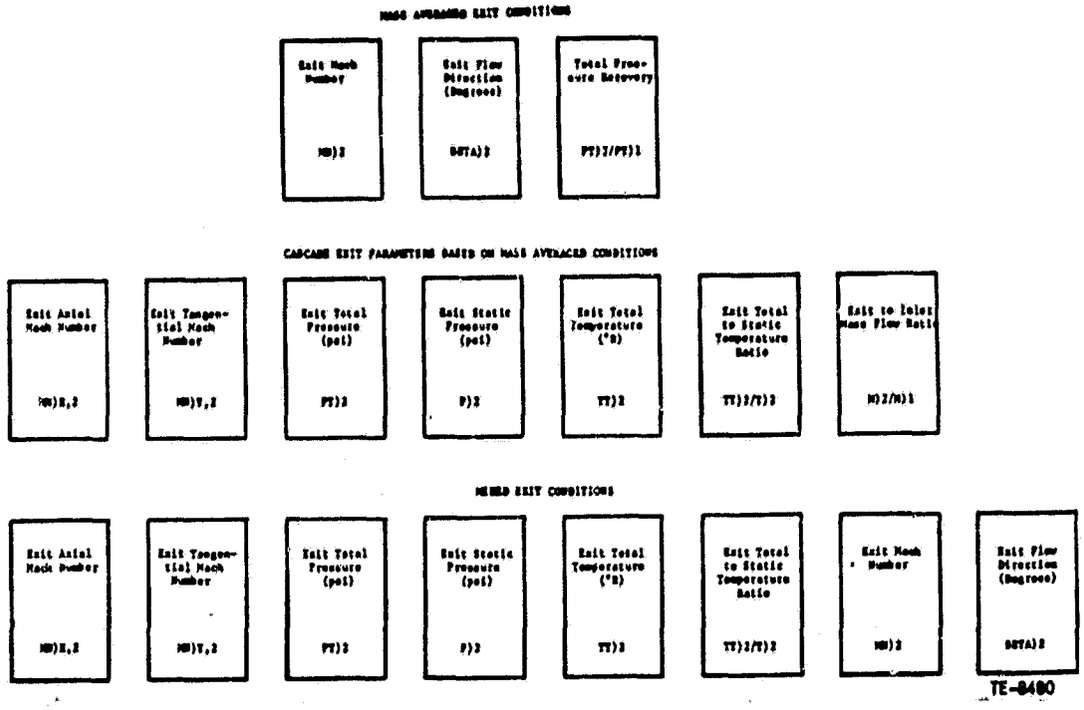

Figure 23. Computer print-out identification - mass averaged and mixed exit conditions.

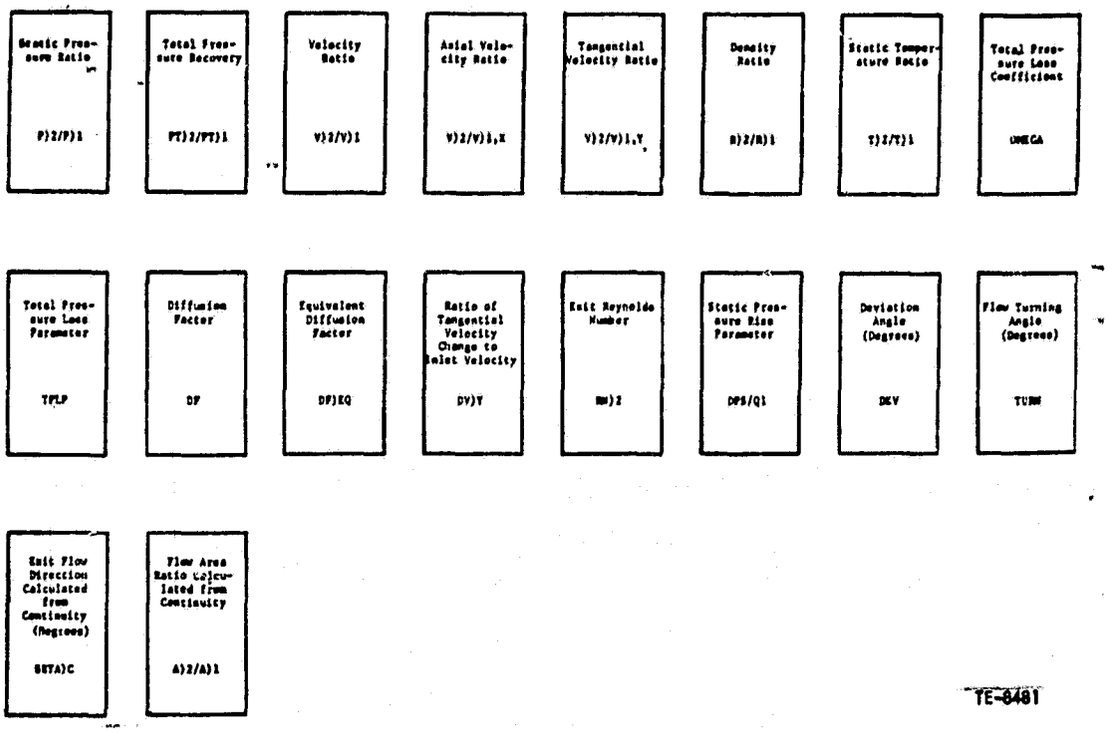

Figure 24. Computer print-out identification overall performance.

The cascade overall performance characteristics relating the inlet and exit properties are presented on the thirteenth page of the computer print-out and are identified in Figure 24.

A sample of the computer print outs for a typical data set is included in Appendix A.

TIME VARIANT AERODYNAMIC DATA

The fundamental time-unsteady data of interest is the complex airfoil surface chordwise pressure distribution. This data, together with the airfoil motion data, determines the aerodynamic stability. The unsteady force (lift) and moment on the airfoil are calculated from this pressure and airfoil motion data.

The instrumentation used to acquire the unsteady data included the following.

- o Strain Gages - Two per airfoil with one on either side of the tunnel.
- o Kulite Pressure Transducers - Six flush-mounted per surface on the center airfoil of the cascade (a total of twelve transducers on blade 3).
- o Heated Film Gages - Five surface-mounted per surface (a total of ten) on the center airfoil of the cascade.

The heated film gages were used to qualitatively examine the transition and flow separation phenomena on the airfoil surfaces for the conditions where the measured unsteady work per cycle attains its maximum and minimum values. The dynamic characteristic of each heated film gage at a particular operating point were determined from the taped oscilloscope traces of the blade motion as defined by the signals from the strain gage and the particular heated film gage. In addition, for the conditions of maximum and minimum unsteady work per cycle, high speed Schlieren movies were taken.

The strain gage and pressure transducer data was acquired simultaneously. The on-line analysis was performed on the strain gage signals concurrent with the magnetic tape recording of the signals from the instrumented blade's strain gage and pressure transducers. The on-line analysis involved eight channels of strain gage data; two per airfoil. The twelve surface dynamic pressure signals, six from the pressure surface and six from the suction surface, along with the reference strain gage signal from the instrumented blade were taped for each data point.

In this investigation an analog-to-digital converter having a rate of 100,000 points per second was used. Data, either real time or taped, was digitized and stored on a magnetic disc for evaluation. An "n" cycle data averaging technique was adapted early in the test program to eliminate background noise from the unsteady pressure signal. This technique is currently used at DDA to reduce data from a low speed, single-stage compressor facility. The data is sampled at a preset time, triggered by a square wave pulse supplied by the airfoil drive system computer. The analog-to-digital converter is triggered by the positive voltage at the leading edge of the pulse, initiating the acquisition of the unsteady pressure data. The data can be sampled for "m" ensembles and "n" cycles and an average data set obtained. The results of this technique can best be presented with the aid of Figure 25, which represents the output signal of the first pressure surface pressure transducer obtained when 100 ensembles of 5 cycles were averaged.

The data analysis comprised the following three techniques:

- o Amplitude calculation
- o Frequency calculation
- o Phase calculation

In the amplitude calculation, a second order least square fit of the data on the positive and negative sides of the time axis was made for each half cycle of motion. The signal amplitude becomes the average of the positive peaks minus the average of the negative peaks.

The frequency of the time-dependent digital data was determined through the autocorrelation function. This function describes the dependence on the values of the data at one time, X_i, on the values at another time, X_{i+r}. The lag time, ΔT, is inversely proportional to the rate at which the data are digitized. An autocorrelogram of the digitized data exhibits the features of a sine wave plus random noise. A second order least square fit function was fit to the data depicting the second positive peak of the autocorrelogram. The inverse of the time at which this least square function is a maximum is equal to the frequency, f, of the time-dependent data. Additionally, the frequency is known from the computer commanded input and an on-line, electronic counter.

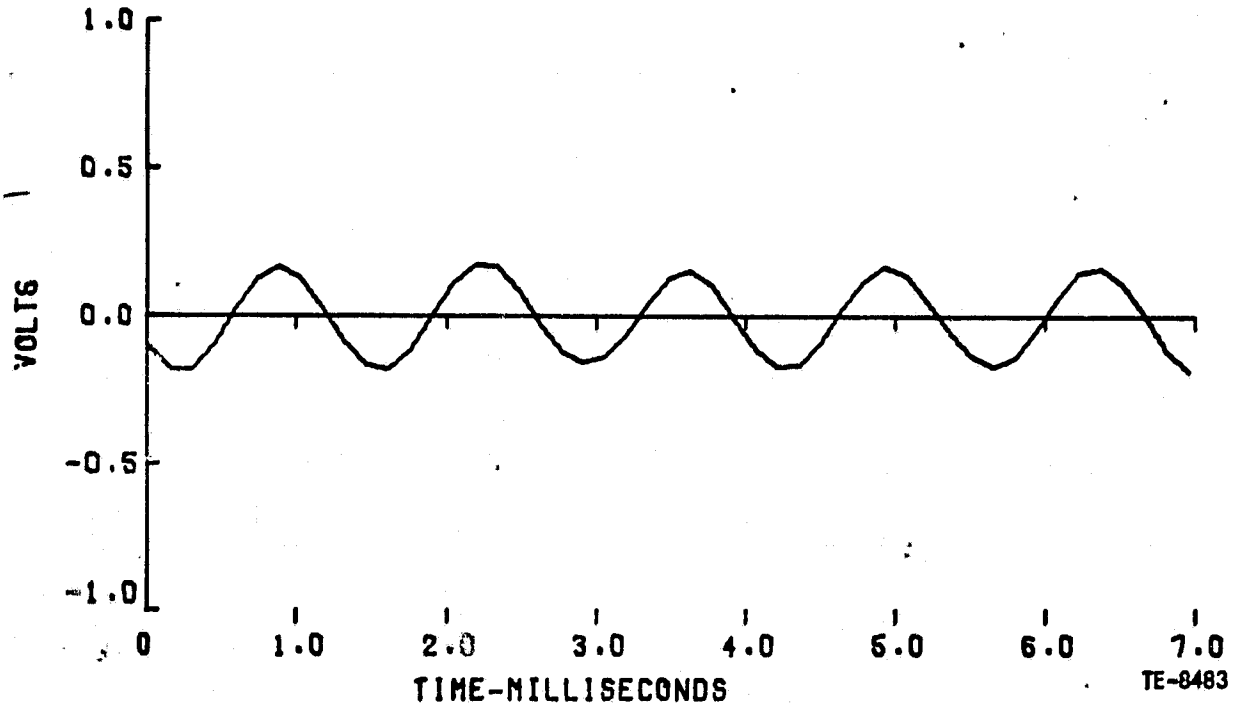

Figure 25. "N" - cycle averaging technique results for first pressure surface Kulite signal.

The phase difference between the time-variant digitized signals was calculated through the cross-correlation function. This function, for two sets of data, X_i, Y_i, describes the dependence of the values of one set of data on the other. As in the frequency calculation, a second order least square curve was fit to the data in the nearest to zero time positive peak of the cross-correlogram. The time, t_p, at which this least square function is a maximum was analytically determined. The phase difference, in degrees, was calculated as

$$\Theta_p = t_p \, f \, 360$$

where f is the frequency calculated for the airfoil motion from the strain gage data.

The reference signal for all of the phase angle determinations was a strain gage signal from the instrumented airfoil. This signal was common in both the on- and the off-line data acquisition.

Figures 26 through 32 present the on-line and off-line unsteady data formats. A summary chart listing the steady aerodynamic operating characteristics of the cascade together with the desired frequency, interblade phase angle, reduced frequency, and multiplexer rate, was printed on the first page, as indicated in Figure 26.

The next pages, indicated in Figures 27 and 28, present the cyclic summaries of the positive and negative peaks of the signals, respectively.

The auto and cross-correlation results are presented on the following pages, as indicated in Figures 29 and 30.

Figure 31 shows a summary of the dynamic pressure transducer data. Included herein are the raw values of phase (after electronic calibration) and unsteady pressure, as well as the corresponding values after correction for acceleration effects.

Figure 32 depicts the last page of the time variant data set. This includes the airfoil surface unsteady pressure distributions, as well as the resultant real and imaginary parts of the lift and moment coefficients.

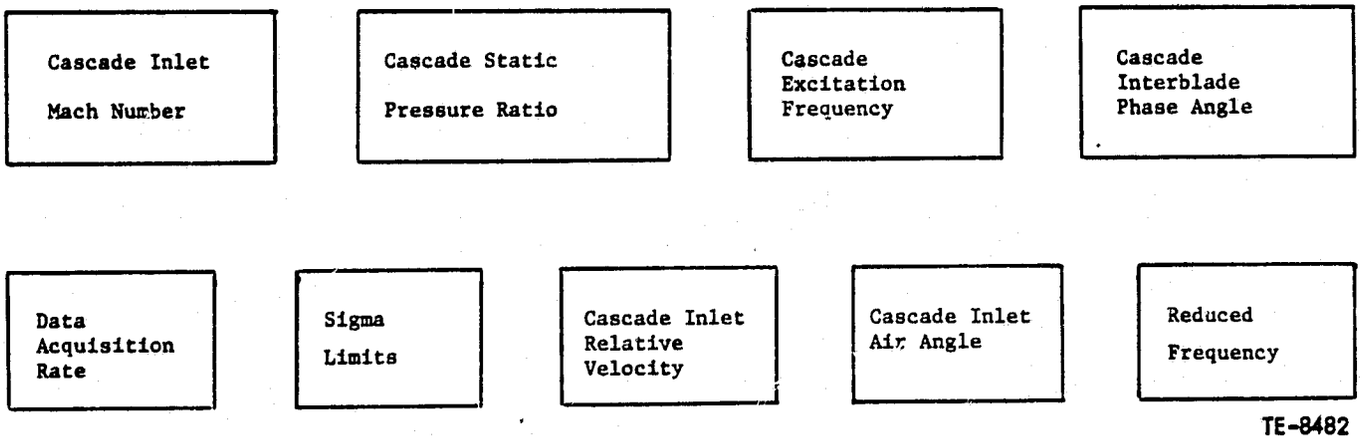

Figure 26. Unsteady data output format page 1.

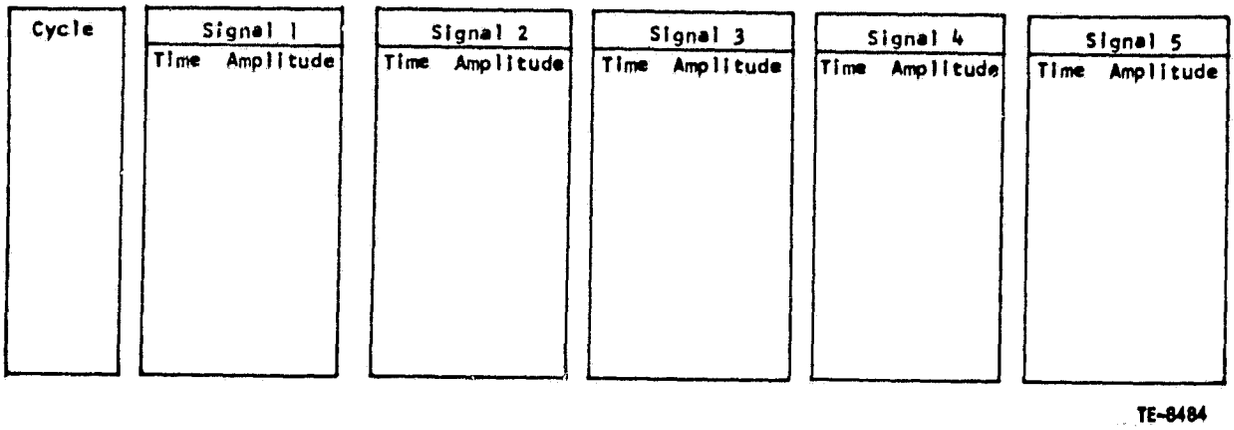

Figure 27. Unsteady data output format page 2.

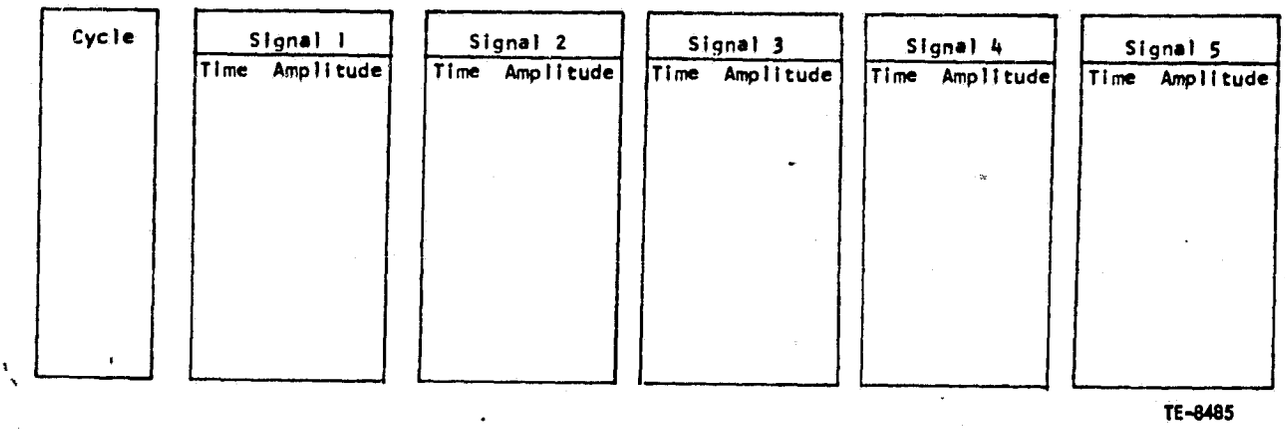

Figure 28. Unsteady data output format page 3.

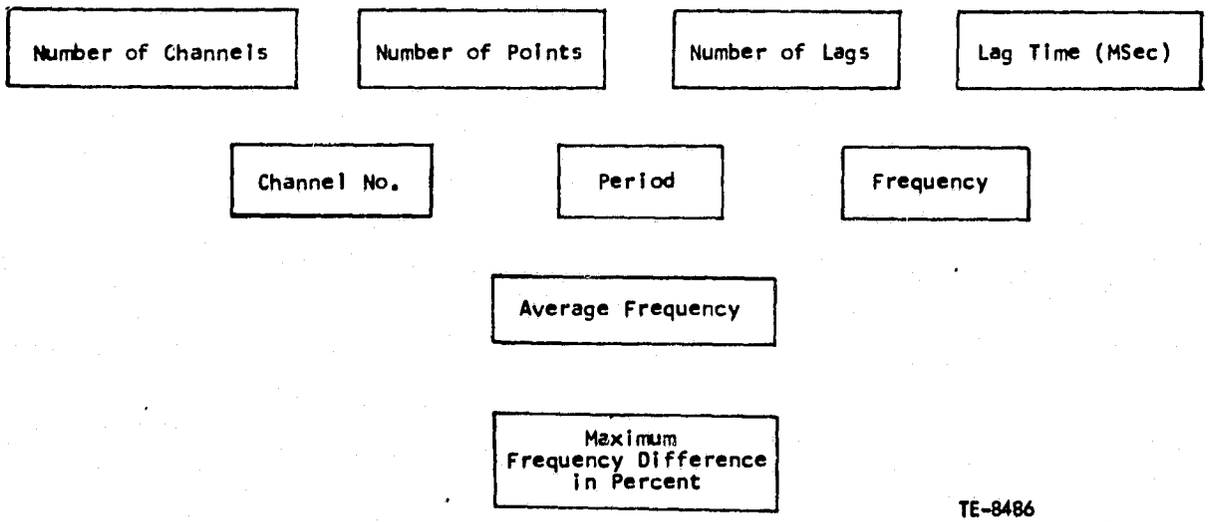

Figure 29. Unsteady data output format page 4.

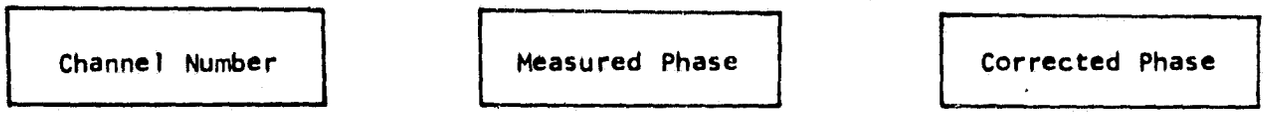

Figure 30. Unsteady data output format page 5.

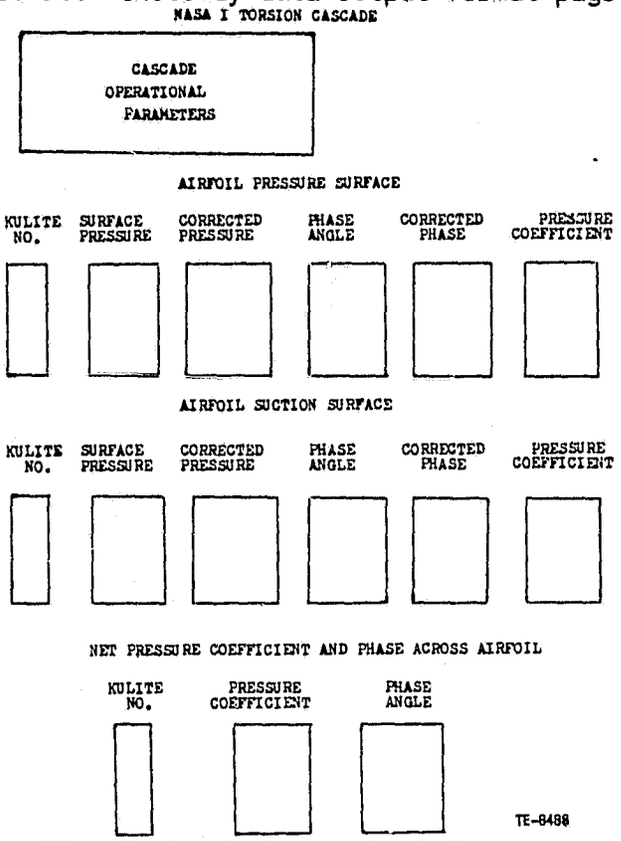

Figure 31. Unsteady data output format page 6.

A sample of the aforementioned data sheets for a typical data set is included in Appendix B.

The time-variant aerodynamic data are correlated against the DDA in-house developed method for a supersonic cascade utilizing a finite-difference/pressure-amplitude-function technique. This technique was further modified[1]* to allow for variable blade-to-blade amplitudes of harmonic oscillation. The

*Numbers are references which are listed at the end of this volume.

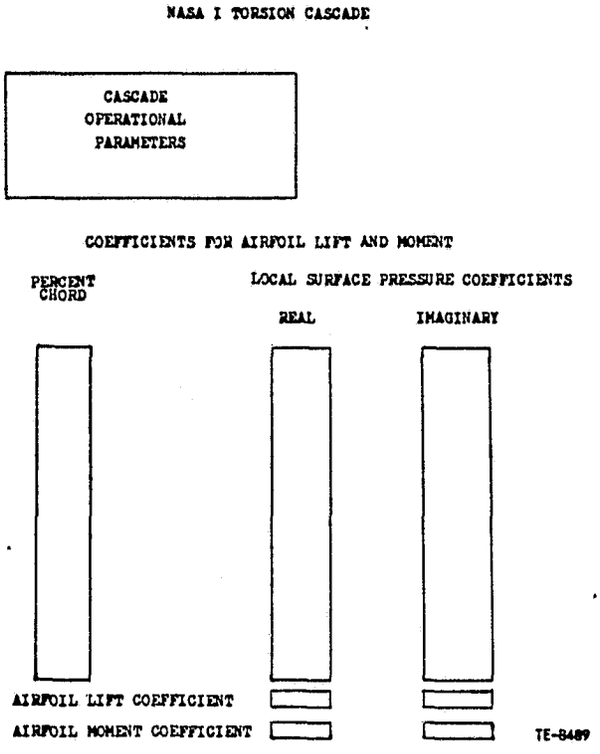

Figure 32. Unsteady data output format page 7.

flow model is inviscid and assumes an operating pressure ratio of unity. The airfoils are assumed to be zero camber, zero thickness, flat plates. The theoretical results obtained from this numerical method have been compared to the published results of Garrick and Rubinow[2], Chalkley[3], Verdon and McCune[4] and Platzer and Brix[5] in the Ph. D. Thesis of John Caruthers at Georgia Institute of Technology[6]. All of the torsional mode cascade time-variant data was correlated against the analysis.

VIII. RESULTS AND DISCUSSION

The steady state aerodynamic test computer print-outs for all three torsion mode cascades are included in the supplement to Volume I a sample of which is included in Appendix A. Included herein are the schlieren photographs and associated data plots for each steady-state data point. The data plots include definitions of the inlet and exit periodicity based on sidewall static pressure measurements, wake survey total pressure variations and the instrumented airfoil static pressure distribution. The time variant aerodynamic test print-outs are also included in the supplement to Volume I and a sample output is presented in Appendix B.

BASELINE CASCADE

The baseline torsion cascade steady-state overall performance results are summarized in Table IV. The mass averaged results are based on an exit survey of the second and third airfoil.

Table IV. Baseline Torsion Mode Cascade Steady-State Performance Summary

	Far away from flutter	Near boundary outside	Near boundary inside	Deep into flutter
Inlet Mach Number	1.315	1.315	1.315	1.315
Mass Averaged Static Pressure Ratio	1.04	1.20	1.35	1.45
Mass Averaged Exit Mach Number	1.25	1.14	1.05	0.99
Mass Averaged Exit Air Angle	1.13 rad (64.8^{o})	1.14 rad (65.4^{o})	1.14 rad (65.3^{o})	1.14 rad (65.6^{o})
Mass Averaged Total Pressure Loss	0.065	0.069	0.068	0.067

The baseline cascade steady-state schlieren photographs are included in Figures 33 through 36. These schlierens correspond to cascade mass averaged static pressure ratios of 1.04, 1.20, 1.35 and 1.45 respectively. As the cascade is back-pressured the shock system moves up into the airfoil passage, until at 1.45:1 it becomes almost normal to the airfoil surface. At this pressure ratio one can observe a boundary layer separation on the suction surface (lower surface) downstream of the shock wave intersection with the airfoil.

The cascade periodicity is a measure of the uniformity of the blade-to-blade flow. Figures 37 through 40 are the baseline cascade inlet and exit periodicity plots based on sidewall static pressure measurements. As can be seen from these plots the flow field is quite uniform throughout the cascade. This is further qualified by the cascade wake surveys presented in Figures 41 through 44. These data result from the cone probe survey downstream of the second and third (instrumented) cascade airfoil. The measured local value of total pressure is normalized to the cascade inlet total pressure.

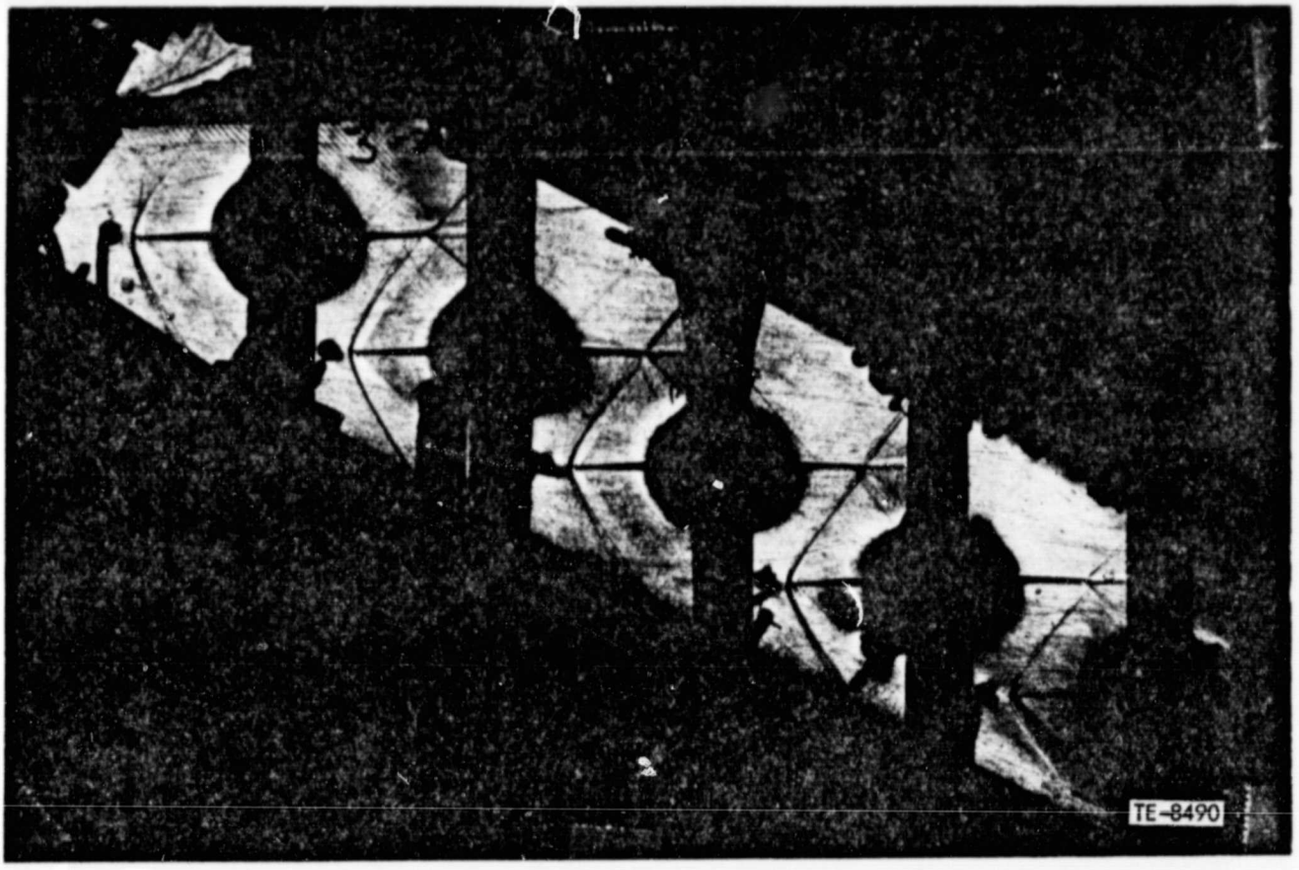

Figure 33. NASA I torsion baseline cascade schlieren at 1.04:1 mass average pressure ratio.

Figure 34. NASA I torsion baseline cascade schlieren at 1.20:1 mass average pressure ratio.

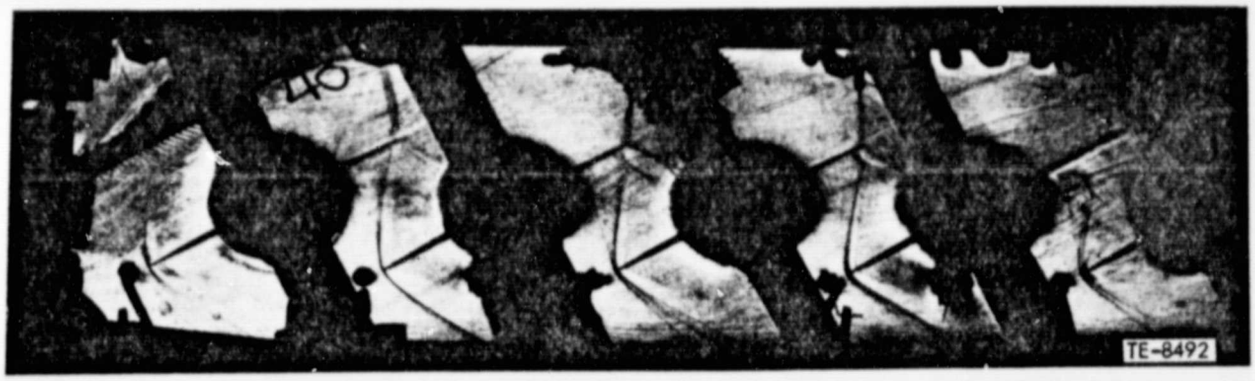

Figure 35. NASA I torsion baseline cascade schlieren at 1.35:1 mass average pressure ratio.

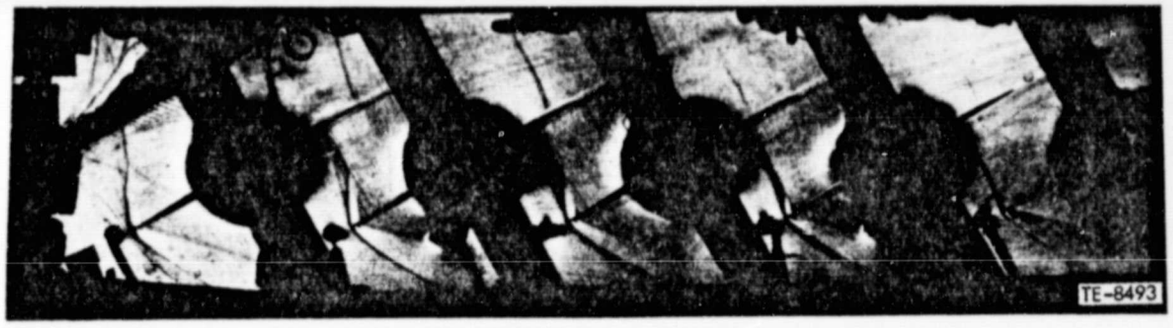

Figure 36. NASA I torsion baseline cascade schlieren at 1.45:1 mass average pressure ratio.

Figures 45 through 48 are the instrumented (middle) airfoil surface pressure distributions referenced to the inlet total pressure. These data plots correspond to cascade static pressure ratios of 1.04, 1.20, 1.35 and 1.45 respectively.

In addition to the schlieren flow visualization, a technique utilizing alcohol injection through the surface static taps was used to define flow separation regions. This technique resulted in the location of a separation region downstream of the intersection of the passage shock with the suction surface boundary layer. As the cascade static pressure ratio was increased this passage shock moved forward on the suction surface causing the length of the separated region to increase. At the 1.45 static pressure ratio, indications were that the aft 40% of the airfoil's suction surface was separated.

After completion of the steady-state testing, the static tap airfoil was removed and the Kulite instrumented airfoil was installed. The time variant aerodynamics computer output data sheets for the torsion mode cascades are included in the supplement and a sample data set is included in Appendix B. This includes the print-out of the raw and corrected data. Plots of the

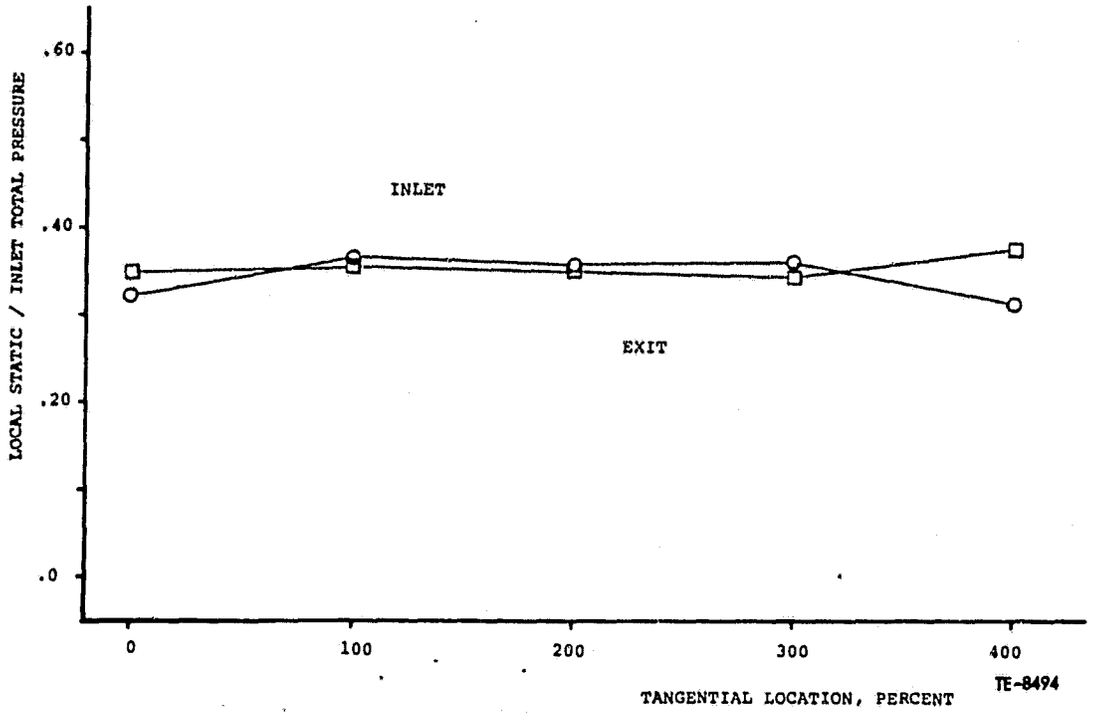

Figure 37. Baseline cascade sidewall static periodicity plots at R_c = 1.04.

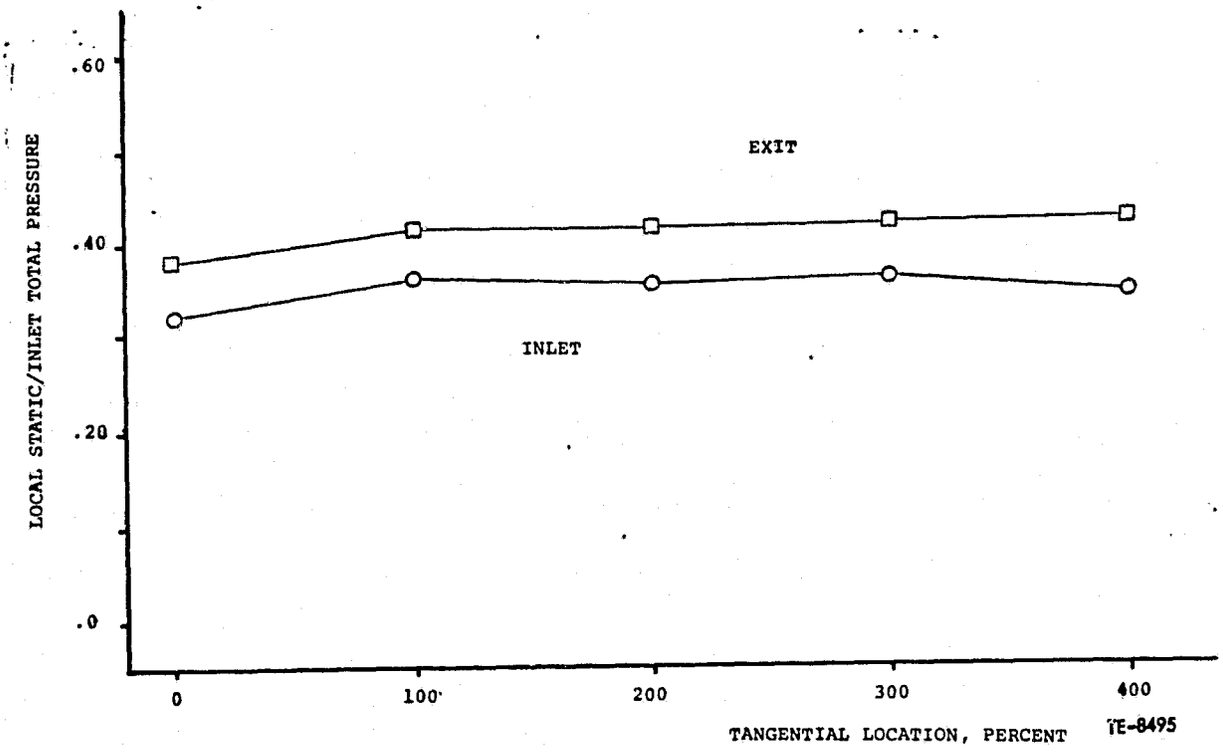

Figure 38. Baseline cascade sidewall static periodicity plots at R_c = 1.20.

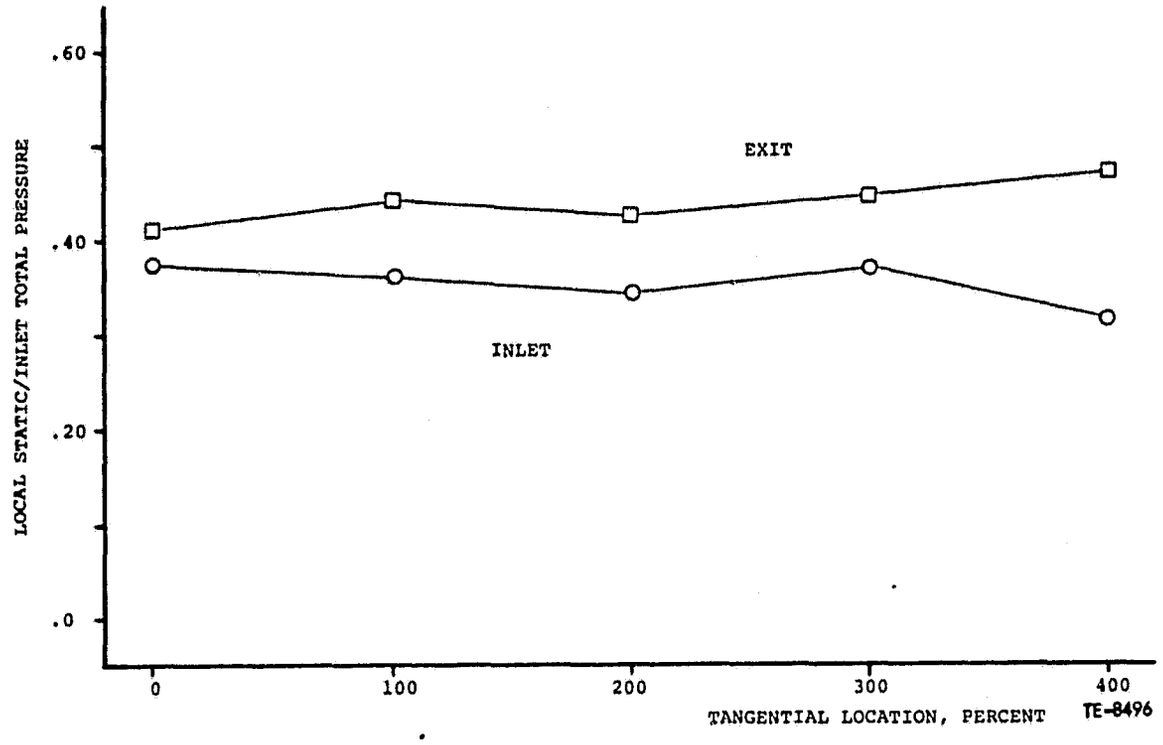

Figure 39. Baseline cascade sidewall static periodicity plots at R_c = 1.35.

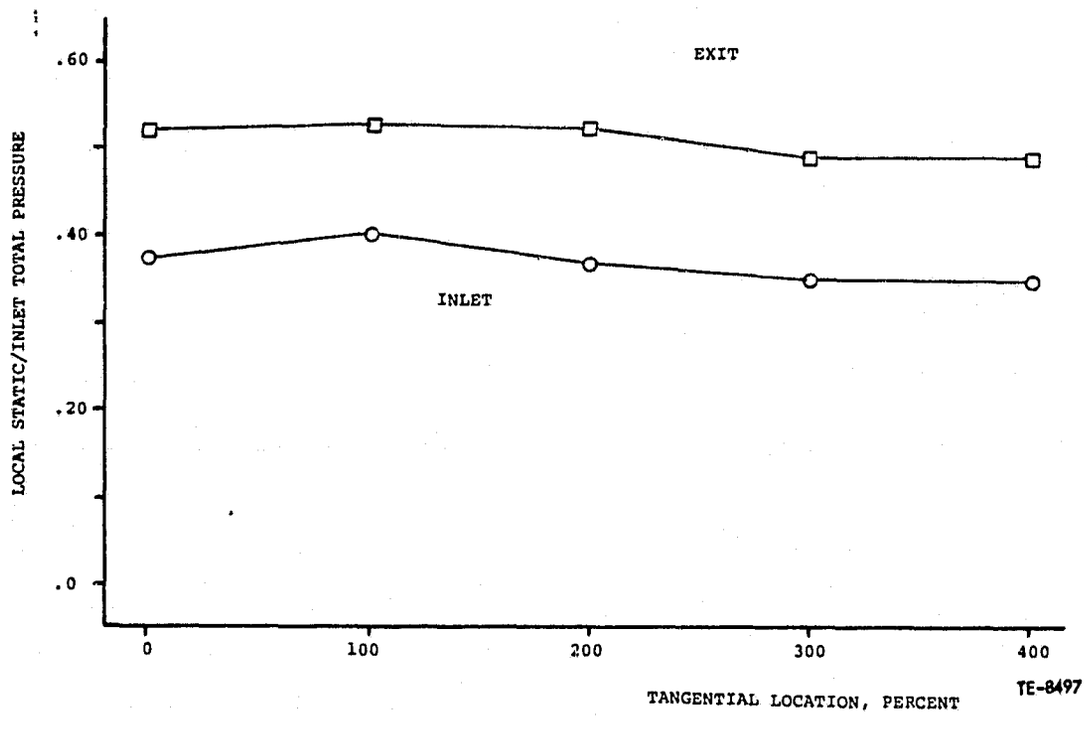

Figure 40. Baseline cascade sidewall static periodicity plots at R_c = 1.45.

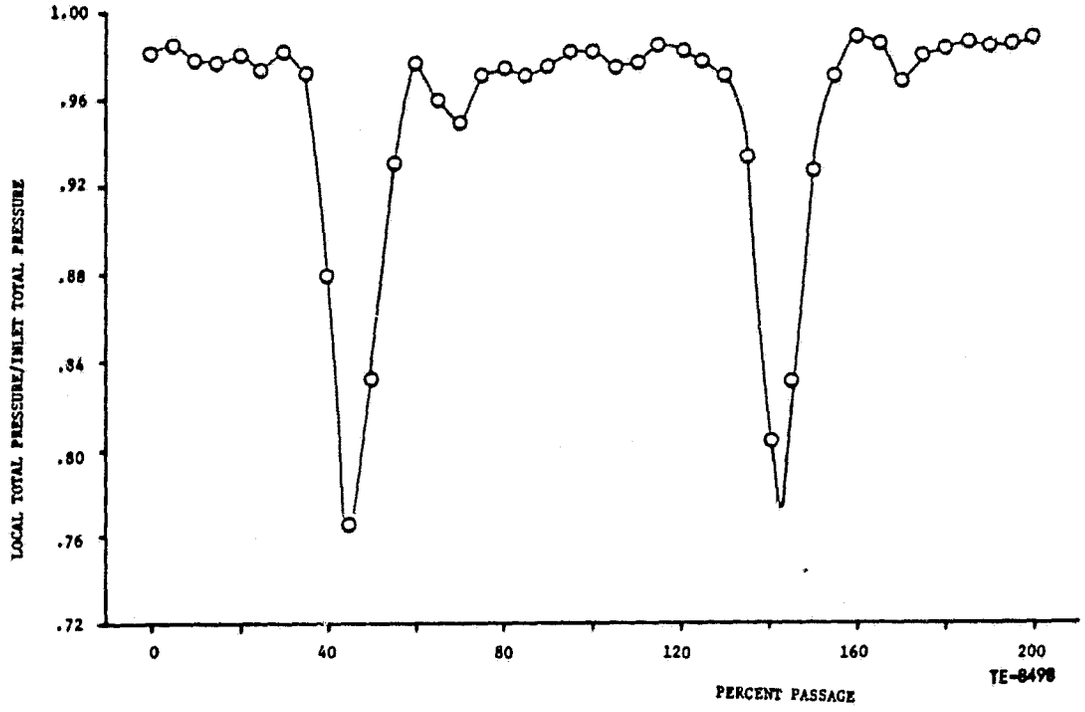

Figure 41. Baseline cascade exit survey at 1.04:1.

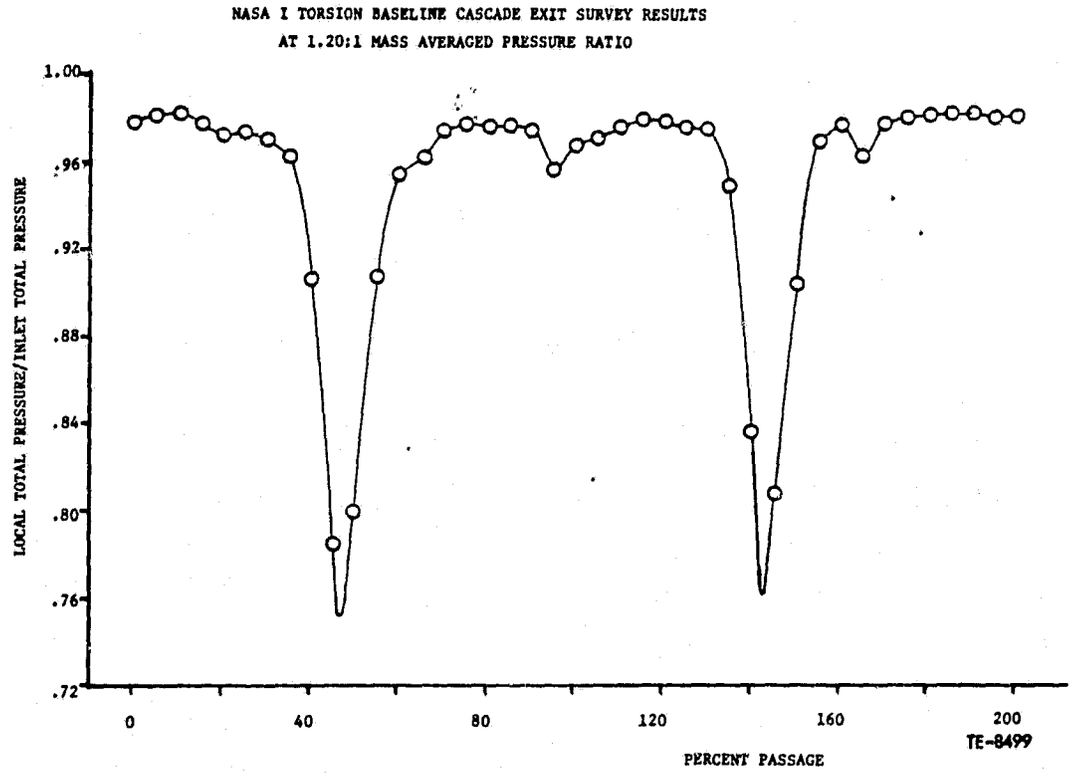

Figure 42. Baseline cascade exit survey at 1.20:1.

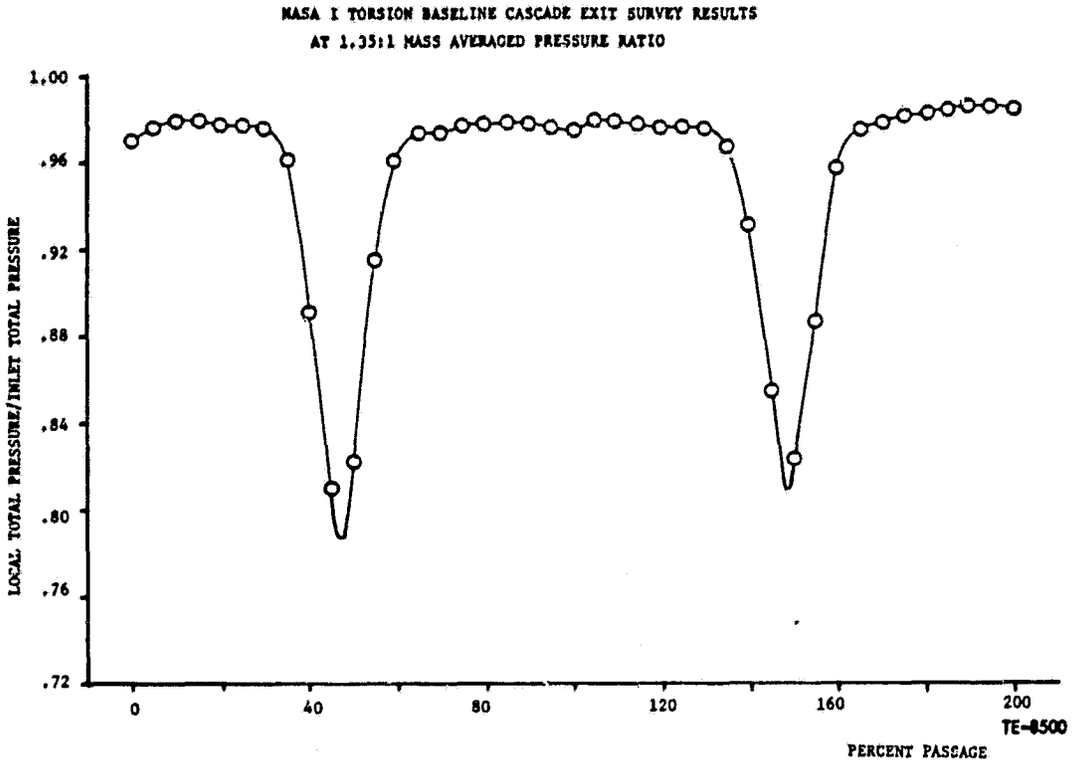

Figure 43. Baseline cascade exit survey at 1.35:1.

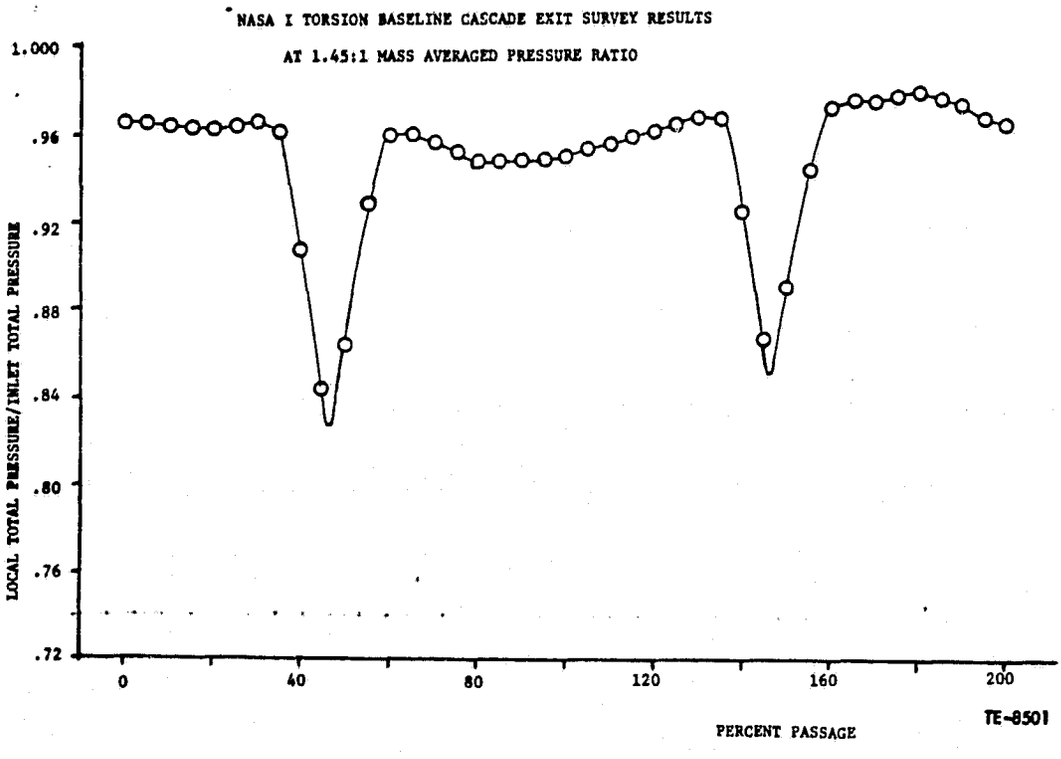

Figure 44. Baseline cascade exit survey at 1.45:1.

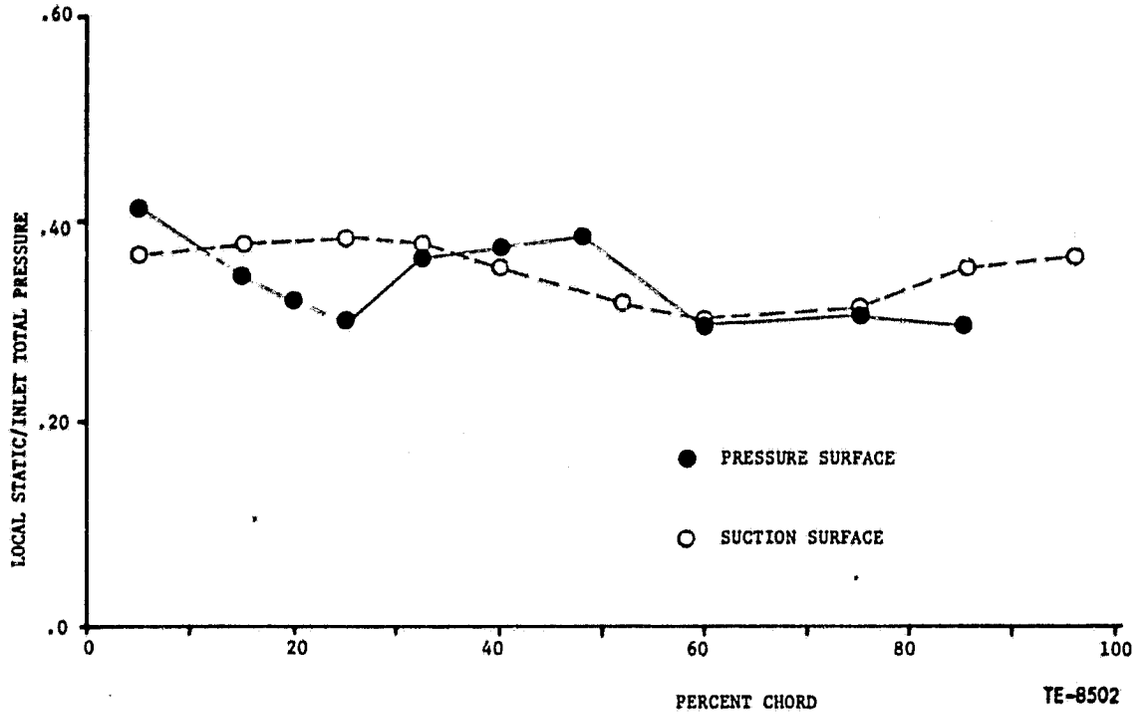

Figure 45. Baseline cascade instrumented airfoil static pressure distribution at 1.04:1.

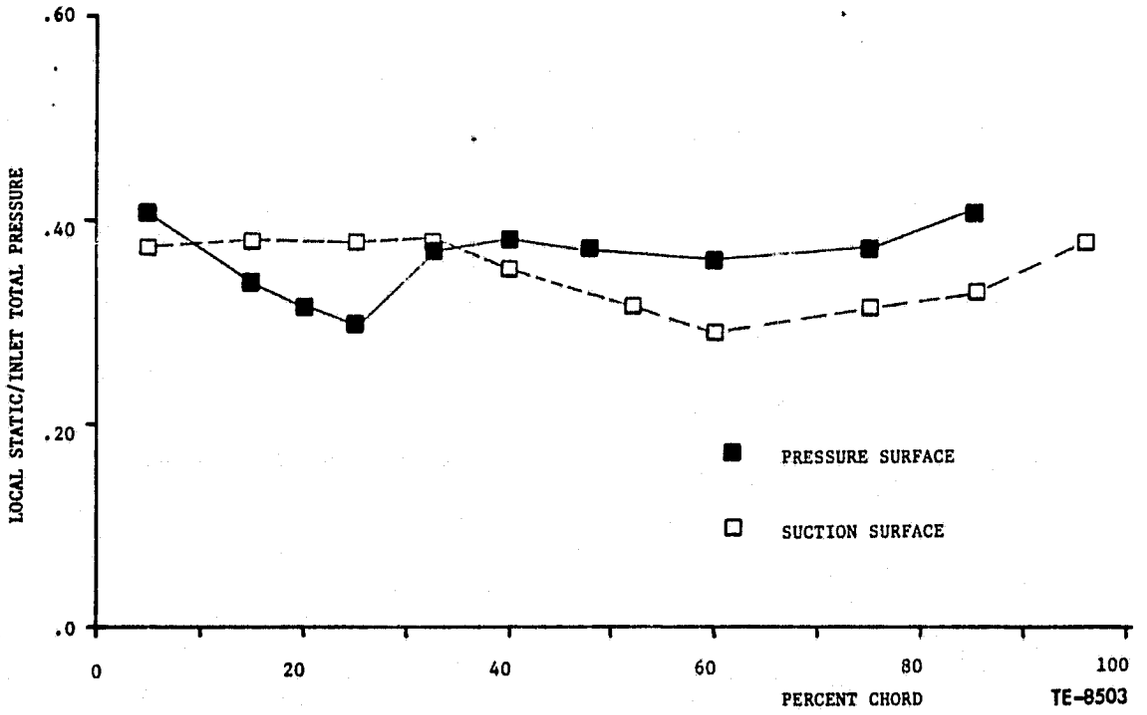

Figure 46. Baseline cascade instrumented airfoil static pressure distribution at 1.20:1.

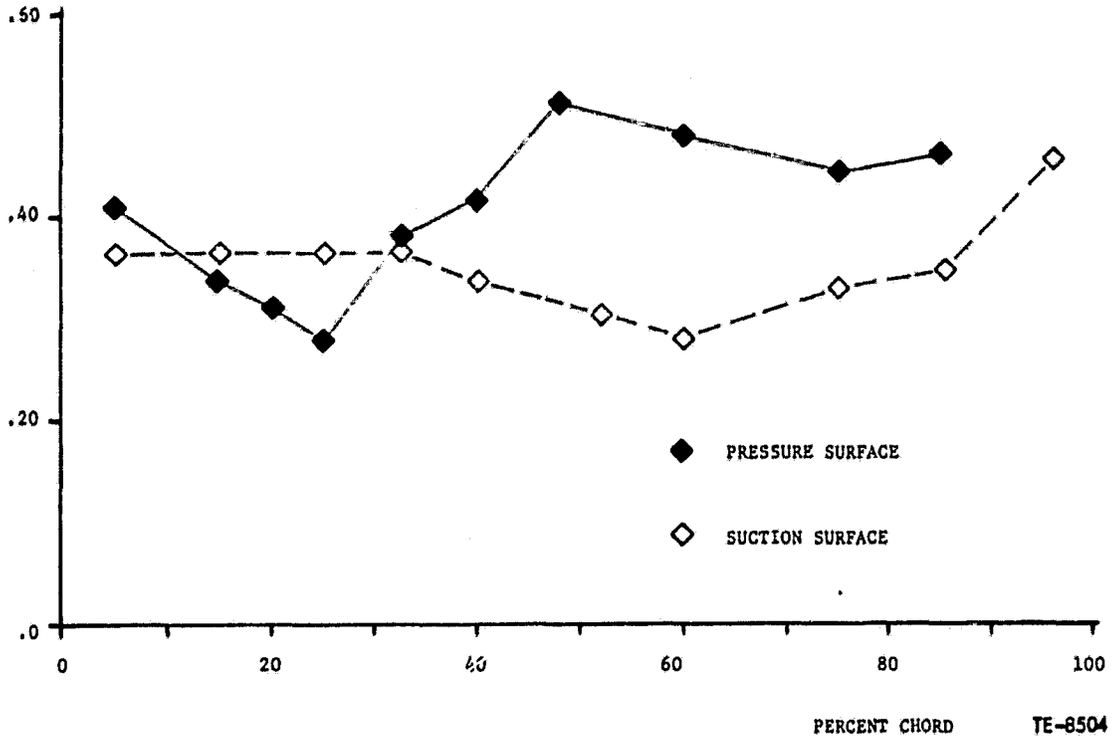

Figure 47. Baseline cascade instrumented airfoil static pressure distribution at 1.35:1.

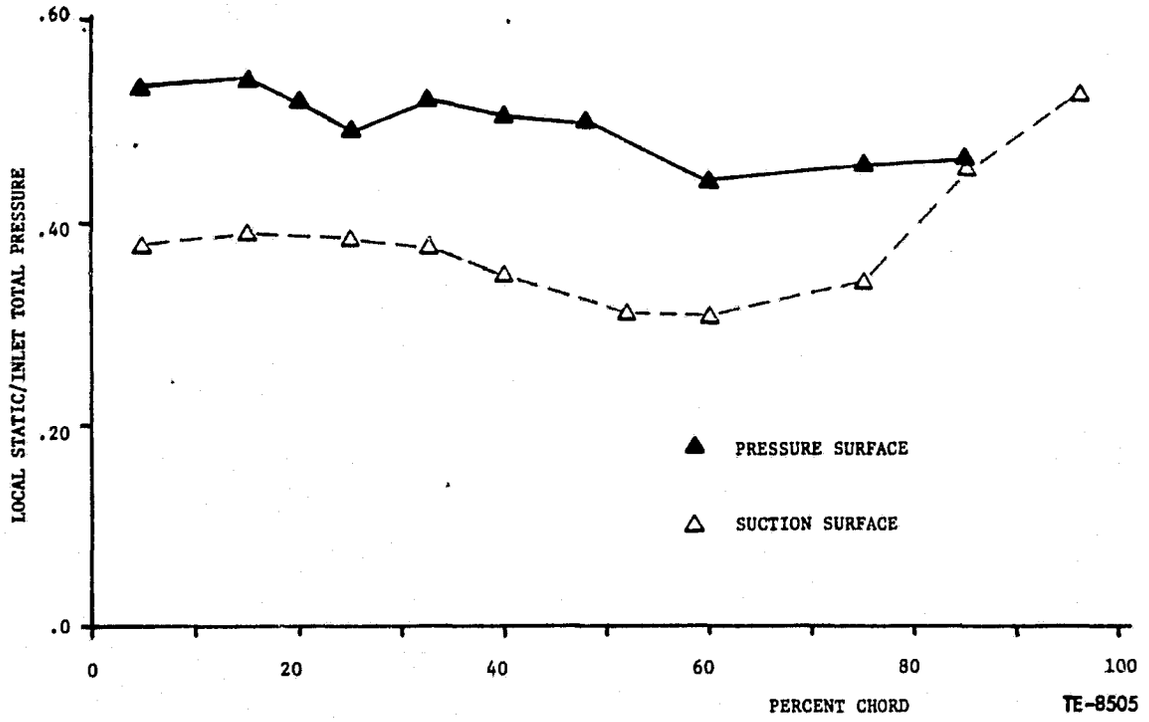

Figure 48. Baseline cascade instrumented airfoil static pressure distribution at 1.45:1.

chordwise variation of the measured surface unsteady pressure and the corresponding phase lag are included herein. These data plots also include the correlation with the aforementioned variable amplitude analysis. All pressure surface data is plotted as a solid symbol and the corresponding variable amplitude theory is represented by a solid line. All suction surface data is plotted as an open symbol and the theory is a dashed line.

At each steady state cascade operating point a total of six interblade phase angles between +3.14 rad (+180°) and -3.14 rad (-180°) were tested. A tabulation of the baseline torsion cascade test phase angles along with other pertinent operational characteristics are included in Table V. The first column in the figure is the average test interblade phase angle to the nearest 0.09 rad (5°). Positive phase angles means that the first airfoil, leads the second airfoil, leads the third airfoil, etc., and is equivalent to a backward traveling wave. The static pressure ratios in the table are cascade mass averaged values.

Table V. NASA I torsion baseline cascade time variant testing results summary.

Phase Radians	Cascade Static Press Ratio R_c	Interblade Phase Angle--Radians ϕ_{1-2}	ϕ_{2-3}	ϕ_{3-4}	Average Phase Radians $\bar{\phi}$	σ_ϕ	Blade Torsional Amplitude α_3 Radians	α_1/α_3	α_2/α_3	α_4/α_3	Frequency, Hz f	Reduced Frequency k
3.142	1.04	3.026	3.257	3.103	3.124	±0.131	0.001	0.76	0.52	1.27	725	0.44
1.396		1.590	1.136	1.407	1.377	±0.229	0.001	0.87	0.20	0.67	714	0.43
0.0		0.075	-0.103	0.140	0.012	±0.133	0.004	0.34	0.61	0.75	724	0.44
-0.524		-0.450	-0.604	-0.541	-0.532	±0.077	0.002	0.31	0.26	0.69	725	0.44
-0.873		-0.833	-0.927	-0.939	-0.899	±0.058	0.002	0.71	0.78	0.32	745	0.45
-1.571		-1.588	-1.585	-1.468	-1.546	±0.068	0.002	0.56	0.59	0.97	724	0.44
3.142	1.20	3.227	-3.168	3.094	3.196	±0.031	0.001	0.46	0.43	1.32	725	0.44
1.571		1.803	1.422	1.534	1.574	±0.115	0.001	0.50	0.56	1.16	725	0.44
0.0		-0.054	0.045	0.115	0.042	±0.075	0.001	0.67	0.40	1.10	724	0.44
-0.698		-0.791	-0.682	-0.654	-0.709	±0.073	0.002	0.26	0.22	0.53	725	0.44
-1.047		-0.925	-1.119	-1.059	-1.035	±0.099	0.002	0.23	0.37	0.61	725	0.44
-1.571		-1.710	-1.454	-1.674	-1.613	±0.138	0.002	0.35	0.41	1.20	725	0.44
3.142	1.35	3.278	-3.187	3.215	3.087	±0.093	0.001	0.84	0.34	1.95	710	0.43
1.571		1.494	1.482	1.555	1.510	±0.040	0.001	0.87	0.50	2.80	730	0.44
0.0		0.157	-0.117	0.136	0.033	±0.164	0.003	0.22	0.59	0.25	725	0.44
-0.349		-0.417	-0.365	-0.370	-0.384	±0.030	0.002	0.31	1.02	1.53	730	0.44
-0.698		-0.740	-0.654	-0.632	-0.675	±0.056	0.002	0.34	0.94	0.29	725	0.44
-0.873		-0.780	-0.936	-0.869	-0.862	±0.079	0.002	0.34	1.53	1.41	725	0.44
2.967	1.45	2.997	2.936	2.843	2.925	±0.079	0.001	1.21	0.85	0.60	724	0.44
1.134		1.155	1.213	1.065	1.145	±0.075	0.002	0.54	0.44	0.34	725	0.44
0.0		0.072	-0.134	0.087	-0.009	±0.122	0.002	0.64	0.96	1.11	724	0.44
-1.047		-1.150	-1.037	-1.052	-1.080	±0.061	0.004	0.36	0.65	0.50	724	0.44
-1.488		-1.606	-1.293	-1.508	-1.470	±0.161	0.002	0.66	0.96	0.73	725	0.44
-1.745		-1.676	-2.007	-1.707	-1.796	±0.178	0.001	0.35	0.40	0.25	725	0.44

The individual phase angles (ϕ_{1-2}, ϕ_{2-3} and ϕ_{3-4}) tabulated are the measured blade-to-blade test values. The average phase tabulation includes the average of the three individual phases and the deviation ($\pm\sigma_\phi$) from this average. The blade amplitude tabulation includes the instrumented (third) airfoil zero-to-peak torsional amplitude (α_3), and the amplitudes of airfoils 1, 2 and 4 as normalized to the instrumented airfoil. Test frequencies are tabulated with their respective reduced frequency value (k).

Figures 49 through 52 are plots of the chordwise variation of the unsteady pressures and their corresponding phase lags at the low (1.04:1) static pressure ratio and a 3.14 rad (180^{o}) interblade phase angle. The data is correlated to DDA's variable amplitude analysis. The experimental variation in the magnitude of the unsteady pressure signal phase lag was found to be within $\pm$0.17 rad ($\pm 10^{o}$). This variation was obtained by making data analysis runs over segments of taped unsteady pressure signals obtained when the test conditions were identical. The corresponding variation in the unsteady pressure signal amplitude was within $\pm$7%. As can be seen from these figures the correlation is excellent. The 40% chord pressure surface phase lag discrepancy can be traced to the passage shock reflection. The constant amplitude results are also presented for reference. Additional data plots are included in Appendix A.

The appropriate unsteady lift and moment coefficients were calculated from the measured blade amplitude and the unsteady pressure coefficient and its phase relative to the blade motion. Figures 53 and 54 are typical chordwise phase lag and unsteady pressure coefficient data used in the lift and moment coefficient analyses. A linear interpolation was assumed between Kulite locations. The leading edge and trailing edge values were obtained by extrapolating the 15% and 85% chord data. The real and imaginary unsteady pressure components were obtained from the following relations:

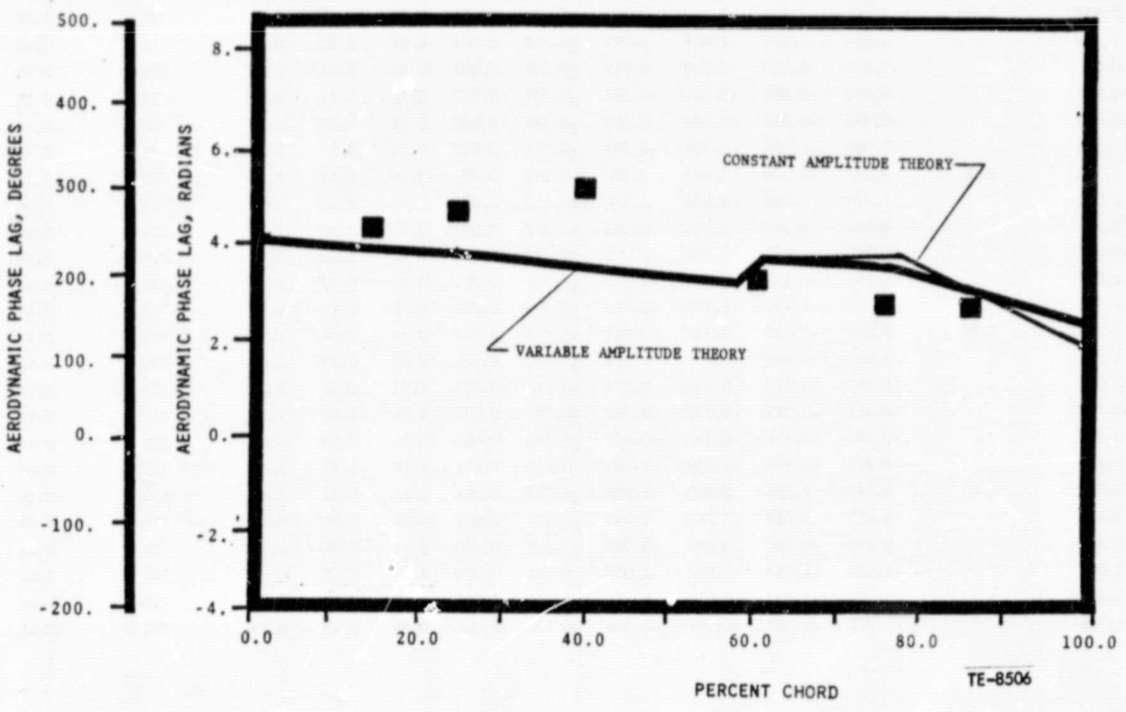

Figure 49. NASA I torsion pressure surface phase lag distribution at 1.04:1 and 3.14 rad (180^{o}) interblade phase angle.

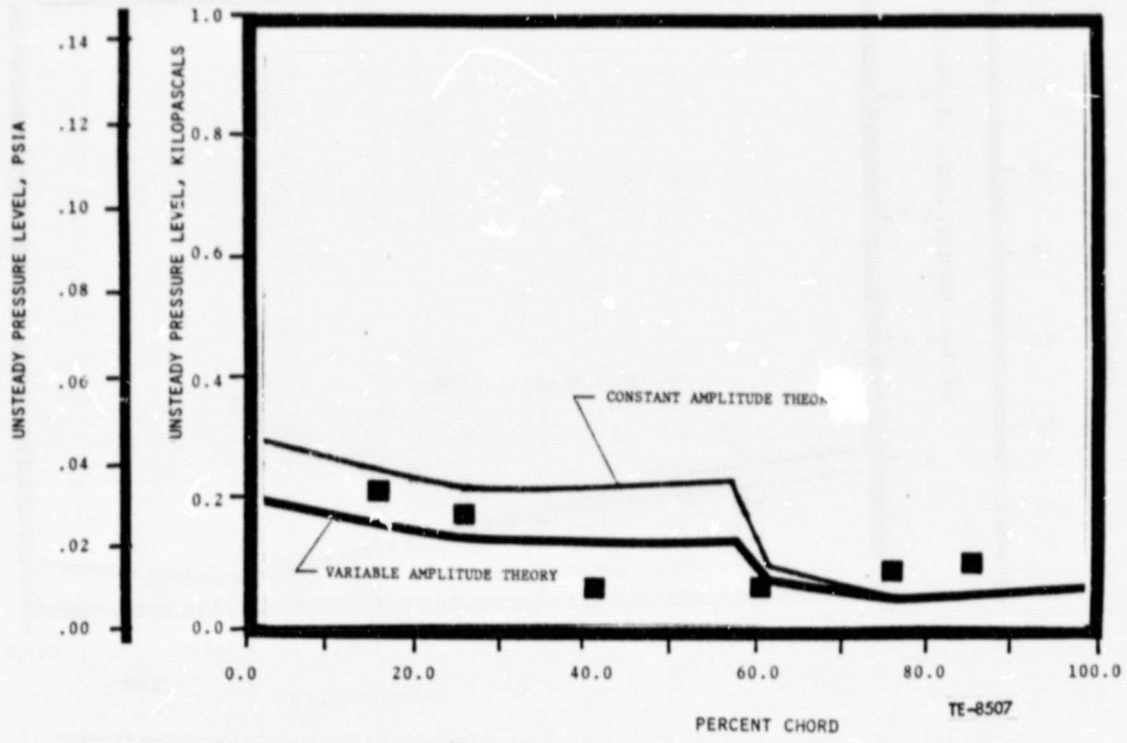

Figure 50. NASA I torsion pressure surface unsteady pressure distribution at 1.04:1 and 3.14 rad (180^{o}) interblade phase angle.

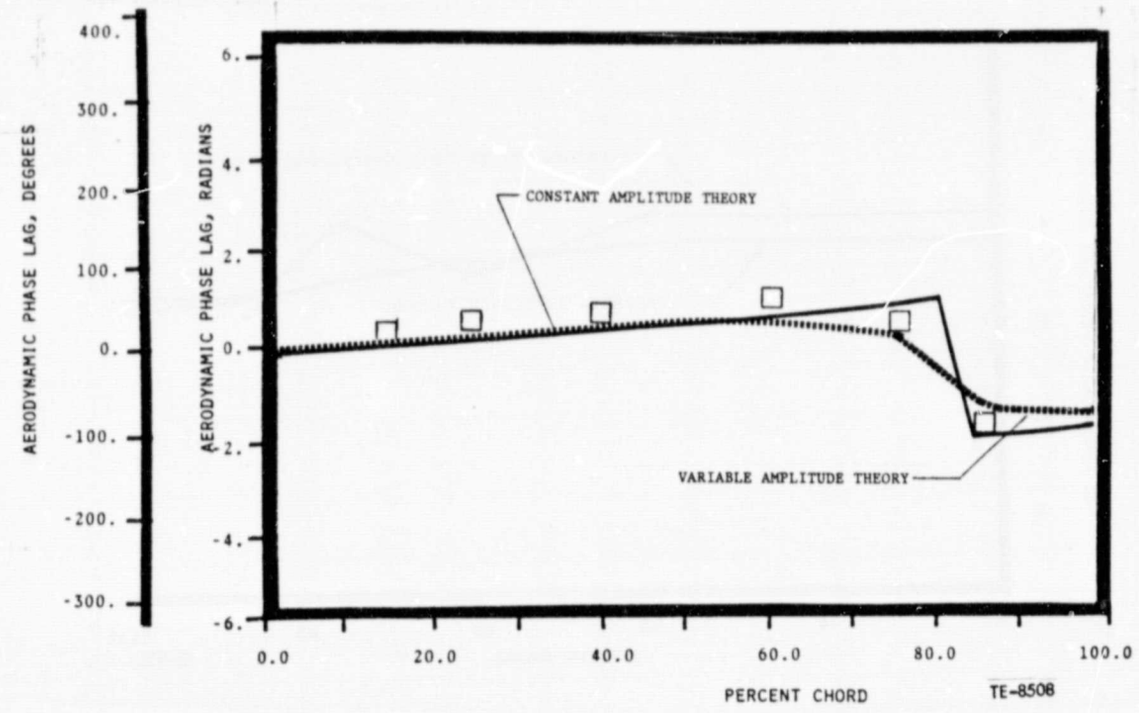

Figure 51. NASA I torsion suction surface phase lag distribution at 1.04:1 and 3.14 rad (180^{o}) interblade phase angle.

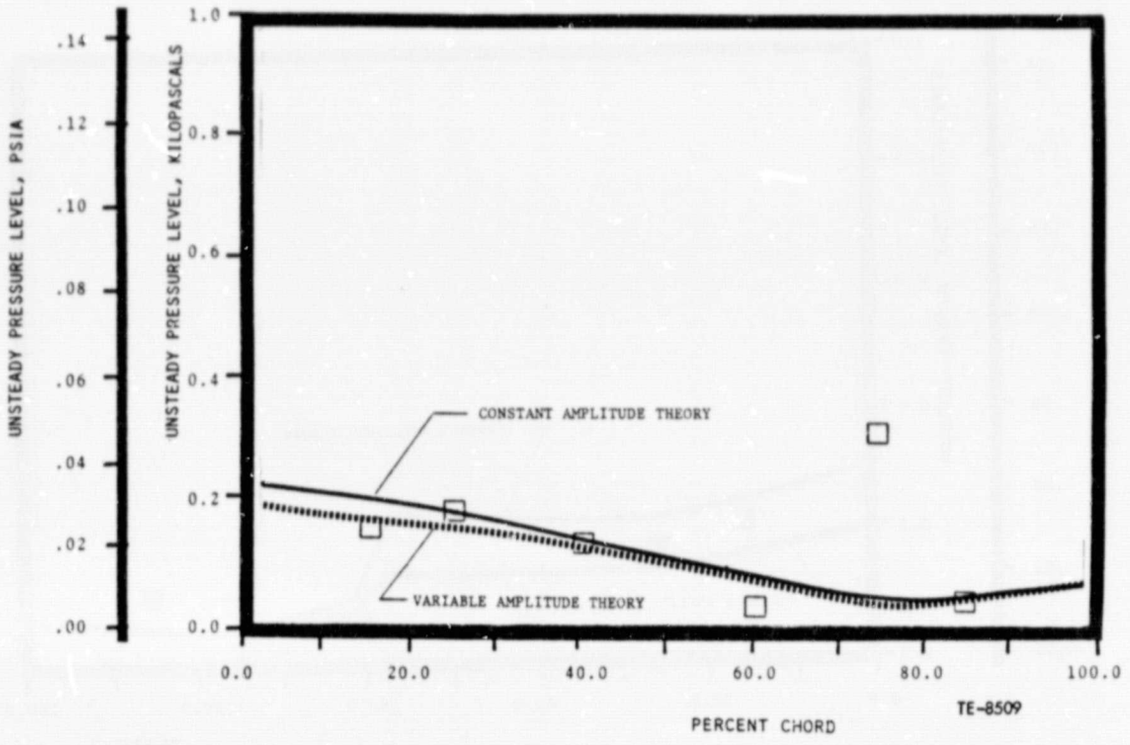

Figure 52. NASA I torsion suction surface unsteady pressure distribution at 1.04:1 and 3.14 rad (180^{o}) interblade phase angle.

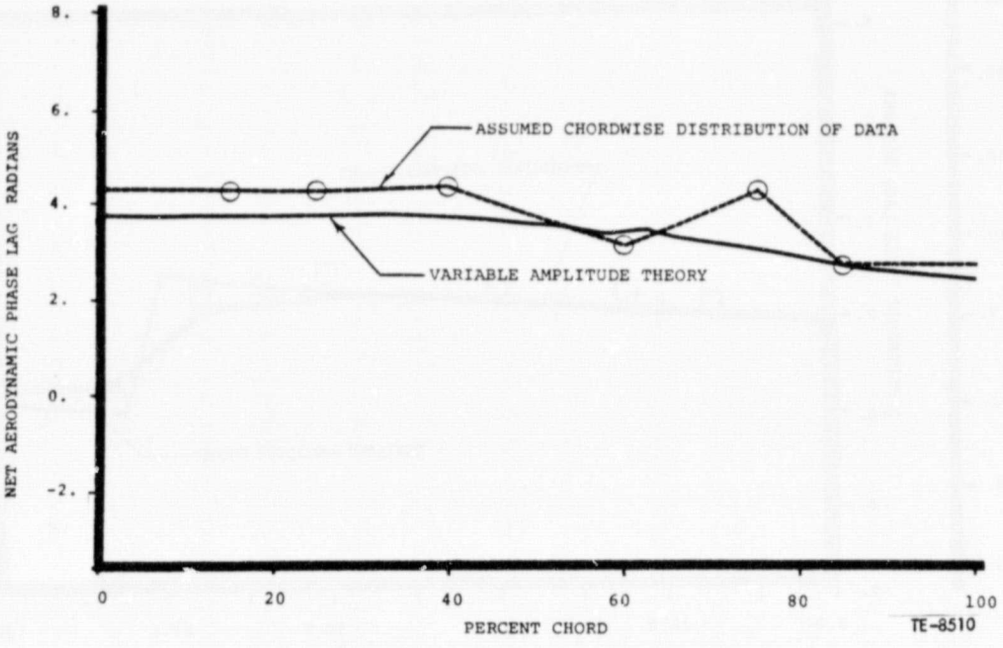

Figure 53. Typical phase lag plot illustrating assumed chordwise data distribution for lift and moment calculation.

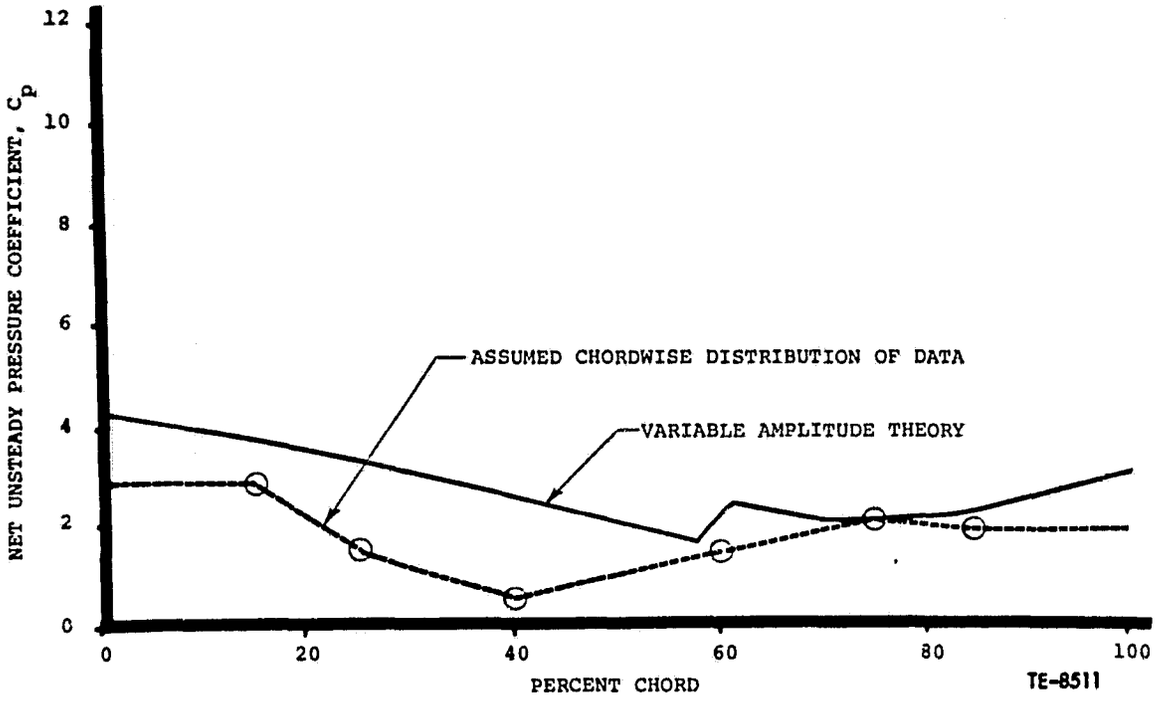

Figure 54. Typical pressure coefficient plot illustrating assumed chordwise data distribution for lift and moment calculation.

$$C_p)_{real} = (C_p)_{net} \cos \phi_{net}$$

$$C_p)_{imag.} = (C_p)_{net} \sin \phi_{net}$$

Where C_p = the unsteady pressure coefficient and ϕ = the aerodynamic phase lag. Net is the resultant difference between the pressure and suction surface values.

The unsteady lift coefficient components were obtained by direct integration of the resulting real and imaginary distributions. The unsteady moment coefficient was obtained by applying the appropriate moment arm to the data. The airfoil trunnions are at the 50% chord location and therefore all moments are about the midchord. Airfoil torsional stability is related to the imaginary part of the unsteady moment coefficient (CM_i). As this value increases into the positive regime the airfoil damping becomes insufficient and the airstream imparts energy into the airfoil resulting in an aeroelastic instability.

Figures 55 through 58 are the stability plots obtained at the four test pressure ratios over a range of phase angles. As can be seen from Figures 55 and 56 the cascade was stable over the entire phase range tested. This is in agreement with the flutter map as at these two pressure ratios no flutter was present. The variable amplitude theory line is included on the low pressure ratio plot (Figure 55). As can be seen the agreement is excellent trendwise, with the theory yielding a somewhat higher value of moment coefficient.

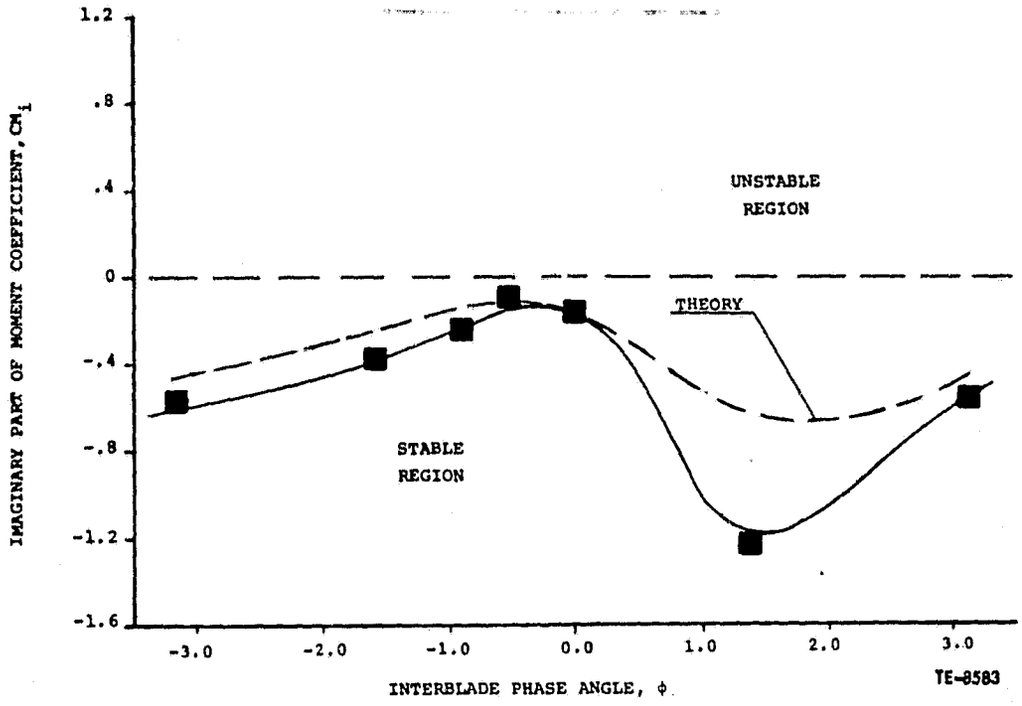

Figure 55. Baseline cascade stability curve at 1.04:1 static pressure ratio.

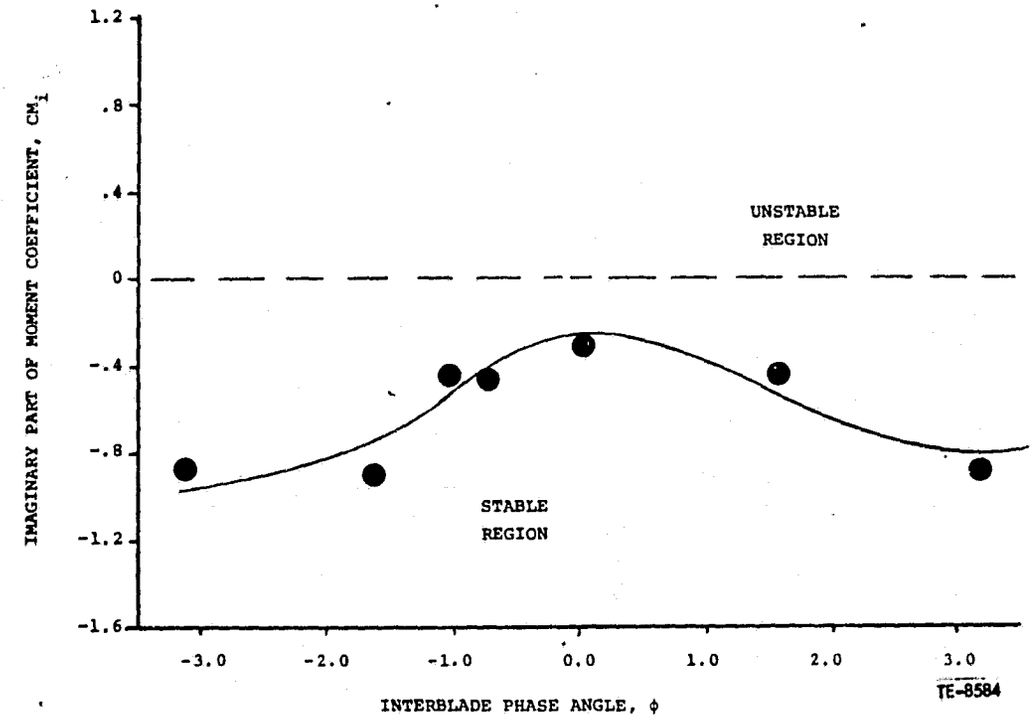

Figure 56. Baseline cascade stability curve at 1.20:1 static pressure ratio.

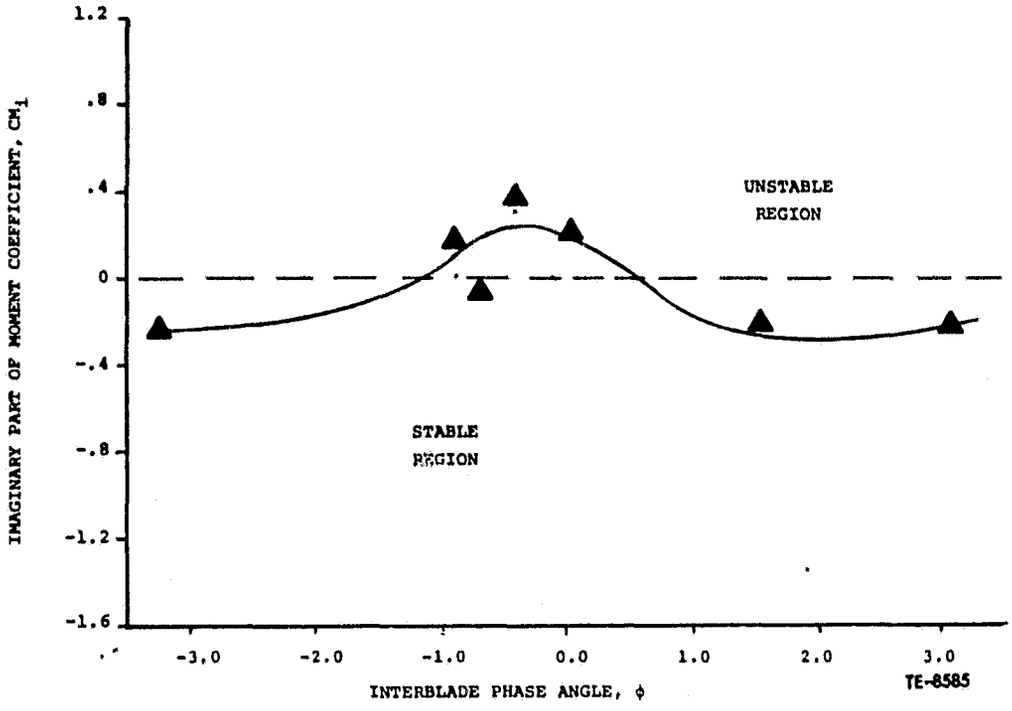

Figure 57. Baseline cascade stability curve at 1.35:1 static pressure ratio.

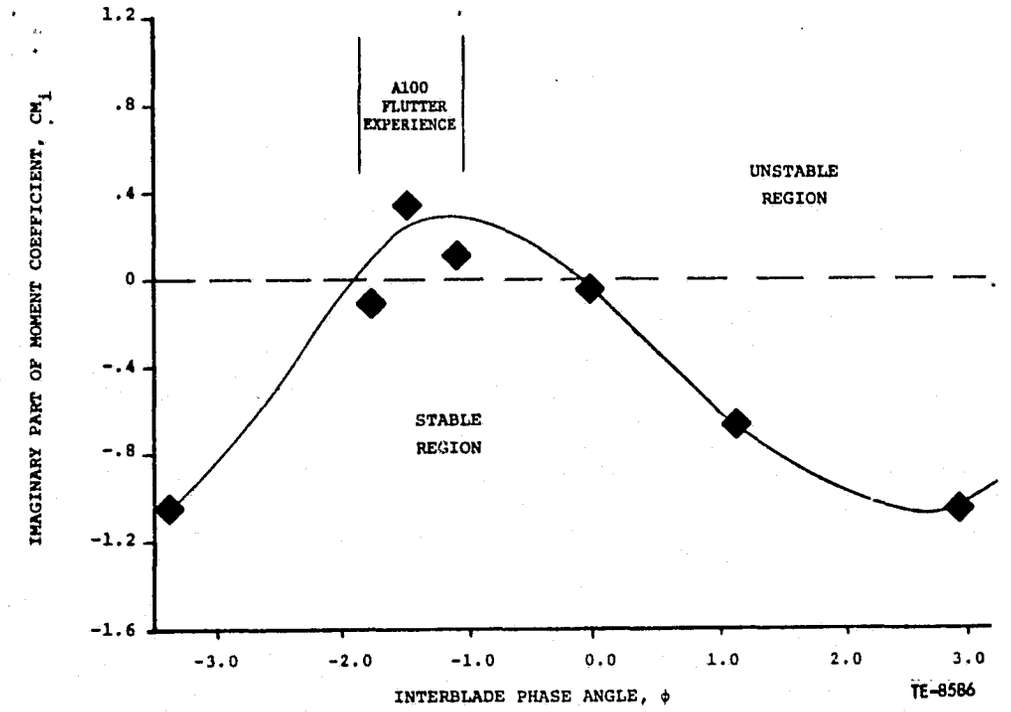

Figure 58. Baseline cascade stability curve at 1.45:1 static pressure ratio.

In Figures 57 and 58, for negative phase angles a small region of instability (positive CM_i) was evident. The unstable region was largest at the highest (1.45:1) pressure ratio and was unstable between 0 rad (0^o) and -1.66 rad (-95^o) phase angle. The stability levels of the two higher pressure ratios exhibits the same excellent agreement with the flutter map as the lower pressure ratios. The 1.45:1 pressure ratio point was the most unstable point and was also the data point deepest into the flutter area. The phase angle at the most unstable point also compares to the A100 rotor test value.

The effect of cascade loading on the unsteady pressure data is demonstrated with the aid of Figures 59 through 62. These chordwise time variant data plots are for a range of static pressure ratios between 1.04 and 1.45:1 at approximately -1.57 rad (-90^o) interblade phase angle. Theoretical analysis performed with the blade-to-blade amplitude variations noted in testing are represented by a shaded band. Figure 59 presents the chordwise phase lag distribution on the pressure surface at the four pressure ratios. The correlation between theory and experiment at the low pressure ratio (1.04:1) is excellent, with the possible exception of the 40% chord data station. At this location, the presence of the reflected passage shock wave onto the pressure surface is present in the form of an increased phase lag. As the cascade pressure ratio is increased, the forward 25% of the airfoil remains unaffected. At the 40% chord location, increased pressure ratio diminishes the influence of the reflected passage shock. The effect of increased pressure ratio is most noticeable on the trailing portion of the airfoil. As the pressure ratio is increased, the deviation from the unity pressure ratio theory line increases. The suction surface phase lag data as presented in Figure 61,

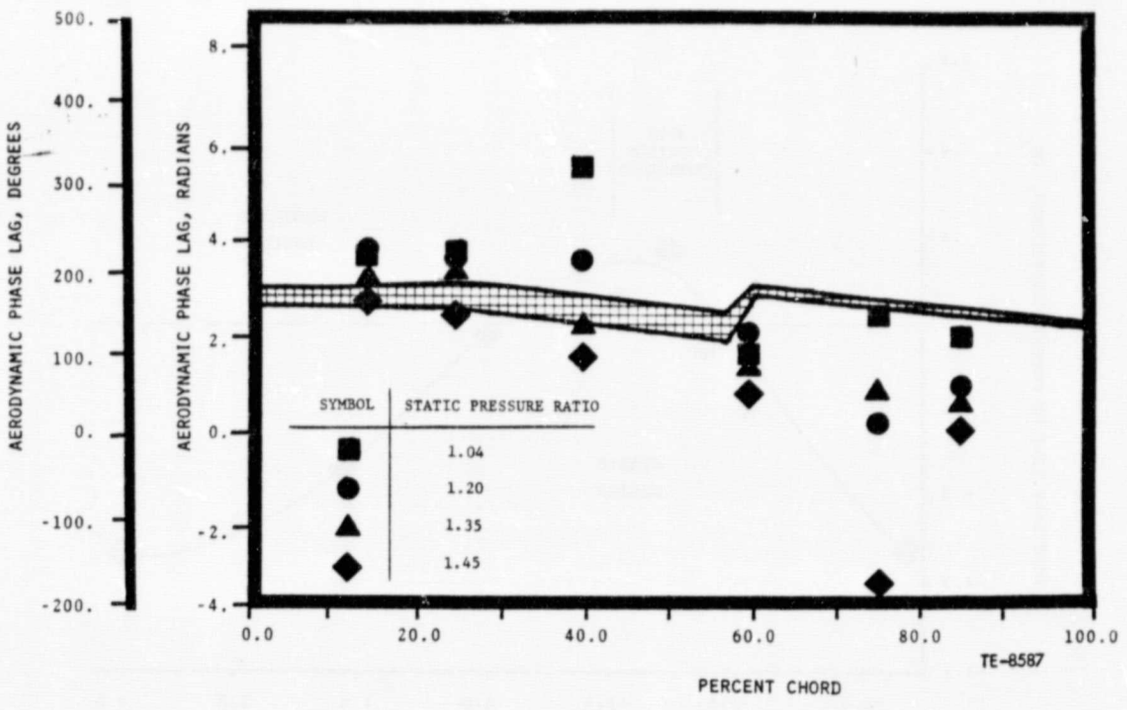

Figure 59. NASA I torsion pressure surface phase lag data at 4 static pressure ratios and -1.57 rad (-90^o) interblade phase angle.

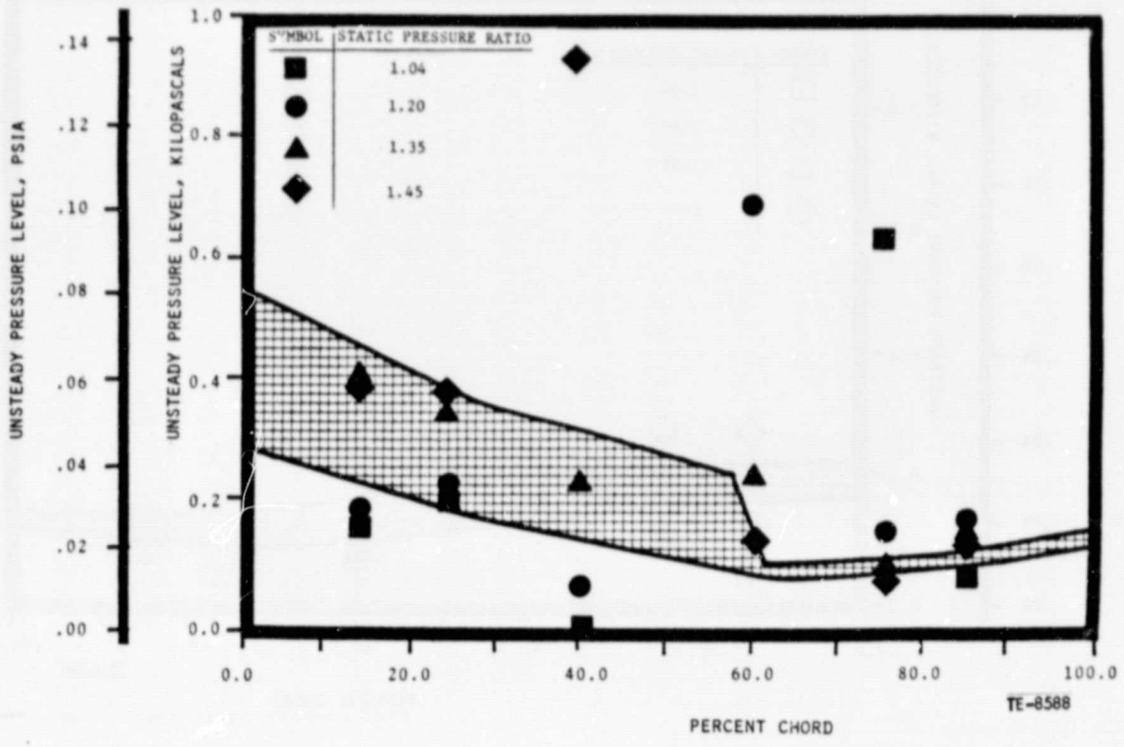

Figure 60. NASA I torsion pressure surface unsteady pressure data at 4 static pressure ratios and -1.57 rad (-90^{o}) interblade phase angle.

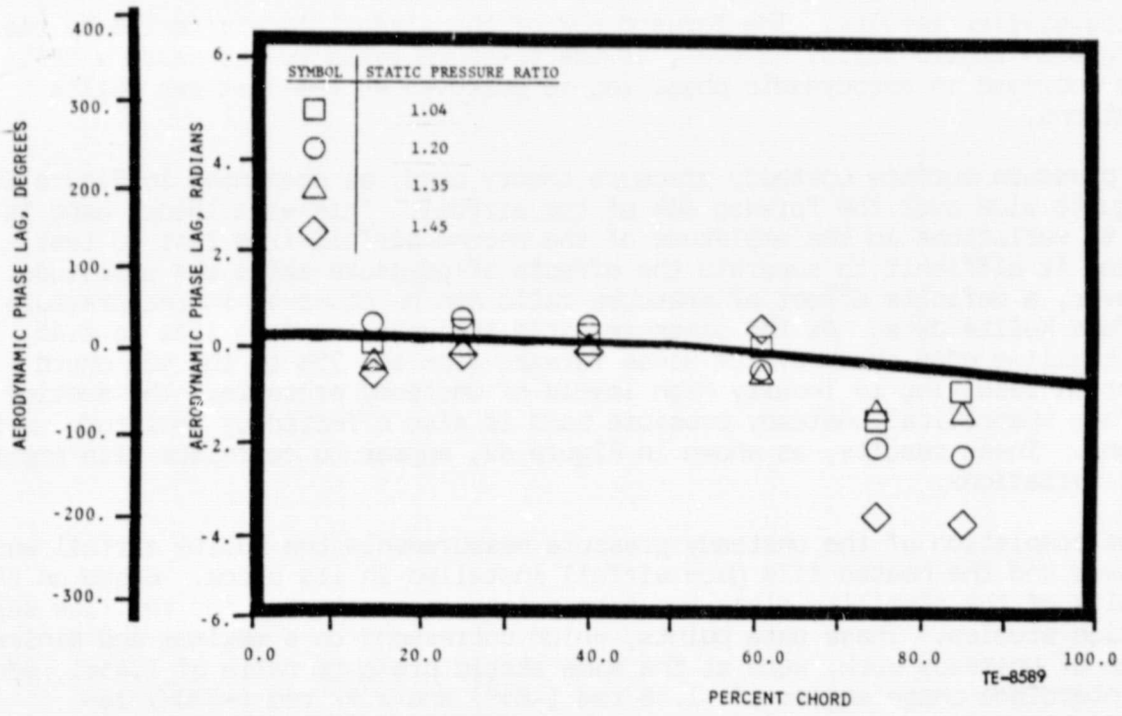

Figure 61. NASA I torsion suction surface phase lag data at 4 static pressure ratios and -1.57 rad (-90^{o}) interblade phase angle.

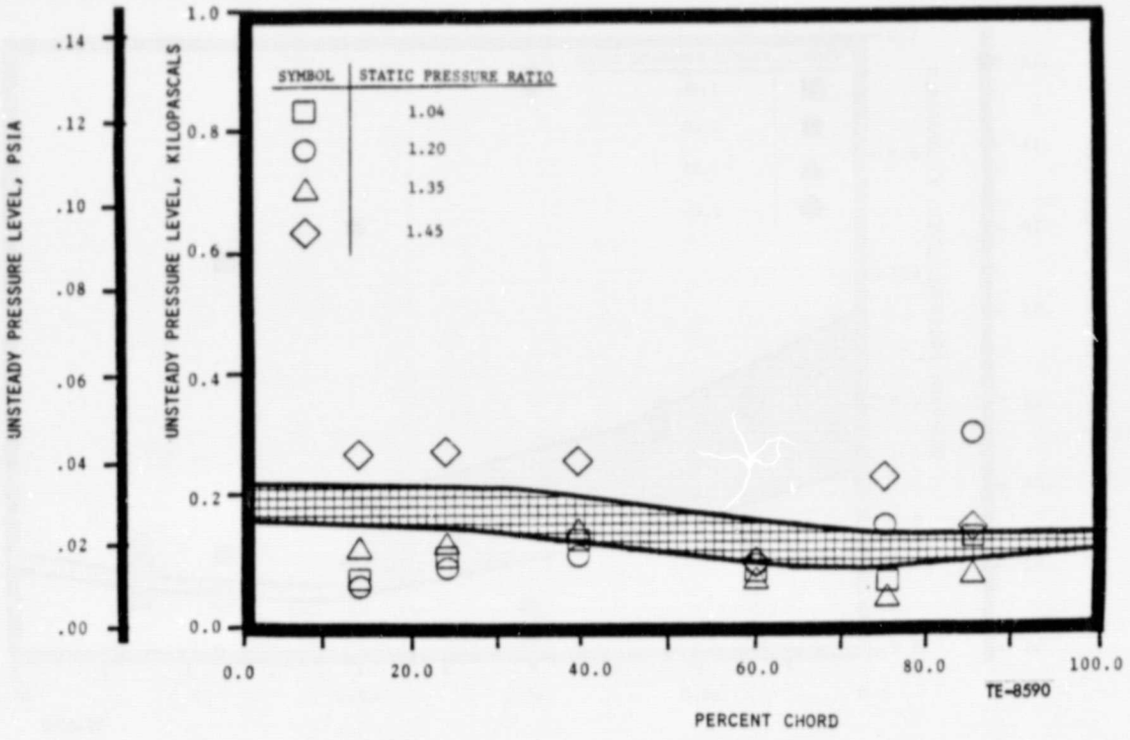

Figure 62. NASA I torsion suction surface unsteady pressure data at 4 static pressure ratios and -1.57 rad (-90^{o}) interblade phase angle.

yields similar results. The forward 60% of the airfoil is unaffected by the changes in static ratio, however, as the pressure ratio is increased a definite increase in aerodynamic phase lag is observed at the last two Kulite locations.

The pressure surface unsteady pressure theory band, as presented in Figure 60, is quite wide over the forward 60% of the airfoil. This wide theory band is due to variations in the amplitude of the second airfoil from test to test, making it difficult to separate the effects of pressure ratio and amplitude. However, a definite effect of pressure ratio can be observed in the pressure surface Kulite data. As the pressure ratio is increased from 1.04 to 1.45, the trailing edge shock system moves forward from the 75% to the 40% chord location resulting in locally high levels of unsteady pressure. The suction surface theoretical unsteady pressure band is also effected by amplitude variations. These results, as shown in Figure 62, appear to correlate with amplitude variations.

After completion of the unsteady pressure measurements the Kulite airfoil was removed and the heated film gage airfoil installed in its place. Based on the results of the stability plots two data points were selected for the flow separation studies. These data points, which correspond to a maximum and minimum value of unsteady work, were at the same static pressure ratio of 1.45:1, and at interblade phase angles of -1.48 rad (-85^{o}) and 2.97 rad ($+170^{o}$) respectively. These data points are represented graphically in Figure 58 in terms of the unsteady moment coefficient level; which is directly proportional to the level of unsteady work.

The measured chordwise distribution of the shear stress intensity for the baseline cascade at the maximum and minimum unsteady work levels are presented in Figures 63 and 64. The separation level of the shear stress intensity is noted on the figures and was based on the heated film gage airfoil calibration. The pressure surface intensity distribution is presented in Figure 63, and with the exception of the 40% chord location, the flow was attached over the entire surface for both interblade phase angles. The increased intensity at the 40% location is due to the direct impingement of the trailing edge shock from airfoil 2 onto the airfoil 3 pressure surface. The suction surface shear stress intensity is presented in Figure 64 and a region of separated flow is indicated downstream of the 60% chord location. This is consistent with the alcohol injection flow visualization results obtained during the steady state testing. As mentioned previously, during these investigations a separated flow region was observed on the suction surface downstream of the impinging wake shock. At the test cascade pressure ratio of 1.45:1 this shock wave hits the suction surface near the 60% chord location.

The taped heated film gage output signals were analyzed and have been found to have no significant signal variation at the 725 Hz, or driving frequency range. This would indicate that there is no significant shock wave and/or boundary layer movement in the regions surrounding these gages for these test conditions. The high speed schlieren movies have also yielded negligible motion at 725 Hz frequency and both interblade phase angle conditions. These results indicate that large amplitude shock wave motion is not a requirement for an unstable cascade.

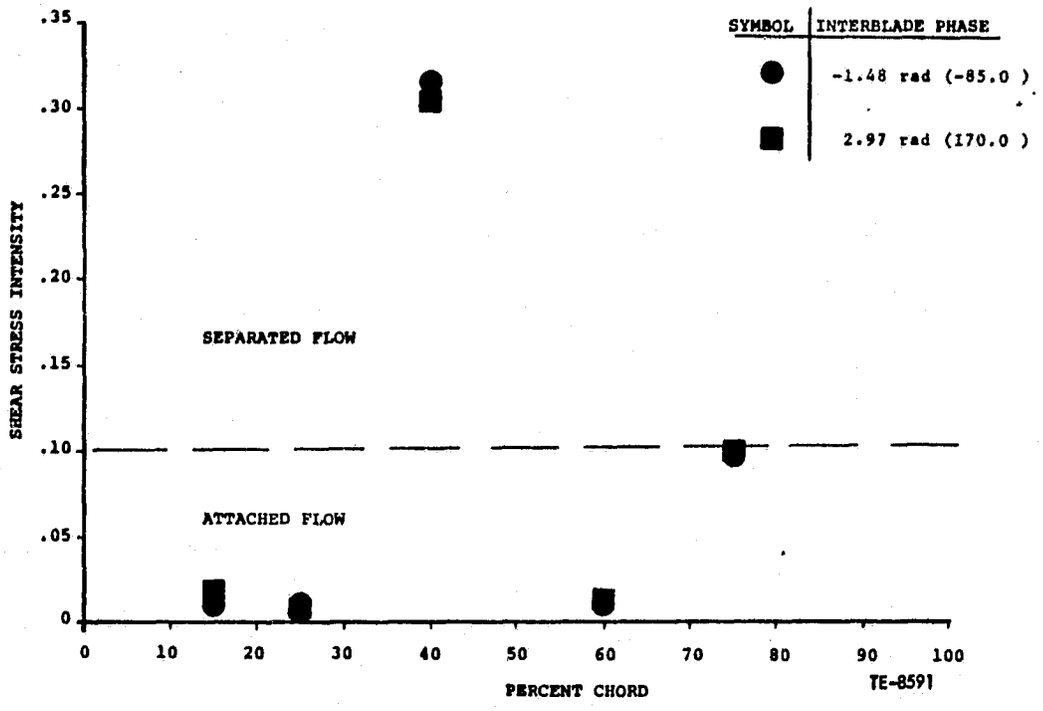

Figure 63. NASA I torsion baseline pressure surface chordwise distribution of shear stress intensity parameter.

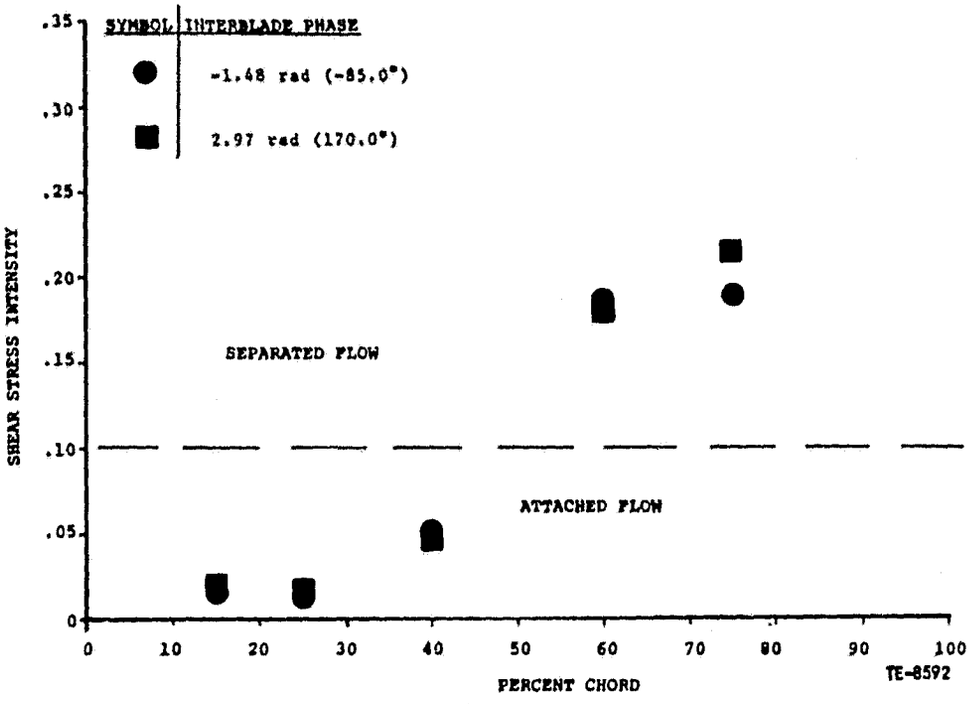

Figure 64. NASA I torsion baseline cascade suction surface chordwise distribution of shear stress intensity parameter.

REDUCED SOLIDITY CASCADES

The reduced solidity cascade steady state performance was evaluated at only two static pressure ratios at each of the setting angles tested. These conditions were selected to be analagous to those of the baseline torsion cascade. The first or low pressure ratio corresponded to the baseline cascade's "far away from flutter" condition. The second pressure ratio was equivalent to the baseline's "near flutter inside" test condition. This condition was selected over the "deep into flutter" condition because of the reduced pressure ratio capability of the cascade. The reduction in the cascade's solidity and setting angle decreased its ability to support a static pressure gradient. The reduced solidity cascade's overall steady state performance parameters are summarized in Table VI.

Table VI. Reduced Solidity Torsion Mode Cascade Steady State Performance Summary

	Far away from flutter		Near flutter inside	
	Nominal setting	Open setting	Nominal setting	Open setting
Inlet Mach Number	1.315	1.315	1.315	1.315
Mass Averaged Static Pressure Ratio	1.03	1.06	1.35	1.33
Mass Averaged Exit Mach Number	1.26	1.24	1.06	1.05
Mass Averaged Exit Air Angle	1.07 rad (61.3^{o})	1.05 rad (60.4^{o})	1.07 rad (61.5^{o})	1.05 rad (59.9^{o})
Mass Averaged Total Pressure Loss	.059	.076	.054	.082

The steady state schlieren photographs for both setting angle configurations of the reduced solidity cascade are included in Figures 65 through 68. Figures 65 and 66 are at the nominal setting angle and correspond to static pressure ratios of 1.03 and 1.35. The 0.052 rad (3^{0}) open reset schlierens at 1.06 and 1.33 are presented in Figures 67 and 68.

Figure 65. Reduced solidity nominal setting angle torsion cascade schlieren at 1.03:1 mass average pressure ratio.

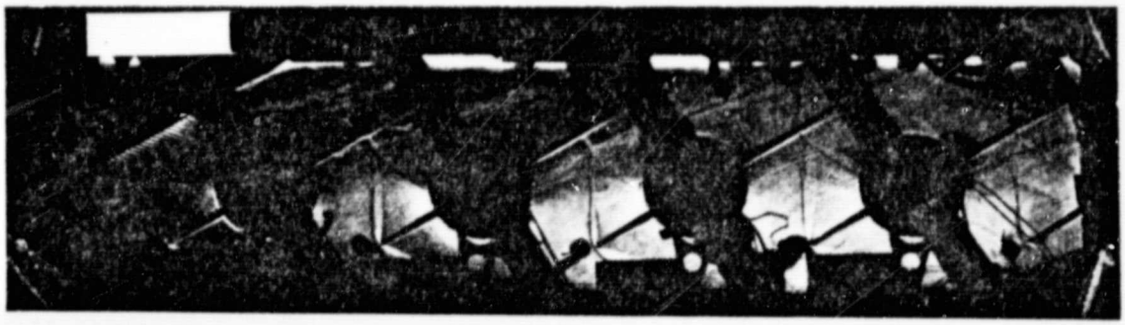

Figure 66. Reduced solidity nominal setting angle torsion cascade schlieren at 1.35:1 mass average pressure ratio.

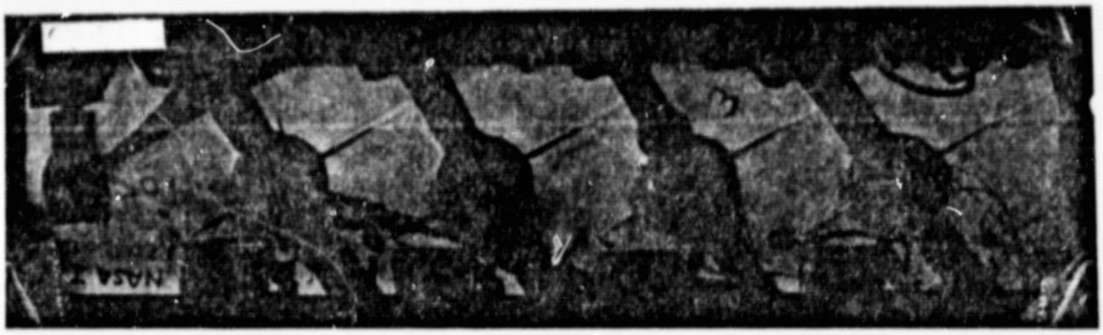

Figure 67. Reduced solidity open setting angle torsion cascade schlieren at 1.06:1 mass average pressure ratio.

Figure 68. Reduced solidity open setting angle torsion cascade schlieren at 1.33:1 mass average pressure ratio.

The steady state periodicity plots for the nominal setting angle cascade at the low and high pressure ratio are shown in Figures 69 and 70. Figures 71 and 72 are the corresponding plots for the open setting configuration. The number of exit sidewall static pressure taps downstream of the airfoils trailing edge was limited by hardware restrictions to the first three airfoils. The value indicated at the 260% tangential location is 60% of the way between airfoils No. 3 and No. 4. The cascade exit wake survey results for the low and high pressure ratios are presented in Figures 73 and 74 for the nominal setting angle cascade and 75 and 76 for the open configuration. All of the aforementioned data plots are normalized to the cascade inlet total pressure.

The static pressure tap instrumented airfoil surface pressure distributions for the reduced solidity cascade are shown in Figures 77 through 80. These data are also normalized to the inlet total pressure. As with the baseline cascade, the alcohol injection technique was used to identify regions of flow separation within the reduced solidity cascade. The alcohol was injected back through the airfoil surface pressure taps using the same procedure as before. The results this time were not as clear as with the baseline investigation. No well defined regions of separation were observed on the airfoil surface during the reduced solidity testing at either setting angle level.

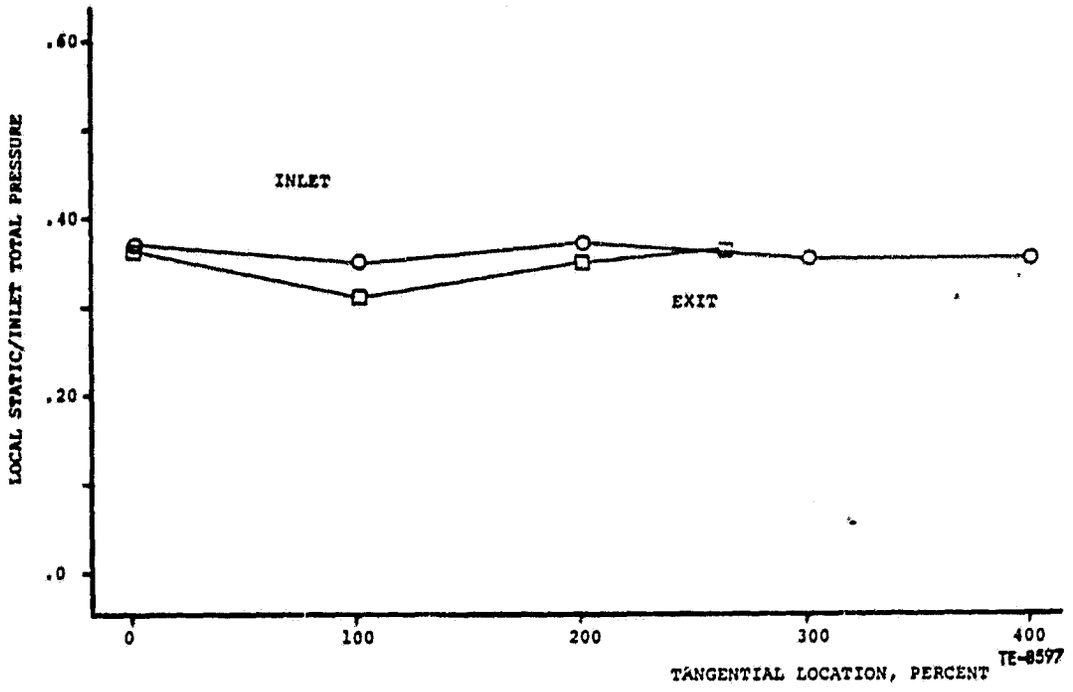

Figure 69. Reduced solidity nominal setting sidewall static periodicity plots at 1.03:1.

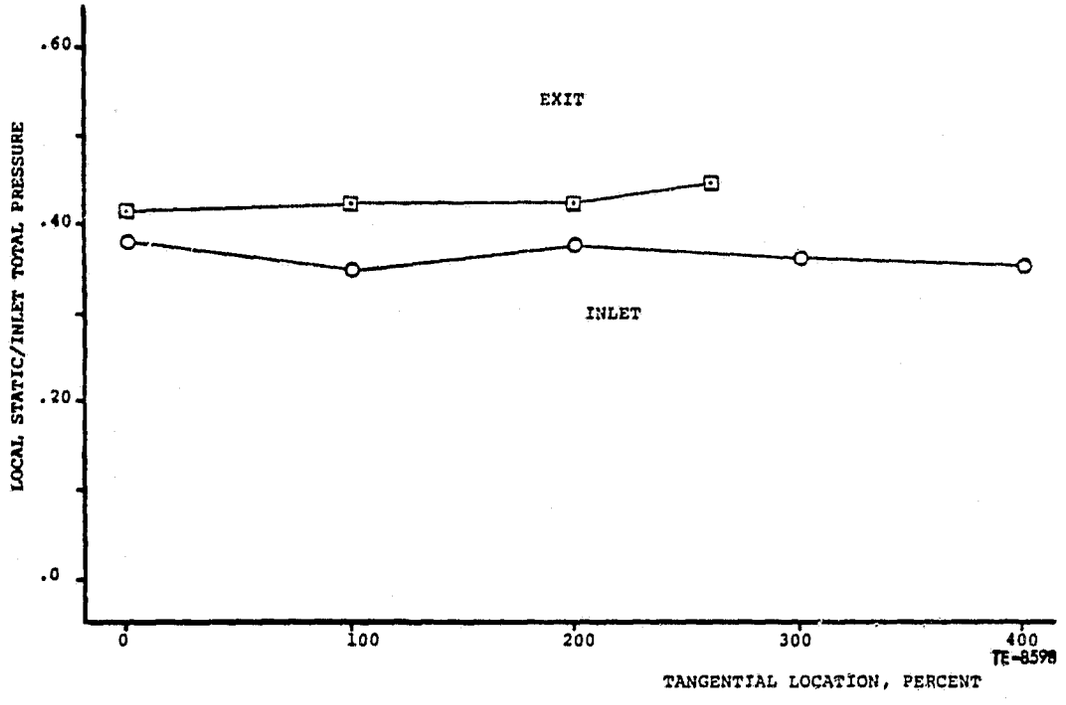

Figure 70. Reduced solidity nominal setting sidewall static periodicity plots at 1.35:1.

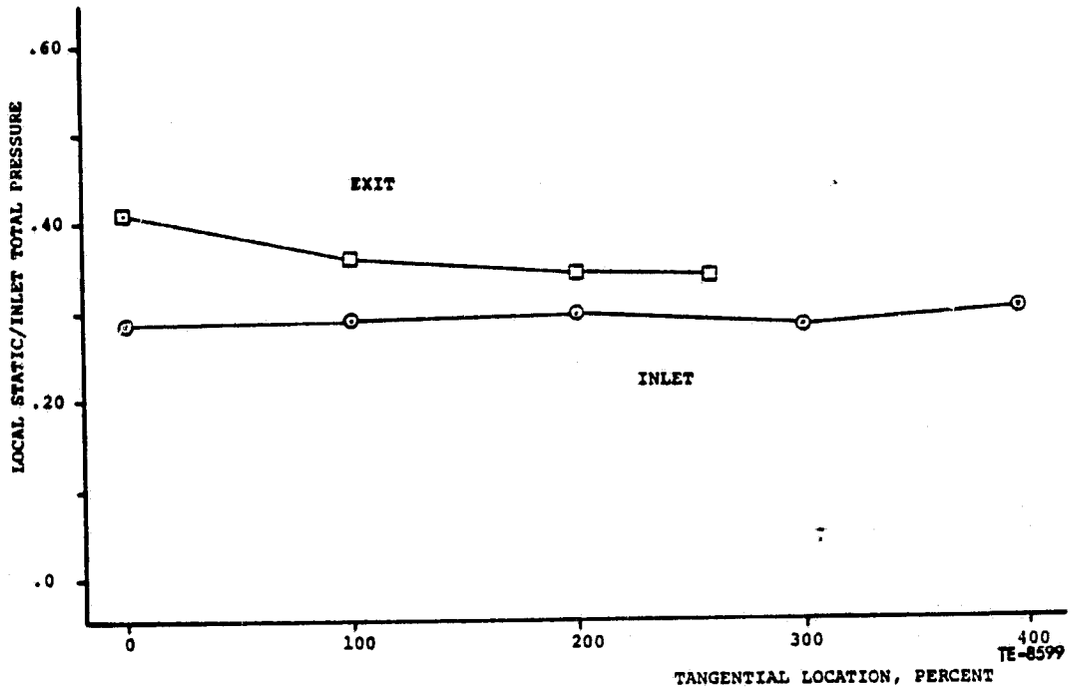

Figure 71. Reduced solidity open setting sidewall static periodicity plots at 1.06:1.

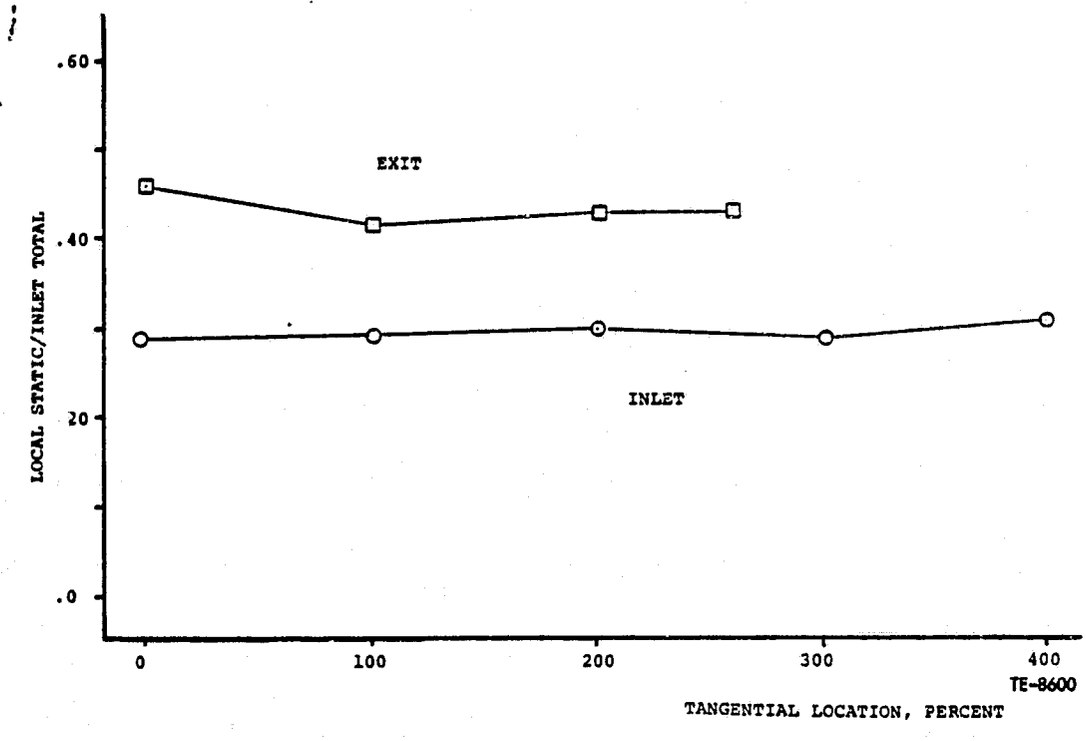

Figure 72. Reduced solidity open setting sidewall static periodicity plots at 1.33:1.

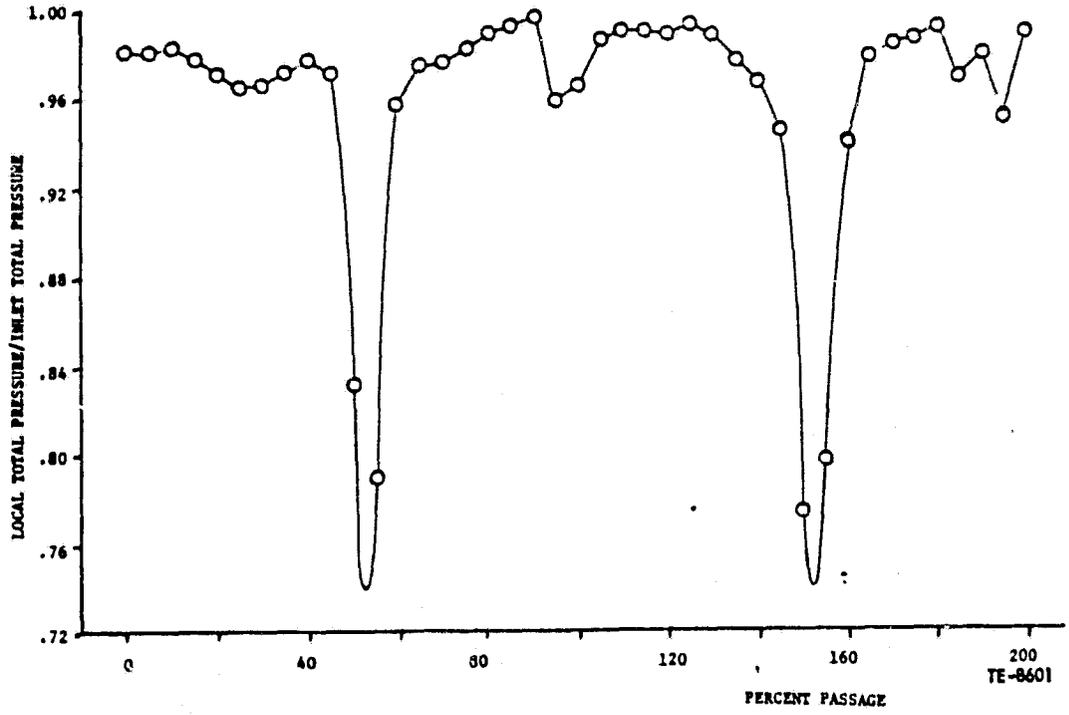

Figure 73. Reduced solidity nominal setting cascade exit survey at 1.03:1.

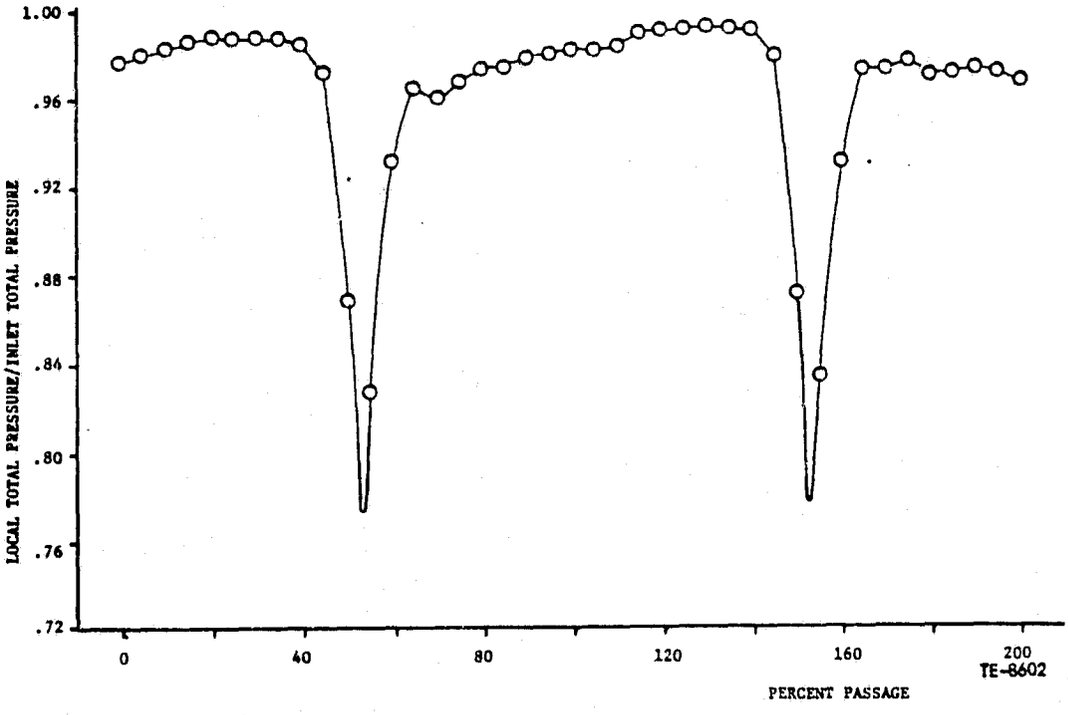

Figure 74. Reduced solidity nominal setting cascade exit survey at 1.35:1.

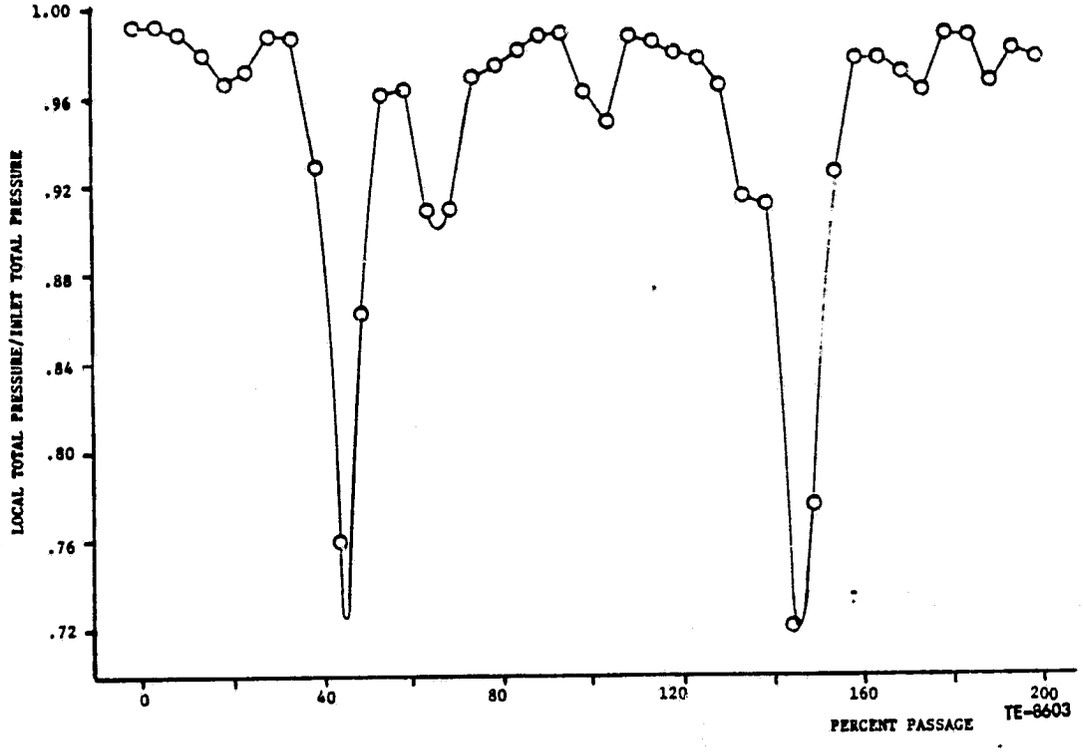

Figure 75. Reduced solidity open setting cascade exit survey at 1.06:1.

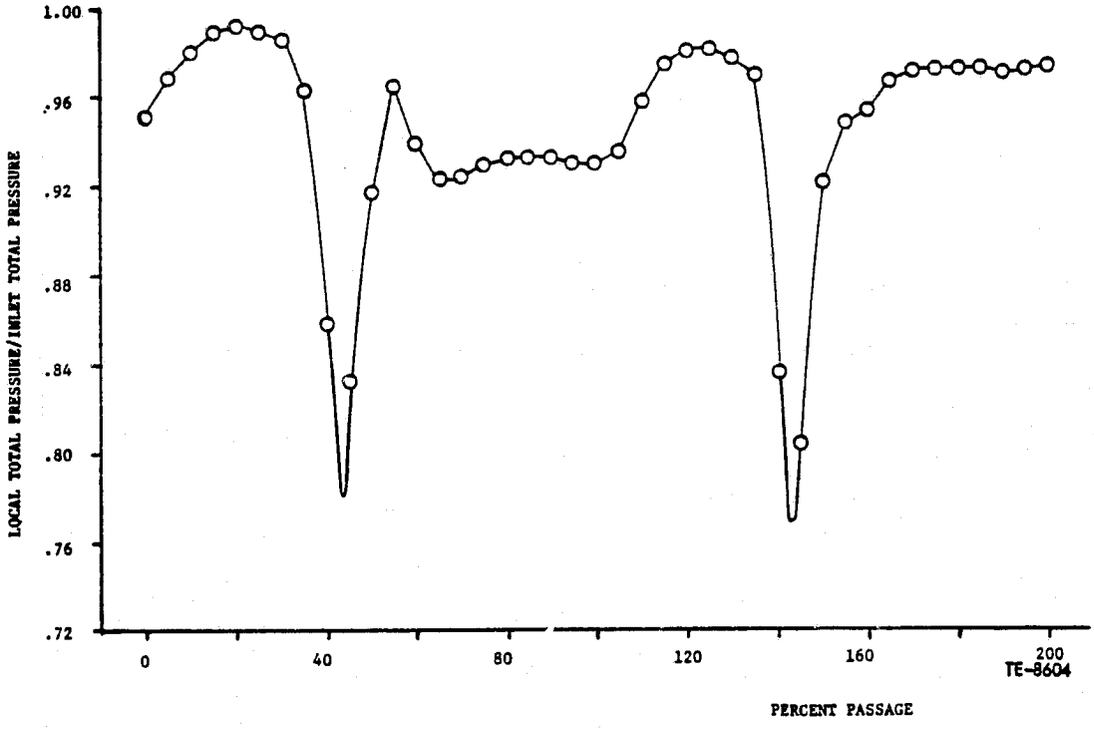

Figure 76. Reduced solidity open setting cascade exit survey at 1.33:1.

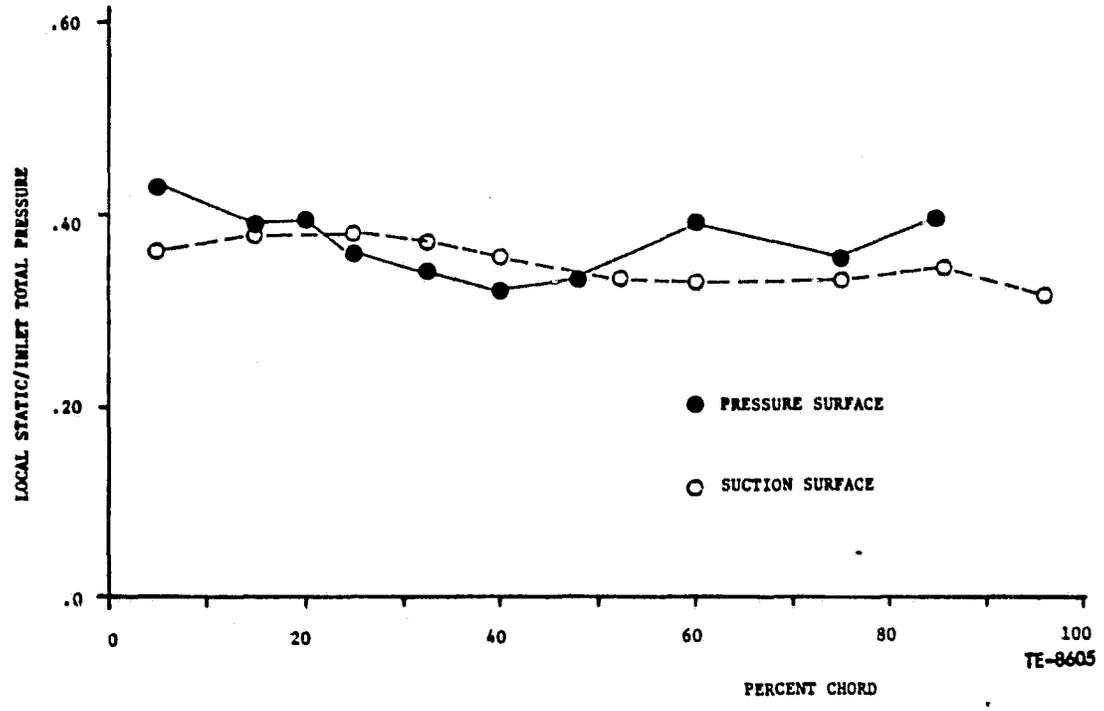

Figure 77. Reduced solidity nominal setting cascade instrumented airfoil static pressure distribution at 1.03:1.

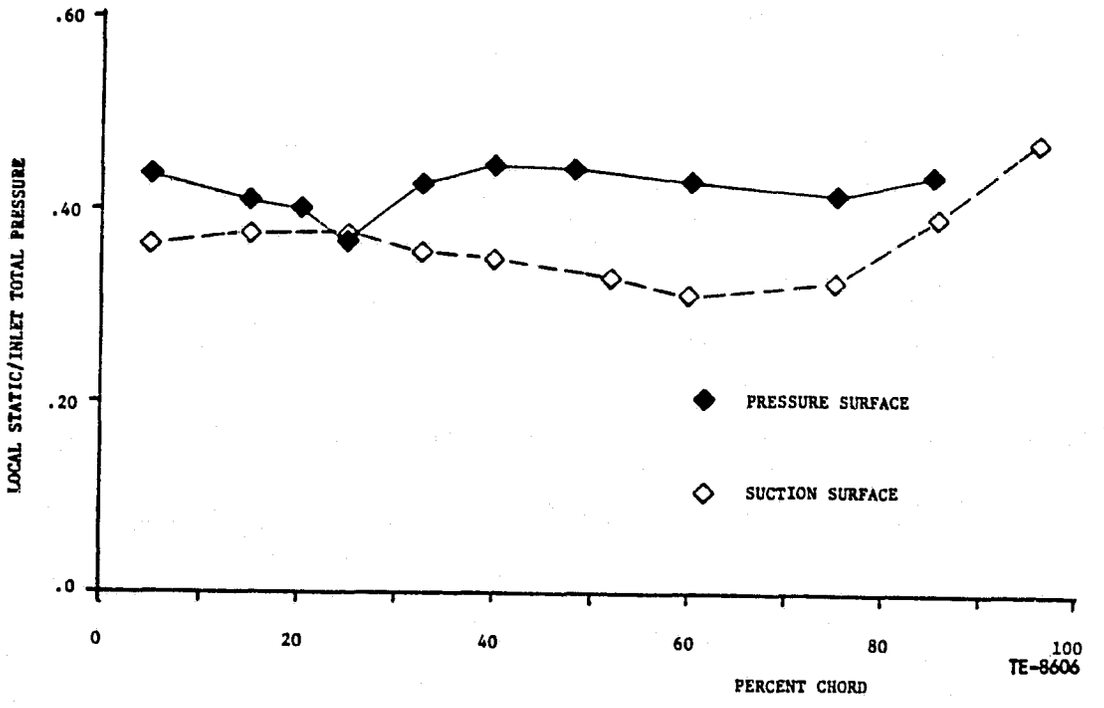

Figure 78. Reduced solidity nominal setting cascade instrumented airfoil static pressure distribution at 1.35:1.

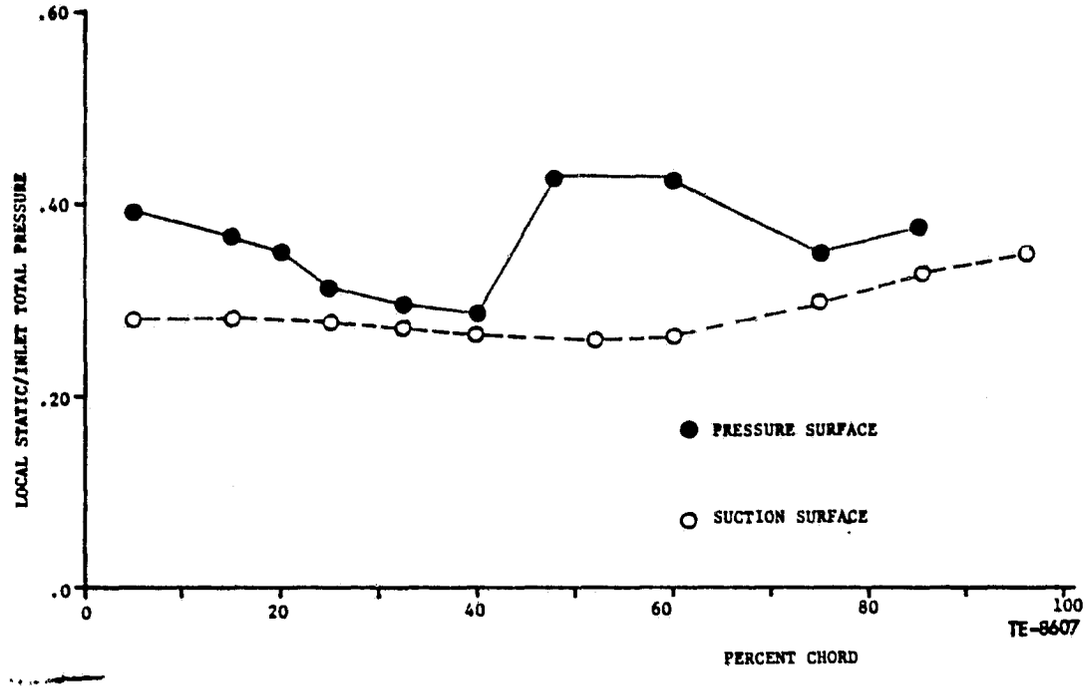

Figure 79. Reduced solidity open setting cascade instrumented airfoil static pressure distribution at 1.06:1.

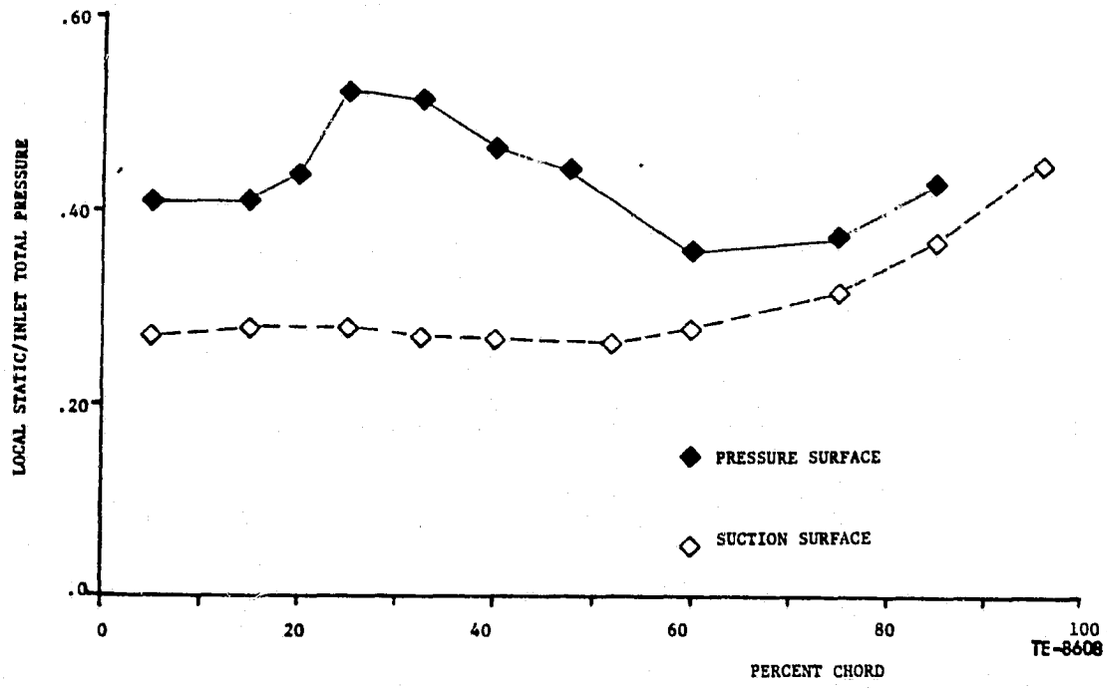

Figure 80. Reduced solidity open setting cascade instrumented airfoil static pressure distribution at 1.33:1.

After the steady state tests were finished the Kulite instrumented airfoil was installed and the time variant testing resumed. A tabulation of the reduced solidity cascade time variant operational characteristics is included in Table VII. The nomenclature is the same as used in Table V. Plots of the chordwise variation of the measured surface unsteady pressure and their corresponding phase lag are included in Appendix D.

Table VII. Reduced solidity cascade time variant testing results summary.

Phase Radians	Cascade Setting Angle Configuration	Cascade Static Press Ratio R_c	Interblade Phase Angle--Radians ϕ_{1-2}	ϕ_{2-3}	ϕ_{3-4}	Average Phase Radians $\bar{\phi}$	σ_{ϕ}	Blade Torsional Amplitude a_3 Radians	a_1/a_3	a_2/a_3	a_4/a_3	Frequency, Hz f	Reduced Frequency k
3.142	Nominal	1.03	3.156	3.194	3.110	3.154	±0.042	0.001	1.680	0.344	2.934	725	0.44
1.571			1.449	1.573	1.618	1.546	±0.087	0.001	1.932	1.284	0.311	725	0.44
0.0			-0.126	0.026	0.059	-0.014	±0.099	0.002	0.727	1.200	0.782	725	0.44
-0.524			-0.553	-0.499	-0.510	-0.520	±0.028	0.002	0.564	0.906	0.427	725	0.44
-1.047			-1.127	-1.004	-1.066	-1.068	±0.061	0.002	0.609	0.985	0.369	725	0.44
-1.571			-1.548	-1.477	-1.682	-1.569	±0.105	0.001	0.438	1.466	1.068	725	0.44
2.967	Nominal	1.35	3.185	2.780	2.906	2.958	±0.208	0.001	1.092	0.382	0.895	725	0.44
1.571			1.820	1.405	1.693	1.639	±0.213	0.001	1.706	1.858	1.764	725	0.44
-0.087			-0.089	-0.086	-0.080	-0.086	±0.005	0.002	0.411	1.082	0.861	725	0.44
-0.436			-0.499	-0.466	-0.414	-0.459	±0.042	0.002	0.546	0.972	0.766	725	0.44
-1.047			-1.100	-0.997	-1.093	-1.063	±0.058	0.002	0.564	1.053	0.890	725	0.44
-1.571			-1.620	-1.538	-1.583	-1.578	±0.058	0.001	0.971	1.844	0.796	725	0.44
3.142	Open Reset	1.06	3.033	3.241	3.087	3.121	±0.108	0.001	1.731	0.548	1.231	725	0.44
1.571			1.593	1.525	1.621	1.580	±0.049	0.001	1.944	0.356	2.000	725	0.44
0.0			-0.140	0.052	0.054	-0.010	±0.112	0.002	0.708	0.977	1.215	725	0.44
-0.524			-0.539	-0.501	-0.464	-0.504	±0.037	0.002	0.739	1.066	1.159	725	0.44
-1.047			-1.070	-0.979	-1.049	-1.033	±0.047	0.001	0.321	1.105	1.080	725	0.44
-1.571			-1.663	-1.497	-1.546	-1.573	±0.091	0.001	0.426	1.417	1.361	725	0.44
3.142	Open Reset	1.33	3.330	3.135	2.967	3.143	±0.182	0.001	1.692	0.771	1.583	725	0.44
1.571			1.670	1.614	1.520	1.602	±0.075	0.001	2.481	1.407	1.278	725	0.44
0.0			-0.113	-0.028	0.094	0.016	±0.103	0.001	0.491	1.358	1.113	725	0.44
-0.524			-0.607	-0.497	-0.524	-0.543	±0.058	0.002	0.609	1.106	0.693	725	0.44
-1.047			-1.070	-1.051	-0.970	-1.030	±0.052	0.001	0.792	1.649	1.078	725	0.44
-1.571			-1.557	-1.566	-1.637	-1.587	±0.049	0.001	1.379	2.879	1.424	725	0.44

Figures 81 through 88 are plots of the chordwise variation of the aerodynamic phase lag and unsteady pressure level, at a 3.14 rad (180 ^{o}) phase angle and the "far away from flutter" condition, for both setting angles. The data is correlated with the variable airfoil amplitude analysis. The reduced solidity unsteady cascade data/theory correlations yielded similar results to the baseline cascade. As can be seen for the above referenced figures, excellent agreement exists at the low static pressure ratios for both setting angle levels.

Figures 89 through 96 are chordwise data plots at test conditions equivalent to the aforementioned data, but at the higher cascade static pressure ratio. The effect of increased pressure ratio on phase lag noticed during the baseline investigation, was not as noticeable in the reduced solidity data. No change with pressure ratio was evident on the pressure surface, and only a

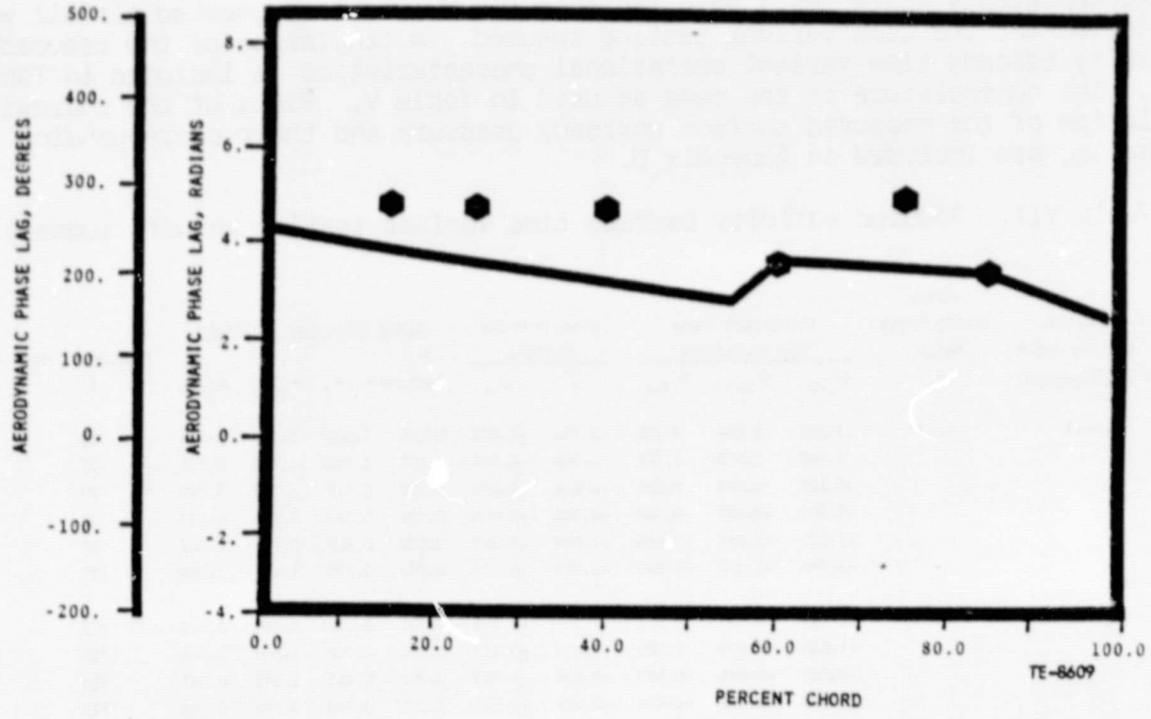

Figure 81. Reduced solidity nominal setting pressure surface phase lag at 1.03:1 and 3.14 rad (180^{o}) phase angle.

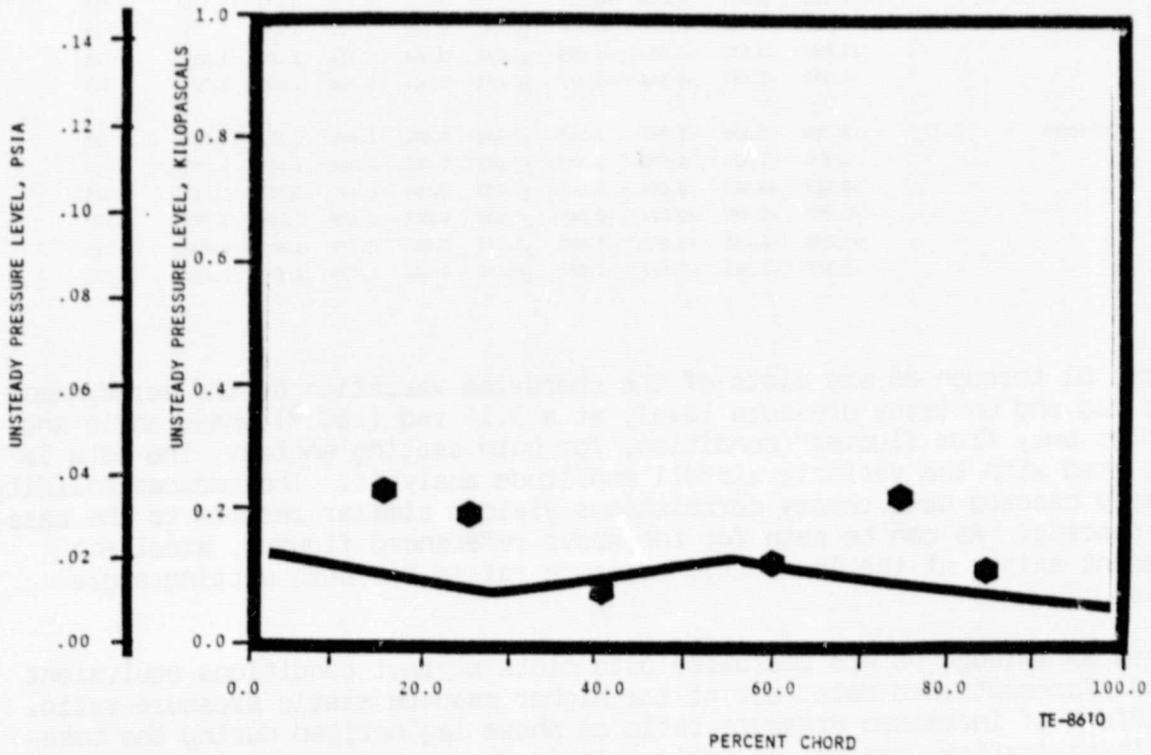

Figure 82. Reduced solidity nominal setting pressure surface unsteady pressure at 1.03:1 and 3.14 rad (180^{o}) phase.

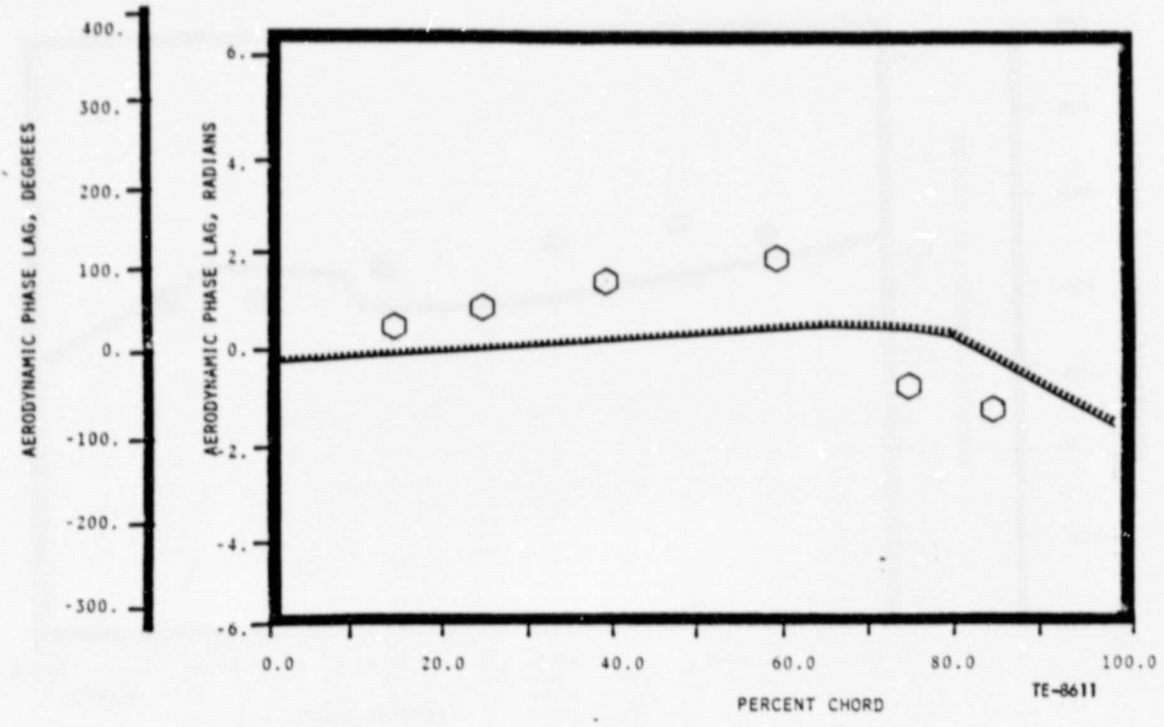

Figure 83. Reduced solidity nominal setting suction surface phase lag at 1.03:1 and 3.14 rad (180°) phase.

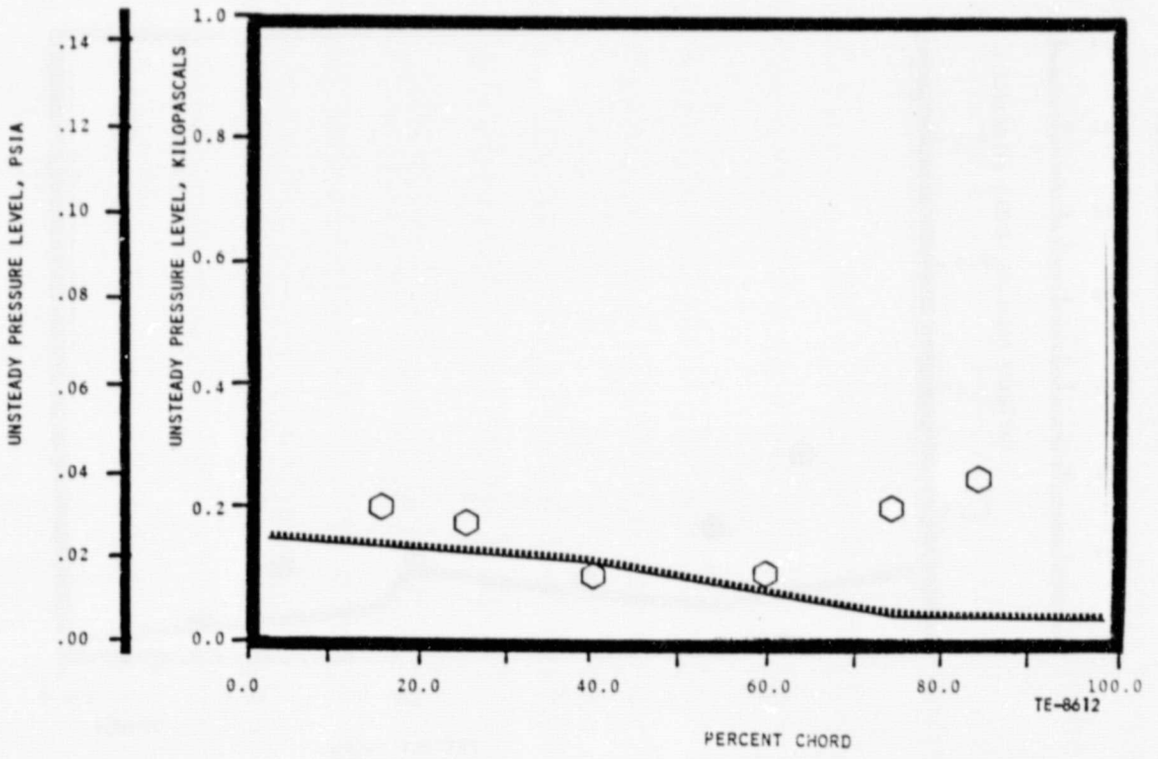

Figure 84. Reduced solidity nominal setting suction surface unsteady pressure at 1.03:1 and 3.14 rad (180°) phase.

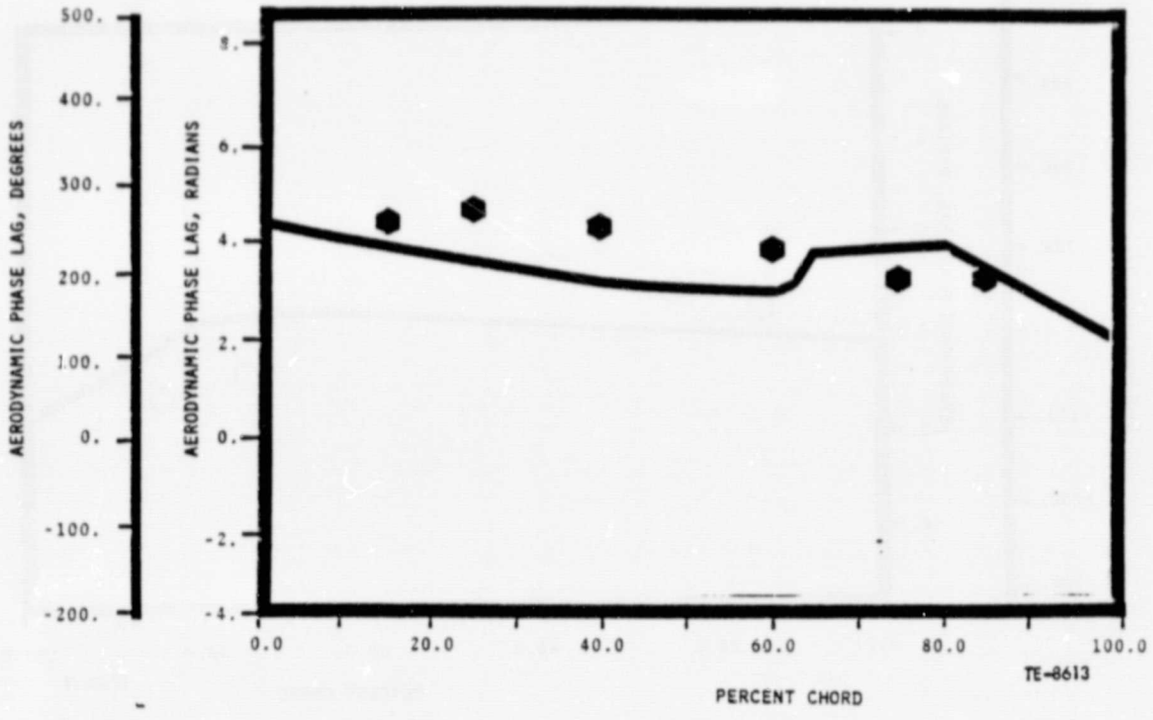

Figure 85. Reduced solidity open setting pressure surface phase lag at 1.06:1 and 3.14 rad (180°) phase.

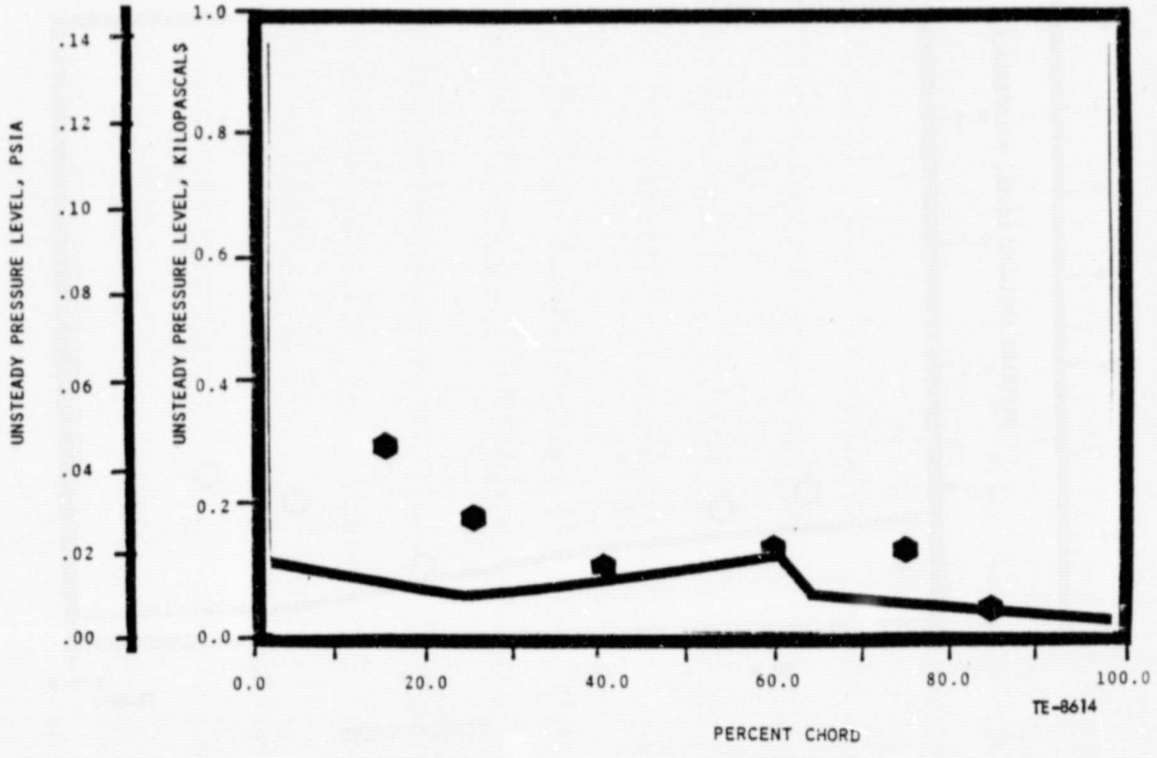

Figure 86. Reduced solidity open setting pressure surface unsteady pressure at 1.06:1 and 3.14 rad (180°) phase.

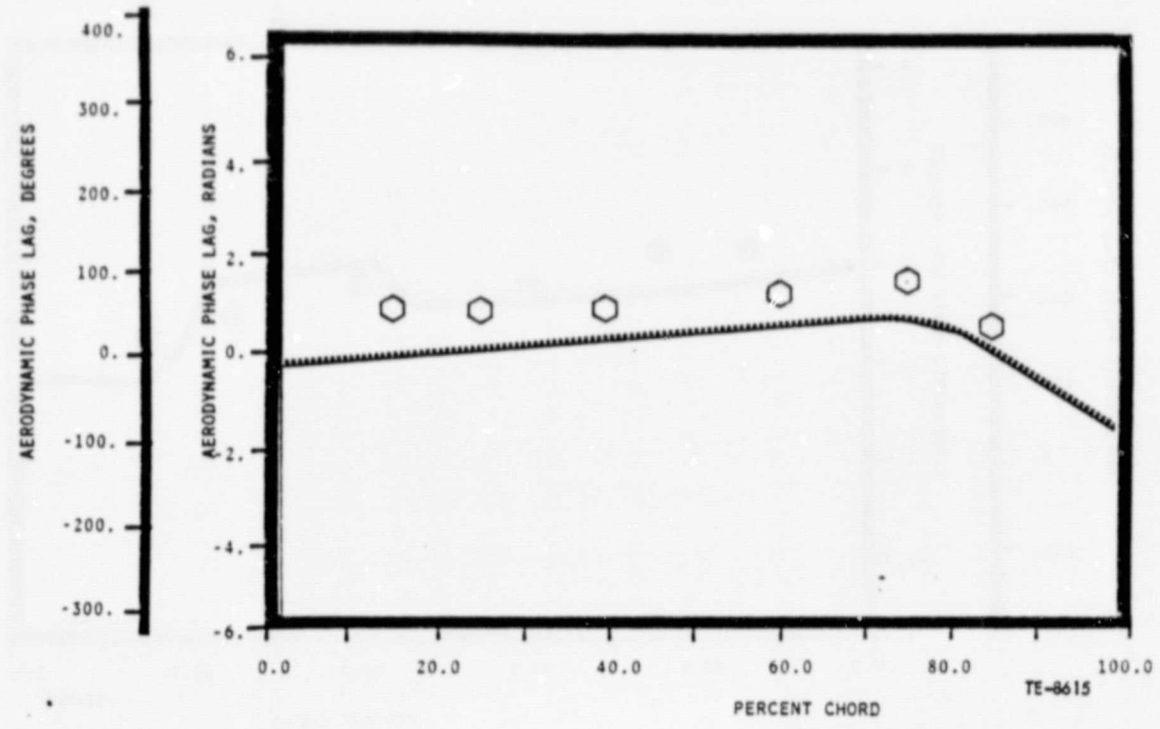

Figure 87. Reduced solidity open setting suction surface phase lag at 1.06:1 and 3.14 rad (180^{o}) phase.

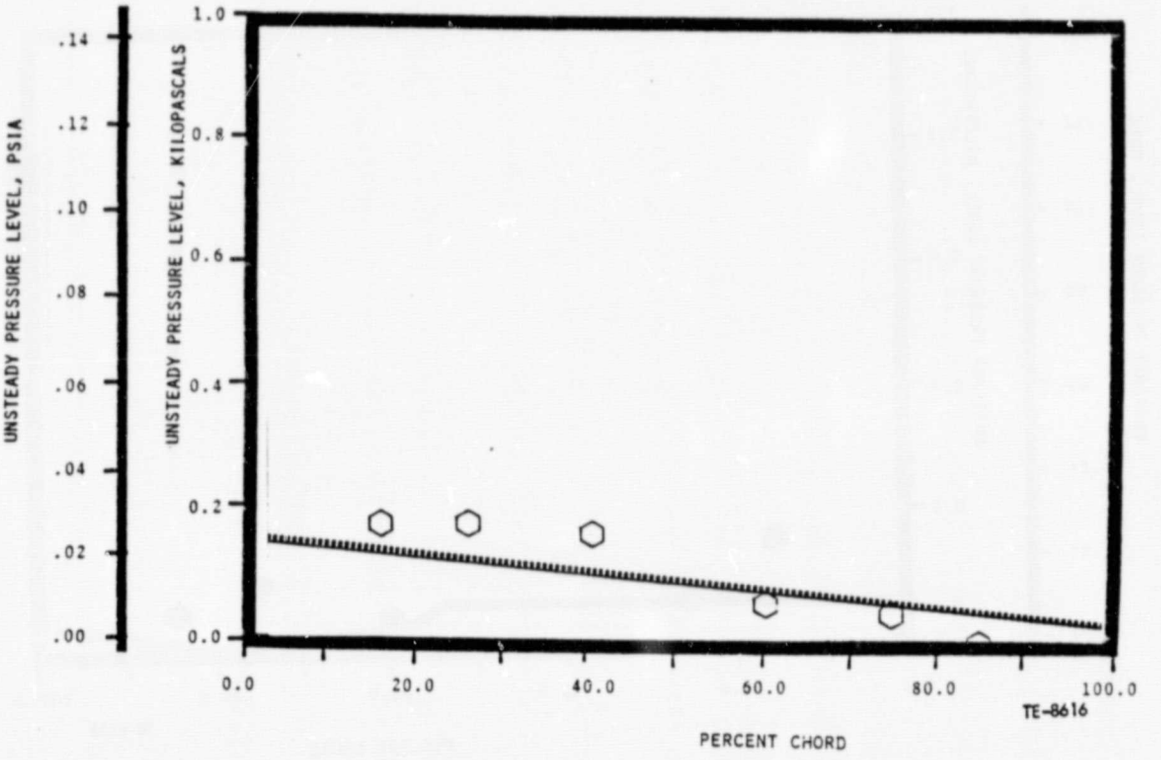

Figure 88. Reduced solidity open setting suction surface unsteady pressure at 1.06:1 and 3.14 rad (180^{o}) phase.

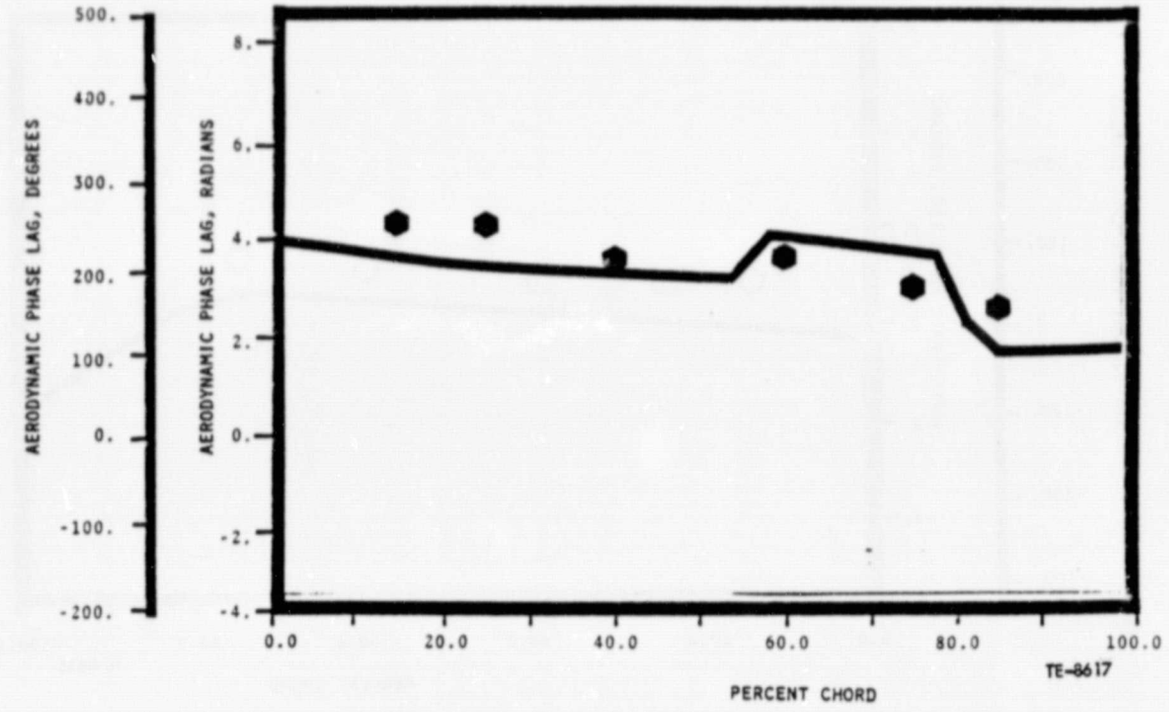

Figure 89. Reduced solidity nominal setting pressure surfce phase lag at 1.35:1 and 2.97 rad (170^{o}) phase.

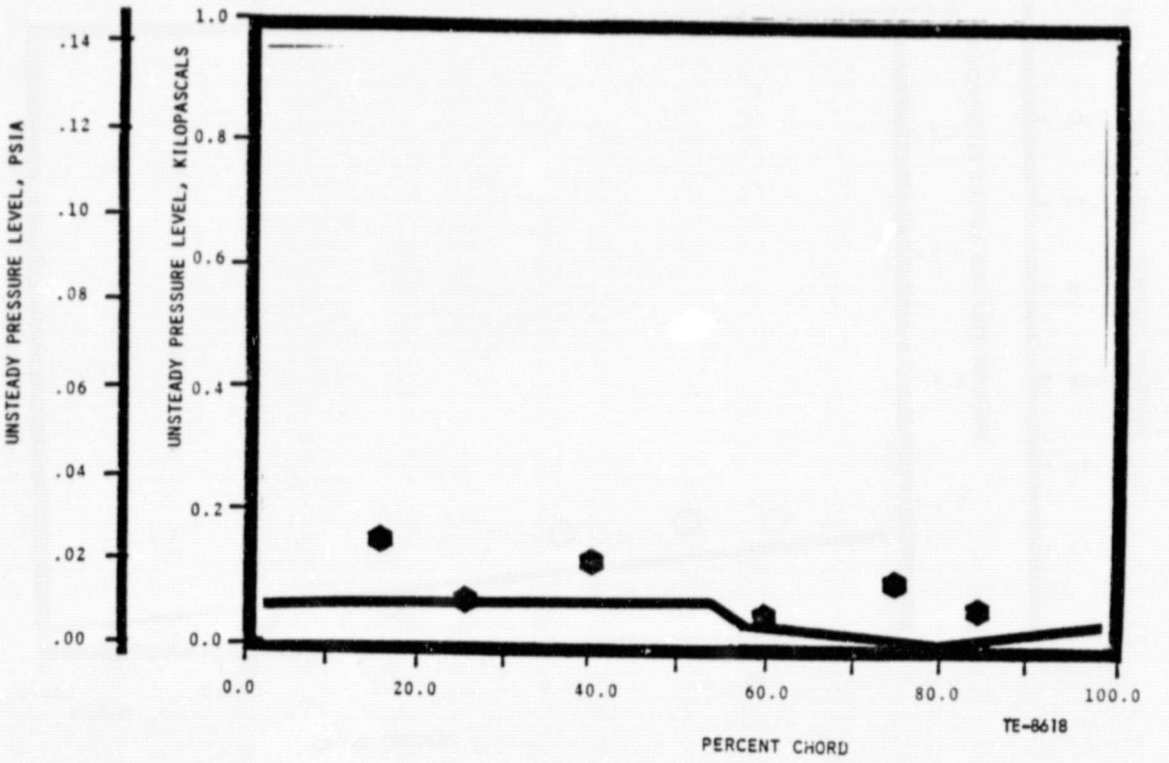

Figure 90. Reduced solidity nominal setting pressure surface unsteady pressure at 1.35 and 2.97 rad (170^{o}) phase.

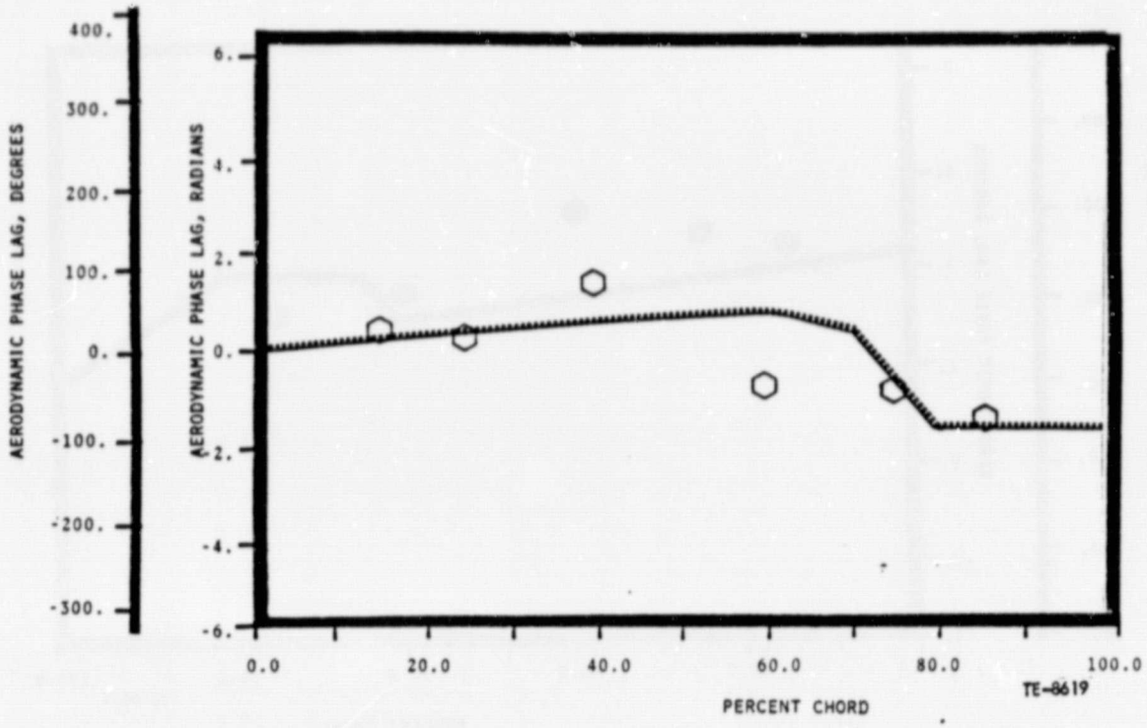

Figure 91. Reduced solidity nominal setting suction surface phase lag at 1.35:1 and 2.97 rad (170^{o}) phase.

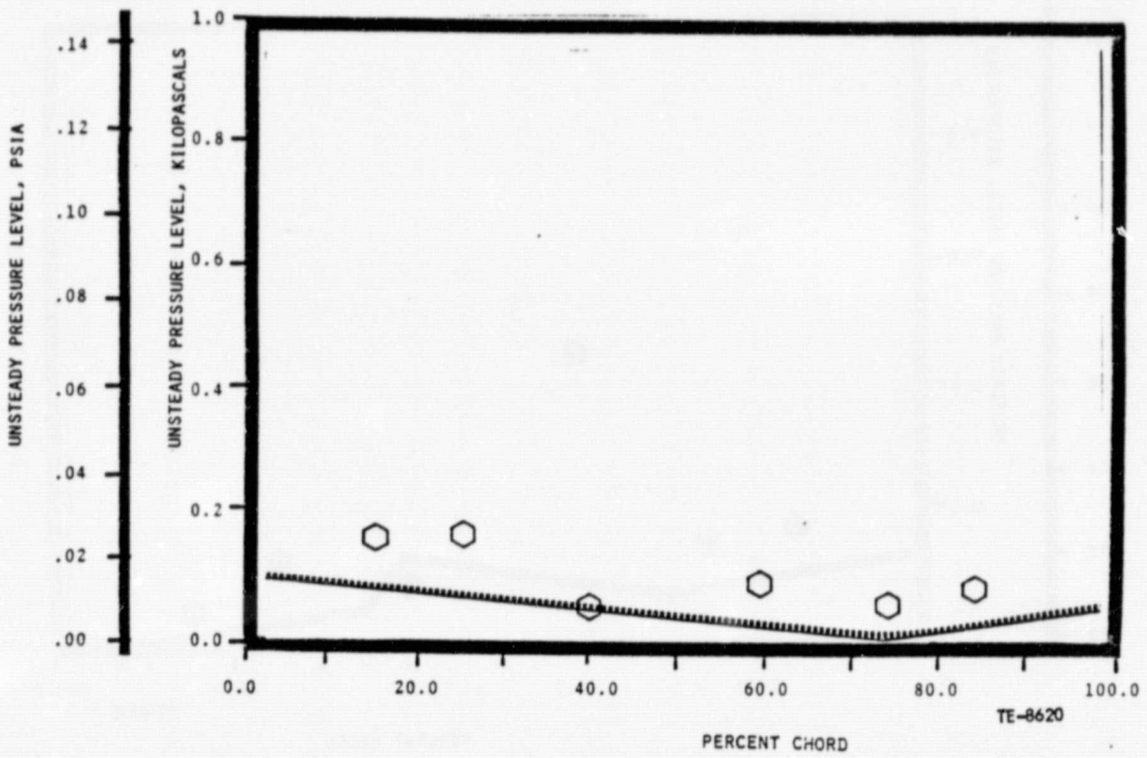

Figure 92. Reduced solidity nominal setting suction surface unsteady pressure at 1.35:1 and 2.97 rad (170^{o}) phase.

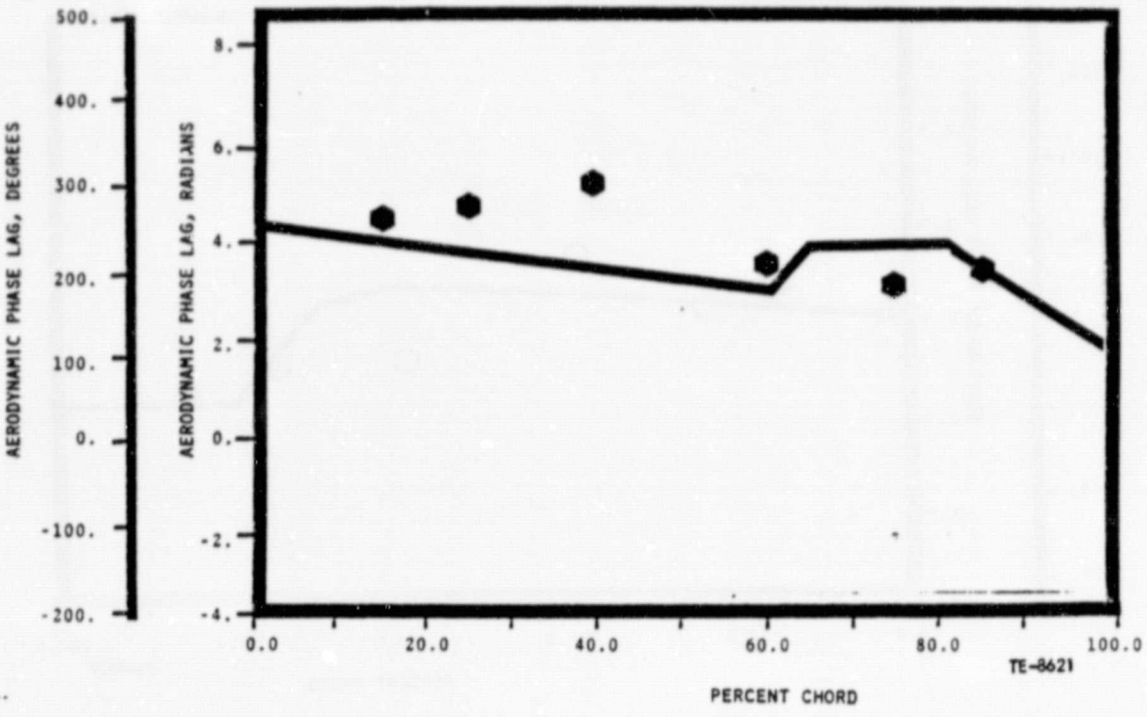

Figure 93. Reduced solidity open setting pressure surface phase lag at 1.33:1 and 3.04 rad (180°) phase.

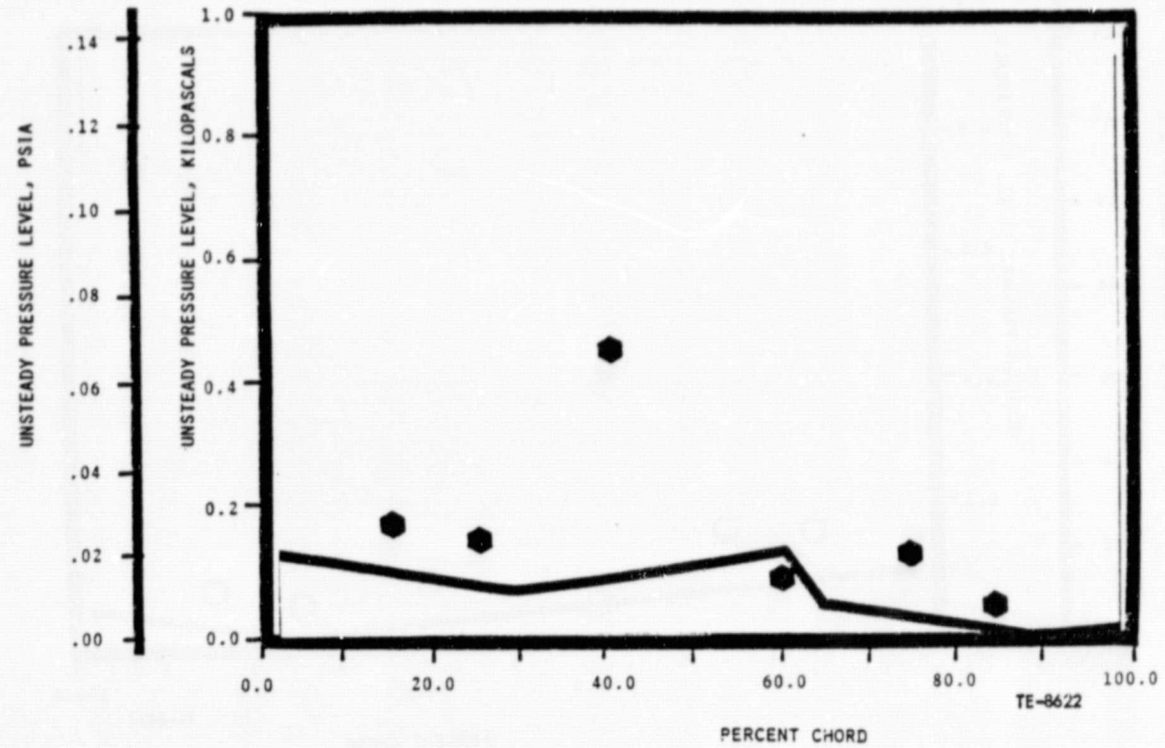

Figure 94. Reduced solidity open setting pressure surface unsteady pressure at 1.33:1 and 3.14 rad (180°) phase.

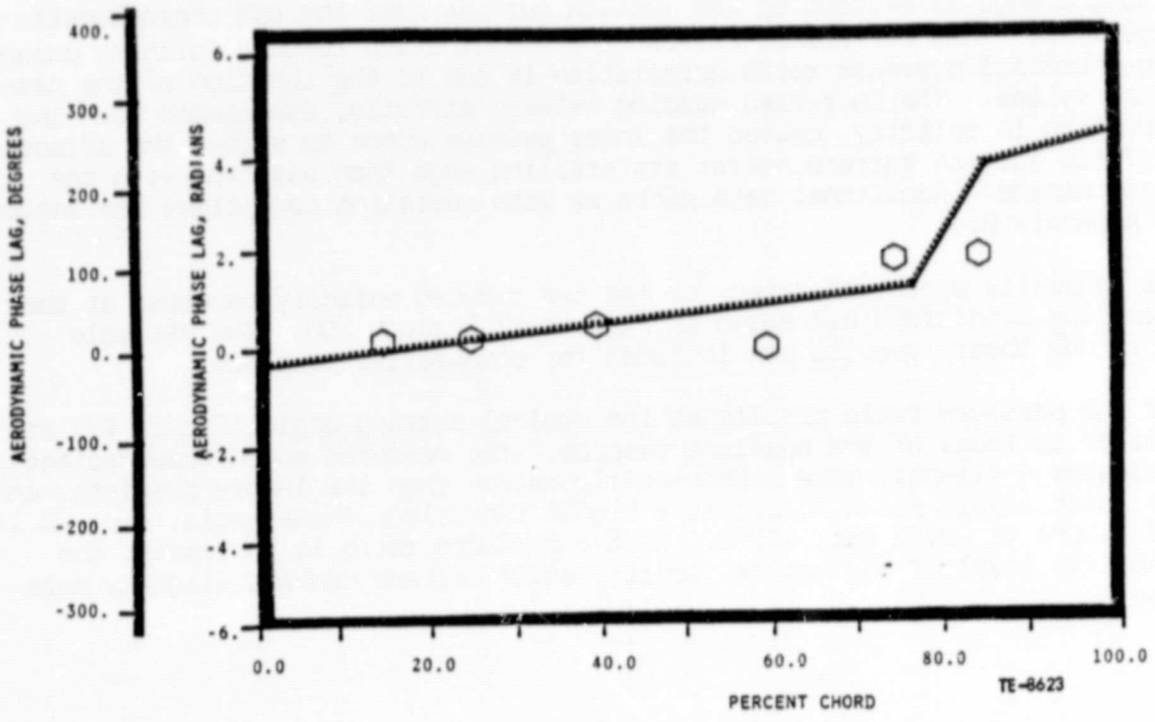

Figure 95. Reduced solidity open setting suction surface phase lag at 1.33:1 and 3.14 rad (180°) phase.

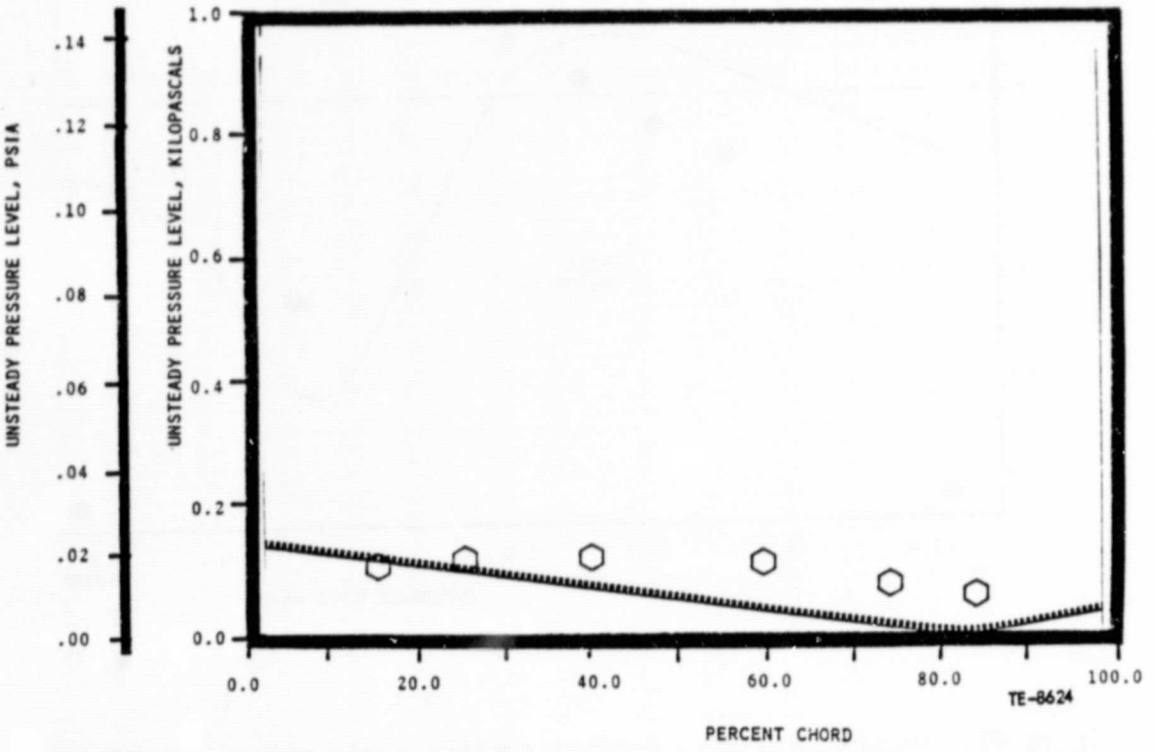

Figure 96. Reduced solidity open setting suction surface unsteady pressure at 1.33:1 and 3.14 rad (180°) phase.

slight change is evident on the suction surface near the 85% chord location in Figure 95. This difference between the baseline and reduced solidity phase lag-increased pressure ratio correlation is due to the location of the passage shock system. The increased spacing between airfoils, associated with the reduction in solidity, causes the inlet passage shock to strike the adjacent airfoils suction surface nearer its trailing edge than was true with the baseline cascade. Additional data plots at both operating conditions are included in Appendix B.

The stability plots generated for the two reduced solidity cascades at the two operating conditions are shown in Figures 97 through 100. The variable amplitude theory results are included for comparative purposes.

The low pressure ratio results at the nominal setting angle (Figure 97) are similar to those of the baseline cascade. The measured moment coefficient indicates a slightly more stable configuration than the theory predicts, and the least stable point occurs at a higher interblade phase angle, i.e. -0.19 rad (-10^{o}) vs -0.52 rad (-30^{o}). As the pressure ratio is increased, the stability level of the nominal setting angle cascade becomes slightly more stable.

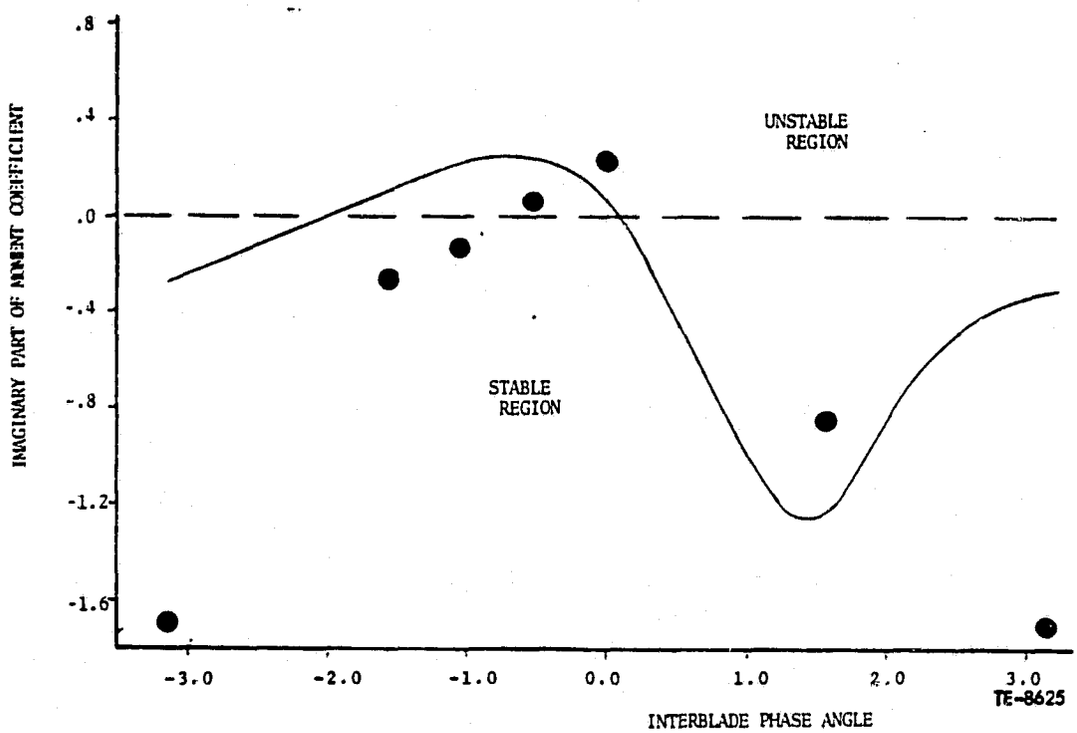

Figure 97. Reduced solidity nominal setting angle cascade stability plot at 1.03:1.

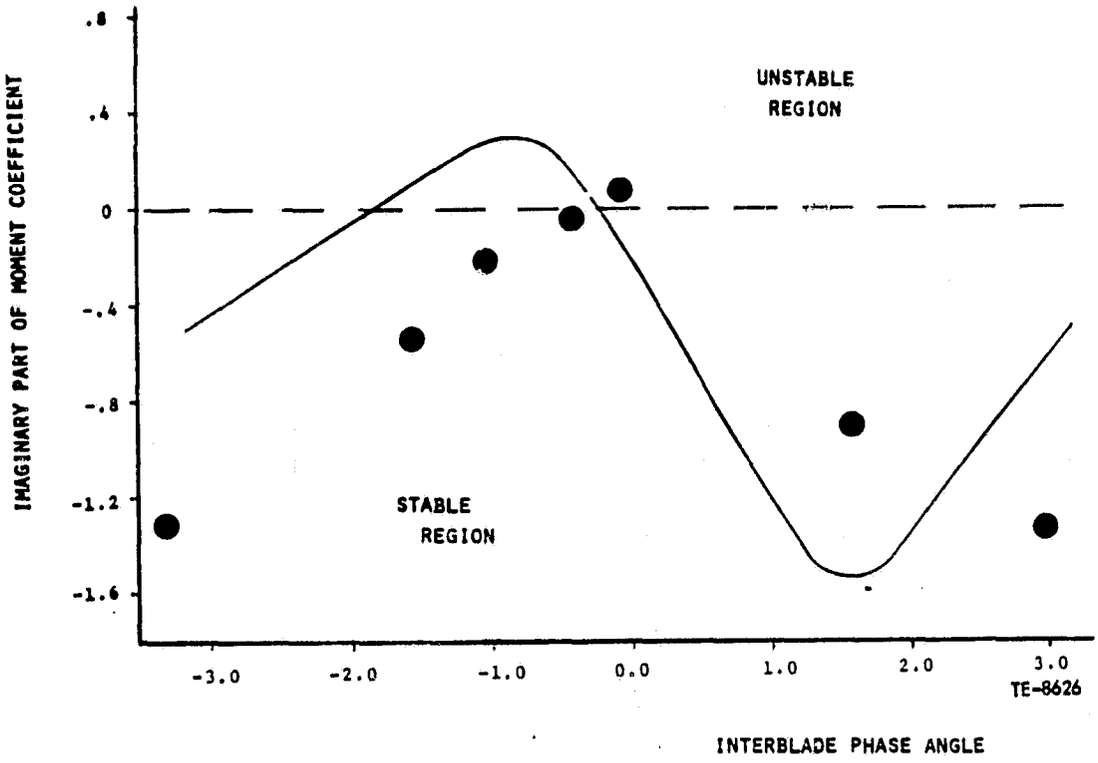

Figure 98. Reduced solidity nominal setting angle cascade stability plot at 1.35:1.

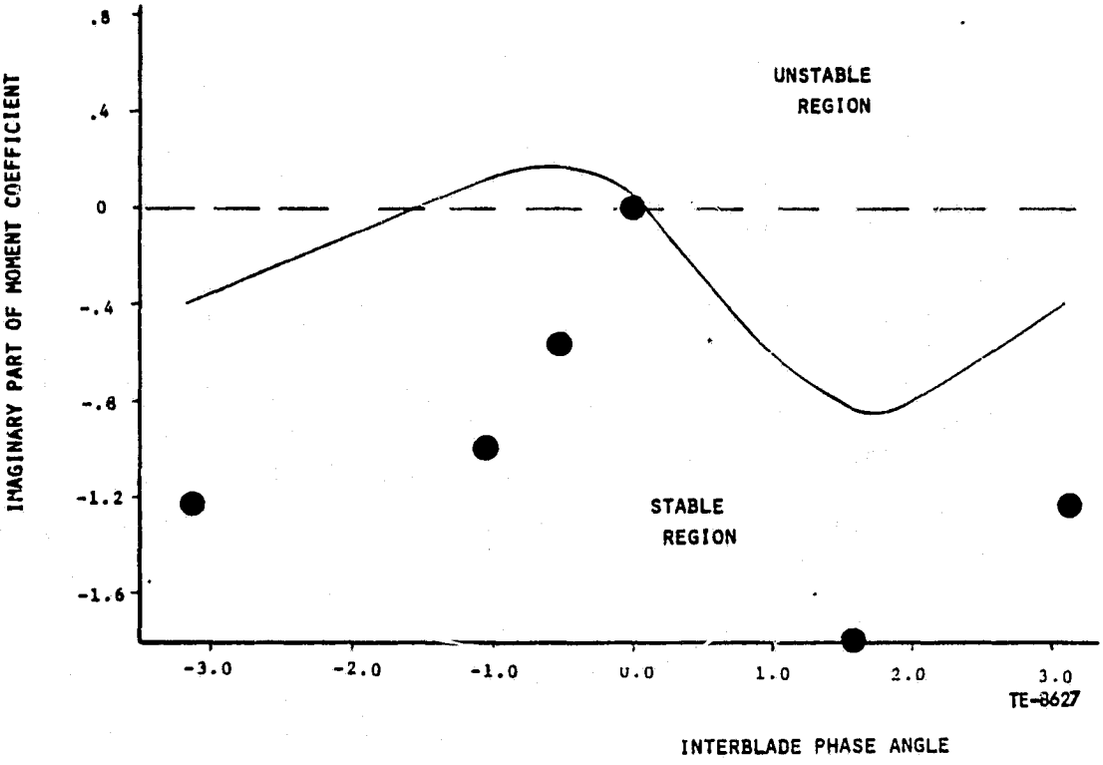

Figure 99. Reduced solidity open setting angle cascade stability plot at 1.06:1.

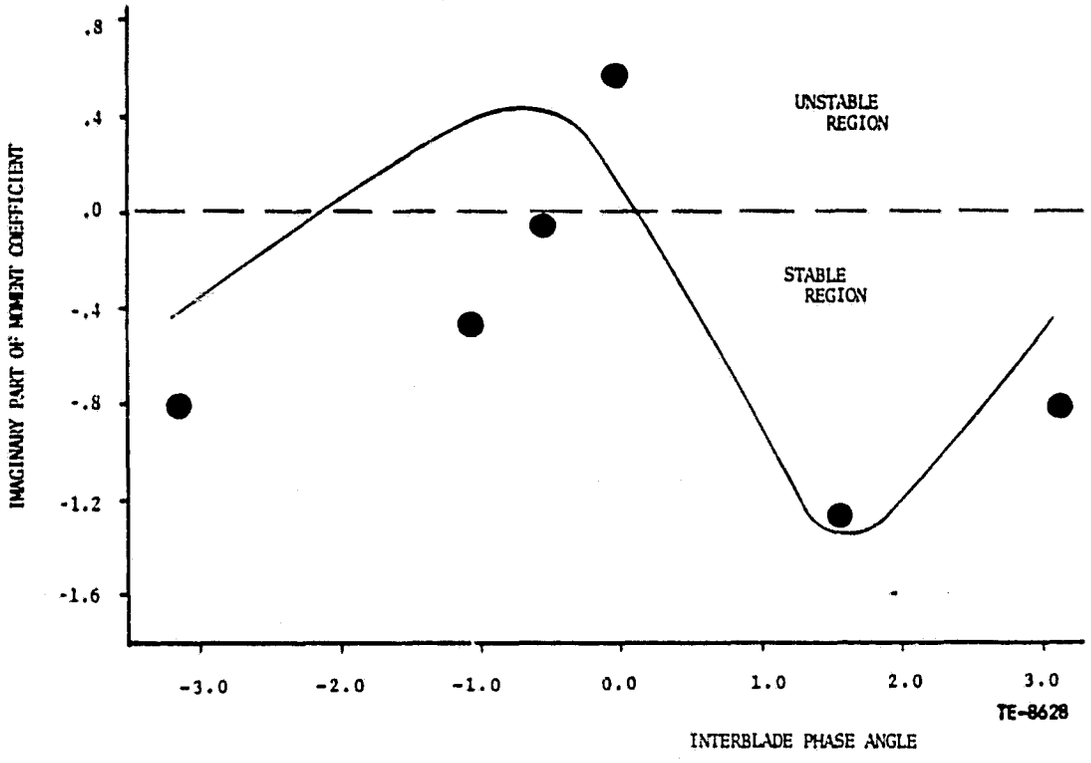

Figure 100. Reduced solidity open setting angle cascade stability plot at 1.33:1.

The open setting angle, reduced solidity cascade stability data at the low pressure ratio is also more stable than theory would predict. This is very noticeable for the -1.05 rad (-60^{o}) interblade phase angle calculated imaginary moment coefficient (CM_i) theory comparison in Figure 99. In general the open reset had a tendency to stabilize the cascade. The level of the calculated CM_i was lower for this open configuration, as compared to the nominal setting, over most of the phase angle range evaluated. Again as with the baseline, pressure ratio had a destabilizing effect as shown in Figure 100. The most unstable phase angle for this configuration was 0 rad (0^{o}). As was true with the low pressure ratio reset cascade data, the +1.57 rad ($+90^{o}$) interblade phase angle was the most stable.

Based on the results of the aforementioned stability plots the data points presented in Table VIII were selected for the flow separation studies.

Table VIII. Reduced Solidity Cascade Flow Separation Study Operating Conditions

	Nominal setting angle	3^{o} open setting angle
Maximum Unsteady Work		
Pressure Ratio	1.03	1.33
Interblade Phase Angle	0 rad (0^{o})	0 rad (0^{o})
Minimum Unsteady Work		
Pressure Ratio	1.03	1.33
Interblade Phase Angle	3.14 rad (180^{o})	+1.57 rad ($+90^{o}$)

The measured chordwise distribution of the shear stress intensity parameter for the four separation data points are presented in Figures 101 through 104. The nominal setting angle pressure surface data is presented in Figure 101. The flow is attached along this surface, with the possible exception of some local effects at the 60% chord location caused by the direct impingement of the adjacent airfoil's wake shock. The nominal setting angle cascade's suction surface shear stress intensity distribution, as shown in Figure 102, indicates no separation along the surface.

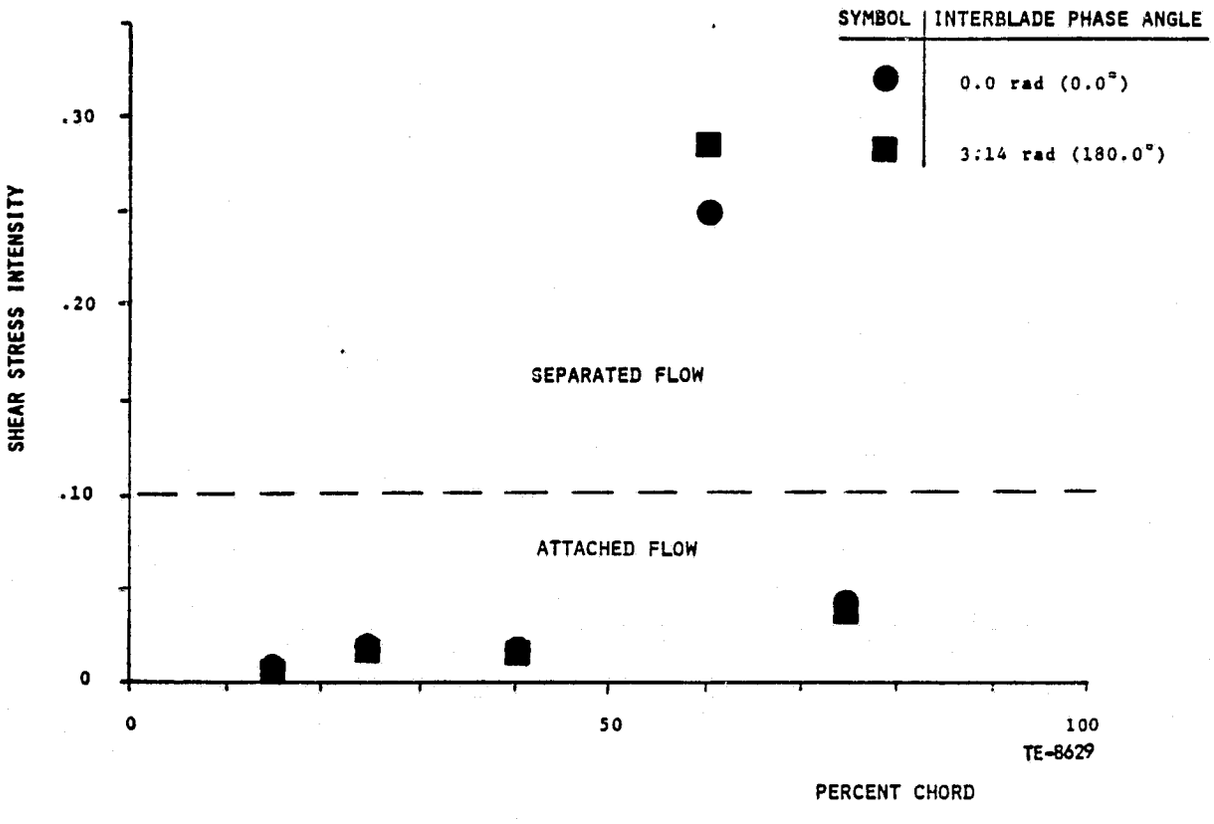

Figure 101. Reduced solidity nominal setting angle pressure surface chordwise distribution of shear stress intensity parameter.

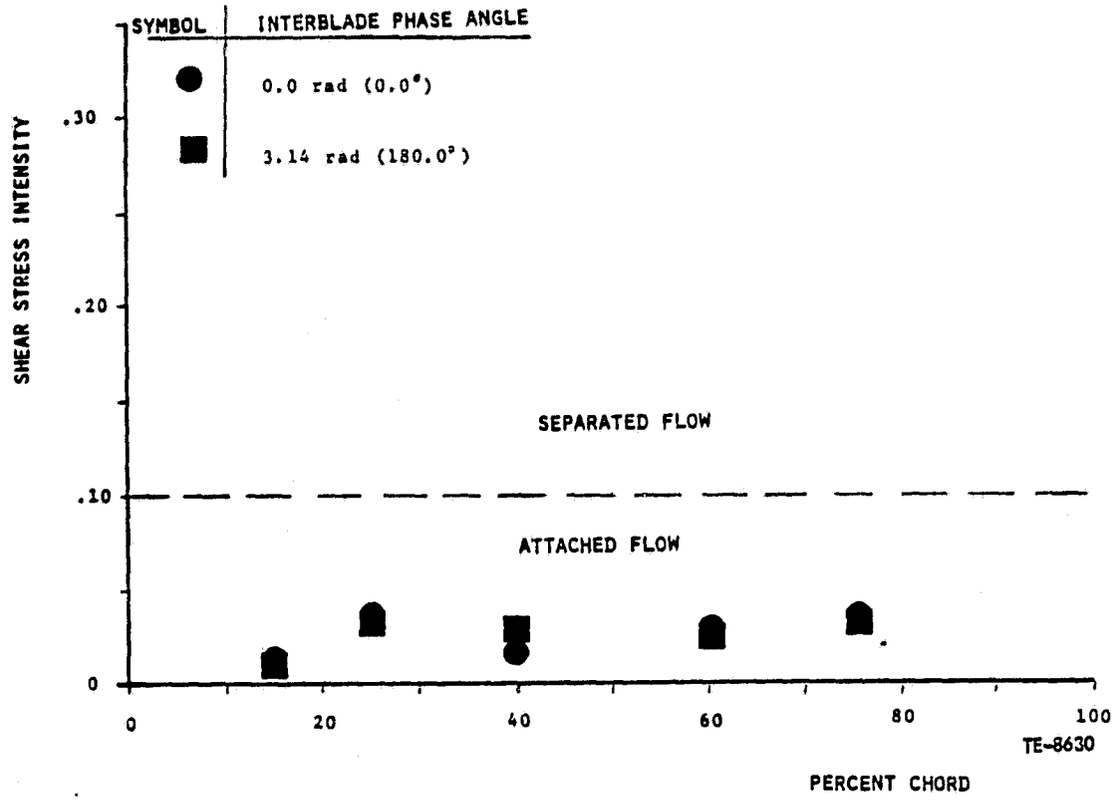

Figure 102. Reduced solidity nominal setting angle suction surface chordwise distribution of shear stress intensity parameter.

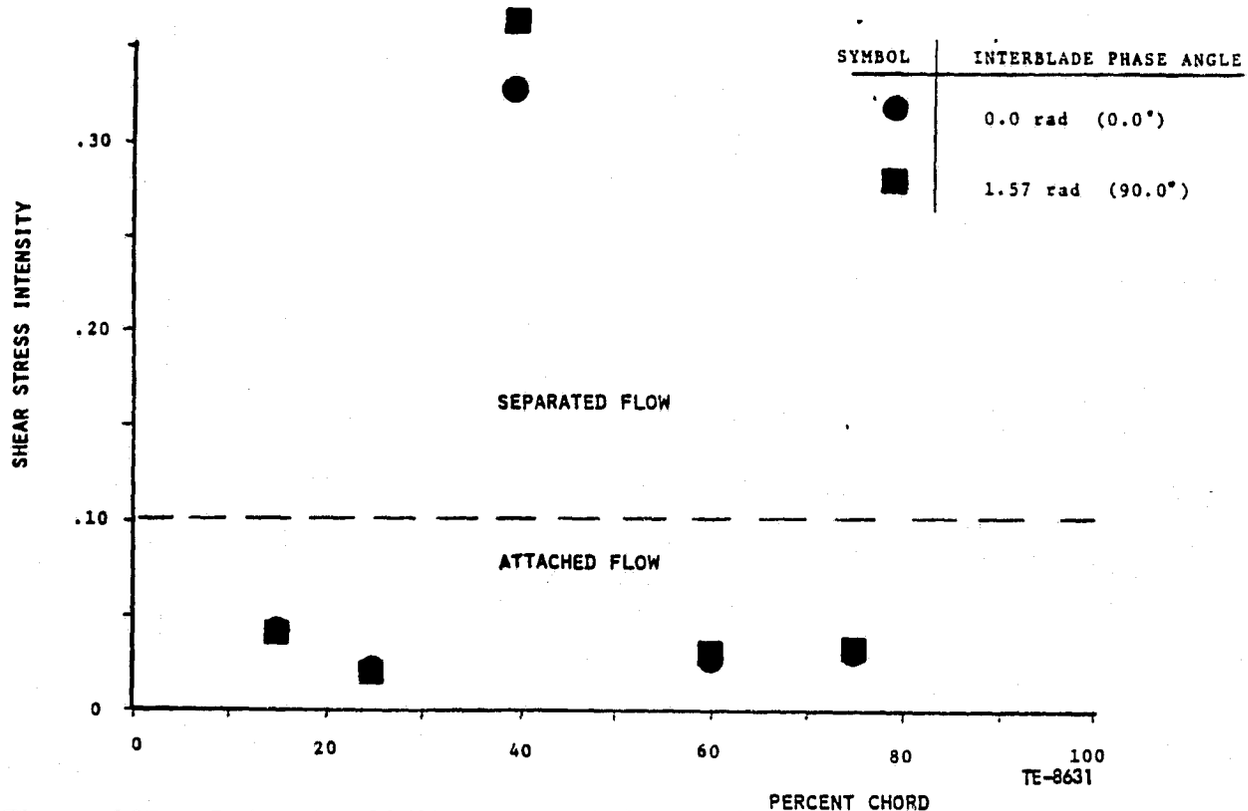

Figure 103. Reduced solidity open setting angle pressure surface chordwise distribution of shear stress intensity parameter.

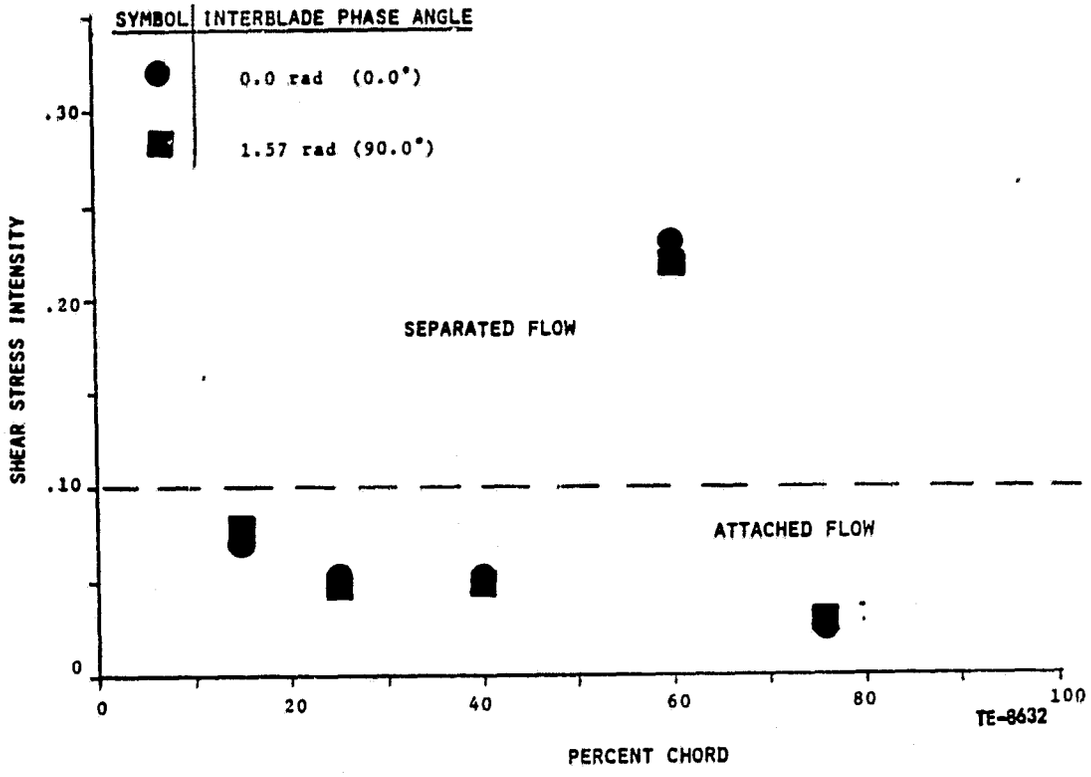

Figure 104. Reduced solidity open setting angle suction surface chordwise distribution of shear stress intensity parameter.

The open setting angle cascade's pressure surface shear stress intensity distribution also indicates the presence of a shock wave. The wave is located at 40% chord (Figure 103). This is due primarily to the increased back pressure causing the wave system to move further up into the passage. The suction surface distribution presented in Figure 104 indicates a separation at 60% chord, but by the 75% chord location the flow is reattached. Since there are no shock waves impinging on the suction surface in this region, this separation must be related to local flow effects.

EDR 10119

APPENDIX A

Sample of Steady State Aerodynamics Computer Print Out

Refer to Section VII for item identification and explanation of meanings.

SUPERSONIC COMPRESSOR CASCADE
NASA CASCADE

CASCADE INLET MACH NUMBER	CASCADE IDEAL STATIC PRESSURE RATIO	PROBE DATA TAKEN BEHIND BLADE	PROBE AXIAL LOCATION (IN.)
1.315	1.425	3	2.250

PRESSURE DATA FROM SCANIVALVE - PSIA

SCANIVALVE PORT #	SCANIVALVE NO. 3	SCANIVALVE NO. 2	SCANIVALVE NO. 4	SCANIVALVE NO. 1
9	17.485	17.469	17.456	17.478
11	16.969	9.114	9.251	6.529
13	10.354	8.877	9.562	4.072
15	10.180	8.854	9.044	6.627
17	10.363	8.715	8.541	6.574
19	10.206	16.915	9.088	6.054
21	17.386	16.898	8.746	5.416
23	8.550	5.994	8.654	5.287
25	8.498	5.910	7.660	5.921
27	8.844	6.507	7.907	7.923
29	9.077	6.238	8.054	9.272
31	9.176	5.919	17.426	17.437
33	8.851	6.347	2.131	2.120
35	9.044	6.703	5.019	4.950
37	8.888	5.982	5.011	4.792
39	8.480	6.298	5.705	5.916
41	9.066	5.699	6.376	6.258
43	17.450	5.484	5.797	5.662
45	4.743	7.971	8.858	8.295
47	17.467	17.479	17.493	17.492

MISCELLANEOUS TEST SECTION DATA

PROBE TANGENTIAL POSITION (IN.)	PROBE SPANWISE POSITION (IN.)	PROBE ANGLE (REF. TANG.) (DEG.)	TEST SECTION ANGLE (REF. HORIZ) (DEG.)	TUNNEL TOTAL TEMPERATURE (DEG.R)
11.656	.908	26.720	25.714	552.823

SUPERSONIC COMPRESSOR CASCADE
NASA CASCADE

NOZZLE EXIT CONDITIONS

MN)O	PT)O	TT)O	M)O	BETA)O
1.300	17.446	552.803	7.955	64.286

TEST SECTION AND CASCADE INLET PERFORMANCE
BASED ON SIDEWALL STATIC PRESSURES

	SCANIVALVE PORT #	SCANIVALVE NO. 2	MACH NUMBER
BLADE	27	6.507	1.276
BLADE	29	6.238	1.307
BLADE	31	5.919	1.345
BLADE	33	6.347	1.294
BLADE	35	6.703	1.254

SUPERSONIC FLOW PROPERTIES ACROSS LEADING WEDGE

WEDGE UPSTREAM MACH NO.	+ COMPRESSION - EXPANSION OF FLOW	WAVE ANGLE	DOWNSTREAM MACH NUMBER	TOTAL PRESSURE RATIO	STATIC PRESSURE RATIO
1.300	-.326	49.665	1.312	1.000	.984

SUPERSONIC COMPRESSOR CASCADE
NASA CASCADE

CASCADE PHYSICAL DESIGN PARAMETERS

STAGGER ANGLE (DEG)	CHORD (IN)	BLADE SPACING (IN)	T/C RATIO	EXIT TO INLET SPAN RATIO (BLADE EXIT)	EXIT TO INLET SPAN RATIO (PROBE MEASURING PLANE)
61.550	3.000	2.564	.034	1.000	1.000

INLET METAL ANGLE PS (DEGREES)	INLET METAL ANGLE SS (DEGREES)	INLET METAL ANGLE ML (DEGREES)	EXIT METAL ANGLE ML (DEG.)
58.890	62.940	60.460	61.760

CASCADE INLET CONDITIONS

MN)1	PT)1	TT)1	BETA)1	P)1	M)1	G)1
1.312	17.446	552.803	63.960	6.196	.415	7.464

I)SS	I)ML	MN)X,1	MN)Y,1	TT/T)1	PT/P)1	NR/10**6
1.020	3.500	.576	1.179	1.344	2.816	1.314

SUPERSONIC COMPRESSOR CASCADE
NASA CASCADE

CASCADE IDEAL PERFORMANCE
BASED ON SIDEWALL STATIC PRESSURES

PRESSURE DATA FROM SCANIVALVE - PSIA

SCANIVALVE PORT #	SCANIVALVE NO. 3	SCANIVALVE PORT #	SCANIVALVE NO. 3
23	8.550	33	8.851
25	8.498	35	9.044
27	8.844	37	8.888
29	9.077	39	8.480
31	9.176	41	9.066

MEAN EXIT STATIC PRESSURE (PSIA)	RMS DEVIATION	MEAN EXIT MID-PASSAGE STATIC PRESSURE (PSIA)	RMS DEVIATION	IDEAL EXIT MACH NO.	CASCADE IDEAL STATIC PRESSURE RATIO (P)2/P)1)
8.829	.272	8.866	.210	1.036	1.425

SUPERSONIC COMPRESSOR CASCADE
NASA CASCADE

INSTRUMENTED BLADE PARAMETERS

	PRESSURE SURFACE (PS)	SUCTION SURFACE (SS)	DPS/Q1 (PS)	DFS/Q1 (SS)	PS/PT)1	SS/PT)1	PERCENT CHORD (PS)	PERCENT CHORD (SS)
11	9.251	6.529	.429	.045	.530	.374	5.00	5.00
13	9.562	7.058	.451	.116	.548	.405	15.00	15.00
15	9.044	5.627	.382	.058	.518	.380	20.00	25.00
17	8.541	6.574	.314	.051	.490	.377	25.00	32.50
19	9.058	6.054	.384	-.019	.519	.347	32.50	40.00
21	8.746	5.416	.342	-.105	.501	.310	40.00	52.00
23	8.654	5.287	.329	-.122	.496	.303	48.00	60.00
25	7.660	5.921	.196	-.037	.439	.339	60.00	75.00
27	7.907	7.923	.229	.231	.453	.454	75.00	85.53
29	8.054	9.272	.249	.412	.462	.531	85.00	96.15

SUPERSONIC COMPRESSOR CASCADE
NASA CASCADE

LOCAL CASCADE EXIT PERFORMANCE

PERCT	Y DEV PT)YP	MN)2 TURN P)TP	MN)X,2 M)2 P)RP	MN)Y,2 P)2/P)1 P)AP	FT)2 V)2 P)SP	P)2 PT)C BETA)P	FT)2/PT)1 FT)C PT)1	BETA)2 PT)C,A TT)1
.20	6.522 1.811 16.964	.994 .389 10.310	.443 .020 10.256	.850 1.455 10.450	16.966 1047.171 10.192	9.013 17.446 .291	.972 17.437 17.442	63.571 17.442 552.459
4.59	6.650 1.921 17.062	1.008 .279 10.333	.447 .022 10.258	.904 1.440 10.456	17.063 1059.365 10.215	8.919 17.446 .401	.978 17.413 17.430	63.661 17.430 552.459
9.98	6.778 2.147 17.077	1.015 .053 10.350	.446 .022 10.233	.911 1.439 10.435	17.079 1064.745 10.204	8.861 17.446 .627	.979 17.398 17.422	63.907 17.422 552.459
14.98	6.906 2.346 17.062	1.014 -.146 10.358	.443 .022 10.203	.912 1.430 10.424	17.063 1064.370 10.205	8.858 17.446 .826	.978 17.391 17.419	64.106 17.419 552.459
20.21	7.035 2.444 17.048	1.008 -.244 10.371	.439 .022 10.199	.907 1.440 10.435	17.050 1058.786 10.231	8.919 17.446 .924	.977 17.409 17.428	64.204 17.428 552.459
25.20	7.163 2.696 17.070	1.017 -.486 10.382	.439 .021 10.164	.917 1.426 10.410	17.072 1066.662 10.226	8.836 17.446 1.166	.979 17.432 17.439	64.446 17.439 552.459
29.99	7.291 3.152 17.044	1.031 -.952 10.364	.437 .021 10.055	.933 1.400 10.361	17.047 1078.811 10.188	8.678 17.446 1.632	.977 17.400 17.423	64.912 17.423 552.459

SUPERSONIC COMPRESSOR CASCADE
NASA CASCADE

LOCAL CASCADE EXIT PERFORMANCE

PERCT	Y DEV PT)YP	MN)2 TURN P)TP	MN)X,2 M)2 P)BP	MN)Y,2 P)2/P)1 P)MP	PT)2 V)2 P)SP	P)2 PT)C BETA)P	PT)2/PT)1 PT)C PT)1	BETA)2 PT)C,A TT)1
	7.419	1.235	.425	.944	16.890	8.549	.968	65.762
34.98	4.902	-1.802	.020	1.380	1062.837	17.446	17.412	17.429
	16.885	10.329	9.862	10.253	10.085	2.482	17.429	552.459
	7.547	.919	.370	.841	15.917	9.215	.912	66.238
39.98	4.478	-2.278	.019	1.487	979.377	17.446	17.417	17.431
	15.911	10.214	9.743	10.056	9.888	2.958	17.431	552.459
	7.676	.831	.359	.750	14.811	9.410	.849	64.443
44.01	2.693	-.483	.018	1.519	898.001	17.446	17.423	17.434
	14.810	9.980	9.825	9.877	9.719	1.163	17.434	552.114
	7.804	.844	.408	.739	15.020	9.418	.861	61.102
50.00	-.658	2.858	.019	1.520	910.066	17.446	17.438	17.442
	15.017	9.789	10.088	9.930	9.748	-2.178	17.442	552.459
	7.932	.932	.459	.811	16.094	9.181	.922	60.478
54.99	-1.282	3.482	.022	1.482	991.504	17.446	17.387	17.417
	16.088	9.796	10.253	10.118	9.901	-2.802	17.417	552.114
	8.060	1.012	.486	.888	16.855	8.772	.966	61.290
59.98	-.470	2.670	.023	1.416	1062.511	17.446	17.422	17.434
	16.851	9.969	10.335	10.323	10.058	-1.990	17.434	552.459
	8.188	1.012	.473	.895	16.956	8.820	.972	62.146
64.98	.386	1.814	.023	1.424	1062.929	17.446	17.390	17.418
	16.953	10.117	10.327	10.396	10.098	-1.134	17.418	552.114

SUPERSONIC COMPRESSOR CASCADE
NASA CASCADE

LOCAL CASCADE EXIT PERFORMANCE

PERCT	Y DEV PT)YP	MN)2 TURN P)TP	MN)X,2 M)2 P)BP	MN)Y,2 P)2/P)1 P)AP	PT)2 V)2 P)SP	P)2 PT)D BETA)P	PT)2/PT)1 PT)D PT)1	BETA)2 PT)D,A TT)1
	8.317	.992	.458	.880	16.883	8.994	.968	62.510
70.01	.750	1.450	.023	1.452	1045.139	17.446	17.387	17.417
	16.880	10.176	10.315	10.420	10.109	-.770	17.417	552.459
	8.445	.981	.450	.872	16.840	9.088	.965	62.682
75.00	.922	1.278	.022	1.467	1035.270	17.446	17.437	17.442
	16.837	10.203	10.310	10.441	10.121	-.598	17.442	552.459
	8.573	.982	.448	.874	16.815	9.063	.964	62.870
79.99	1.110	1.090	.022	1.463	1036.227	17.446	17.436	17.441
	16.812	10.200	10.273	10.431	10.091	-.410	17.441	552.459
	8.701	.980	.445	.873	16.752	9.054	.960	63.013
84.98	1.253	.947	.022	1.461	1034.042	17.446	17.417	17.432
	16.750	10.183	10.231	10.402	10.057	-.267	17.432	552.114
	8.829	.967	.437	.862	16.616	9.113	.952	63.130
89.98	1.370	.830	.022	1.471	1022.750	17.446	17.425	17.436
	16.614	10.156	10.183	10.371	10.033	-.150	17.436	552.114
	8.958	.966	.436	.861	16.566	9.097	.950	63.135
95.01	1.375	.825	.022	1.468	1021.754	17.446	17.426	17.436
	16.564	10.135	10.160	10.346	9.998	-.145	17.436	552.459
	9.086	.974	.439	.869	16.575	9.020	.950	63.219
100.00	1.459	.741	.022	1.456	1028.879	17.446	17.401	17.424
	16.572	10.117	10.129	10.315	9.973	-.061	17.424	552.114

C-2

SUPERSONIC COMPRESSOR CASCADE
NASA CASCADE

LOCAL CASCADE EXIT PERFORMANCE

PERCT	Y DEV PT)YP	MN)2 TURN P)TP	MN)X,2 M)2 P)BP	MN)Y,2 P)2/P)1 P)NP	PT)2 V)2 P)SP	P)2 PT)C BETA)P	PT)2/PT)1 PT)C PT)1	BETA)2 PT)C,A TT)1
	9.214	.981	.439	.877	16.622	8.971	.953	63.391
104.59	1.631	.569	.022	1.448	1035.270	17.446	17.397	17.422
	16.629	10.131	10.111	10.317	9.983	.111	17.422	552.459
	9.342	.987	.440	.884	16.685	8.941	.956	63.549
109.58	1.789	.411	.022	1.443	1040.628	17.446	17.421	17.433
	16.683	10.151	10.103	10.344	10.009	.269	17.433	552.459
	9.470	.999	.440	.897	16.793	8.877	.963	63.862
114.58	2.102	.098	.021	1.433	1050.889	17.446	17.431	17.439
	16.791	10.205	10.099	10.375	10.032	.522	17.439	552.459
	9.599	1.018	.443	.916	16.942	8.757	.971	64.196
120.01	2.436	-.236	.022	1.413	1067.676	17.446	17.421	17.434
	16.939	10.273	10.102	10.410	10.058	.916	17.434	552.114
	9.727	1.037	.444	.937	17.036	8.608	.976	64.640
125.20	2.880	-.680	.021	1.389	1084.096	17.446	17.413	17.430
	17.031	10.316	10.058	10.430	10.076	1.360	17.430	552.459
	9.855	1.051	.441	.954	17.086	8.491	.979	65.177
129.99	3.417	-1.217	.021	1.371	1096.954	17.446	17.388	17.417
	17.078	10.373	10.008	10.432	10.064	1.897	17.417	552.459
	9.983	1.043	.426	.952	16.972	8.517	.973	65.905
134.98	4.145	-1.945	.020	1.375	1088.969	17.446	17.411	17.428
	16.963	10.372	9.873	10.383	10.016	2.625	17.428	552.114

SUPERSONIC COMPRESSOR CASCADE
NASA CASCADE

LOCAL CASCADE EXIT PERFORMANCE

PERCT	Y DEV PT)YP	MN)2 TURN P)TP	MN)X,2 M)2 P)BP	MN)Y,2 P)2/P)1 P)NP	FT)2 V)2 P)SP	P)2 PT)O BETA)P	PT)2/PT)1 PT)O PT)1	BETA)2 PT)O,A TT)1
	10.111	.945	.377	.867	16.257	9.140	.932	66.491
138.98	4.731	-2.531	.019	1.475	1003.196	17.446	17.433	17.440
	16.247	10.306	9.769	10.227	9.875	3.211	17.440	552.459
	10.240	.850	.358	.771	15.165	9.450	.869	65.109
145.21	3.349	-1.149	.019	1.525	915.731	17.446	17.449	17.448
	15.160	10.103	9.847	10.046	9.752	1.829	17.448	552.114
	10.368	.870	.400	.772	15.395	9.396	.882	62.627
150.00	.867	1.333	.019	1.517	934.270	17.446	17.395	17.422
	15.393	9.946	10.041	10.040	9.771	-.653	17.420	552.114
	10.496	.947	.447	.834	16.274	9.133	.933	61.798
154.99	.038	2.162	.021	1.474	1004.662	17.446	17.387	17.416
	16.271	9.948	10.196	10.190	9.913	-1.482	17.416	552.114
	10.624	1.015	.475	.898	16.923	8.774	.970	62.134
159.98	.374	1.826	.023	1.416	1065.445	17.446	17.390	17.418
	16.920	10.088	10.309	10.378	10.061	-1.146	17.418	552.459
	10.752	1.021	.469	.907	17.112	8.809	.981	62.639
164.98	.879	1.321	.023	1.422	1070.570	17.446	17.440	17.443
	17.110	10.222	10.343	10.493	10.162	-.641	17.443	552.489
	10.881	1.010	.487	.901	17.120	8.932	.981	63.193
170.01	1.343	.857	.023	1.442	1060.769	17.446	17.449	17.448
	17.118	10.305	10.338	10.528	10.201	-.177	17.448	552.459

SUPERSONIC COMPRESSOR CASCADE
NASA CASCADE

LOCAL CASCADE EXIT PERFORMANCE

PERCT	Y DEV PT)YP	MN)2 TURN P)TP	MN)X,2 M)2 P)RP	MN)Y,2 P)2/P)1 P)NP	PT)2 V)2 P)SP	P)2 PT)O BETA)P	PT)2/PT)1 PT)C PT)1	BETA)2 PT)C,A TT)1
	11.009	1.006	.451	.859	17.123	8.972	.981	63.358
178.00	1.598	.602	.022	1.448	1057.504	17.446	17.413	17.430
	17.121	10.340	10.325	10.540	10.216	.078	17.430	552.459
	11.137	1.009	.447	.904	17.129	8.949	.982	63.669
179.99	1.909	.291	.022	1.444	1059.713	17.446	17.402	17.424
	17.127	10.371	10.299	10.525	10.213	.389	17.424	552.459
	11.265	1.010	.445	.907	17.105	8.922	.980	63.844
184.98	2.084	.116	.022	1.440	1060.931	17.446	17.392	17.419
	17.103	10.370	10.265	10.492	10.209	.564	17.419	552.459
	11.393	1.007	.441	.905	17.061	8.932	.978	64.025
189.98	2.265	-.065	.022	1.442	1058.237	17.446	17.388	17.417
	17.059	10.375	10.237	10.455	10.201	.745	17.417	552.459
	11.522	.999	.436	.899	16.987	8.974	.974	64.117
195.01	2.357	-.157	.022	1.448	1051.344	17.446	17.405	17.425
	16.986	10.362	10.208	10.415	10.200	.837	17.425	552.114
	11.650	.999	.435	.899	16.971	8.969	.973	64.206
200.00	2.446	-.246	.021	1.448	1051.019	17.446	17.428	17.437
	16.970	10.362	10.192	10.379	10.221	.926	17.437	552.114

SUPERSONIC COMPRESSOR CASCADE
NASA CASCADE

MASS AVERAGED EXIT CONDITIONS

MN)2	BETA)2	PT)2/PT)1
.985	63.564	.957

CASCADE EXIT PARAMETERS
BASED ON MASS AVERAGED CONDITIONS

MN)X,2	MN)Y,2	PT)2	P)2	TT)2	TT)2/T)2	M)2/M)1
.438	.882	16.690	8.975	552.803	1.194	1.032

MIXED EXIT CONDITIONS

MN)X,2	MN)Y,2	PT)2	P)2	TT)2	TT)2/T)2	MN)2	BETA)2
.436	.881	16.657	8.978	552.803	1.193	.983	63.680

SUPERSONIC COMPRESSOR CASCADE
NASA CASCADE

OVERALL PERFORMANCE

MASS AVERAGED EXIT CONDITIONS

P)2/P)1	PT)2/PT)1	V)2/V)1	V)2/V)1,X	V)2/V)1,Y	R)2/R)1	T)2/T)1	OMEGA
TPLP	DF	DF)EQ	CV)Y	RN)2	CPS/Q1	DEV	TURN
BETA)C	A)2/A)1						
1.449	.957	.796	.808	.794	1.287	1.126	.067
.013	.283	1.460	.185	1.232	.372	1.804	.356
64.635	.962						

OVERALL PERFORMANCE

MIXED EXIT CONDITIONS

P)2/P)1	PT)2/PT)1	V)2/V)1	V)2/V)1,X	V)2/V)1,Y	R)2/R)1	T)2/T)1	OMEGA
TPLP	DF	DF)EQ	CV)Y	RN)2	CPS/Q1	DEV	TURN
BETA)C	A)2/A)1						
1.449	.955	.795	.803	.793	1.286	1.127	.070
.013	.284	1.462	.186	1.229	.373	1.920	.280
64.580	.968						

EOR 10119

APPENDIX B

Sample of Time Variant Aerodynamics Computer Print Out

Refer to Section VII for item identification and explanation of meanings.

SUPERSONIC COMPRESSOR CASCADE
NASA-I TORSION REDUCED SOLIDITY CASCADE - OPEN

FILE NAME NAS01

CASCADE INLET MACH NUMBER	CASCADE IDEAL STATIC PRESSURE RATIO	CASCADE EXCITATION FREQUENCY	INTERBLADE PHASE ANGLE
1.315	1.33	725	-90.

DATA AQUISITION RATE PER CHANNEL (PTS/SEC)	SIGMA LIMITS	RELATIVE VELOCITY (FT/SEC)	INLET AIR ANGLE	REDUCED FREQUENCY
6923	2.00	1315.	62.06	0.44

DATA ANALYSIS OF POSITIVE PEAK

		1		2		3		4		5		6
1	1.4	.019	.7	.061	.8	.050	.4	.040	.6	.019	.4	.014
2	2.8	.018	2.1	.058	2.2	.049	3.2	.026	2.0	.017	1.8	.015
3	4.2	.018	3.5	.062	3.6	.051	6.0	.023	3.4	.019	3.2	.013
4	5.6	.018	4.9	.058	5.0	.049	7.3	.039	4.7	.013	4.6	.019
UNCORR MEAN		.018		.060		.050		.032		.017		.015
CORR MEAN		.018		.060		.050		.032		.017		.015
WITHIN 2.0 SIGMA		4		4		4		4		4		4

		7		8		9		10		11		12
1	.5	.019	-.0	.030	.2	.025	1.4	.028	.3	.009	1.1	.007
2	1.8	.025	1.4	.035	1.6	.032	2.8	.031	1.6	.008	2.4	.006
3	3.2	.021	2.8	.038	2.9	.026	4.2	.031	3.0	.010	3.9	.010
4	4.6	.023	4.2	.029	4.3	.032	5.6	.030	8.6	.008	5.3	.013
UNCORR MEAN		.022		.033		.028		.030		.009		.009
CORR MEAN		.022		.033		.028		.030		.009		.009
WITHIN 2.0 SIGMA		4		4		4		4		4		4

```
                  13
 1     1.1    .016
 2     2.5    .019
 3     3.9    .014
 4     5.3    .018

UNCORR
 MEAN         .017

 CORR
 MEAN         .017

WITHIN
2.0 SIGMA      4
```

DATA ANALYSIS OF NEGATIVE PEAK

		1		2		3		4		5		6
1	.8	.045	.0	.070	.1	.055	1.5	.032	1.3	.015	1.1	.023
2	2.2	.046	1.4	.072	1.5	.055	4.0	.058	2.7	.016	2.5	.019
3	3.5	.048	2.8	.068	2.9	.058	5.3	.058	4.1	.021	3.8	.021
4	4.9	.045	4.2	.070	4.3	.055	6.5	.018	5.4	.020	5.3	.014
5	6.3	.046	5.6	.071	5.7	.057	8.7	.058	6.8	.015	6.6	.019
6	7.7	.048	7.0	.068	7.1	.054	10.7	.017	8.2	.015	8.0	.024
UNCORR MEAN		.046		.070		.056		.040		.017		.020
CORR MEAN		.046		.070		.056		.040		.017		.020
WITHIN 2.0 SIGMA		6		6		6		6		6		6

AVERAGE OF POSITIVE AND NEGATIVE PEAKS

UNCORR AVG	.032	.065	.053	.036	.017	.018
CORR AVG	.032	.065	.053	.036	.017	.018

		7		8		9		10		11		12
1	1.1	.029	.7	.032	.9	.035	.7	.034	1.0	.012	.4	.012
2	2.5	.024	2.1	.024	2.3	.036	2.1	.028	2.4	.012	1.8	.011
3	3.9	.025	3.5	.030	3.6	.031	3.5	.028	3.7	.015	3.1	.011
4	5.3	.019	4.9	.035	5.0	.032	4.9	.029	5.8	.009	4.6	.009
5	6.7	.019	6.3	.029	6.4	.032	6.3	.022	7.8	.014	5.9	.005
6	8.1	.024	7.7	.034	7.8	.030	7.7	.026	9.4	.012	8.6	.010
UNCORR MEAN		.023		.030		.033		.028		.012		.010
CORR MEAN		.023		.030		.033		.028		.012		.010
WITHIN 2.0 SIGMA		6		6		6		6		6		6

AVERAGE OF POSITIVE AND NEGATIVE PEAKS

UNCORR AVG	.023	.032	.031	.029	.010	.009
CORR AVG	.023	.032	.031	.029	.010	.009

		13
1	.4	.014
2	1.8	.014
3	3.2	.016
4	4.6	.013
5	6.0	.015
6	7.3	.014

UNCORR	
MEAN	.014
CORR	
MEAN	.014
WITHIN	
2.0 SIGMA	6

AVERAGE OF POSITIVE AND NEGATIVE PEAKS

UNCORR	
AVG	.015
CORR	
AVG	.015

AUTO-CORRELATION OF

TIME DEPENDENT DATA

NUMBER OF CHANELS	NUMBER OF POINTS	NUMBER OF LAGS	LAG TIME (MSEC)
13	76	15	.1444

CHANEL #	CYCLE TIME (MSEC)	FREQUENCY (HERTZ)
1	1.3946	717.028
2	1.3895	719.664
3	1.3950	716.871
4	1.1124	898.941
5	1.3790	725.186
6	1.3793	725.023
7	1.3928	723.172
8	1.3908	719.012
9	1.3922	718.265
10	1.3813	723.942
11	1.4105	708.945
12	1.3824	723.367
13	1.3902	719.302
MEAN		733.748
STANDARD DEVIATION		49.831

CROSS CORRELATION OF

TIME DEPENDENT DATA

CHANNEL NUMBER	PHASE (DEG)	CORRECTED PHASE
2	174.416	196.192
3	196.036	182.307
4	105.896	124.605
5	130.613	115.667
6	84.671	102.371
7	94.294	78.525
8	-4.955	12.068
9	23.844	5.911
10	-10.779	5.076
11	46.422	26.797
12	269.008	282.501
13	266.420	247.355

NASA I TORSION CASCADE

TAPE COUNT: NASA I-6, 4195-4255
INLET MACH NO: 1.315
STATIC PRESSURE RATIO: 1.330
INLET STATIC PRESSURE: 5.400
FREQUENCY: 725.000
PHASE: -90
BLADE AMPLITUDE: .032

AIRFOIL PRESSURE SURFACE

KULITE NO.	SURFACE PRESSURE (PSI)	CORRECTED PRESSURE (PSI)	PHASE ANGLE (DEG)	CORRECTED PHASE (DEG)	PRESSURE COEFFICIENT
1	.0648	.0602	196.192	-161.766	16.3541
2	.0526	.0493	182.307	-176.950	13.3955
3	.0362	.0358	124.695	121.937	9.7265
4	.0171	.0174	115.667	116.663	4.7411
5	.0177	.0185	102.371	115.443	5.0341
6	.0226	.0219	78.525	83.540	5.9621

AIRFOIL SUCTION SURFACE

KULITE NO.	SURFACE PRESSURE (PSI)	CORRECTED PRESSURE (PSI)	PHASE ANGLE (DEG)	CORRECTED PHASE (DEG)	PRESSURE COEFFICIENT
1	.0319	.0278	12.068	8.627	7.5555
2	.0306	.0274	5.911	4.110	7.4428
3	.0290	.0264	5.076	3.977	7.1639
4	.0105	.0113	26.797	25.033	3.0568
5	.0093	.0101	282.501	-59.029	2.7380
6	.0154	.0151	247.355	-98.857	4.1091

NET PRESSURE COEFFICIENT AND PHASE ACROSS AIRFOIL

KULITE NO	PRESSURE COEFFICIENT	PHASE ANGLE (DEG)
1	23.8370	-164.799
2	20.8375	-176.571
3	14.5350	147.744
4	5.7136	148.991
5	7.7638	117.389
6	10.0691	82.562

NASA I TORSION CASCADE

TAPE COUNT: NASA I-6, 4195-4255
INLET MACH NO: 1.315
STATIC PRESSURE RATIO: 1.330
INLET STATIC PRESSURE: 5.400
FREQUENCY: 725.000
PHASE: -90
BLADE AMPLITUDE: .032

COEFFICIENTS FOR AIRFOIL LIFT AND MOMENT

PERCENT CHORD	LOCAL SURFACE LIFT COEFFICIENTS REAL	IMAGINARY
.0	-23.003	6.2503
5.0	-23.003	6.2503
10.0	-23.003	6.2503
15.0	-23.003	6.2503
20.0	-22.043	3.6155
25.0	-20.800	1.2462
30.0	-18.532	-2.7585
35.0	-15.596	-5.7882
40.0	-12.292	-7.7573
45.0	-10.462	-6.5235
50.0	-8.6201	-5.3095
55.0	-6.7650	-4.1165
60.0	-4.8971	-2.9435
65.0	-4.7879	-4.2424
70.0	-4.3517	-5.5853
75.0	-3.5716	-6.8935
80.0	-1.5446	-8.7817
85.0	1.3035	-9.9844
90.0	1.3035	-9.9844
95.0	1.3035	-9.9844
100.0	1.3035	-9.9844
AIRFOIL LIFT COEFFICIENT	-10.8106	-3.4454
AIRFOIL MOMENT COEFFICIENT	2.5389	-1.4412

EDR 10119

APPENDIX C

Baseline Cascade Time Variant Data/Theory Correlation Plots

NASA I TORSION CASCADE

PRESSURE SURFACE AERODYNAMIC PHASE LAG DISTRIBUTION
1.315 INLET MACH NUMBER
1.04 STATIC PRESSURE RATIO
3.14 rad (180.9) INTERBLADE PHASE ANGLE

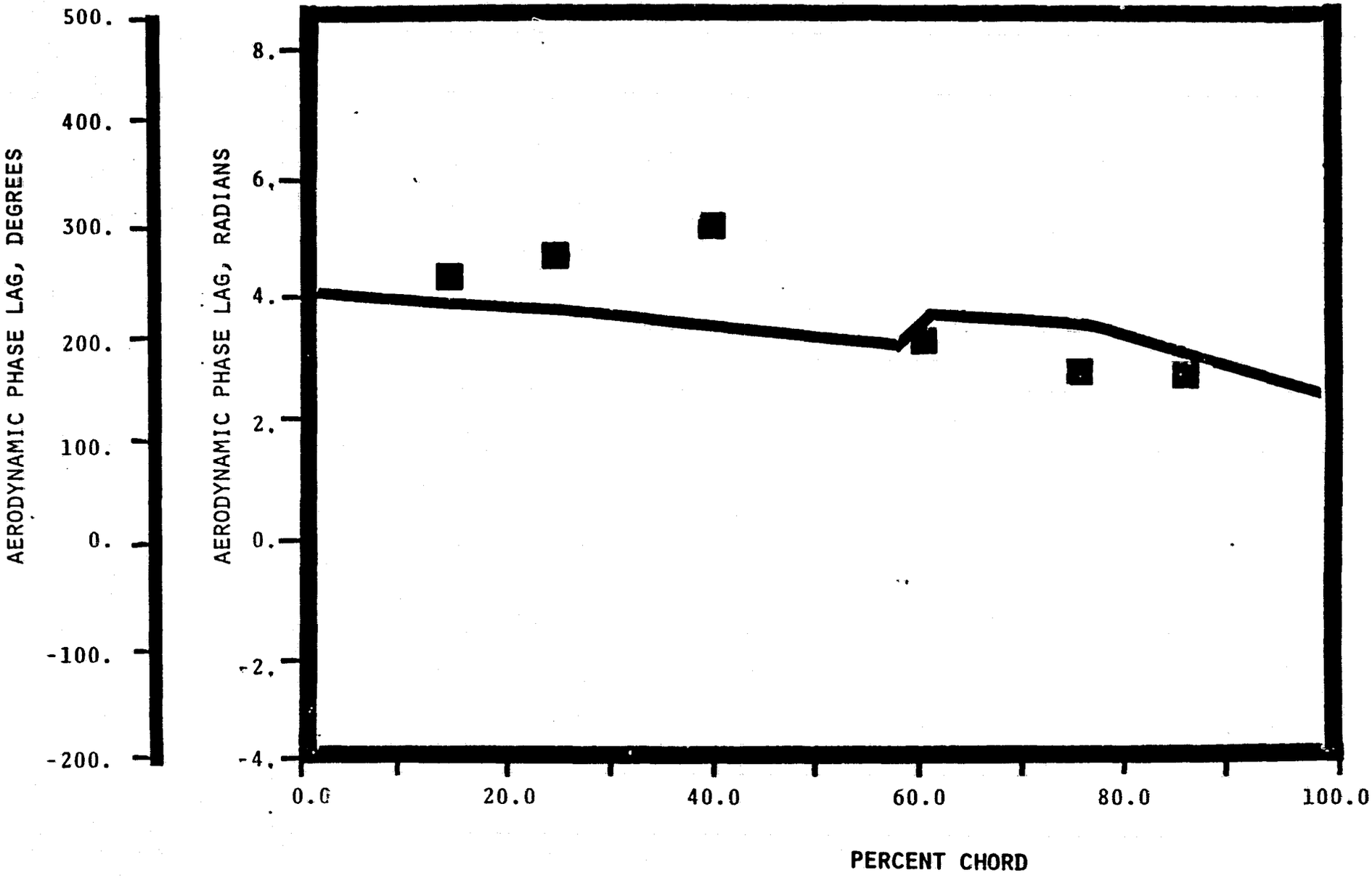

NASA I TORSION CASCADE

PRESSURE SURFACE UNSTEADY PRESSURE DISTRIBUTION

1.315 INLET MACH NUMBER

1.04 STATIC PRESSURE RATIO

3.14 rad (180.°) INTERBLADE PHASE ANGLE

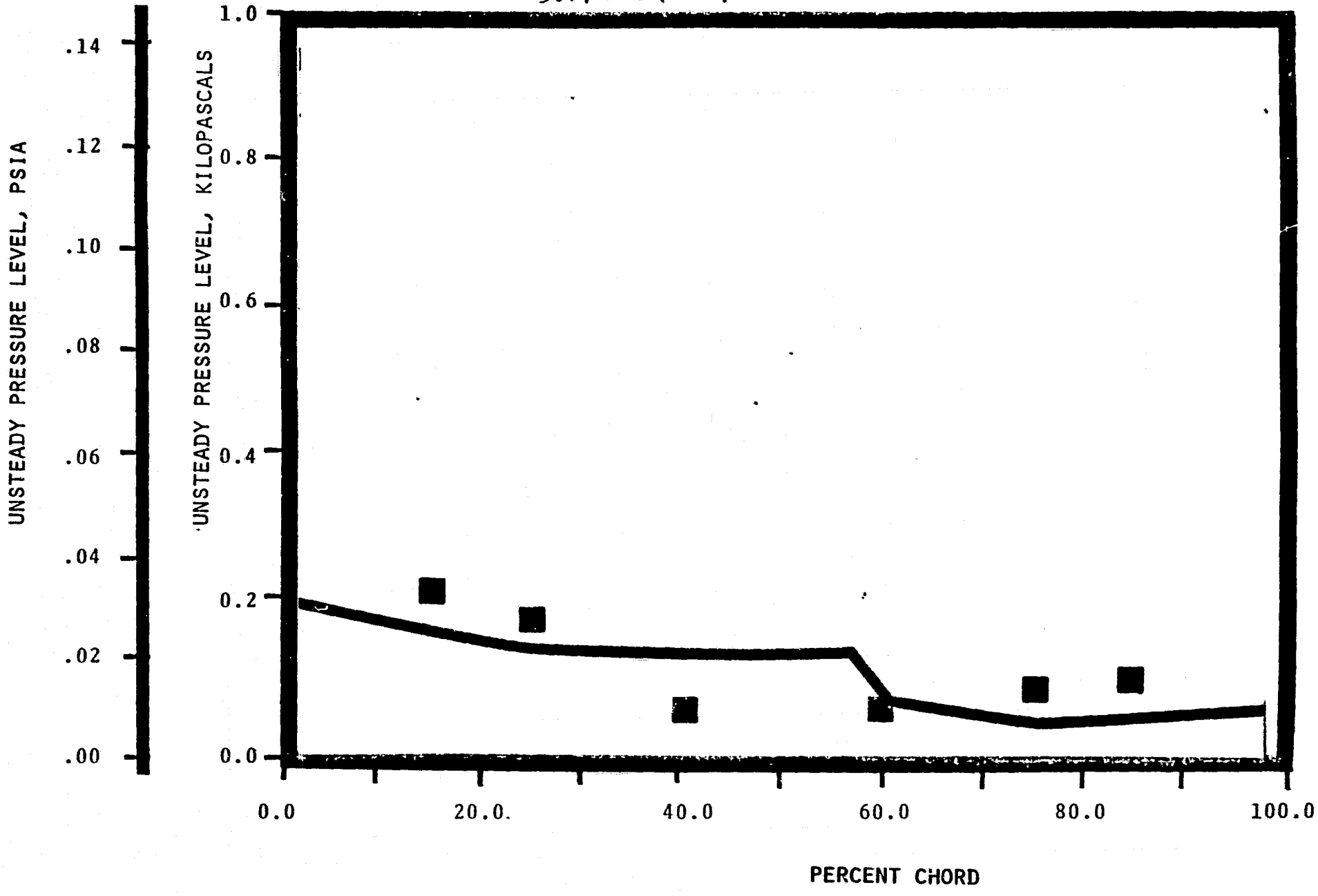

NASA I TORSION CASCADE

SUCTION SURFACE AERODYNAMIC PHASE LAG DISTRIBUTION

1.315 INLET MACH NUMBER

1.04 STATIC PRESSURE RATIO

3.14 rad (180.) INTERBLADE PHASE ANGLE

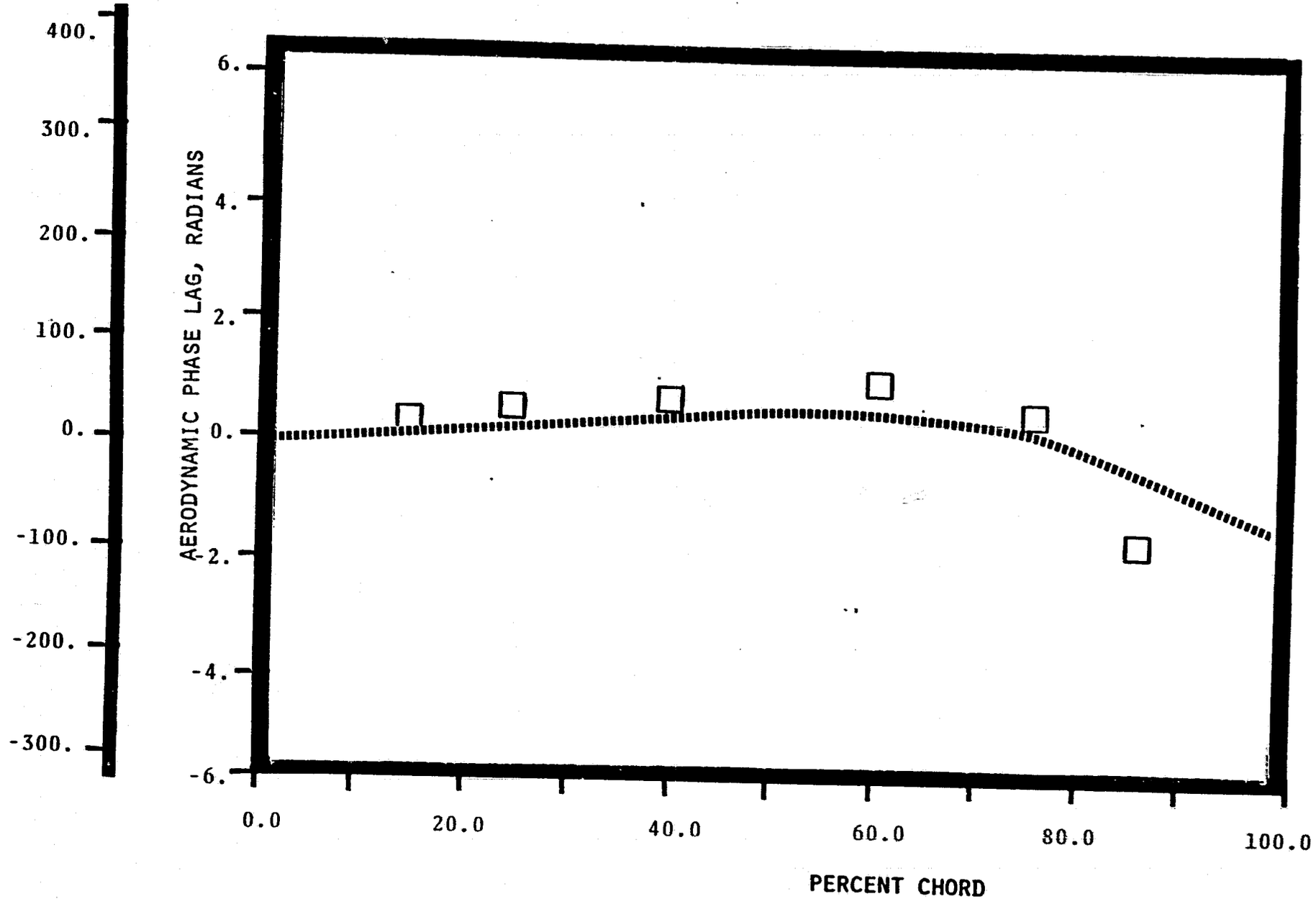

NASA I TORSION CASCADE

SUCTION SURFACE UNSTEADY PRESSURE DISTRIBUTION

1.315 INLET MACH NUMBER

1.04 STATIC PRESSURE RATIO

3.14 rad (180.°)INTERBLADE PHASE ANGLE

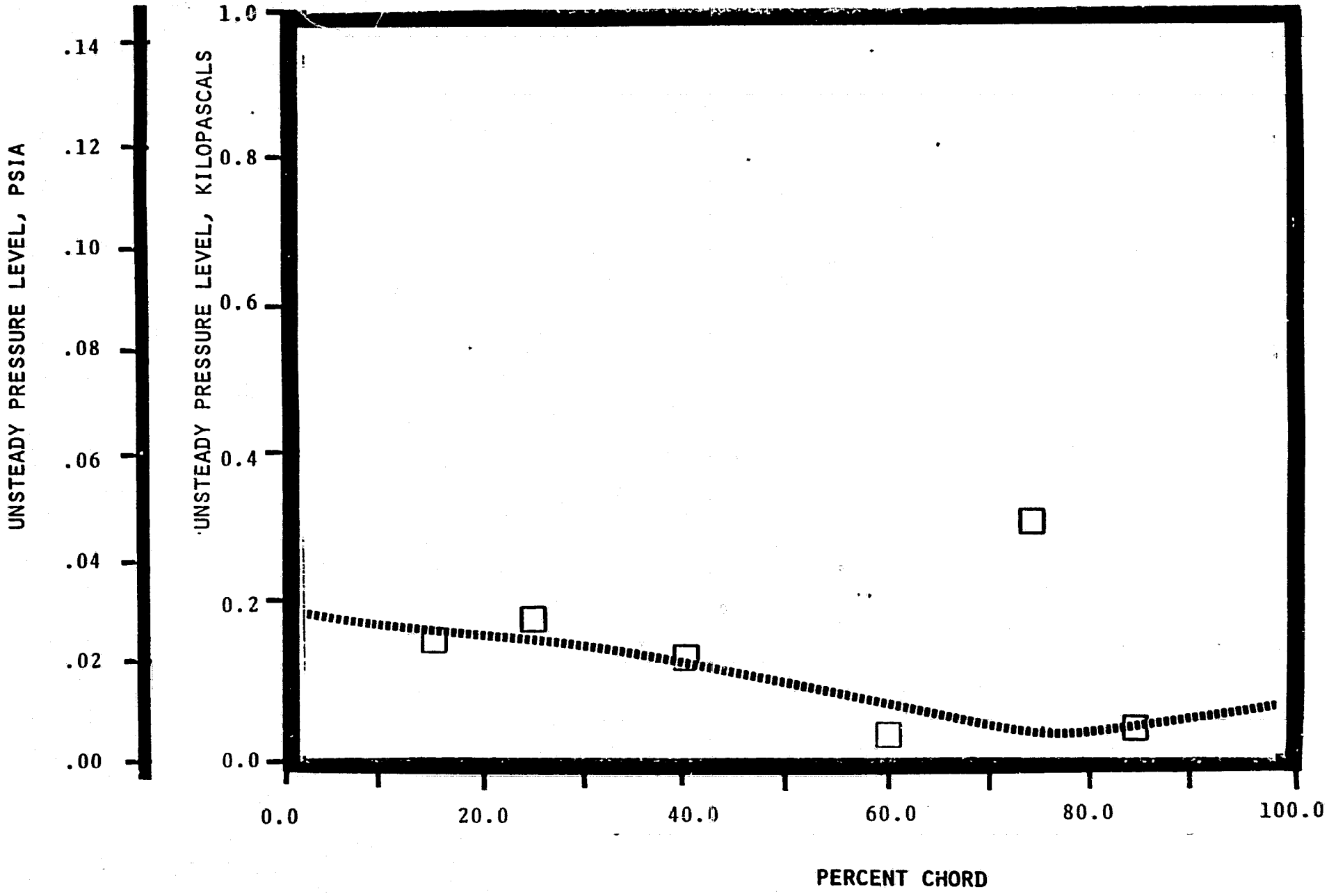

NASA I TORSION CASCADE

PRESSURE SURFACE AERODYNAMIC PHASE LAG DISTRIBUTION
1.315 INLET MACH NUMBER
1.04 STATIC PRESSURE RATIO
1.40 rad(80.°) INTERBLADE PHASE ANGLE

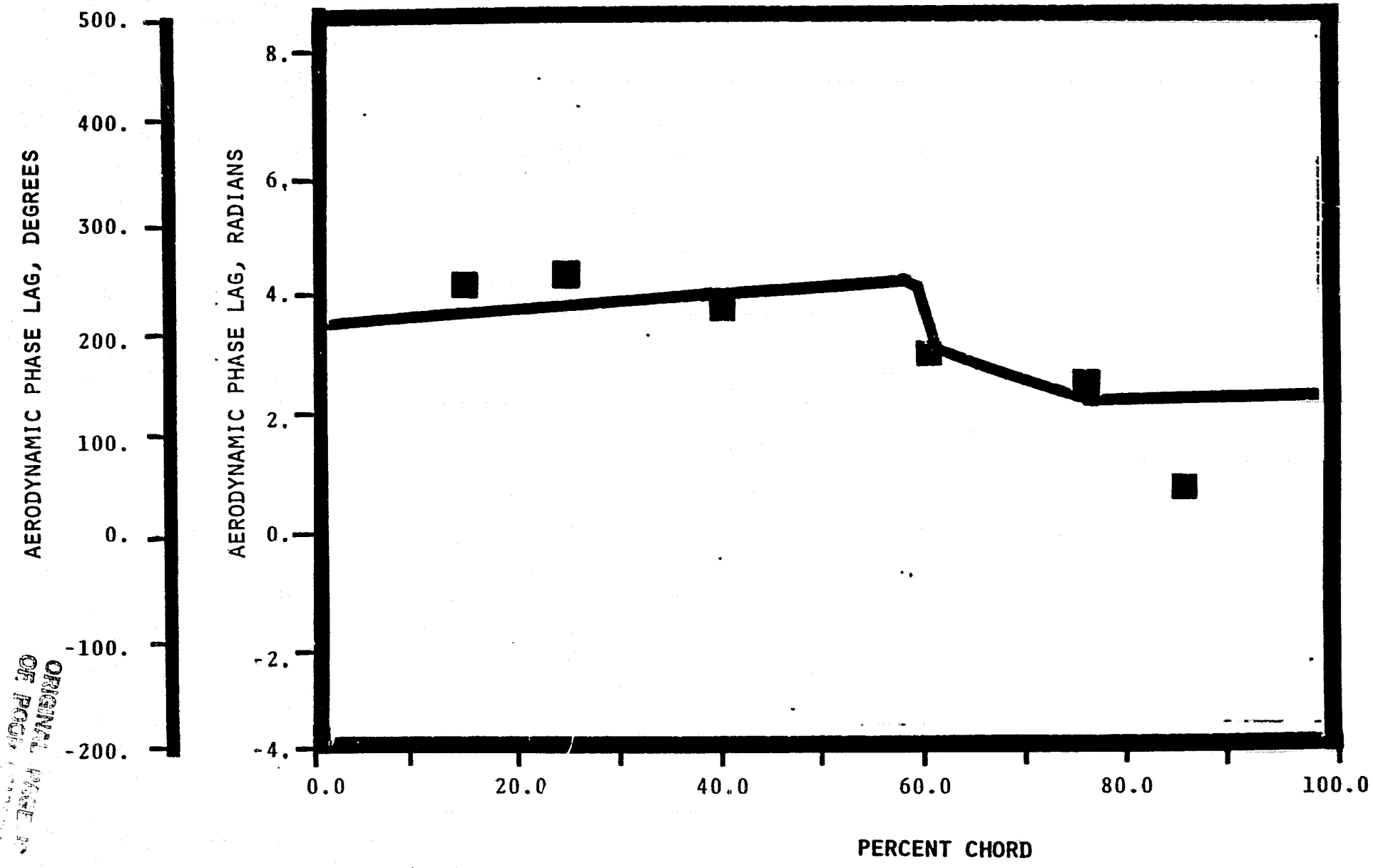

NASA I TORSION CASCADE

PRESSURE SURFACE UNSTEADY PRESSURE DISTRIBUTION

1.315 INLET MACH NUMBER

1.04 STATIC PRESSURE RATIO

1.40 rad (80.°) INTERBLADE PHASE ANGLE

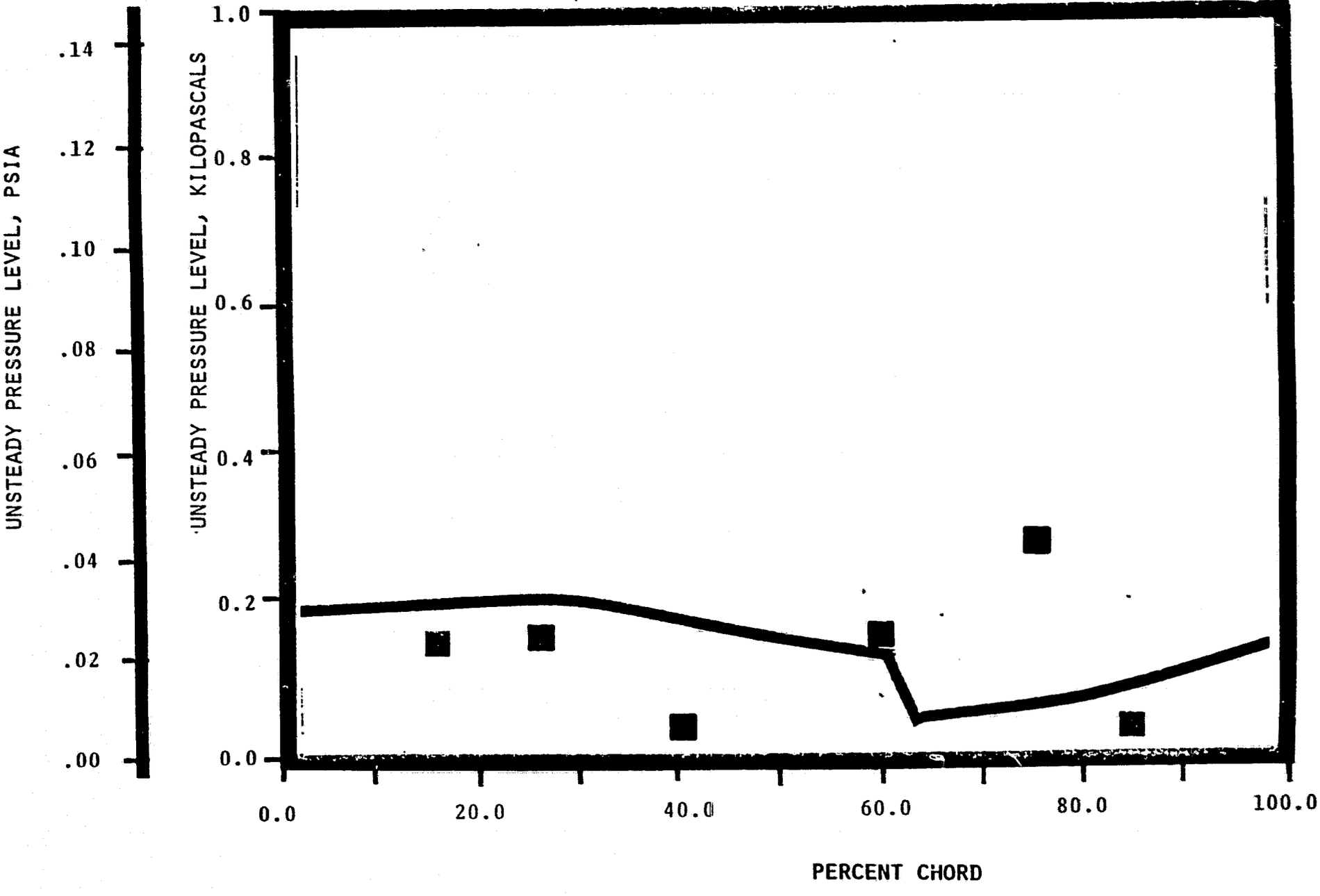

NASA I TORSION CASCADE
SUCTION SURFACE AERODYNAMIC PHASE LAG DISTRIBUTION
1.315 INLET MACH NUMBER
1.04 STATIC PRESSURE RATIO
1.40 rad (80.°) INTERBLADE PHASE ANGLE

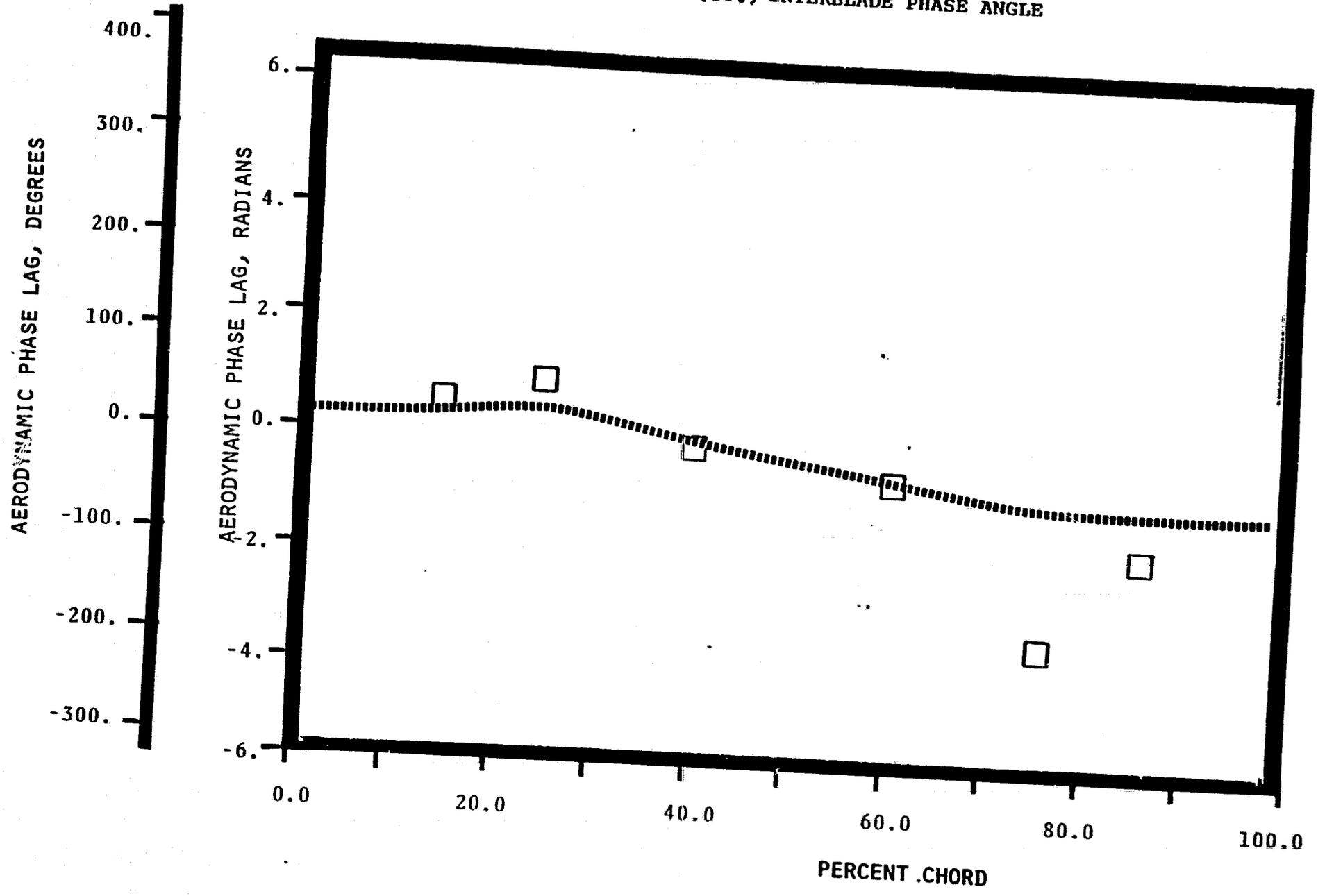

NASA I TORSION CASCADE

SUCTION SURFACE UNSTEADY PRESSURE DISTRIBUTION

1.315 INLET MACH NUMBER

1.04 STATIC PRESSURE RATIO

1.40 rad (80°) INTERBLADE PHASE ANGLE

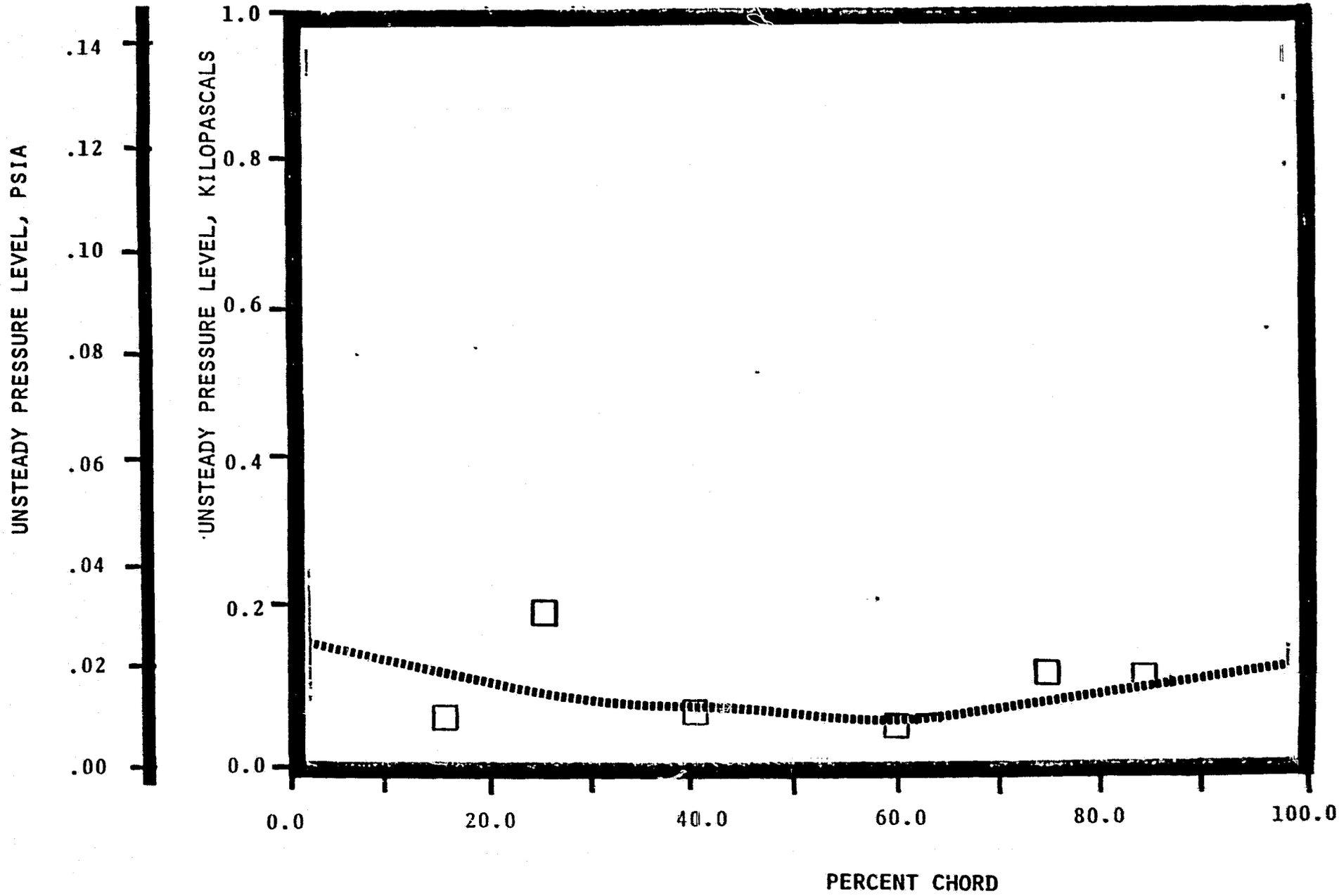

NASA I TORSION CASCADE

PRESSURE SURFACE AERODYNAMIC PHASE LAG DISTRIBUTION
1.315 INLET MACH NUMBER
1.04 STATIC PRESSURE RATIO
0.0 rad (0^{o}) INTERBLADE PHASE ANGLE

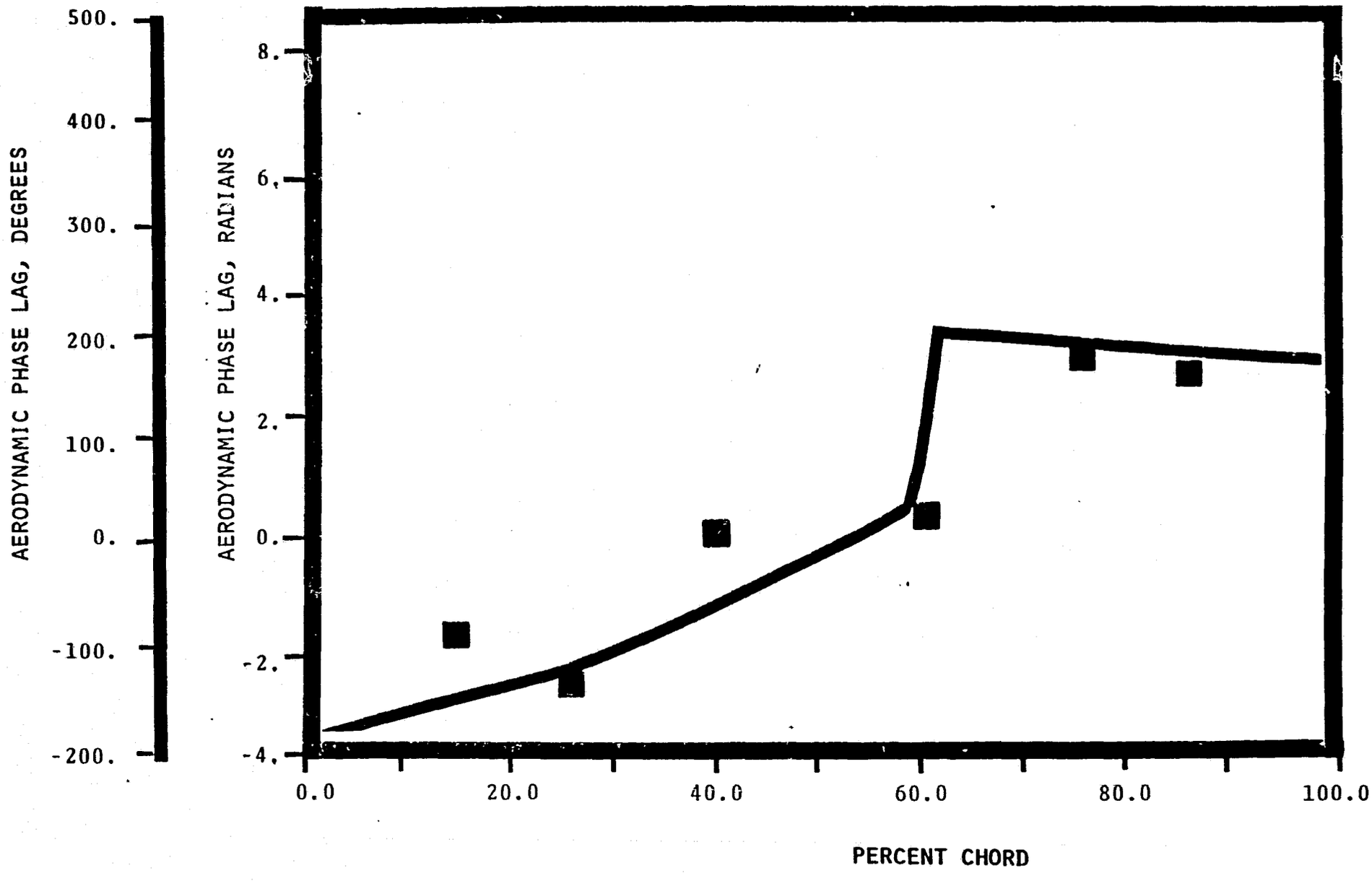

NASA I TORSION CASCADE

PRESSURE SURFACE UNSTEADY PRESSURE DISTRIBUTION

1.315 INLET MACH NUMBER

1.04 STATIC PRESSURE RATIO

0.0 rad (0^{o}) INTERBLADE PHASE ANGLE

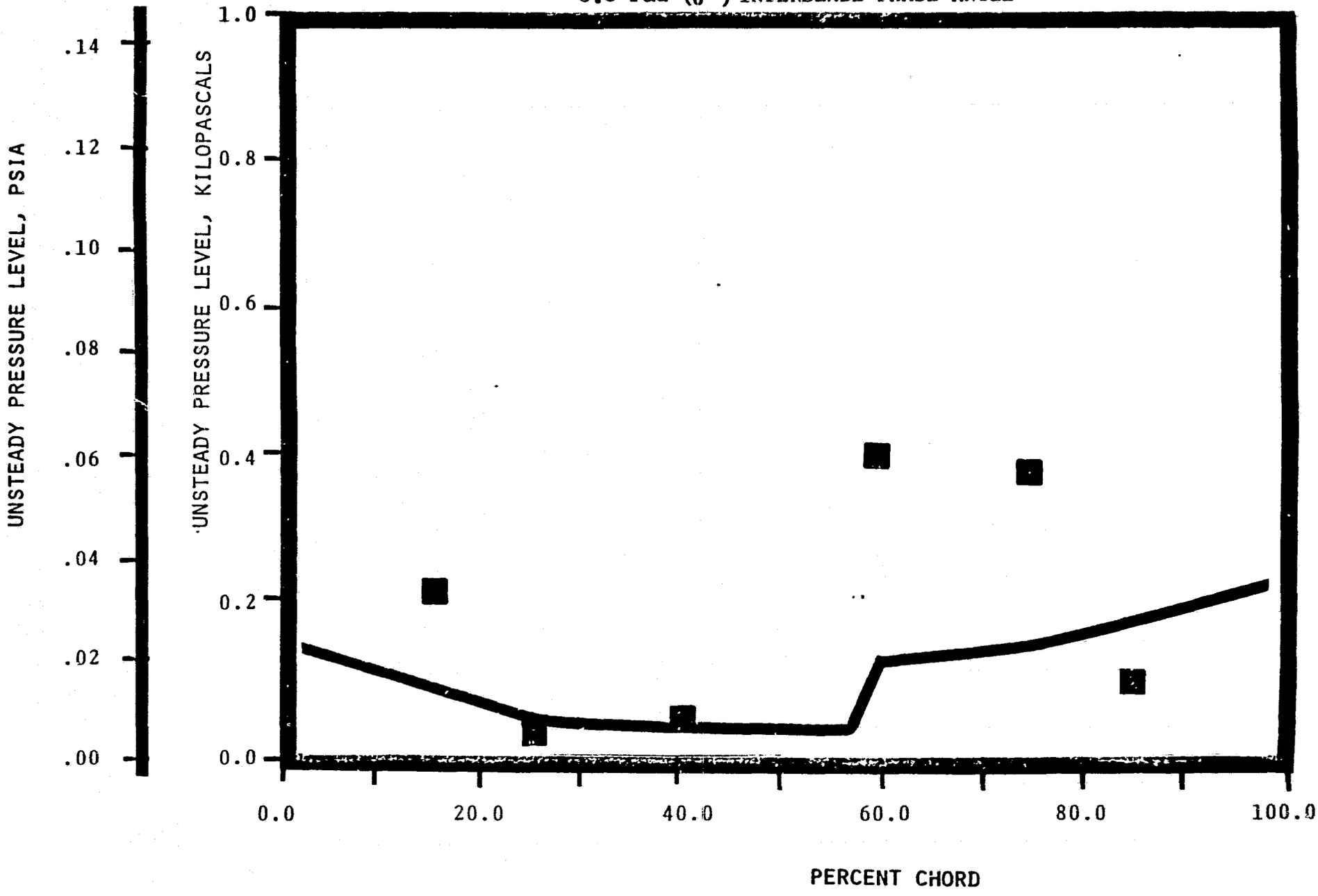

NASA I TORSION CASCADE

SUCTION SURFACE AERODYNAMIC PHASE LAG DISTRIBUTION

1.315 INLET MACH NUMBER

1.04 STATIC PRESSURE RATIO

0.0 rad (0^{o}) INTERBLADE PHASE ANGLE

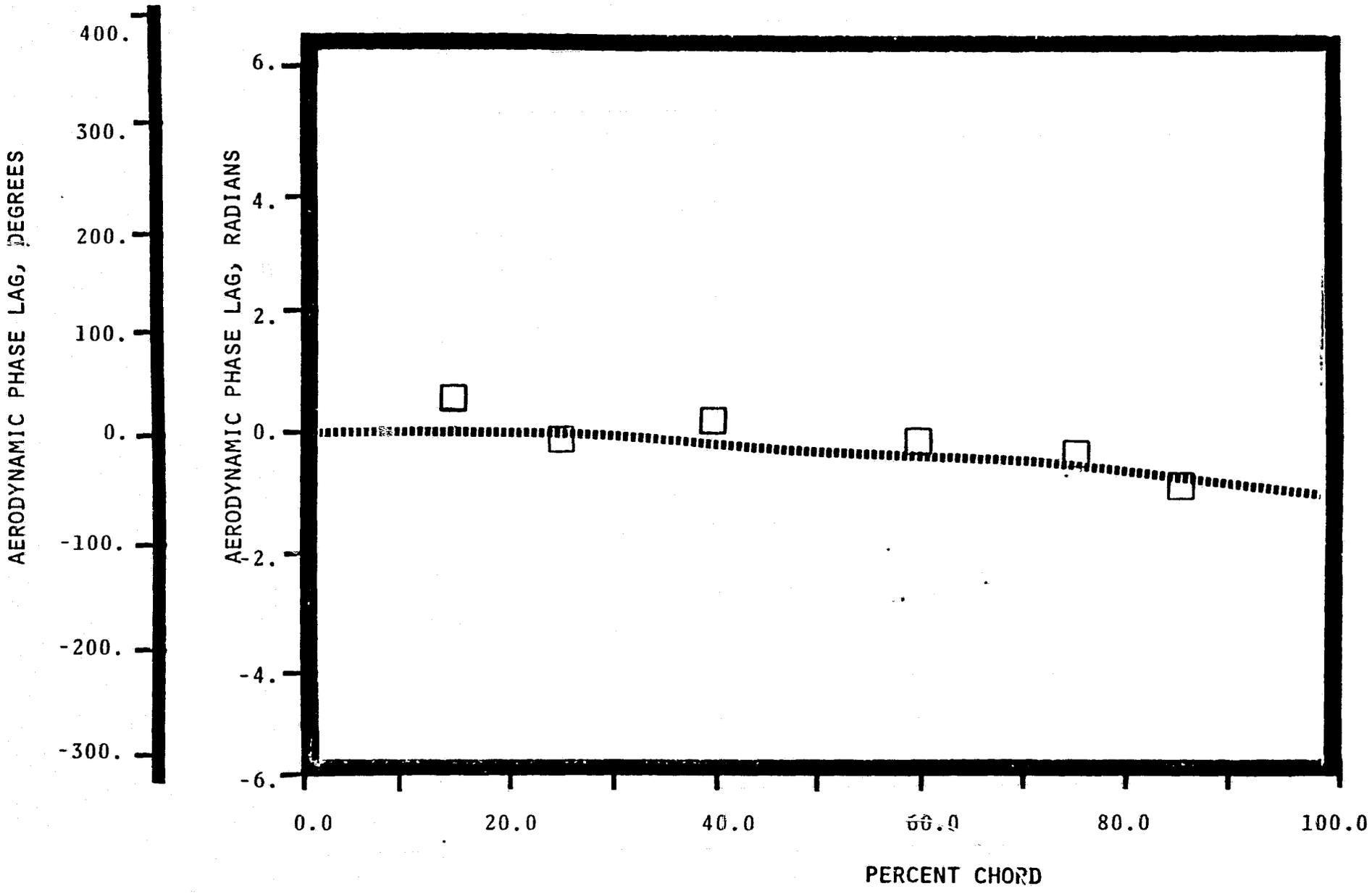

NASA I TORSION CASCADE

SUCTION SURFACE UNSTEADY PRESSURE DISTRIBUTION

1.315 INLET MACH NUMBER

1.04 STATIC PRESSURE RATIO

0.0 rad (0^{o}) INTERBLADE PHASE ANGLE

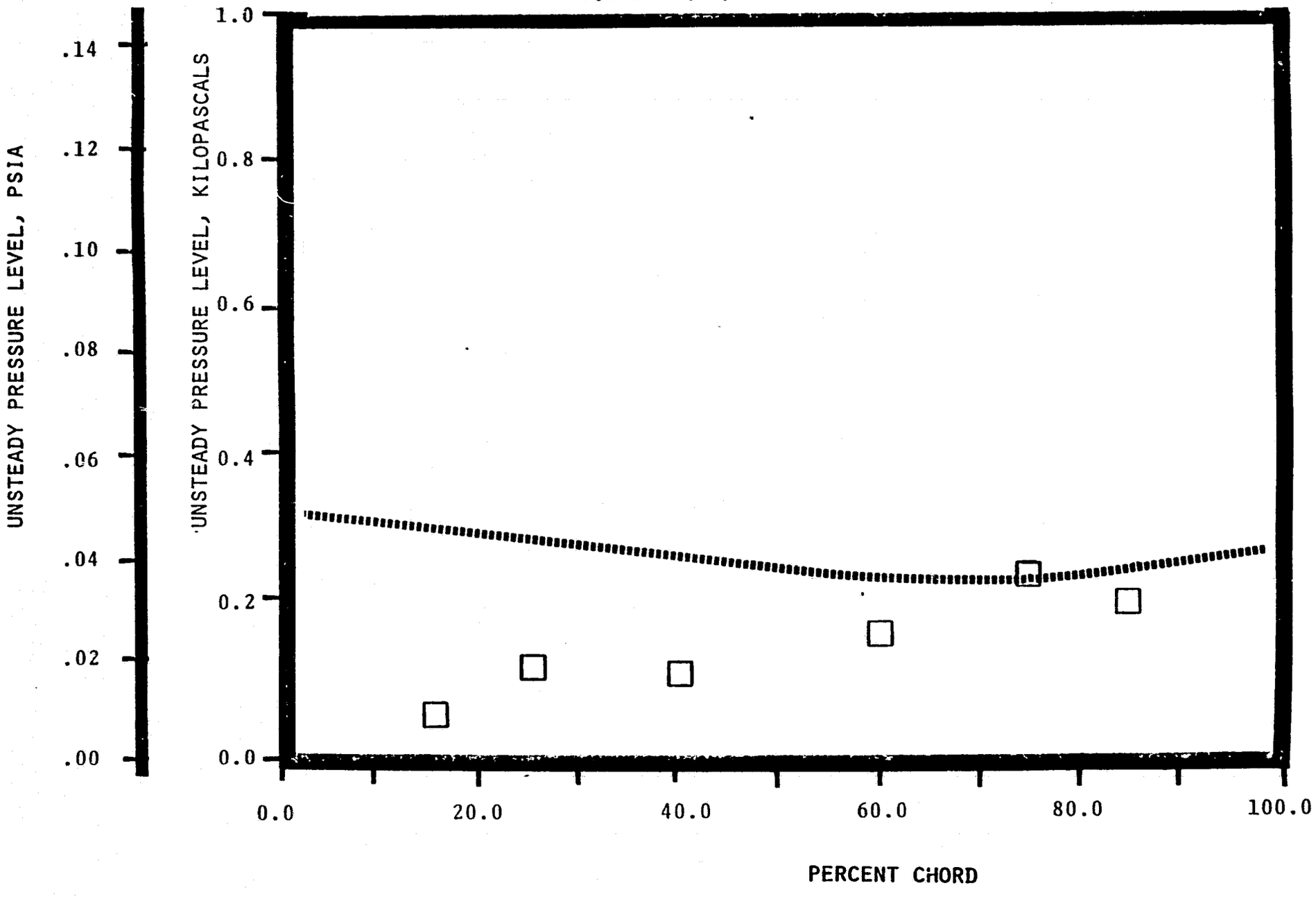

NASA I TORSION CASCADE

PRESSURE SURFACE AERODYNAMIC PHASE LAG DISTRIBUTION

1.315 INLET MACH NUMBER

1.04 STATIC PRESSURE RATIO

-.52 rad (-30.°) INTERBLADE PHASE ANGLE

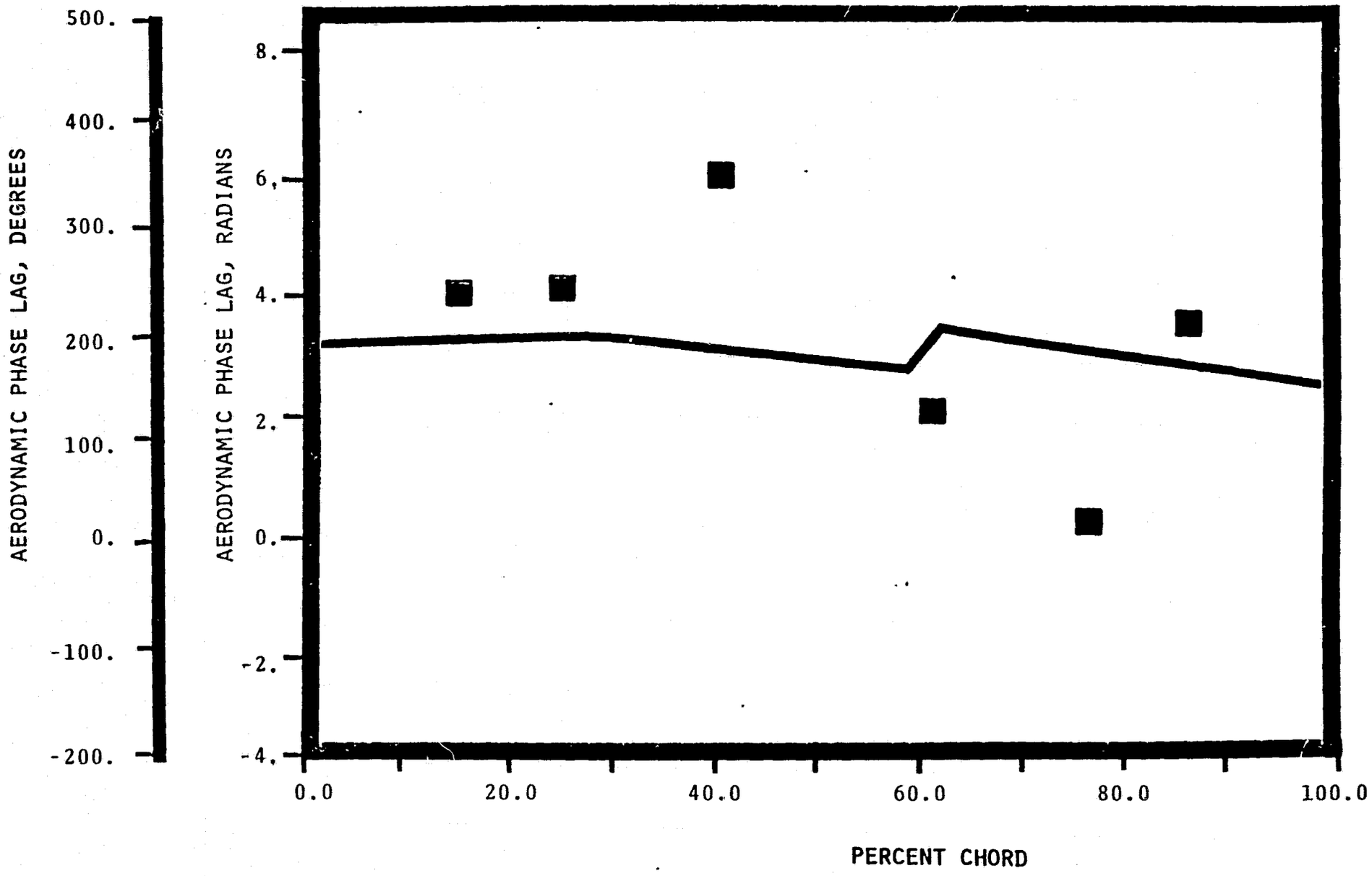

NASA I TORSION CASCADE

PRESSURE SURFACE UNSTEADY PRESSURE DISTRIBUTION

1.315 INLET MACH NUMBER

1.014 STATIC PRESSURE RATIO

-.52 rad (-30.°) INTERBLADE PHASE ANGLE

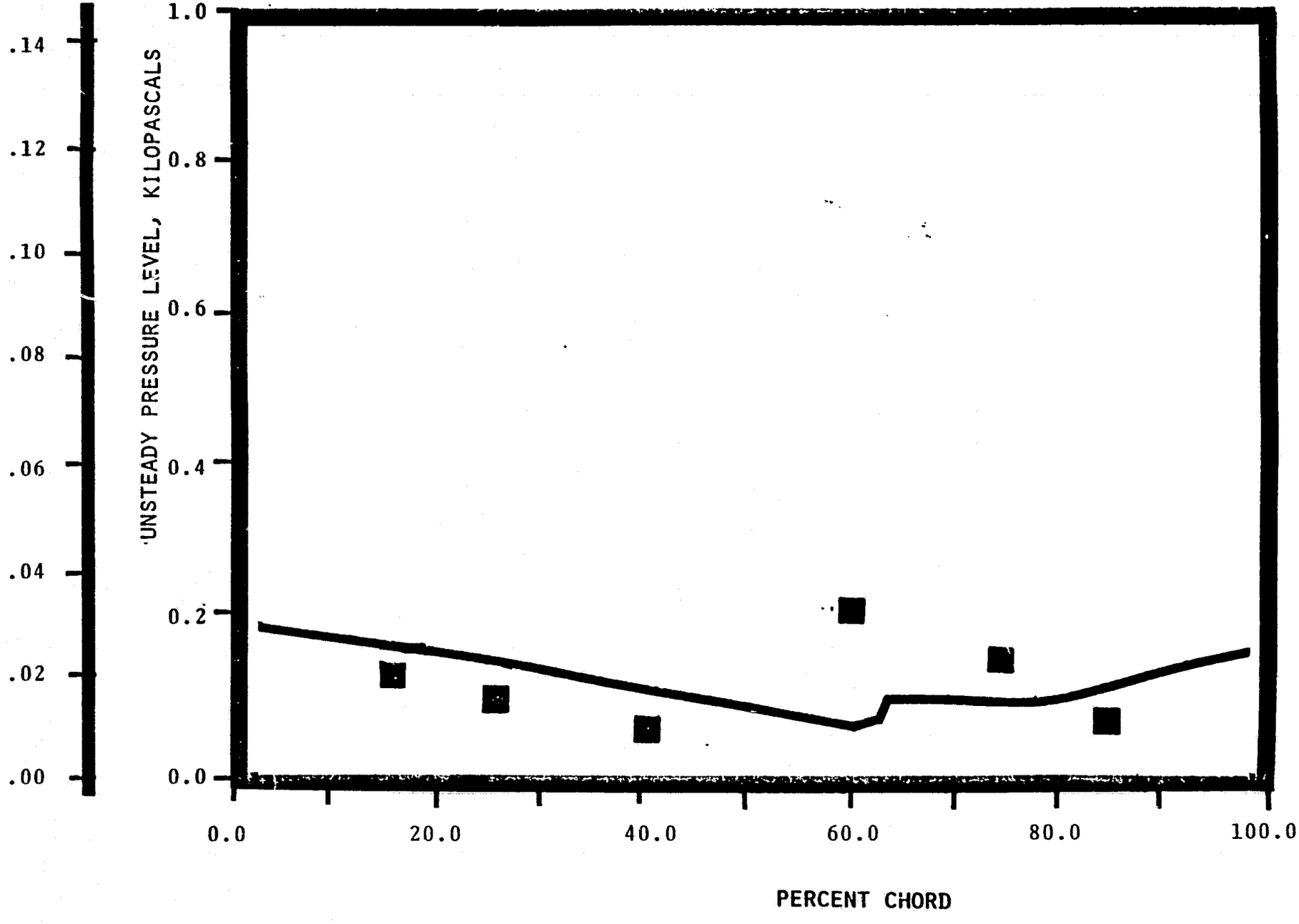

NASA I TORSION CASCADE

SUCTION SURFACE AERODYNAMIC PHASE LAG DISTRIBUTION

1.315 INLET MACH NUMBER

1.04 STATIC PRESSURE RATIO

-.52 rad (-30.) INTERBLADE PHASE ANGLE

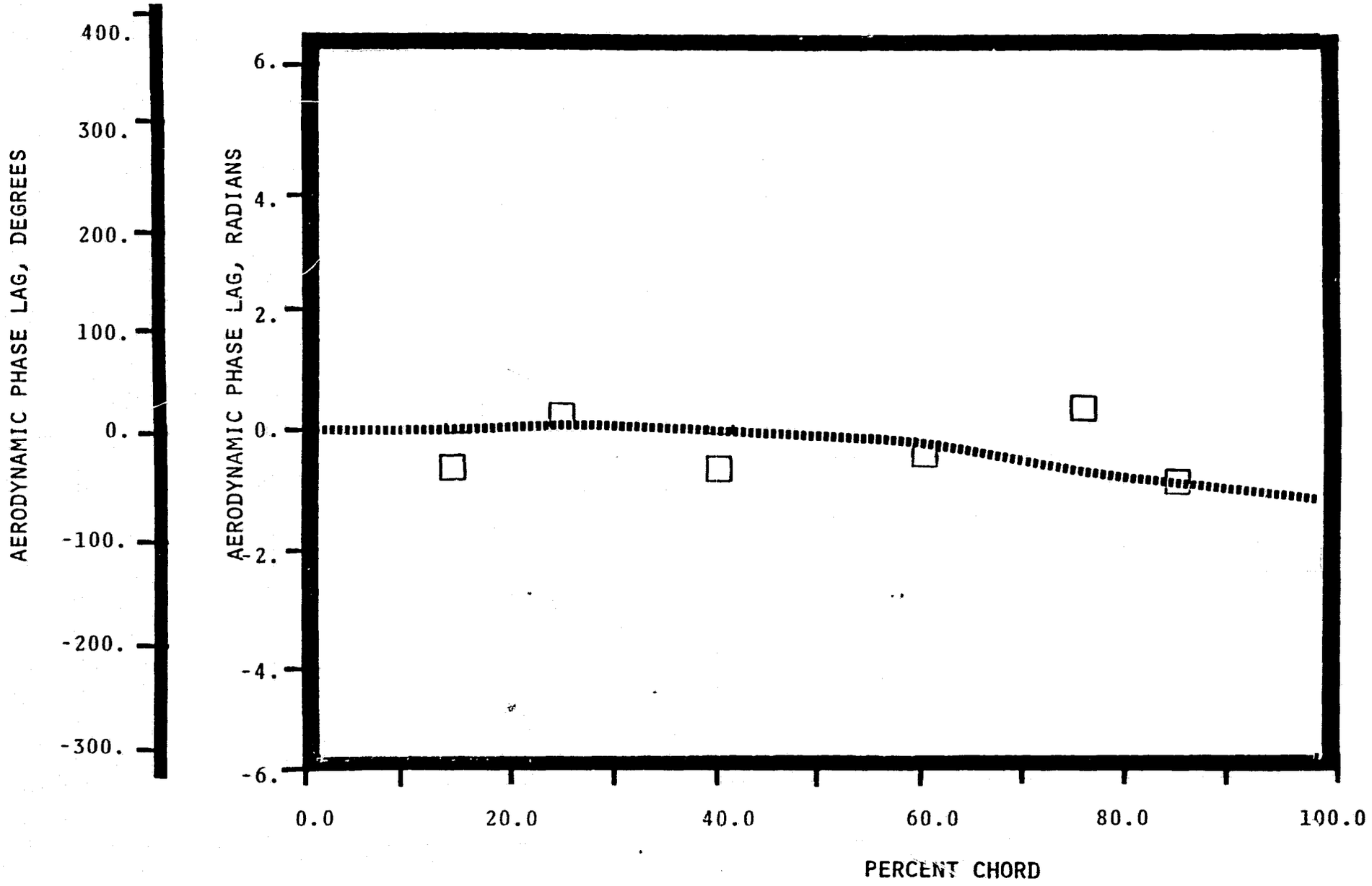

6TI

NASA I TORSION CASCADE

SUCTION SURFACE UNSTEADY PRESSURE DISTRIBUTION

1.315 INLET MACH NUMBER

1.0, STATIC PRESSURE RATIO

-.52 rad (-30°) INTERBLADE PHASE ANGLE

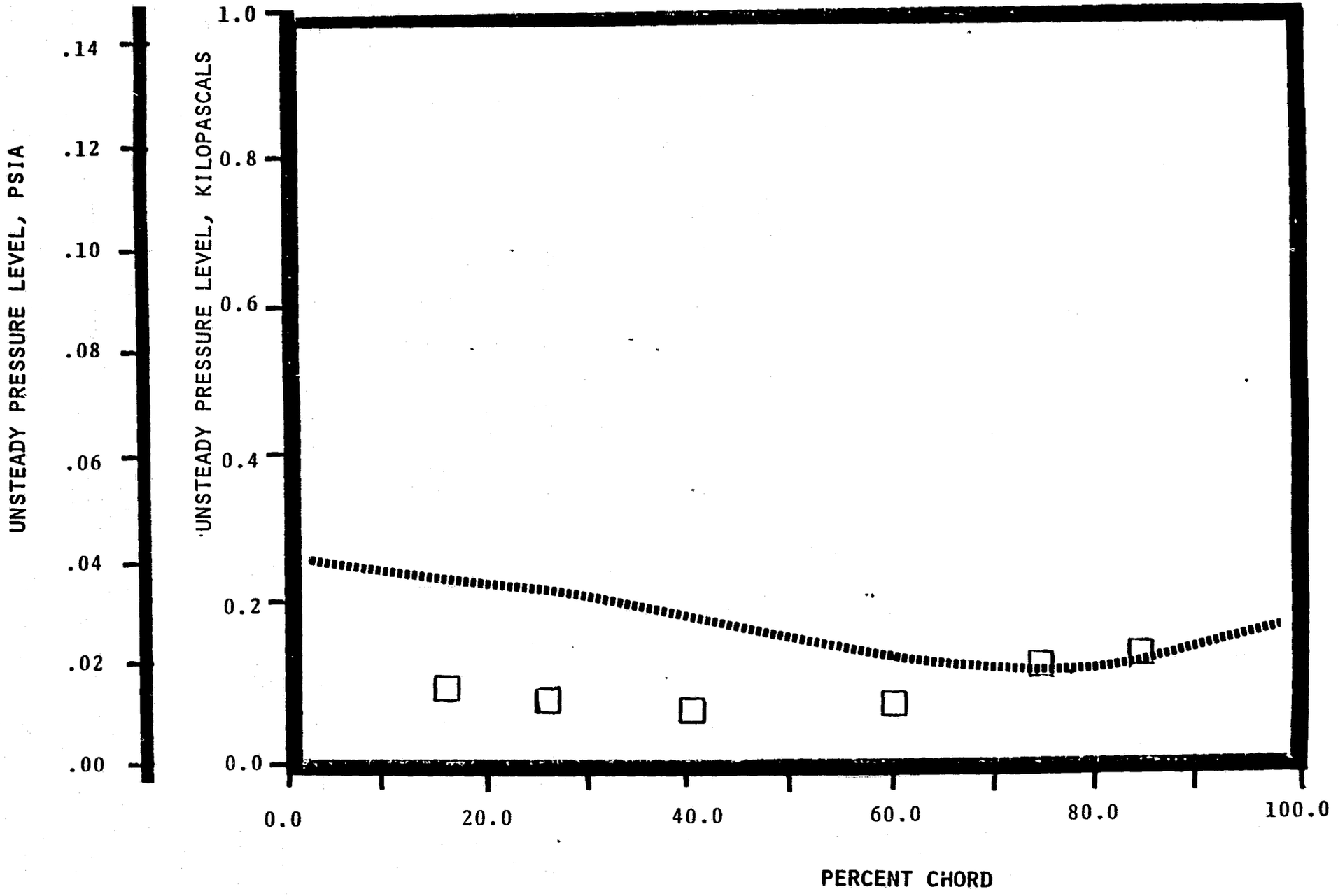

NASA I TORSION CASCADE

PRESSURE SURFACE AERODYNAMIC PHASE LAG DISTRIBUTION
1.315 INLET MACH NUMBER
1.04 STATIC PRESSURE RATIO
-.87 rad (-50.°) INTERBLADE PHASE ANGLE

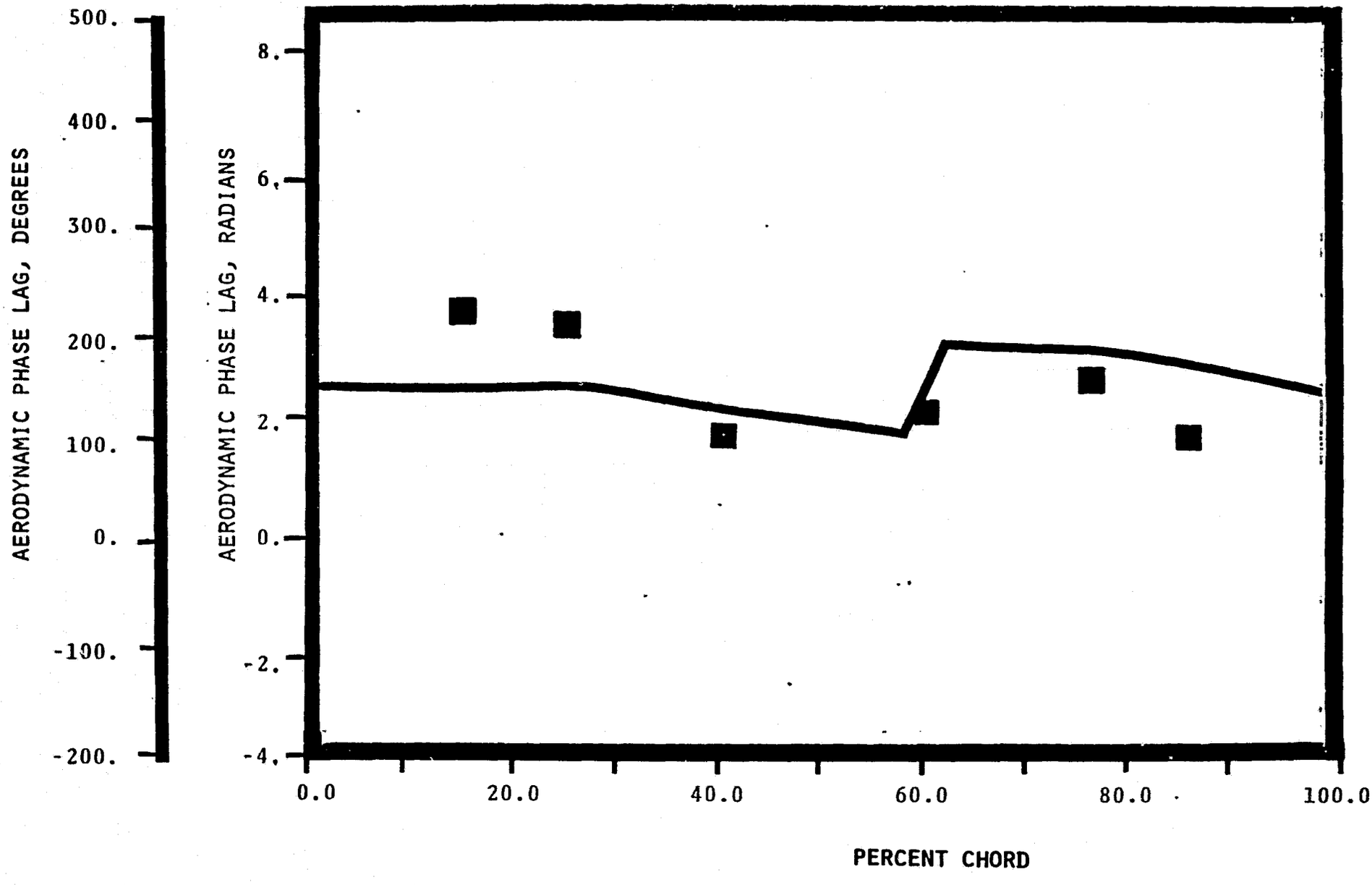

NASA I TORSION CASCADE

PRESSURE SURFACE UNSTEADY PRESSURE DISTRIBUTION

1.315 INLET MACH NUMBER

1.04 STATIC PRESSURE RATIO

-.87 rad (-50.°) INTERBLADE PHASE ANGLE

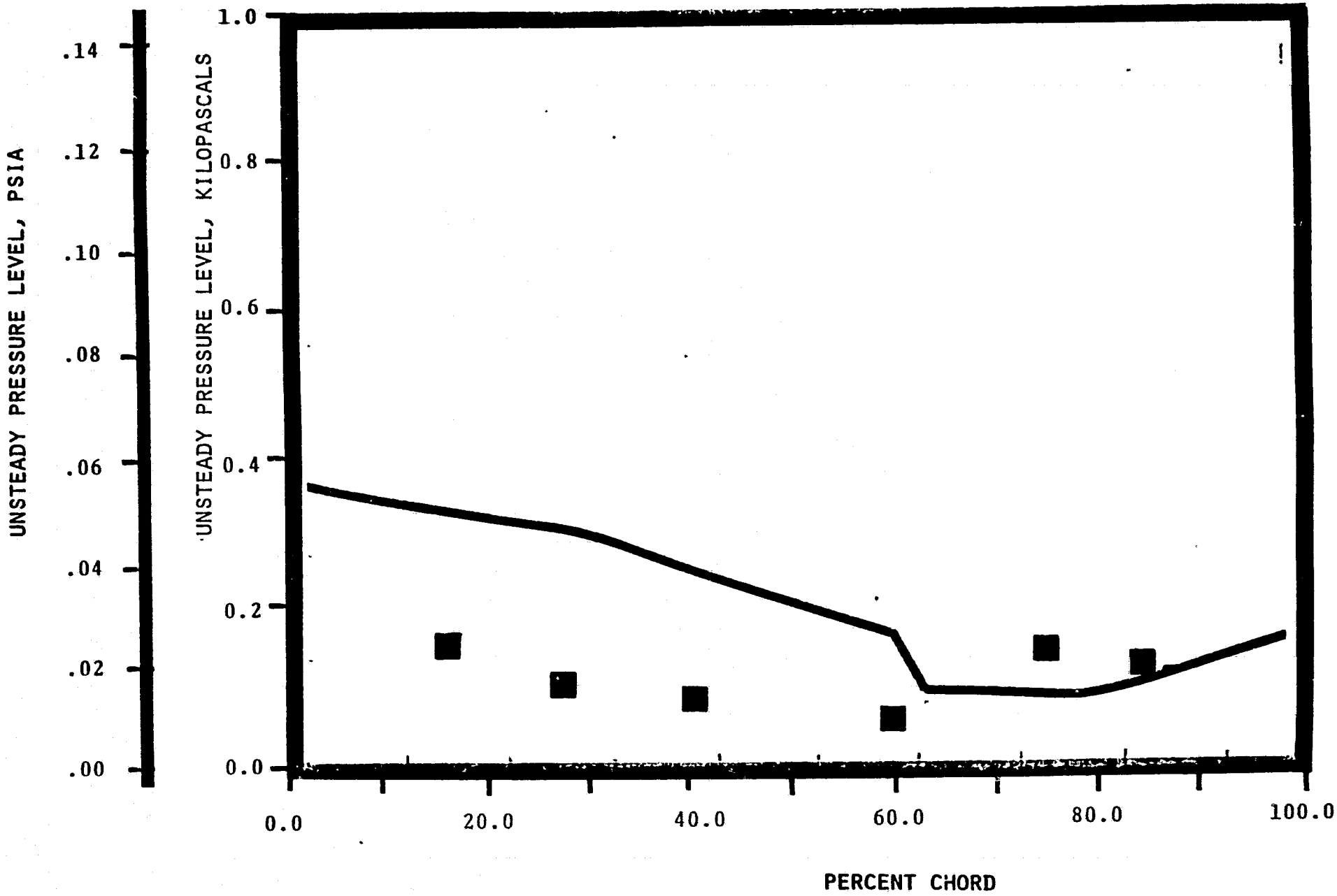

NASA I TORSION CASCADE

SUCTION SURFACE AERODYNAMIC PHASE LAG DISTRIBUTION

1.315 INLET MACH NUMBER

1.04 STATIC PRESSURE RATIO

-.87 rad (-50.°) INTERBLADE PHASE ANGLE

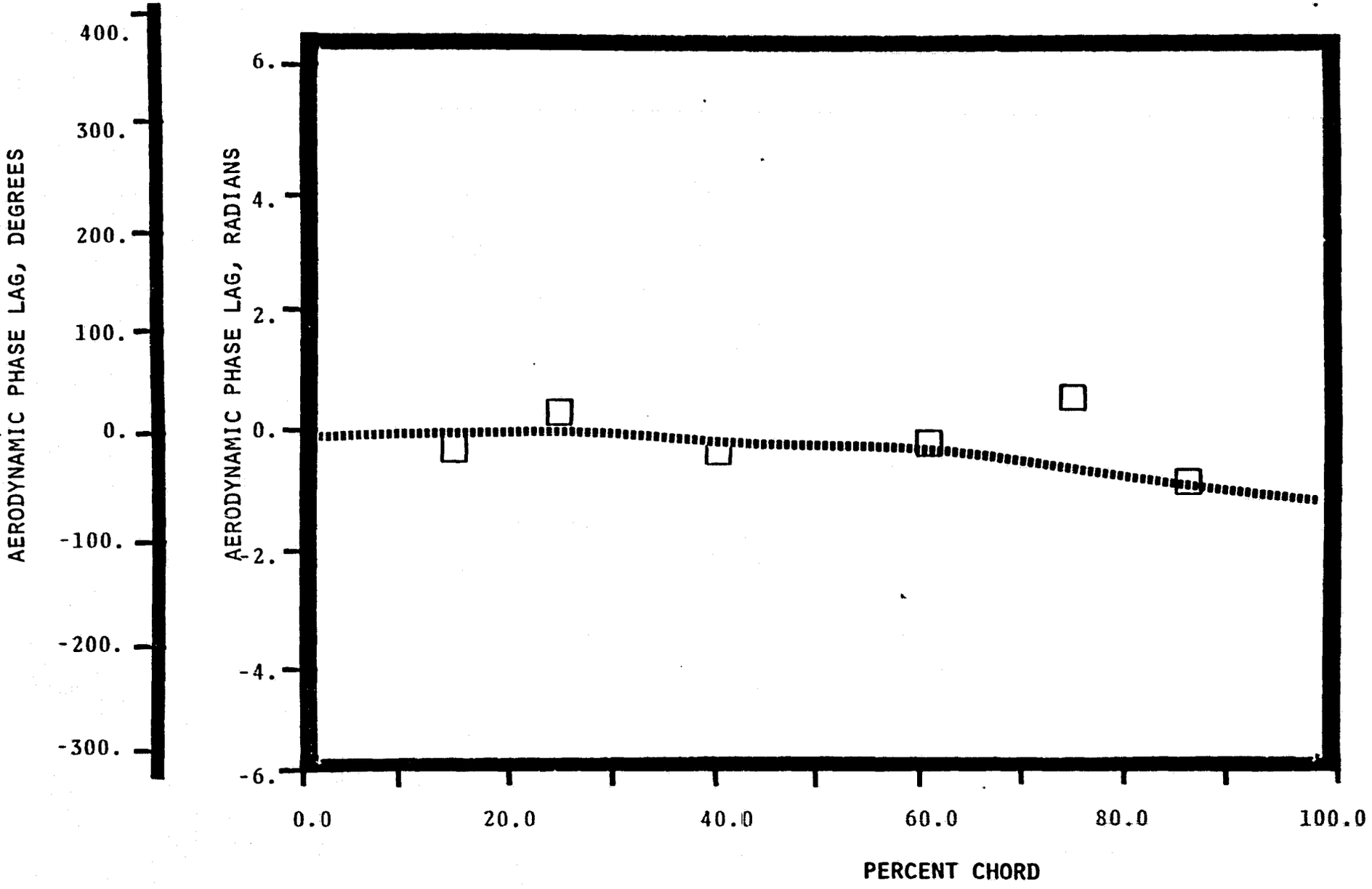

NASA I TORSION CASCADE

SUCTION SURFACE UNSTEADY PRESSURE DISTRIBUTION

1.315 INLET MACH NUMBER

1.04 STATIC PRESSURE RATIO

-.87 rad(-50.°)INTERBLADE PHASE ANGLE

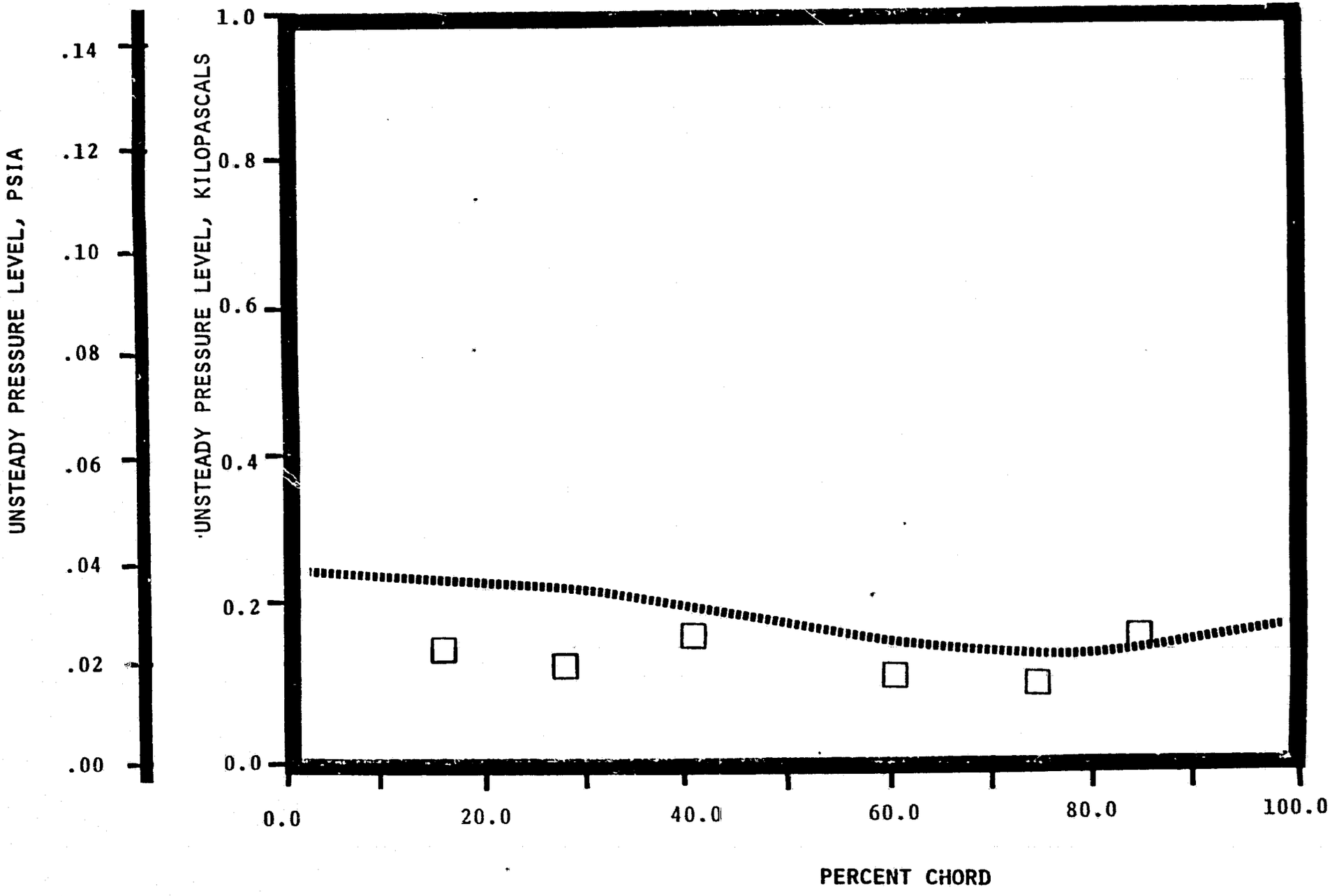

NASA I TORSION CASCADE

PRESSURE SURFACE AERODYNAMIC PHASE LAG DISTRIBUTION

1.315 INLET MACH NUMBER

1.04 STATIC PRESSURE RATIO

-1.57 rad(-90°) INTERBLADE PHASE ANGLE

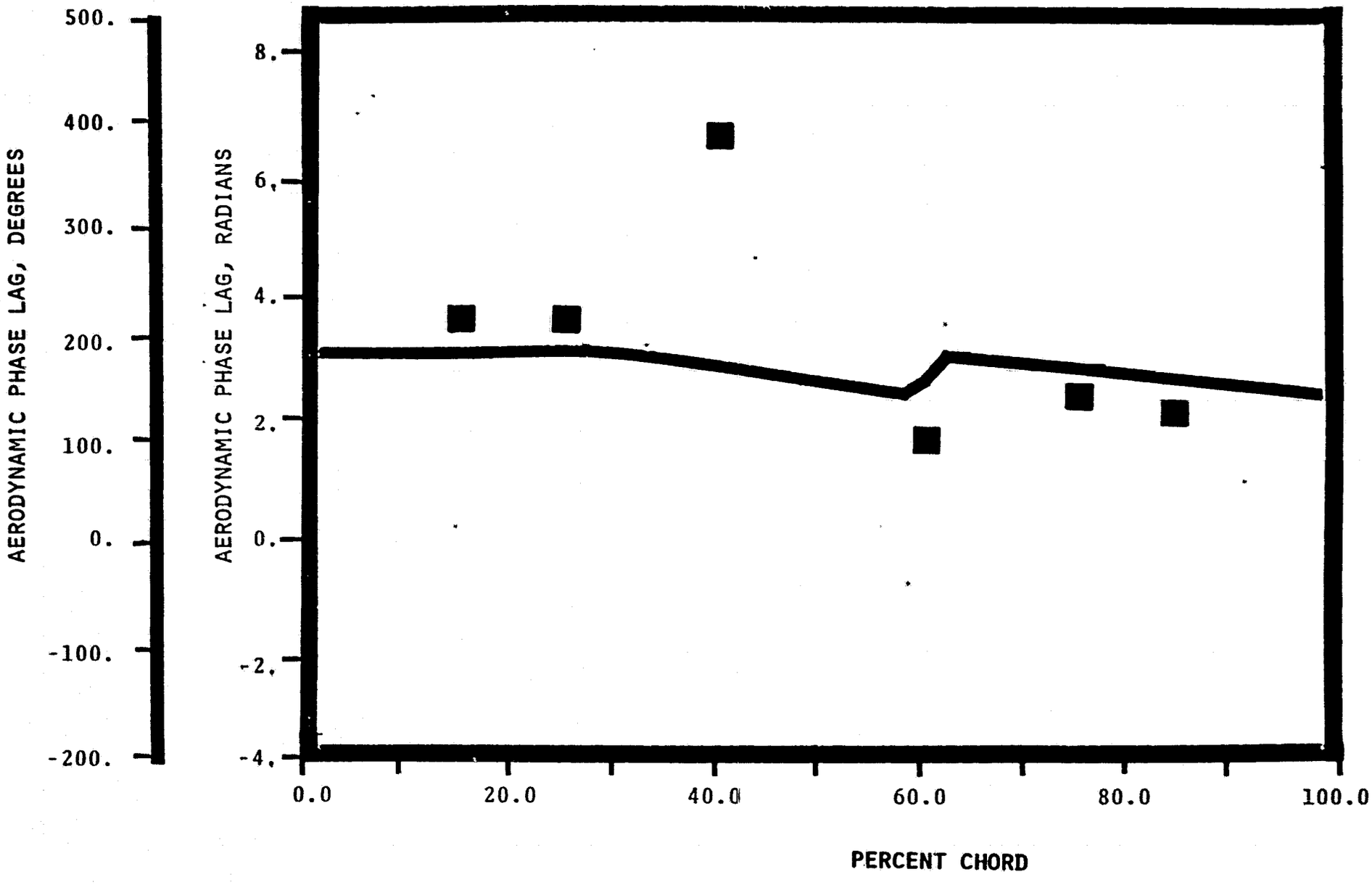

NASA I TORSION CASCADE

PRESSURE SURFACE UNSTEADY PRESSURE DISTRIBUTION

1.315 INLET MACH NUMBER

1.04 STATIC PRESSURE RATIO

-1.57 rad (-90.°) INTERBLADE PHASE ANGLE

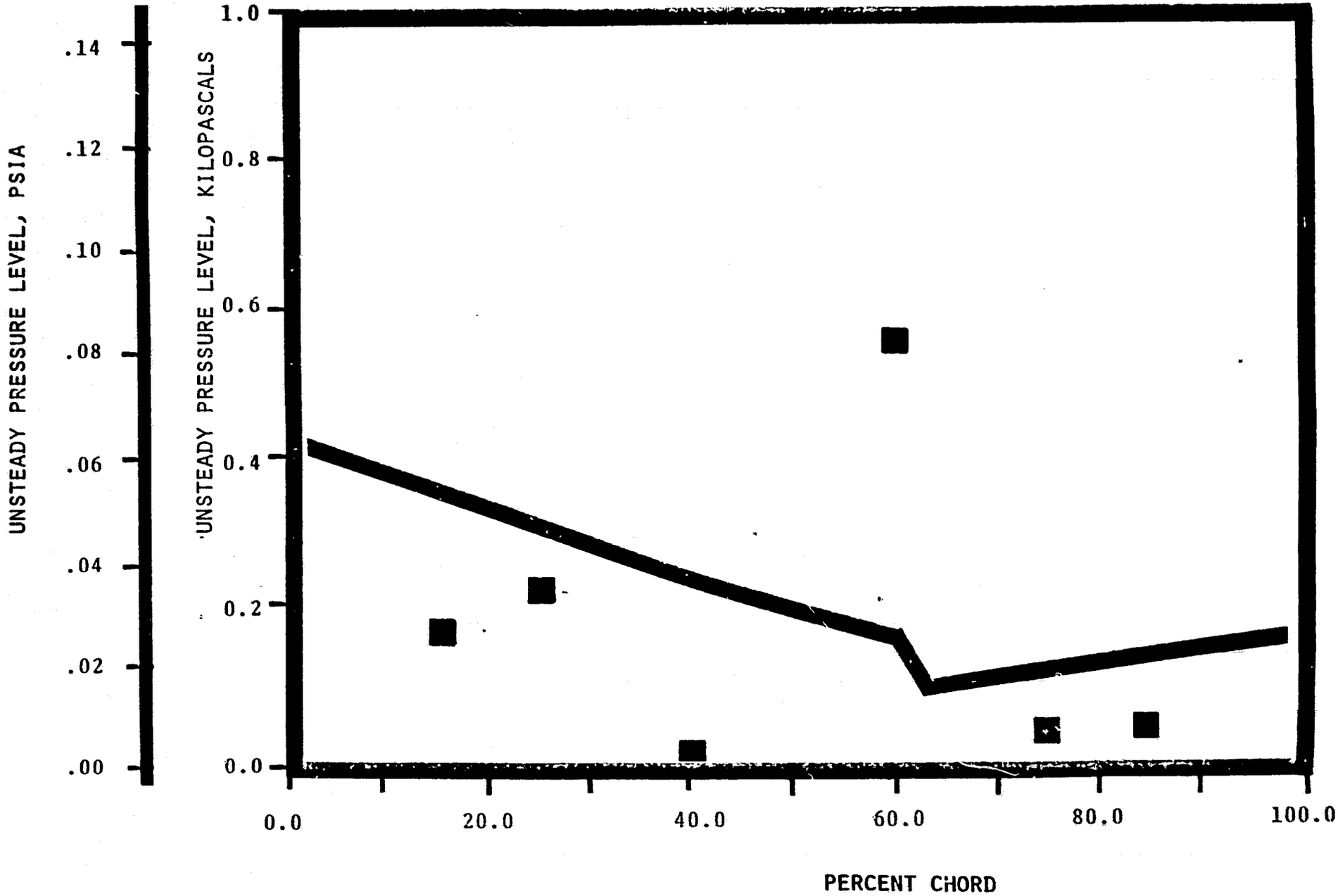

NASA I TORSION CASCADE

SUCTION SURFACE AERODYNAMIC PHASE LAG DISTRIBUTION

1.315 INLET MACH NUMBER

1.04 STATIC PRESSURE RATIO

-1.57 rad (-90°) INTERBLADE PHASE ANGLE

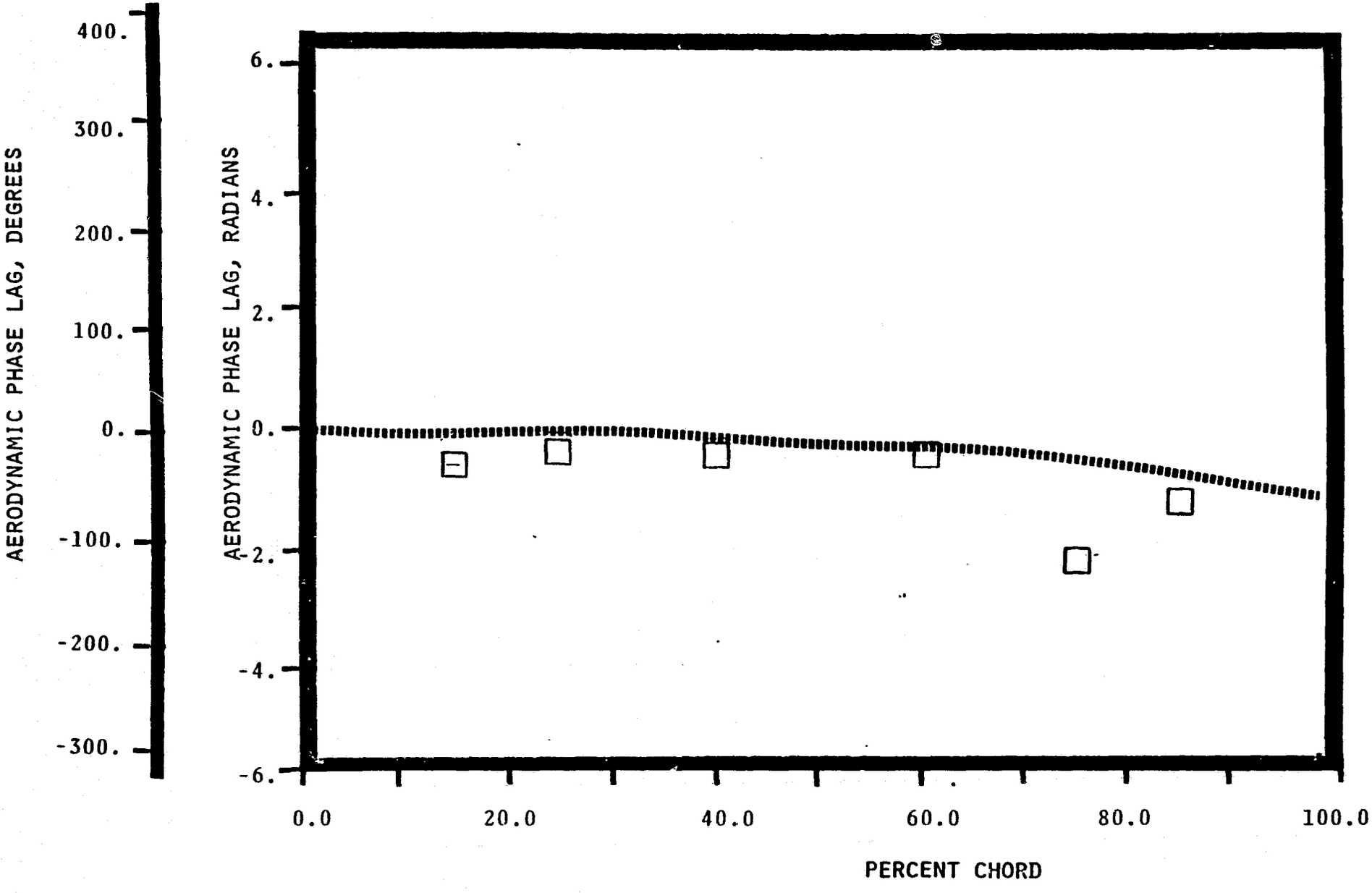

NASA I TORSION CASCADE

SUCTION SURFACE UNSTEADY PRESSURE DISTRIBUTION

1.315 INLET MACH NUMBER

1.04 STATIC PRESSURE RATIO

-1.57 rad(-90°) INTERBLADE PHASE ANGLE

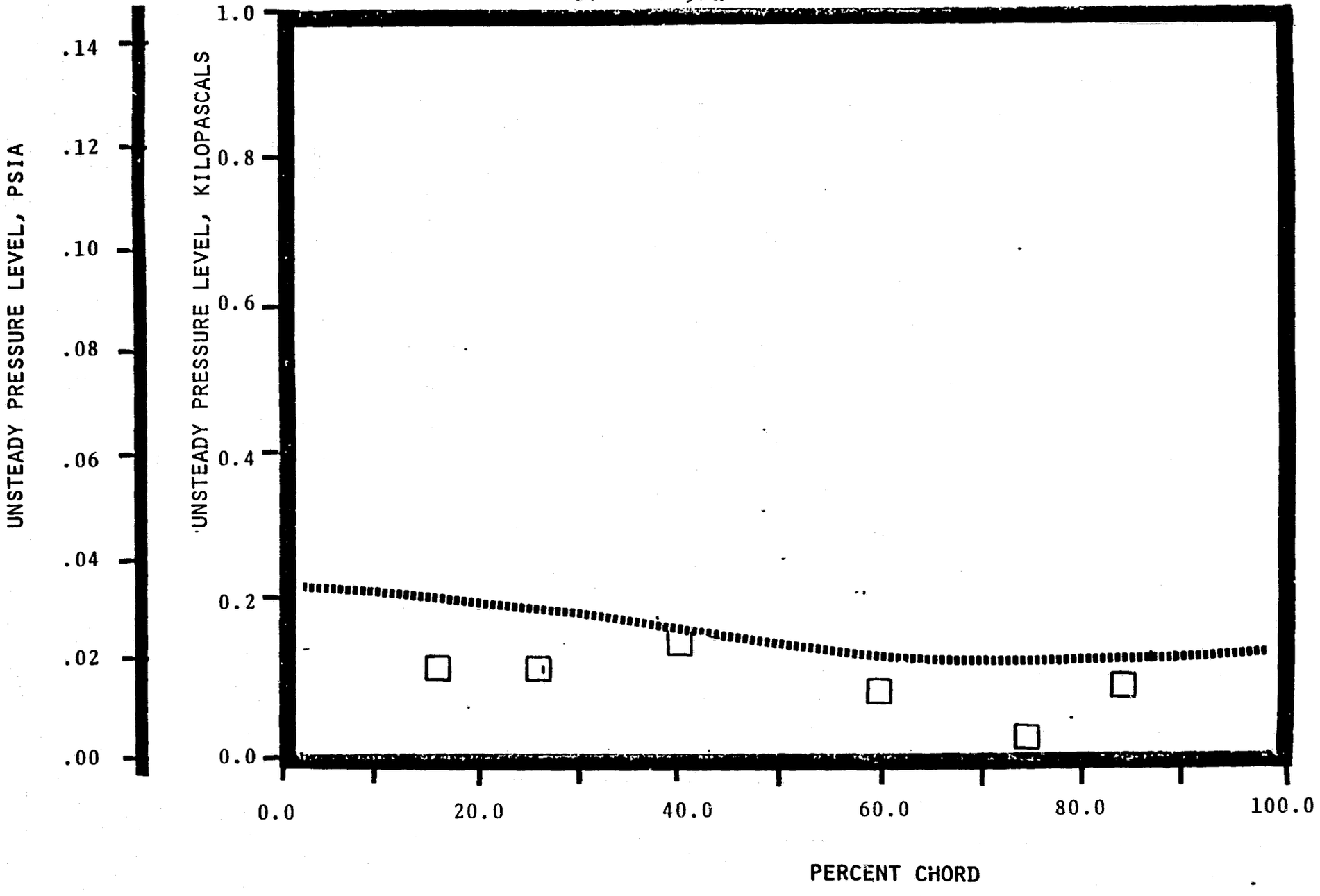

NASA I TORSION CASCADE

PRESSURE SURFACE AERODYNAMIC PHASE LAG DISTRIBUTION

1.315 INLET MACH NUMBER

1.20 STATIC PRESSURE RATIO

3.14 rad (180.°) INTERBLADE PHASE ANGLE

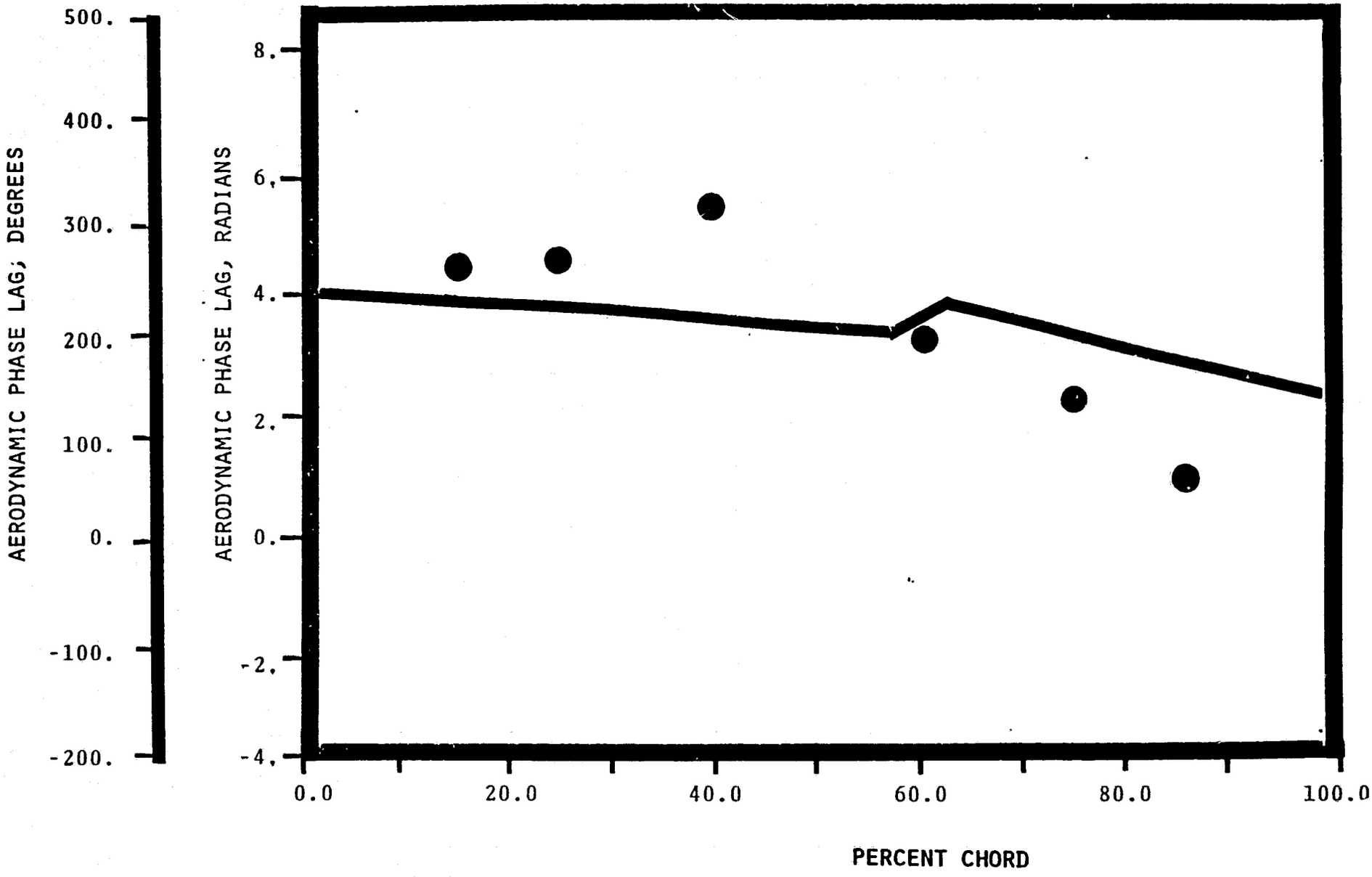

NASA I TORSION CASCADE

PRESSURE SURFACE UNSTEADY PRESSURE DISTRIBUTION

1.315 INLET MACH NUMBER

1.20 STATIC PRESSURE RATIO

3.14 rad (180.°) INTERBLADE PHASE ANGLE

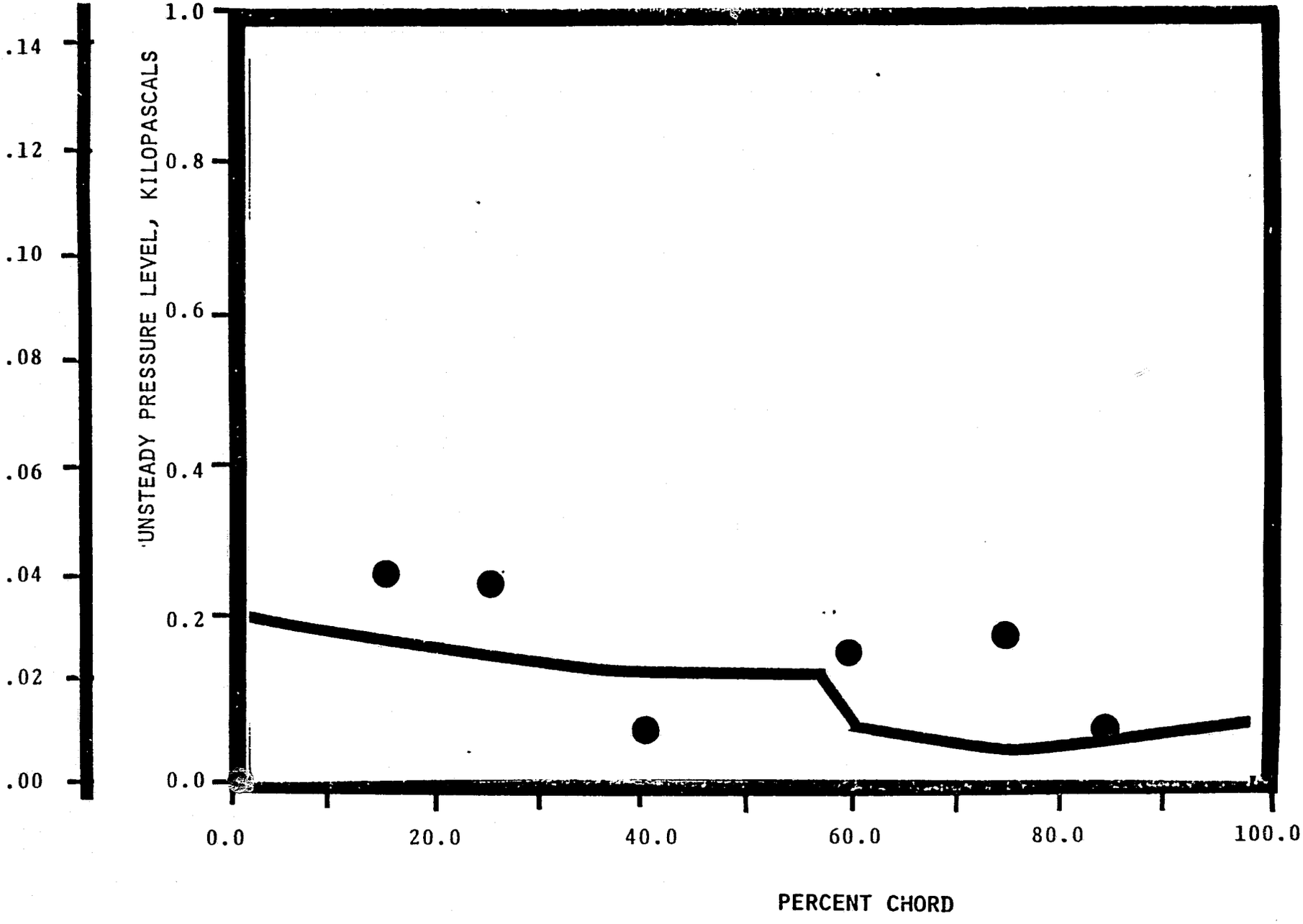

NASA I TORSION CASCADE

SUCTION SURFACE AERODYNAMIC PHASE LAG DISTRIBUTION

1.315 INLET MACH NUMBER

1.20 STATIC PRESSURE RATIO

3.14 rad (180.°) INTERBLADE PHASE ANGLE

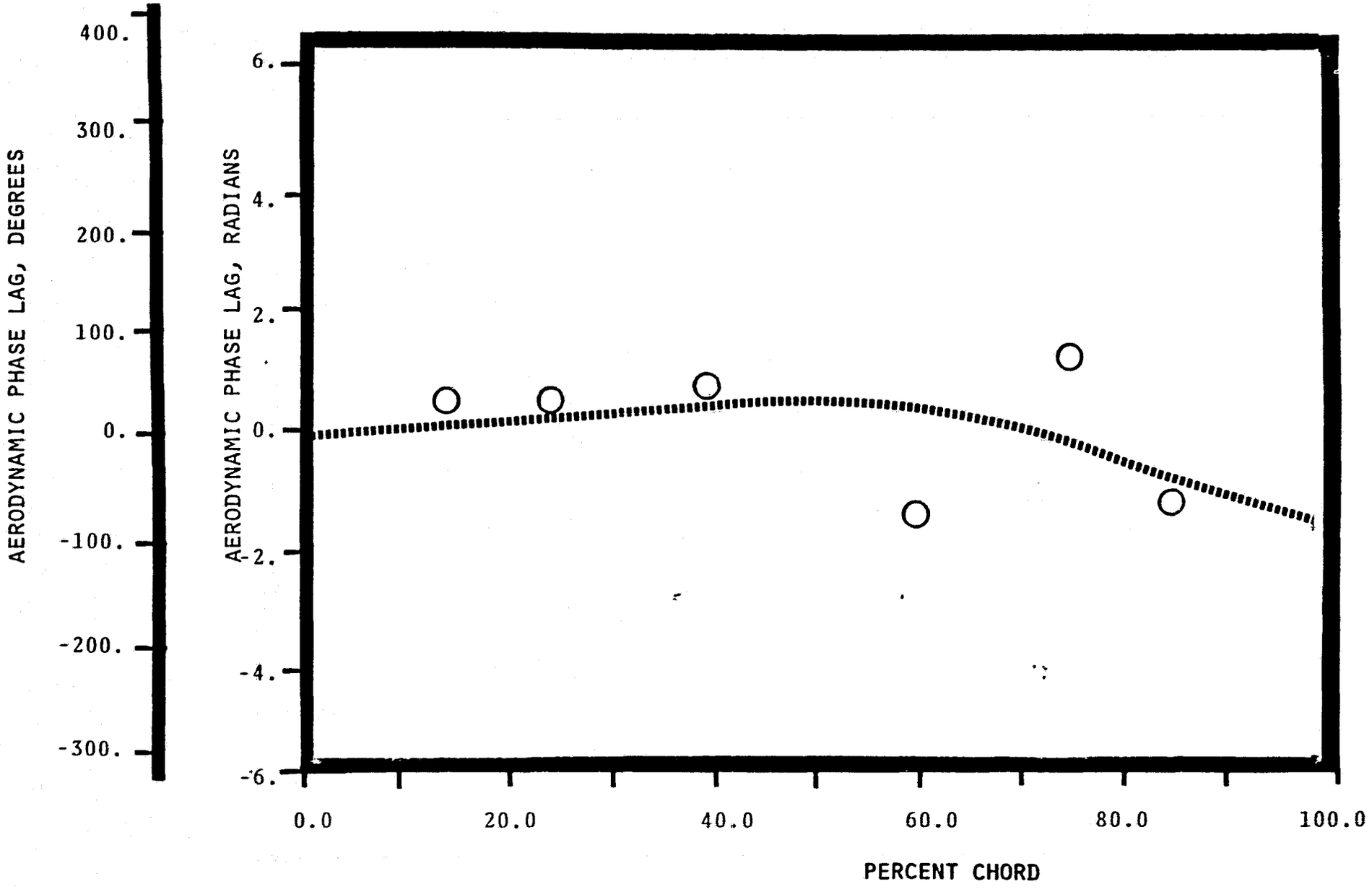

NASA I TORSION CASCADE

SUCTION SURFACE UNSTEADY PRESSURE DISTRIBUTION

1.315 INLET MACH NUMBER

1.20 STATIC PRESSURE RATIO

3.14 rad (180.°)INTERBLADE PHASE ANGLE

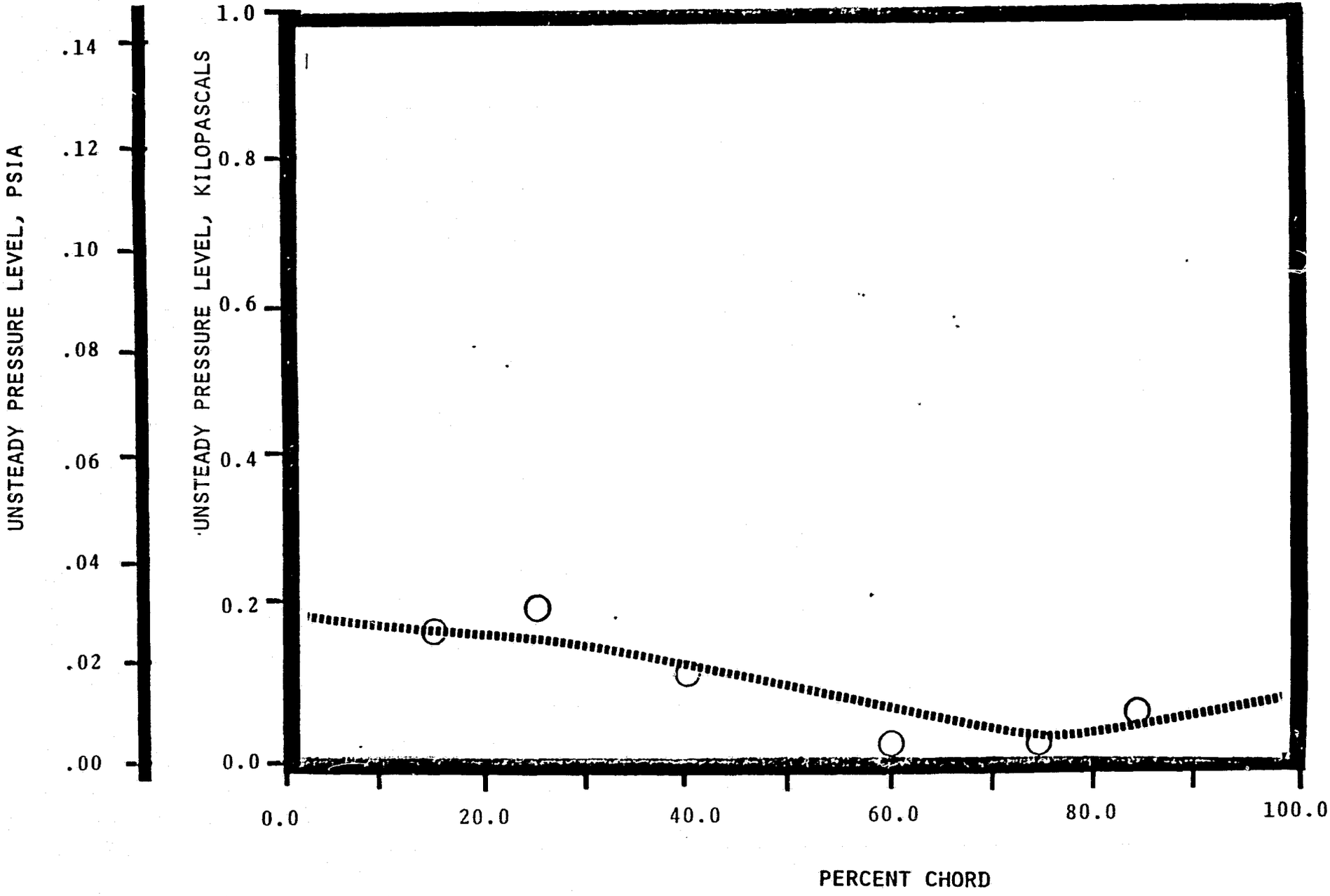

NASA I TORSION CASCADE

PRESSURE SURFACE AERODYNAMIC PHASE LAG DISTRIBUTION

1.315 INLET MACH NUMBER

1.20 STATIC PRESSURE RATIO

1.57 rad (90.°) INTERBLADE PHASE ANGLE

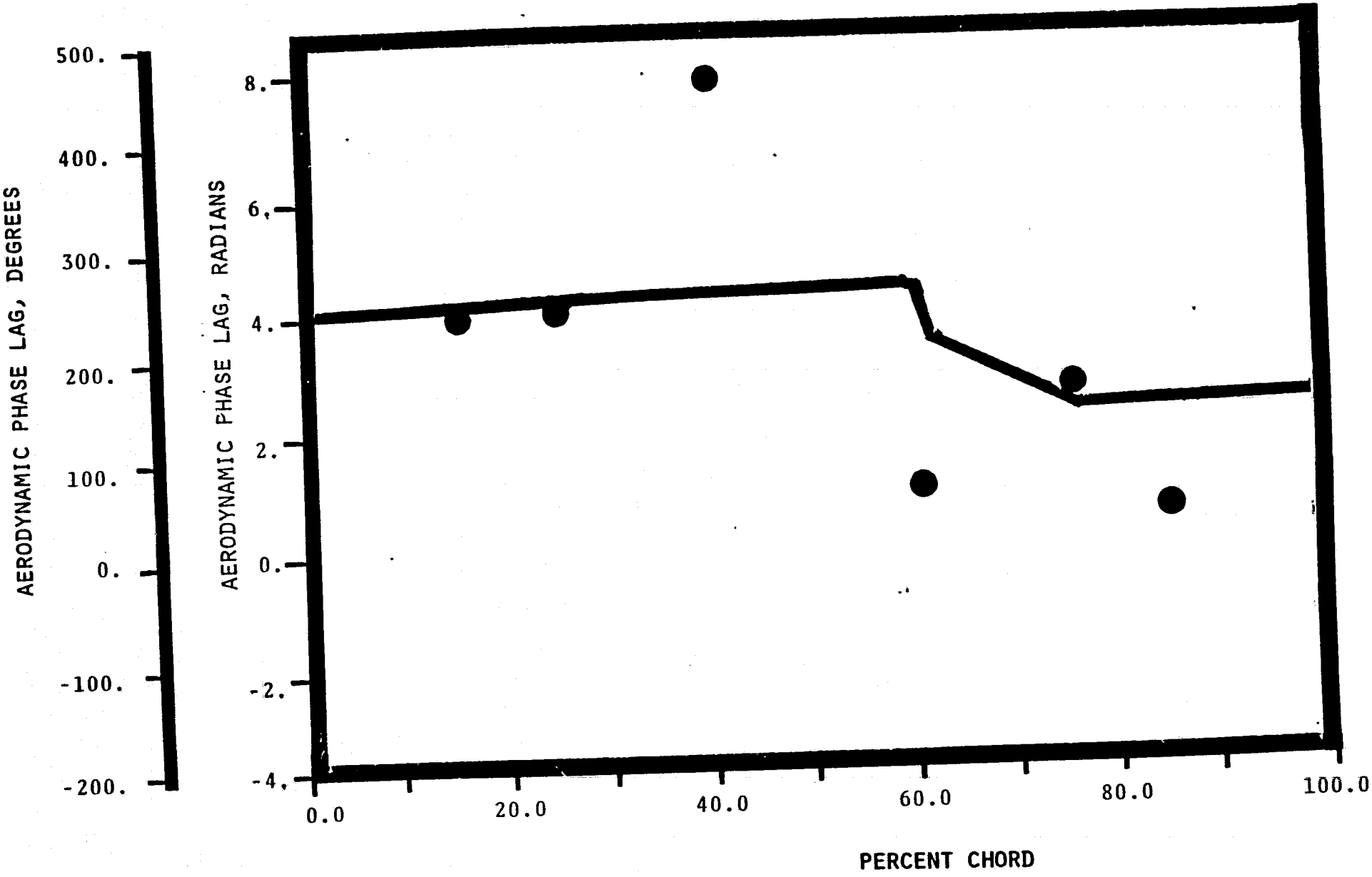

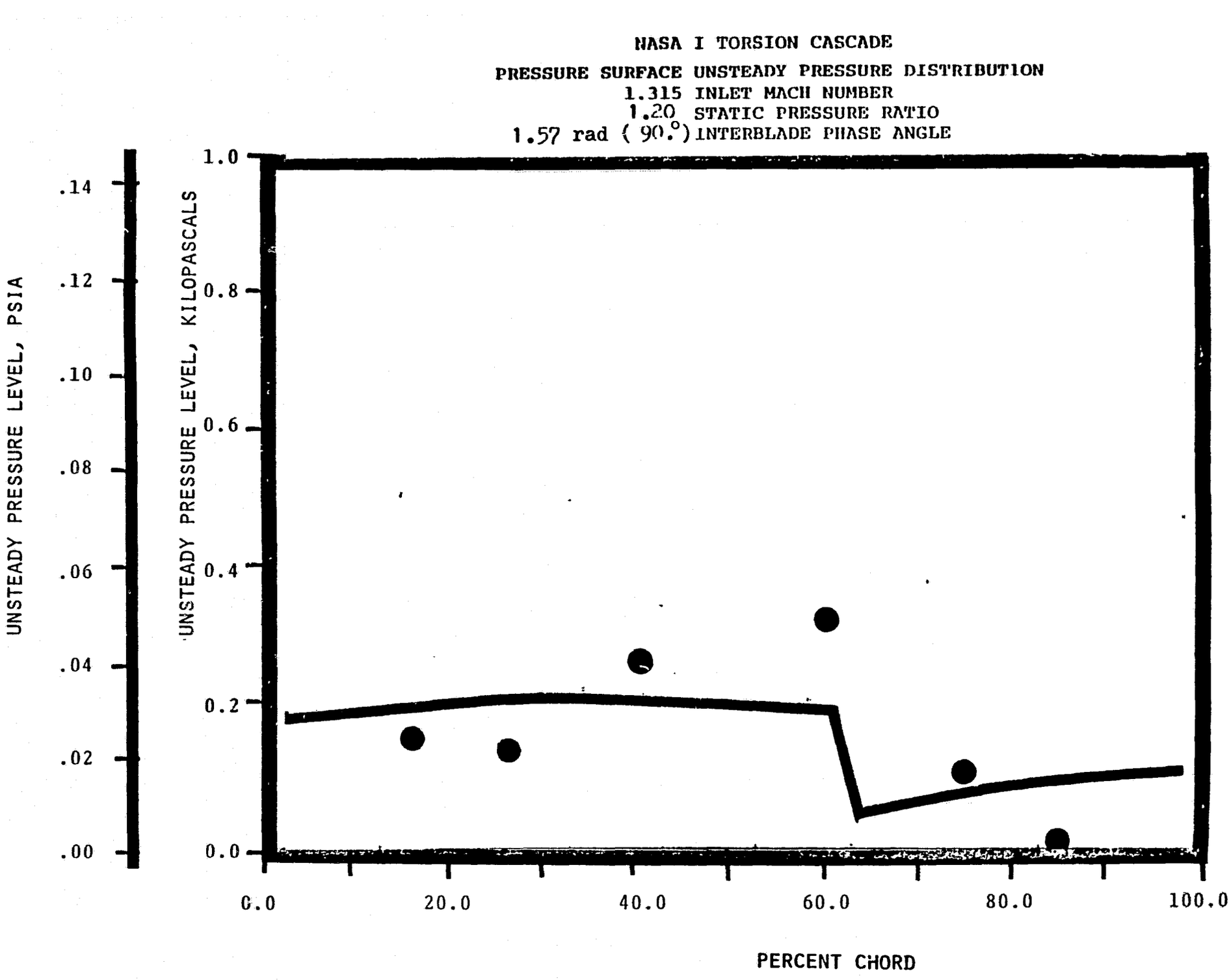
NASA I TORSION CASCADE
PRESSURE SURFACE UNSTEADY PRESSURE DISTRIBUTION
1.315 INLET MACH NUMBER
1.20 STATIC PRESSURE RATIO
1.57 rad (90.°) INTERBLADE PHASE ANGLE
UNSTEADY PRESSURE LEVEL, PSIA
.14
.12
.10
.08
.06
.04
.02
.00
UNSTEADY PRESSURE LEVEL, KILOPASCALS
1.0
0.8
0.6
0.4
0.2
0.0
0.0
20.0
40.0
60.0
80.0
100.0
PERCENT CHORD

NASA I TORSION CASCADE

SUCTION SURFACE AERODYNAMIC PHASE LAG DISTRIBUTION

1.315 INLET MACH NUMBER

1.20 STATIC PRESSURE RATIO

1.57 rad (90.°) INTERBLADE PHASE ANGLE

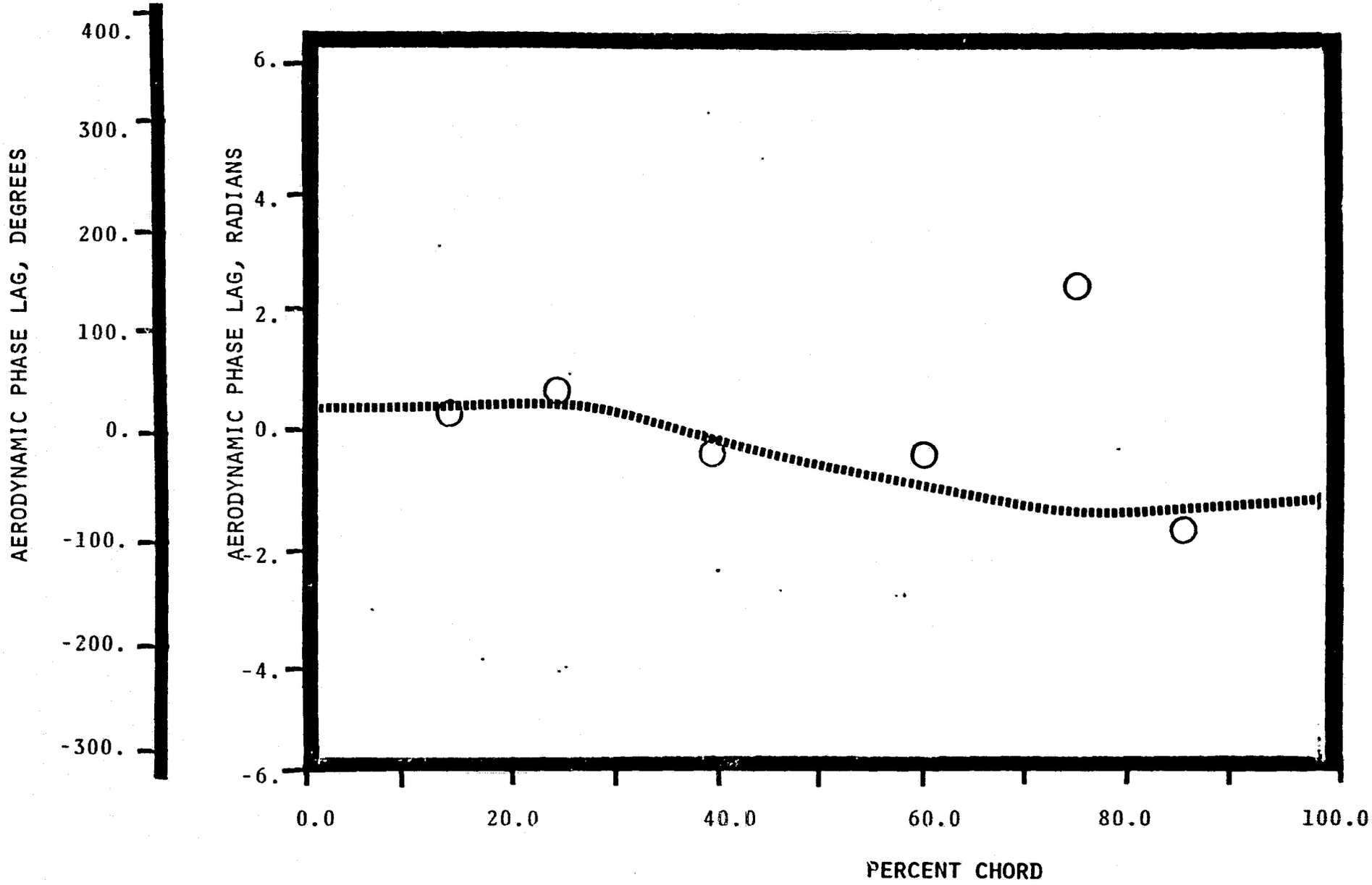

NASA I TORSION CASCADE

SUCTION SURFACE UNSTEADY PRESSURE DISTRIBUTION

1.315 INLET MACH NUMBER

1.20 STATIC PRESSURE RATIO

1.57 rad (90.°)INTERBLADE PHASE ANGLE

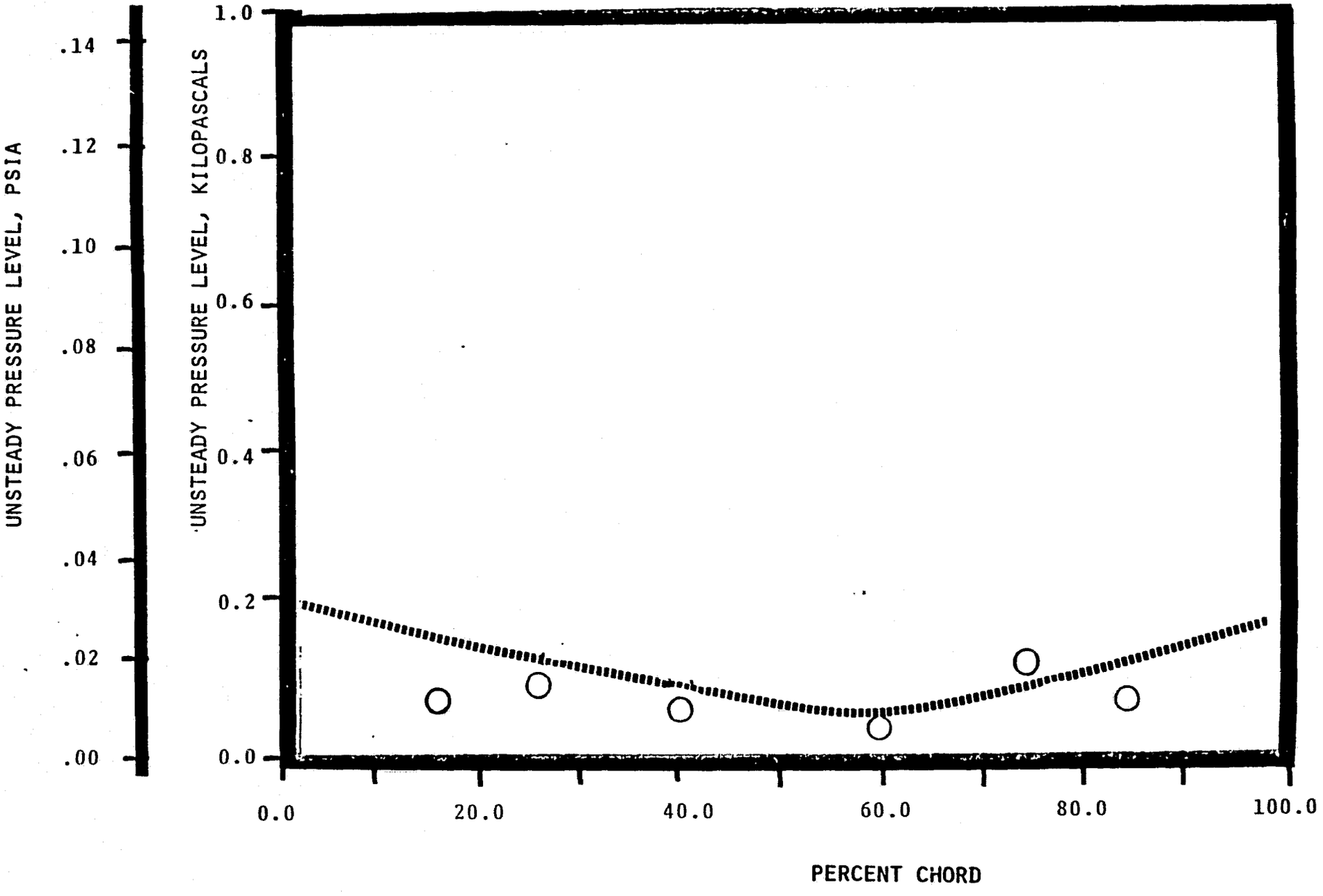

NASA I TORSION CASCADE

PRESSURE SURFACE AERODYNAMIC PHASE LAG DISTRIBUTION
1.315 INLET MACH NUMBER
1.20 STATIC PRESSURE RATIO
0.0 rad (0^{o}) INTERBLADE PHASE ANGLE

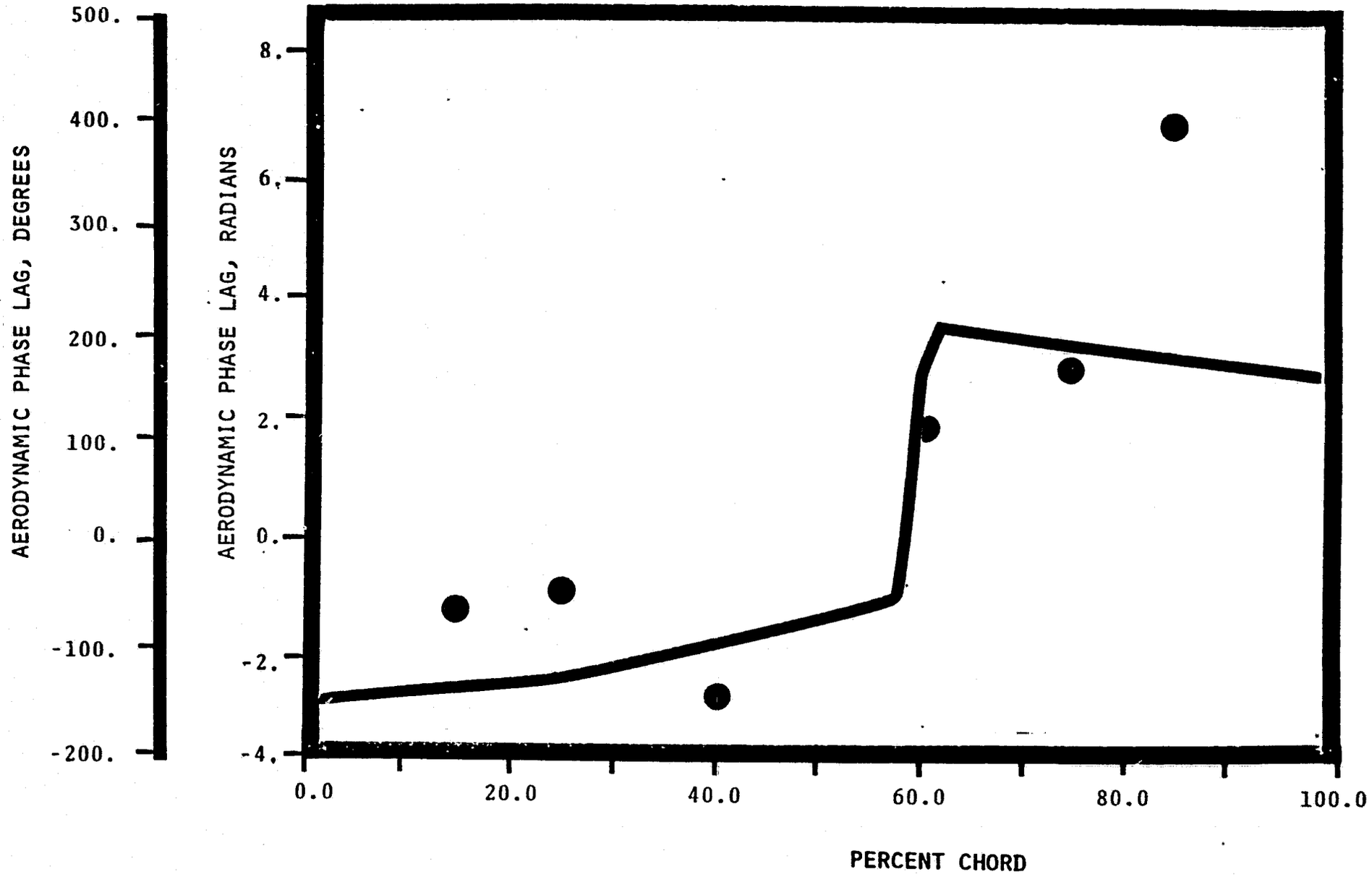

NASA I TORSION CASCADE

PRESSURE SURFACE UNSTEADY PRESSURE DISTRIBUTION

1.315 INLET MACH NUMBER

1.20 STATIC PRESSURE RATIO

0.0 rad (0°) INTERBLADE PHASE ANGLE

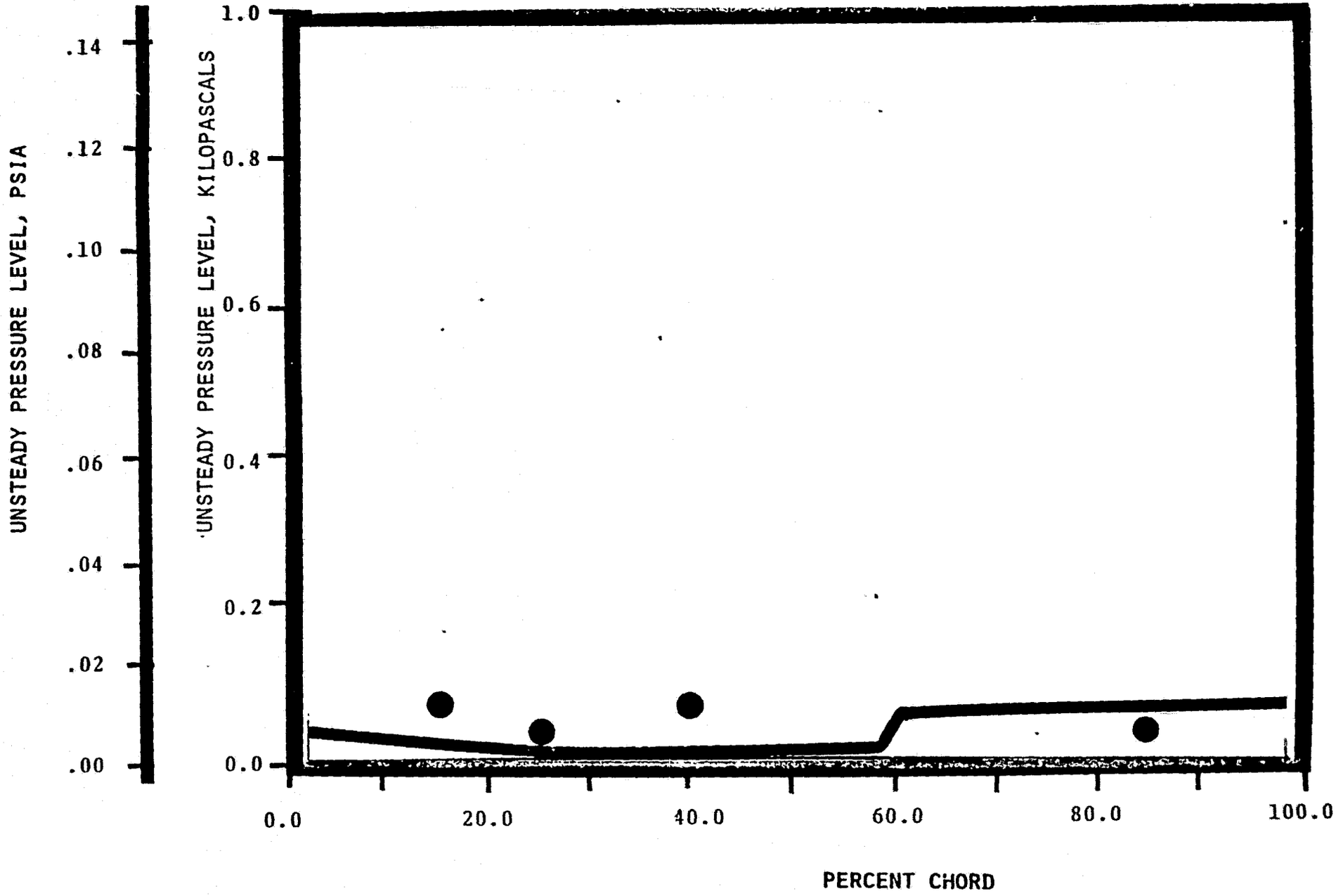

NASA I TORSION CASCADE

SUCTION SURFACE AERODYNAMIC PHASE LAG DISTRIBUTION

1.315 INLET MACH NUMBER

1.20 STATIC PRESSURE RATIO

0.0 rad (0^{o}) INTERBLADE PHASE ANGLE

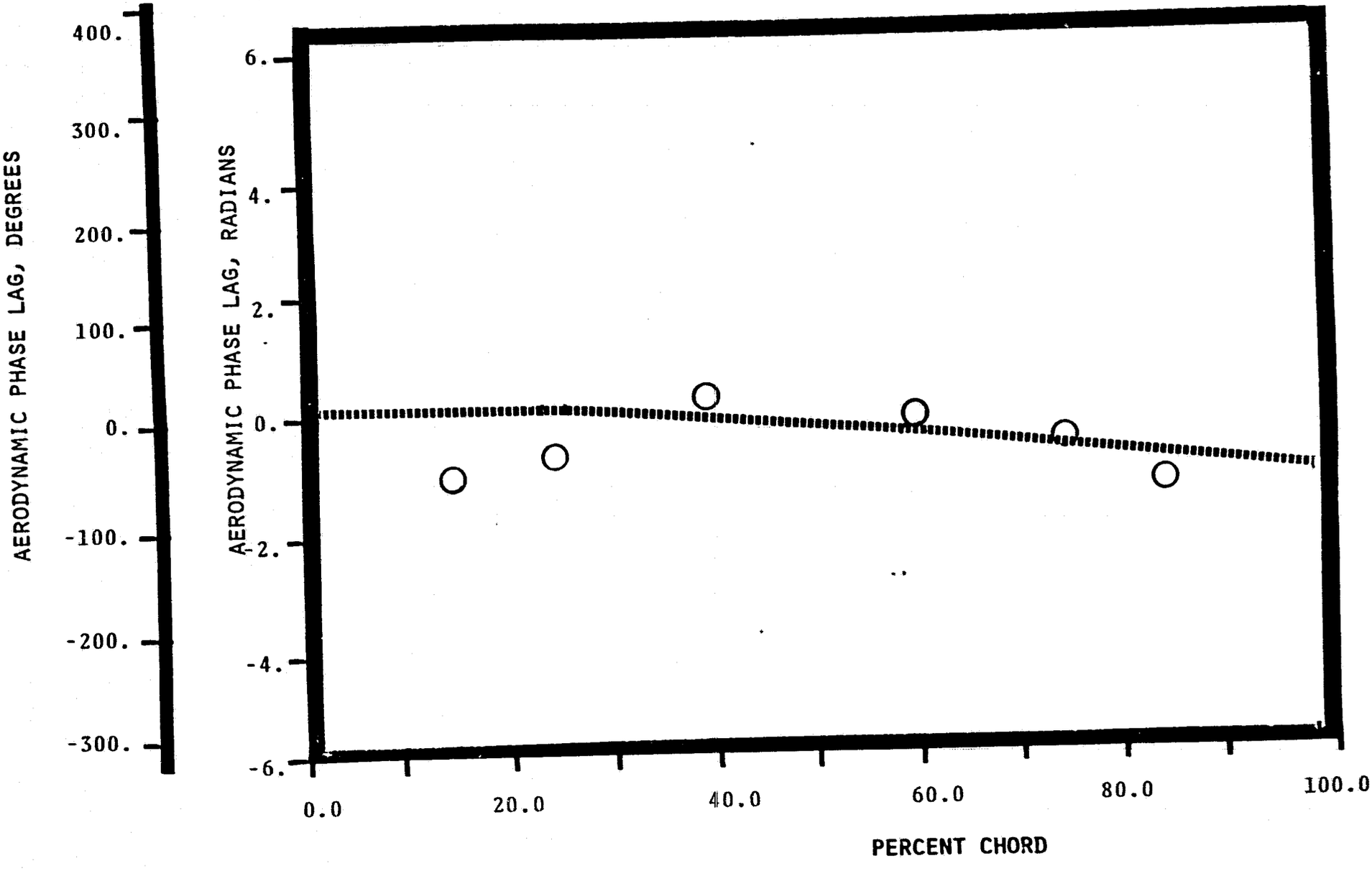

NASA I TORSION CASCADE

SUCTION SURFACE UNSTEADY PRESSURE DISTRIBUTION

1.315 INLET MACH NUMBER

1.20 STATIC PRESSURE RATIO

0.0 rad (0^{o}) INTERBLADE PHASE ANGLE

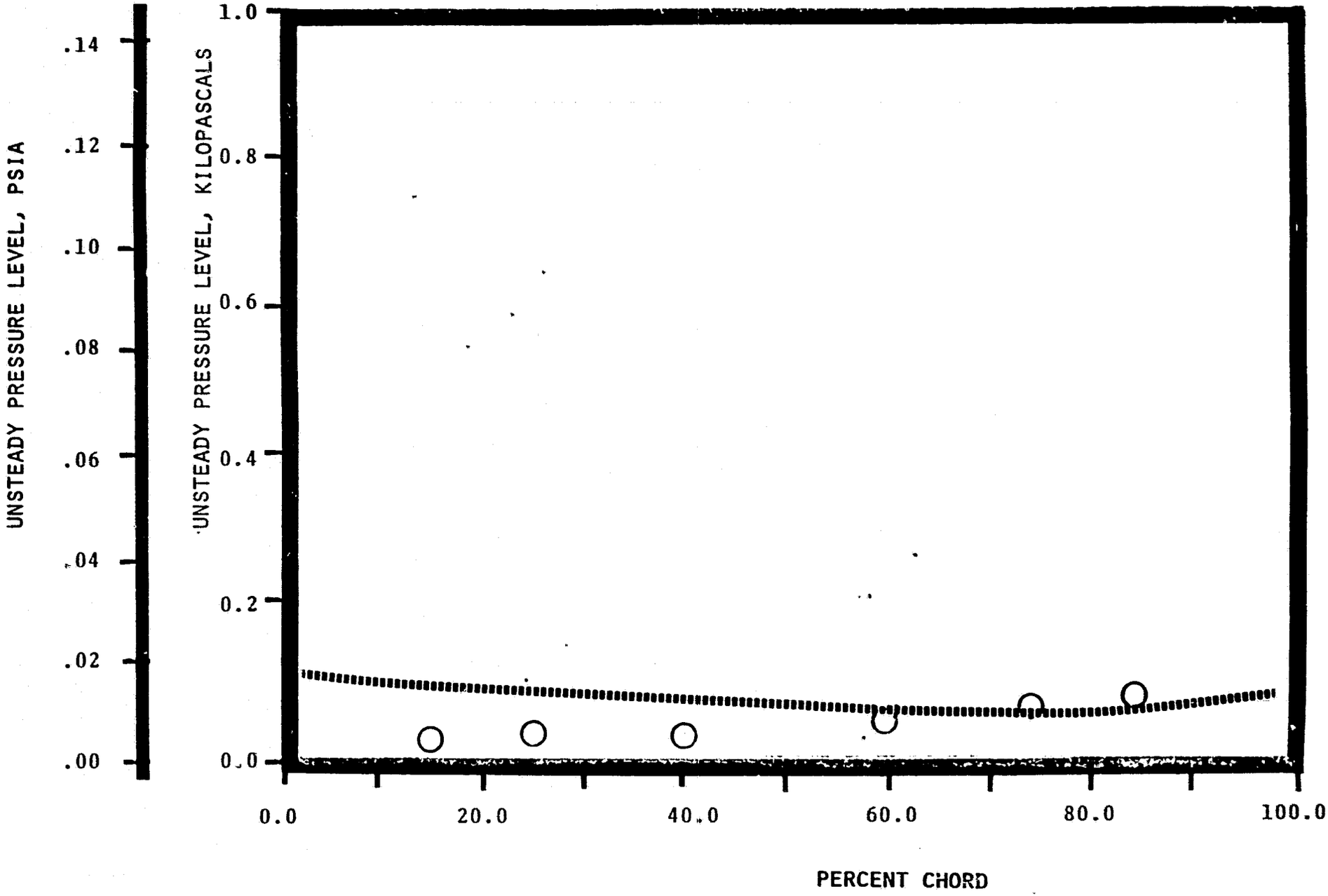

NASA I TORSION CASCADE

PRESSURE SURFACE AERODYNAMIC PHASE LAG DISTRIBUTION
1.315 INLET MACH NUMBER
1.20 STATIC PRESSURE RATIO
-.70 rad (-40.°) INTERBLADE PHASE ANGLE

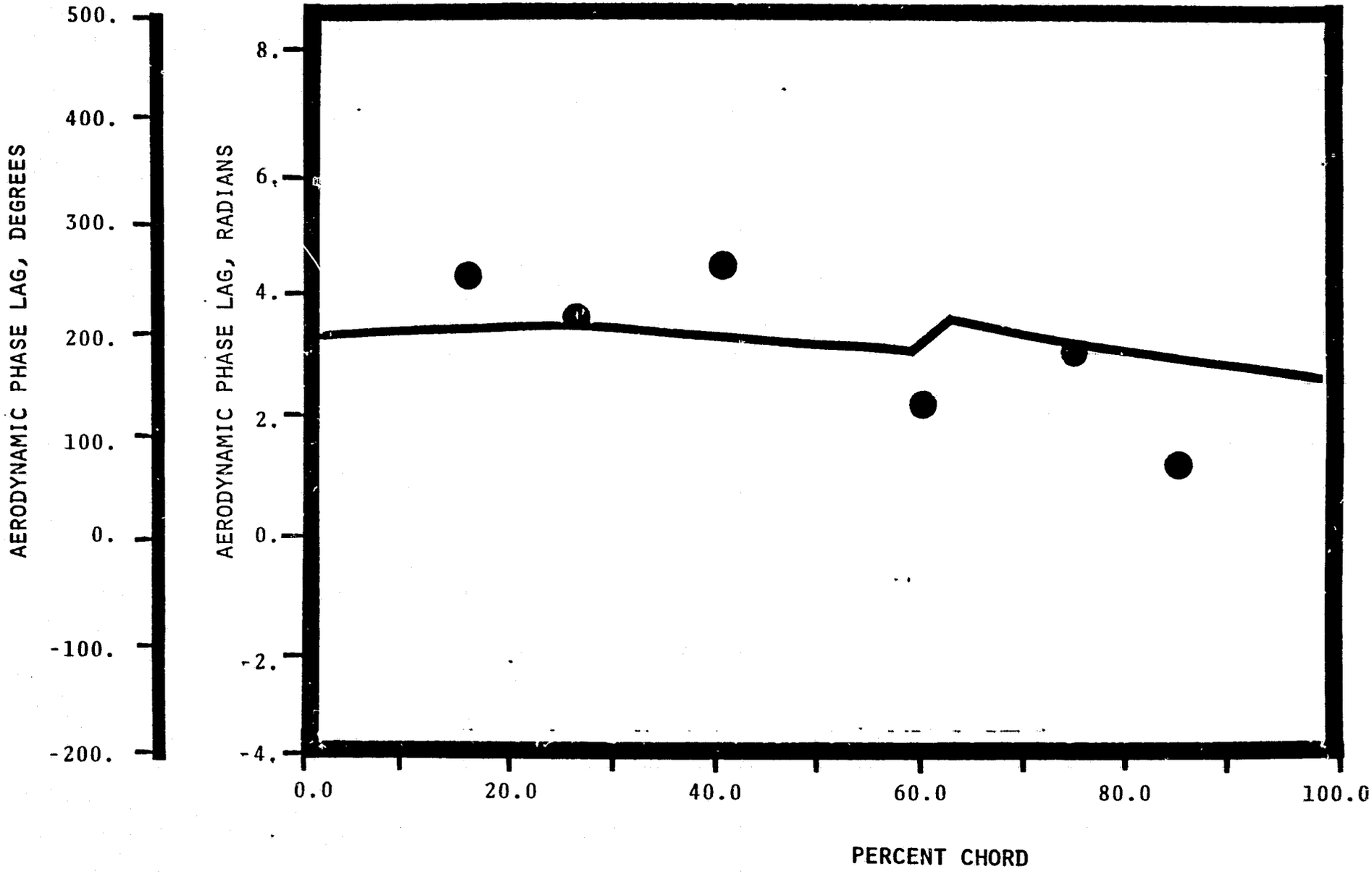

NASA I TORSION CASCADE

PRESSURE SURFACE UNSTEADY PRESSURE DISTRIBUTION

1.315 INLET MACH NUMBER

1.20 STATIC PRESSURE RATIO

-.70 rad (-40°) INTERBLADE PHASE ANGLE

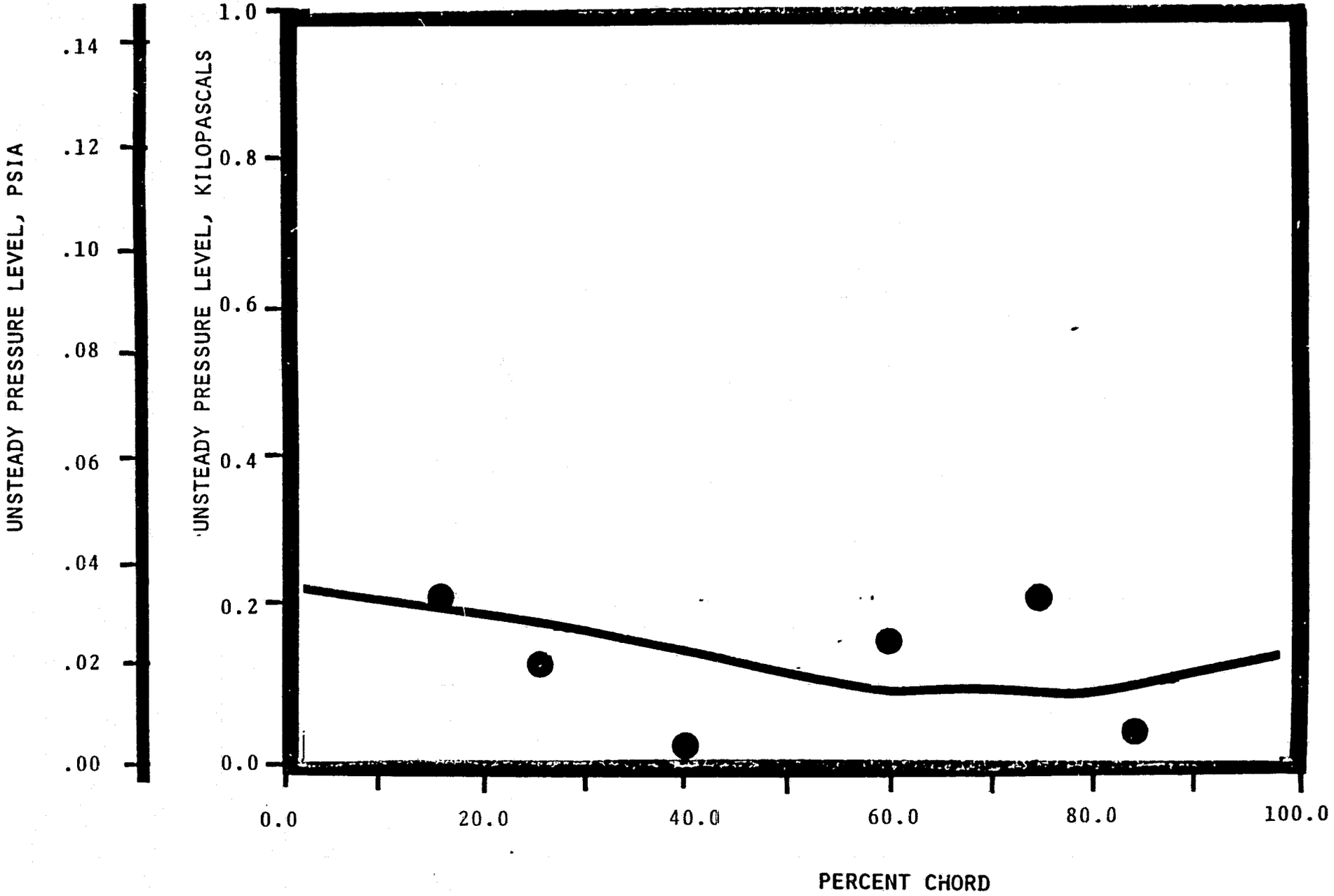

NASA I TORSION CASCADE

SUCTION SURFACE AERODYNAMIC PHASE LAG DISTRIBUTION

1.315 INLET MACH NUMBER

1.20 STATIC PRESSURE RATIO

-.70 rad(-40°) INTERBLADE PHASE ANGLE

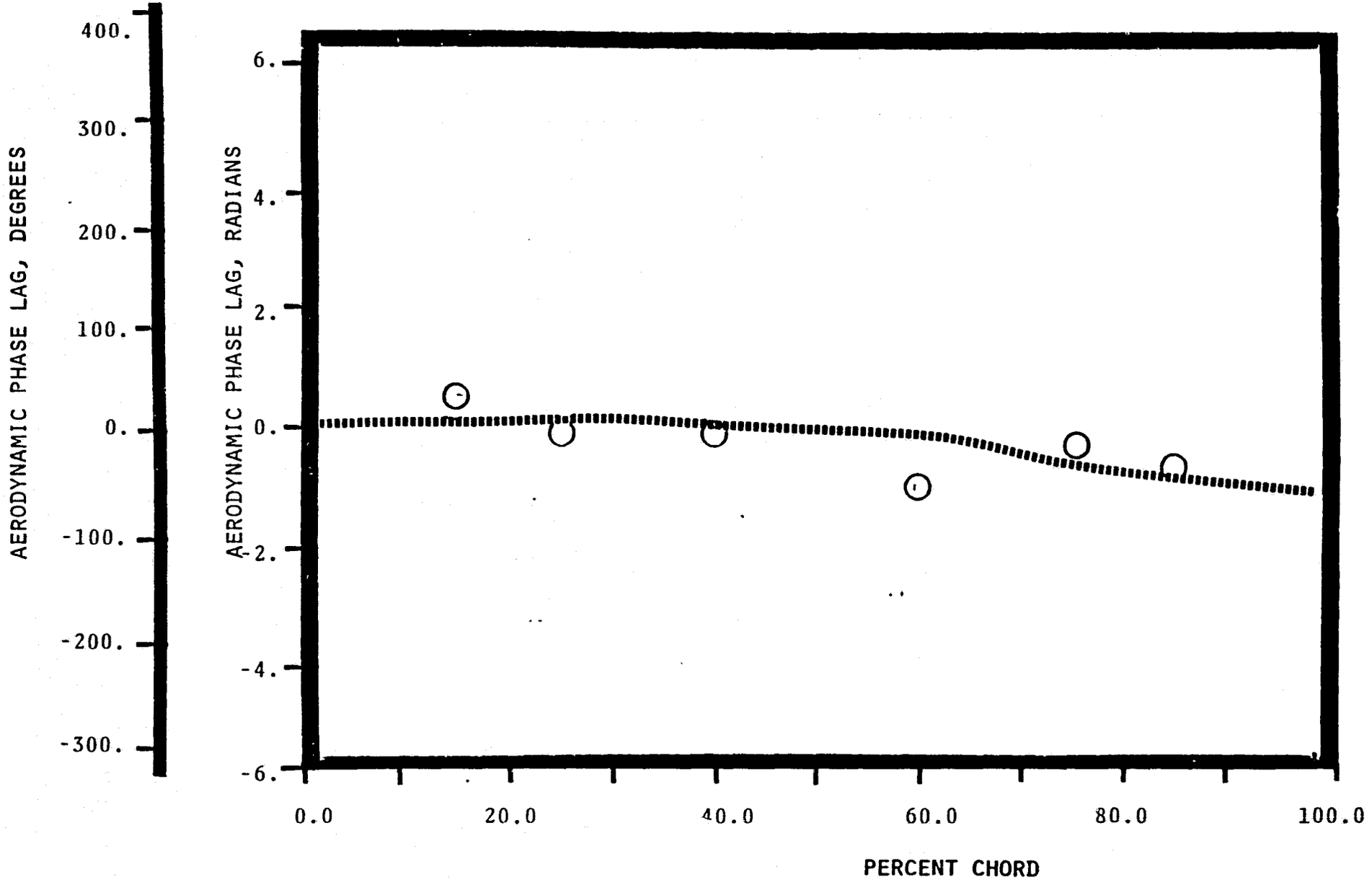

NASA I TORSION CASCADE

SUCTION SURFACE UNSTEADY PRESSURE DISTRIBUTION

1.315 INLET MACH NUMBER

1.20 STATIC PRESSURE RATIO

-.70 rad (-40.°) INTERBLADE PHASE ANGLE

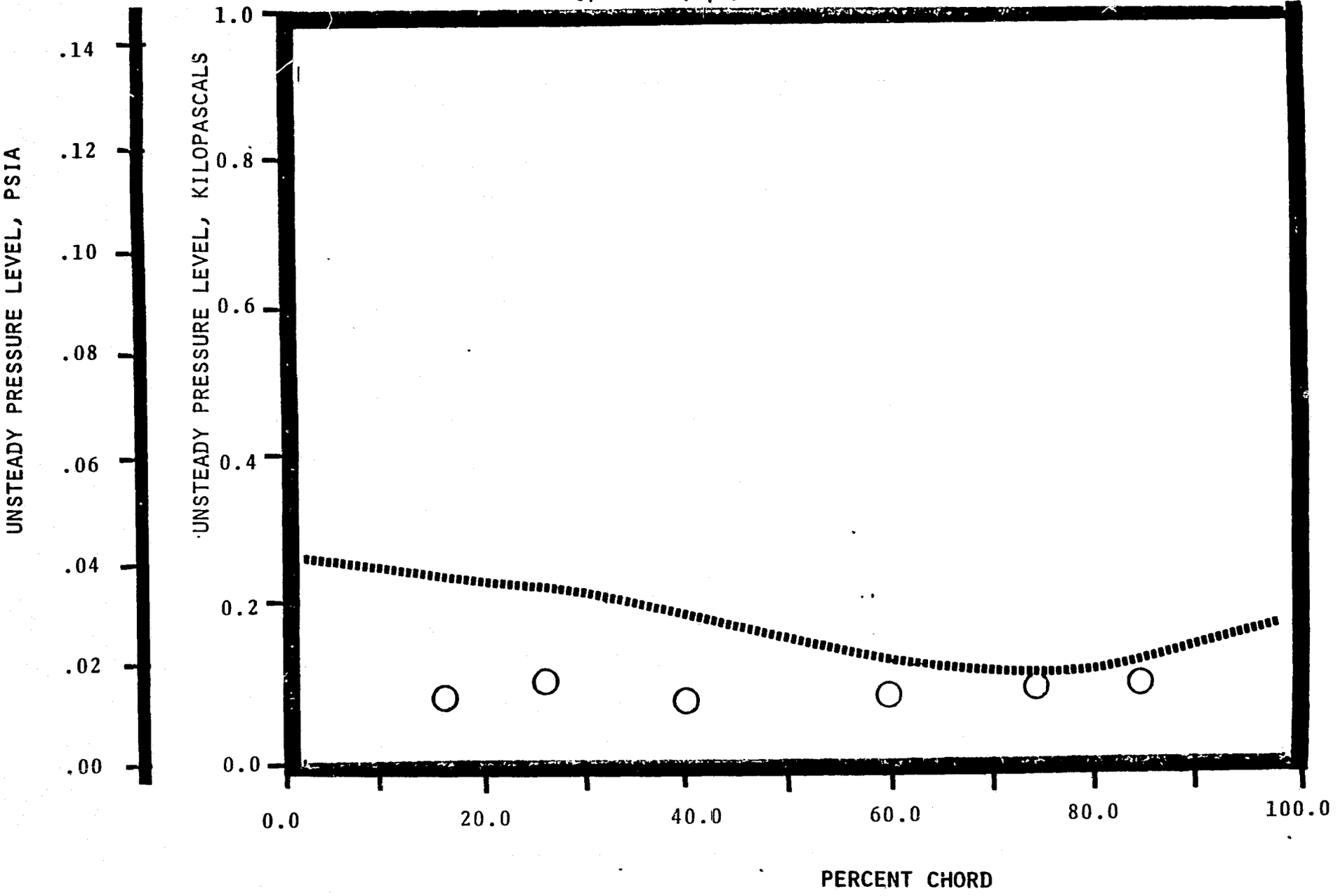

NASA I TORSION CASCADE

PRESSURE SURFACE AERODYNAMIC PHASE LAG DISTRIBUTION
1.315 INLET MACH NUMBER
1.20 STATIC PRESSURE RATIO
-1.05 rad (-60°) INTERBLADE PHASE ANGLE

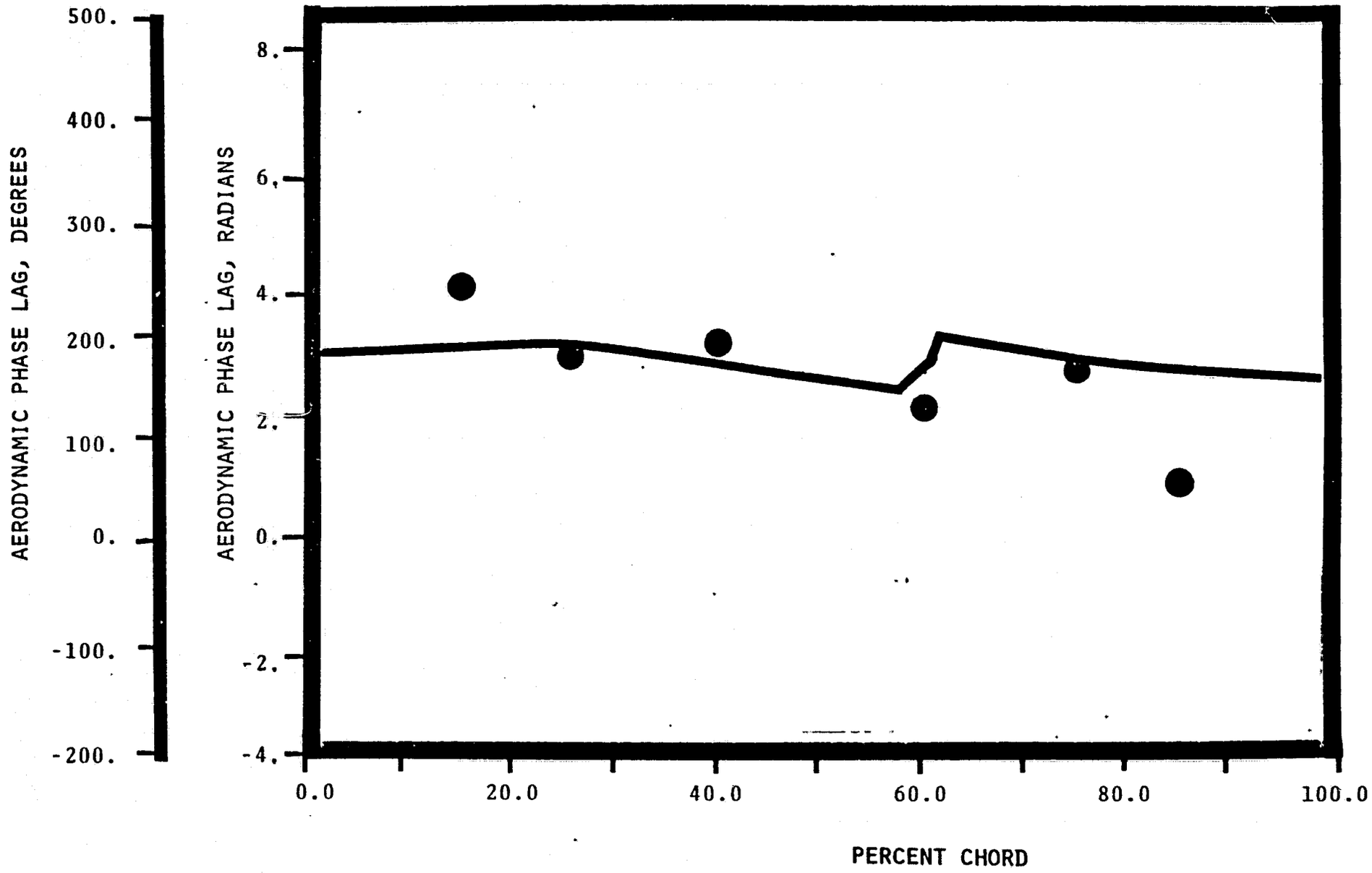

NASA I TORSION CASCADE

PRESSURE SURFACE UNSTEADY PRESSURE DISTRIBUTION

1.315 INLET MACH NUMBER

1.20 STATIC PRESSURE RATIO

-1.05 rad (-60.°) INTERBLADE PHASE ANGLE

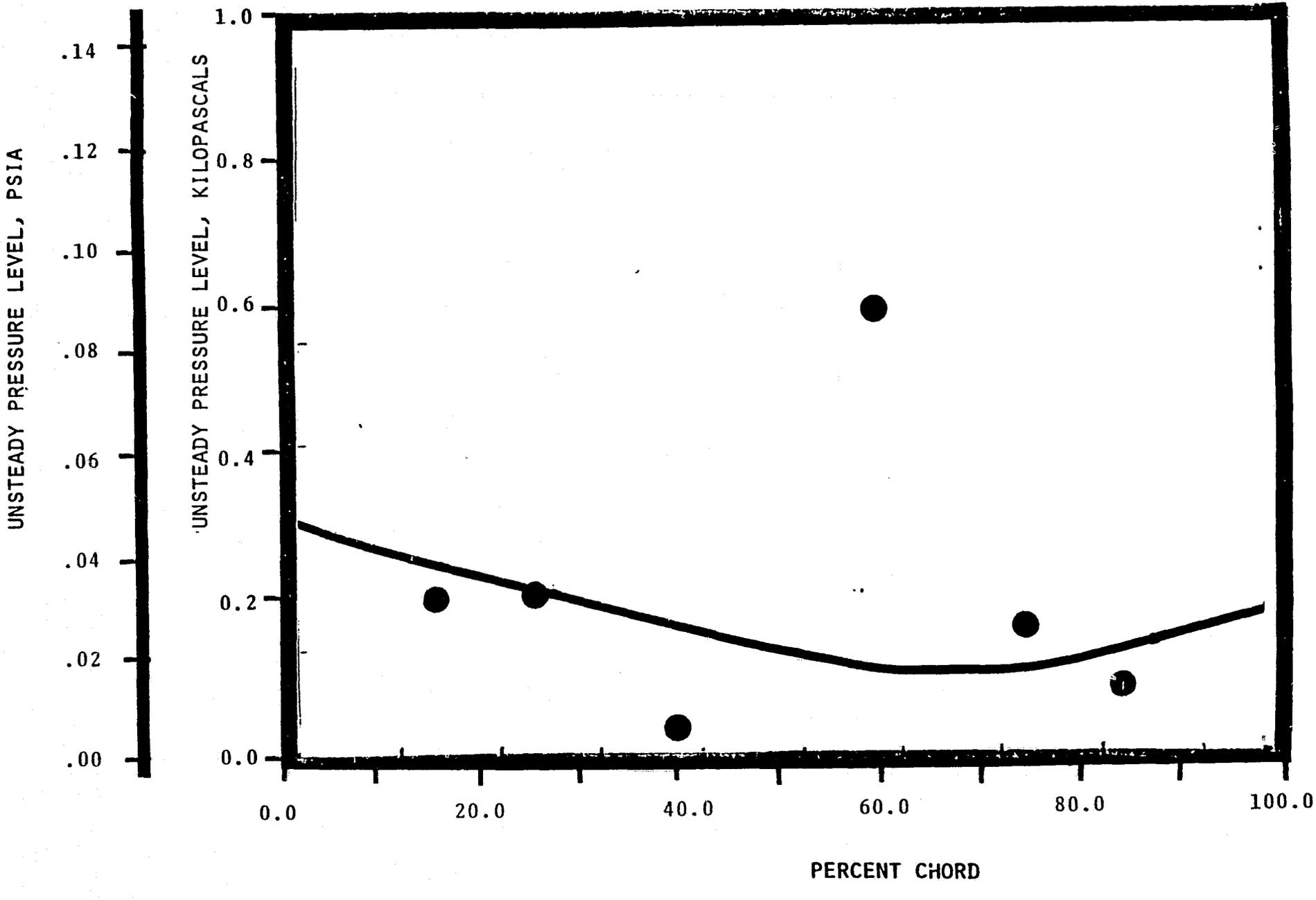

NASA I TORSION CASCADE

SUCTION SURFACE AERODYNAMIC PHASE LAG DISTRIBUTION

1.315 INLET MACH NUMBER

1.20 STATIC PRESSURE RATIO

-1.05 rad (-60°) INTERBLADE PHASE ANGLE

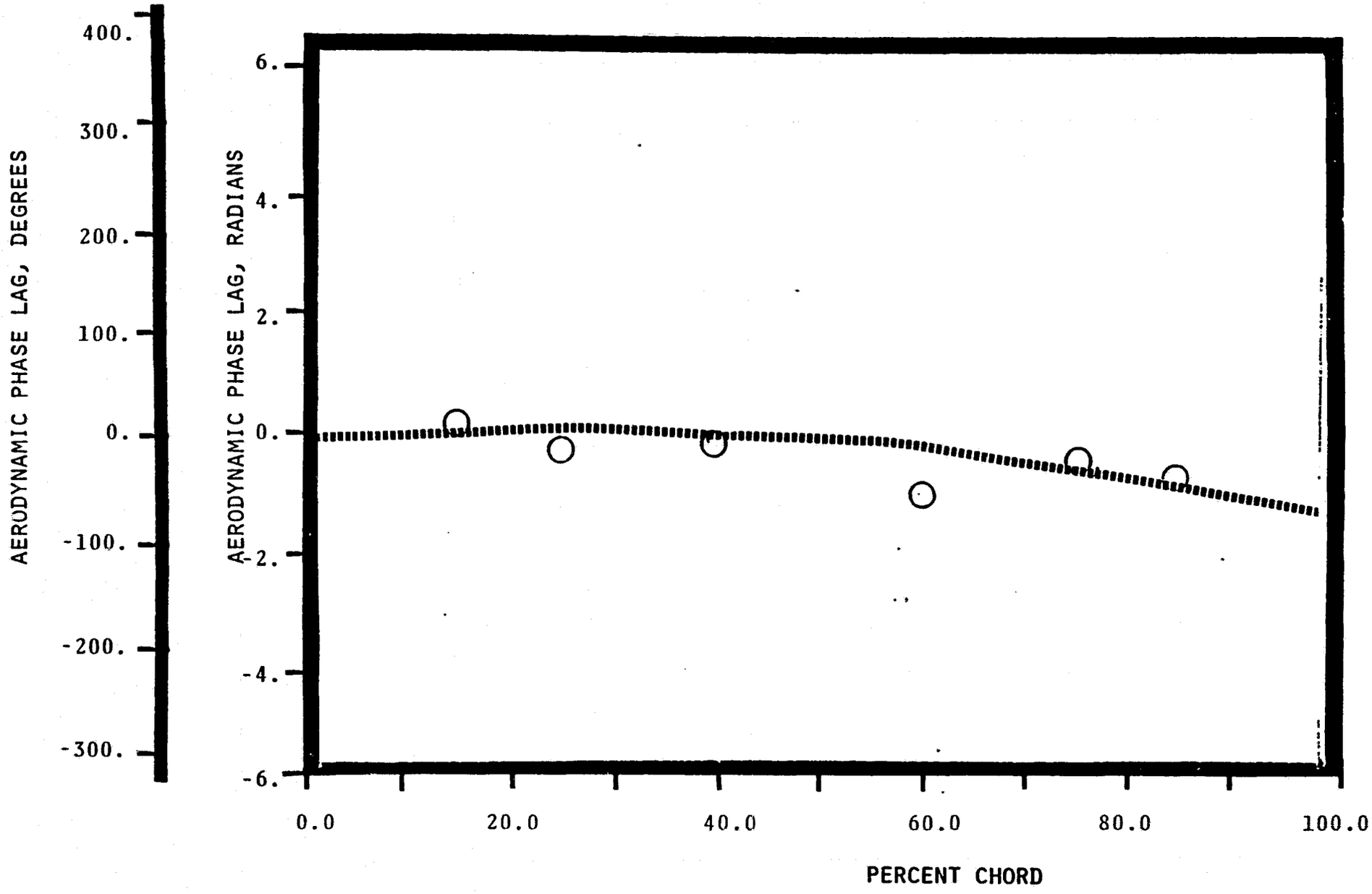

NASA I TORSION CASCADE

SUCTION SURFACE UNSTEADY PRESSURE DISTRIBUTION

1.315 INLET MACH NUMBER

1.20 STATIC PRESSURE RATIO

-1.05 rad (-60°) INTERBLADE PHASE ANGLE

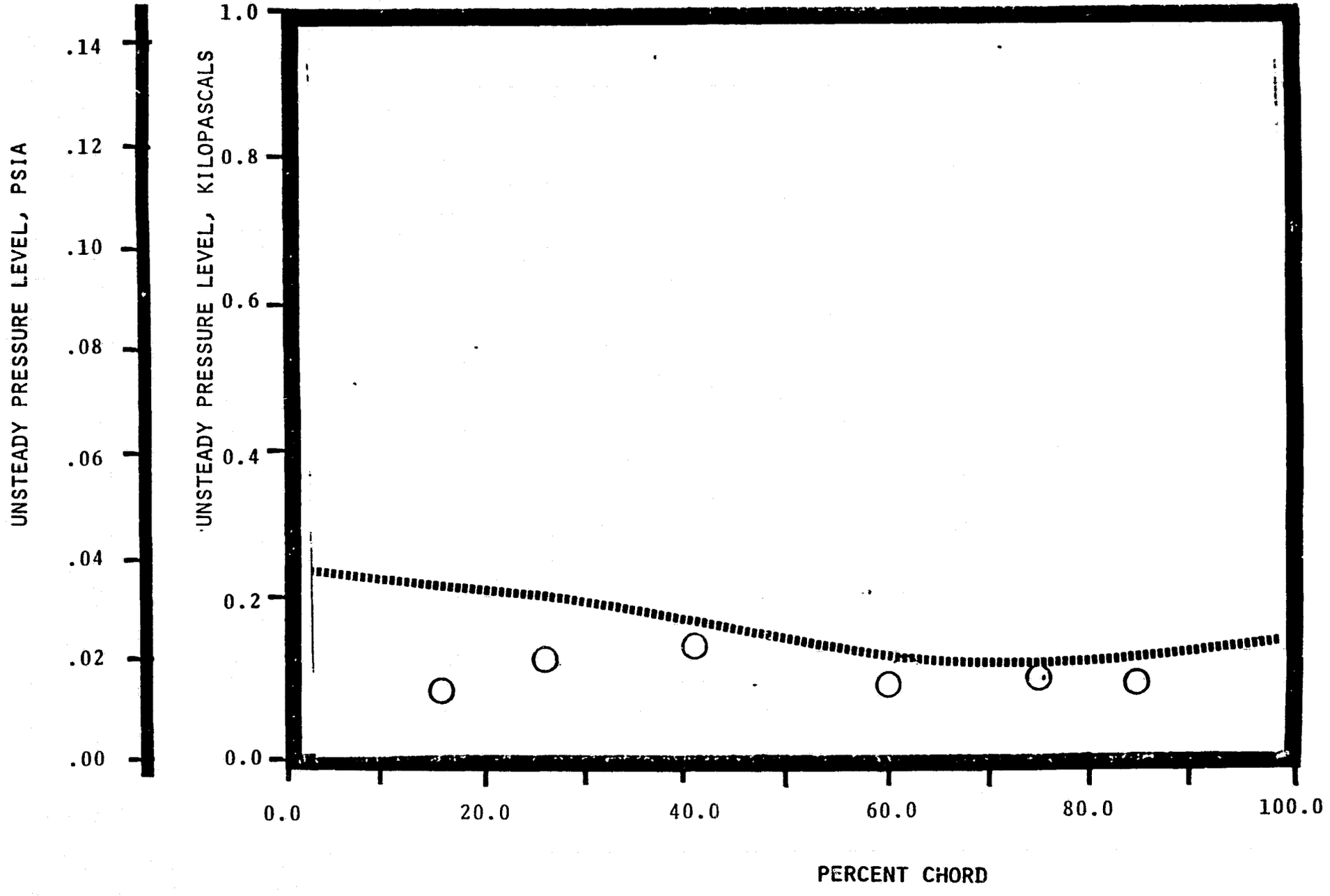

NASA I TORSION CASCADE

PRESSURE SURFACE AERODYNAMIC PHASE LAG DISTRIBUTION
1.315 INLET MACH NUMBER
1.20 STATIC PRESSURE RATIO
-1.57 rad (-90°) INTERBLADE PHASE ANGLE

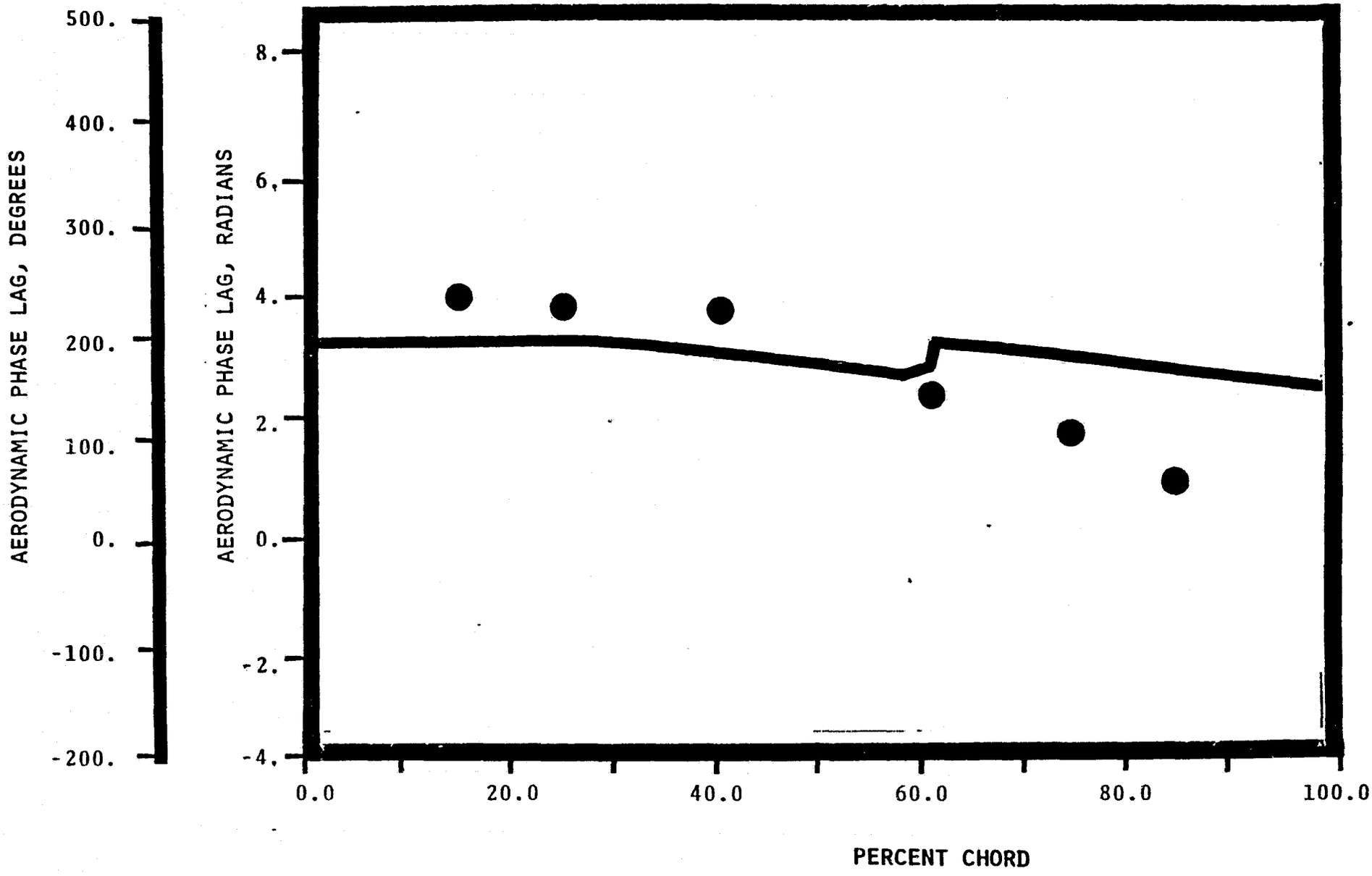

NASA I TORSION CASCADE

PRESSURE SURFACE UNSTEADY PRESSURE DISTRIBUTION

1.315 INLET MACH NUMBER

1.20 STATIC PRESSURE RATIO

-1.57 rad (-90°) INTERBLADE PHASE ANGLE

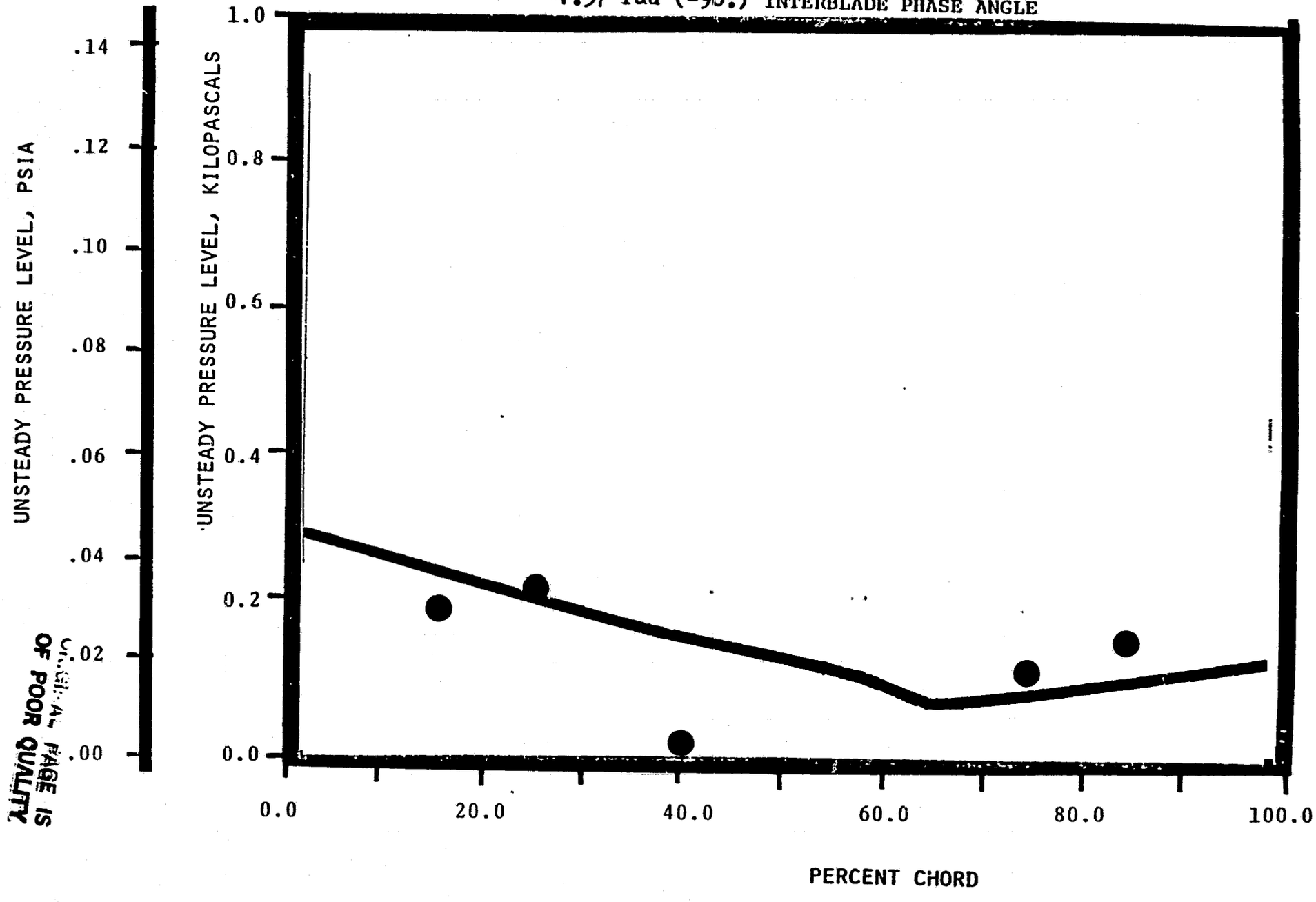

NASA I TORSION CASCADE

SUCTION SURFACE AERODYNAMIC PHASE LAG DISTRIBUTION

1.315 INLET MACH NUMBER

1.20 STATIC PRESSURE RATIO

-1.57 rad (-90.°) INTERBLADE PHASE ANGLE

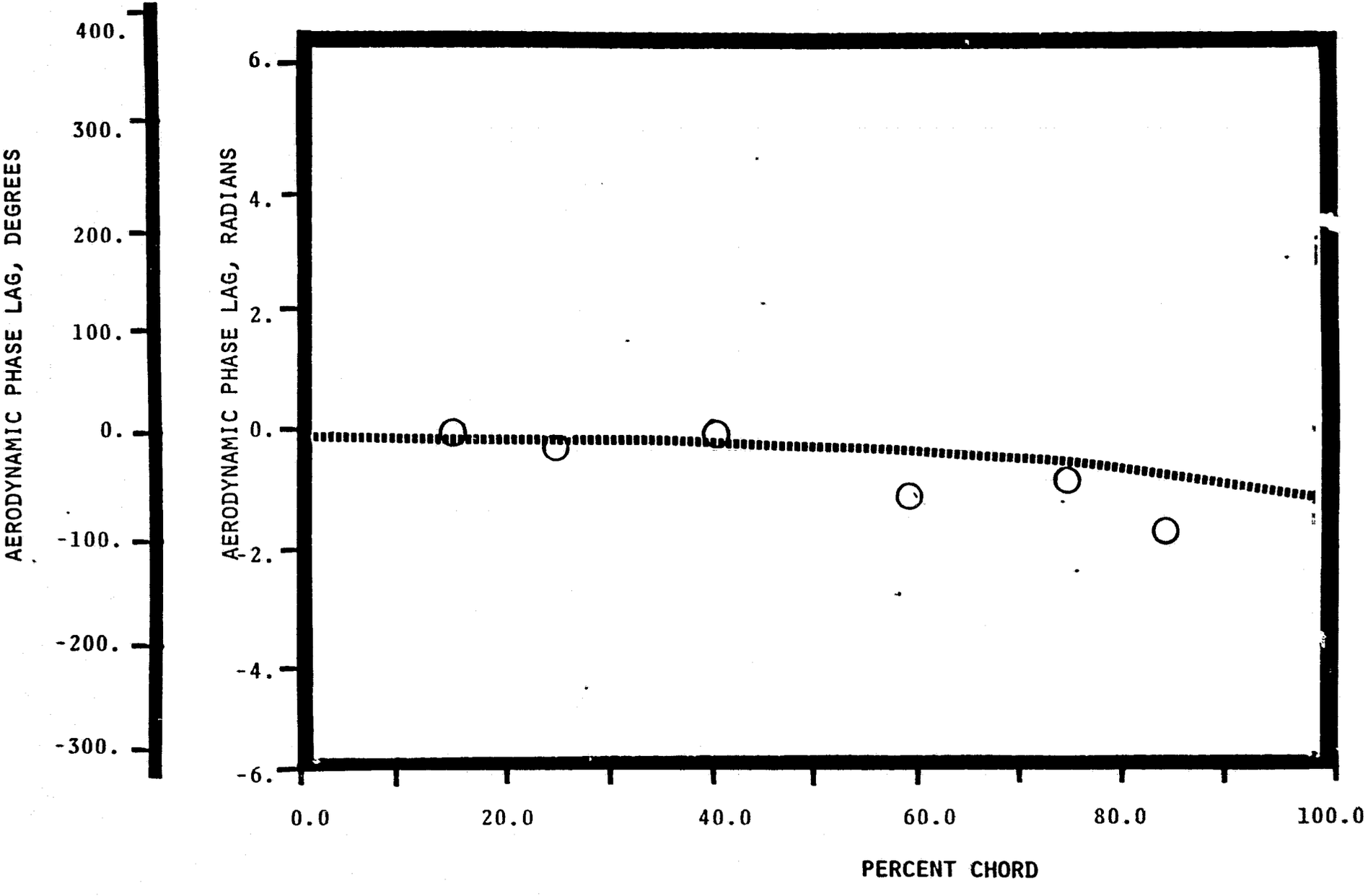

151

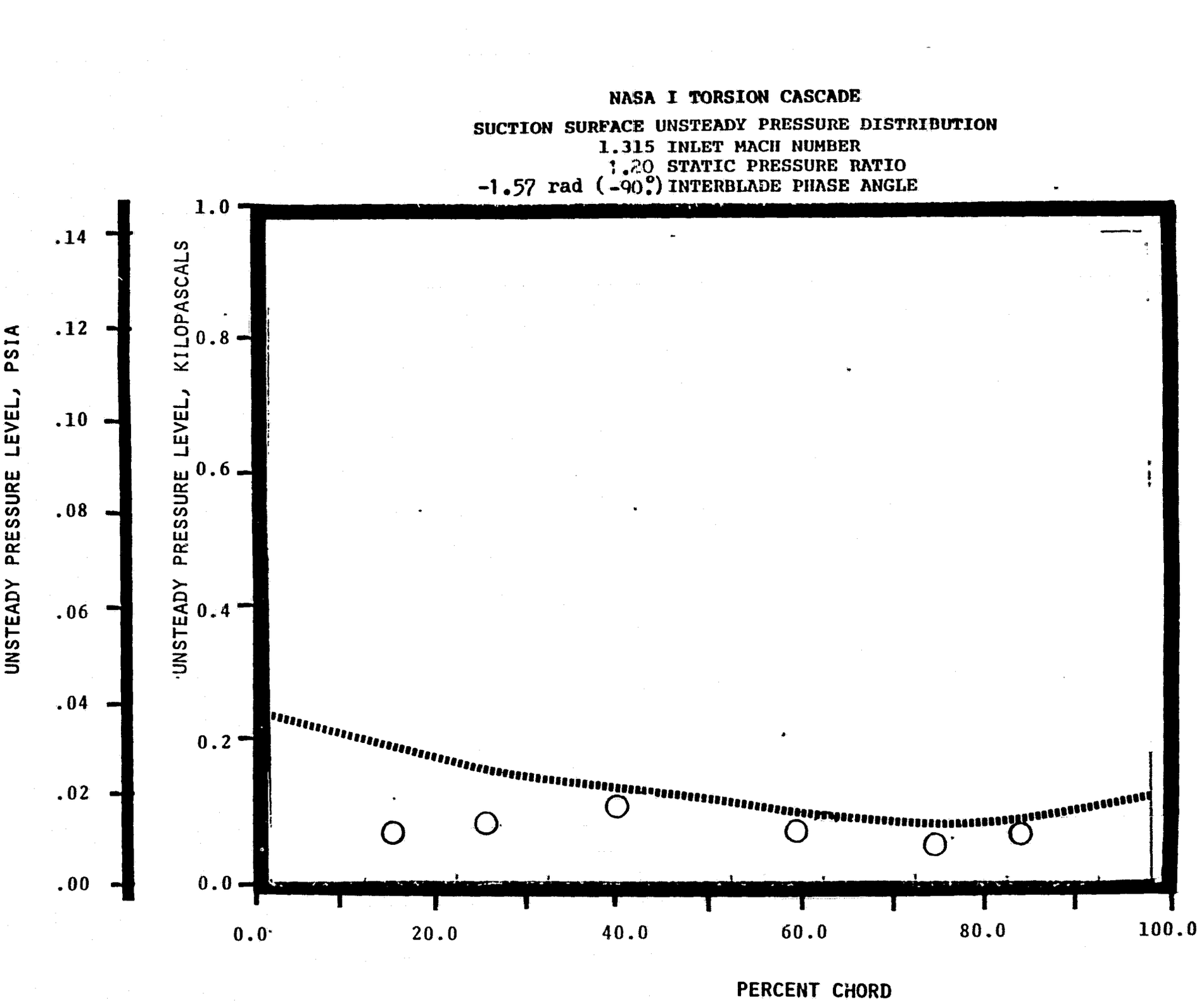
NASA I TORSION CASCADE
SUCTION SURFACE UNSTEADY PRESSURE DISTRIBUTION
1.315 INLET MACH NUMBER
1.20 STATIC PRESSURE RATIO
-1.57 rad (-90°) INTERBLADE PHASE ANGLE
UNSTEADY PRESSURE LEVEL, PSIA
.14
.12
.10
.08
.06
.04
.02
.00
UNSTEADY PRESSURE LEVEL, KILOPASCALS
1.0
0.8
0.6
0.4
0.2
0.0
0.0
20.0
40.0
60.0
80.0
100.0
PERCENT CHORD

NASA I TORSION CASCADE

PRESSURE SURFACE AERODYNAMIC PHASE LAG DISTRIBUTION

1.315 INLET MACH NUMBER

1.35 STATIC PRESSURE RATIO

3.14 rad (180.°)INTERBLADE PHASE ANGLE

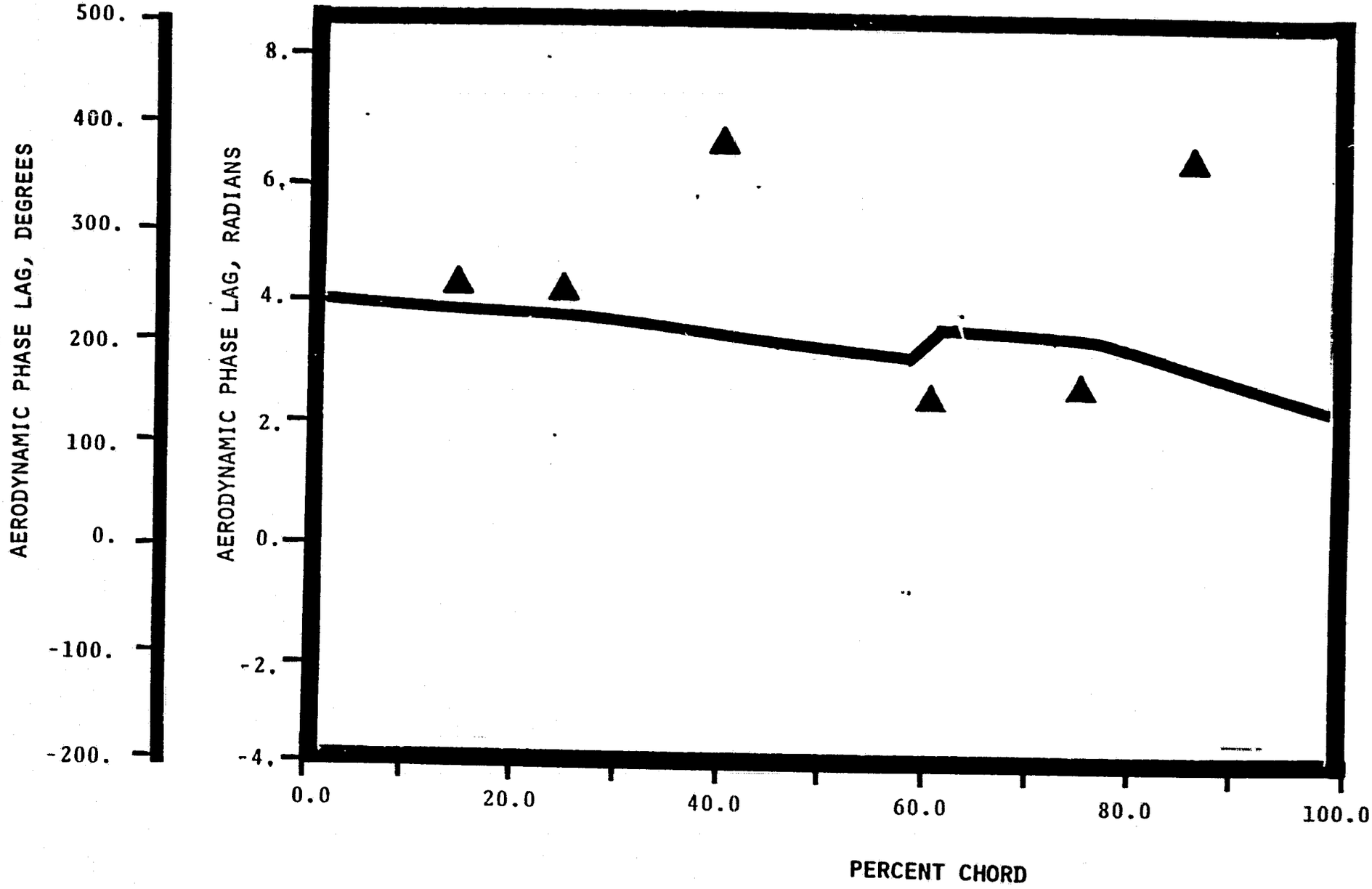

NASA I TORSION CASCADE

PRESSURE SURFACE UNSTEADY PRESSURE DISTRIBUTION

1.315 INLET MACH NUMBER

1.35 STATIC PRESSURE RATIO

3.14 rad (180.°) INTERBLADE PHASE ANGLE

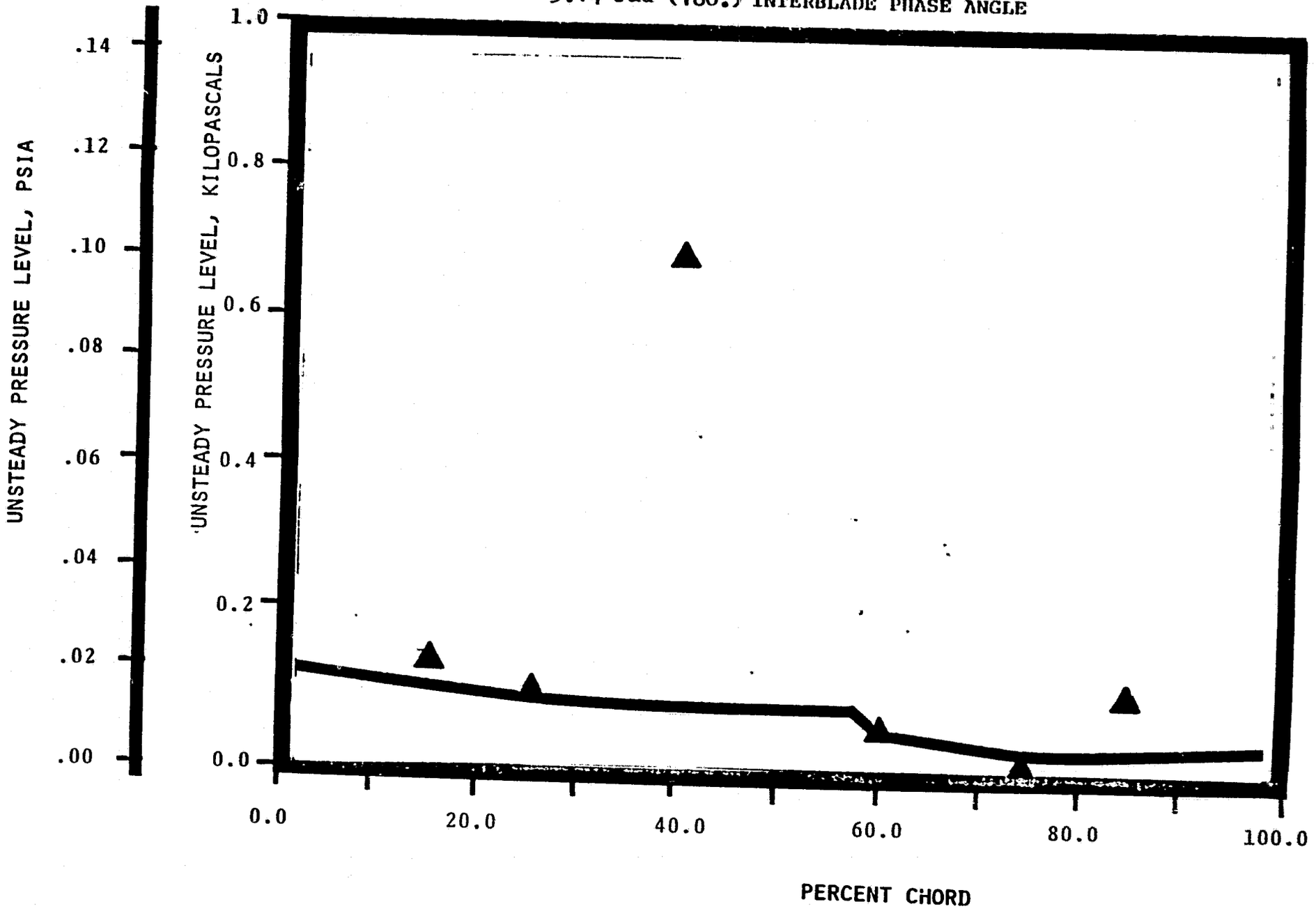

NASA I TORSION CASCADE

SUCTION SURFACE AERODYNAMIC PHASE LAG DISTRIBUTION

1.315 INLET MACH NUMBER

1.35 STATIC PRESSURE RATIO

3.14 rad (180°) INTERBLADE PHASE ANGLE

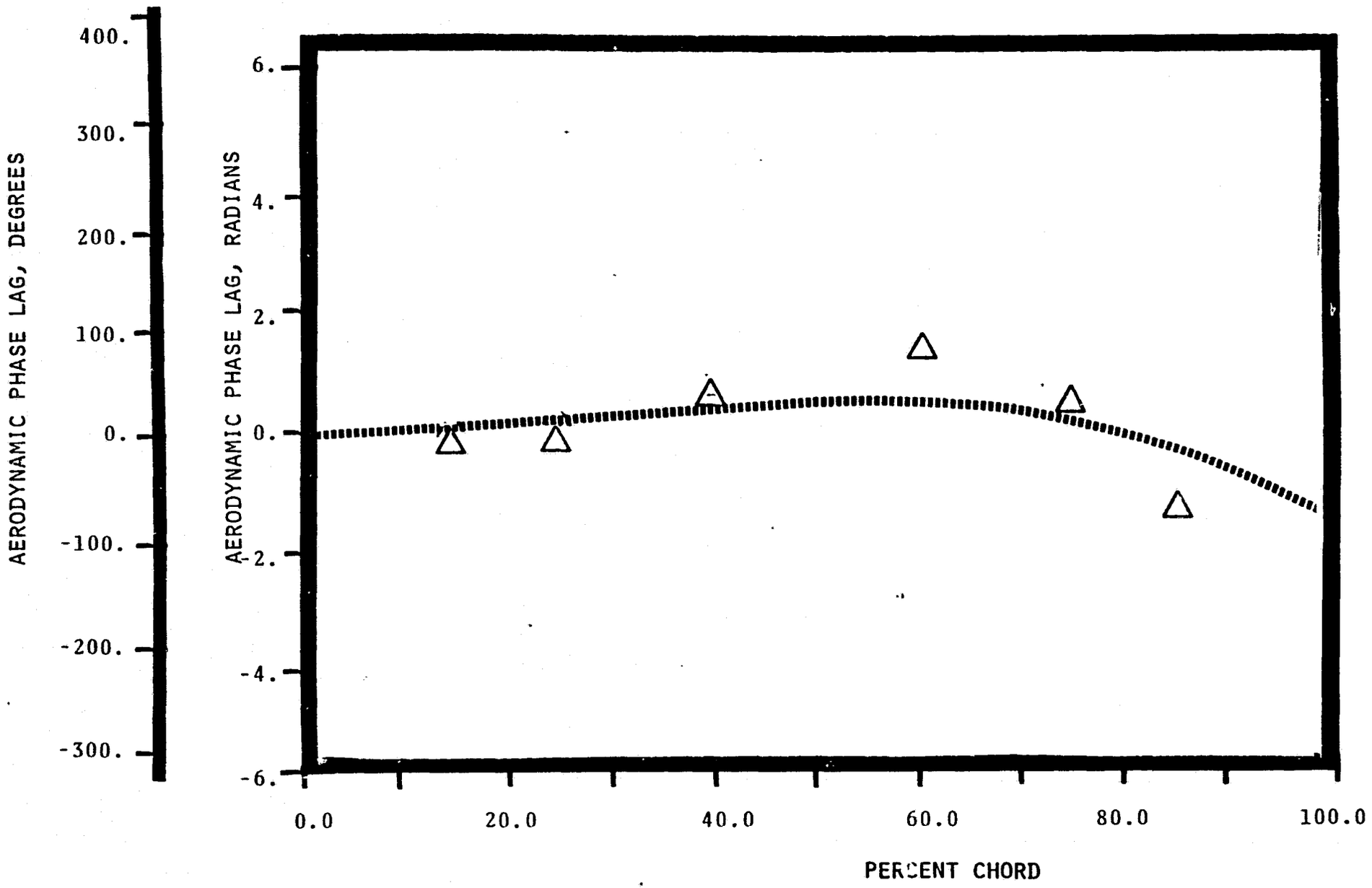

NASA I TORSION CASCADE

SUCTION SURFACE UNSTEADY PRESSURE DISTRIBUTION

1.315 INLET MACH NUMBER

1.35 STATIC PRESSURE RATIO

3.14 rad (180.°) INTERBLADE PHASE ANGLE

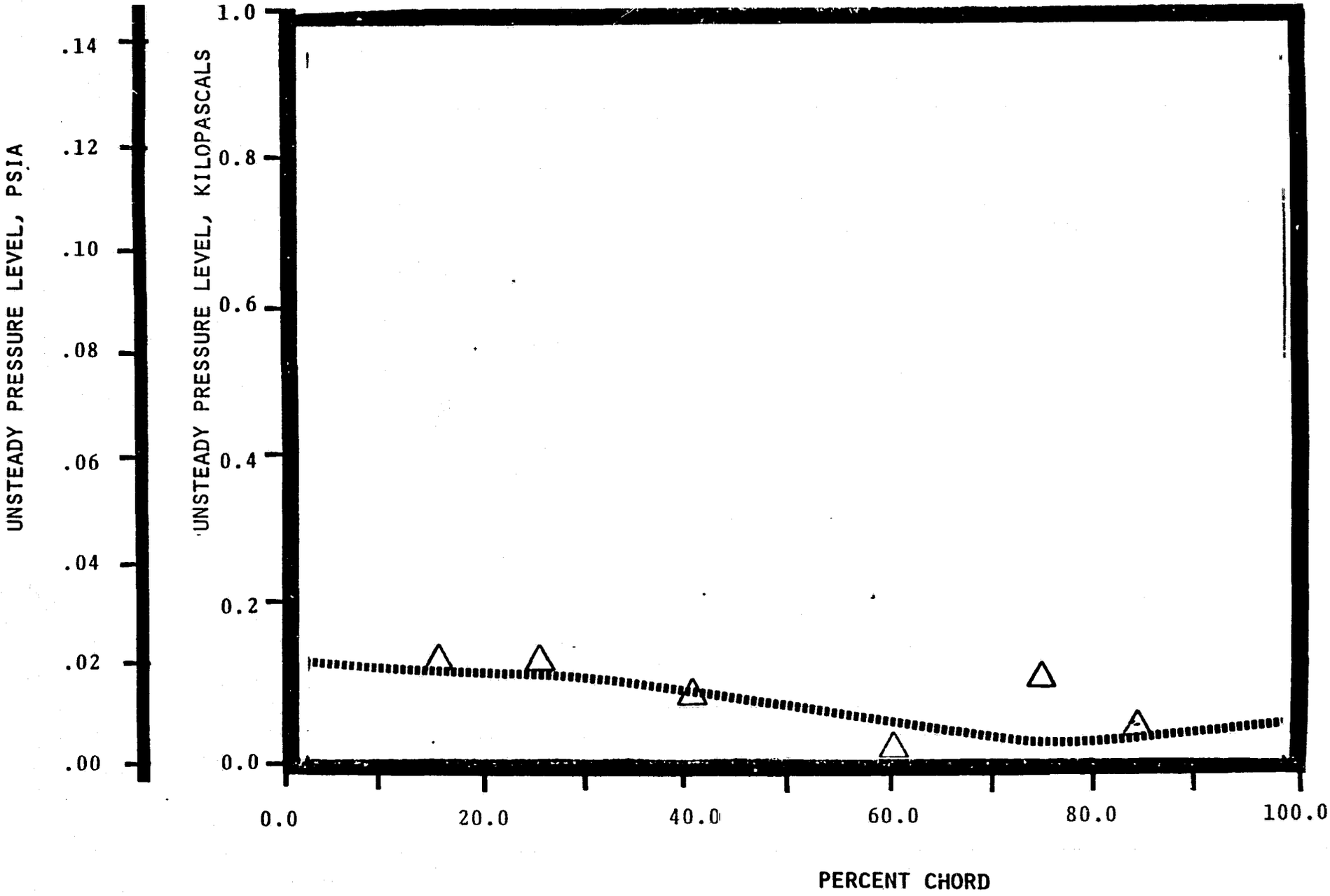

NASA I TORSION CASCADE

PRESSURE SURFACE AERODYNAMIC PHASE LAG DISTRIBUTION
1.315 INLET MACH NUMBER
1.35 STATIC PRESSURE RATIO
1.57 rad (90.°) INTERBLADE PHASE ANGLE (1.57 rad.)

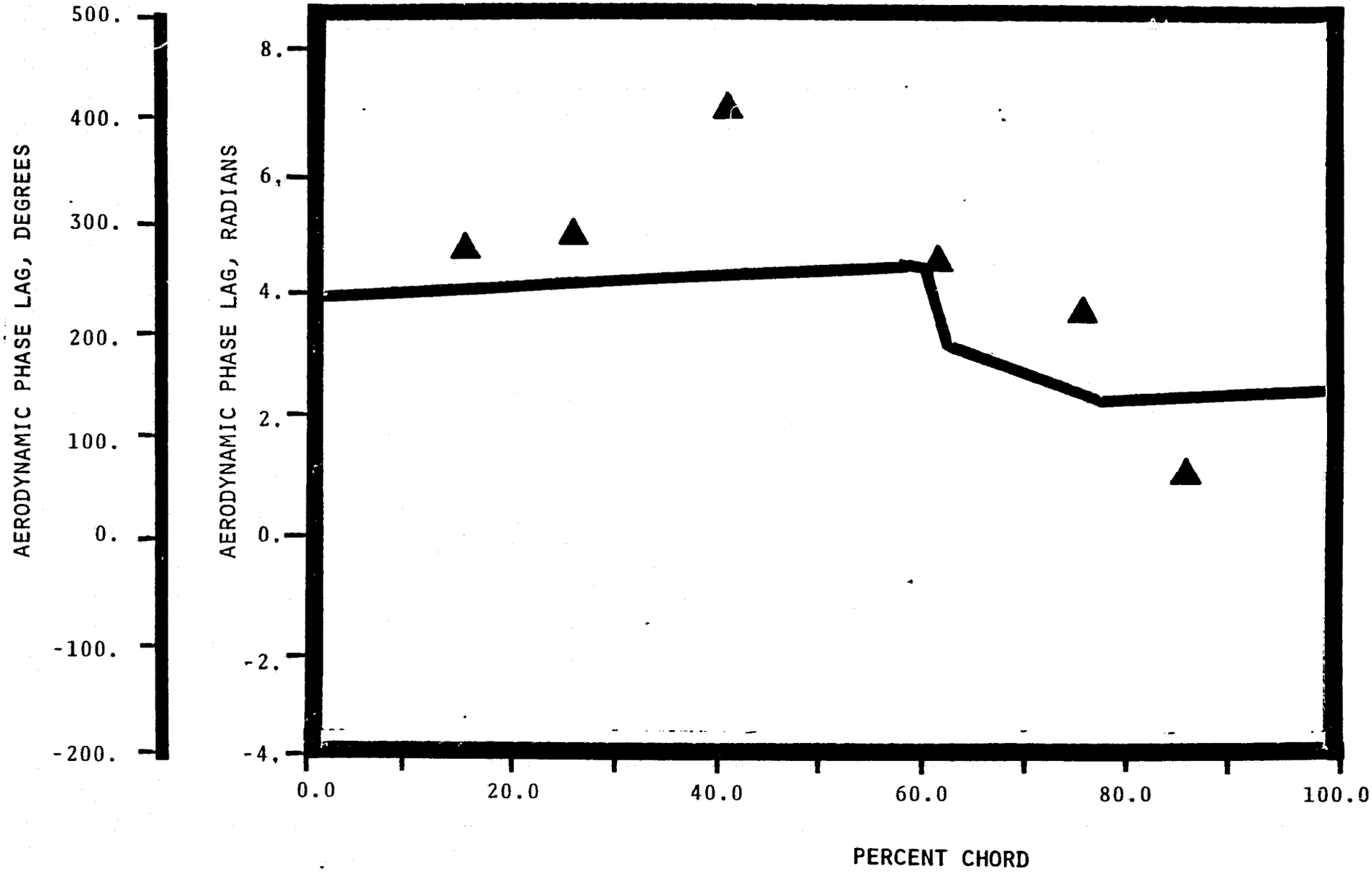

NASA I TORSION CASCADE

PRESSURE SURFACE UNSTEADY PRESSURE DISTRIBUTION

1.315 INLET MACH NUMBER

1.35 STATIC PRESSURE RATIO

1.57 rad (90.°) INTERBLADE PHASE ANGLE (1.57 rad.)

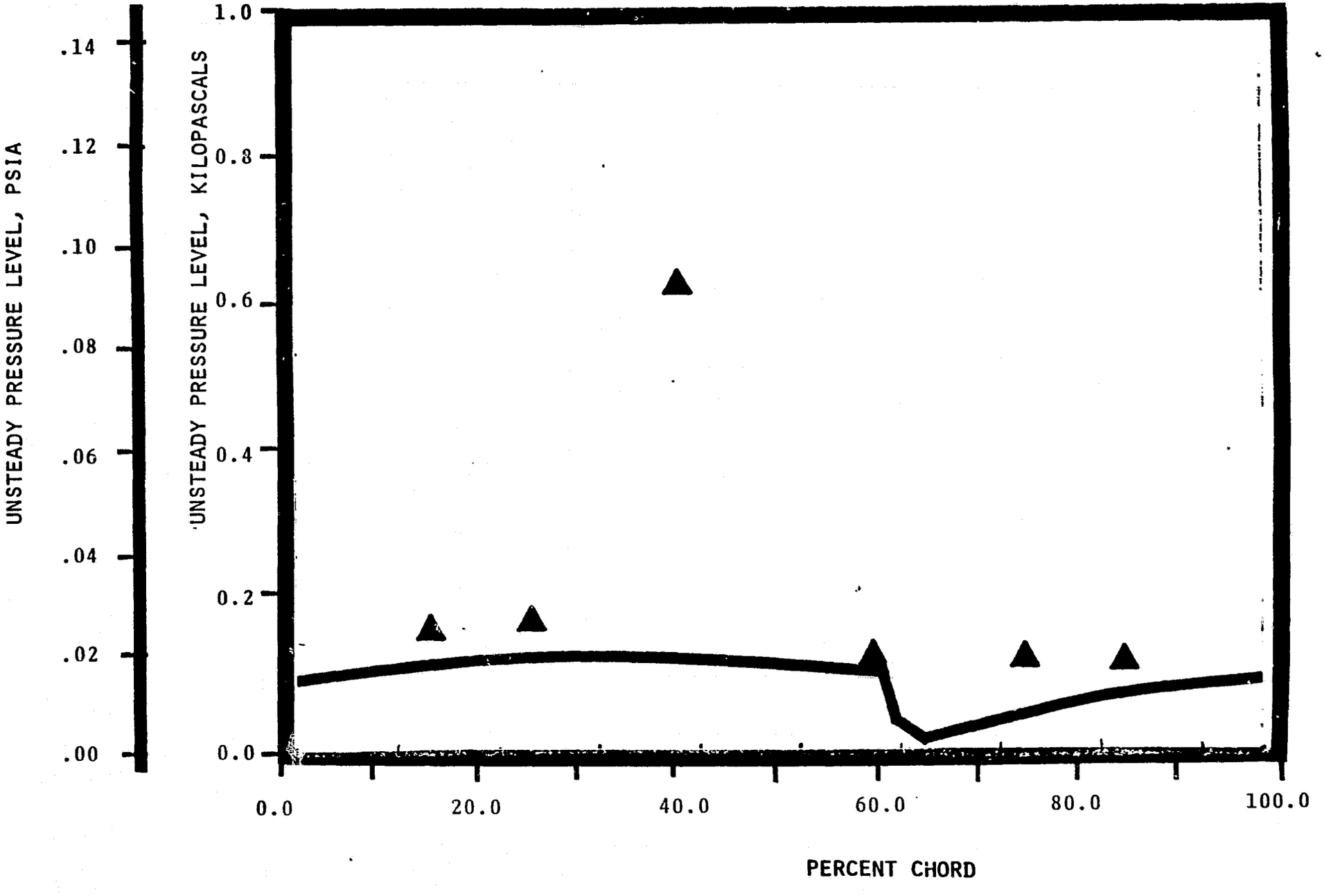

NASA I TORSION CASCADE

SUCTION SURFACE AERODYNAMIC PHASE LAG DISTRIBUTION

1.315 INLET MACH NUMBER

1.35 STATIC PRESSURE RATIO

1.57 rad (90.°) INTERBLADE PHASE ANGLE (1.57 rad.)

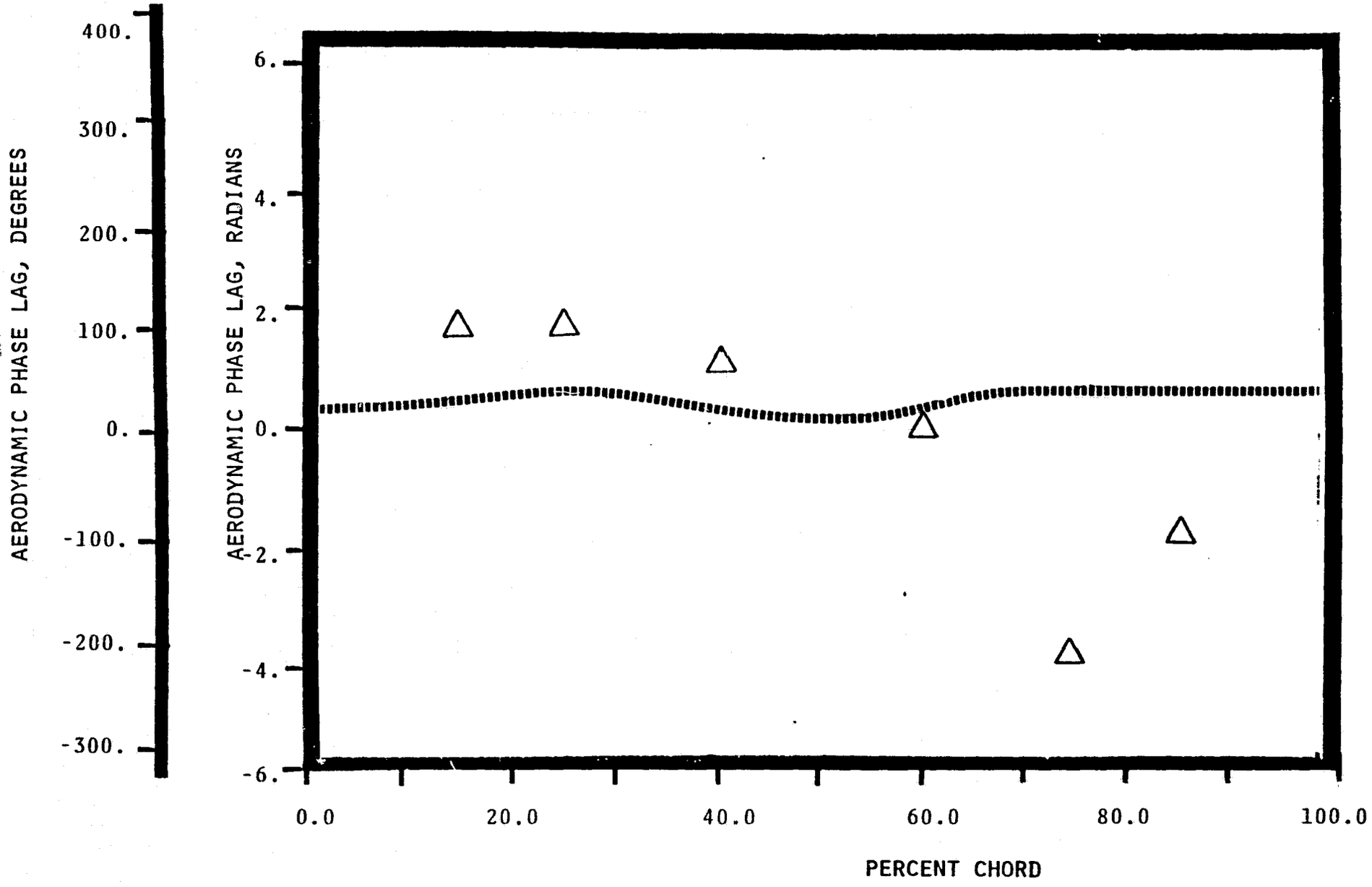

NASA I TORSION CASCADE

SUCTION SURFACE UNSTEADY PRESSURE DISTRIBUTION

1.315 INLET MACH NUMBER

1.35 STATIC PRESSURE RATIO

1.57 rad (90°) INTERBLADE PHASE ANGLE (1.57 rad.)

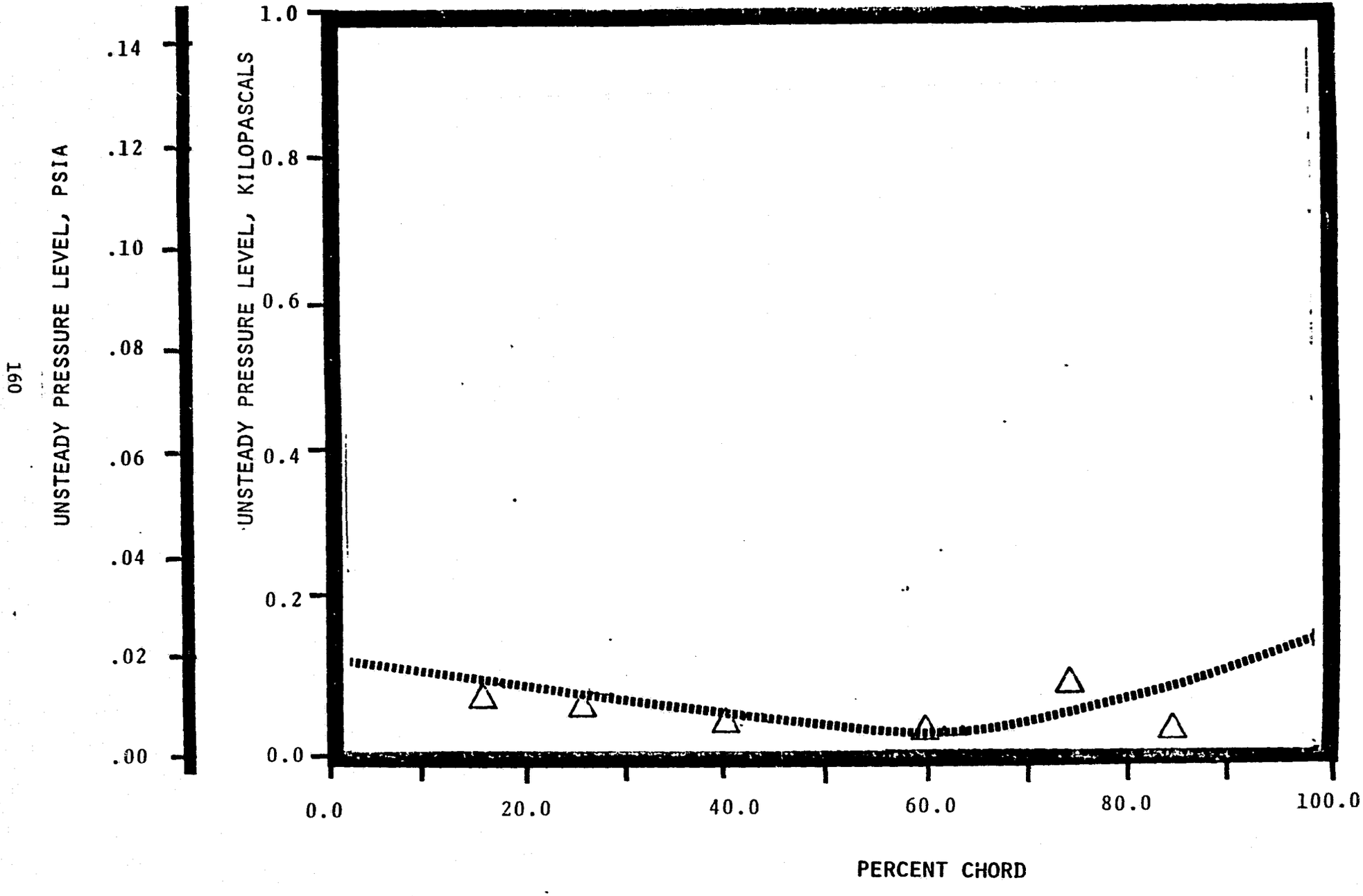

160

NASA I TORSION CASCADE

SUCTION SURFACE UNSTEADY PRESSURE DISTRIBUTION

1.315 INLET MACH NUMBER

1.35 STATIC PRESSURE RATIO

0.0 rad (0^{o}) INTERBLADE PHASE ANGLE

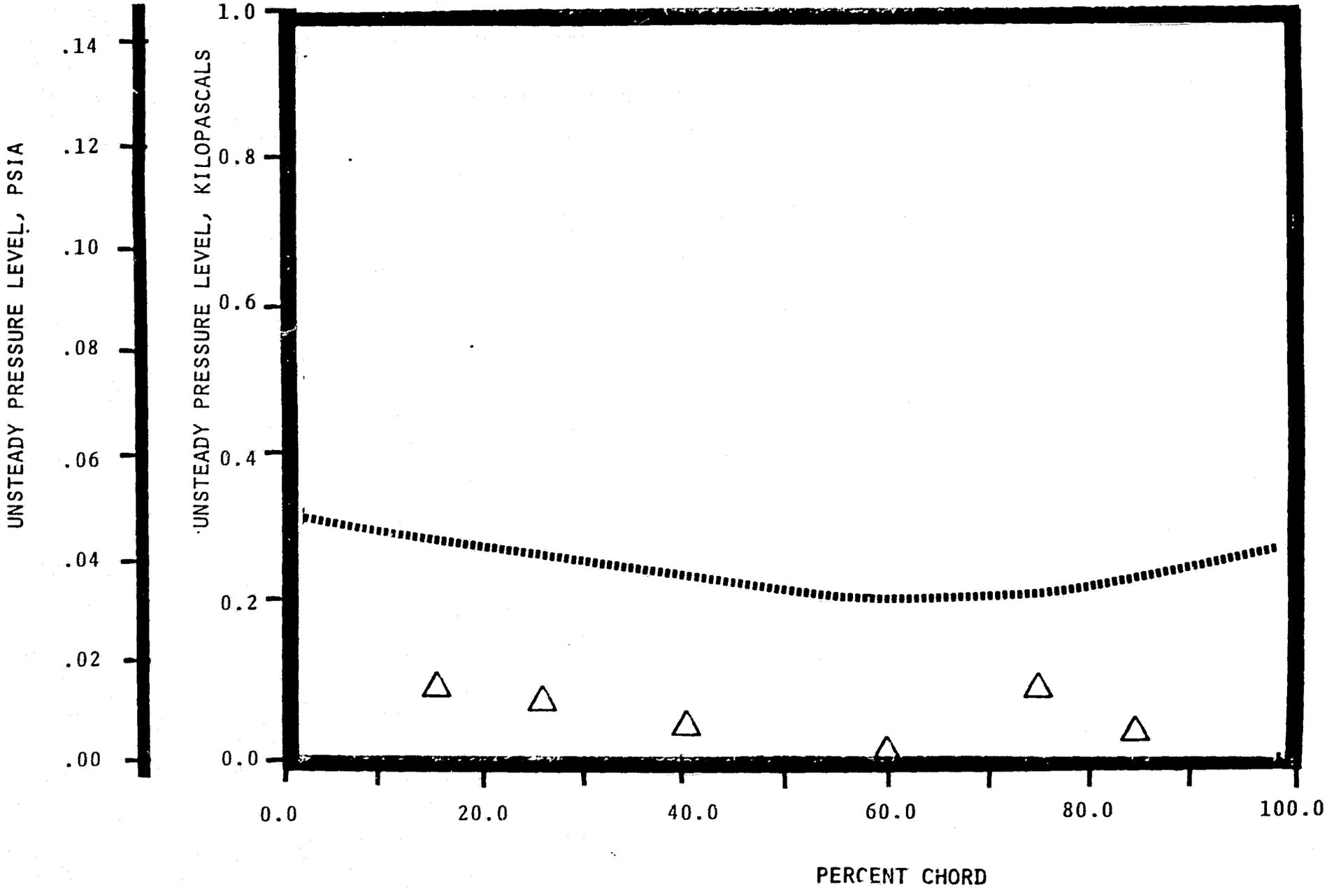

NASA I TORSION CASCADE

PRESSURE SURFACE UNSTEADY PRESSURE DISTRIBUTION
1.315 INLET MACH NUMBER
1.35 STATIC PRESSURE RATIO
0.0 rad (0°) INTERBLADE PHASE ANGLE

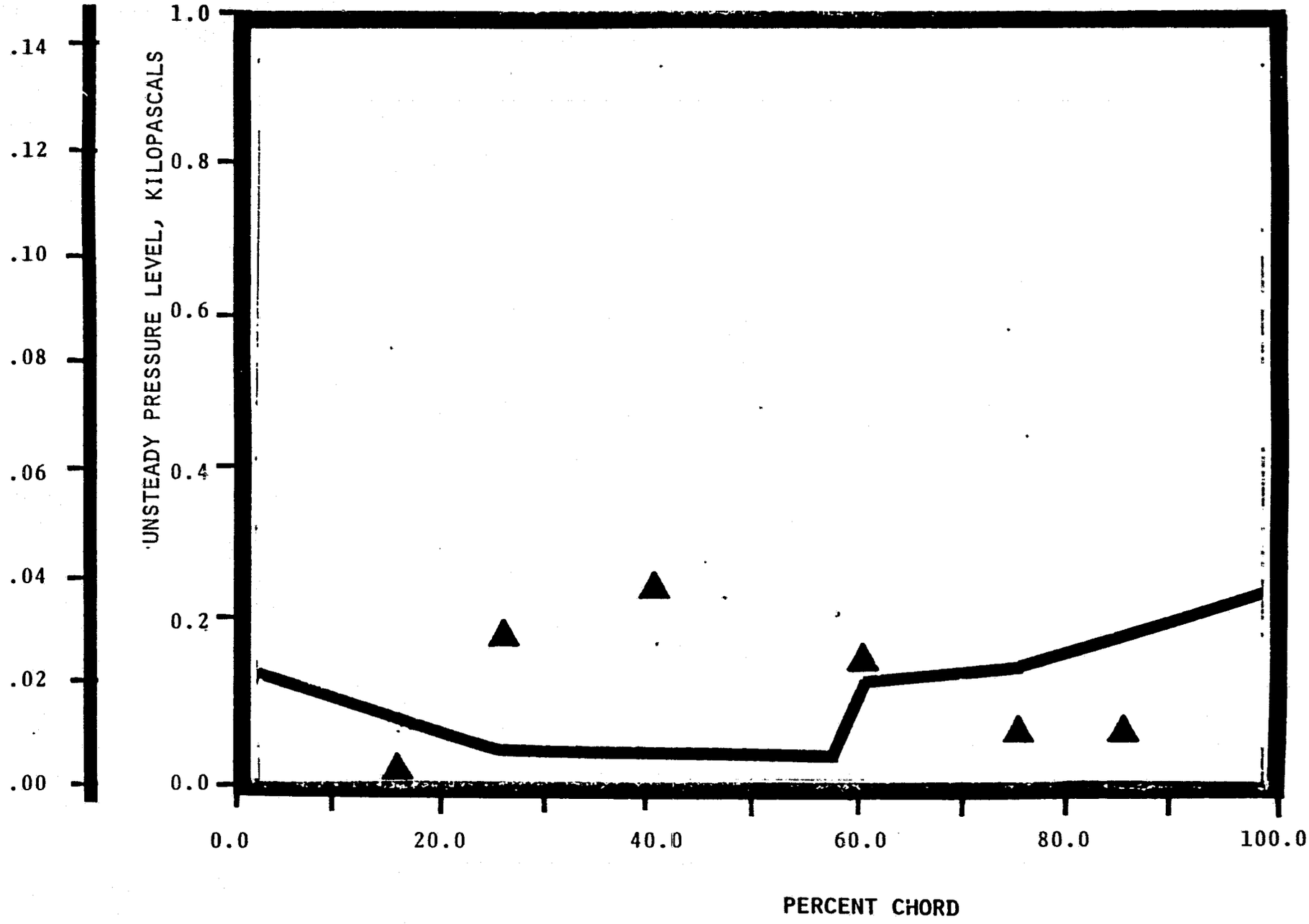

NASA I TORSION CASCADE

SUCTION SURFACE AERODYNAMIC PHASE LAG DISTRIBUTION

1.315 INLET MACH NUMBER

1.35 STATIC PRESSURE RATIO

0.0 rad(0°) INTERBLADE PHASE ANGLE

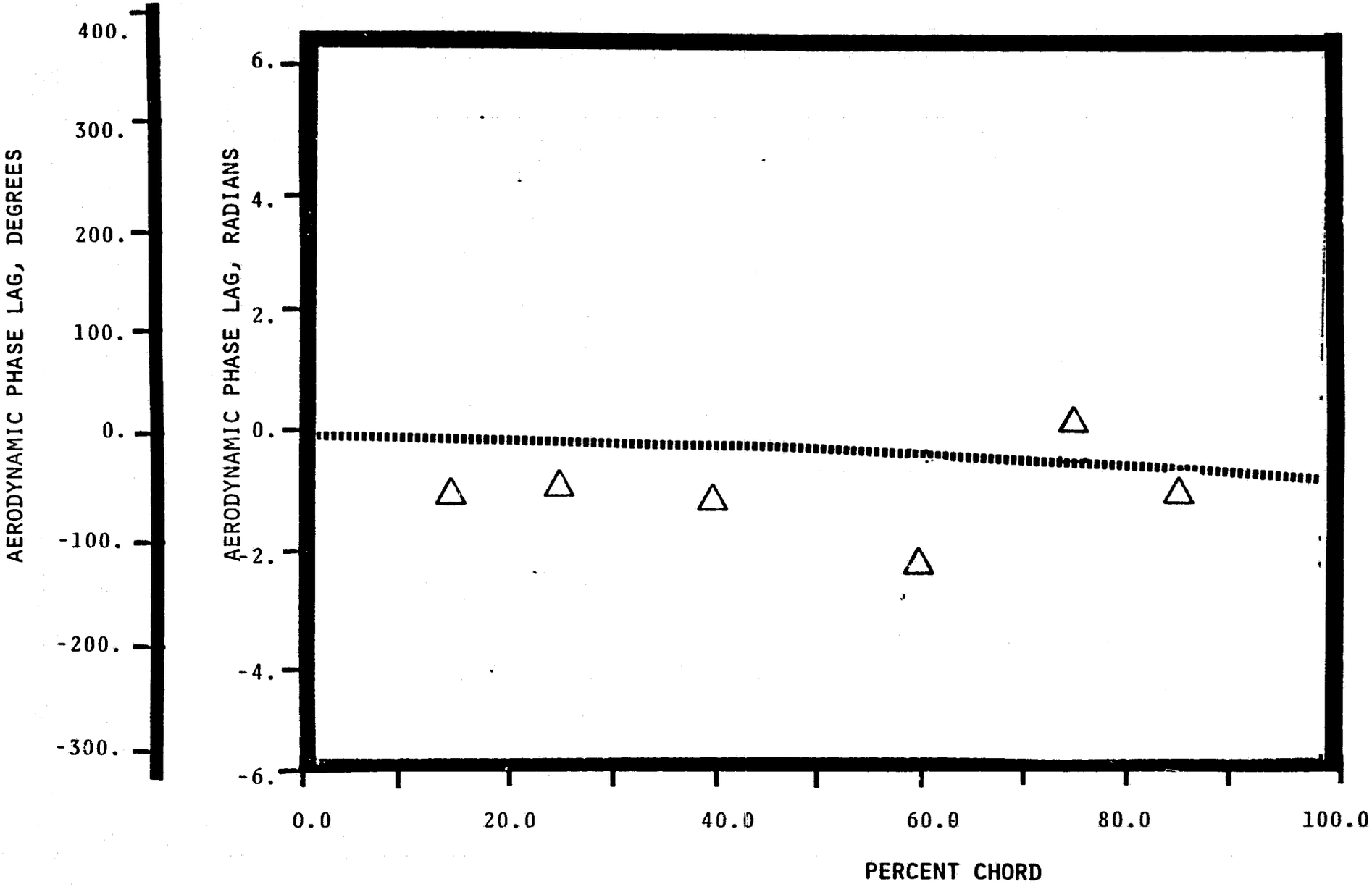

NASA I TORSION CASCADE

PRESSURE SURFACE AERODYNAMIC PHASE LAG DISTRIBUTION
1.315 INLET MACH NUMBER
1.35 STATIC PRESSURE RATIO
0.0 rad(0^{o}) INTERBLADE PHASE ANGLE

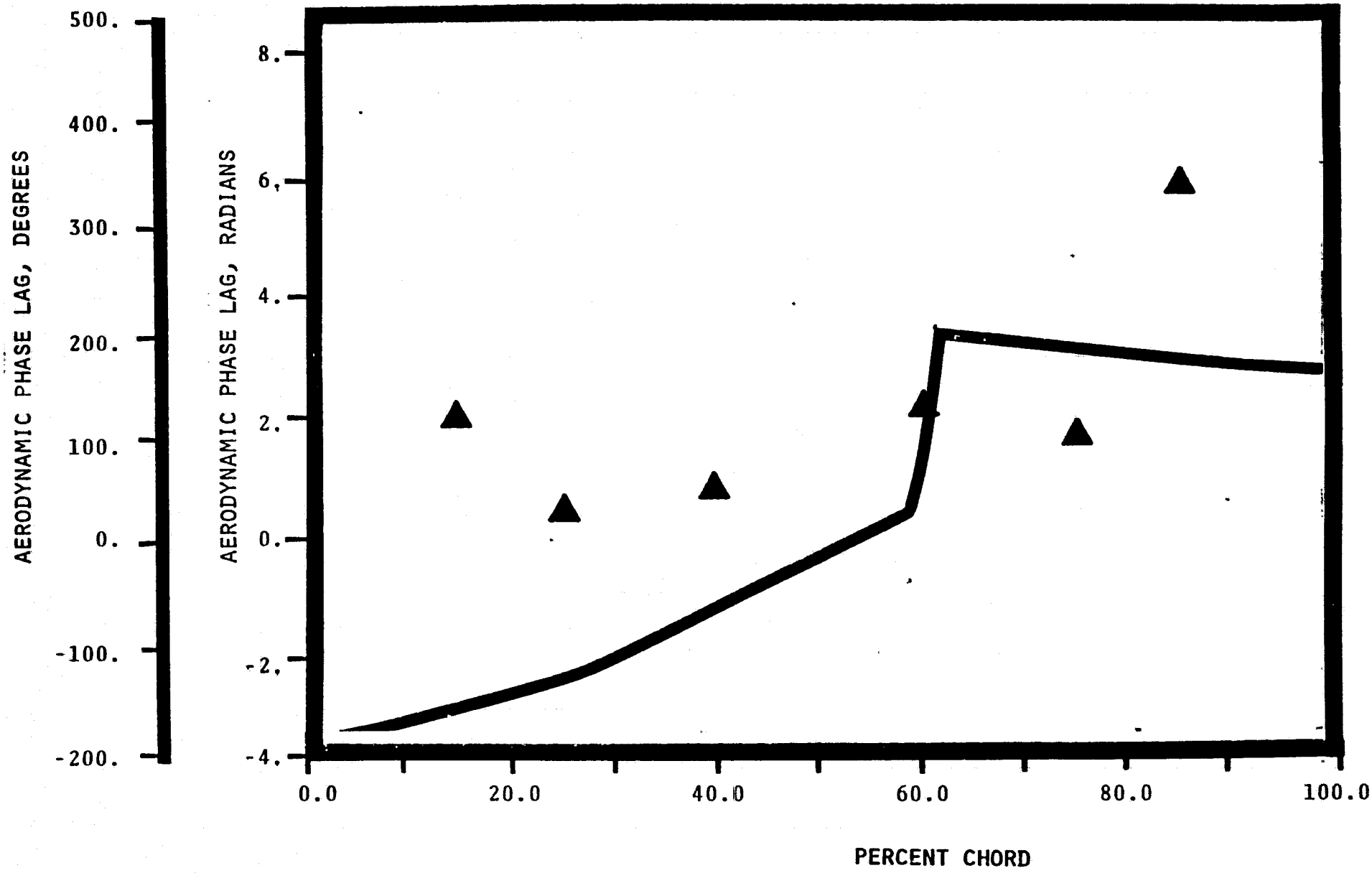

NASA I TORSION CASCADE

PRESSURE SURFACE AERODYNAMIC PHASE LAG DISTRIBUTION

1.315 INLET MACH NUMBER

1.35 STATIC PRESSURE RATIO

-.35 rad (-20°) INTERBLADE PHASE ANGLE

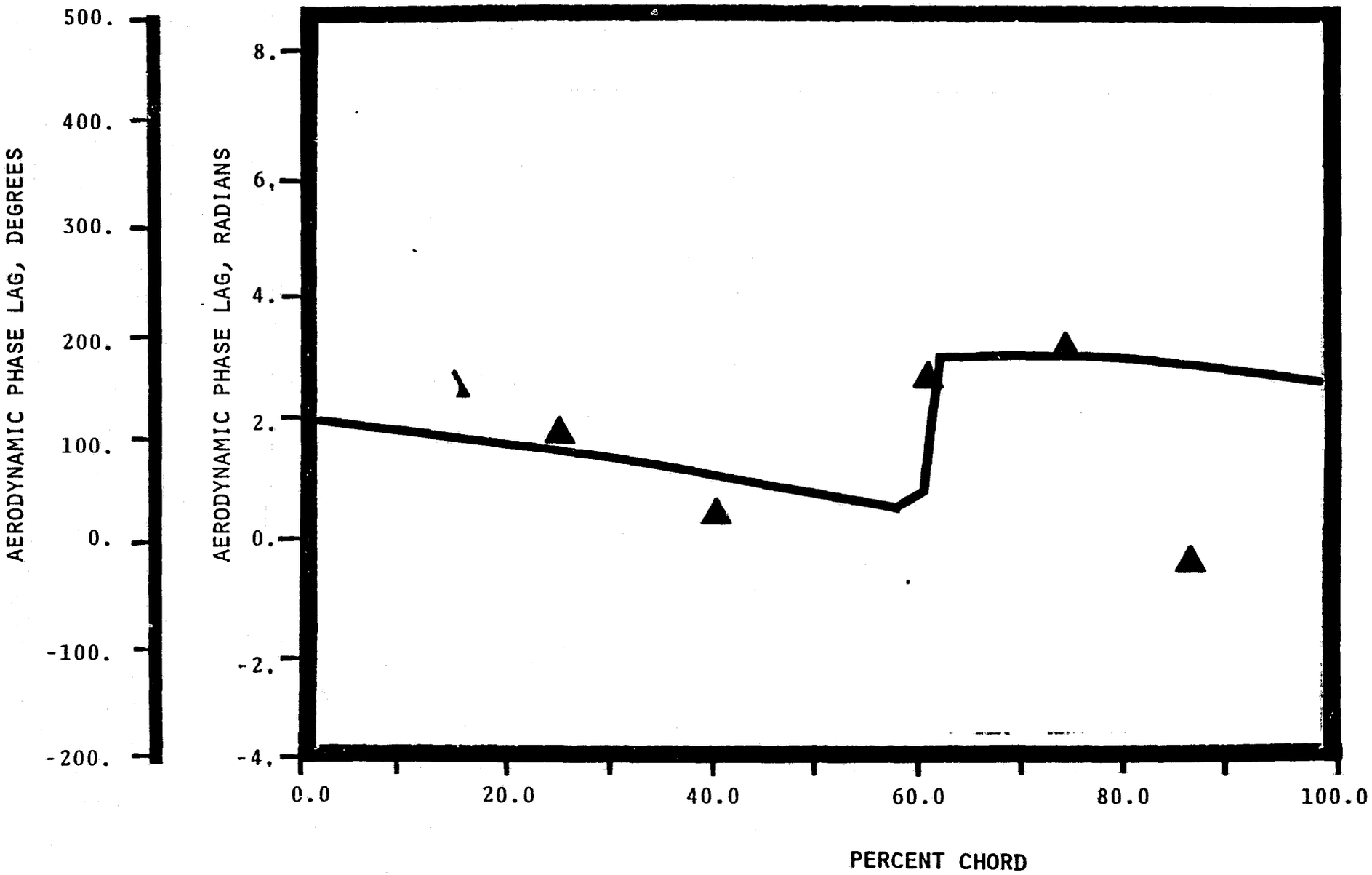

NASA I TORSION CASCADE

PRESSURE SURFACE UNSTEADY PRESSURE DISTRIBUTION
1.315 INLET MACH NUMBER
1.35 STATIC PRESSURE RATIO
-.35 rad (-20°) INTERBLADE PHASE ANGLE

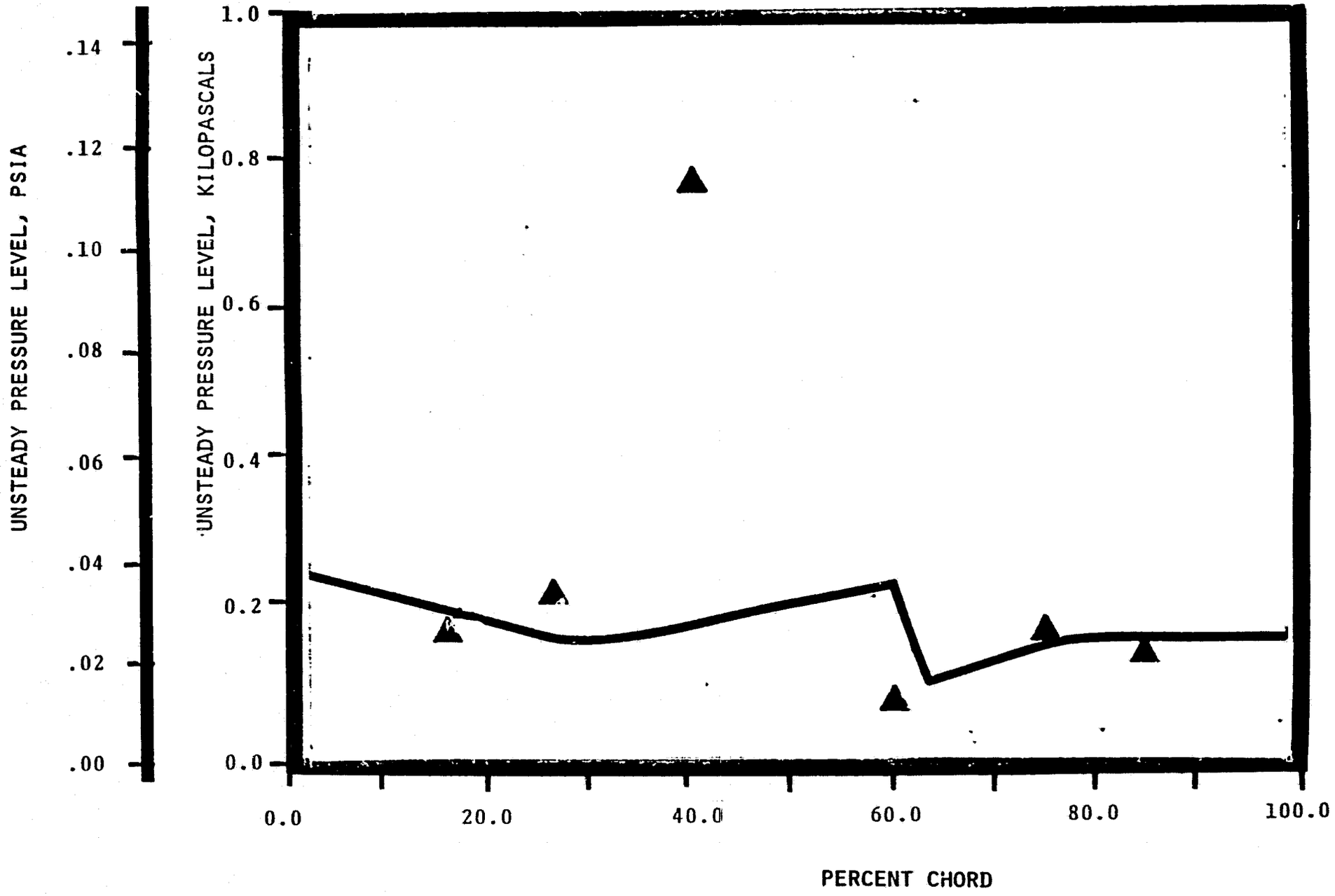

NASA I TORSION CASCADE

SUCTION SURFACE AERODYNAMIC PHASE LAG DISTRIBUTION

1.315 INLET MACH NUMBER

1.35 STATIC PRESSURE RATIO

-.35 rad (-20.°)INTERBLADE PHASE ANGLE

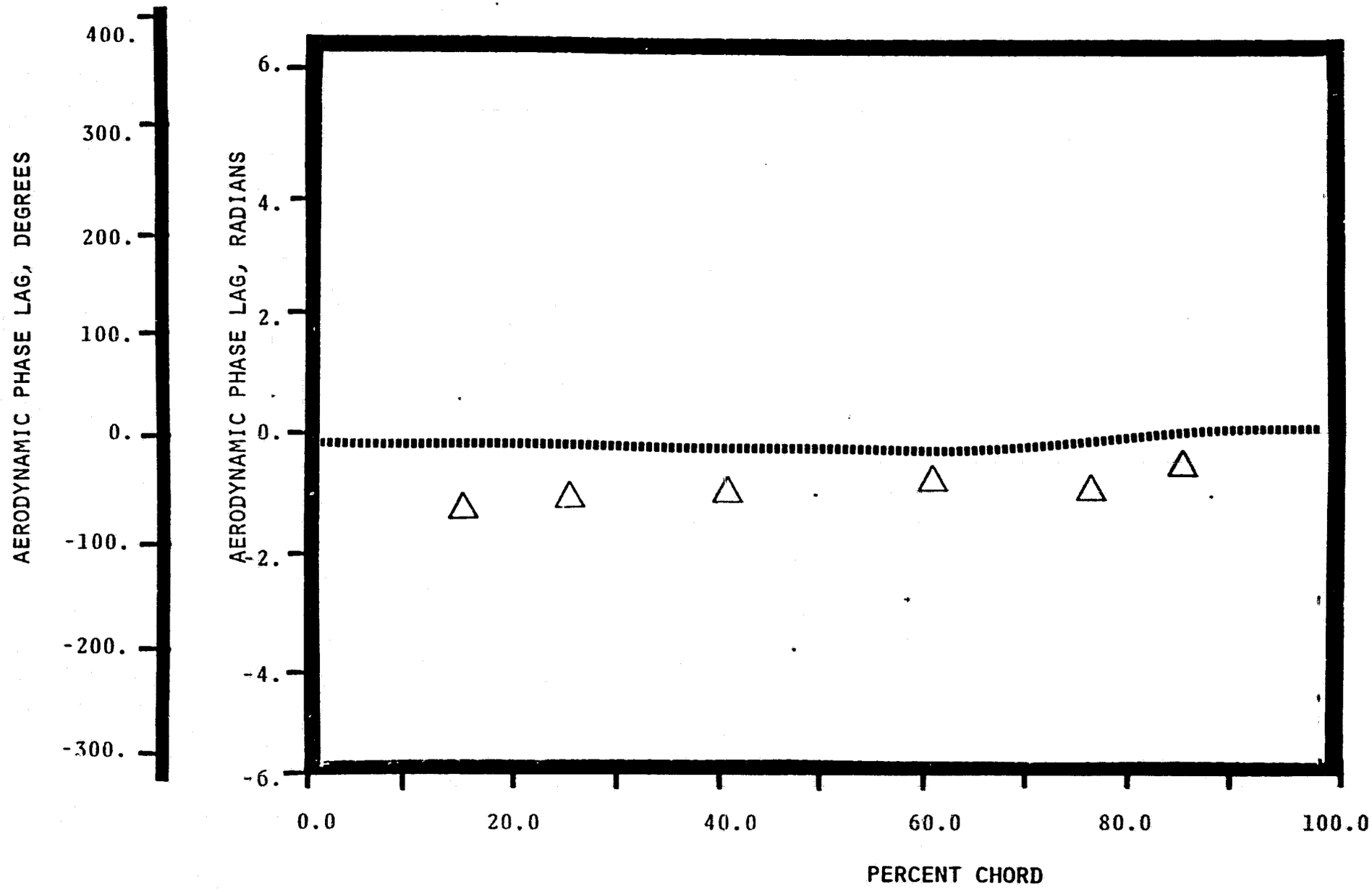

NASA I TORSION CASCADE

SUCTION SURFACE UNSTEADY PRESSURE DISTRIBUTION

1.315 INLET MACH NUMBER

1.35 STATIC PRESSURE RATIO

-.35 rad (-20°) INTERBLADE PHASE ANGLE

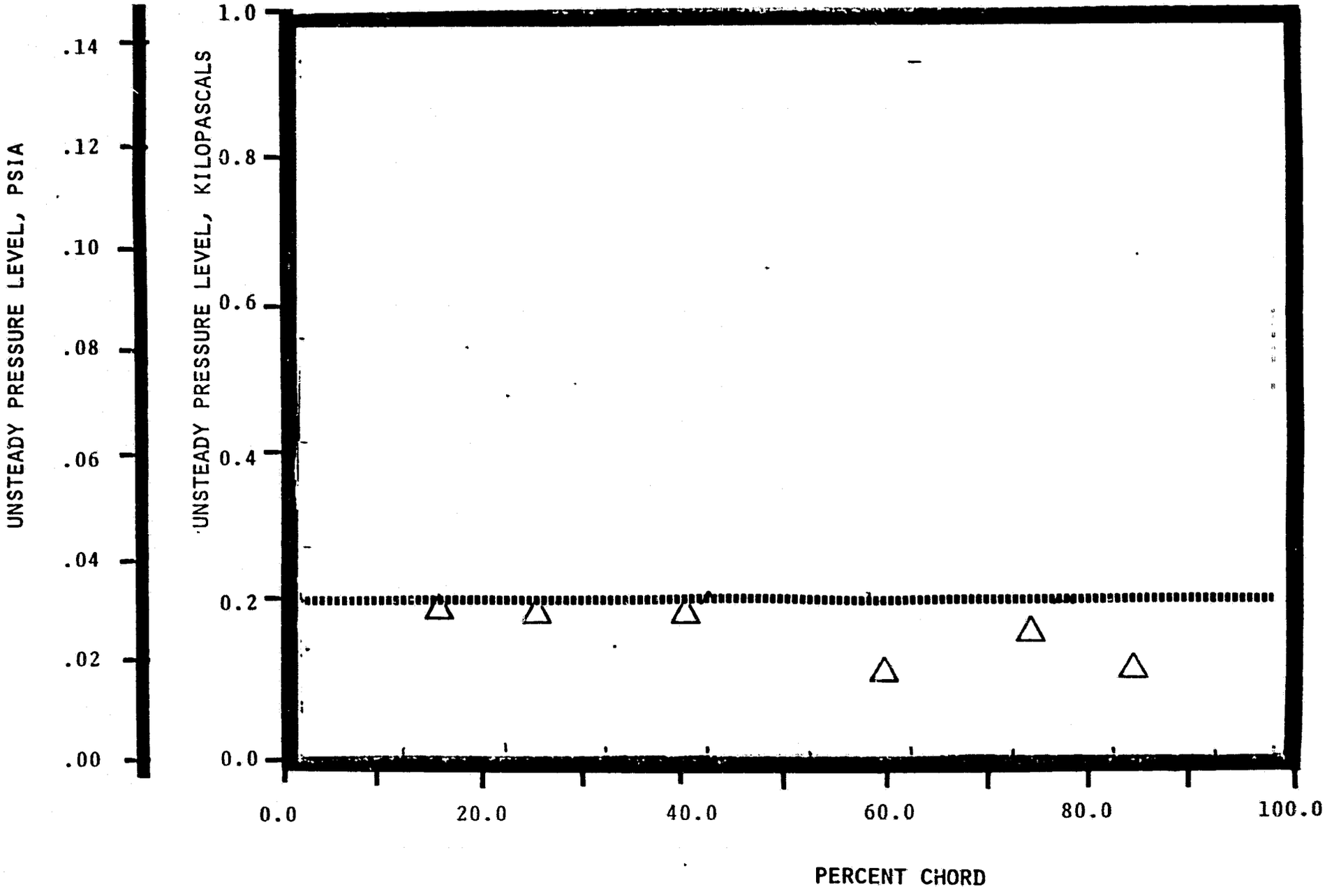

NASA I TORSION CASCADE

PRESSURE SURFACE AERODYNAMIC PHASE LAG DISTRIBUTION
1.315 INLET MACH NUMBER
1.35 STATIC PRESSURE RATIO
-.70 rad (-40.°) INTERBLADE PHASE ANGLE

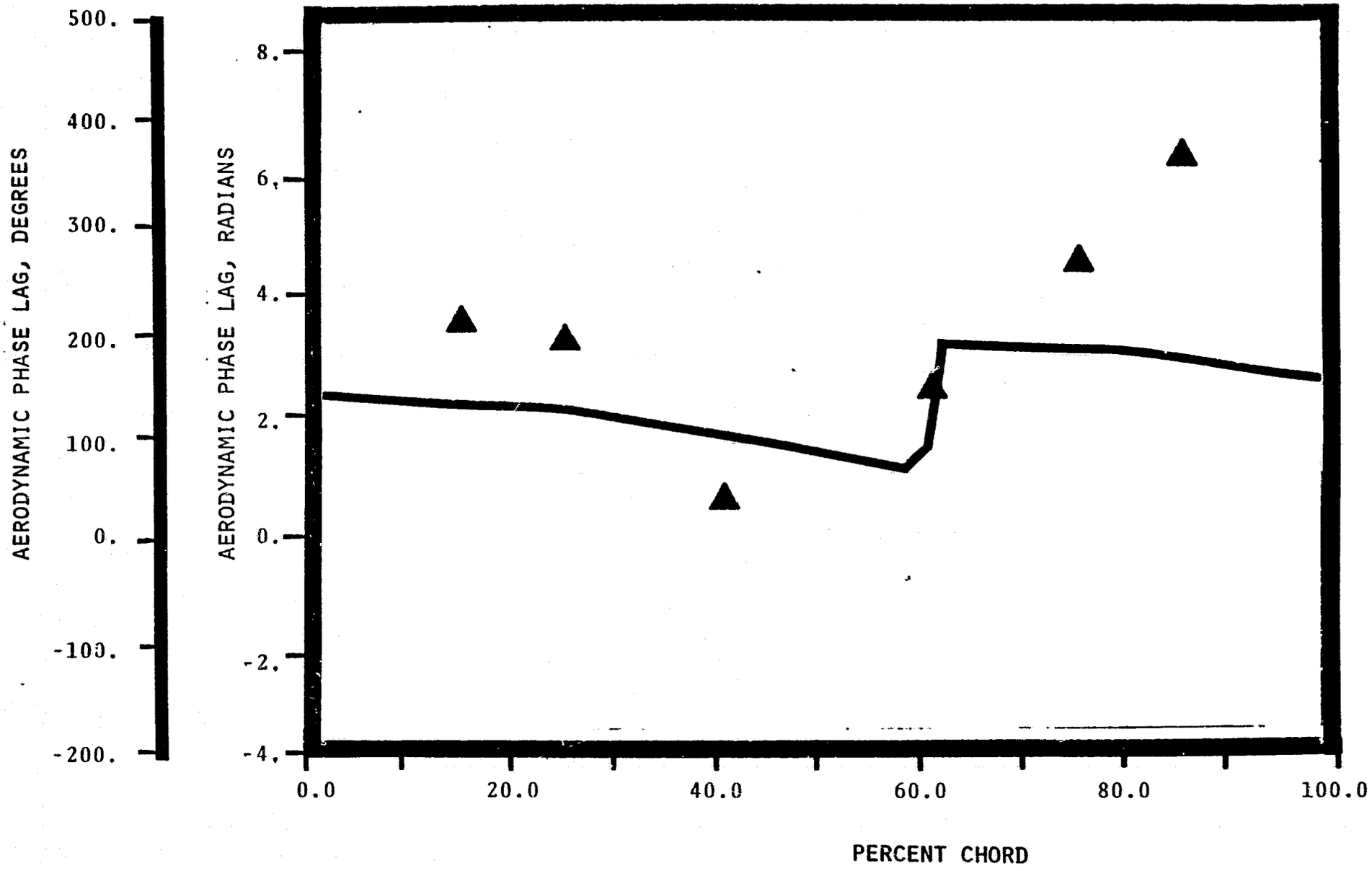

69I

NASA I TORSION CASCADE

PRESSURE SURFACE UNSTEADY PRESSURE DISTRIBUTION
1.315 INLET MACH NUMBER
1.35 STATIC PRESSURE RATIO
-.70 rad (-40°) INTERBLADE PHASE ANGLE

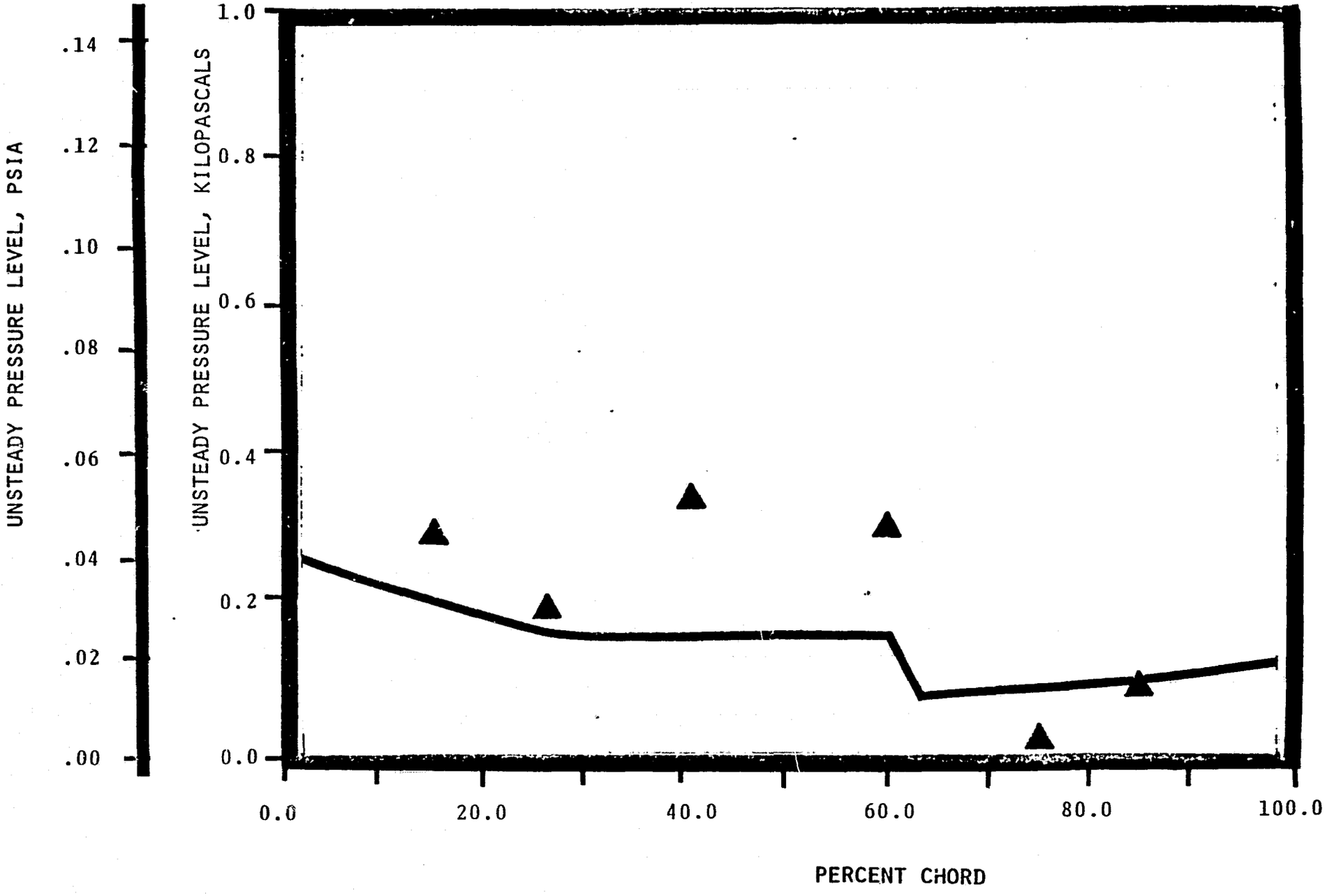

NASA I TORSION CASCADE

SUCTION SURFACE AERODYNAMIC PHASE LAG DISTRIBUTION

1.315 INLET MACH NUMBER

1.35 STATIC PRESSURE RATIO

-.70 rad (-40°) INTERBLADE PHASE ANGLE

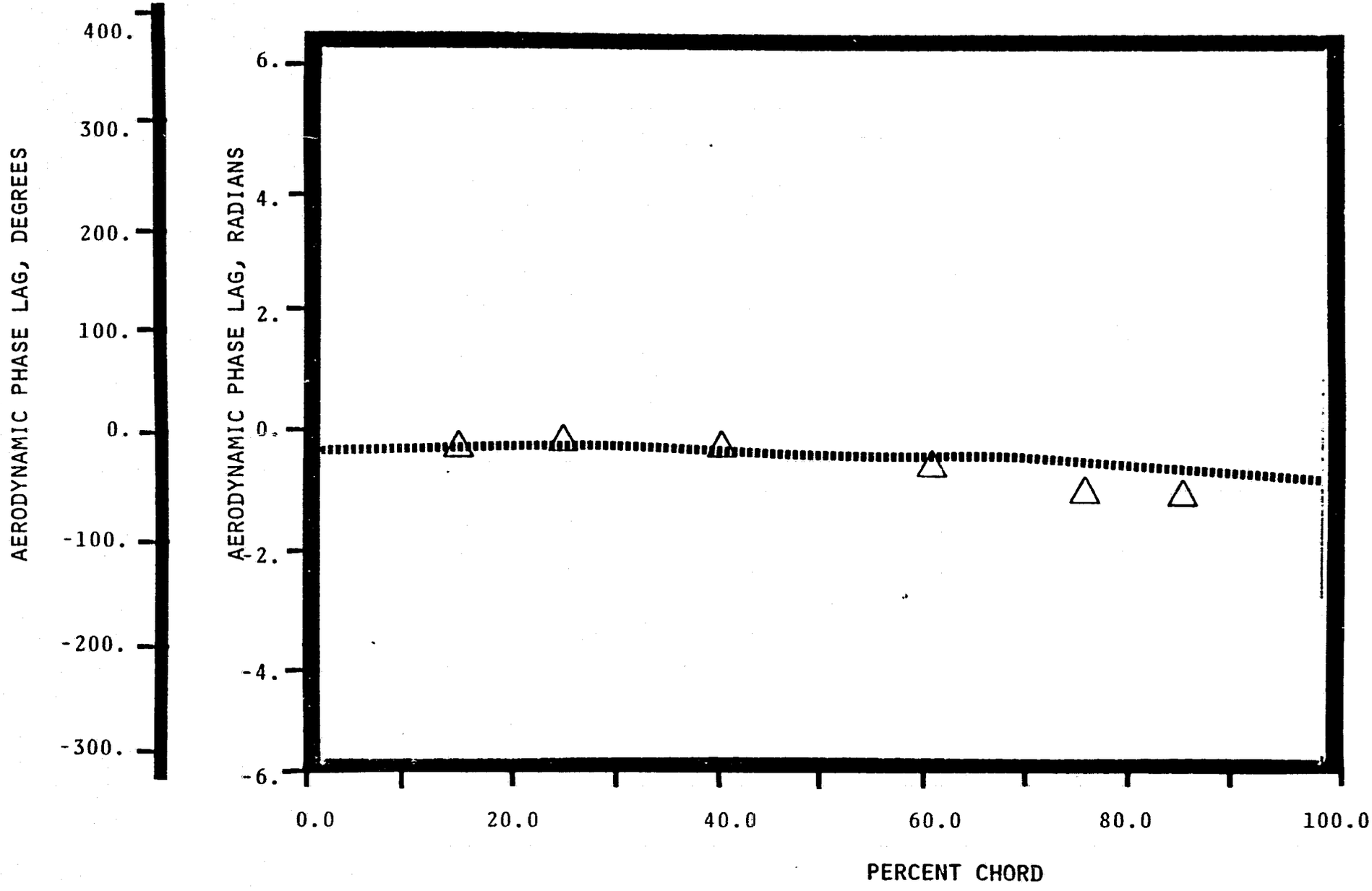

NASA I TORSION CASCADE

SUCTION SURFACE UNSTEADY PRESSURE DISTRIBUTION

1.315 INLET MACH NUMBER

1.35 STATIC PRESSURE RATIO

-.70 rad (-40°) INTERBLADE PHASE ANGLE

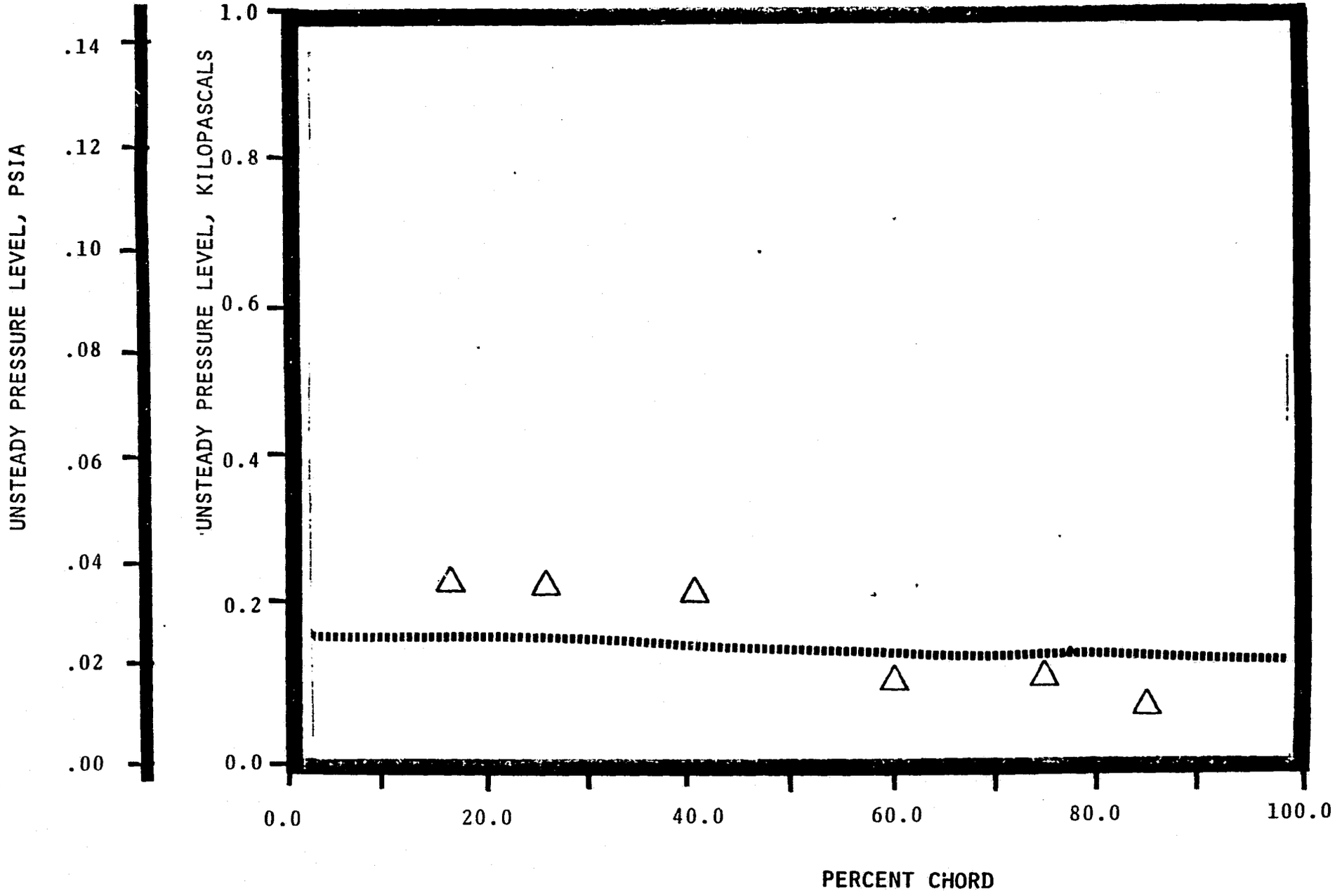

NASA I TORSION CASCADE

PRESSURE SURFACE AERODYNAMIC PHASE LAG DISTRIBUTION
1.315 INLET MACH NUMBER
1.35 STATIC PRESSURE RATIO
-.87 rad (-50.°) INTERBLADE PHASE ANGLE

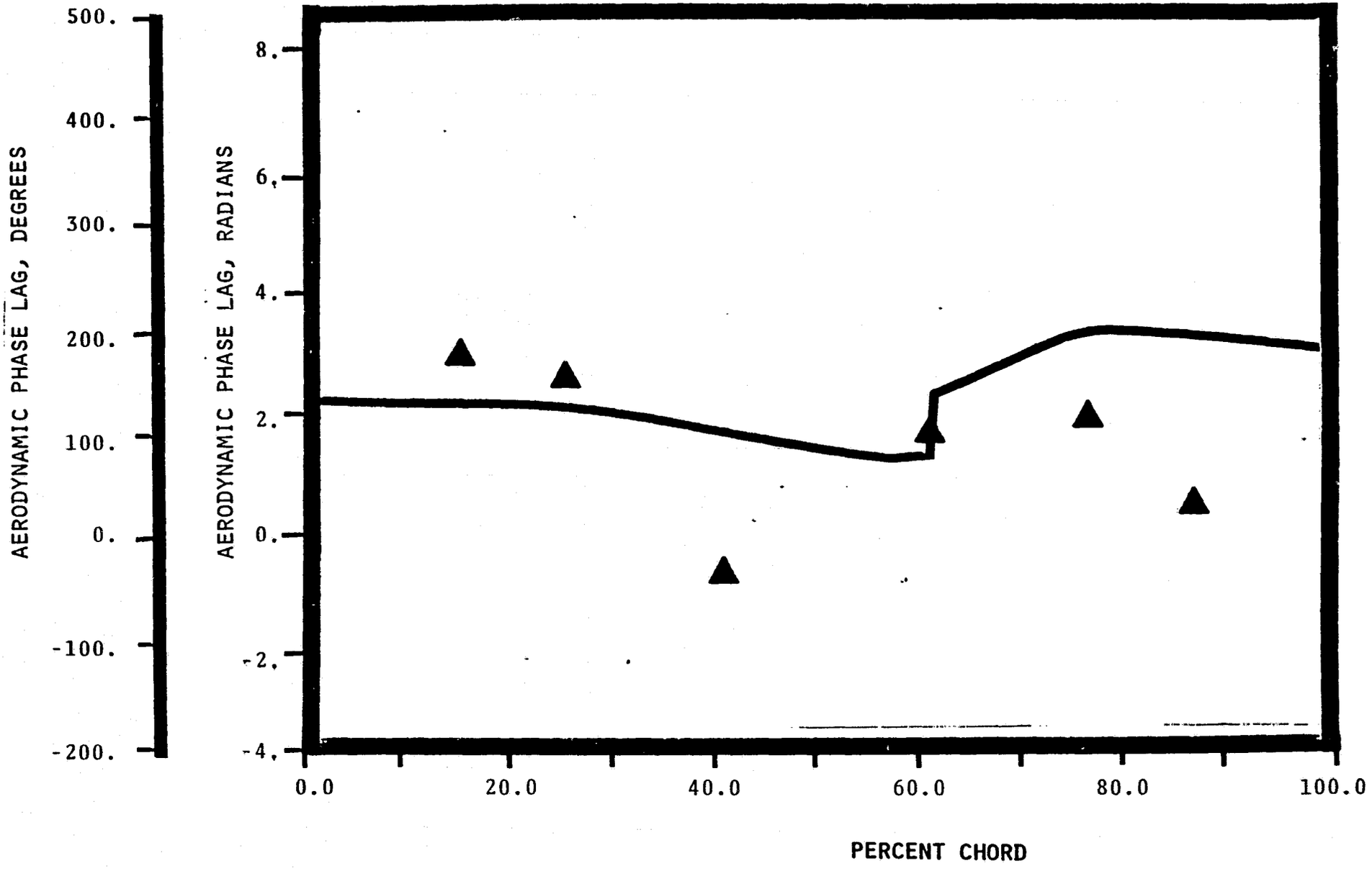

NASA I TORSION CASCADE

PRESSURE SURFACE UNSTEADY PRESSURE DISTRIBUTION

1.315 INLET MACH NUMBER

1.35 STATIC PRESSURE RATIO

-.87 rad (-50°) INTERBLADE PHASE ANGLE

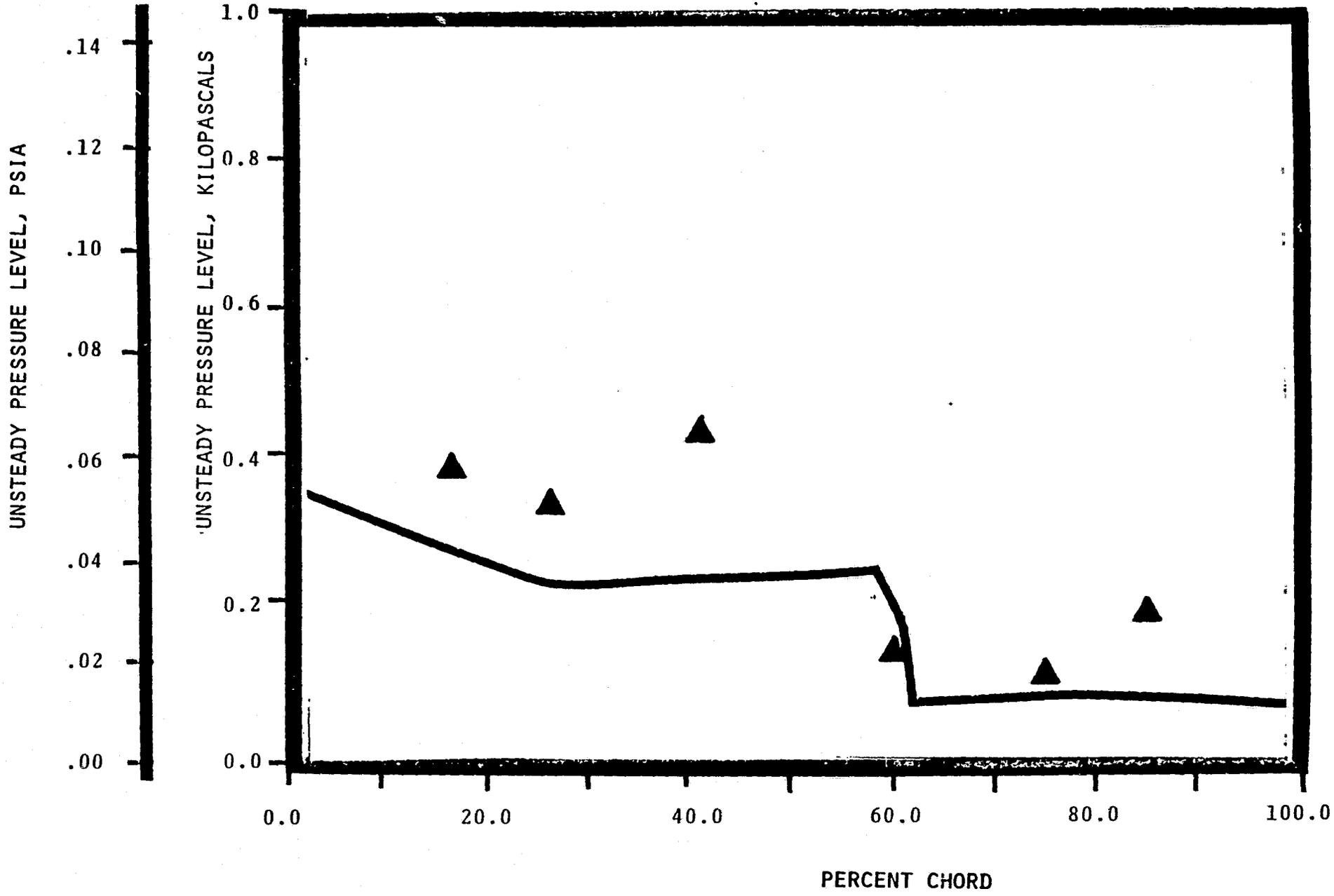

NASA I TORSION CASCADE

SUCTION SURFACE AERODYNAMIC PHASE LAG DISTRIBUTION

1.315 INLET MACH NUMBER

1.35 STATIC PRESSURE RATIO

-.87 rad (-50°) INTERBLADE PHASE ANGLE

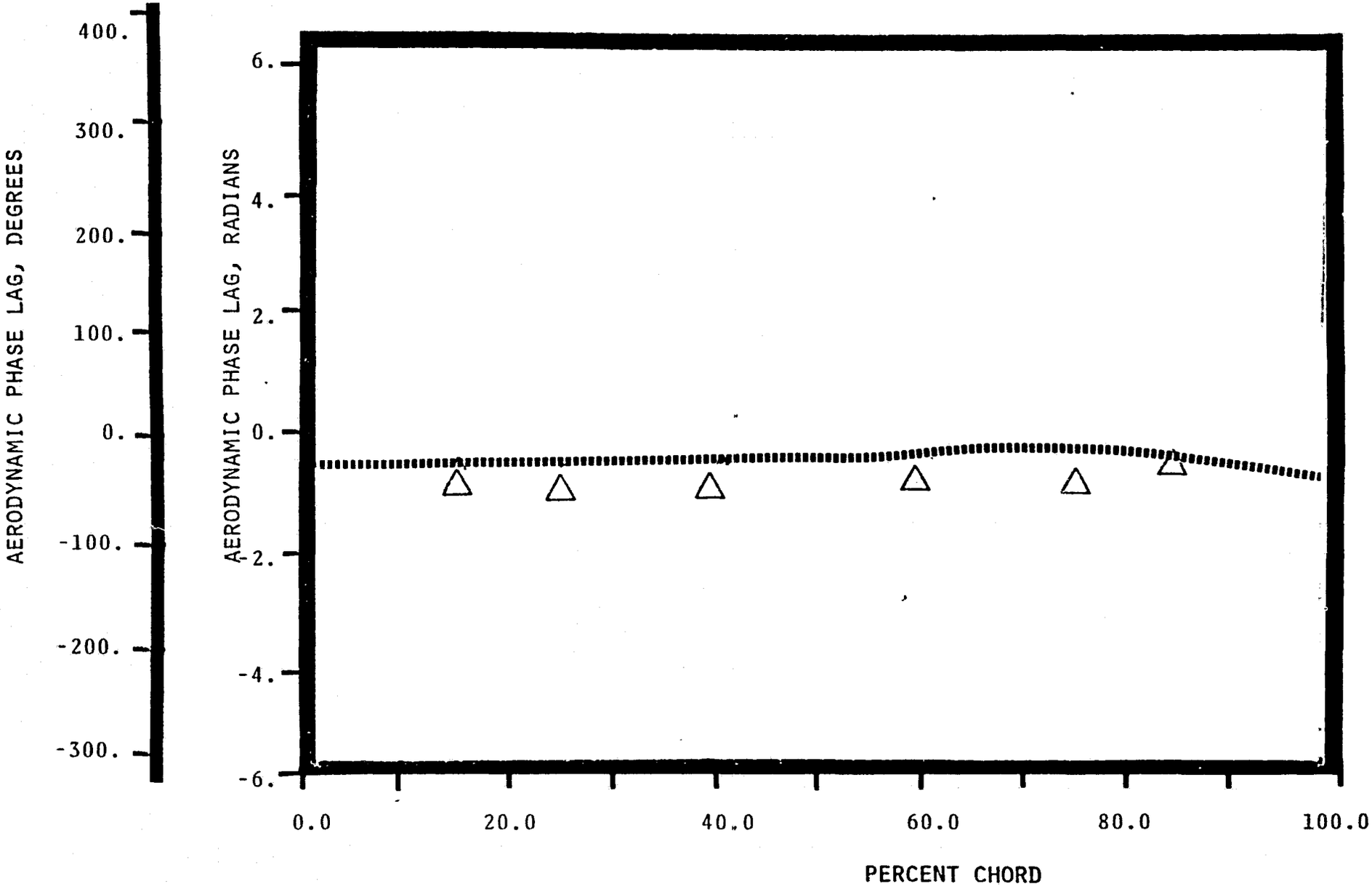

NASA I TORSION CASCADE

SUCTION SURFACE UNSTEADY PRESSURE DISTRIBUTION

1.315 INLET MACH NUMBER

1.35 STATIC PRESSURE RATIO

-.87 rad (-50°)INTERBLADE PHASE ANGLE

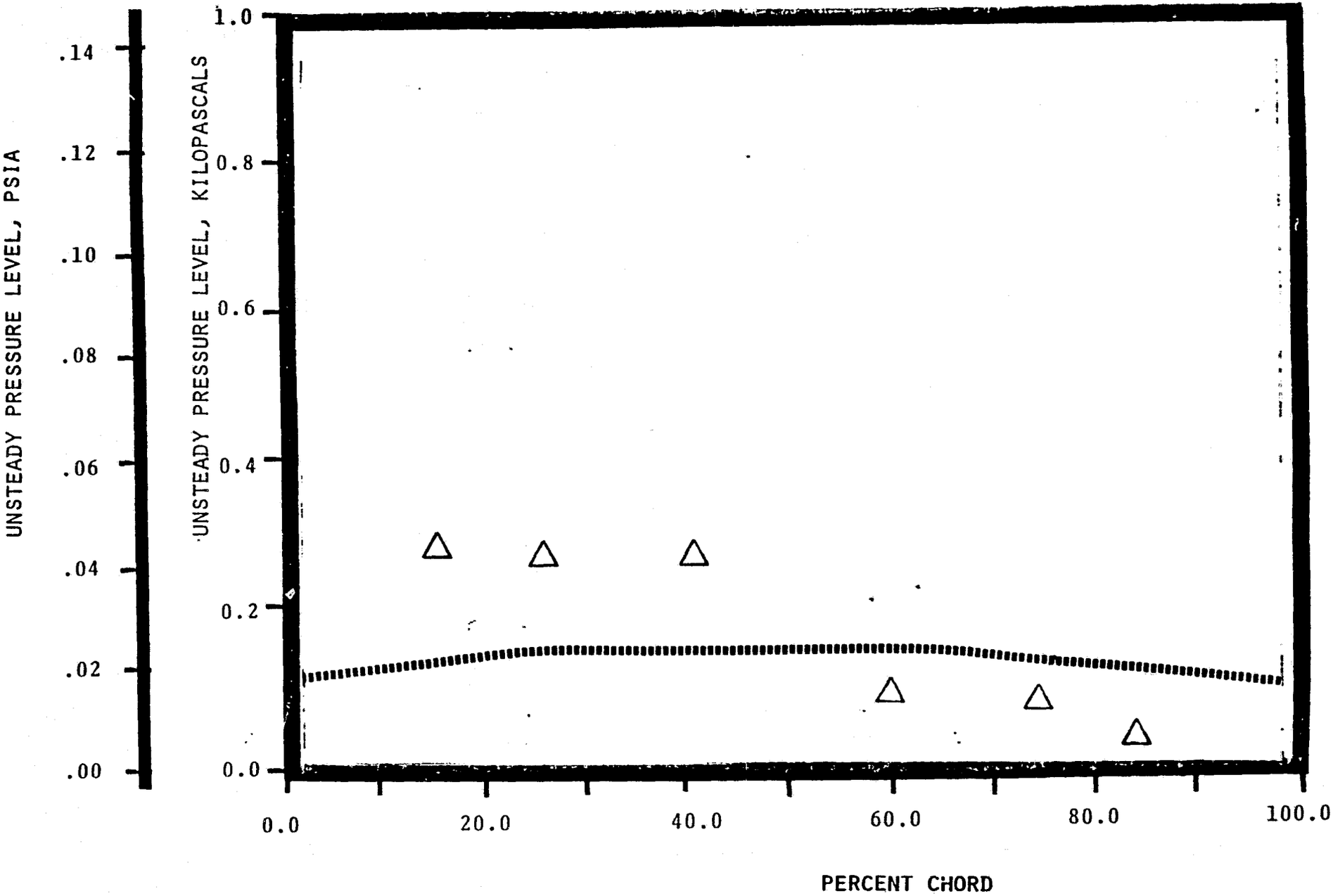

NASA I TORSION CASCADE

PRESSURE SURFACE AERODYNAMIC PHASE LAG DISTRIBUTION

1.315 INLET MACH NUMBER

1.45 STATIC PRESSURE RATIO

2.97 rad (170 °) INTERBLADE PHASE ANGLE

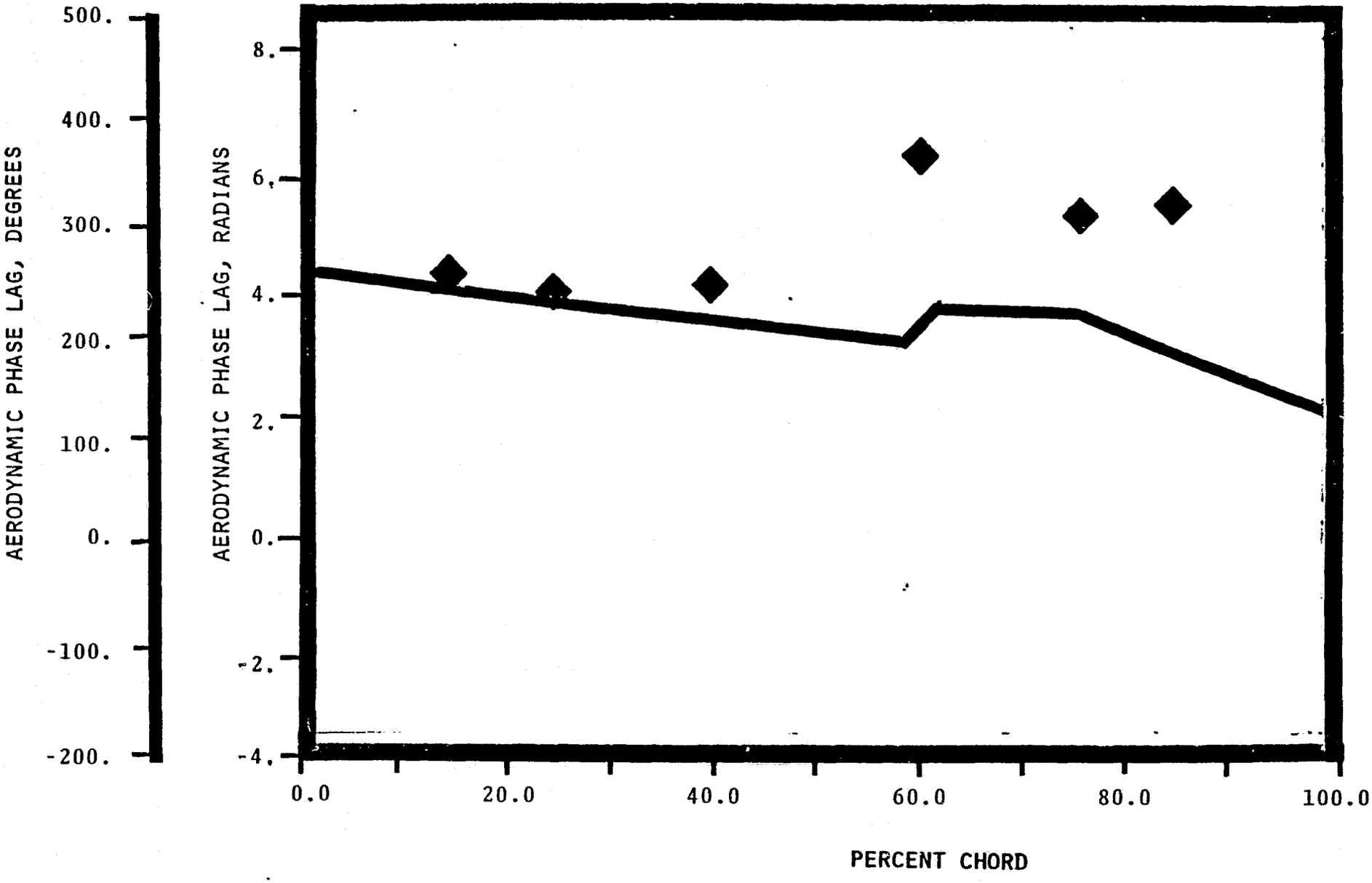

NASA I TORSION CASCADE

PRESSURE SURFACE UNSTEADY PRESSURE DISTRIBUTION

1.315 INLET MACH NUMBER

1.45 STATIC PRESSURE RATIO

2.97 rad (170°) INTERBLADE PHASE ANGLE

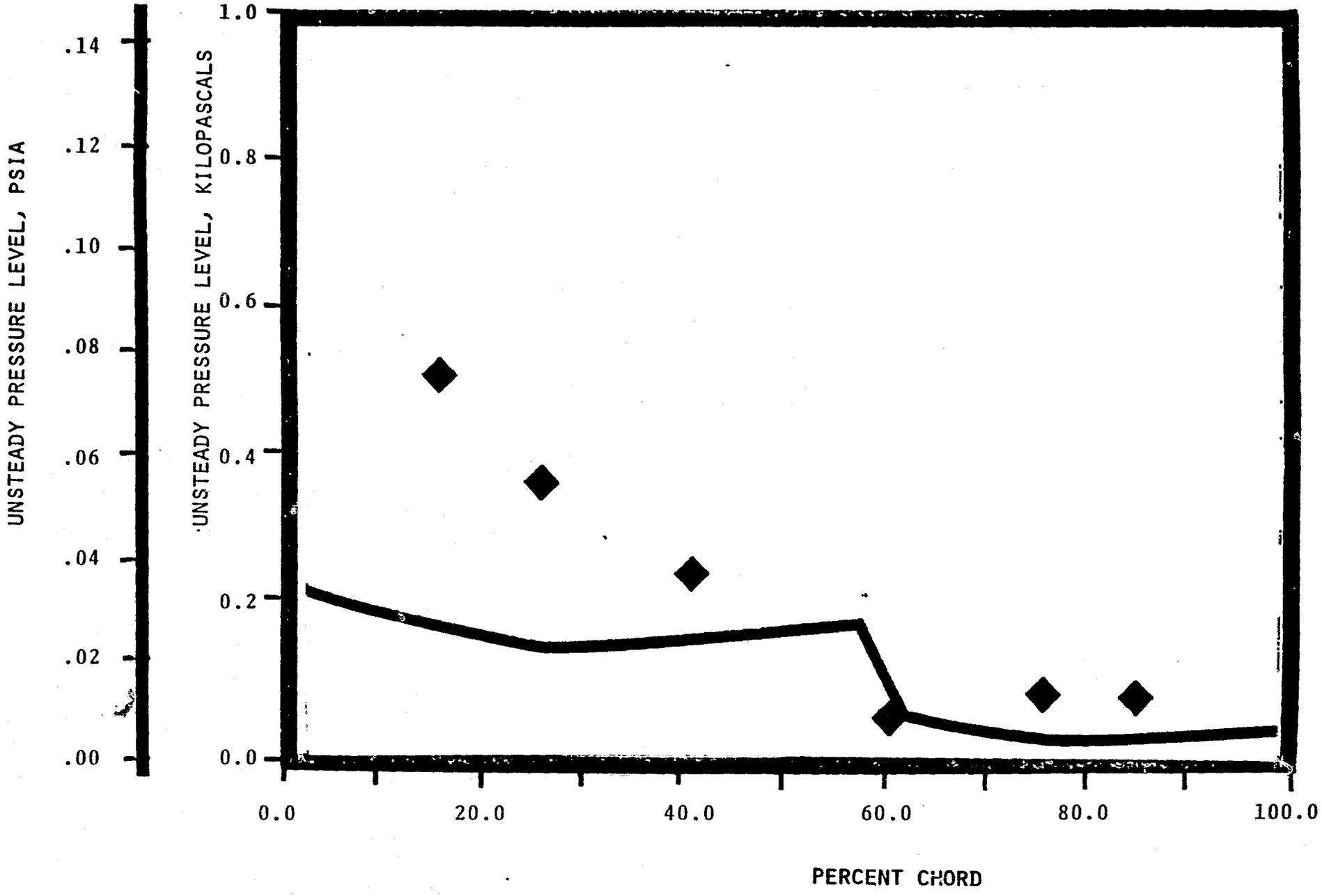

NASA I TORSION CASCADE

SUCTION SURFACE AERODYNAMIC PHASE LAG DISTRIBUTION

1.315 INLET MACH NUMBER

1.45 STATIC PRESSURE RATIO

2.97 rad (170°) INTERBLADE PHASE ANGLE

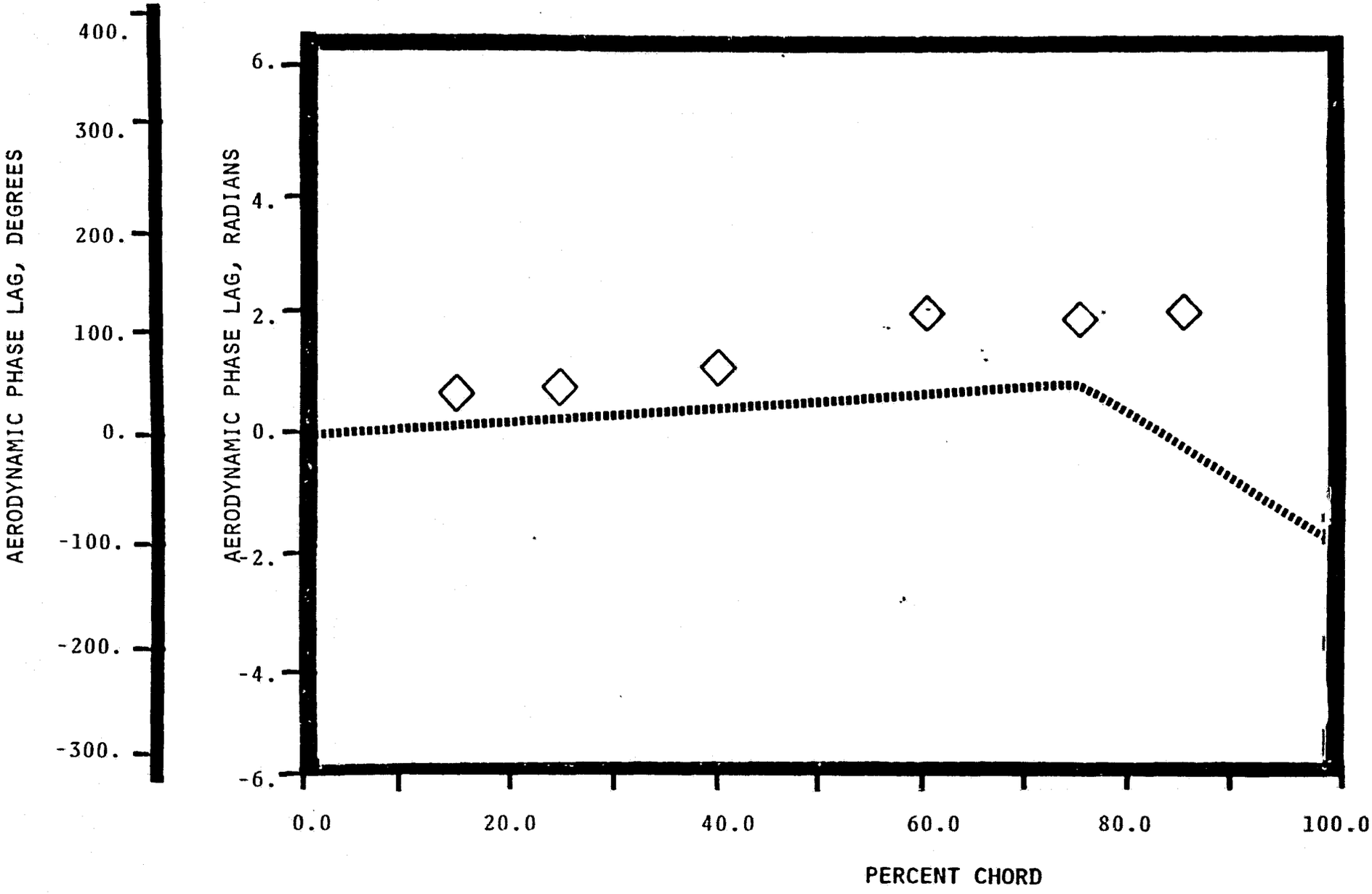

NASA I TORSION CASCADE

SUCTION SURFACE UNSTEADY PRESSURE DISTRIBUTION

1.315 INLET MACH NUMBER

1.45 STATIC PRESSURE RATIO

2.97 rad (170°) INTERBLADE PHASE ANGLE

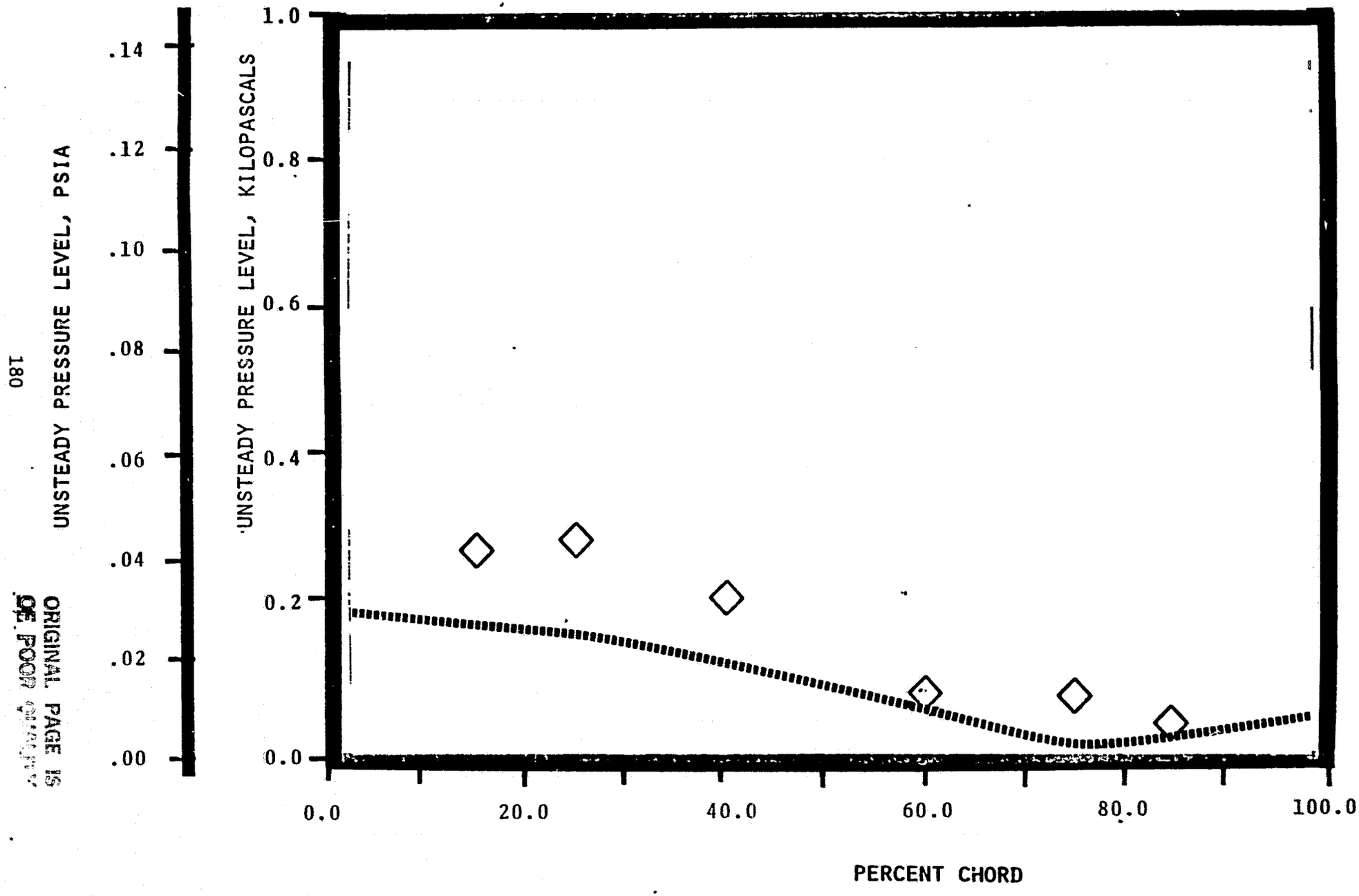

180

NASA I TORSION CASCADE

PRESSURE SURFACE AERODYNAMIC PHASE LAG DISTRIBUTION

1.315 INLET MACH NUMBER

1.45 STATIC PRESSURE RATIO

1.13 rad (65°) INTERBLADE PHASE ANGLE

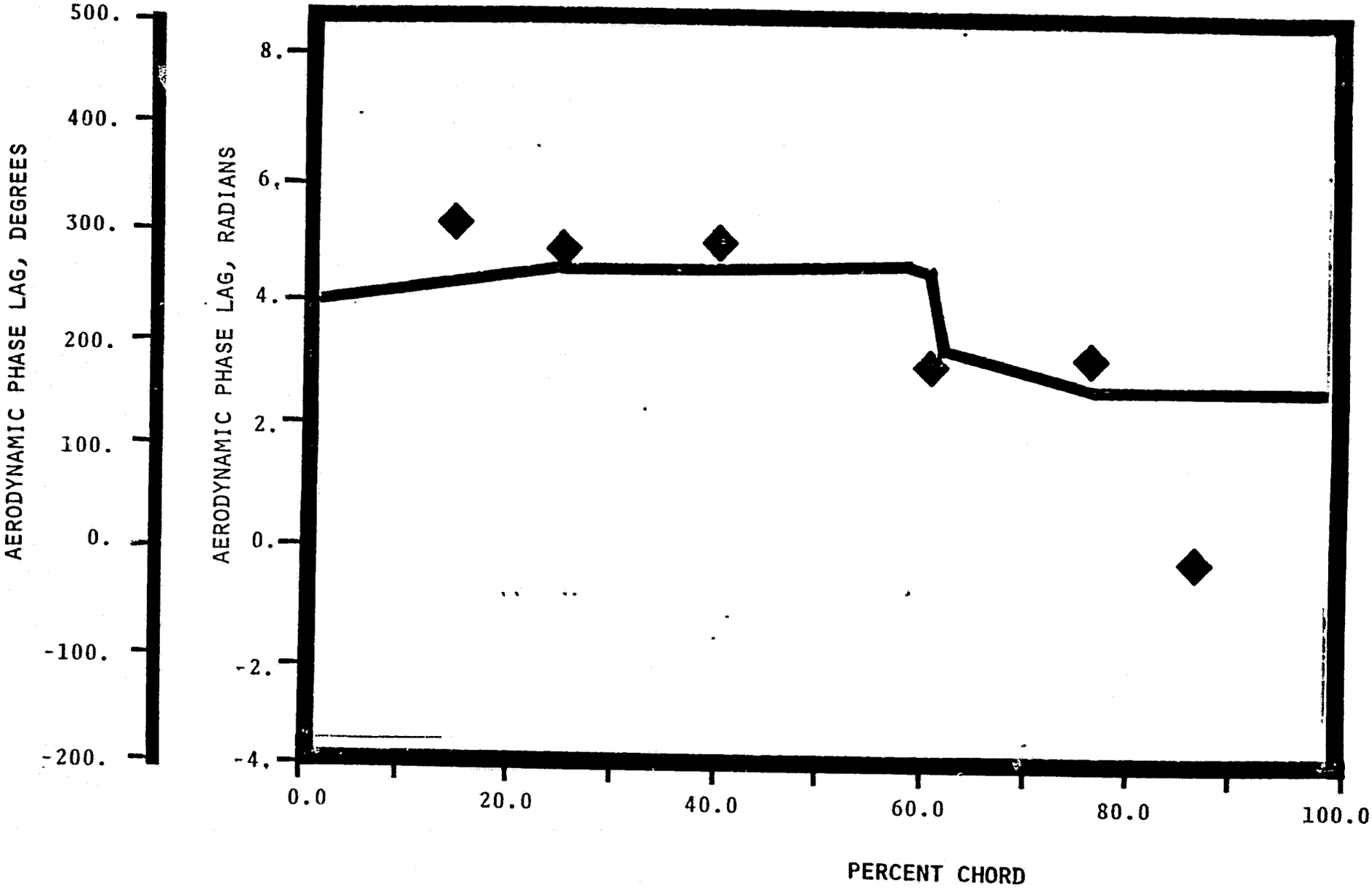

NASA I TORSION CASCADE

PRESSURE SURFACE UNSTEADY PRESSURE DISTRIBUTION

1.315 INLET MACH NUMBER

.45 STATIC PRESSURE RATIO

1.13 rad (65°) INTERBLADE PHASE ANGLE

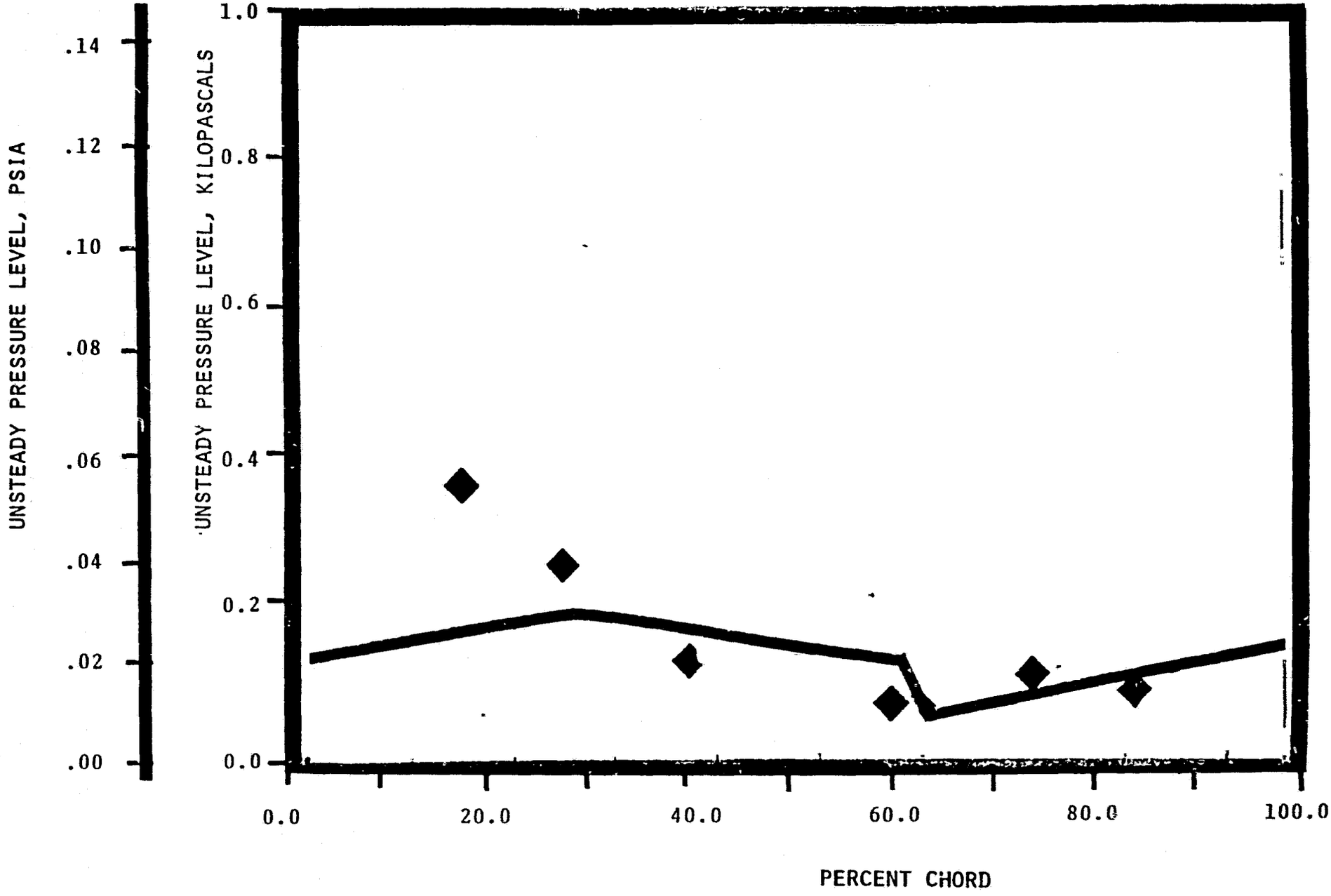

NASA I TORSION CASCADE

SUCTION SURFACE AERODYNAMIC PHASE LAG DISTRIBUTION

1.315 INLET MACH NUMBER

1.45 STATIC PRESSURE RATIO

1.13 rad(65°) INTERBLADE PHASE ANGLE

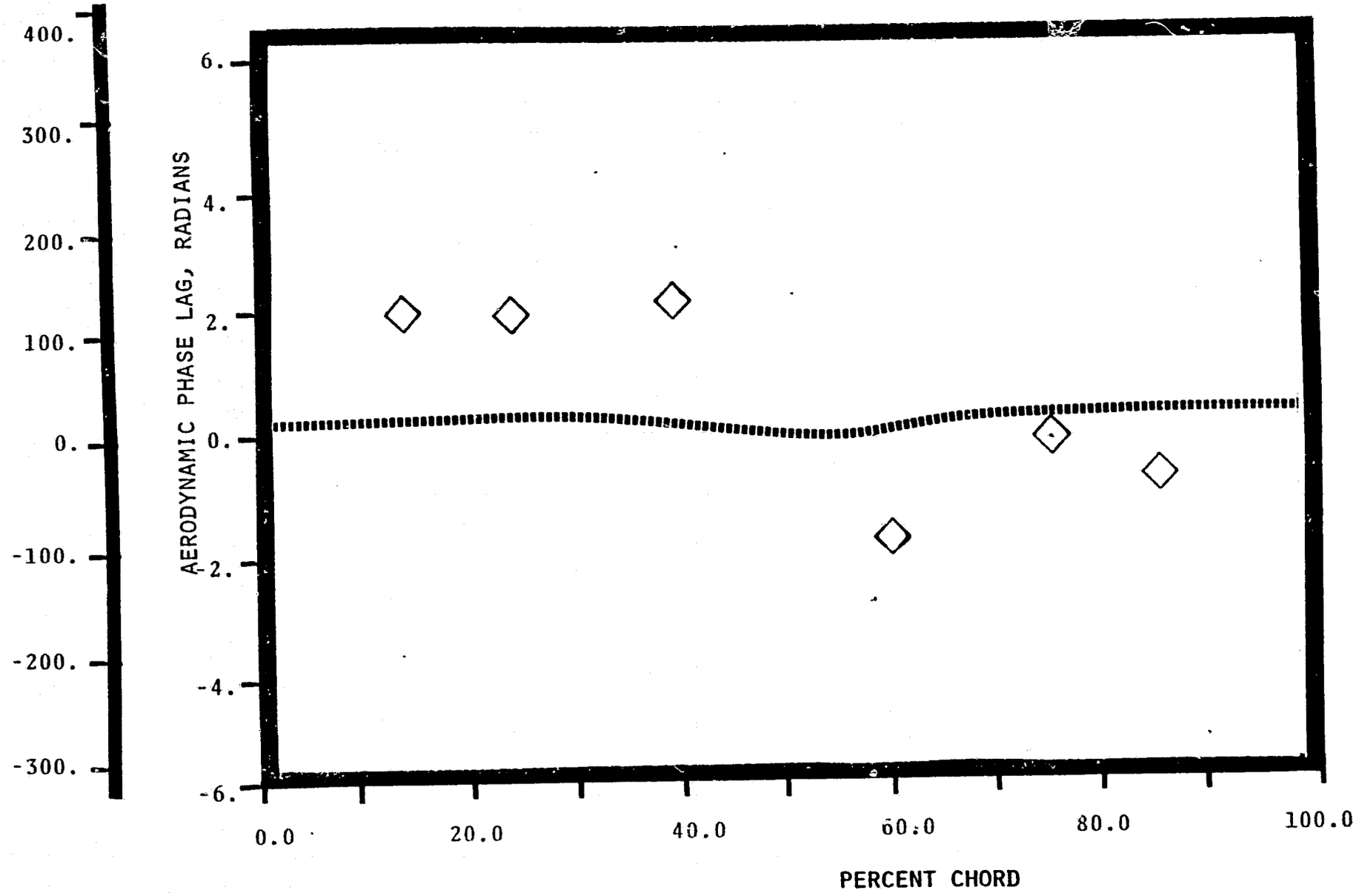

4-7

NASA I TORSION CASCADE

SUCTION SURFACE UNSTEADY PRESSURE DISTRIBUTION

1.315 INLET MACH NUMBER

1.45 STATIC PRESSURE RATIO

1.13 rad (65°) INTERBLADE PHASE ANGLE

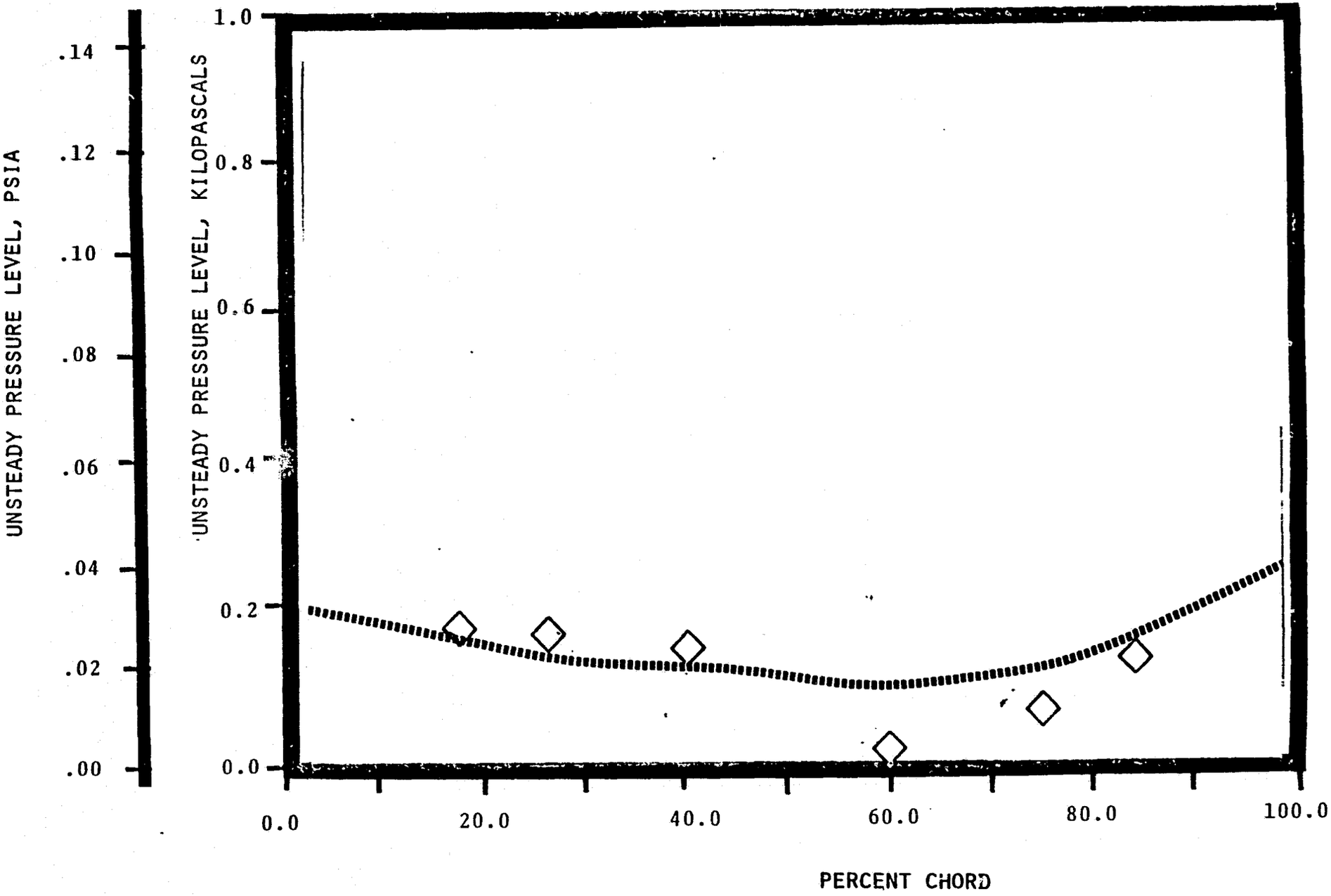

NASA I TORSION CASCADE

PRESSURE SURFACE AERODYNAMIC PHASE LAG DISTRIBUTION
1.315 INLET MACH NUMBER
1.45 STATIC PRESSURE RATIO
0.0 rad (0°) INTERBLADE PHASE ANGLE

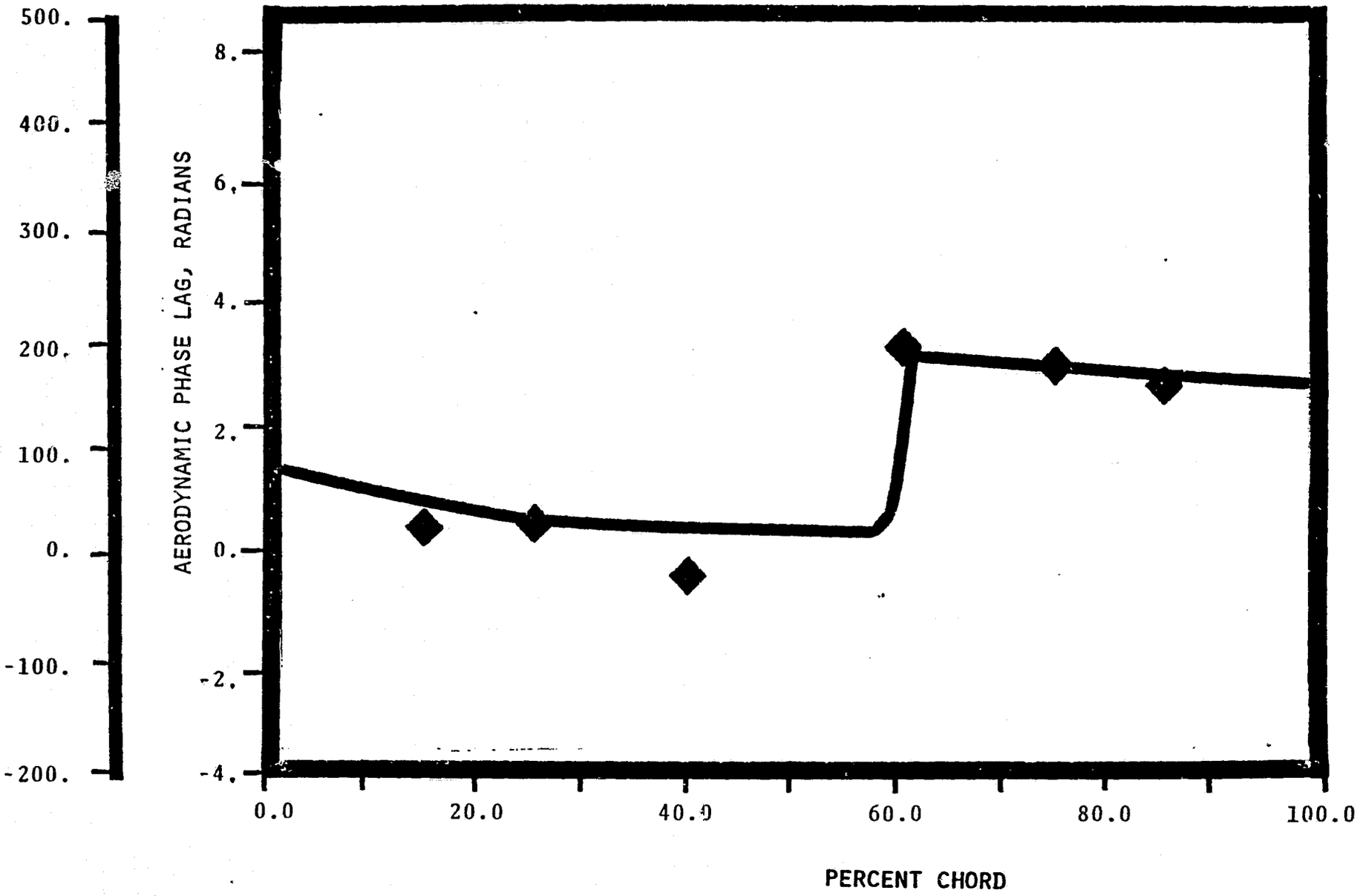

NASA I TORSION CASCADE

PRESSURE SURFACE UNSTEADY PRESSURE DISTRIBUTION

1.315 INLET MACH NUMBER

1.45 STATIC PRESSURE RATIO

0.0 rad (0°) INTERBLADE PHASE ANGLE

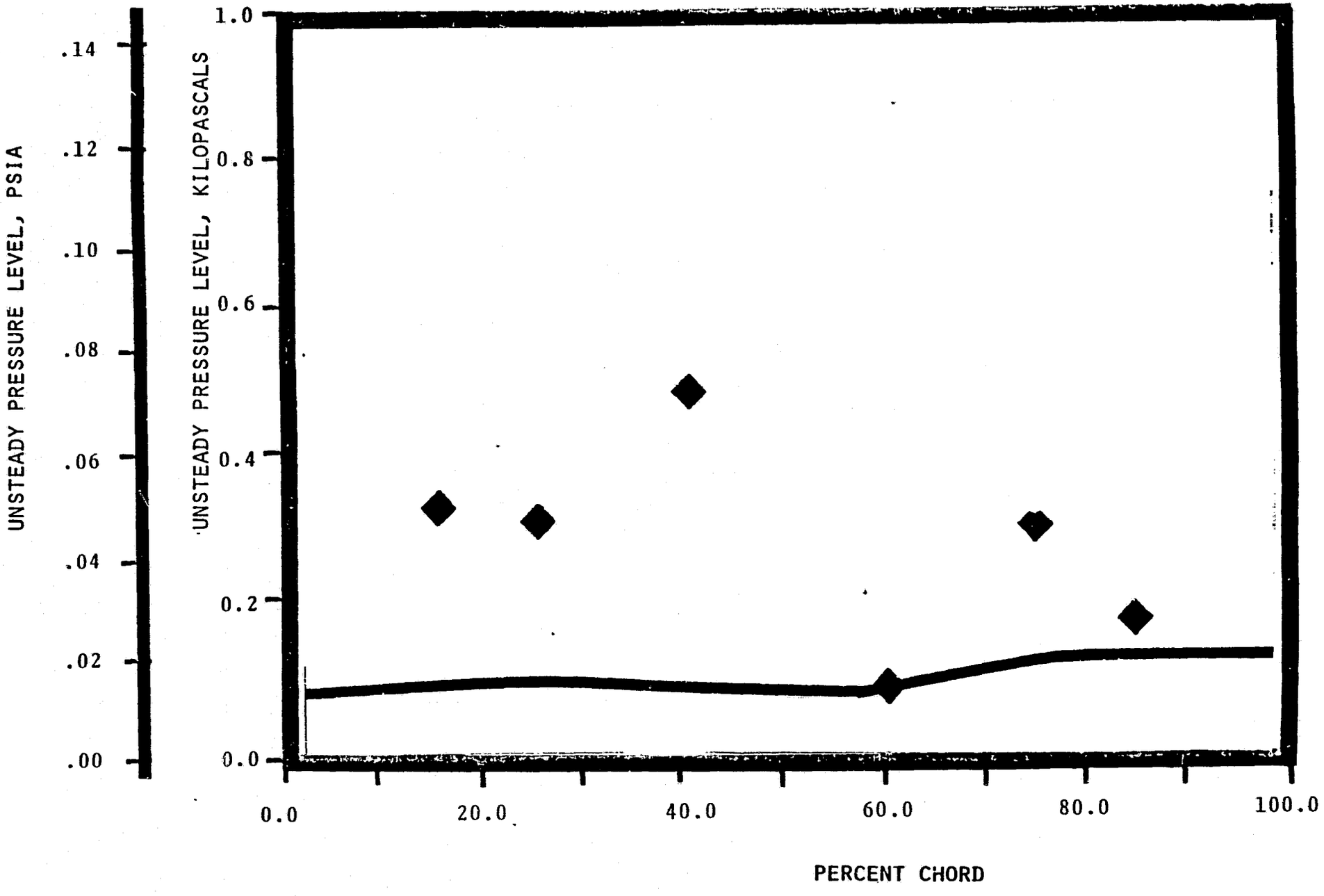

NASA I TORSION CASCADE

SUCTION SURFACE AERODYNAMIC PHASE LAG DISTRIBUTION

1.315 INLET MACH NUMBER

1.45 STATIC PRESSURE RATIO

0.0 rad (0°) INTERBLADE PHASE ANGLE

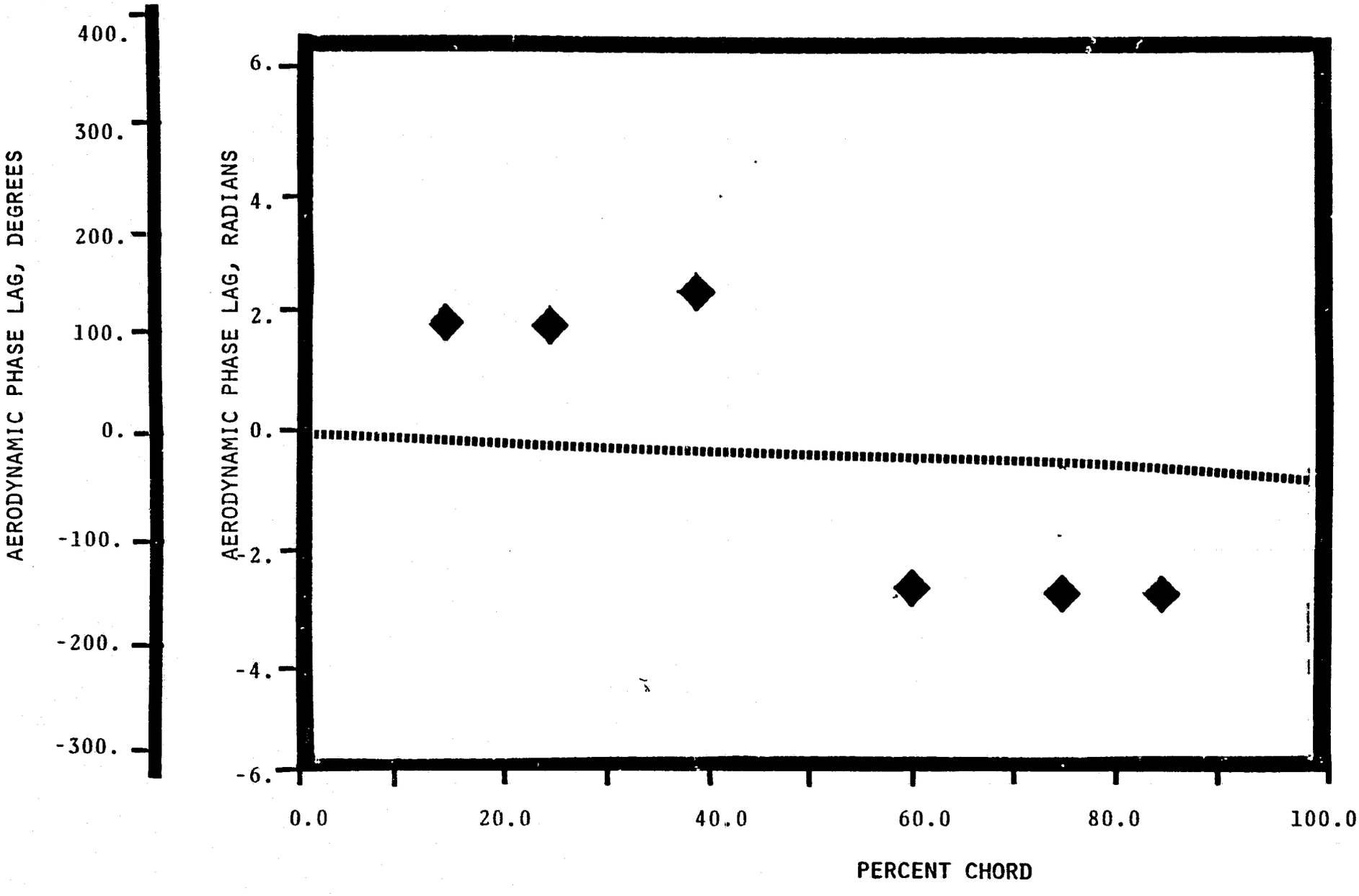

NASA I TORSION CASCADE

SUCTION SURFACE UNSTEADY PRESSURE DISTRIBUTION

1.315 INLET MACH NUMBER

1.45 STATIC PRESSURE RATIO

0.0 rad (0^{o}) INTERBLADE PHASE ANGLE

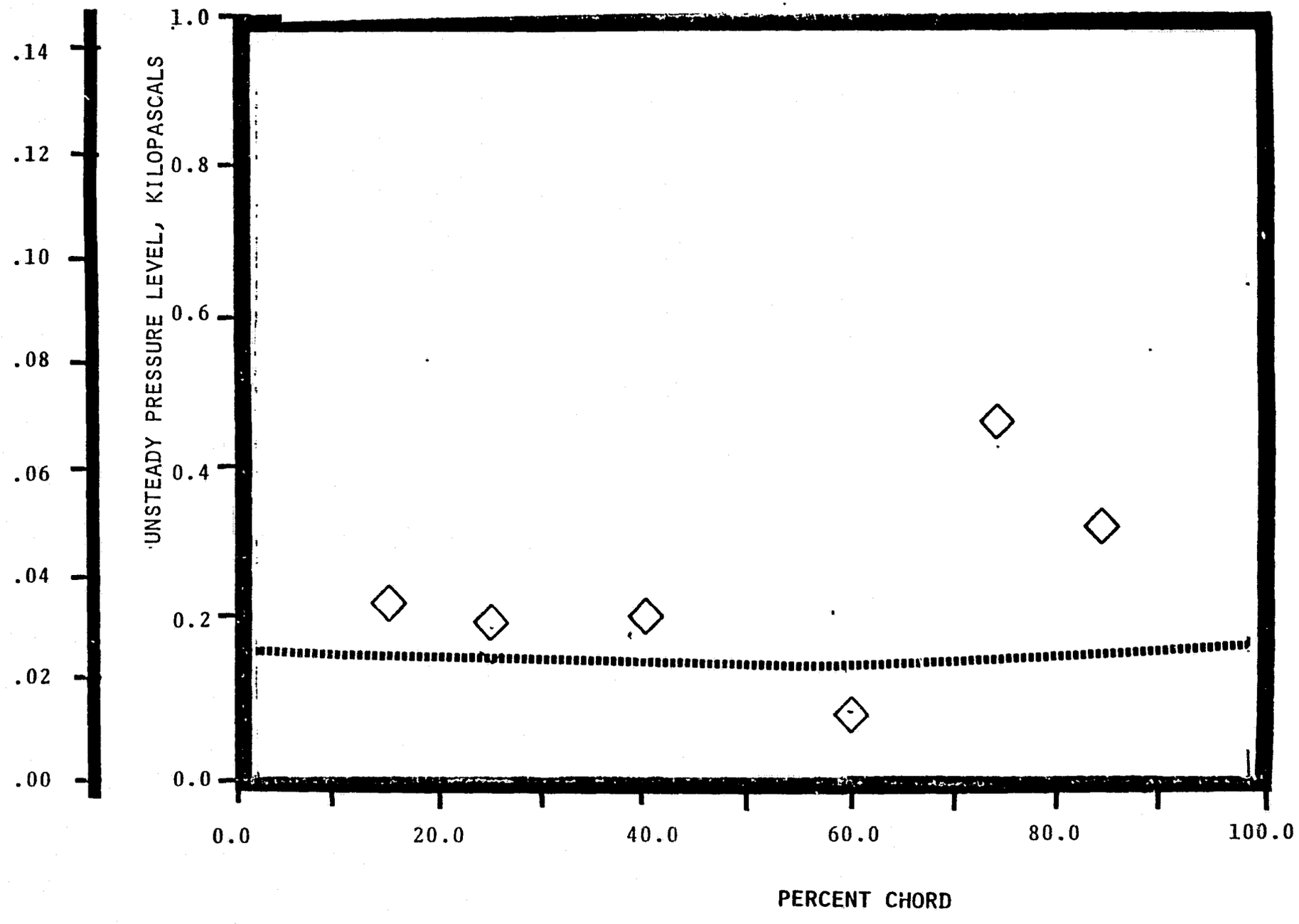

NASA I TORSION CASCADE

PRESSURE SURFACE AERODYNAMIC PHASE LAG DISTRIBUTION
1.315 INLET MACH NUMBER
1.45 STATIC PRESSURE RATIO
-1.05 rad (-60°) INTERBLADE PHASE ANGLE

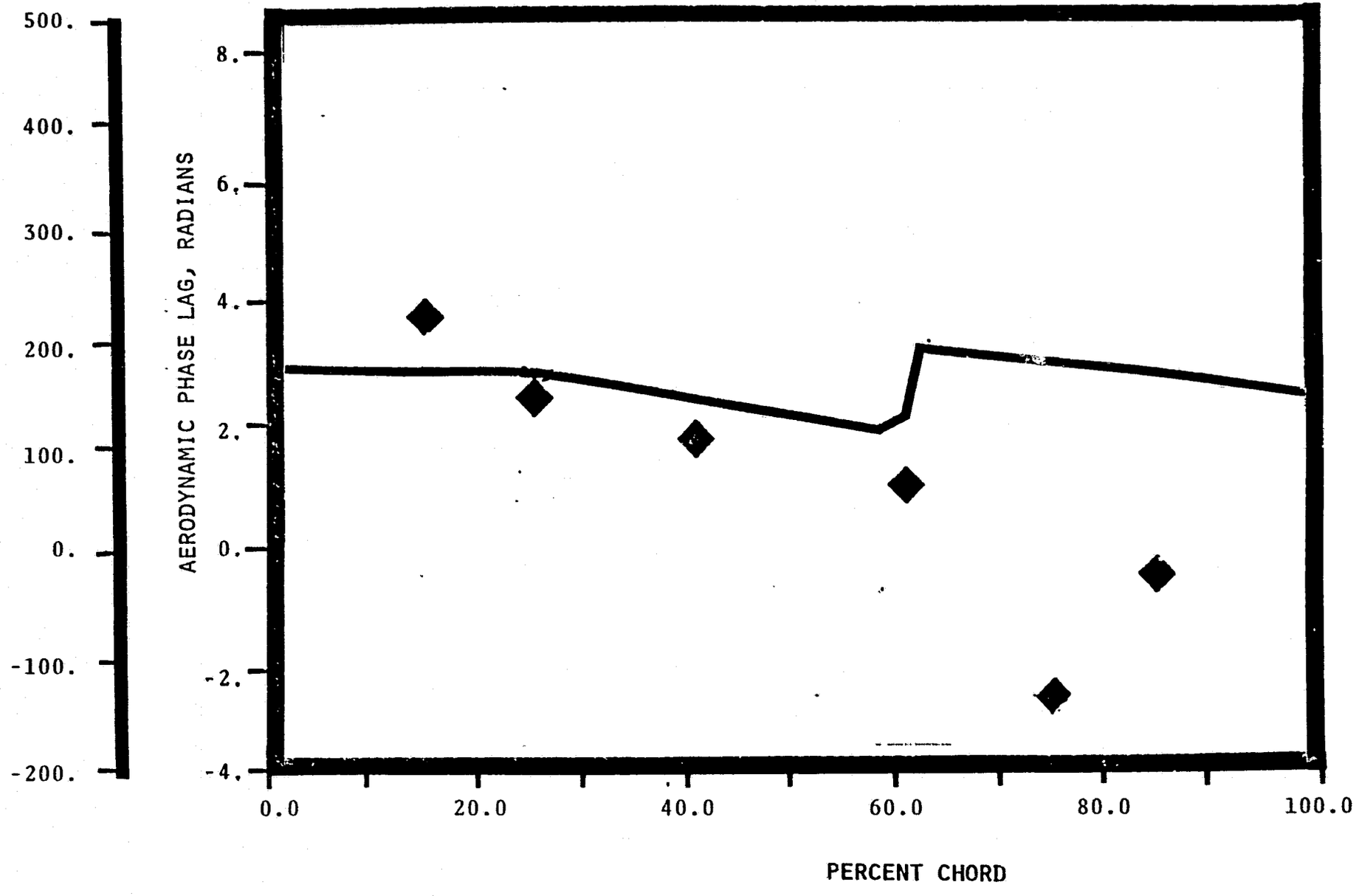

NASA I TORSION CASCADE

PRESSURE SURFACE UNSTEADY PRESSURE DISTRIBUTION

1.315 INLET MACH NUMBER

1.45 STATIC PRESSURE RATIO

-1.05 rad (-60°) INTERBLADE PHASE ANGLE

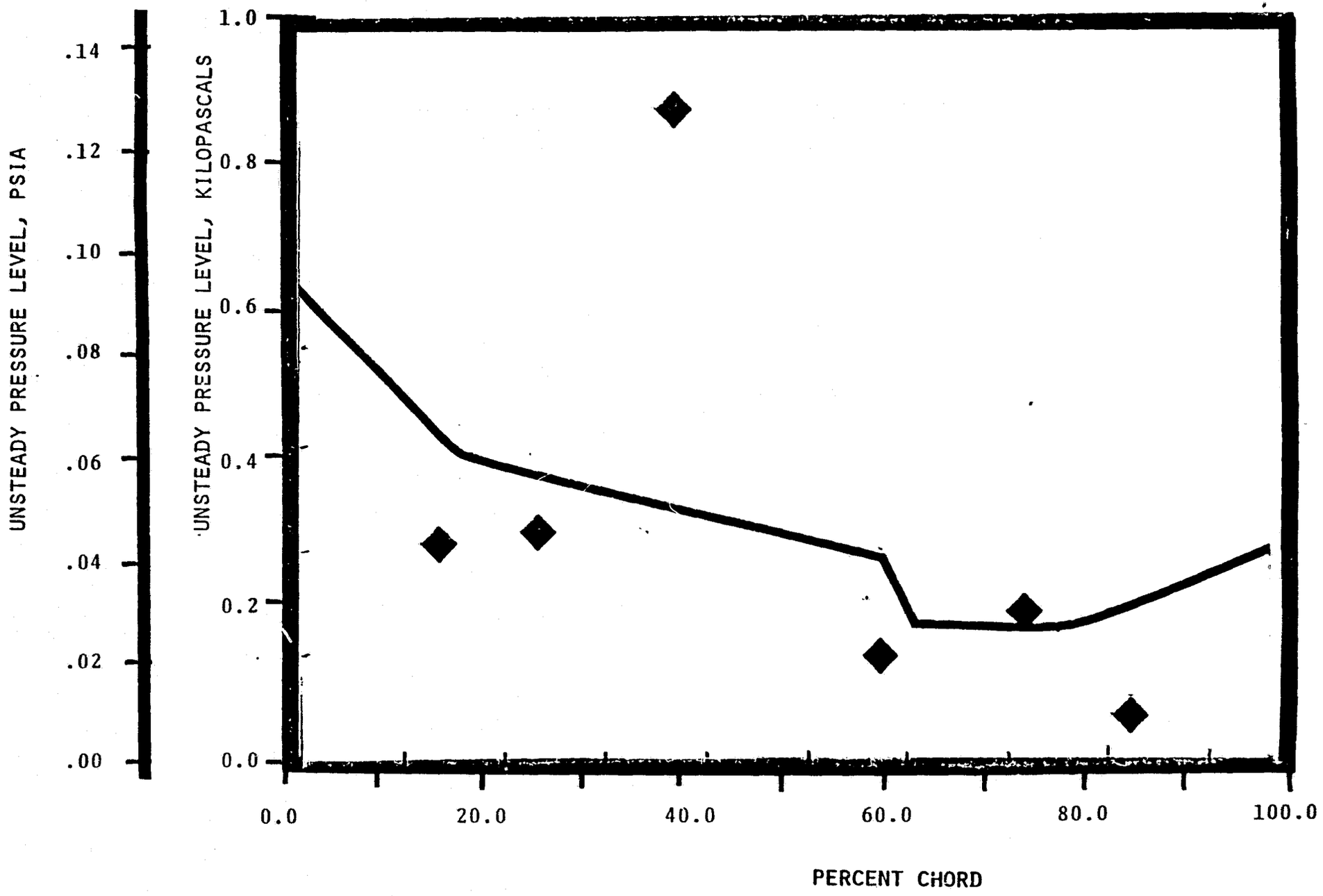

NASA I TORSION CASCADE

SUCTION SURFACE AERODYNAMIC PHASE LAG DISTRIBUTION

1.315 INLET MACH NUMBER

1.45 STATIC PRESSURE RATIO

-1.05 rad (-60°) INTERBLADE PHASE ANGLE

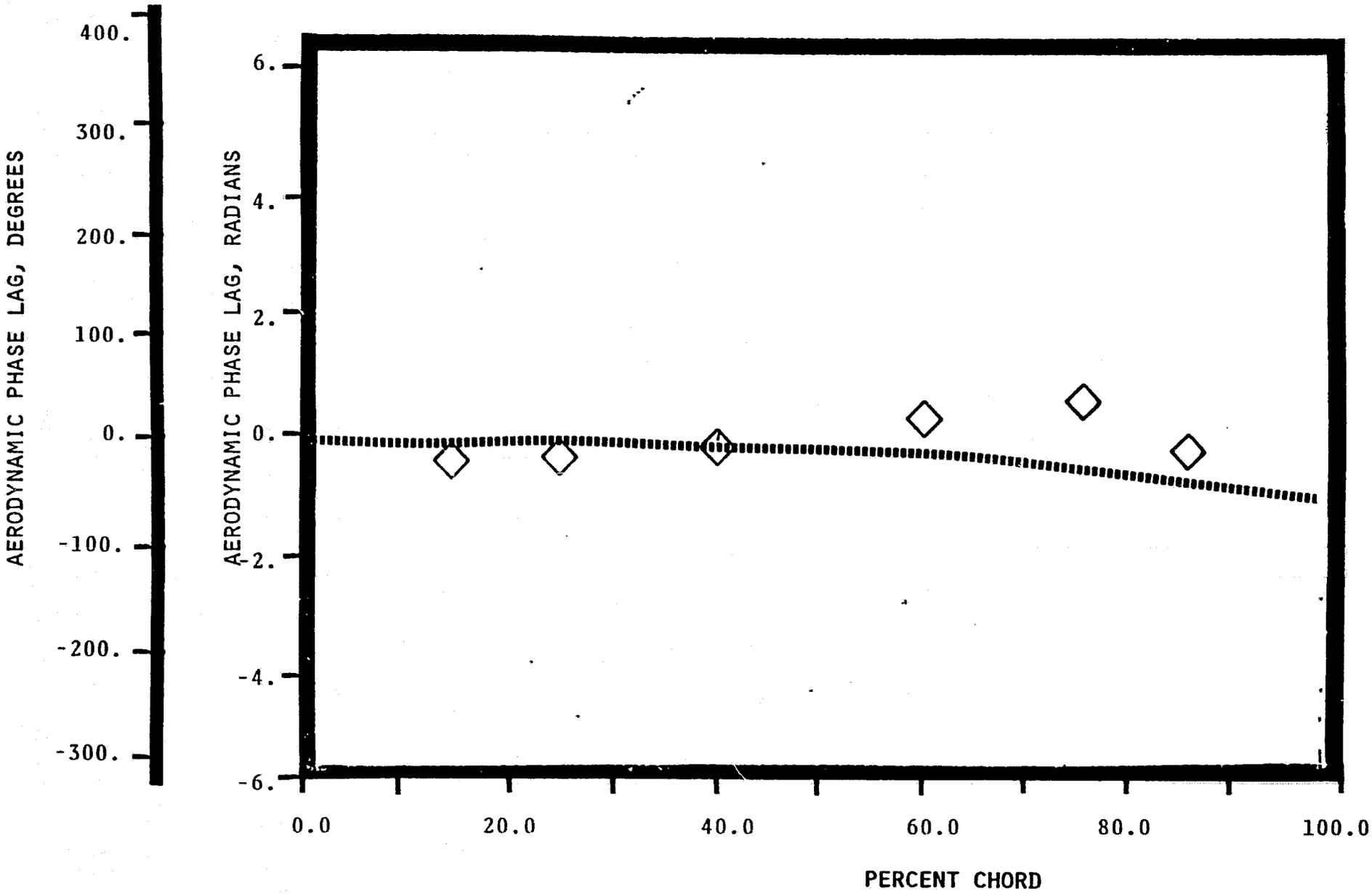

NASA I TORSION CASCADE

SUCTION SURFACE UNSTEADY PRESSURE DISTRIBUTION

1.315 INLET MACH NUMBER

1.45 STATIC PRESSURE RATIO

-1.05 rad (-60°) INTERBLADE PHASE ANGLE

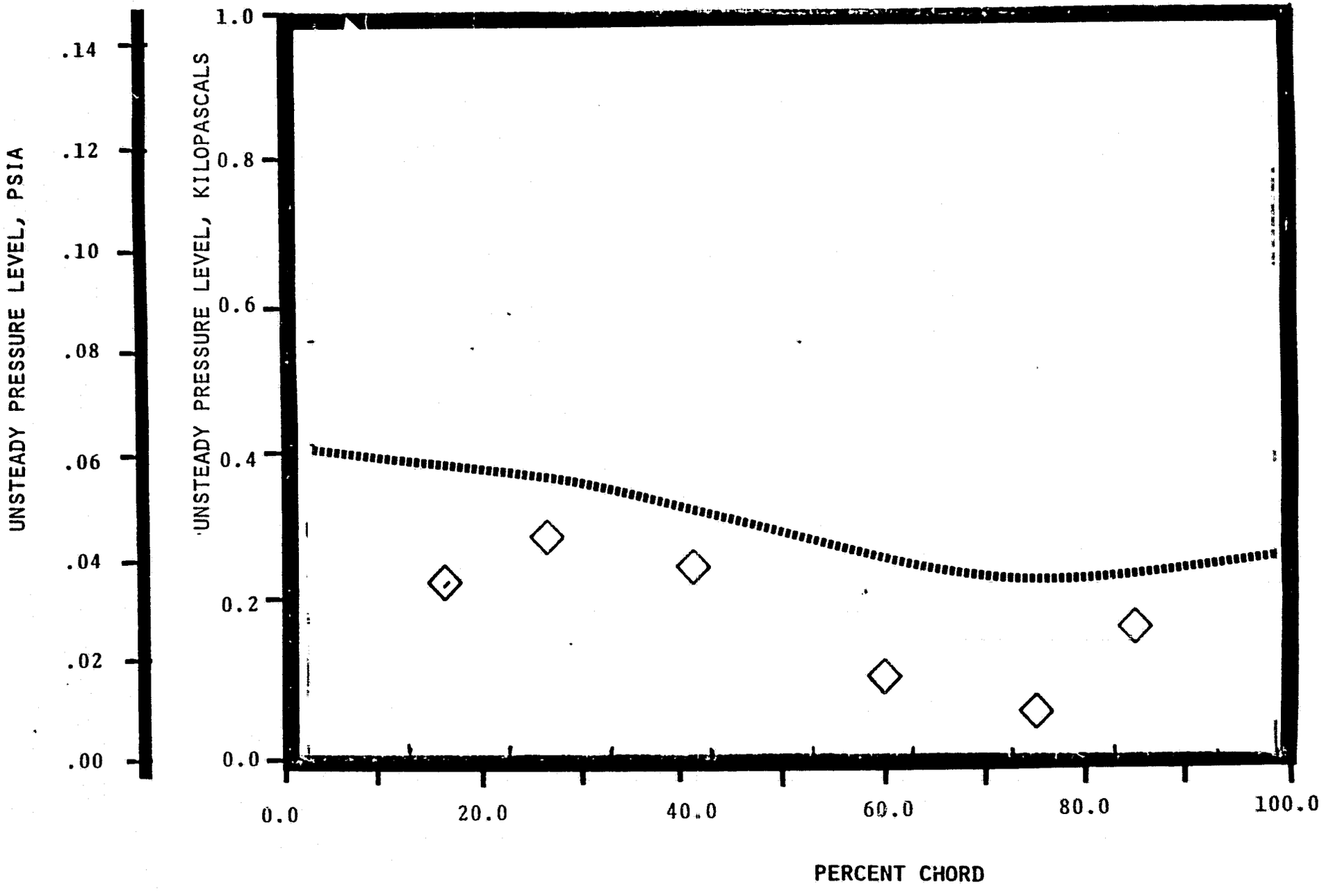

NASA I TORSION CASCADE

PRESSURE SURFACE AERODYNAMIC PHASE LAG DISTRIBUTION
1.315 INLET MACH NUMBER
1.45 STATIC PRESSURE RATIO
-1.48 rad (-85°) INTERBLADE PHASE ANGLE

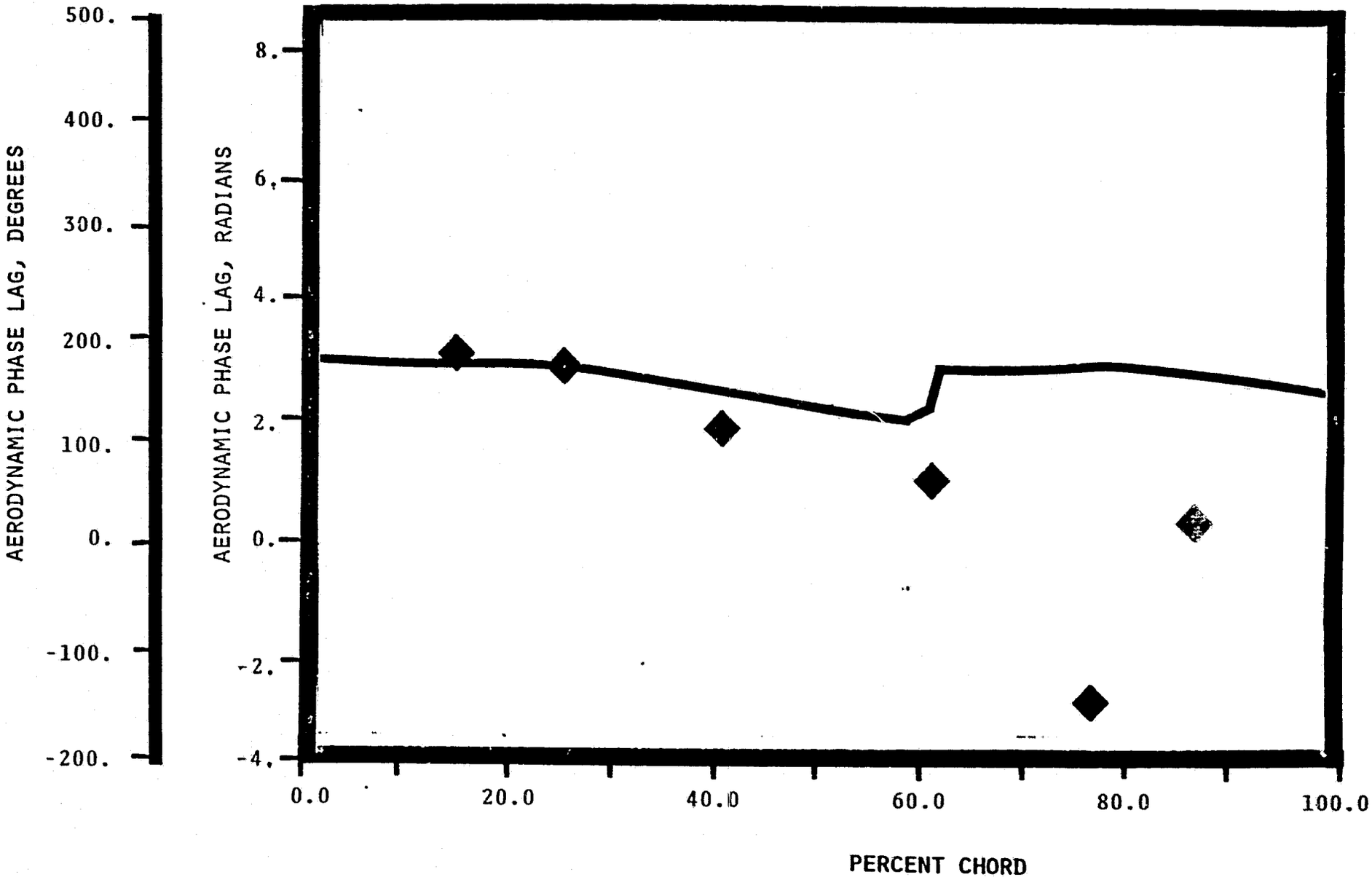

NASA I TORSION CASCADE

PRESSURE SURFACE UNSTEADY PRESSURE DISTRIBUTION

1.315 INLET MACH NUMBER

1.45 STATIC PRESSURE RATIO

-1.48 rad (-85°) INTERBLADE PHASE ANGLE

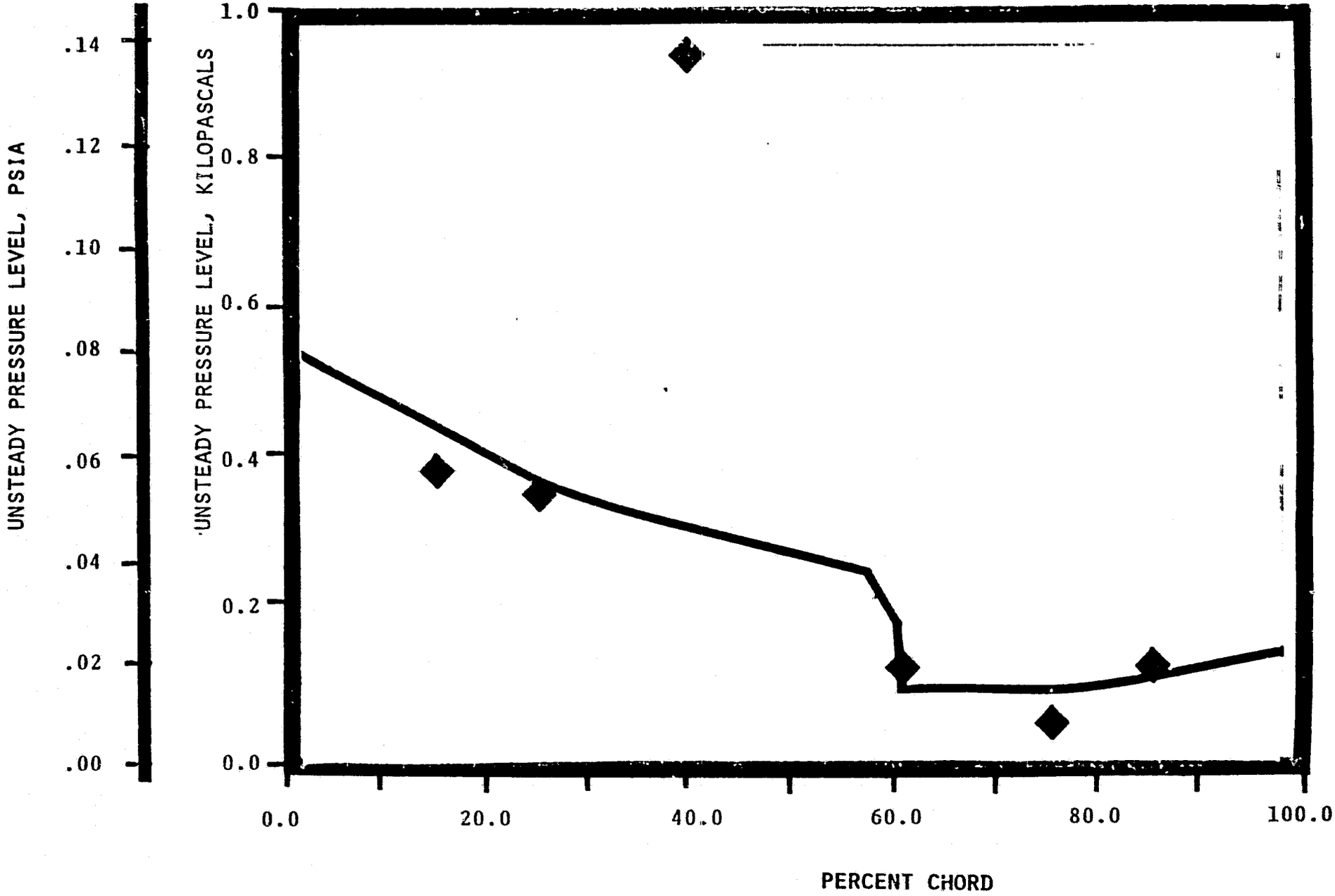

NASA I TORSION CASCADE

SUCTION SURFACE AERODYNAMIC PHASE LAG DISTRIBUTION

1.315 INLET MACH NUMBER

1.45 STATIC PRESSURE RATIO

-1.48 rad (-85°) INTERBLADE PHASE ANGLE

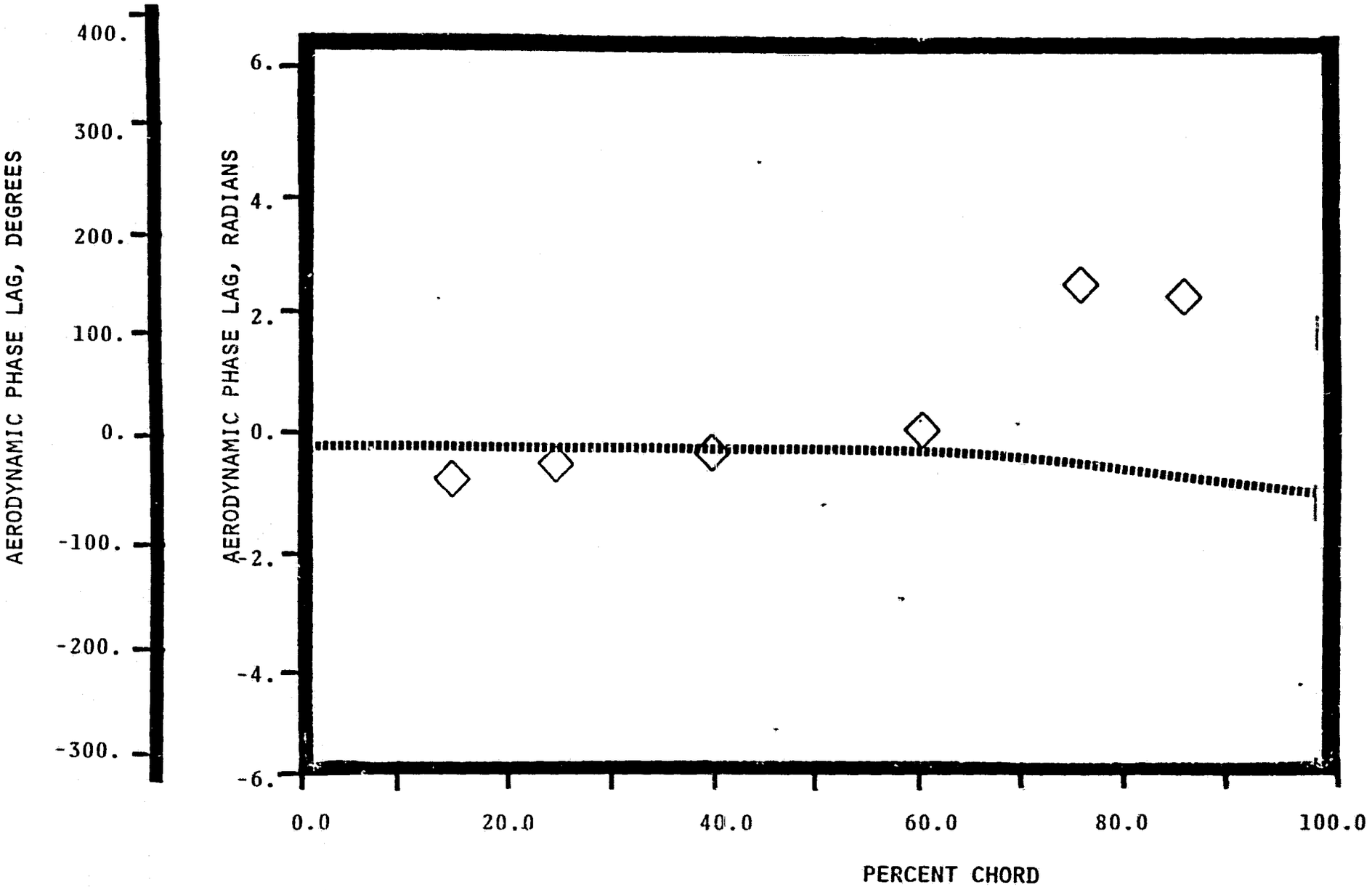

NASA I TORSION CASCADE

SUCTION SURFACE UNSTEADY PRESSURE DISTRIBUTION

1.315 INLET MACH NUMBER

1.45 STATIC PRESSURE RATIO

-1.48 rad (-85°) INTERBLADE PHASE ANGLE

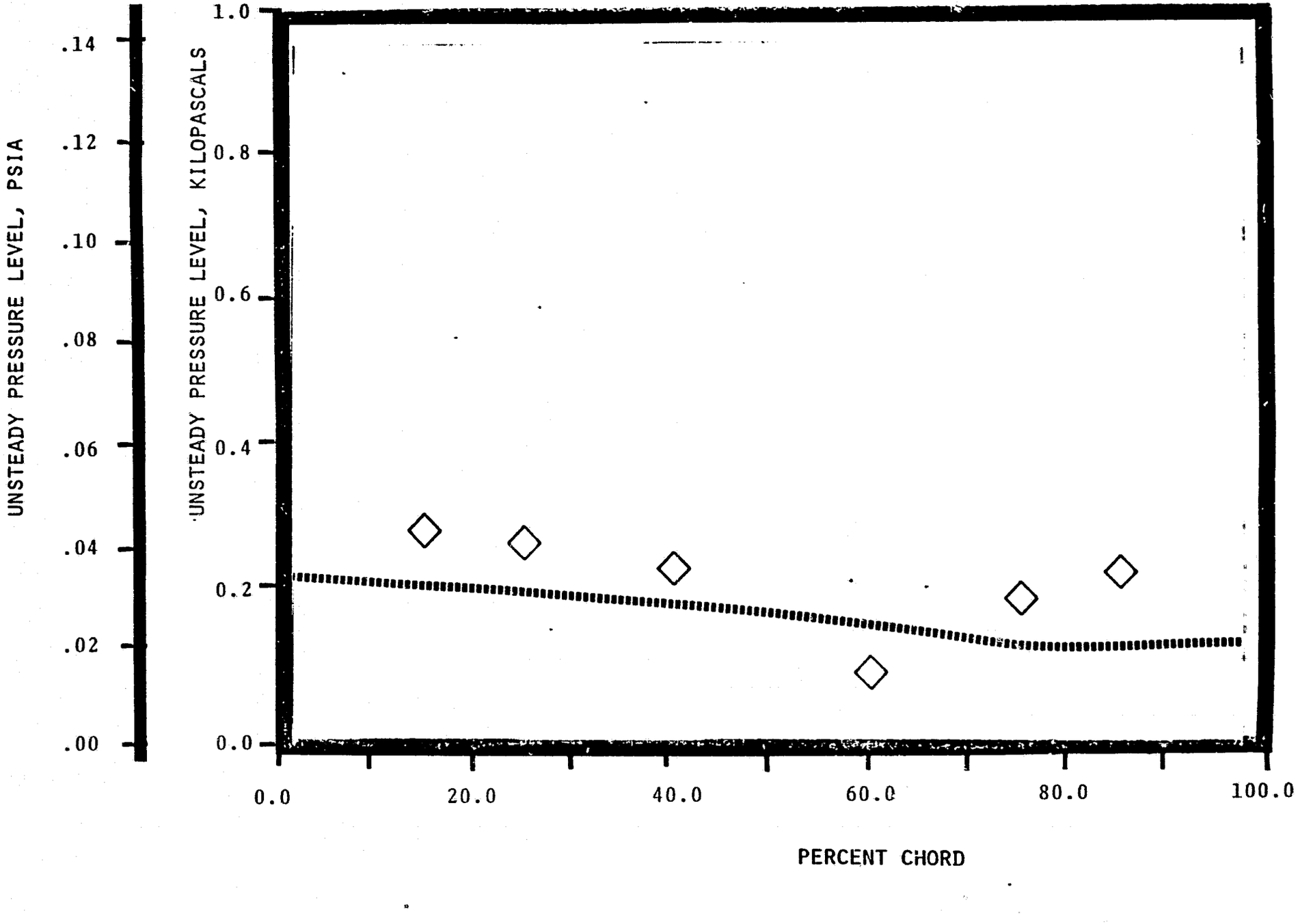

NASA I TORSION CASCADE

PRESSURE SURFACE AERODYNAMIC PHASE LAG DISTRIBUTION
1.315 INLET MACH NUMBER
1.45 STATIC PRESSURE RATIO
-1.75 rad(-100°) INTERBLADE PHASE ANGLE

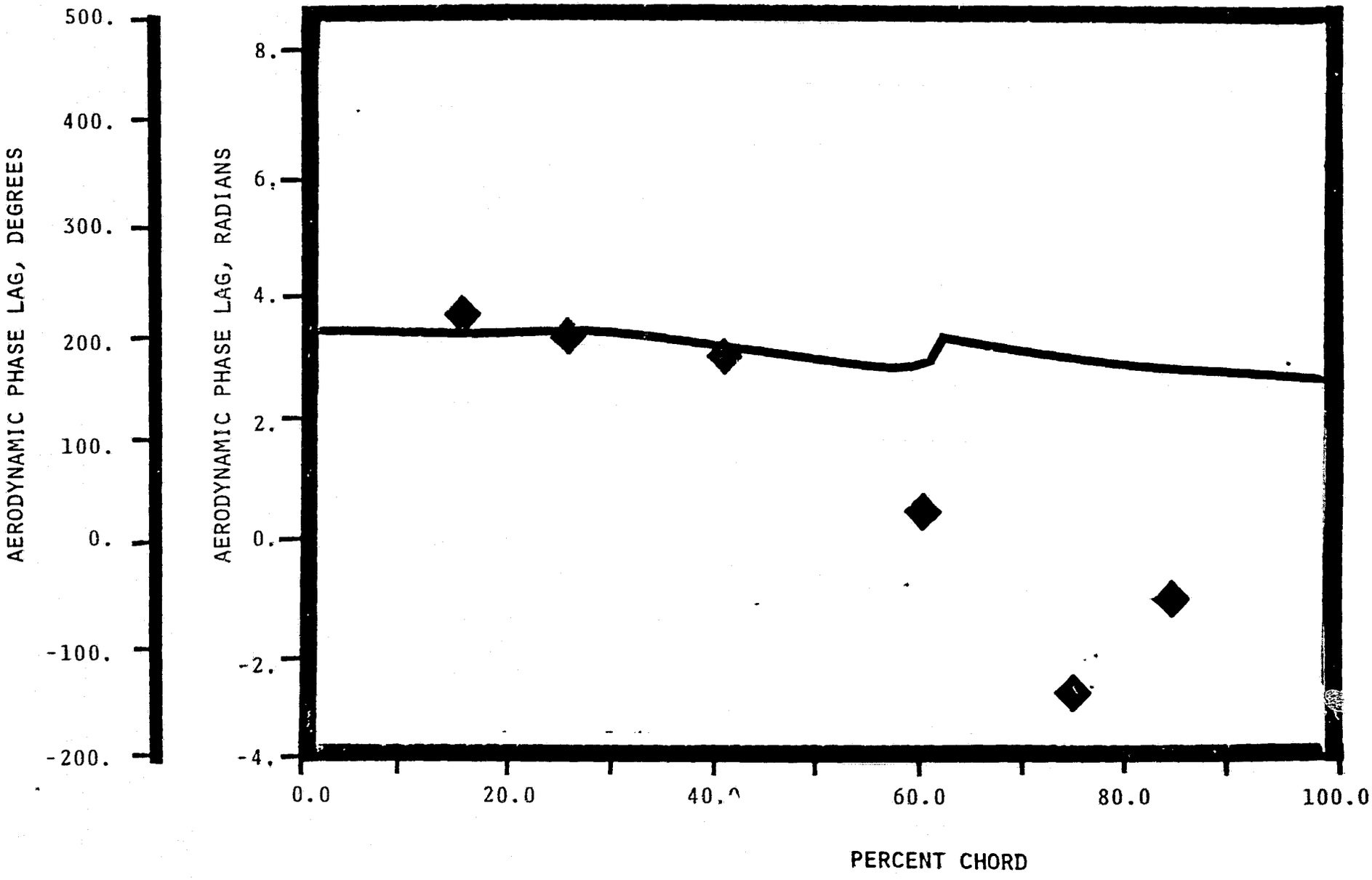

NASA I TORSION CASCADE

PRESSURE SURFACE UNSTEADY PRESSURE DISTRIBUTION

1.315 INLET MACH NUMBER

1.45 STATIC PRESSURE RATIO

-1.75 rad (-100°) INTERBLADE PHASE ANGLE

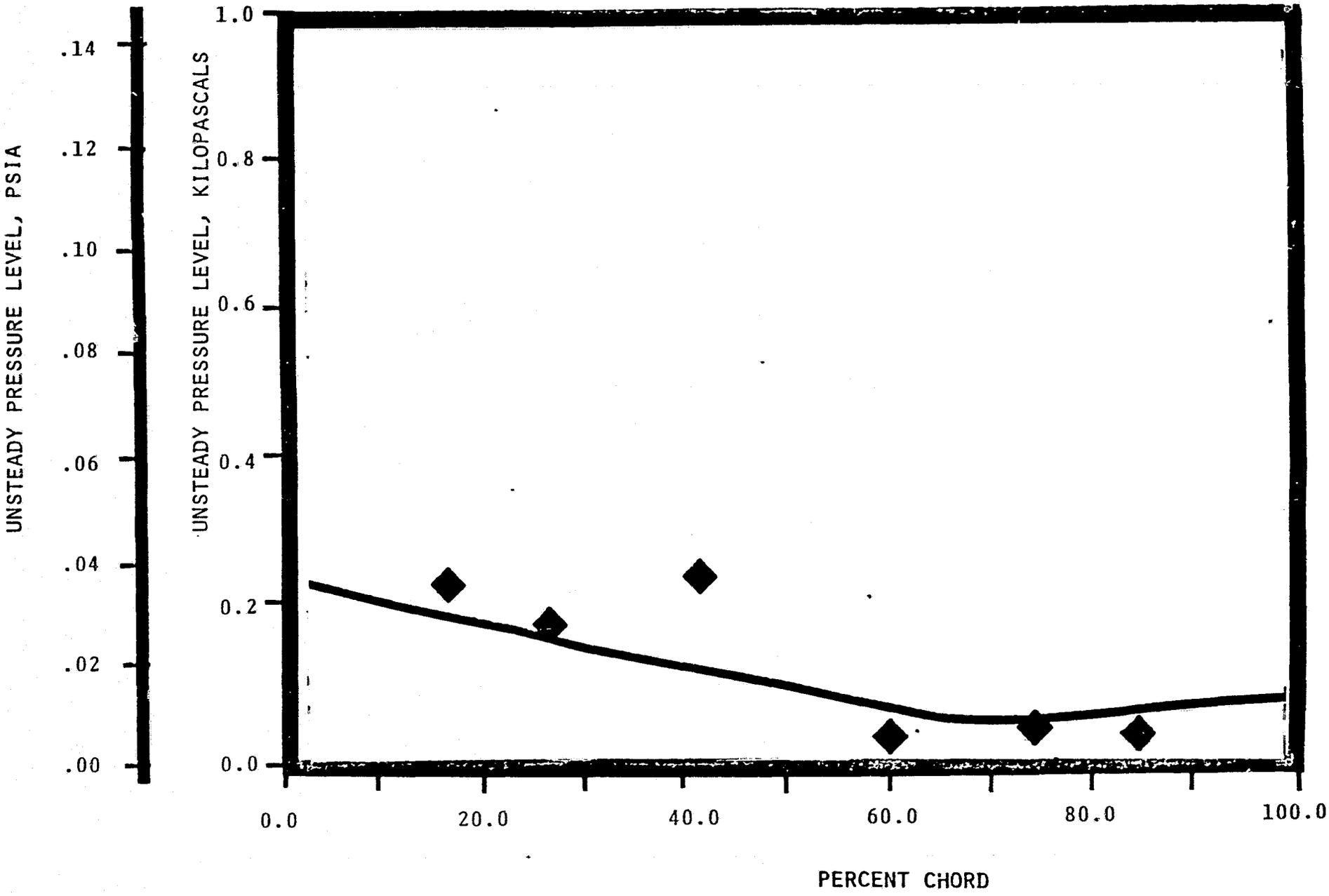

NASA I TORSION CASCADE

SUCTION SURFACE AERODYNAMIC PHASE LAG DISTRIBUTION

1.315 INLET MACH NUMBER

1.45 STATIC PRESSURE RATIO

-1.75 rad (-100°) INTERBLADE PHASE ANGLE

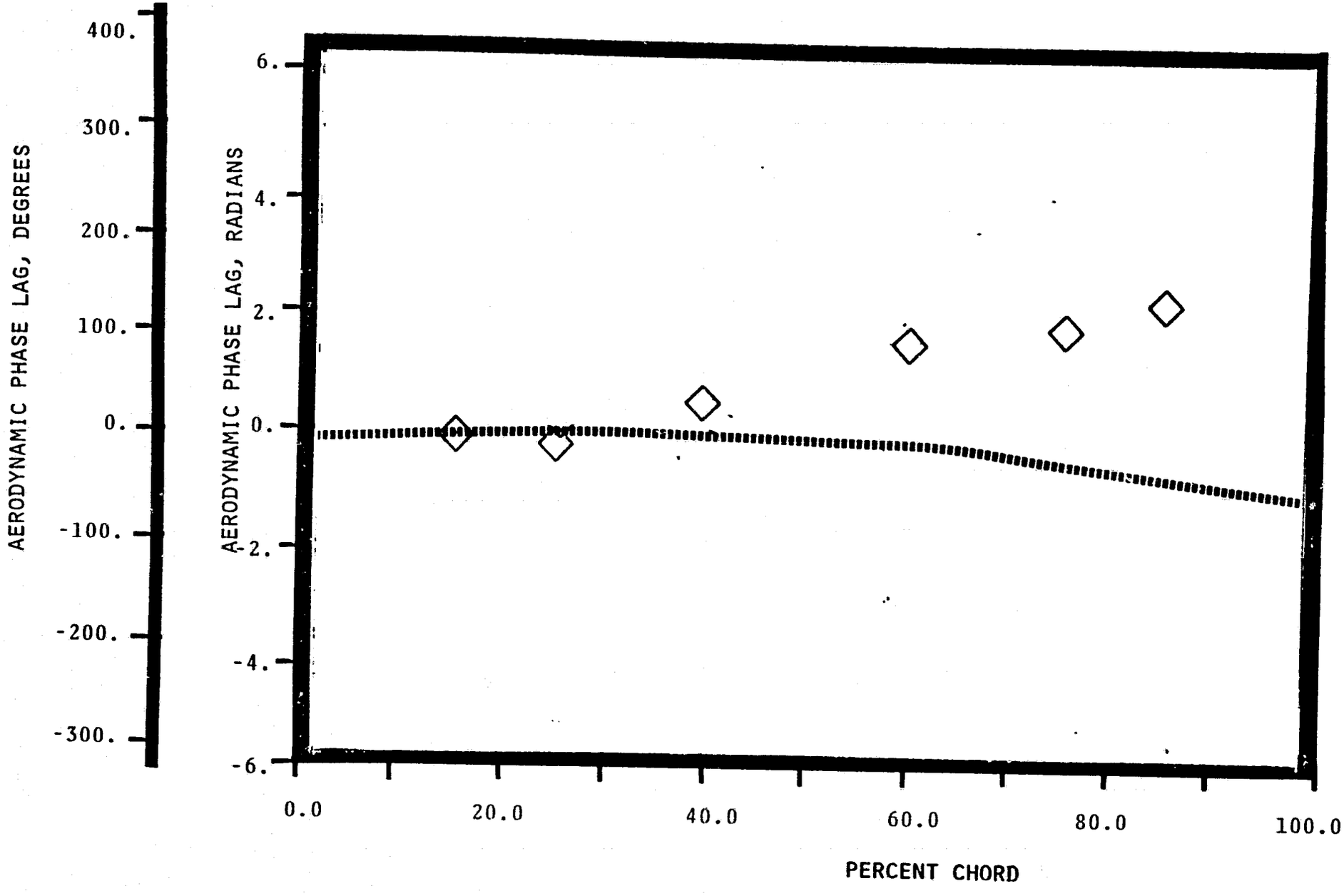

NASA I TORSION CASCADE

SUCTION SURFACE UNSTEADY PRESSURE DISTRIBUTION

1.315 INLET MACH NUMBER

1.45 STATIC PRESSURE RATIO

-1.75 rad (-100°) INTERBLADE PHASE ANGLE

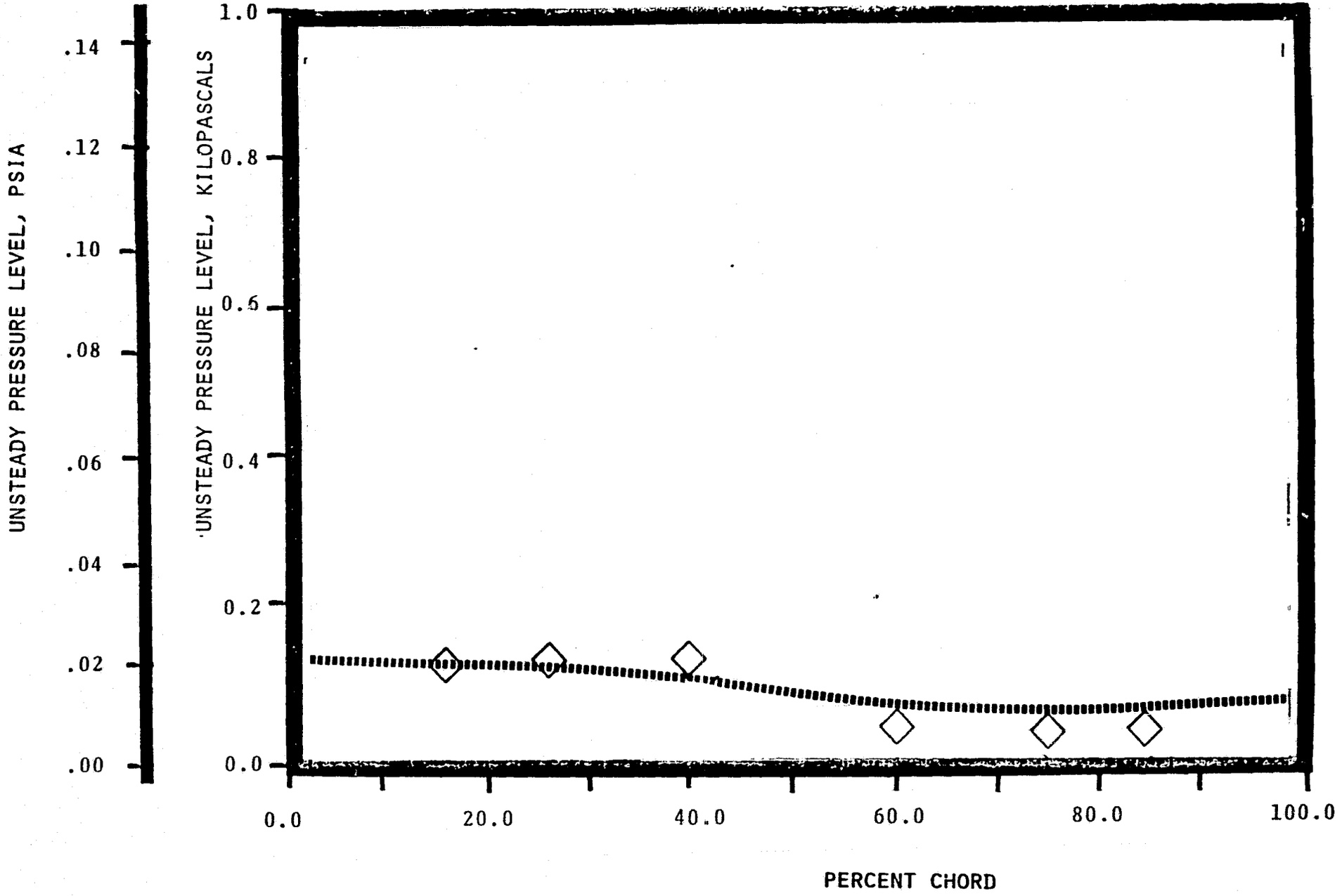

EDR 10119

APPENDIX D

Reduced Solidity Cascades Time Variant Data/Theory Correlation Plots

NASA I TORSION CASCADE - REDUCED SOLIDITY - NOMINAL SETTING

PRESSURE SURFACE AERODYNAMIC PHASE LAG DISTRIBUTION
1.315 INLET MACH NUMBER
1.03 STATIC PRESSURE RATIO
3.14 rad (180°) INTERBLADE PHASE ANGLE

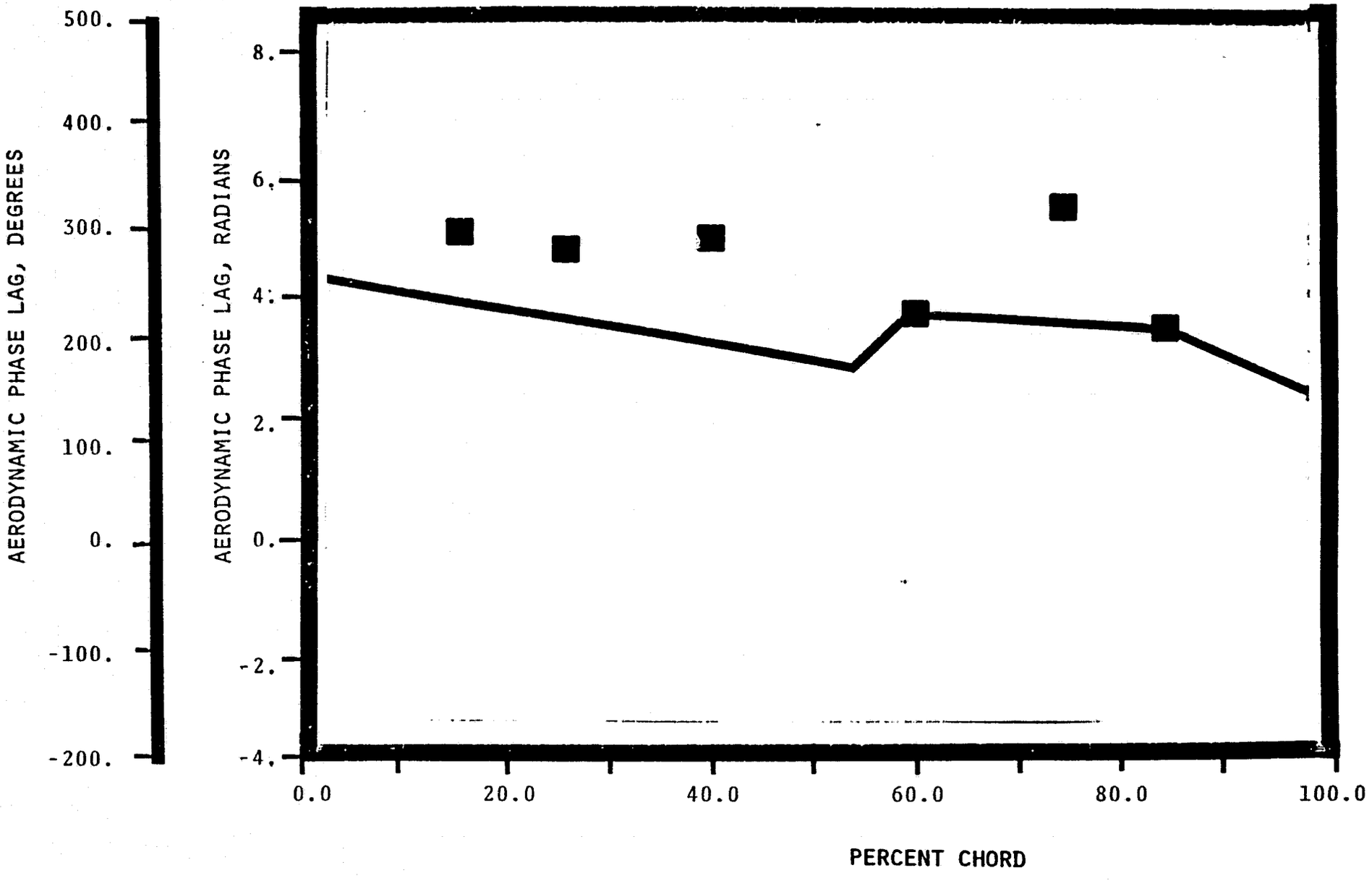

NASA I TORSION CASCADE - REDUCED SOLIDITY - NOMINAL SETTING

PRESSURE SURFACE UNSTEADY PRESSURE DISTRIBUTION

1.315 INLET MACH NUMBER

1.03 STATIC PRESSURE RATIO

3.14 rad (180°) INTERBLADE PHASE ANGLE

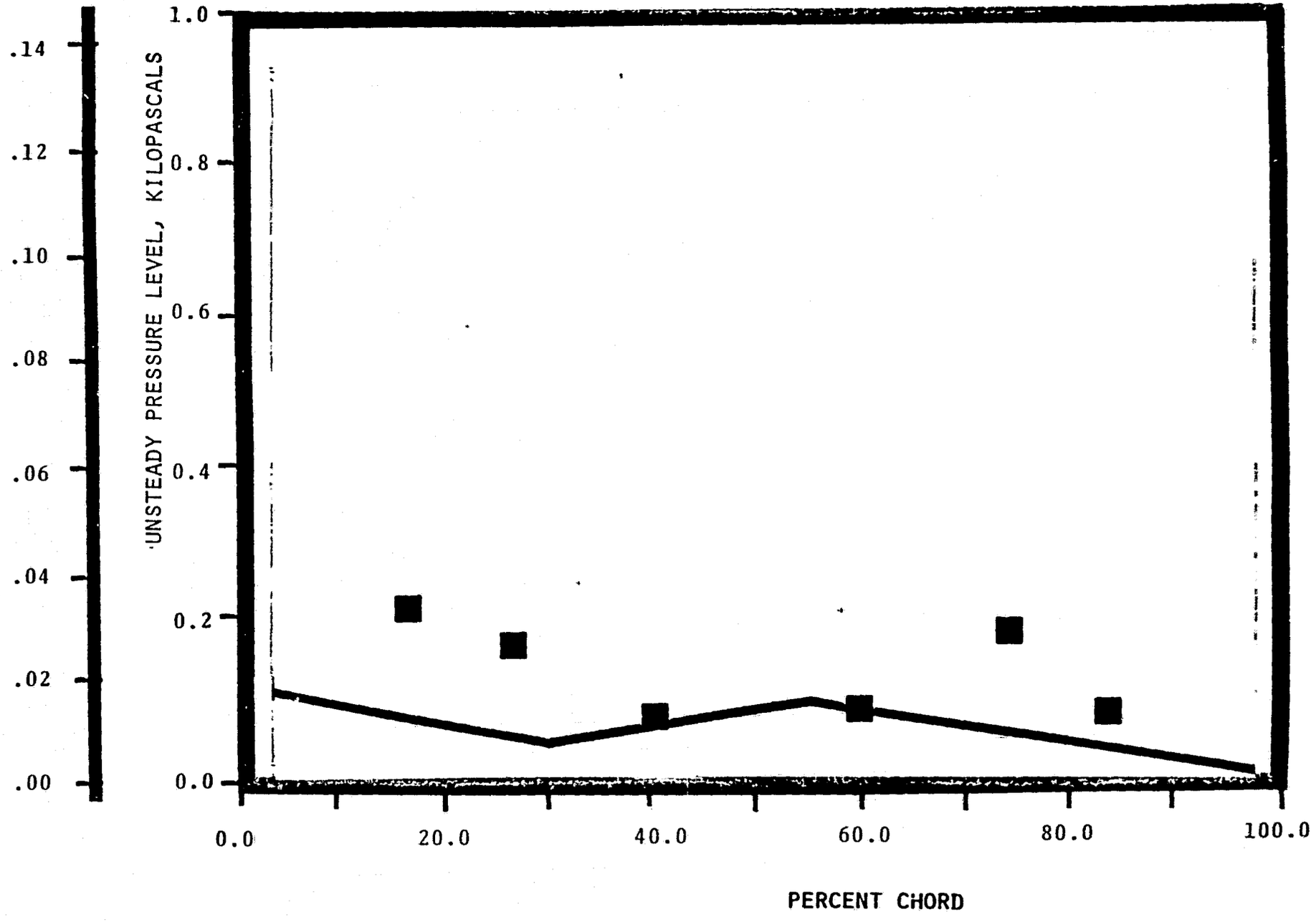

NASA I TORSION CASCADE - REDUCED SOLIDITY - NOMINAL SETTING

SUCTION SURFACE AERODYNAMIC PHASE LAG DISTRIBUTION

1.315 INLET MACH NUMBER

1.03 STATIC PRESSURE RATIO

3.14 rad (180°) INTERBLADE PHASE ANGLE

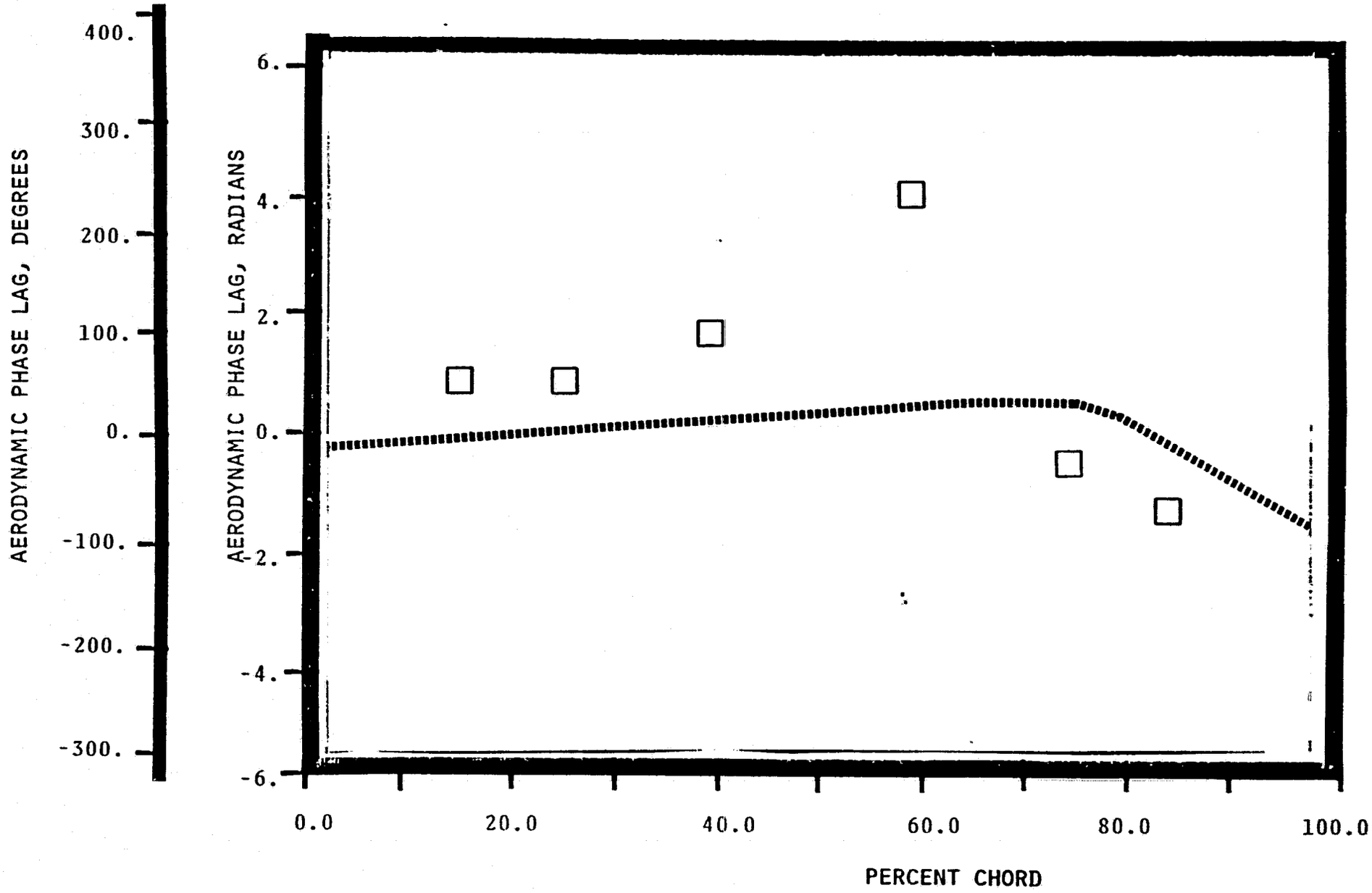

NASA I TORSION CASCADE - REDUCED SOLIDITY - NOMINAL SETTING

SUCTION SURFACE UNSTEADY PRESSURE DISTRIBUTION

1.315 INLET MACH NUMBER

1.03 STATIC PRESSURE RATIO

3.14 rad (180 °) INTERBLADE PHASE ANGLE

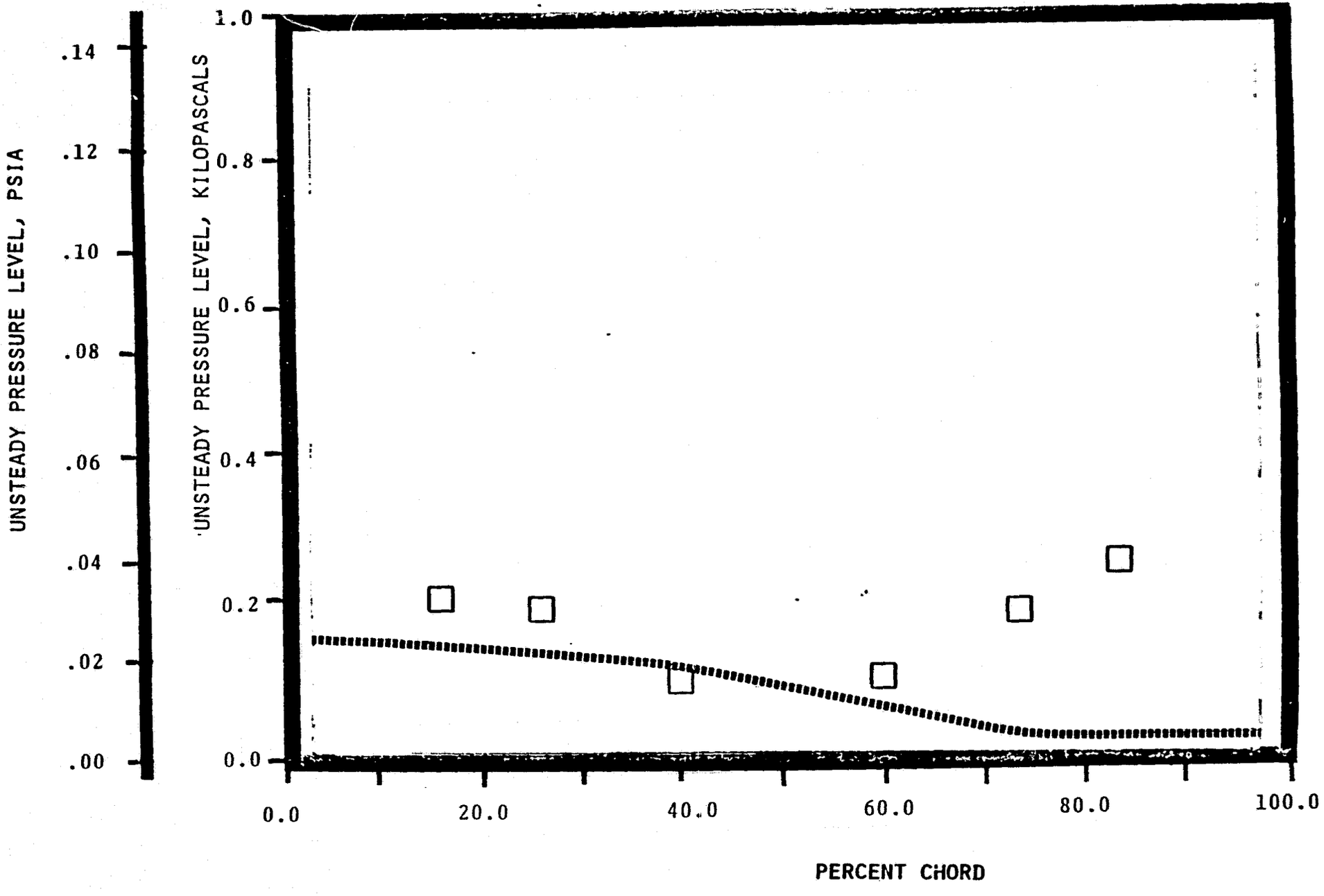

NASA I TORSION CASCADE - REDUCED SOLIDITY - NOMINAL SETTING

PRESSURE SURFACE AERODYNAMIC PHASE LAG DISTRIBUTION
1.315 INLET MACH NUMBER
1.03 STATIC PRESSURE RATIO
1.57 rad (90 °) INTERBLADE PHASE ANGLE

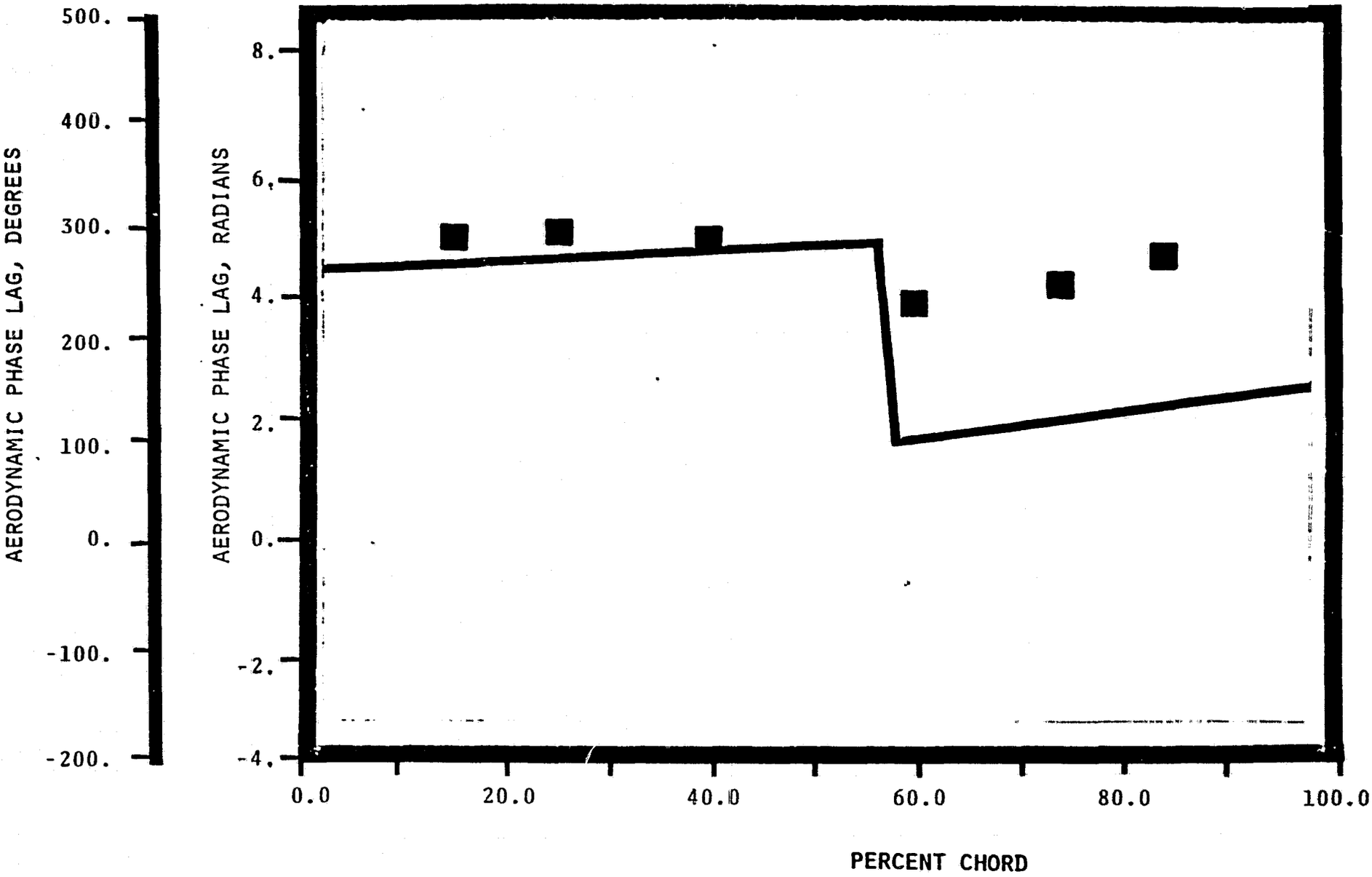

NASA I TORSION CASCADE - REDUCED SOLIDITY - NOMINAL SETTING

PRESSURE SURFACE UNSTEADY PRESSURE DISTRIBUTION

1.315 INLET MACH NUMBER

1.03 STATIC PRESSURE RATIO

1.57 rad (90 °) INTERBLADE PHASE ANGLE

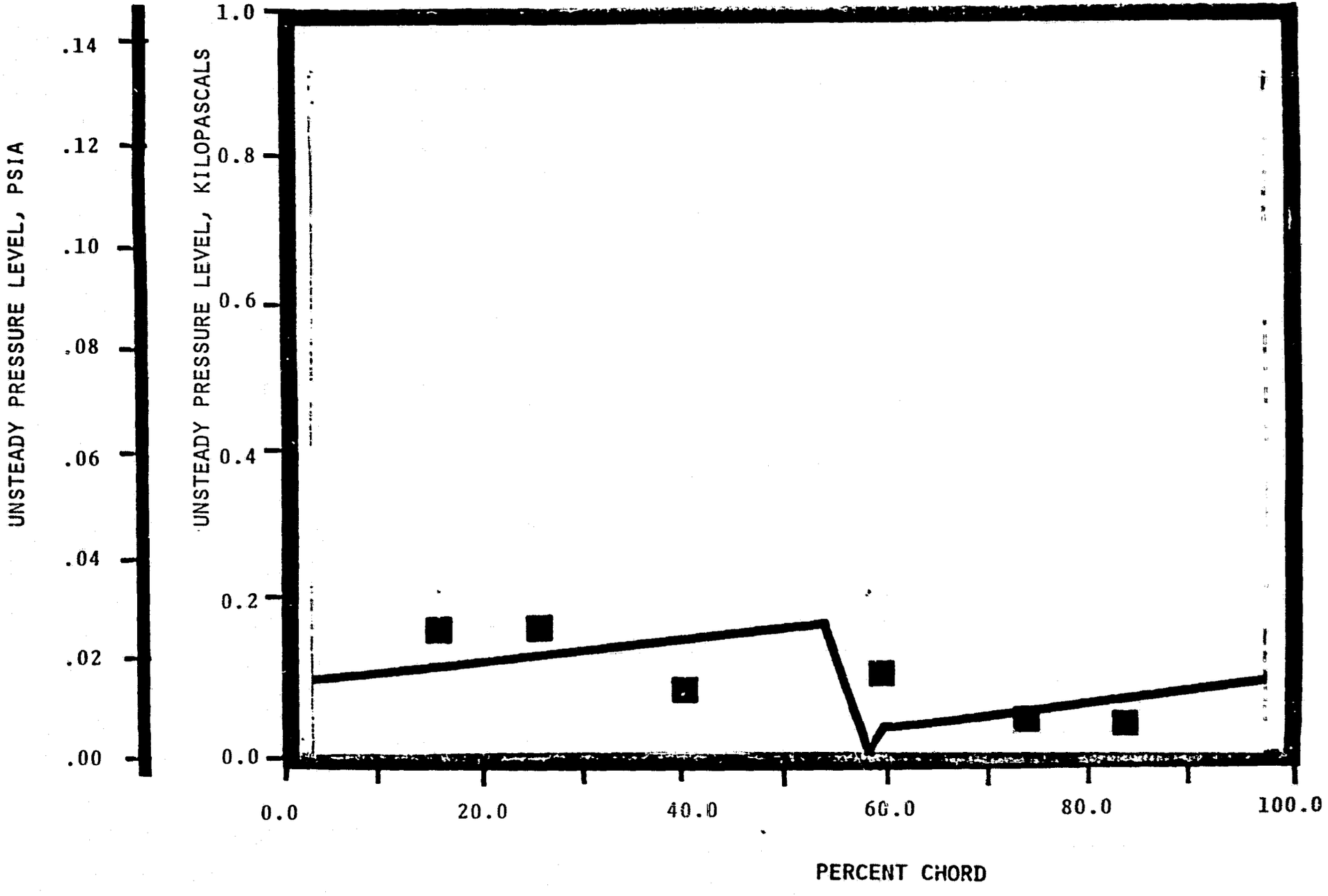

NASA I TORSION CASCADE - REDUCED SOLIDITY - NOMINAL SETTING

SUCTION SURFACE AERODYNAMIC PHASE LAG DISTRIBUTION

1.315 INLET MACH NUMBER

1.03 STATIC PRESSURE RATIO

1.57 rad (90 °) INTERBLADE PHASE ANGLE

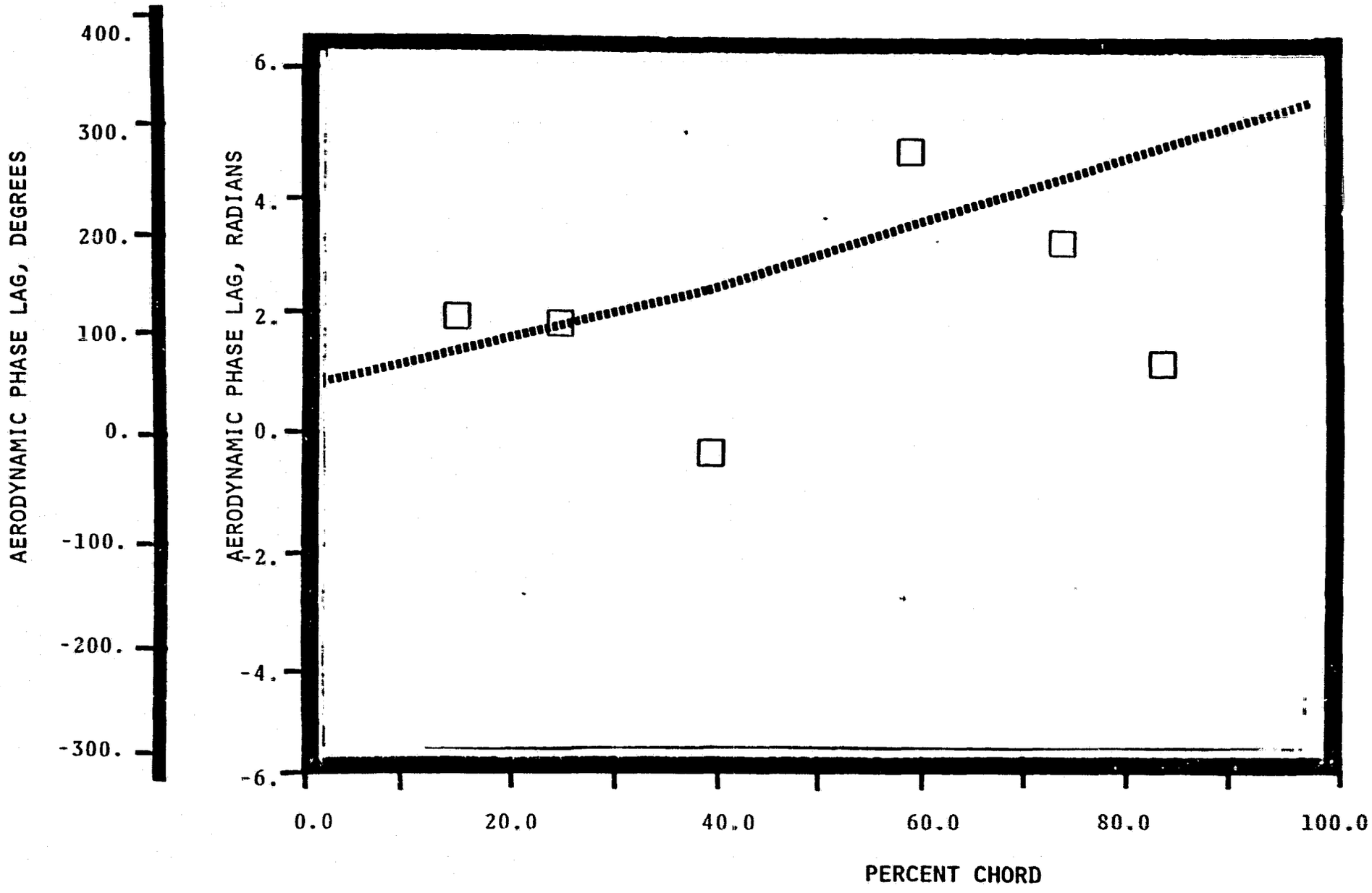

NASA I TORSION CASCADE - REDUCED SOLIDITY - NOMINAL SETTING

SUCTION SURFACE UNSTEADY PRESSURE DISTRIBUTION

1.315 INLET MACH NUMBER

1.03 STATIC PRESSURE RATIO

1.57 rad (90 °) INTERBLADE PHASE ANGLE

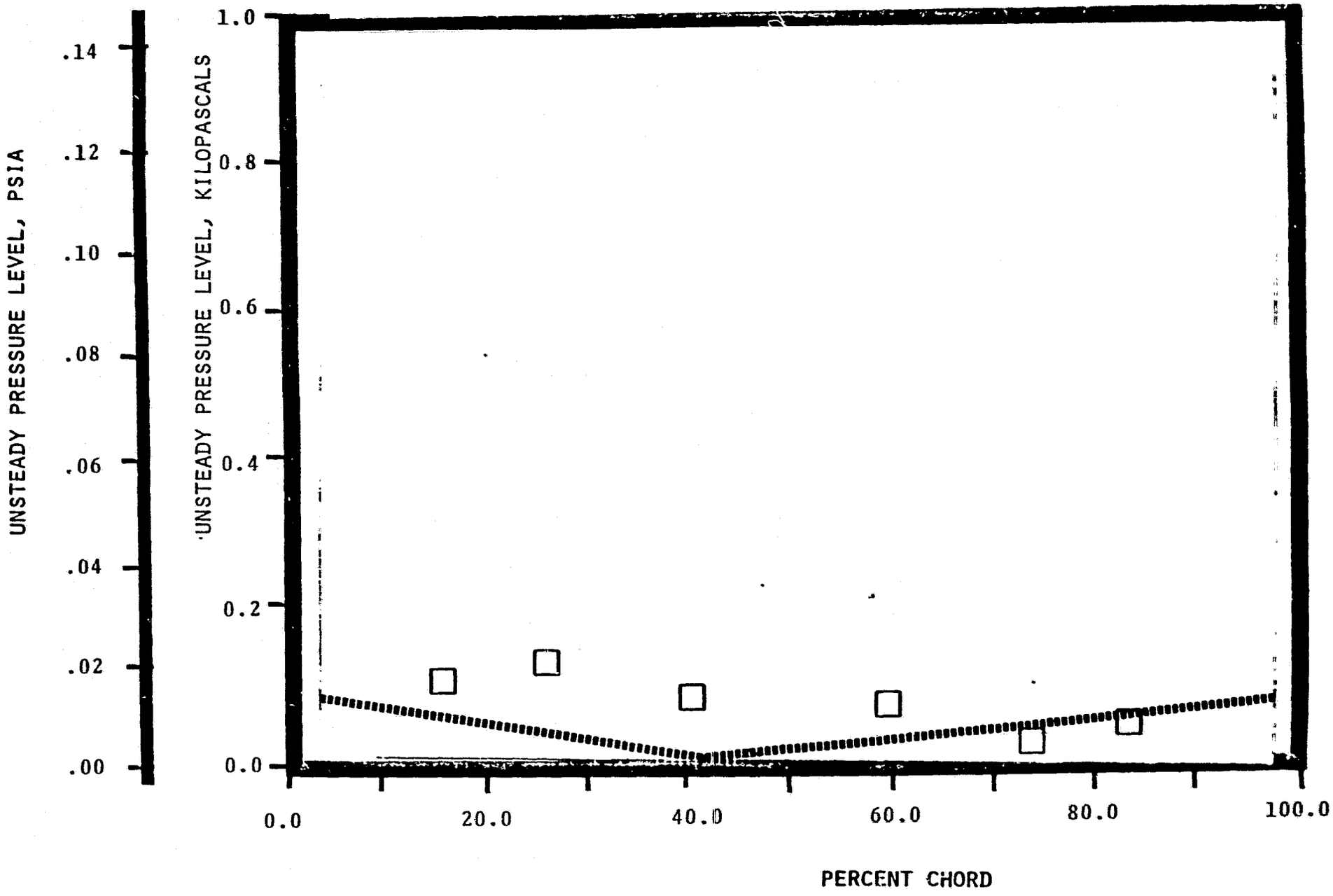

NASA I TORSION CASCADE - REDUCED SOLIDITY - NOMINAL SETTING

PRESSURE SURFACE AERODYNAMIC PHASE LAG DISTRIBUTION
1.315 INLET MACH NUMBER
1.03 STATIC PRESSURE RATIO
0.0 rad (0.°) INTERBLADE PHASE ANGLE

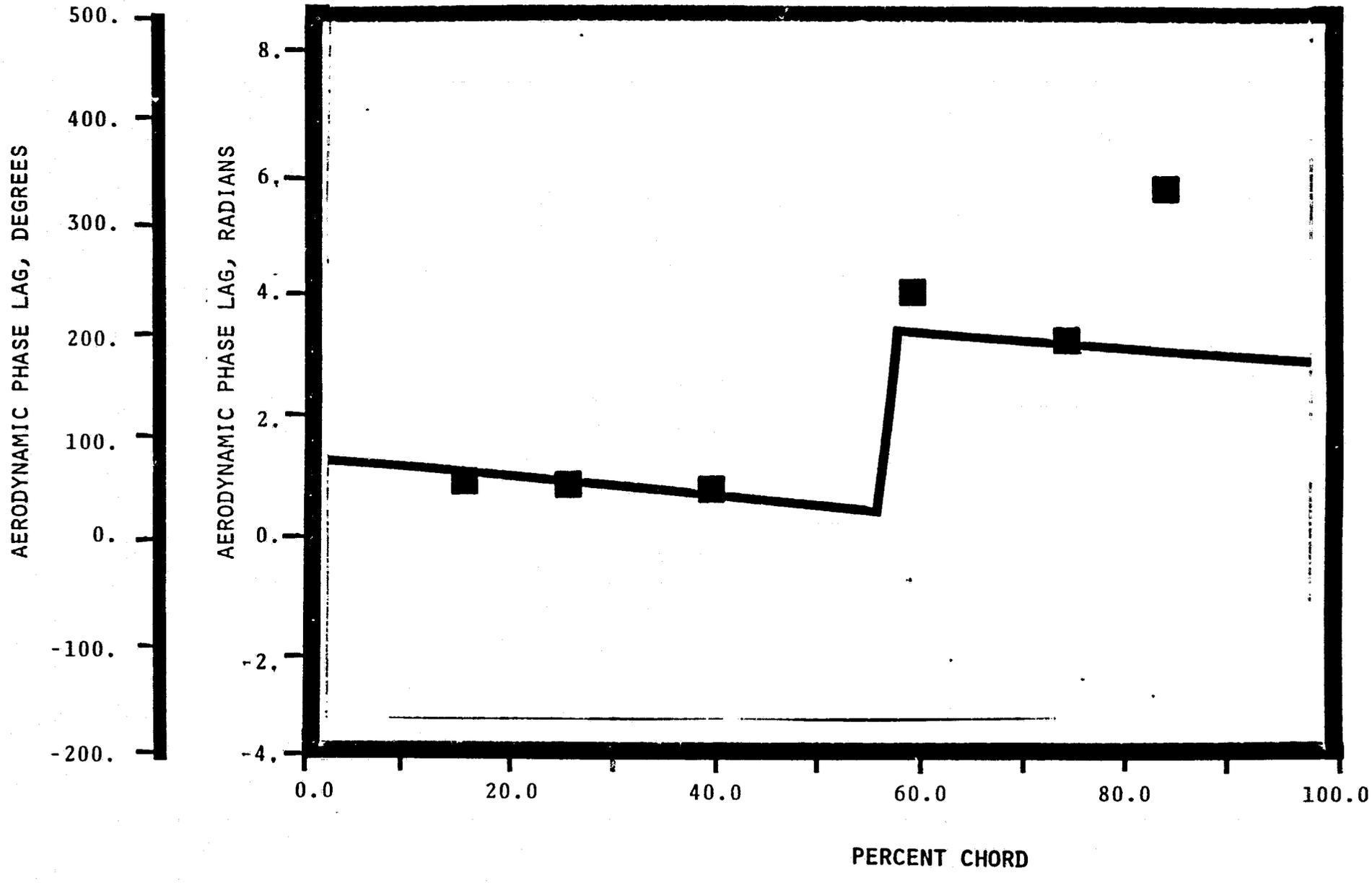

NASA I TORSION CASCADE - REDUCED SOLIDITY - NOMINAL SETTING

PRESSURE SURFACE UNSTEADY PRESSURE DISTRIBUTION

1.315 INLET MACH NUMBER

1.03 STATIC PRESSURE RATIO

0.0 rad (0.°) INTERBLADE PHASE ANGLE

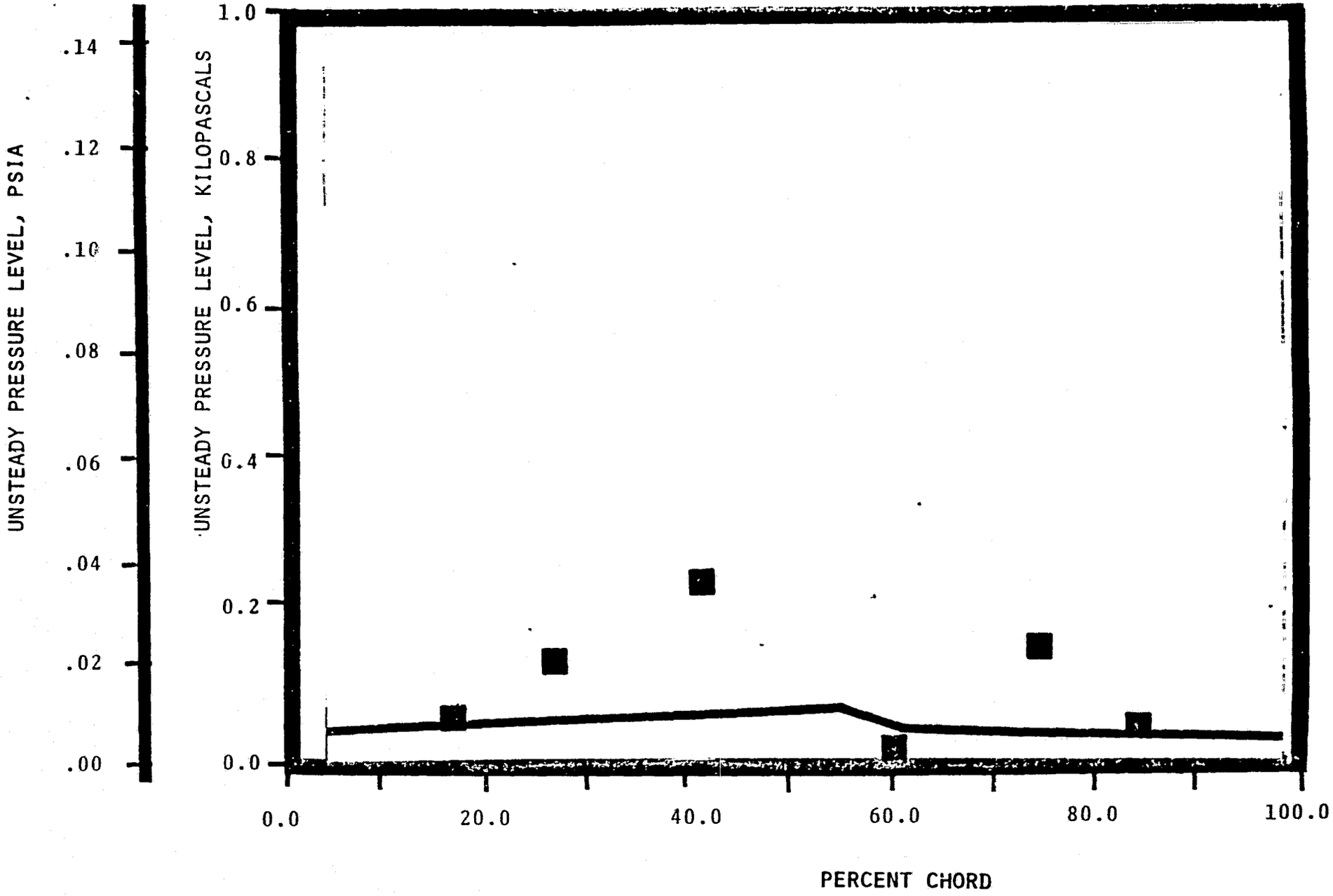

NASA I TORSION CASCADE - REDUCED SOLIDITY - NOMINAL SETTING

SUCTION SURFACE AERODYNAMIC PHASE LAG DISTRIBUTION

1.315 INLET MACH NUMBER

1.03 STATIC PRESSURE RATIO

0.0 rad (0.°)INTERBLADE PHASE ANGLE

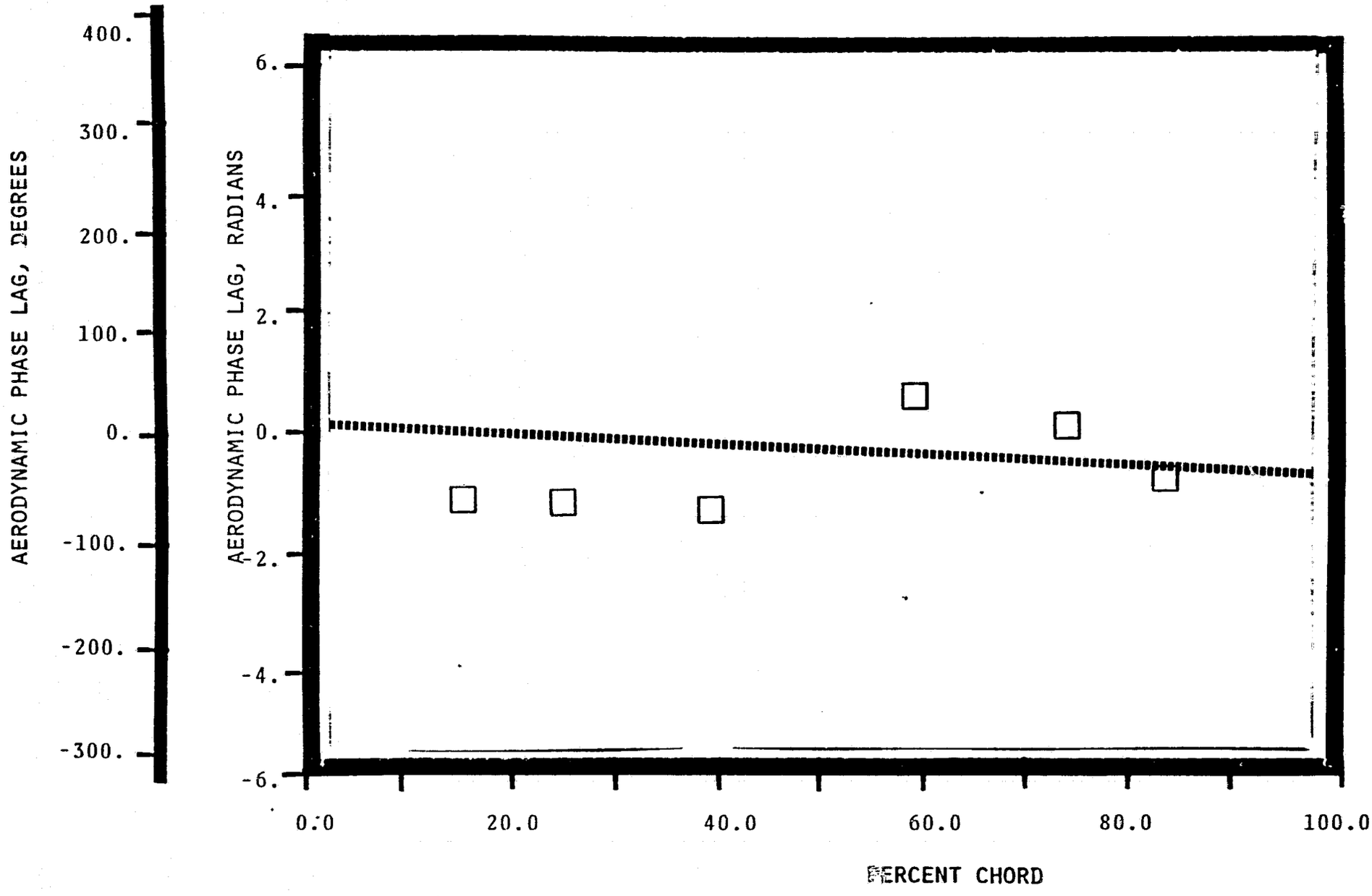

NASA I TORSION CASCADE - REDUCED SOLIDITY - NOMINAL SETTING

SUCTION SURFACE UNSTEADY PRESSURE DISTRIBUTION

1.315 INLET MACH NUMBER

1.03 STATIC PRESSURE RATIO

0.0 rad (0°) INTERBLADE PHASE ANGLE

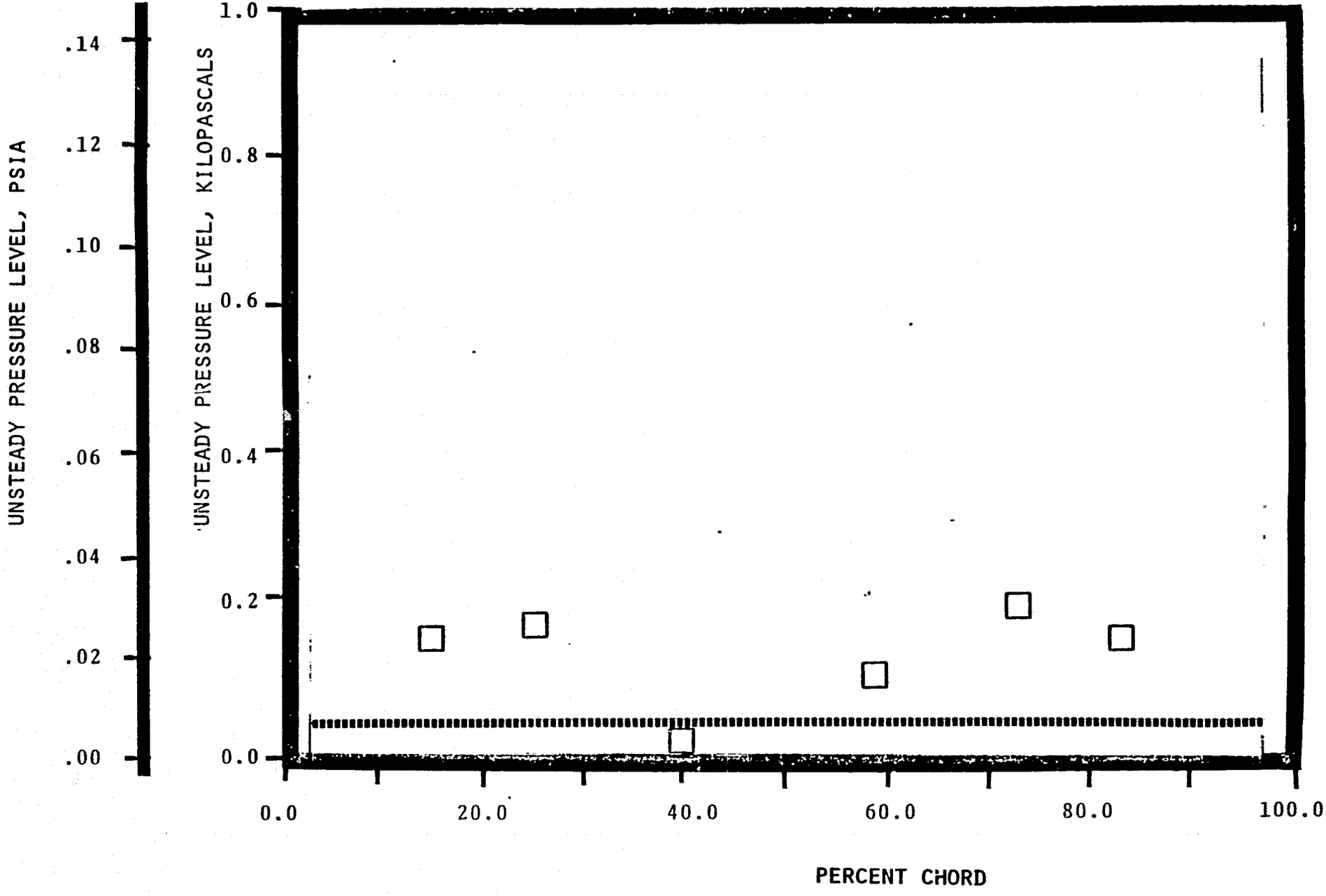

NASA I TORSION CASCADE - REDUCED SOLIDITY - NOMINAL SETTING

PRESSURE SURFACE AERODYNAMIC PHASE LAG DISTRIBUTION

1.315 INLET MACH NUMBER

1.03 STATIC PRESSURE RATIO

-.52 rad (-30) INTERBLADE PHASE ANGLE (-.52 rad.)

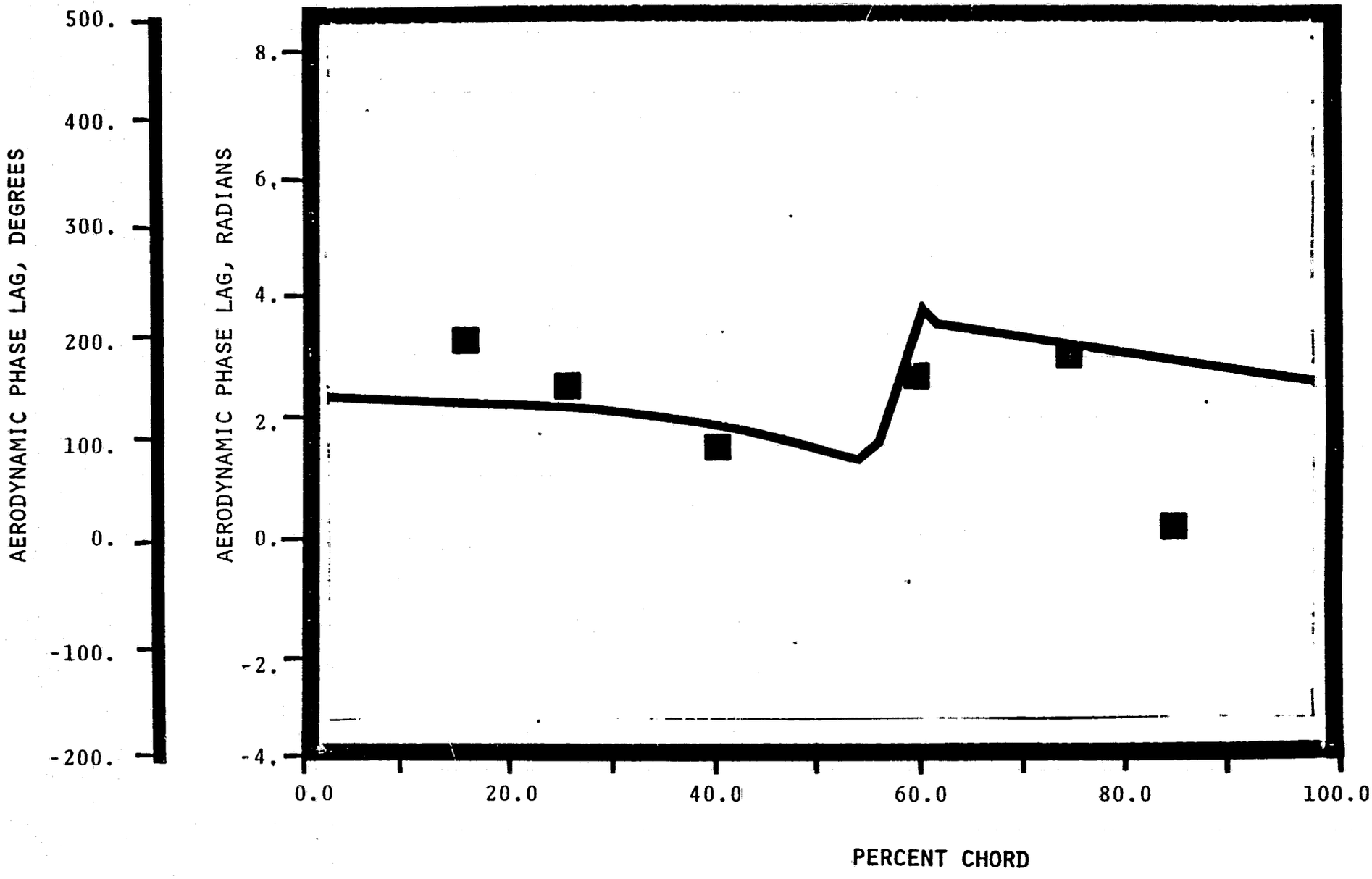

NASA I TORSION CASCADE - REDUCED SOLIDITY - NOMINAL SETTING

PRESSURE SURFACE UNSTEADY PRESSURE DISTRIBUTION
1.315 INLET MACH NUMBER
1.03 STATIC PRESSURE RATIO
-.52 rad (-30°) INTERBLADE PHASE ANGLE

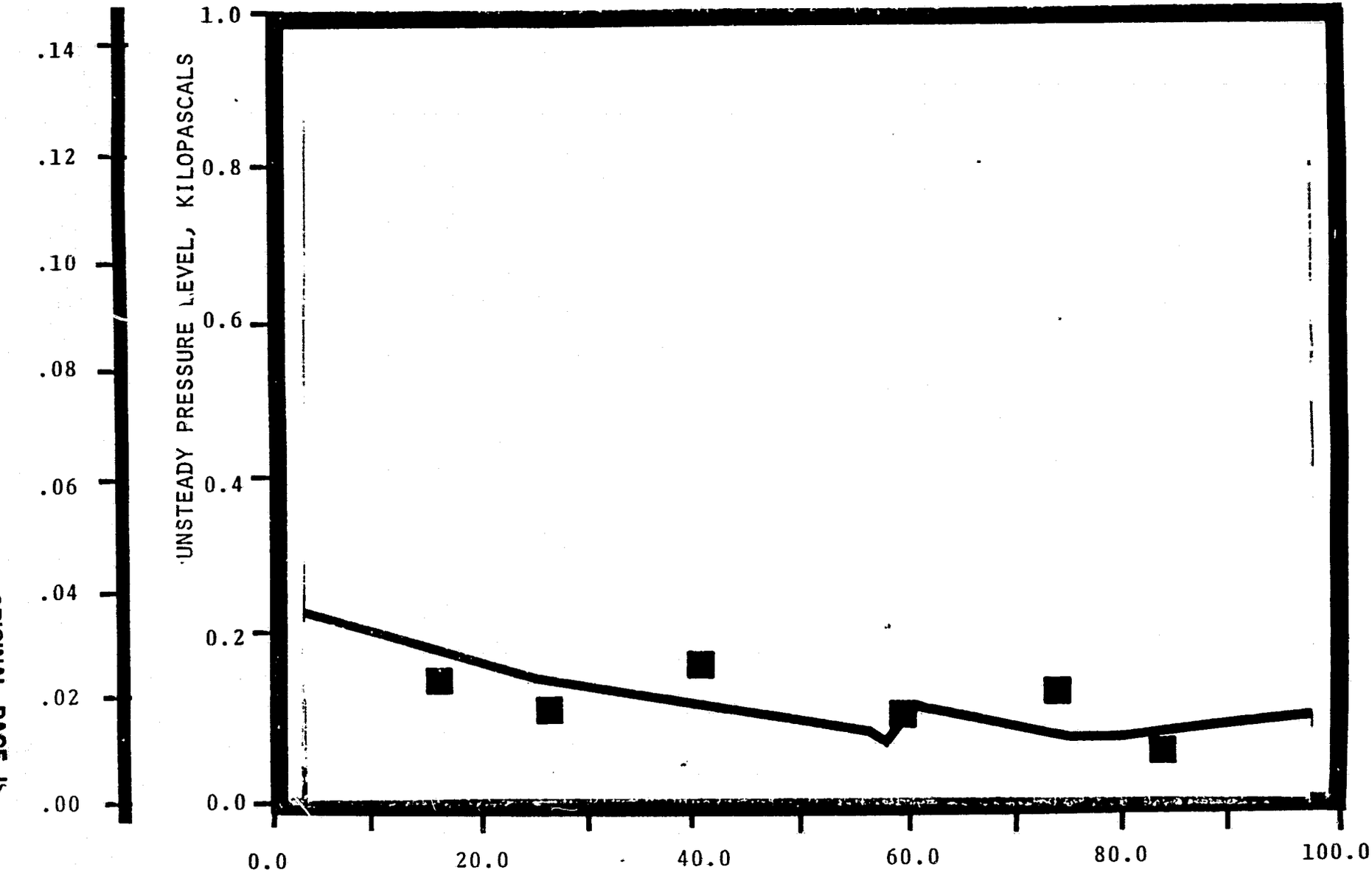

NASA I TORSION CASCADE - REDUCED SOLIDITY - NOMINAL SETTING

SUCTION SURFACE AERODYNAMIC PHASE LAG DISTRIBUTION

1.315 INLET MACH NUMBER

1.03 STATIC PRESSURE RATIO

-.52 rad (-30°) INTERBLADE PHASE ANGLE (-.52 rad.)

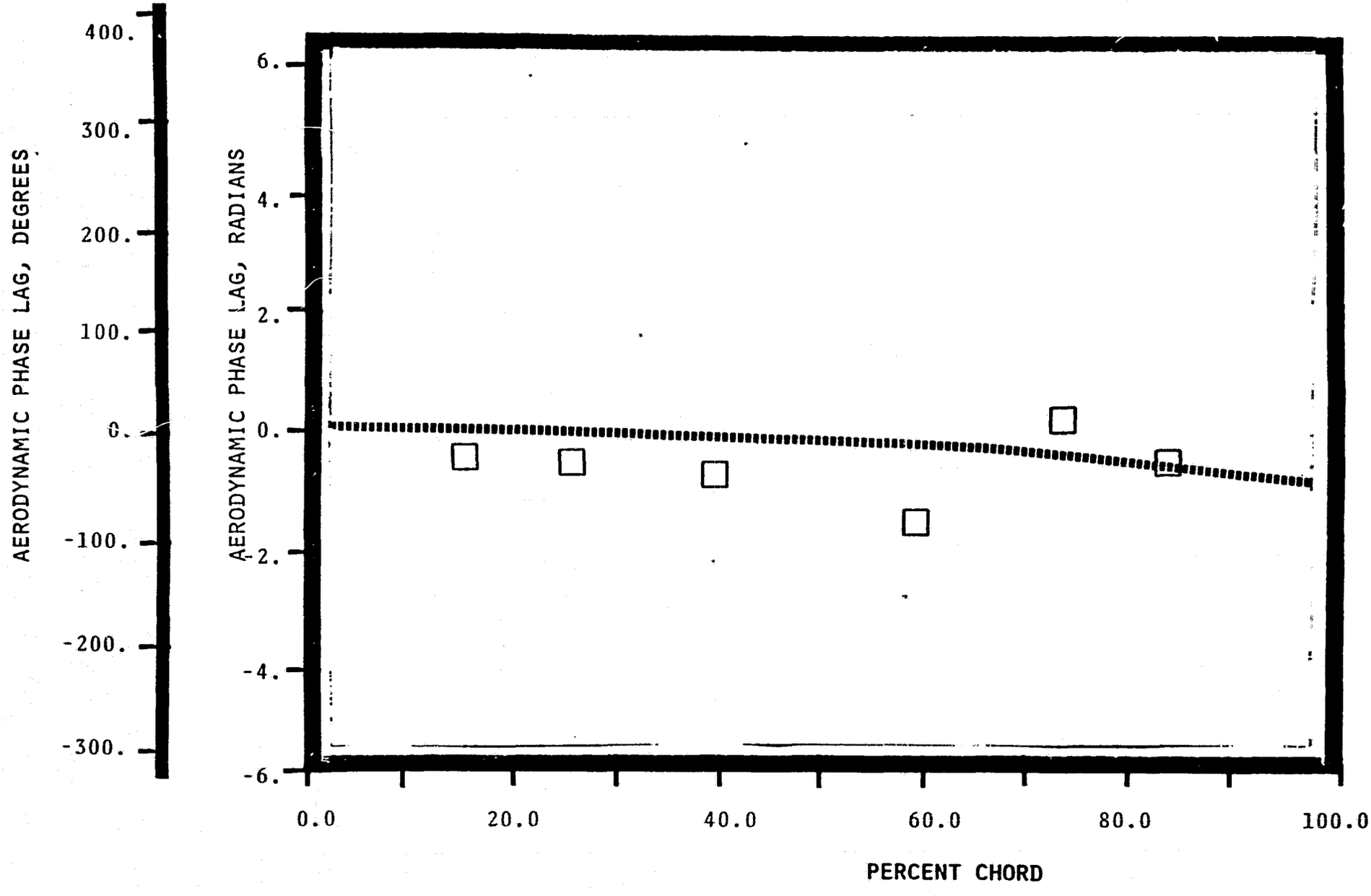

NASA I TORSION CASCADE - REDUCED SOLIDITY - NOMINAL SETTING

SUCTION SURFACE UNSTEADY PRESSURE DISTRIBUTION

1.315 INLET MACH NUMBER

1.03 STATIC PRESSURE RATIO

-.52 rad (-30°) INTERBLADE PHASE ANGLE

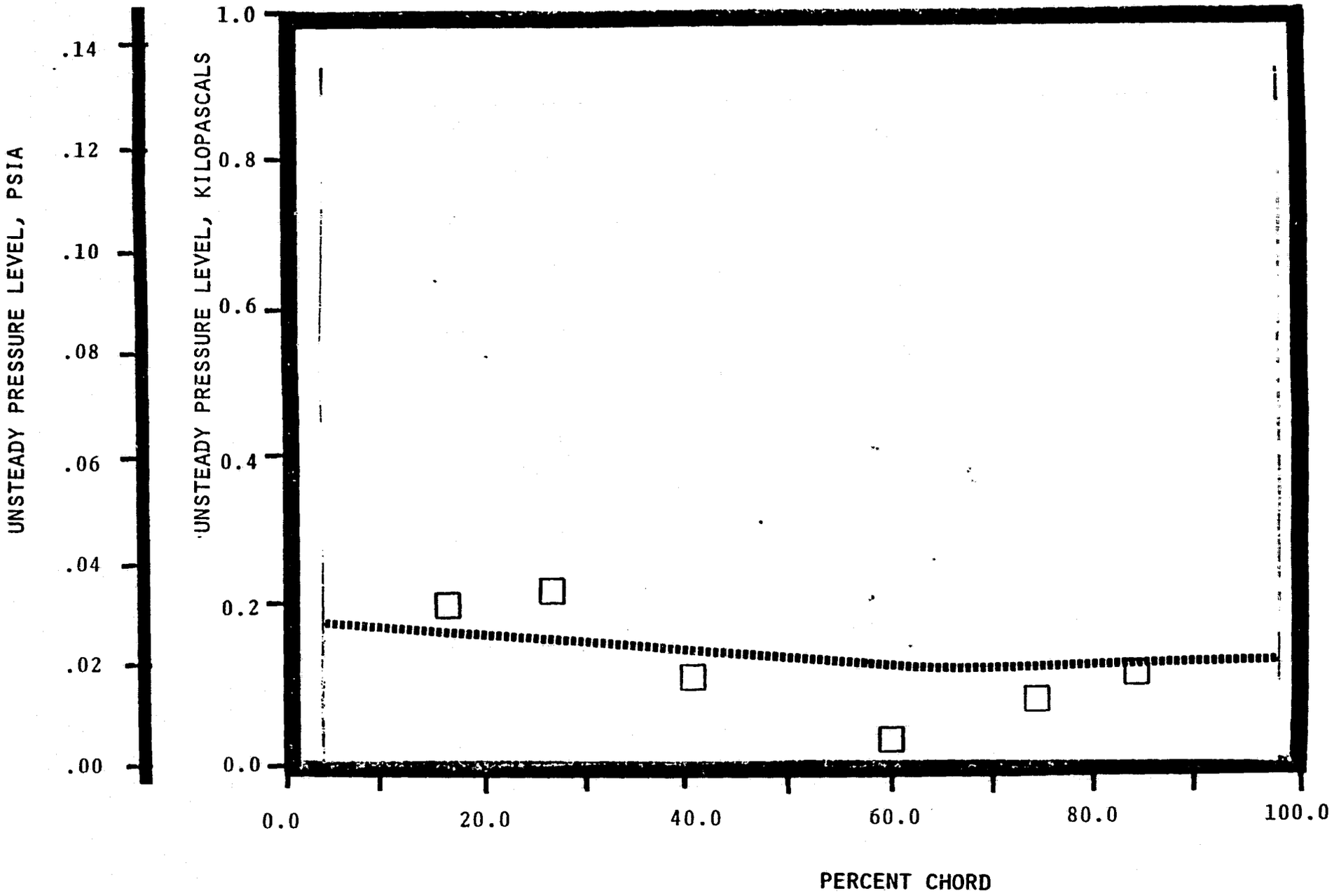

NASA I TORSION CASCADE - REDUCED SOLIDITY - NOMINAL SETTING

PRESSURE SURFACE AERODYNAMIC PHASE LAG DISTRIBUTION
1.315 INLET MACH NUMBER
1.03 STATIC PRESSURE RATIO
-1.05 rad (-60°) INTERBLADE PHASE ANGLE

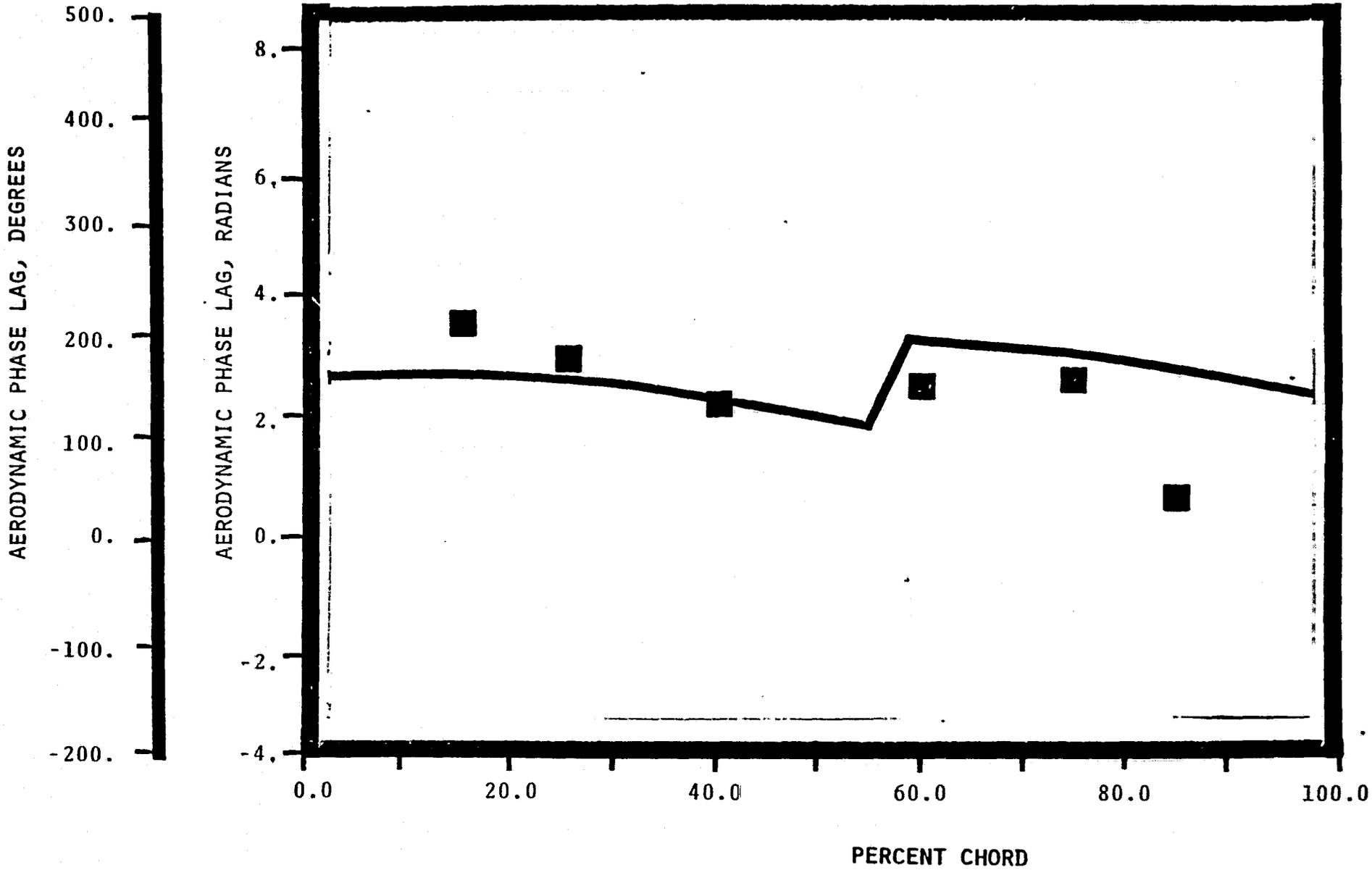

NASA I TORSION CASCADE - REDUCED SOLIDITY - NOMINAL SETTING

PRESSURE SURFACE UNSTEADY PRESSURE DISTRIBUTION

1.315 INLET MACH NUMBER

1.03 STATIC PRESSURE RATIO

-1.05 rad (-60) INTERBLADE PHASE ANGLE

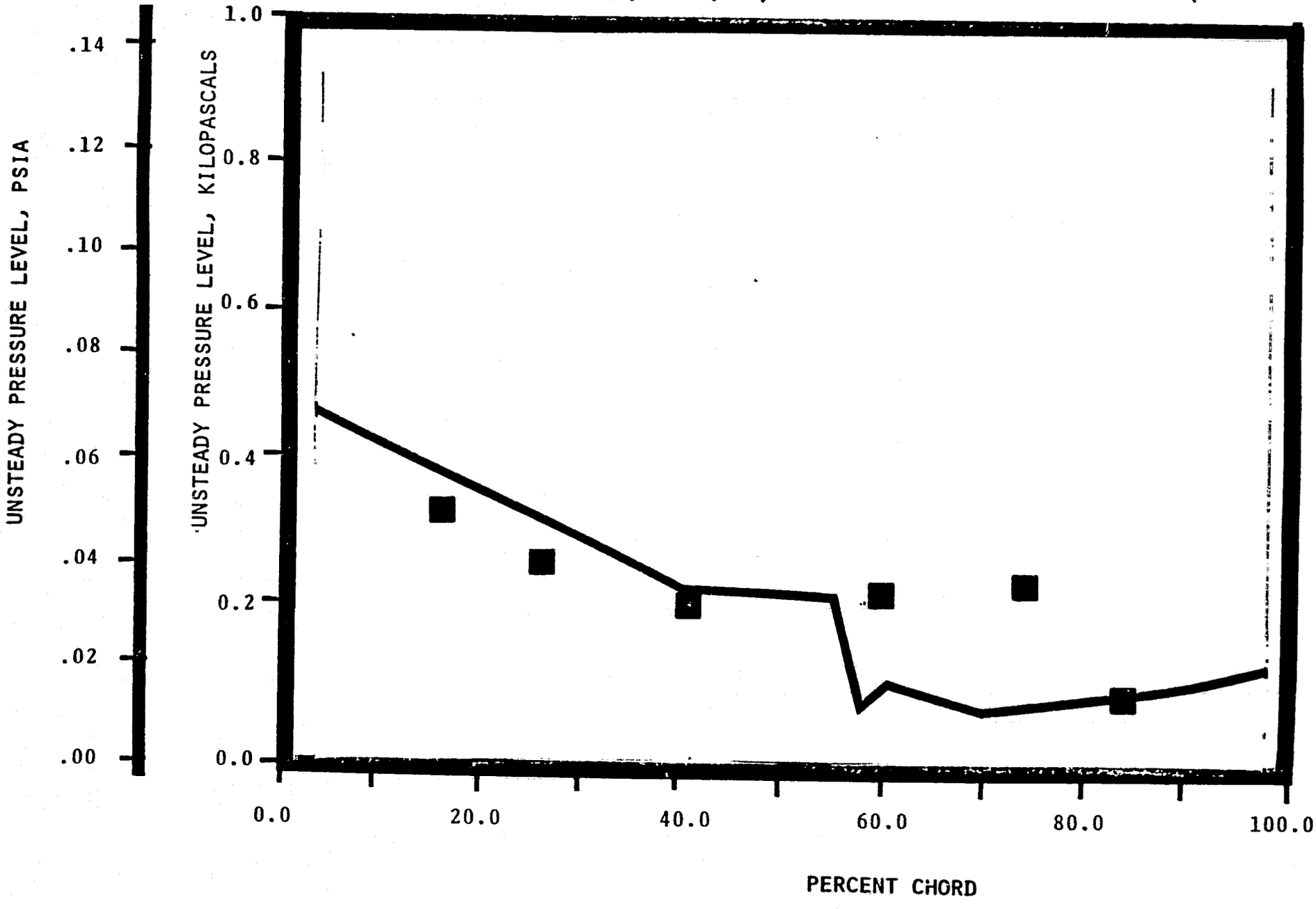

NASA I TORSION CASCADE - REDUCED SOLIDITY - NOMINAL SETTING

SUCTION SURFACE AERODYNAMIC PHASE LAG DISTRIBUTION

1.315 INLET MACH NUMBER

1.03 STATIC PRESSURE RATIO

-1.05 rad (-60°) INTERBLADE PHASE ANGLE

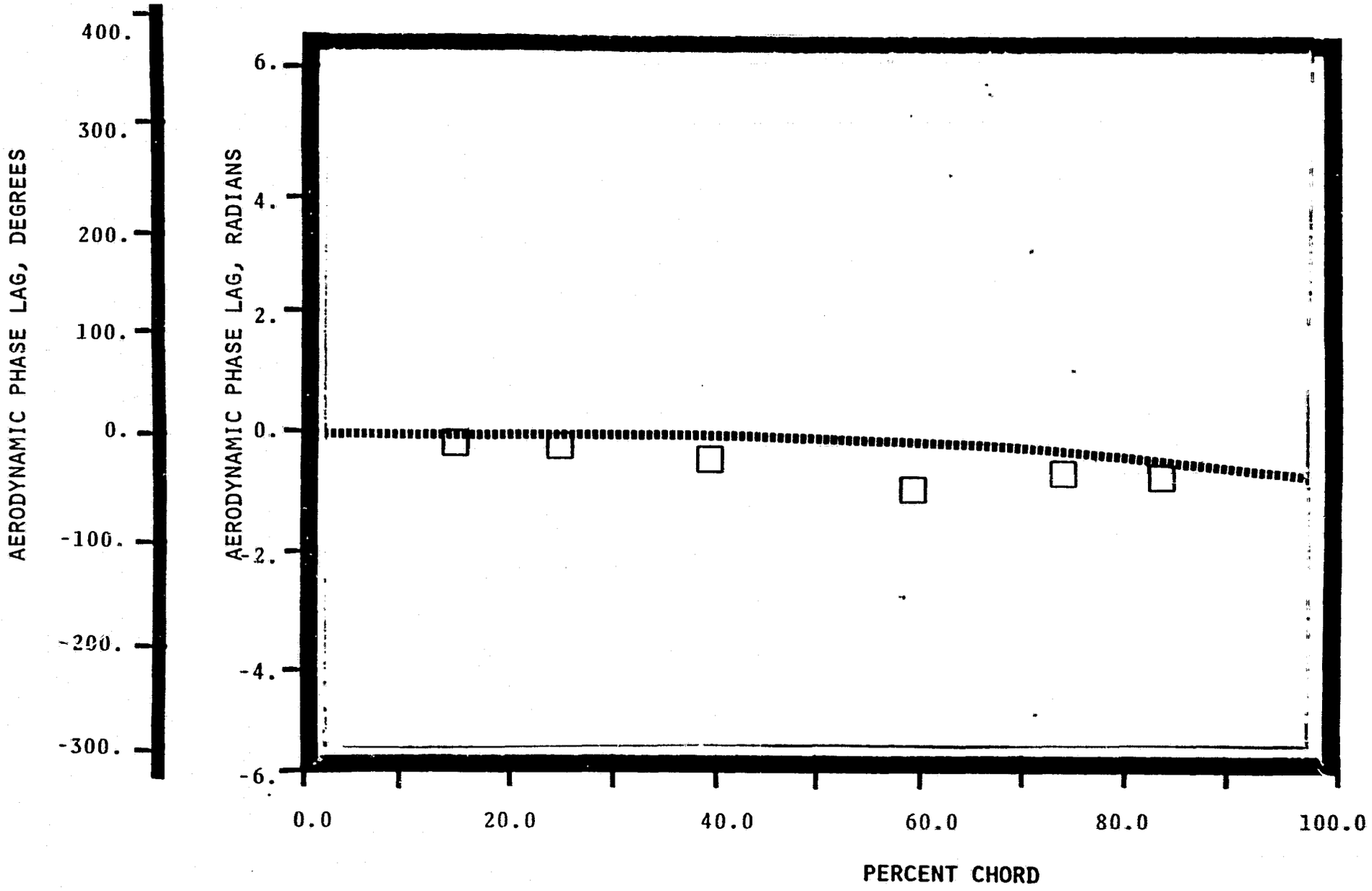

NASA I TORSION CASCADE - REDUCED SOLIDITY - NOMINAL SETTING

SUCTION SURFACE UNSTEADY PRESSURE DISTRIBUTION

1.315 INLET MACH NUMBER

1.03 STATIC PRESSURE RATIO

-1.05 rad (-60.°) INTERBLADE PHASE ANGLE

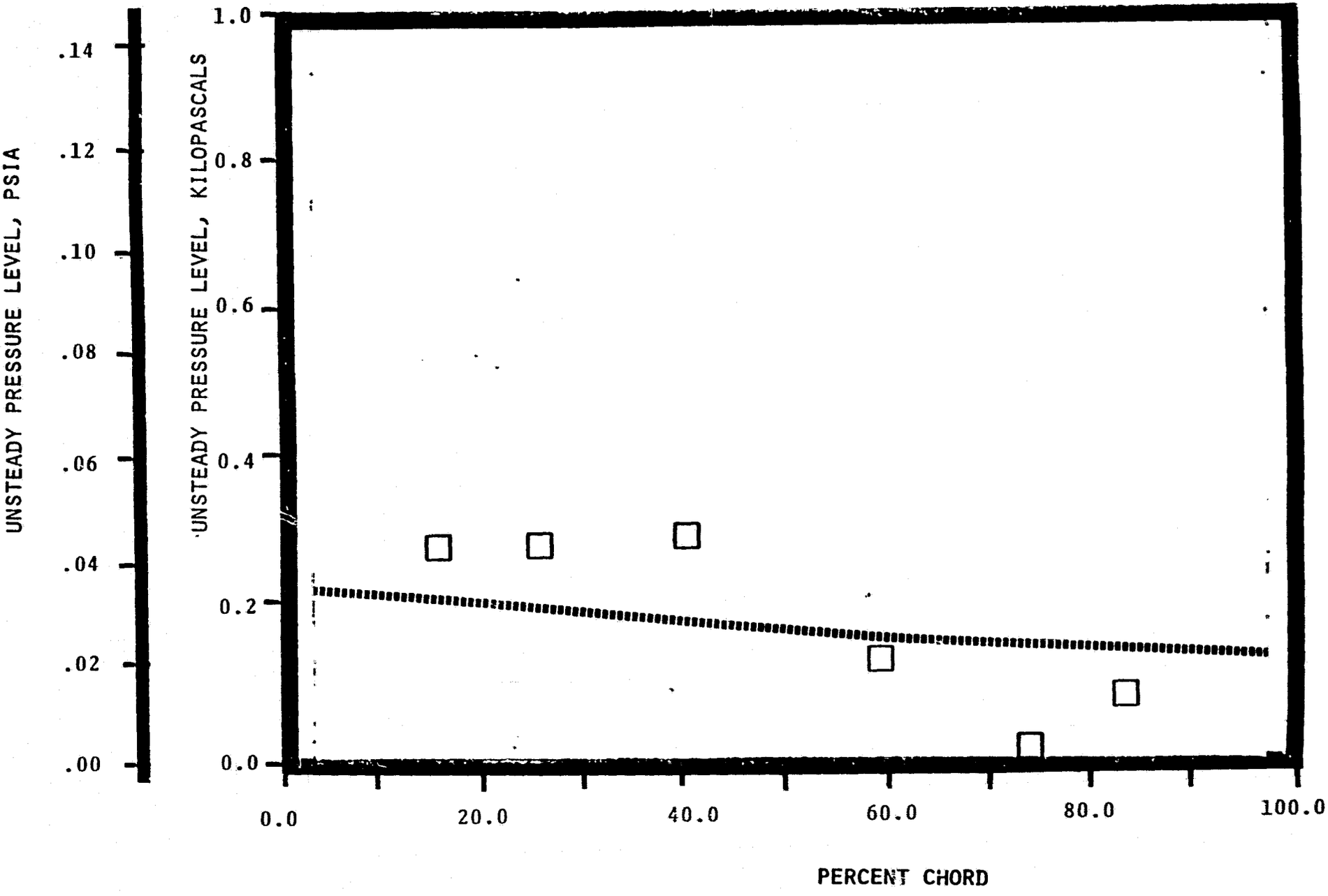

NASA L-TORSION CASCADE - REDUCED SOLIDITY - NOMINAL SETTING

PRESSURE SURFACE AERODYNAMIC PHASE LAG DISTRIBUTION
1.315 INLET MACH NUMBER
1.03 STATIC PRESSURE RATIO
-1.57 rad (-90°) INTERBLADE PHASE ANGLE

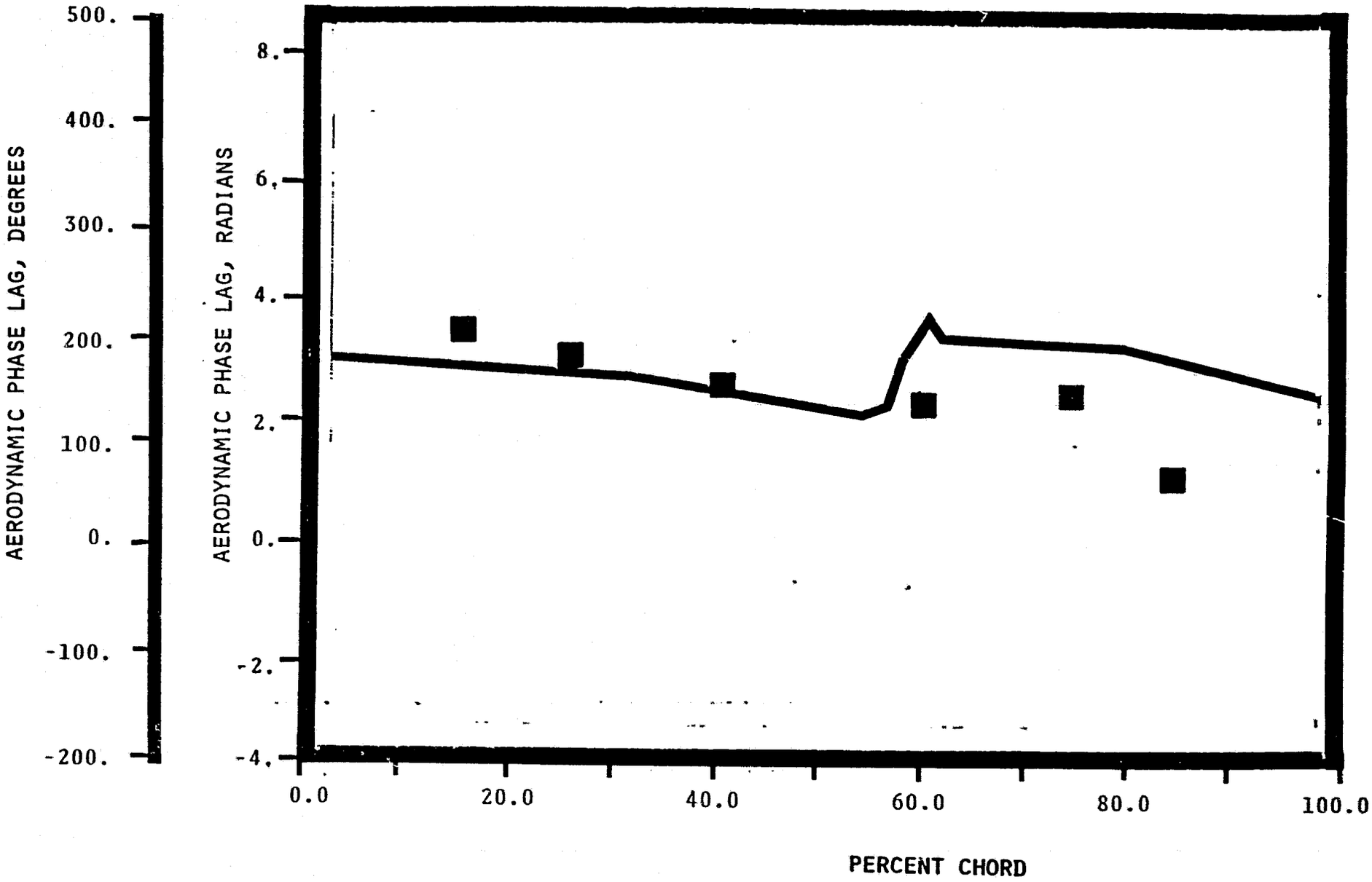

NASA I TORSION CASCADE - REDUCED SOLIDITY - NOMINAL SETTING

PRESSURE SURFACE UNSTEADY PRESSURE DISTRIBUTION

1.315 INLET MACH NUMBER

1.03 STATIC PRESSURE RATIO

-1.57 rad (-90°) INTERBLADE PHASE ANGLE

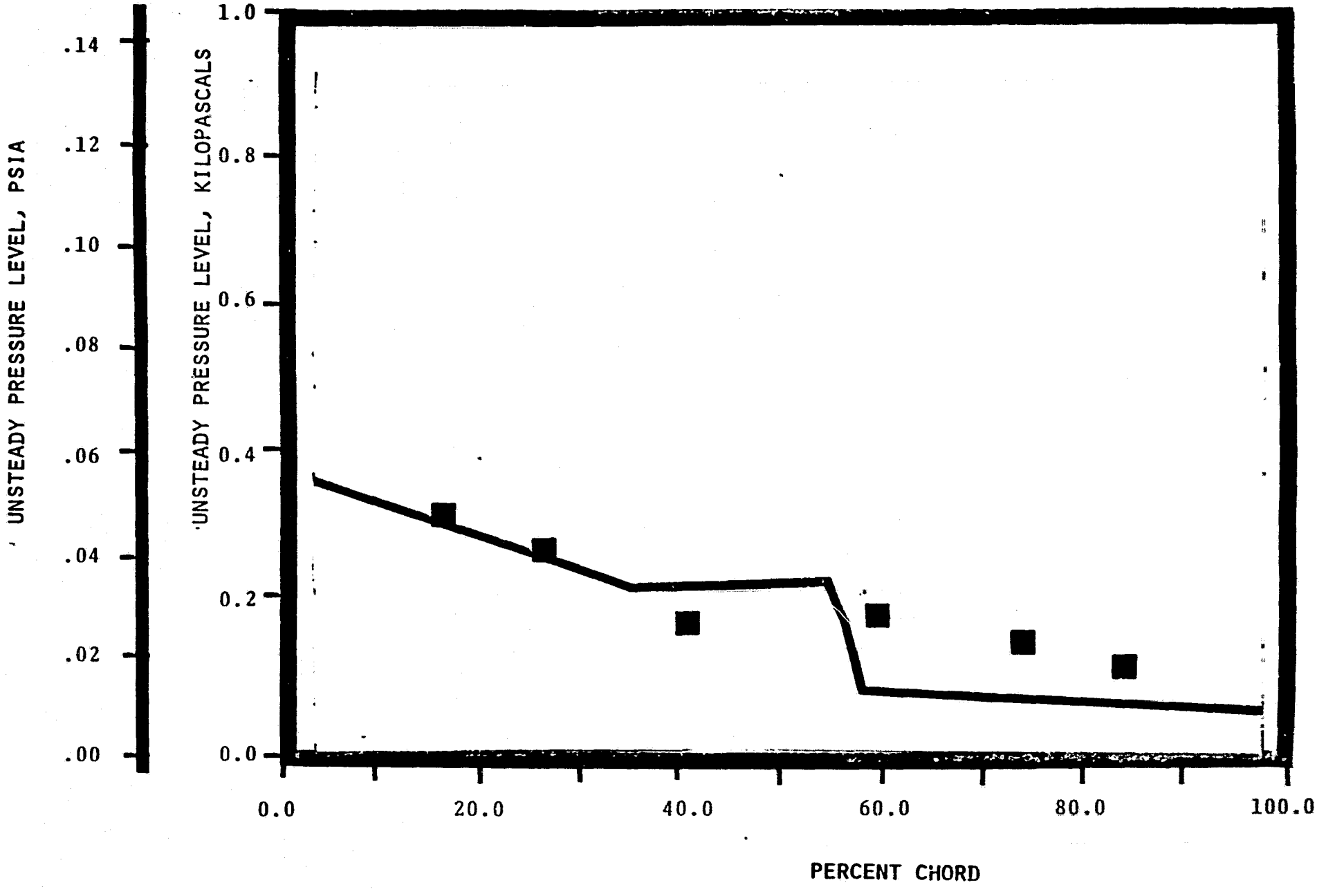

NASA I TORSION CASCADE - REDUCED SOLIDITY - NOMINAL SETTING

SUCTION SURFACE AERODYNAMIC PHASE LAG DISTRIBUTION

1.315 INLET MACH NUMBER

1.03 STATIC PRESSURE RATIO

-1.57 rad (-90°) INTERBLADE PHASE ANGLE

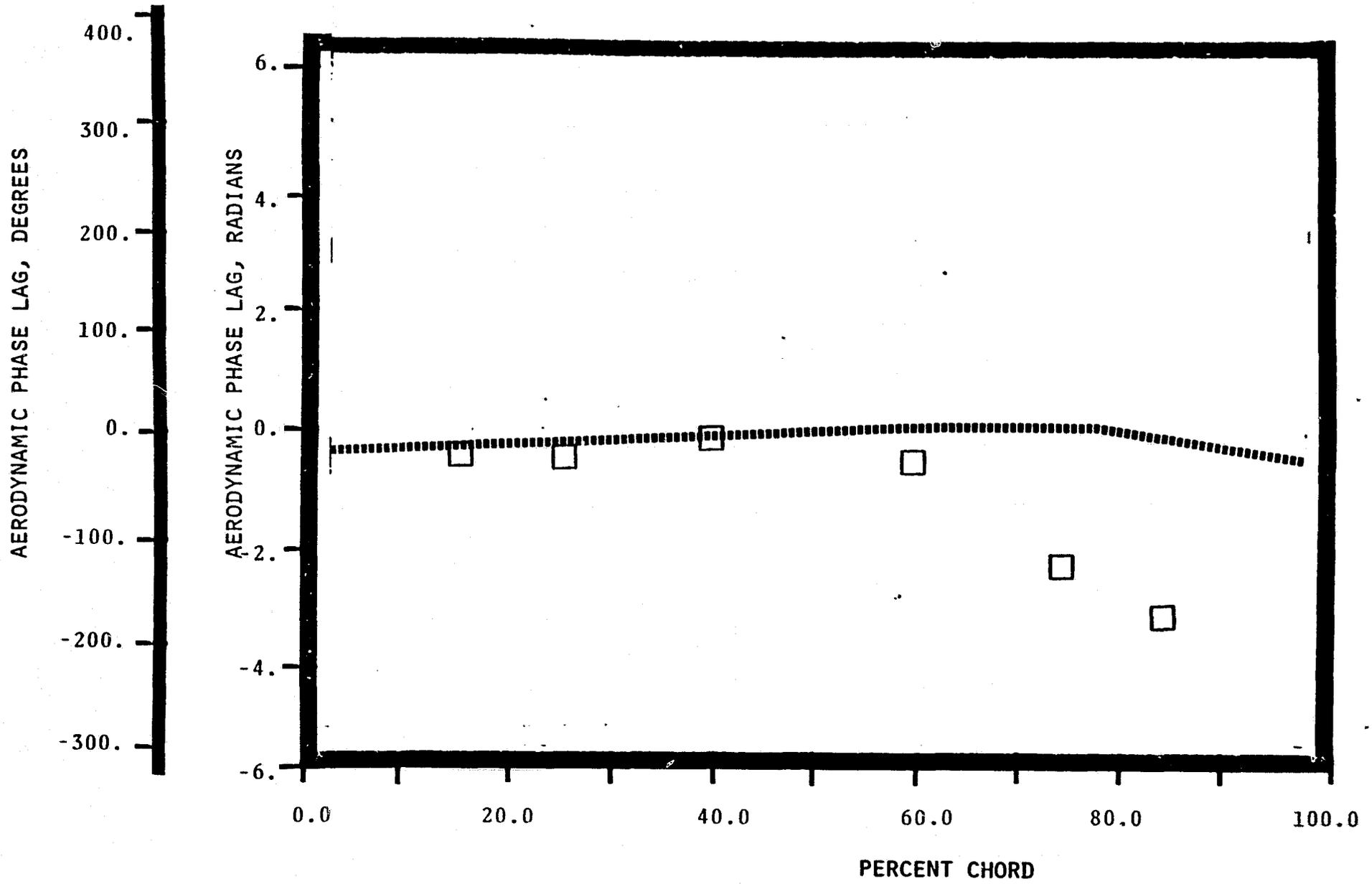

NASA I TORSION CASCADE - REDUCED SOLIDITY - NOMINAL SETTING

SUCTION SURFACE UNSTEADY PRESSURE DISTRIBUTION

1.315 INLET MACH NUMBER

1.03 STATIC PRESSURE RATIO

-1.57 rad (-90°) INTERBLADE PHASE ANGLE

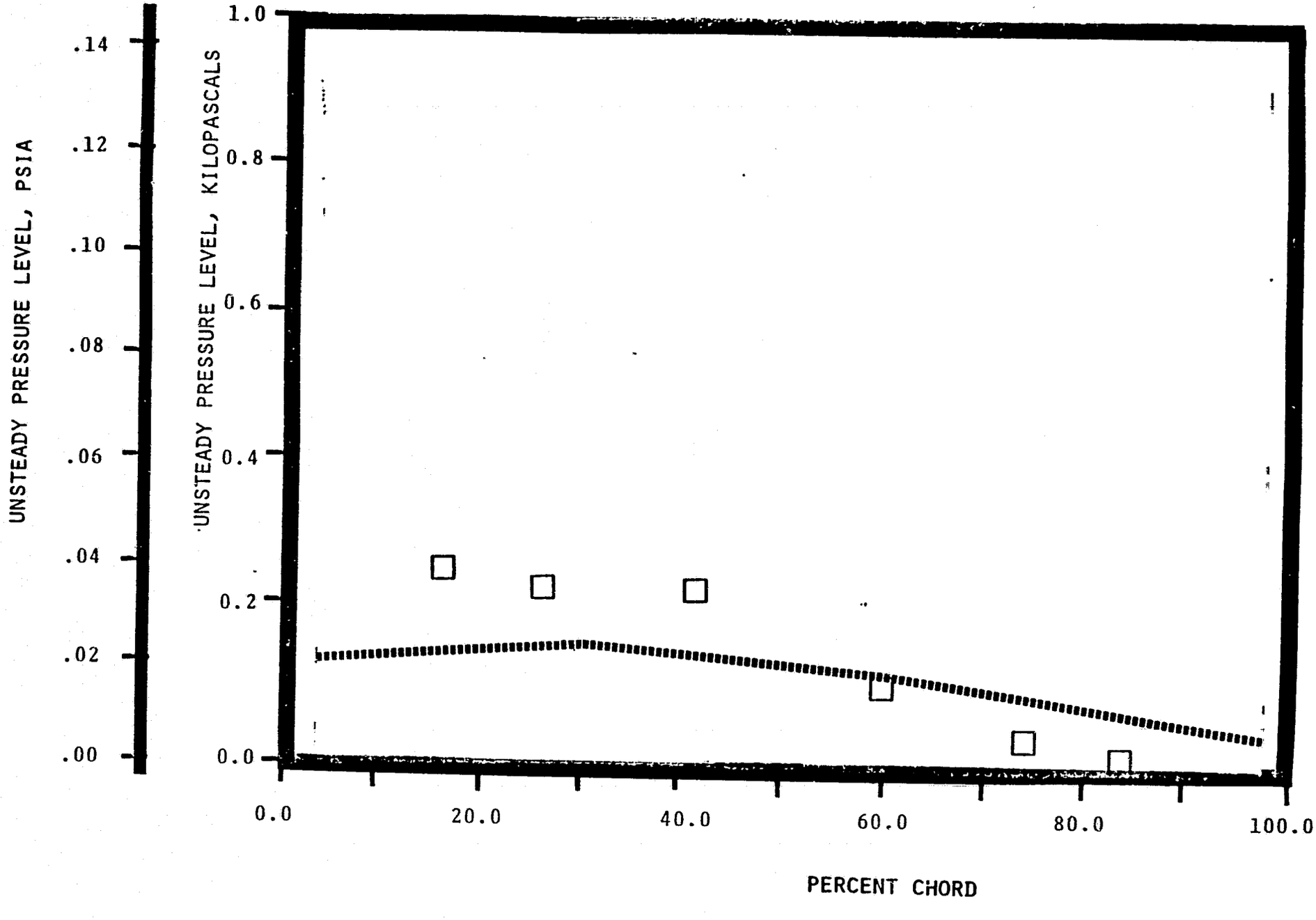

NASA I TORSION CASCADE - REDUCED SOLIDITY - NOMINAL SETTING

PRESSURE SURFACE AERODYNAMIC PHASE LAG DISTRIBUTION
1.315 INLET MACH NUMBER
1.35 STATIC PRESSURE RATIO
2.97 rad (170.°)INTERBLADE PHASE ANGLE

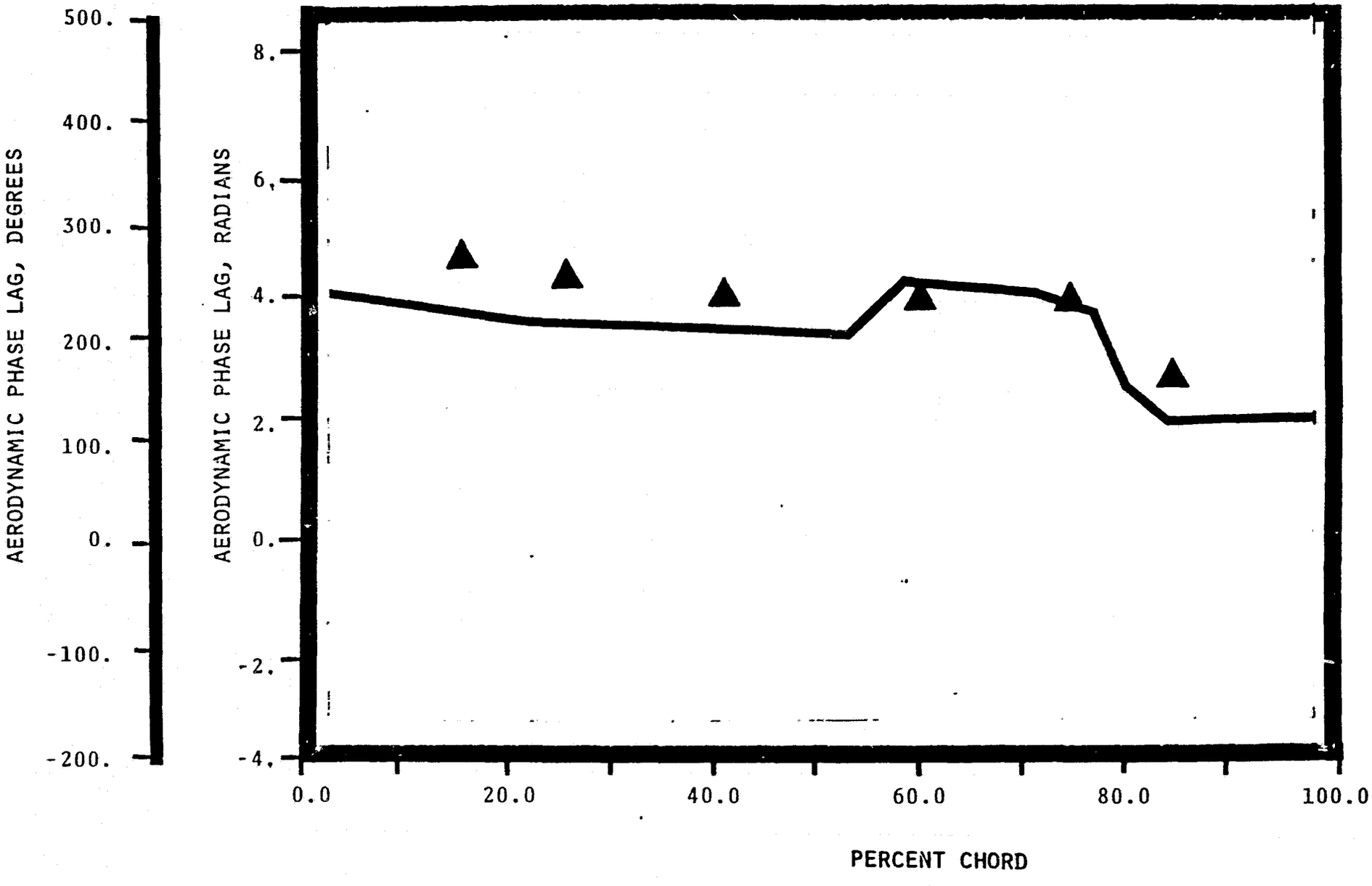

NASA I TORSION CASCADE - REDUCED SOLIDITY - NOMINAL SETTING

PRESSURE SURFACE UNSTEADY PRESSURE DISTRIBUTION

1.315 INLET MACH NUMBER

1.35 STATIC PRESSURE RATIO

2.97 rad (170 °) INTERBLADE PHASE ANGLE

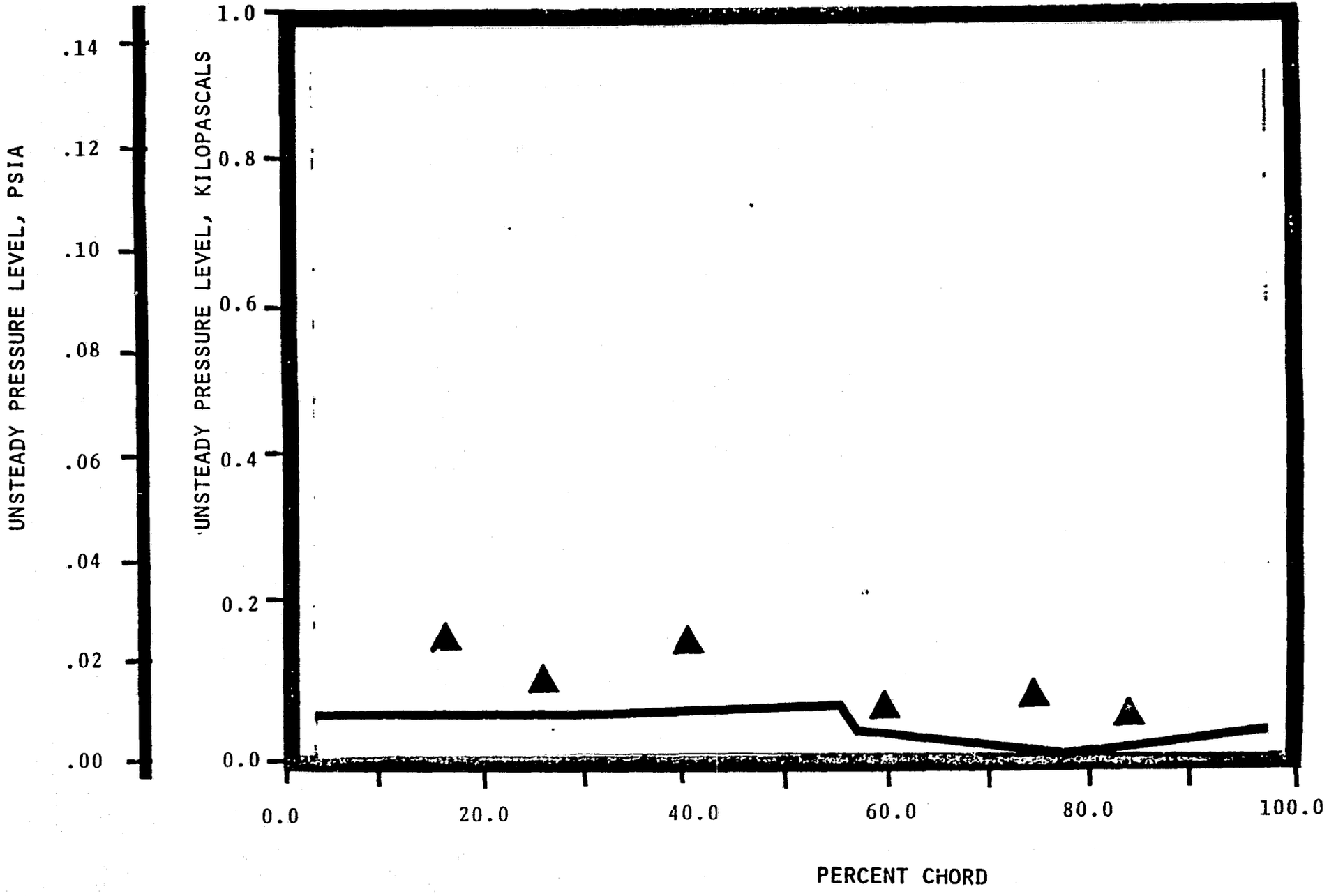

NASA I TORSION CASCADE - REDUCED SOLIDITY - NOMINAL SETTING

SUCTION SURFACE AERODYNAMIC PHASE LAG DISTRIBUTION

1.315 INLET MACH NUMBER

1.35 STATIC PRESSURE RATIO

2.97 rad (170 °) INTERBLADE PHASE ANGLE

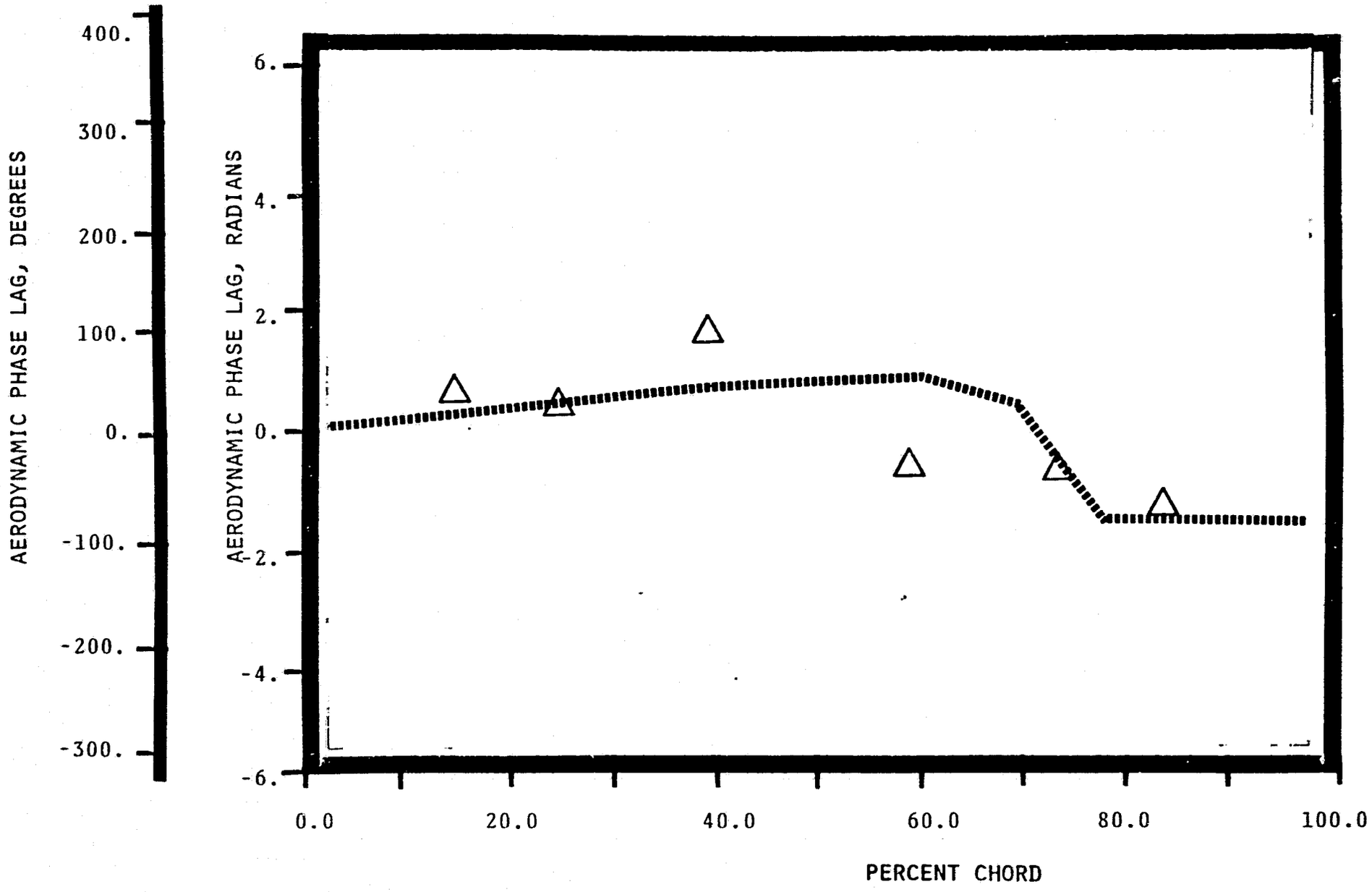

NASA I TORSION CASCADE - REDUCED SOLIDITY - NOMINAL SETTING

SUCTION SURFACE UNSTEADY PRESSURE DISTRIBUTION

1.315 INLET MACH NUMBER

1.35 STATIC PRESSURE RATIO

2.97 rad (170 °) INTERBLADE PHASE ANGLE

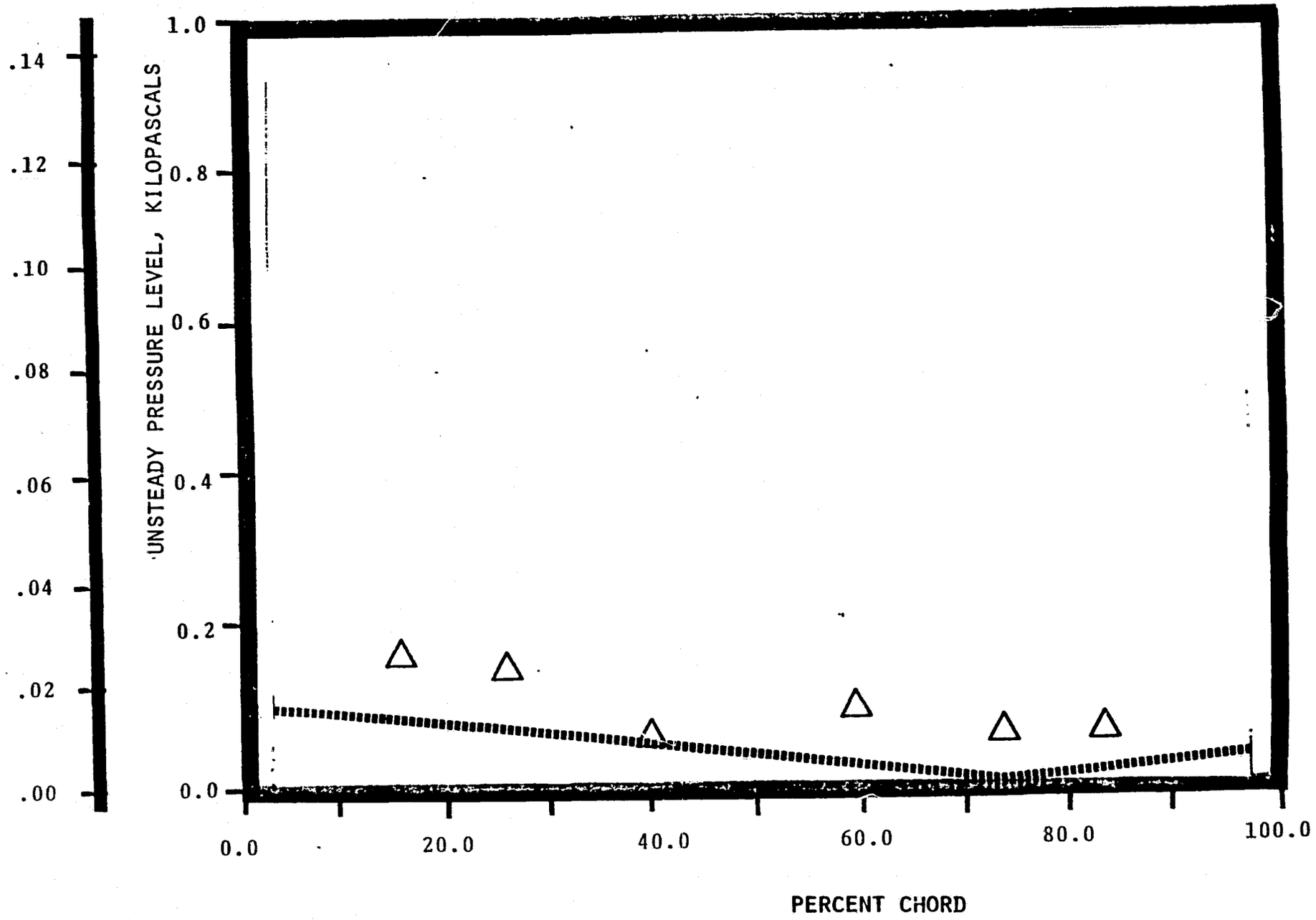

NASA I TORSION CASCADE - REDUCED SOLIDITY - NOMINAL SETTING

PRESSURE SURFACE AERODYNAMIC PHASE LAG DISTRIBUTION
1.315 INLET MACH NUMBER
1.35 STATIC PRESSURE RATIO
1.57 rad (90°) INTERBLADE PHASE ANGLE

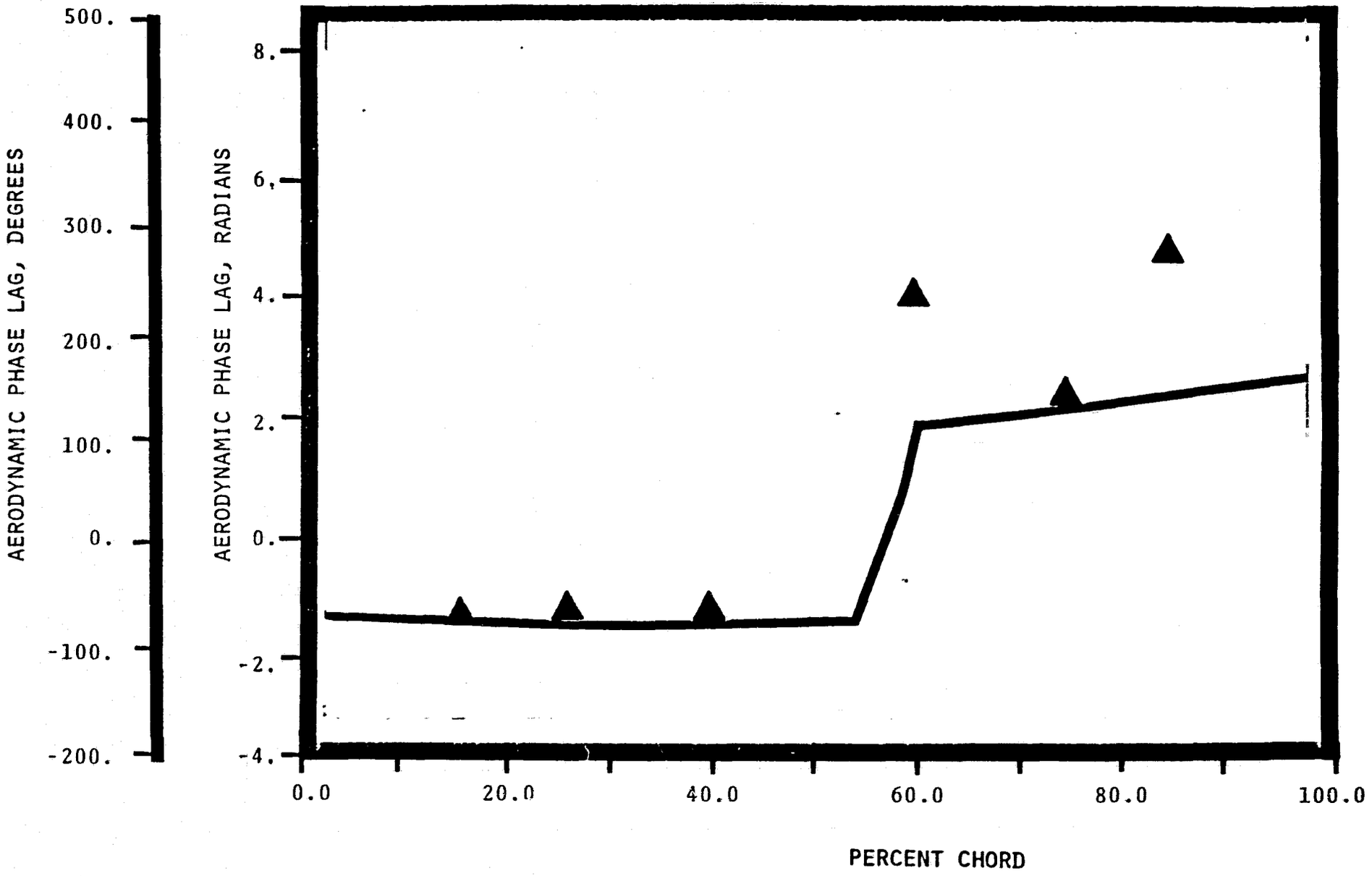

NASA L TORSION CASCADE - REDUCED SOLIDITY - NOMINAL SETTING

PRESSURE SURFACE UNSTEADY PRESSURE DISTRIBUTION

1.315 INLET MACH NUMBER

1.35 STATIC PRESSURE RATIO

1.57 rad (90°) INTERBLADE PHASE ANGLE

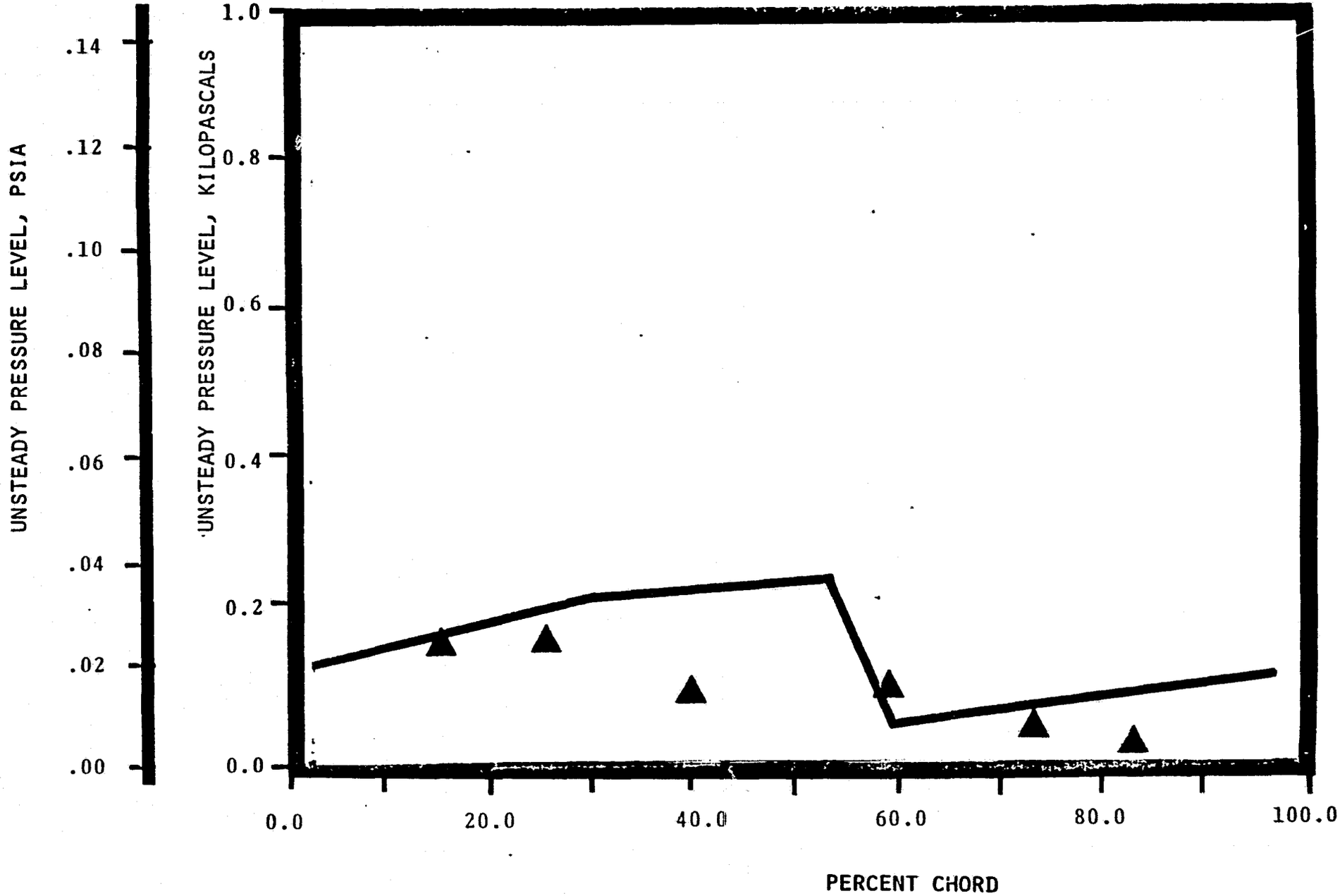

NASA I TORSION CASCADE - REDUCED SOLIDITY - NOMINAL SETTING

SUCTION SURFACE AERODYNAMIC PHASE LAG DISTRIBUTION

1.315 INLET MACH NUMBER

1.35 STATIC PRESSURE RATIO

1.57 rad (90°) INTERBLADE PHASE ANGLE

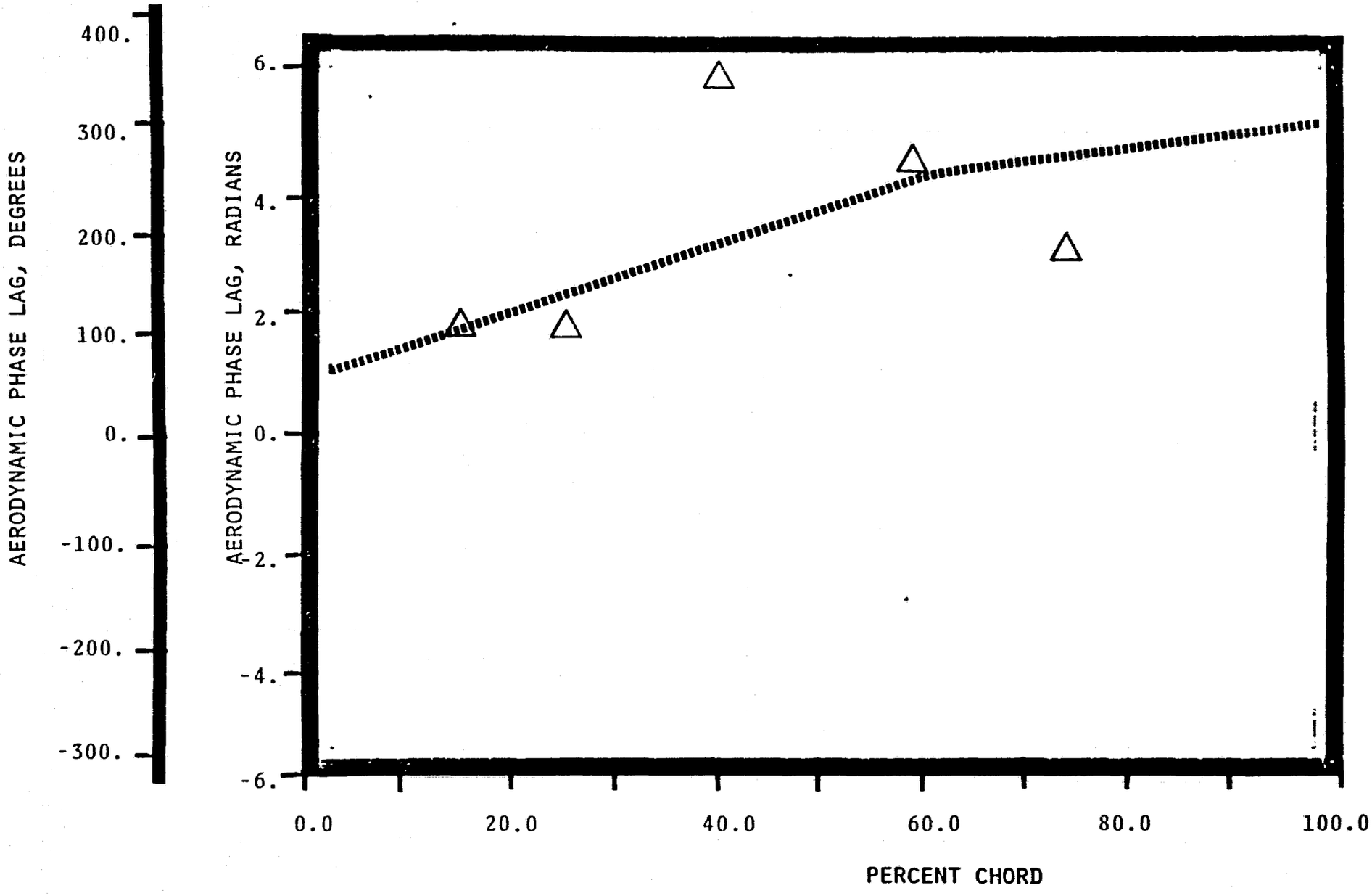

NASA I TORSION CASCADE - REDUCED SOLIDITY - NOMINAL SETTING

SUCTION SURFACE UNSTEADY PRESSURE DISTRIBUTION

1.315 INLET MACH NUMBER

1.35 STATIC PRESSURE RATIO

1.57 rad (90°)INTERBLADE PHASE ANGLE

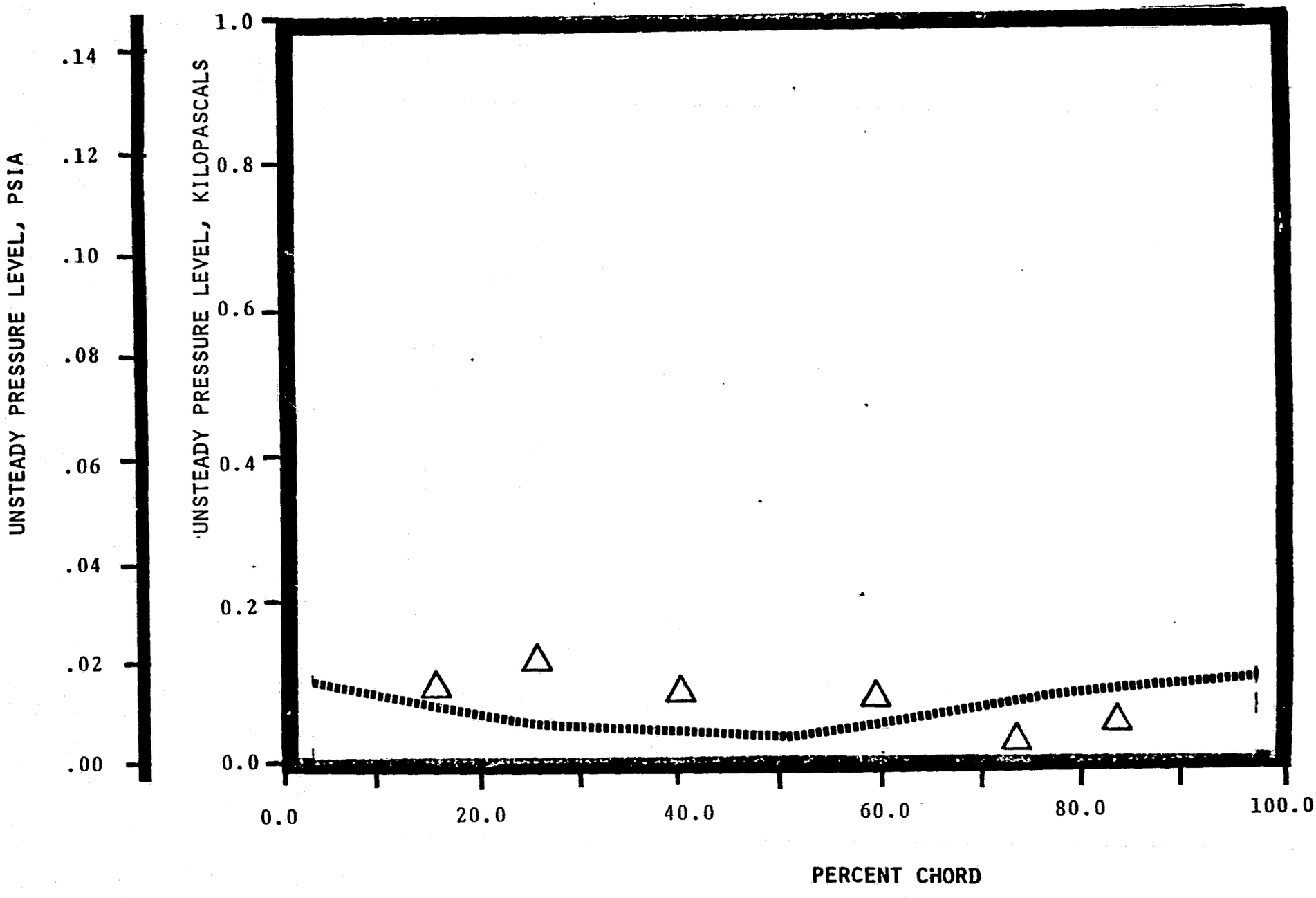

NASA I TORSION CASCADE - REDUCED SOLIDITY - NOMINAL SETTING

PRESSURE SURFACE AERODYNAMIC PHASE LAG DISTRIBUTION
1.315 INLET MACH NUMBER
1.35 STATIC PRESSURE RATIO
-.09 rad (-5 °) INTERBLADE PHASE ANGLE

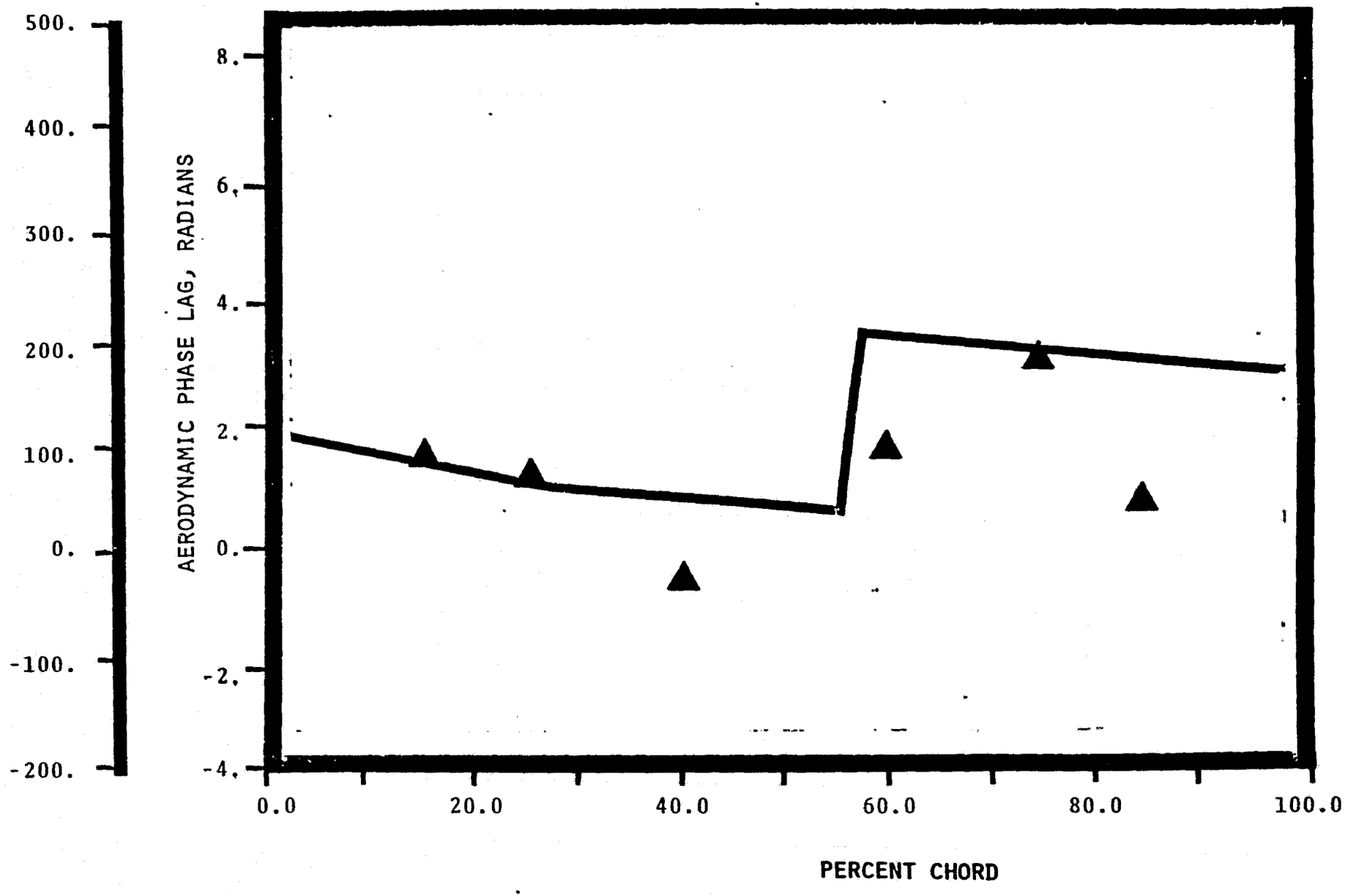

NASA I TORSION CASCADE - REDUCED SOLIDITY - NOMINAL SETTING

PRESSURE SURFACE UNSTEADY PRESSURE DISTRIBUTION

1.315 INLET MACH NUMBER

1.35 STATIC PRESSURE RATIO

-.09 rad (-5°) INTERBLADE PHASE ANGLE

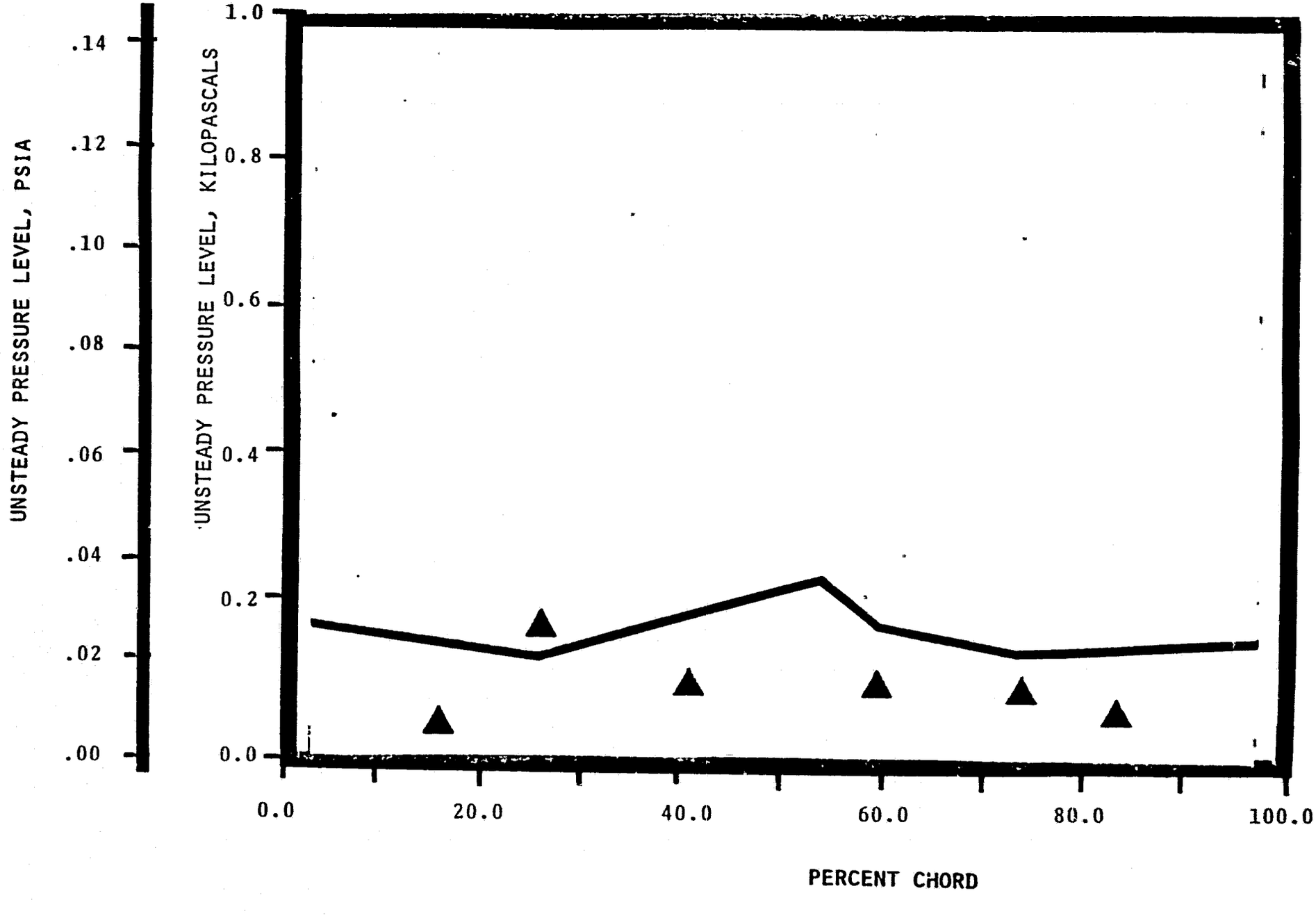

NASA I TORSION CASCADE - REDUCED SOLIDITY - NOMINAL SETTING

SUCTION SURFACE AERODYNAMIC PHASE LAG DISTRIBUTION

1.315 INLET MACH NUMBER

1.35 STATIC PRESSURE RATIO

-.09 rad (-5°) INTERBLADE PHASE ANGLE

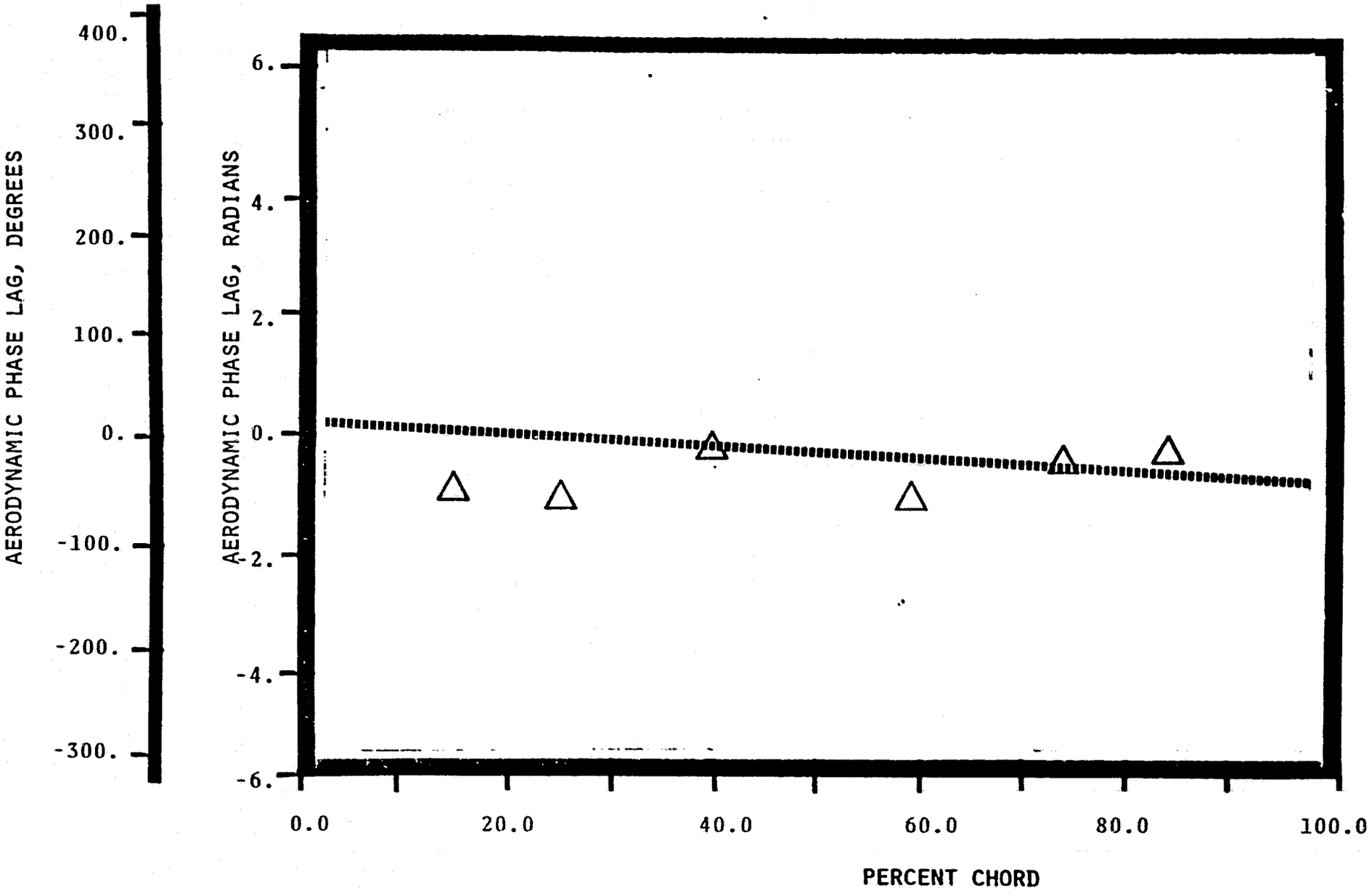

NASA I TORSION CASCADE - REDUCED SOLIDITY - NOMINAL SETTING
SUCTION SURFACE UNSTEADY PRESSURE DISTRIBUTION
1.315 INLET MACH NUMBER
1.35 STATIC PRESSURE RATIO
-.09 rad (-5°) INTERBLADE PHASE ANGLE

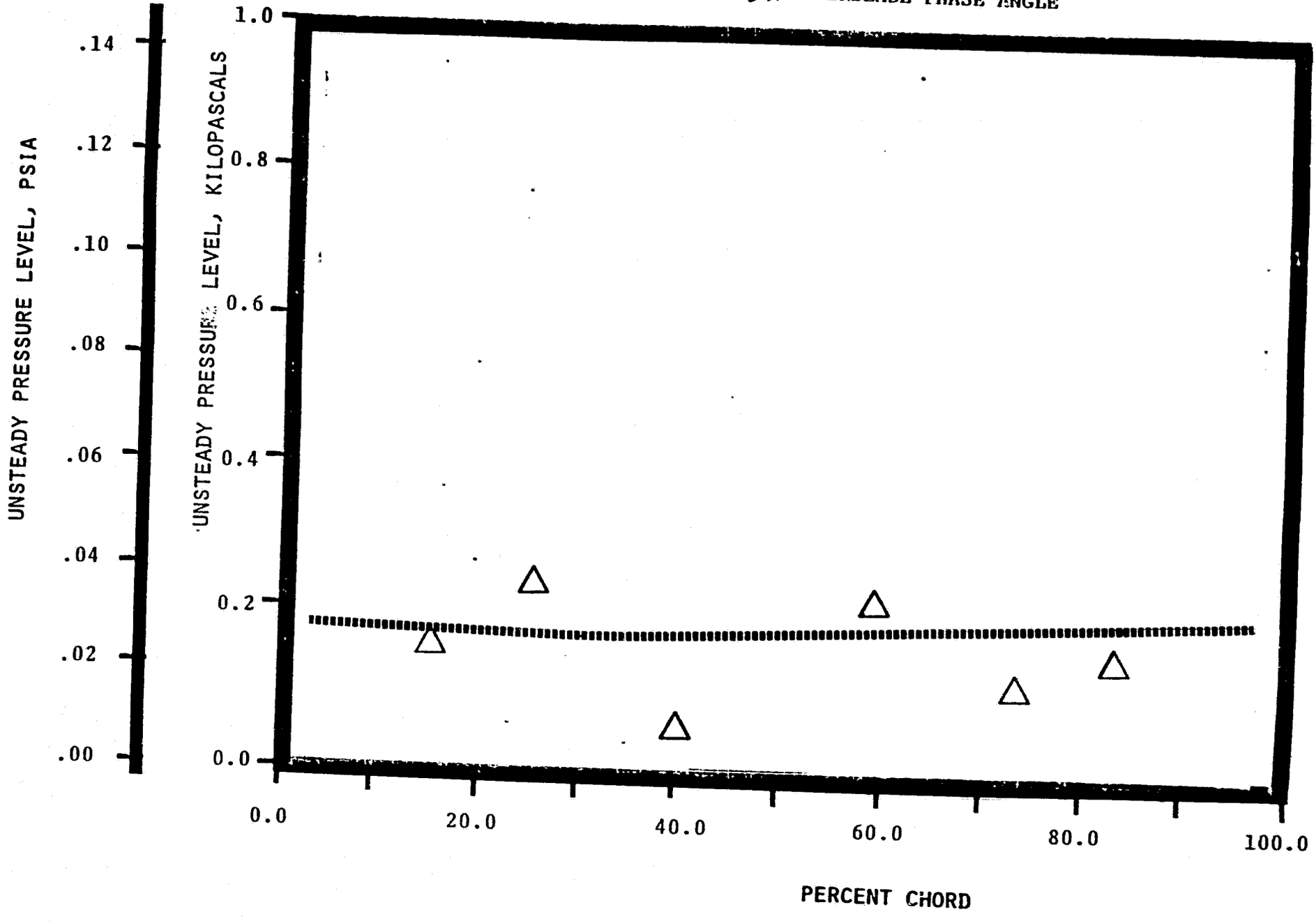

NASA I TORSION CASCADE - REDUCED SOLIDITY - NOMINAL SETTING

PRESSURE SURFACE AERODYNAMIC PHASE LAG DISTRIBUTION
1.315 INLET MACH NUMBER
1.35 STATIC PRESSURE RATIO
-.44 rad (-25°) INTERBLADE PHASE ANGLE

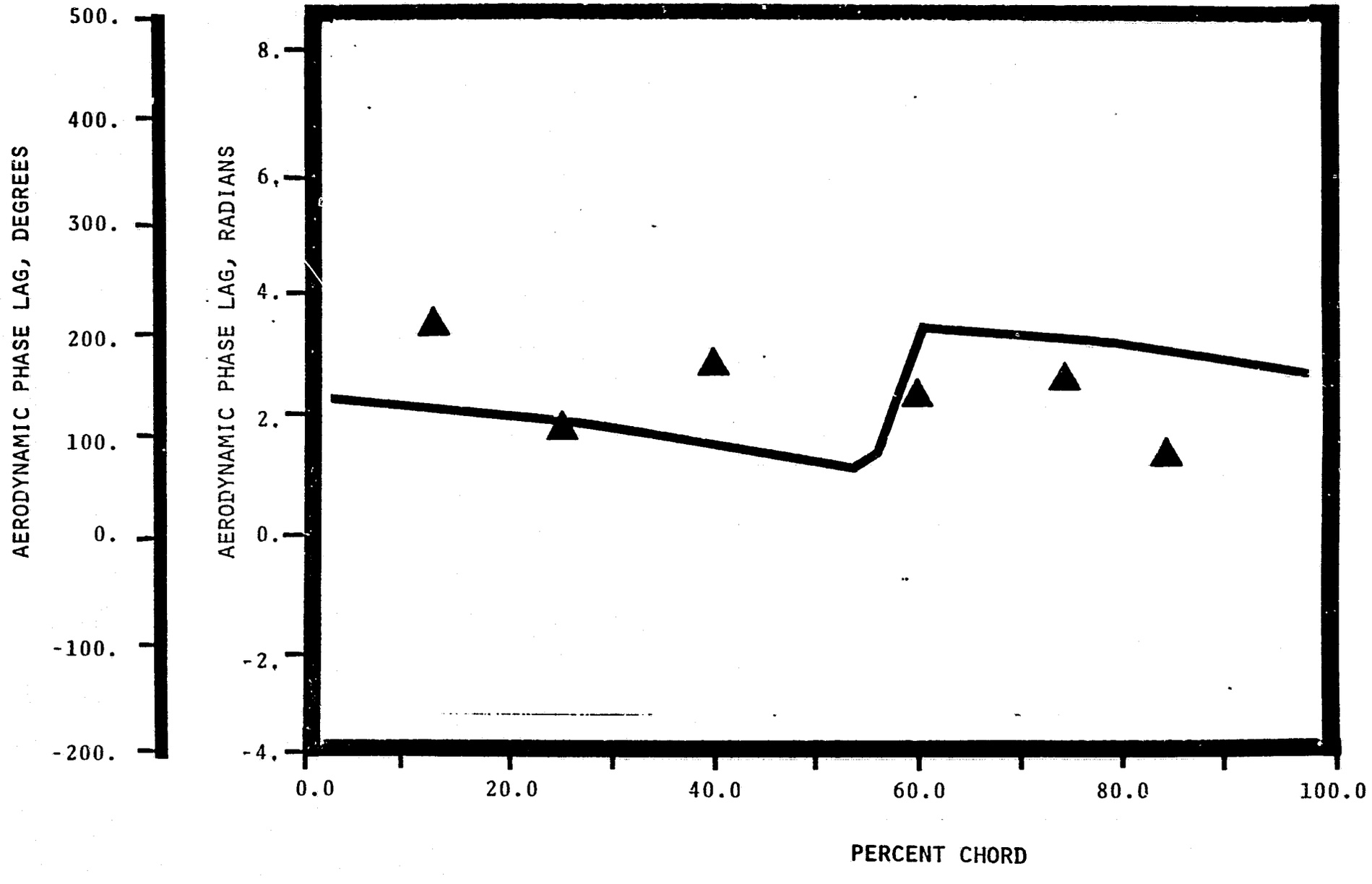

NASA I TORSION CASCADE - REDUCED SOLIDITY - NOMINAL SETTING

PRESSURE SURFACE UNSTEADY PRESSURE DISTRIBUTION
1.315 INLET MACH NUMBER
1.35 STATIC PRESSURE RATIO
-.44 rad (-25°) INTERBLADE PHASE ANGLE

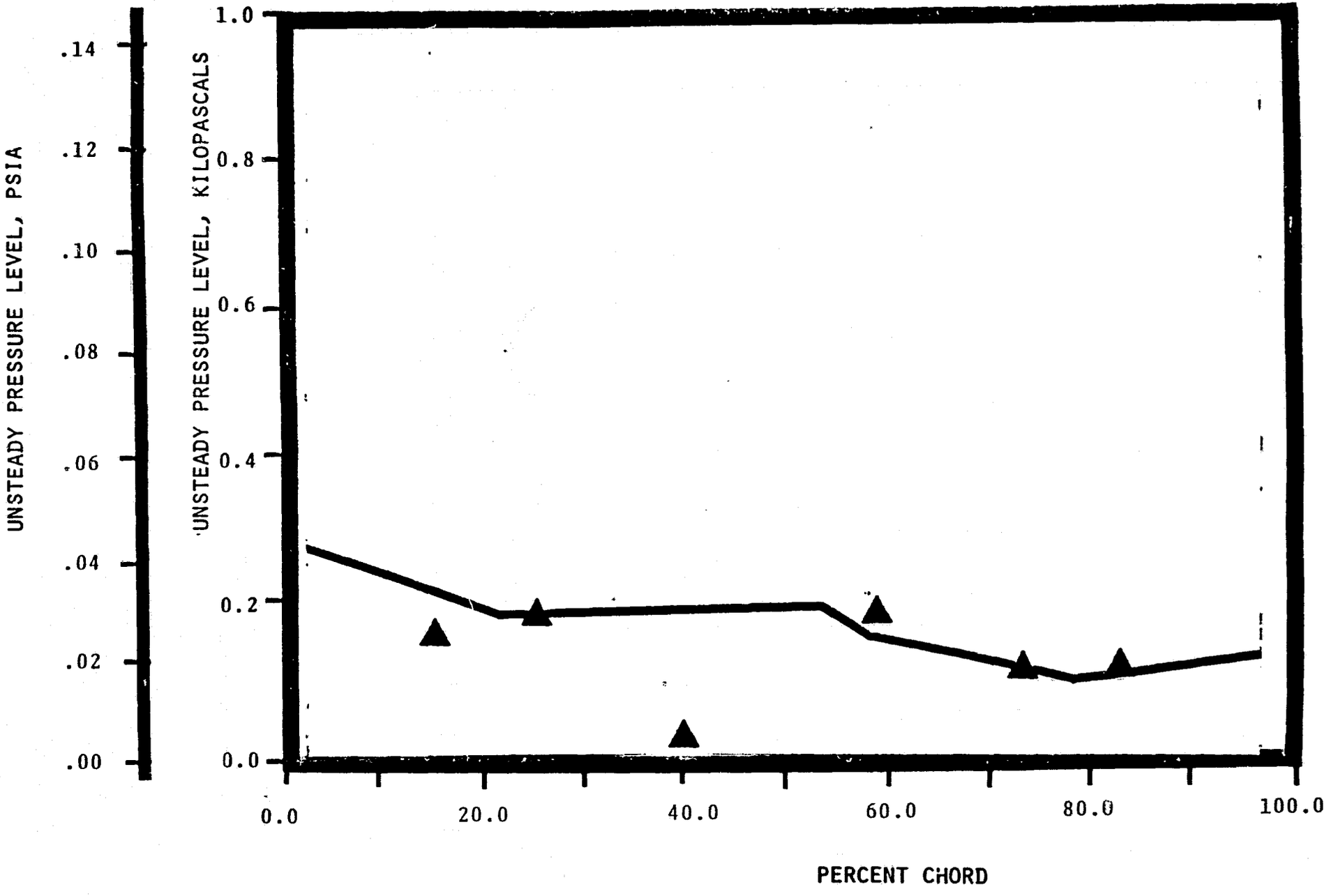

NASA I TORSION CASCADE - REDUCED SOLIDITY - NOMINAL SETTING

SUCTION SURFACE AERODYNAMIC PHASE LAG DISTRIBUTION
1.315 INLET MACH NUMBER
1.35 STATIC PRESSURE RATIO
-.44 rad (-25°) INTERBLADE PHASE ANGLE

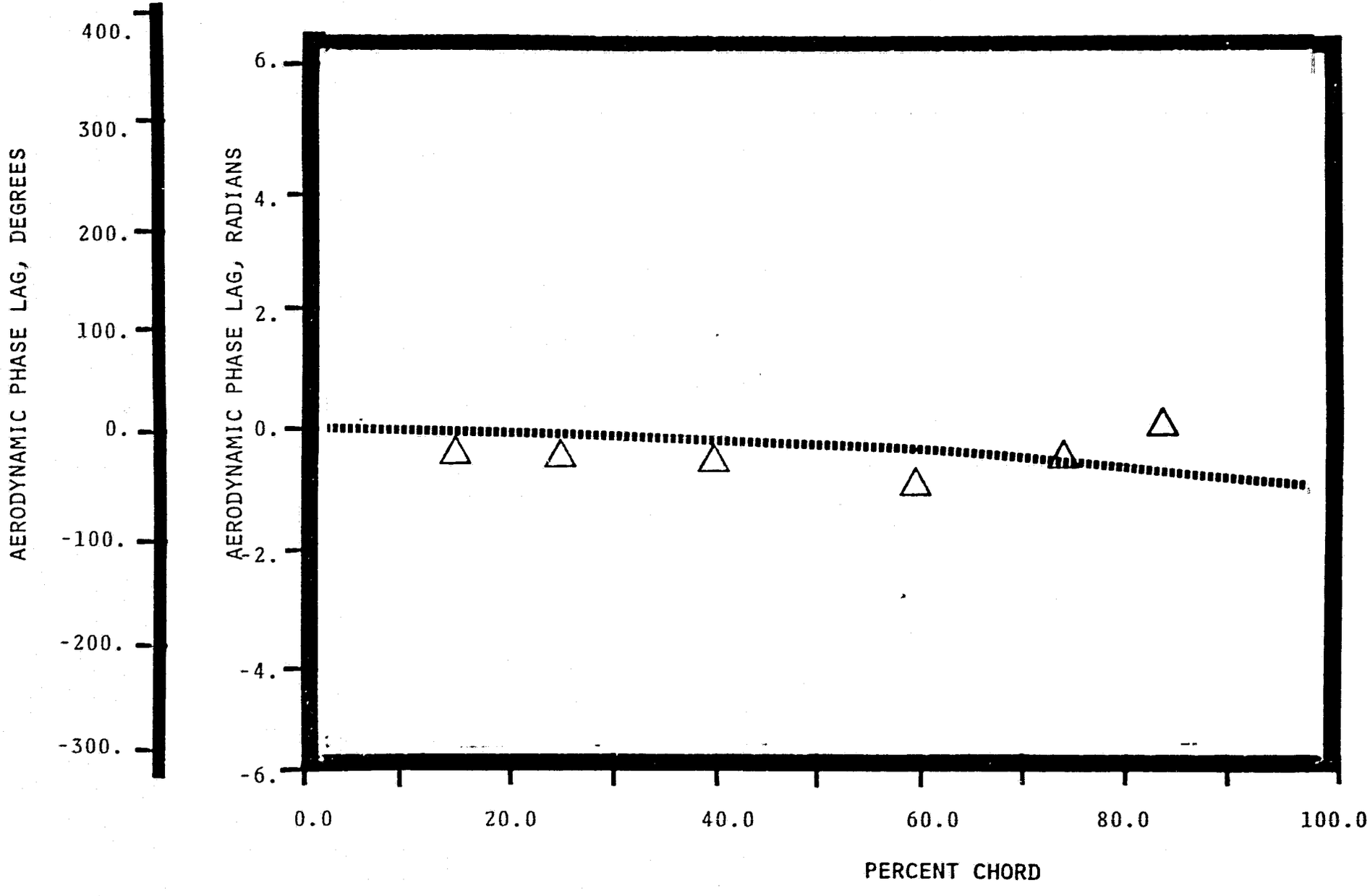

NASA I TORSION CASCADE - REDUCED SOLIDITY - NOMINAL SETTING

SUCTION SURFACE UNSTEADY PRESSURE DISTRIBUTION

1.315 INLET MACH NUMBER

1.35 STATIC PRESSURE RATIO

-.44 rad (-25) INTERBLADE PHASE ANGLE

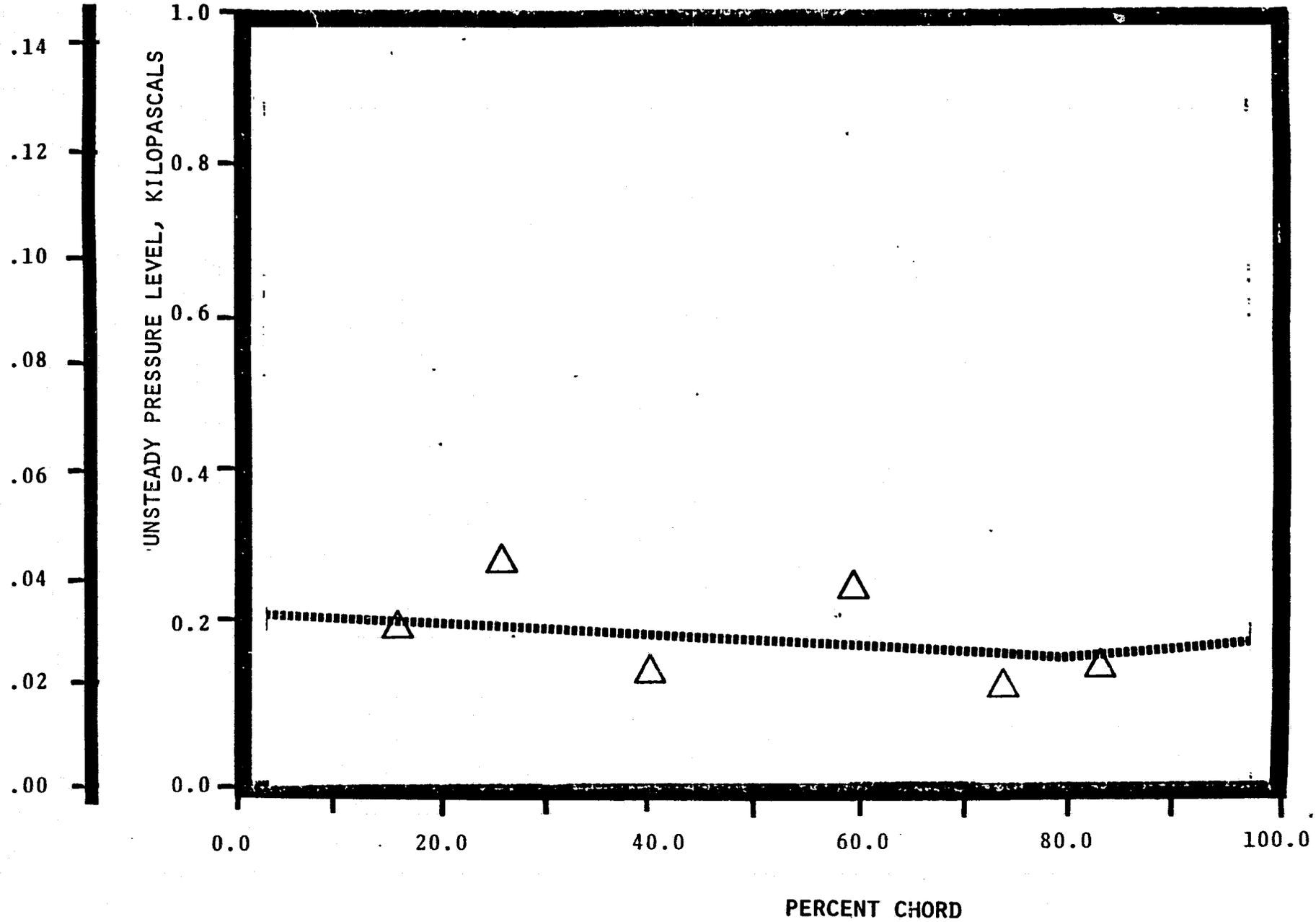

NASA I TORSION CASCADE - REDUCED SOLIDITY - NOMINAL SETTING

PRESSURE SURFACE AERODYNAMIC PHASE LAG DISTRIBUTION
1.315 INLET MACH NUMBER
1.35 STATIC PRESSURE RATIO
-1.05 rad(-60) INTERBLADE PHASE ANGLE

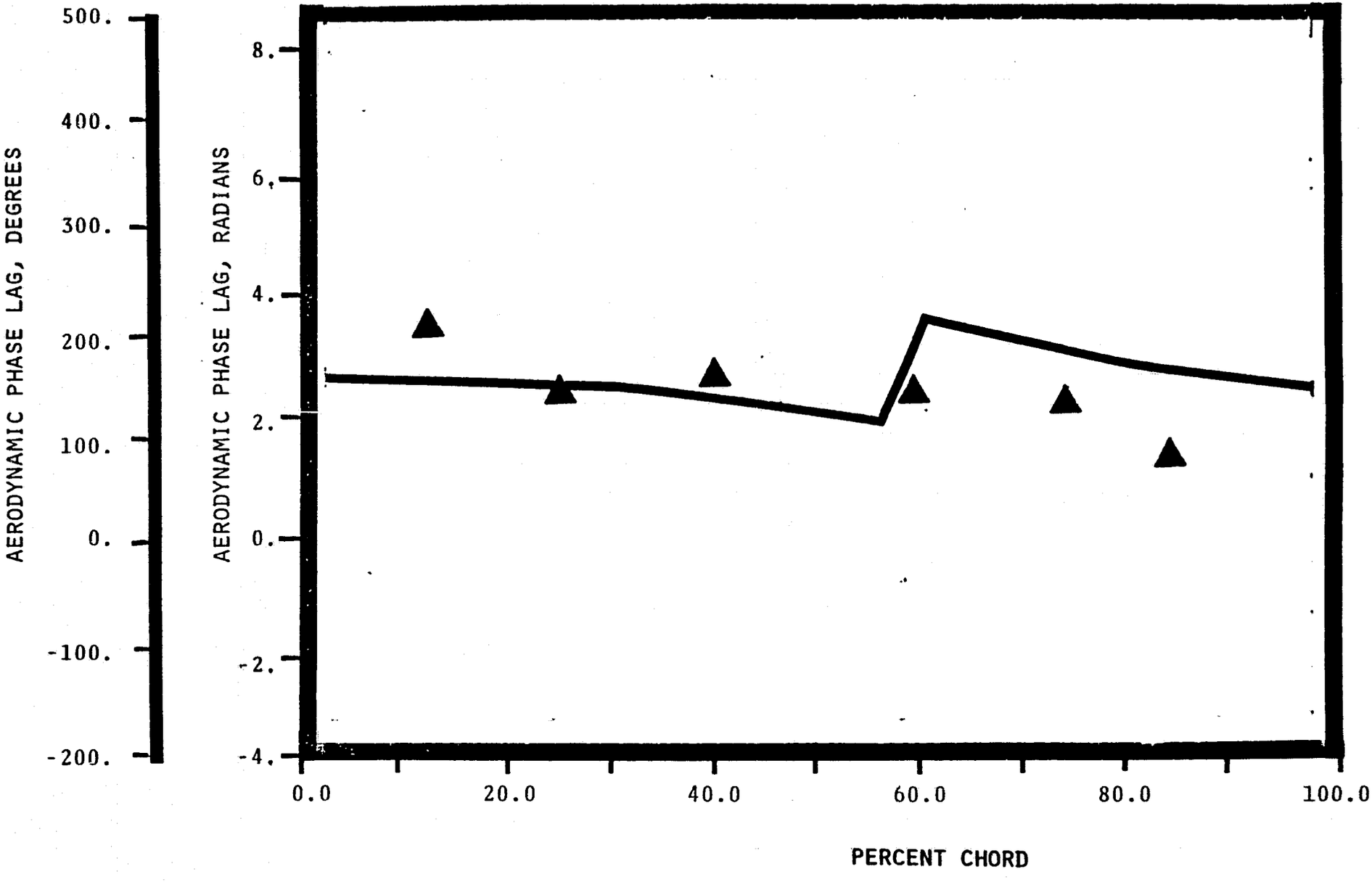

NASA I TORSION CASCADE - REDUCED SOLIDITY - NOMINAL SETTING

PRESSURE SURFACE UNSTEADY PRESSURE DISTRIBUTION

1.315 INLET MACH NUMBER

1.35 STATIC PRESSURE RATIO

-1.05 rad (-60°) INTERBLADE PHASE ANGLE

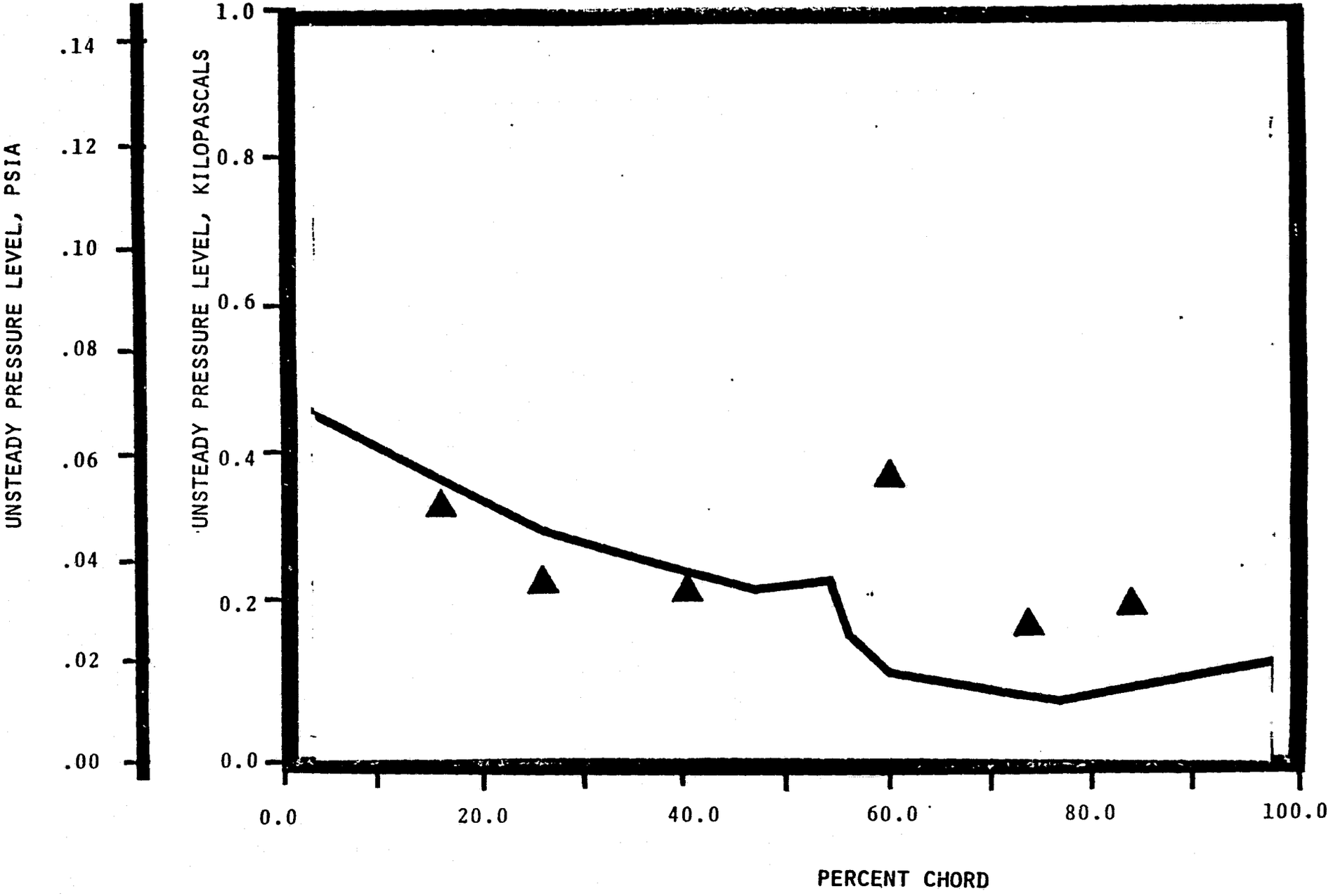

NASA I TORSION CASCADE - REDUCED SOLIDITY - NOMINAL SETTING

SUCTION SURFACE AERODYNAMIC PHASE LAG DISTRIBUTION

1.315 INLET MACH NUMBER

1.35 STATIC PRESSURE RATIO

-1.05 rad (-60)INTERBLADE PHASE ANGLE

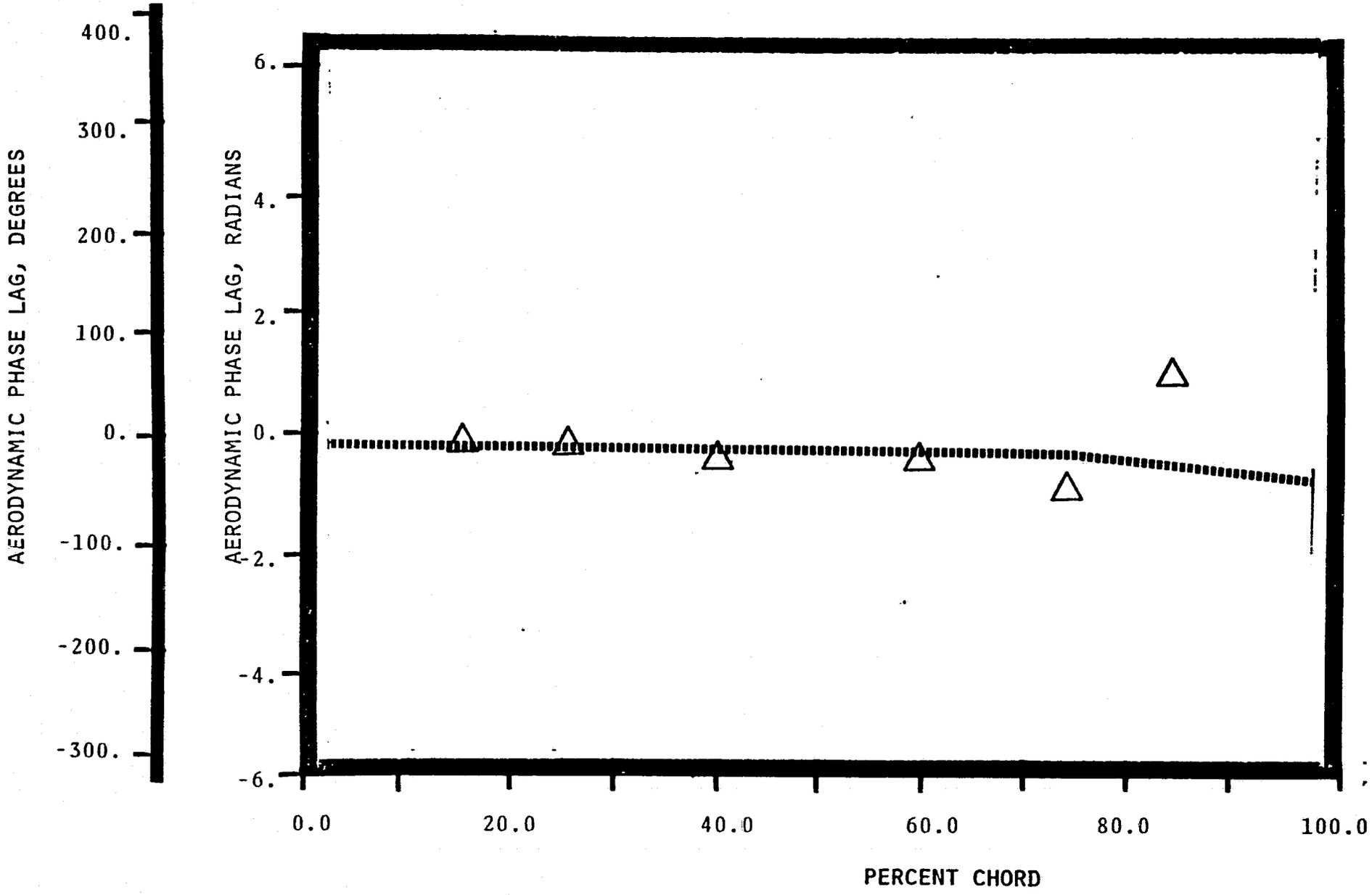

NASA I TORSION CASCADE - REDUCED SOLIDITY - NOMINAL SETTING

SUCTION SURFACE UNSTEADY PRESSURE DISTRIBUTION

1.315 INLET MACH NUMBER

1.35 STATIC PRESSURE RATIO

-1.05 rad (-60) INTERBLADE PHASE ANGLE

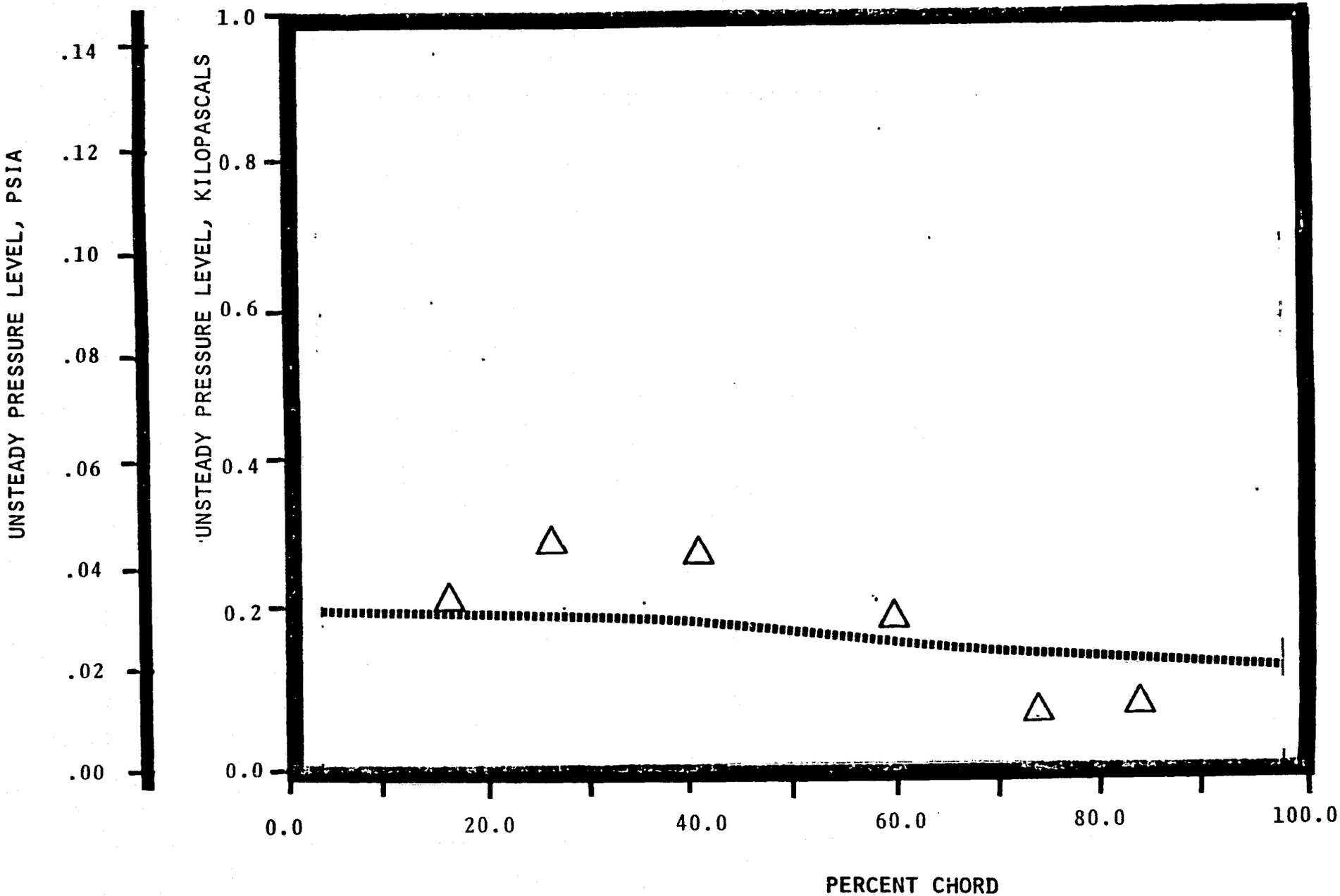

NASA I TORSION CASCADE - REDUCED SOLIDITY - NOMINAL SETTING

PRESSURE SURFACE AERODYNAMIC PHASE LAG DISTRIBUTION
1.315 INLET MACH NUMBER
1.35 STATIC PRESSURE RATIO
-1.05 rad (-90°) INTERBLADE PHASE ANGLE

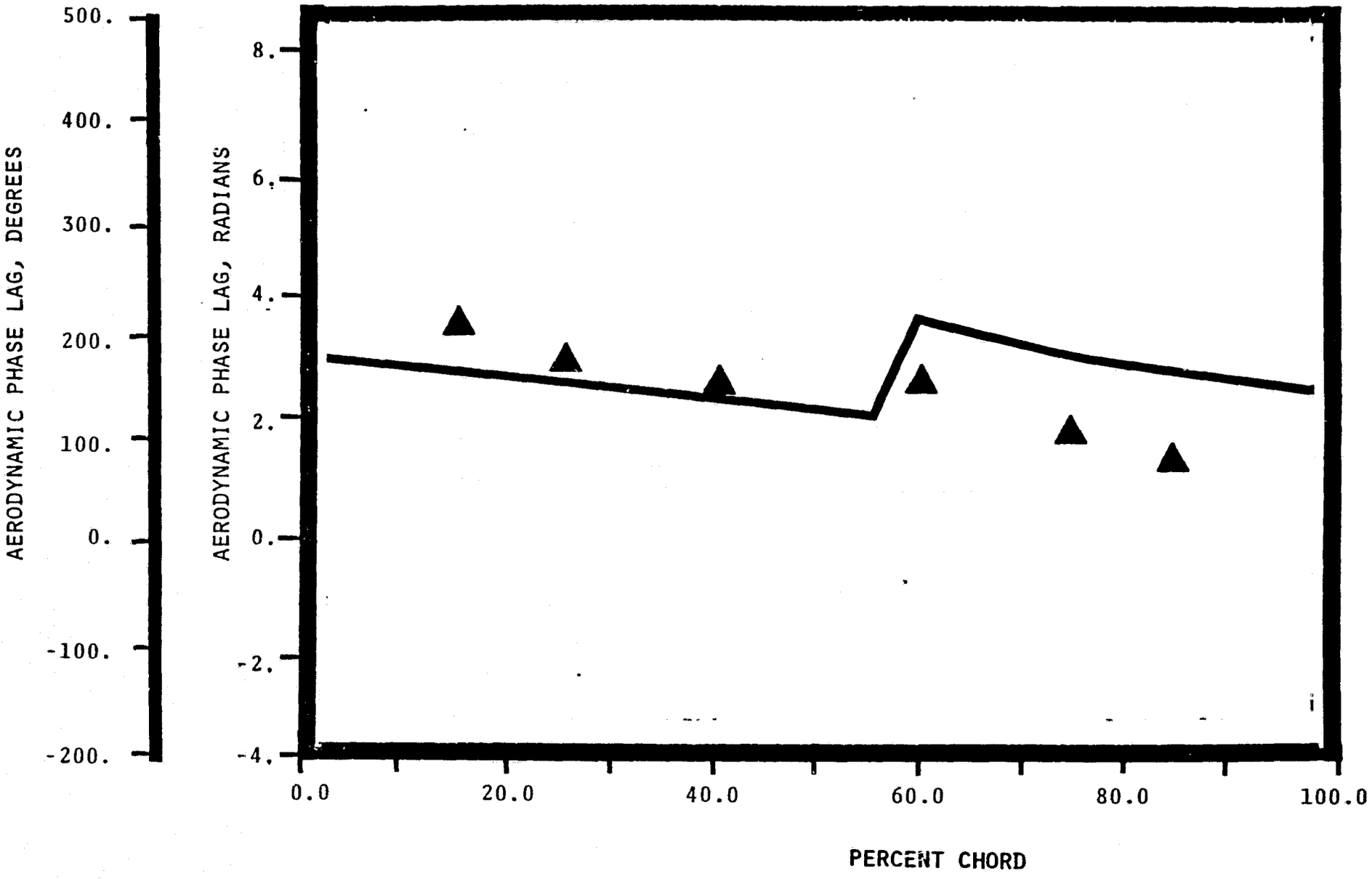

NASA I TORSION CASCADE - REDUCED SOLIDITY - NOMINAL SETTING

PRESSURE SURFACE UNSTEADY PRESSURE DISTRIBUTION
1.315 INLET MACH NUMBER
1.35 STATIC PRESSURE RATIO
-1.05 rad (-90°) INTERBLADE PHASE ANGLE

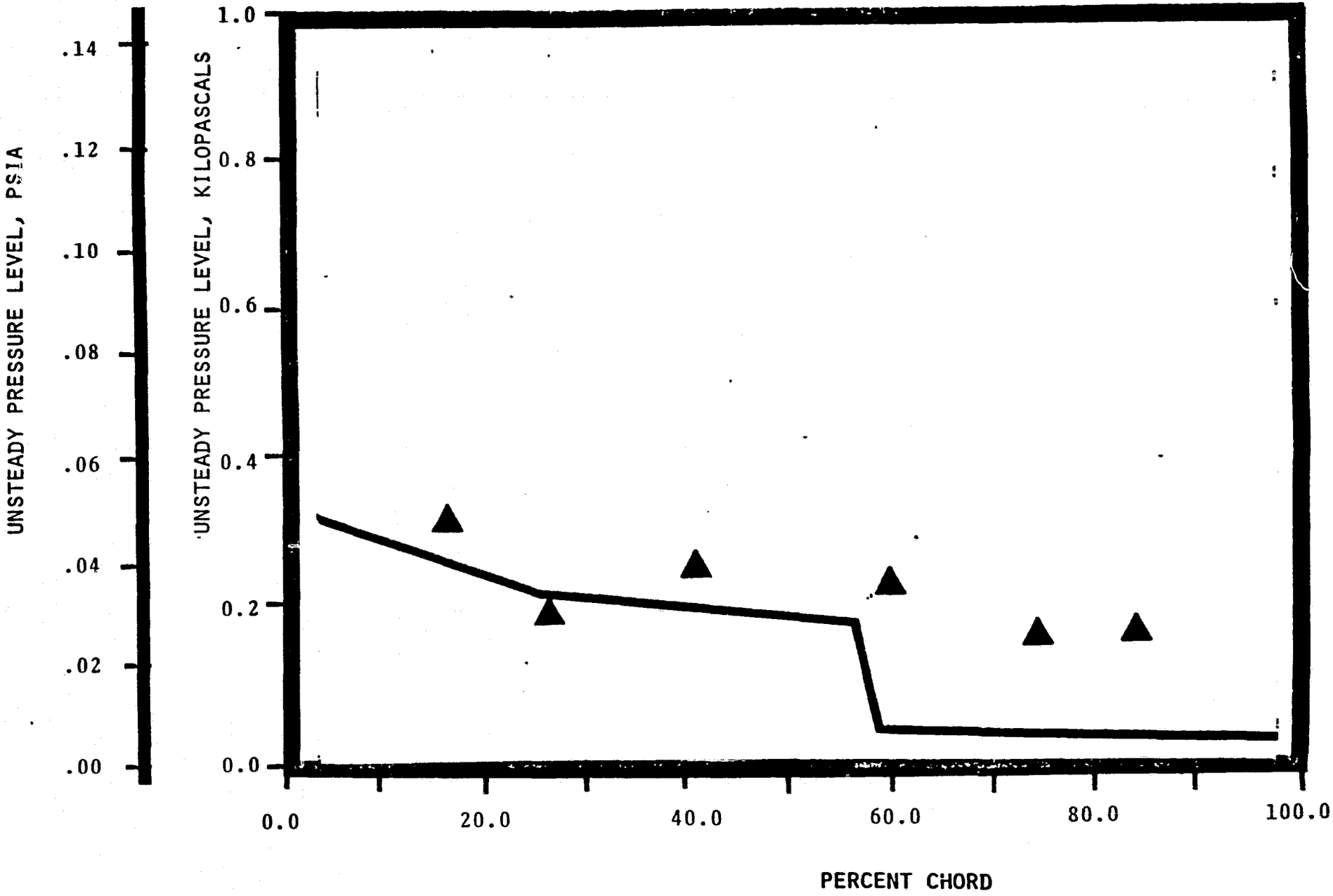

NASA I TORSION CASCADE - REDUCED SOLIDITY - NOMINAL SETTING

SUCTION SURFACE AERODYNAMIC PHASE LAG DISTRIBUTION

1.315 INLET MACH NUMBER

1.35 STATIC PRESSURE RATIO

-1.05 rad (-90^{0}) INTERBLADE PHASE ANGLE

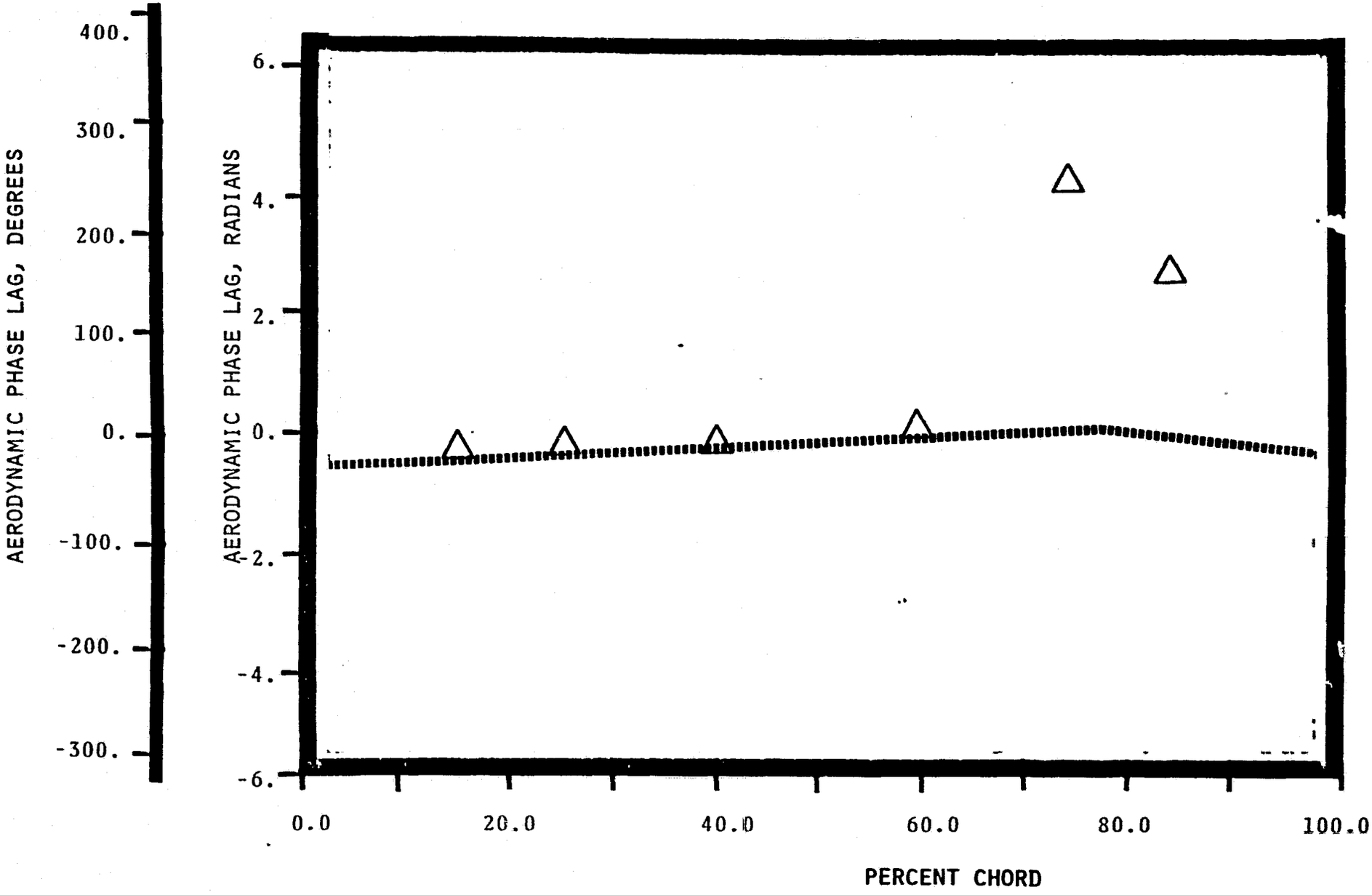

NASA I TORSION CASCADE - REDUCED SOLIDITY - NOMINAL SETTING

SUCTION SURFACE UNSTEADY PRESSURE DISTRIBUTION

1.315 INLET MACH NUMBER

1.35 STATIC PRESSURE RATIO

-1.05 rad (-90) INTERBLADE PHASE ANGLE

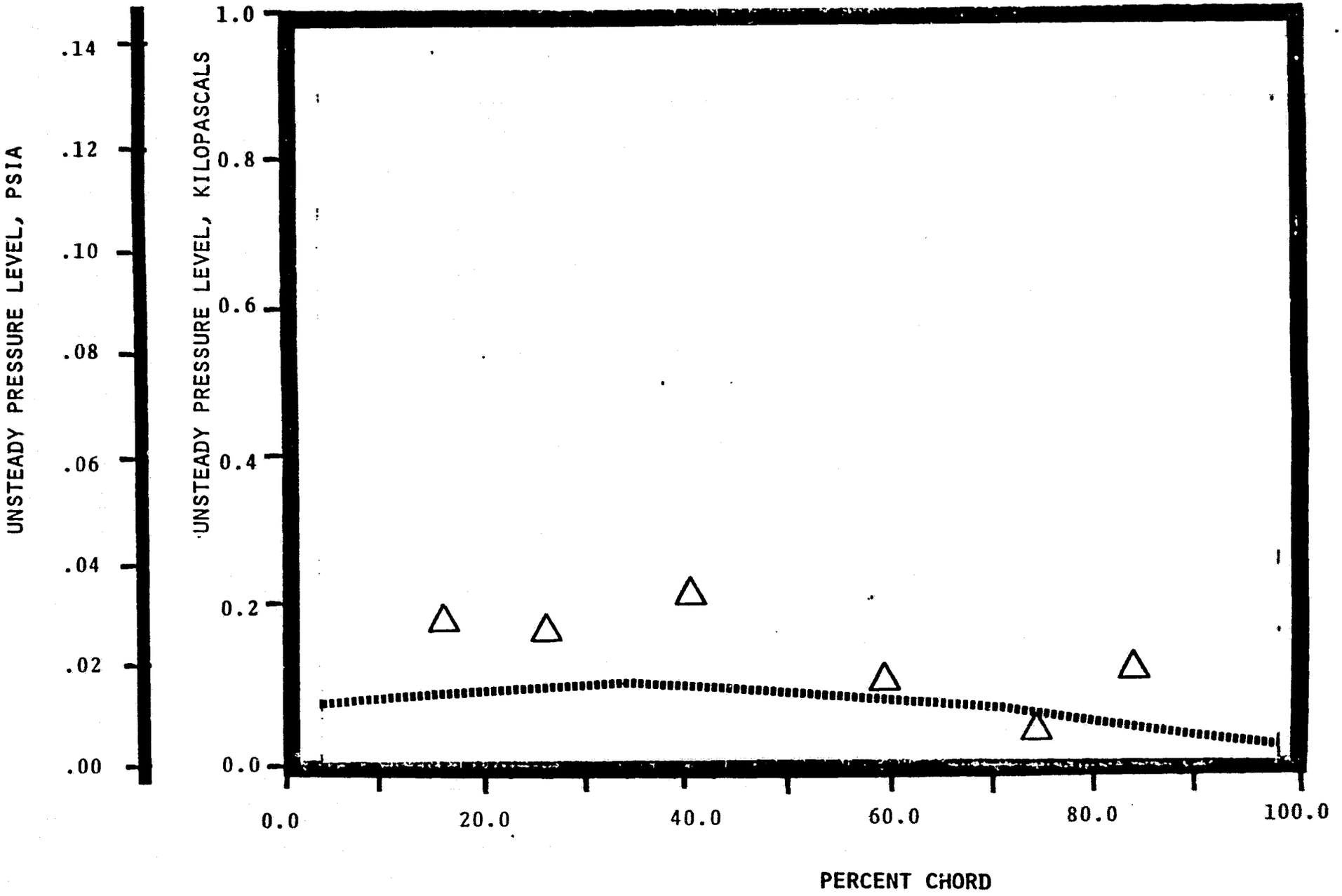

NASA·I TORSION CASCADE - REDUCED SOLIDITY - OPEN SETTING

PRESSURE SURFACE AERODYNAMIC PHASE LAG DISTRIBUTION

1.315 INLET MACH NUMBER

1.06 STATIC PRESSURE RATIO

3.14 rad (180°) INTERBLADE PHASE ANGLE

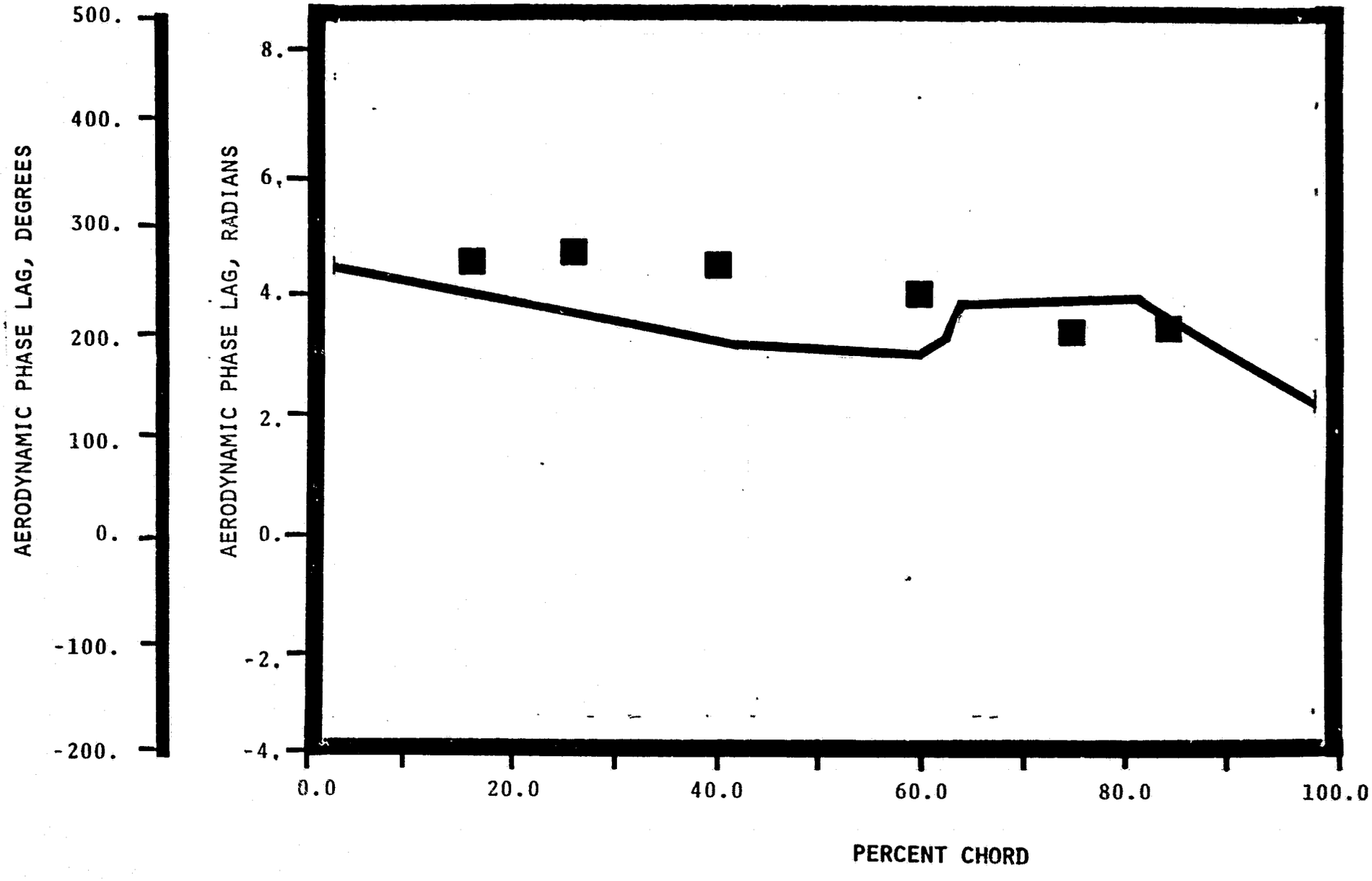

NASA I TORSION CASCADE - REDUCED SOLIDITY - OPEN SETTING

PRESSURE SURFACE UNSTEADY PRESSURE DISTRIBUTION

1.315 INLET MACH NUMBER

1.06 STATIC PRESSURE RATIO

3.14 rad (180^0) INTERBLADE PHASE ANGLE

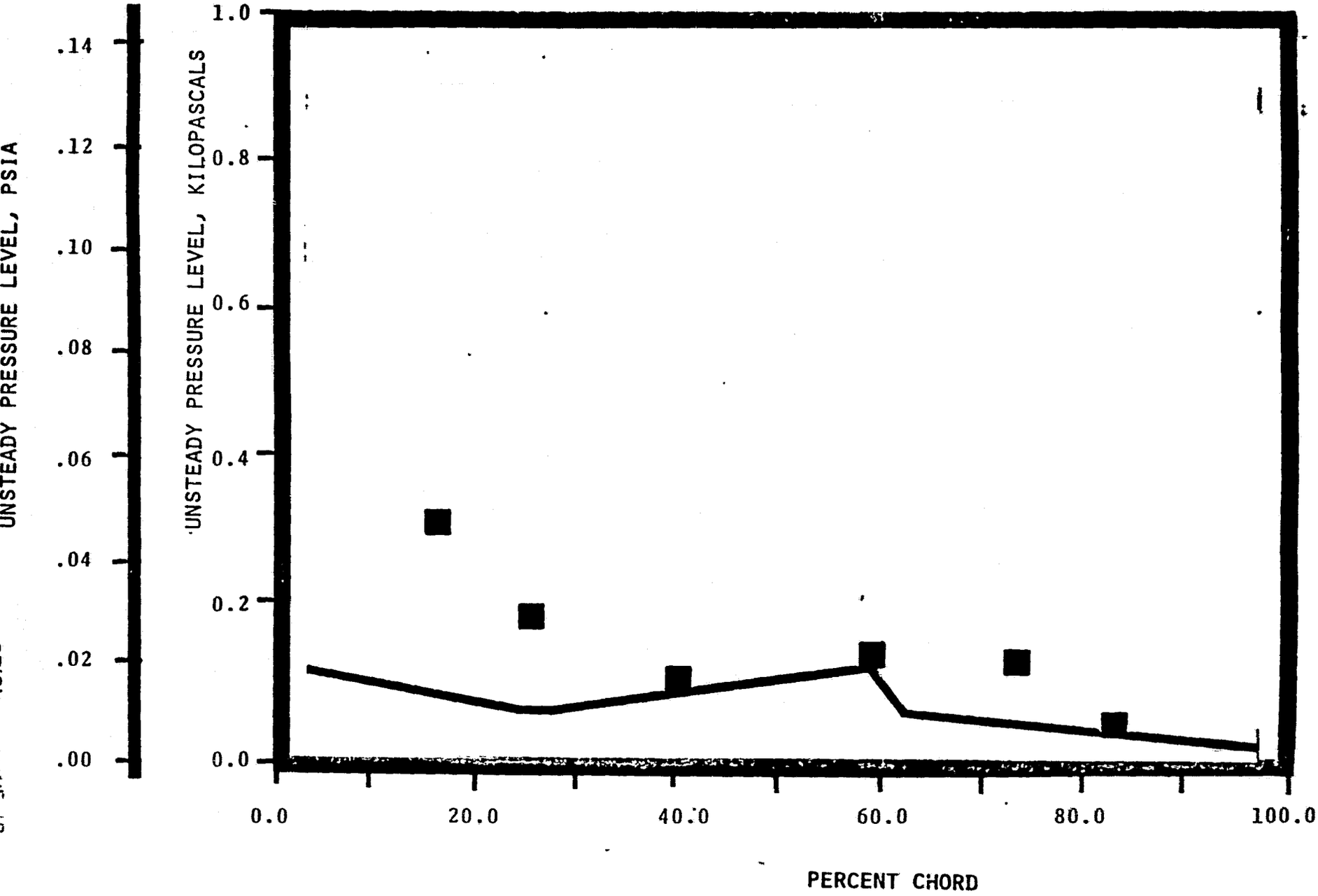

NASA I TORSION CASCADE - REDUCED SOLIDITY - OPEN SETTING

SUCTION SURFACE AERODYNAMIC PHASE LAG DISTRIBUTION

1.315 INLET MACH NUMBER

1.06 STATIC PRESSURE RATIO

3.14 rad (180°) INTERBLADE PHASE ANGLE

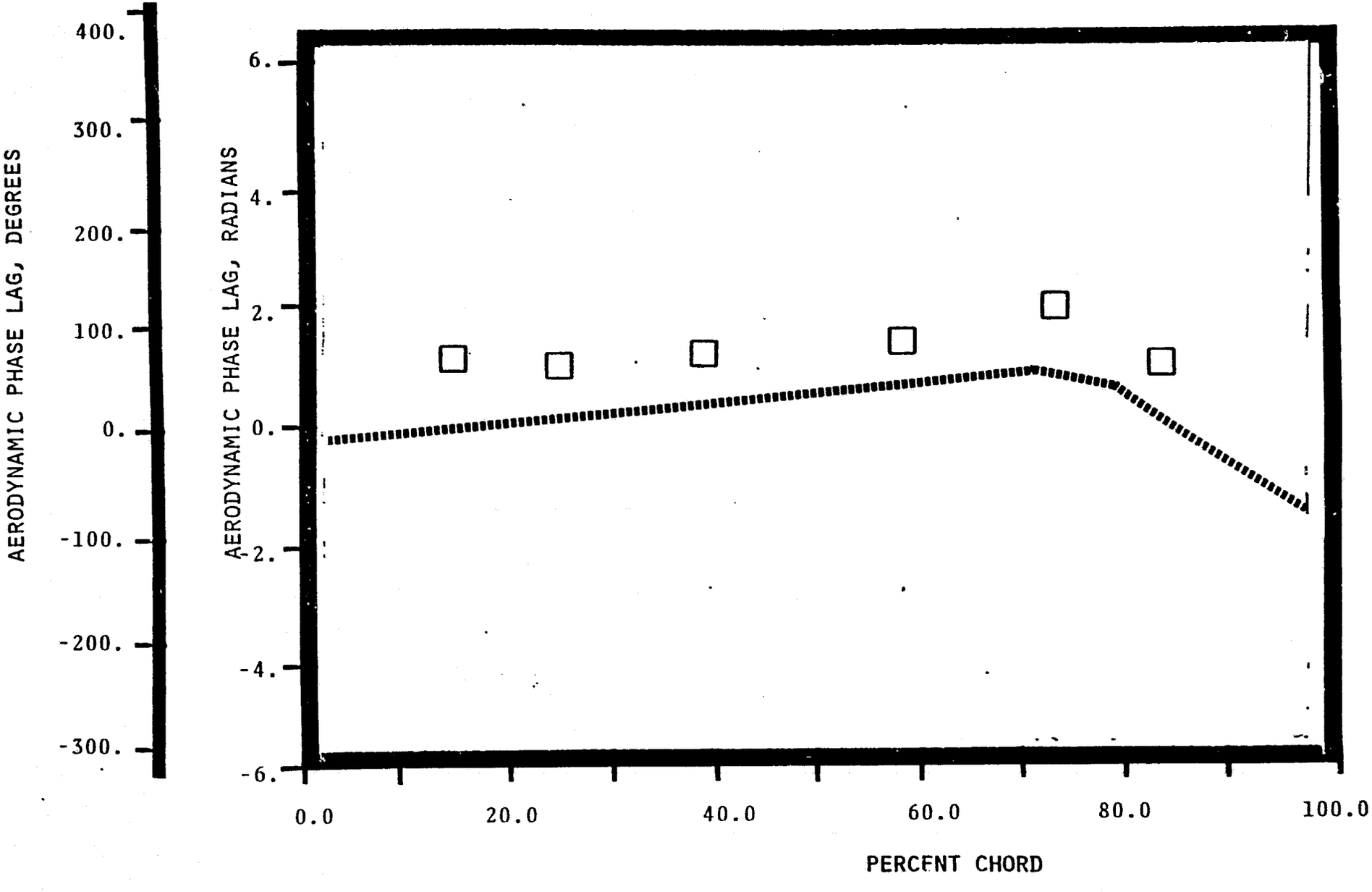

NASA I TORSION CASCADE - REDUCED SOLIDITY - OPEN SETTING

SUCTION SURFACE UNSTEADY PRESSURE DISTRIBUTION

1.315 INLET MACH NUMBER

1.06 STATIC PRESSURE RATIO

3.14 rad (180°) INTERBLADE PHASE ANGLE

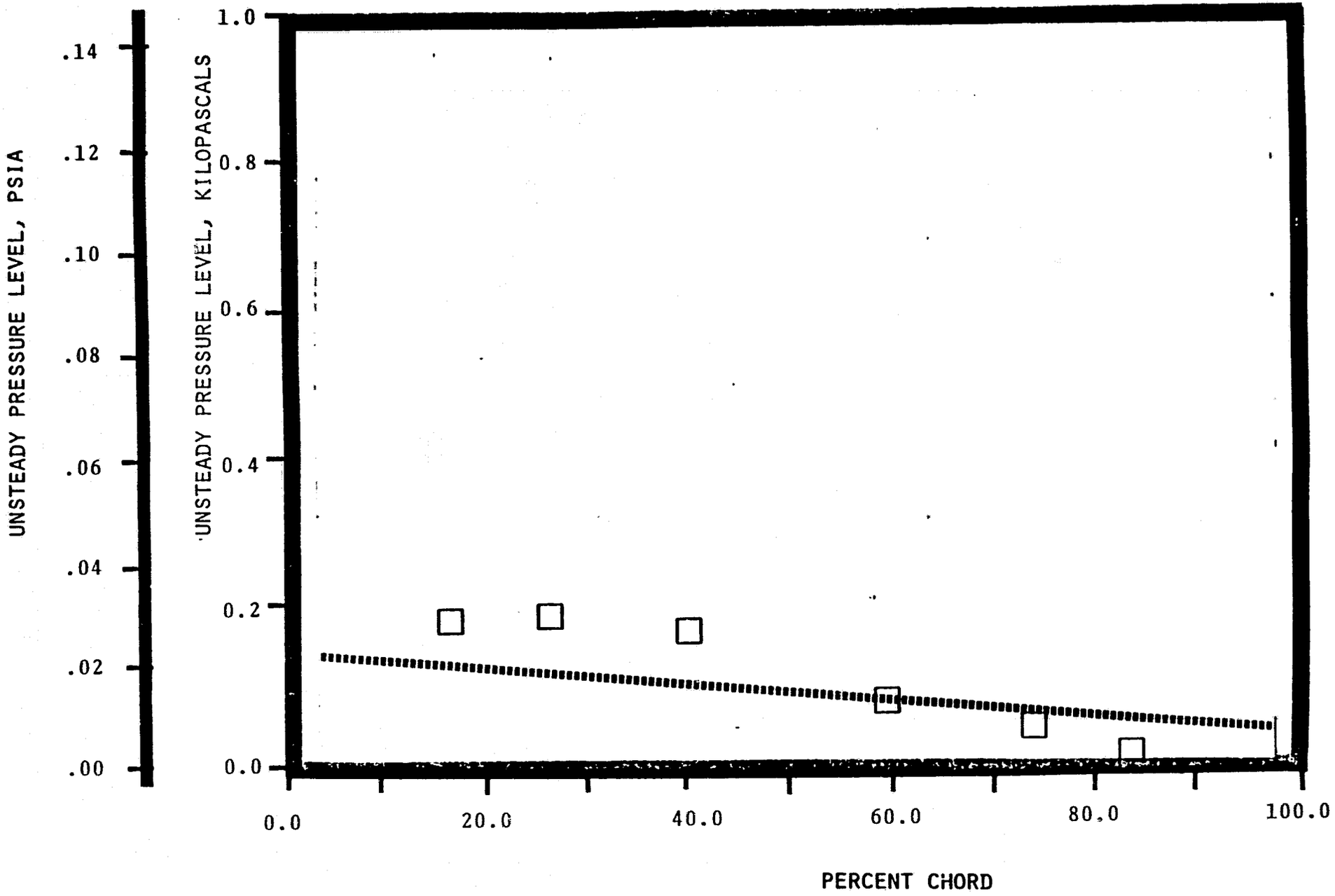

NASA I TORSION CASCADE - REDUCED SOLIDITY - OPEN SETTING

PRESSURE SURFACE AERODYNAMIC PHASE LAG DISTRIBUTION
1.315 INLET MACH NUMBER
1.06 STATIC PRESSURE RATIO
1.05 rad (90°) INTERBLADE PHASE ANGLE

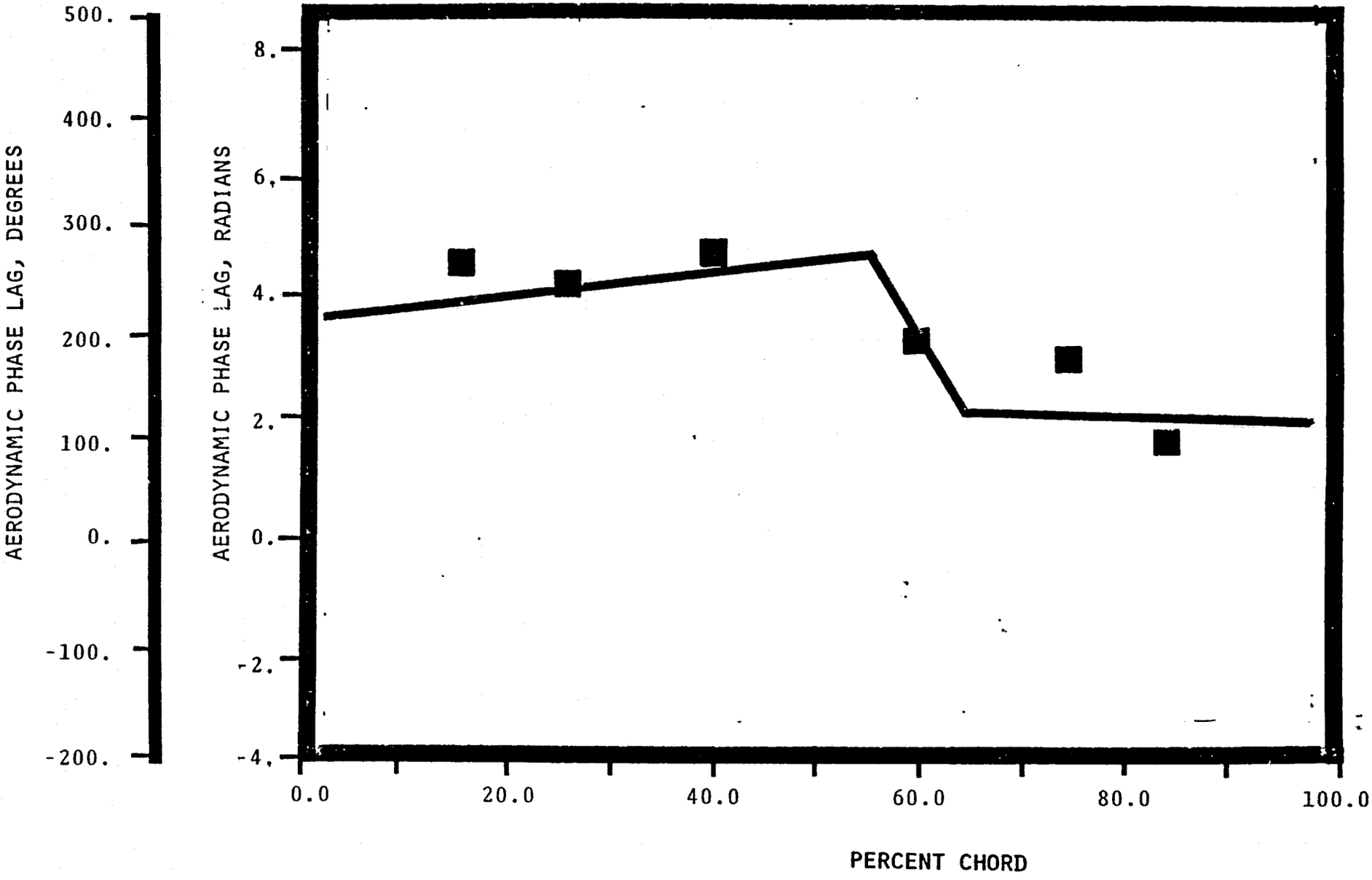

NASA I TORSION CASCADE - REDUCED SOLIDITY - OPEN SETTING

PRESSURE SURFACE UNSTEADY PRESSURE DISTRIBUTION
1.315 INLET MACH NUMBER
1.06 STATIC PRESSURE RATIO
1.05 rad (90°) INTERBLADE PHASE ANGLE

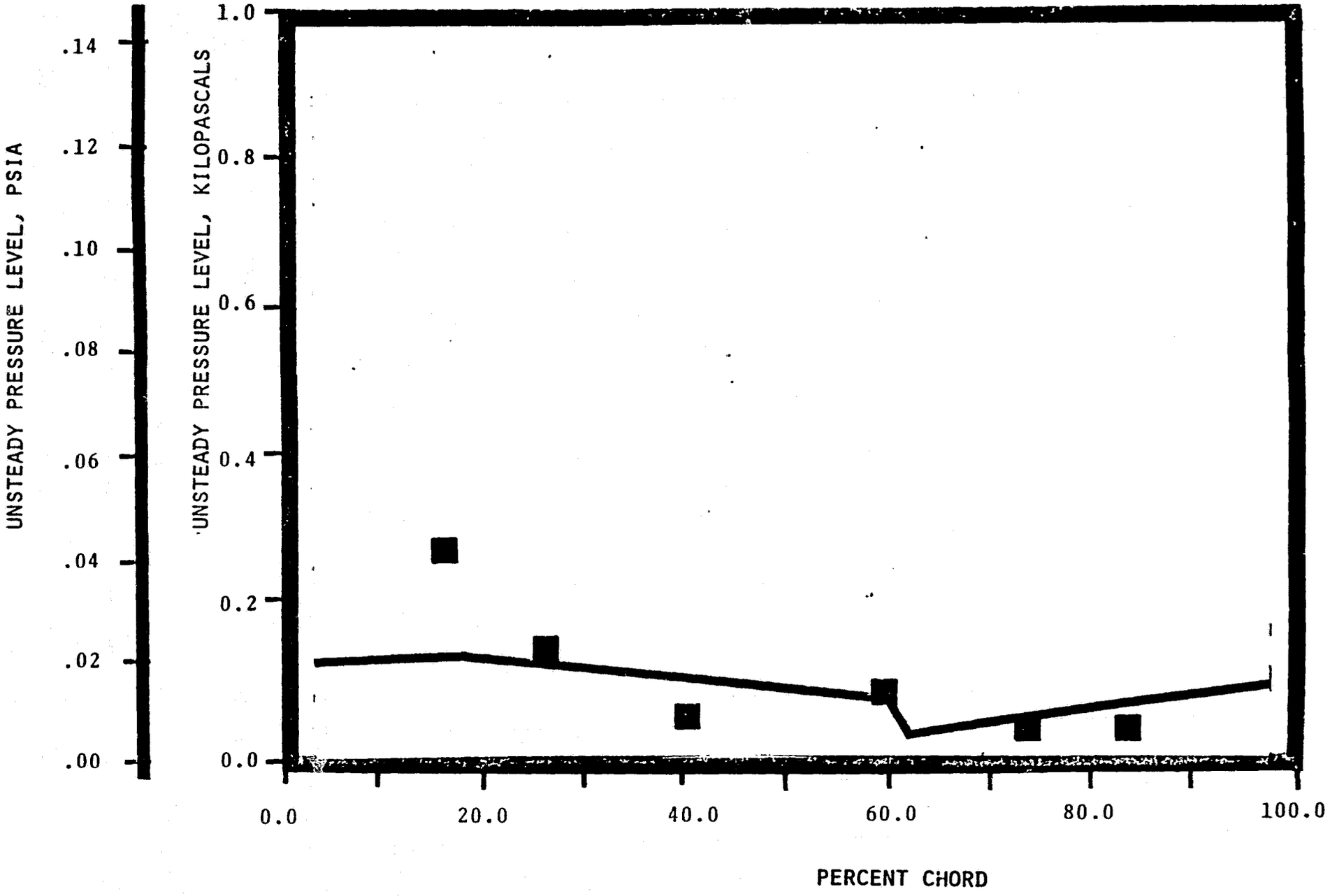

NASA I TORSION CASCADE - REDUCED SOLIDITY - OPEN SETTING

SUCTION SURFACE AERODYNAMIC PHASE LAG DISTRIBUTION

1.315 INLET MACH NUMBER

1.06 STATIC PRESSURE RATIO

1.05 rad (90°) INTERBLADE PHASE ANGLE

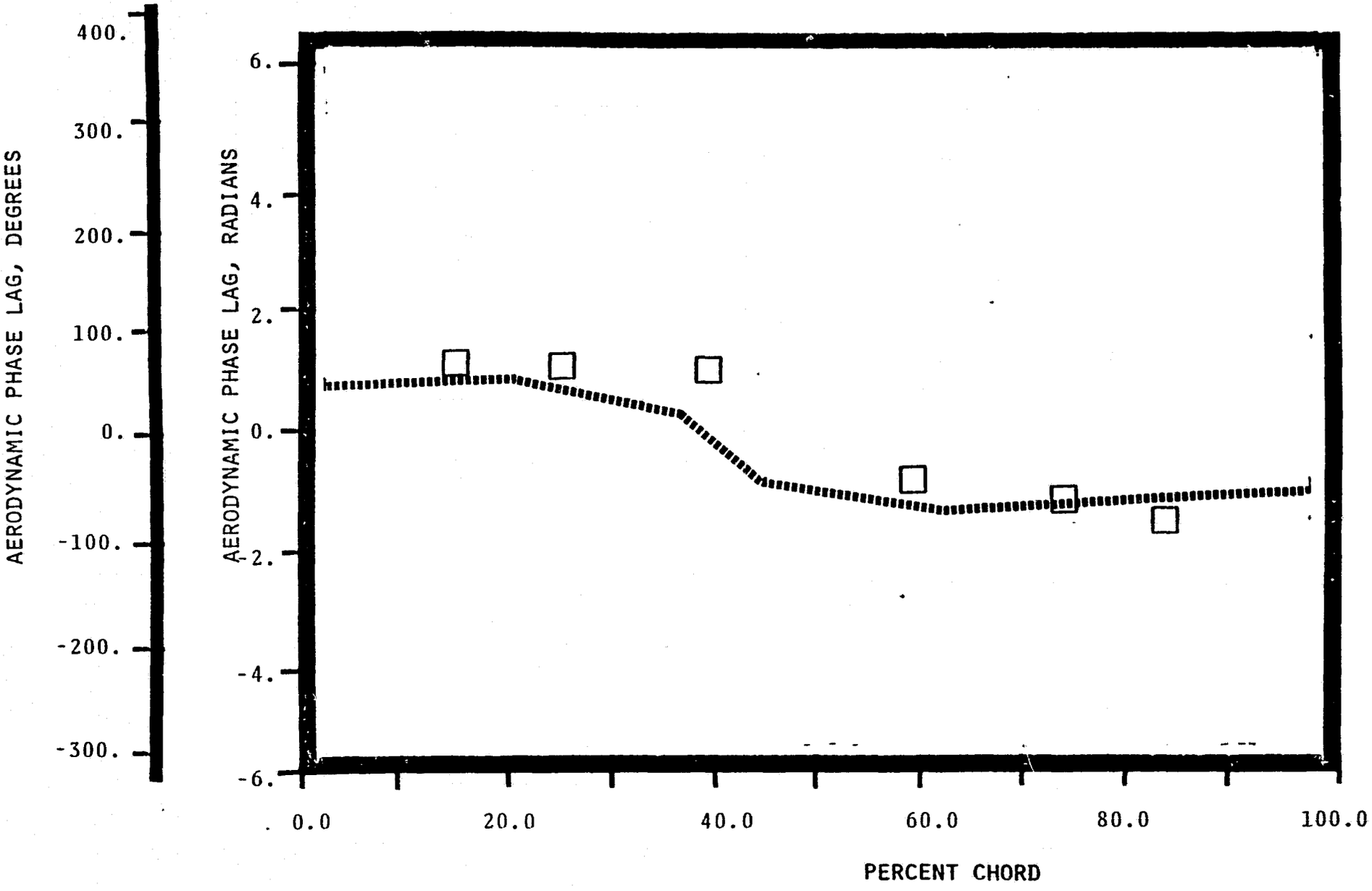

NASA I TORSION CASCADE - REDUCED SOLIDITY - OPEN SETTING

SUCTION SURFACE UNSTEADY PRESSURE DISTRIBUTION

1.315 INLET MACH NUMBER

1.06 STATIC PRESSURE RATIO

1.05 rad (90°) INTERBLADE PHASE ANGLE

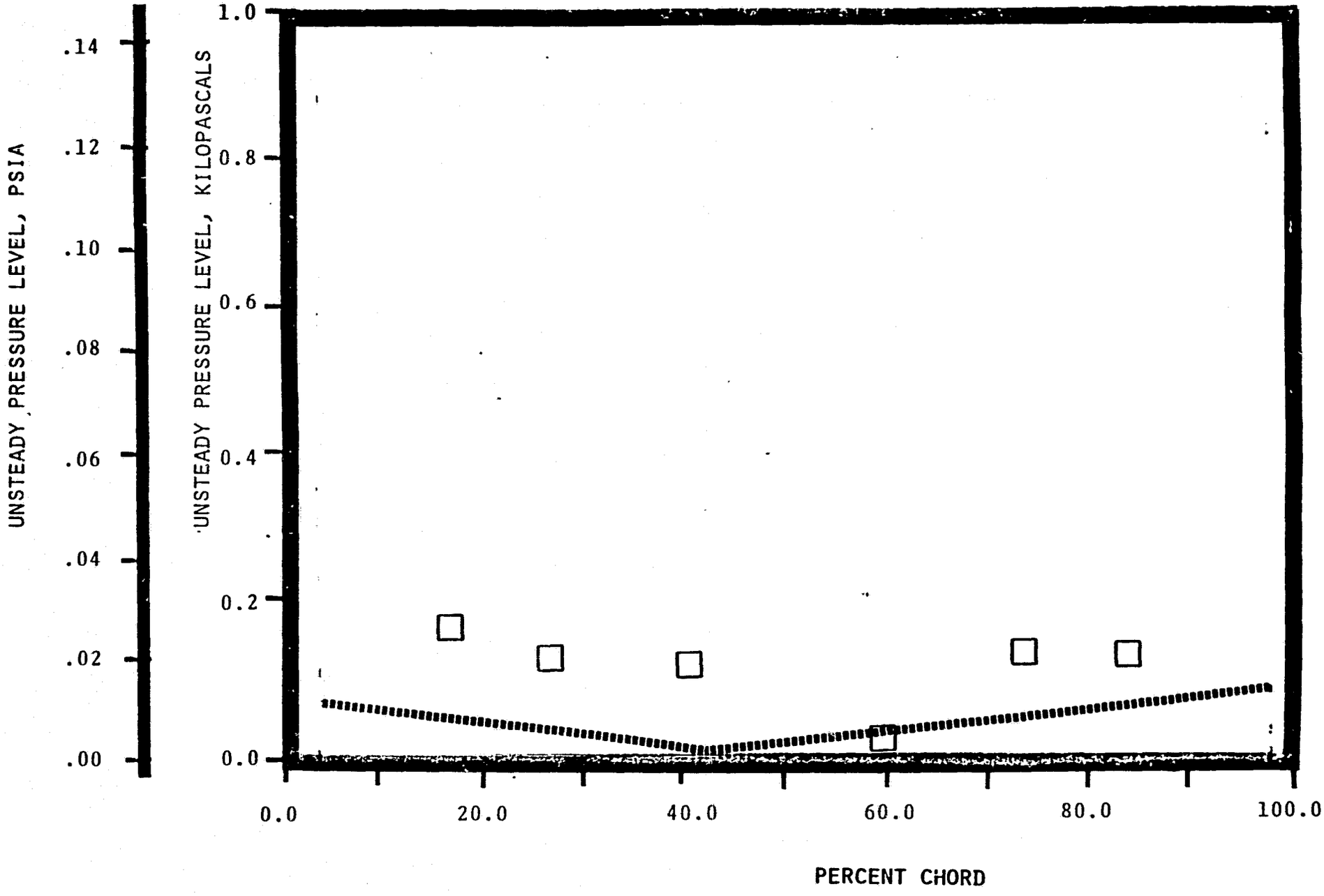

NASA I TORSION CASCADE - REDUCED SOLIDITY - OPEN SETTING

PRESSURE SURFACE AERODYNAMIC PHASE LAG DISTRIBUTION
1.315 INLET MACH NUMBER
1.06 STATIC PRESSURE RATIO
0.0 rad (0) INTERBLADE PHASE ANGLE

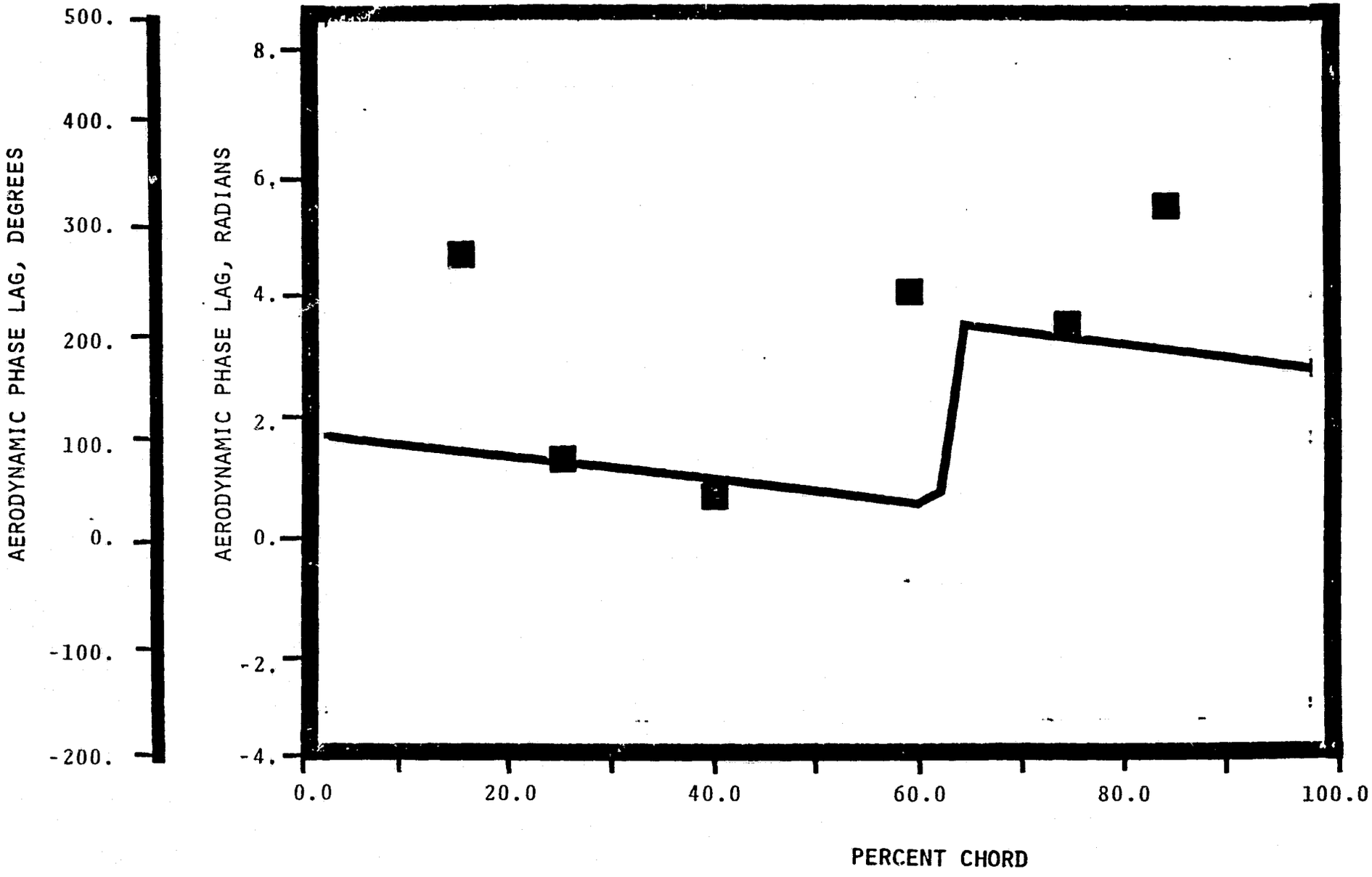

NASA I TORSION CASCADE - REDUCED SOLIDITY - OPEN SETTING

PRESSURE SURFACE UNSTEADY PRESSURE DISTRIBUTION

1.315 INLET MACH NUMBER

1.06 STATIC PRESSURE RATIO

0.0 rad (0°) INTERBLADE PHASE ANGLE

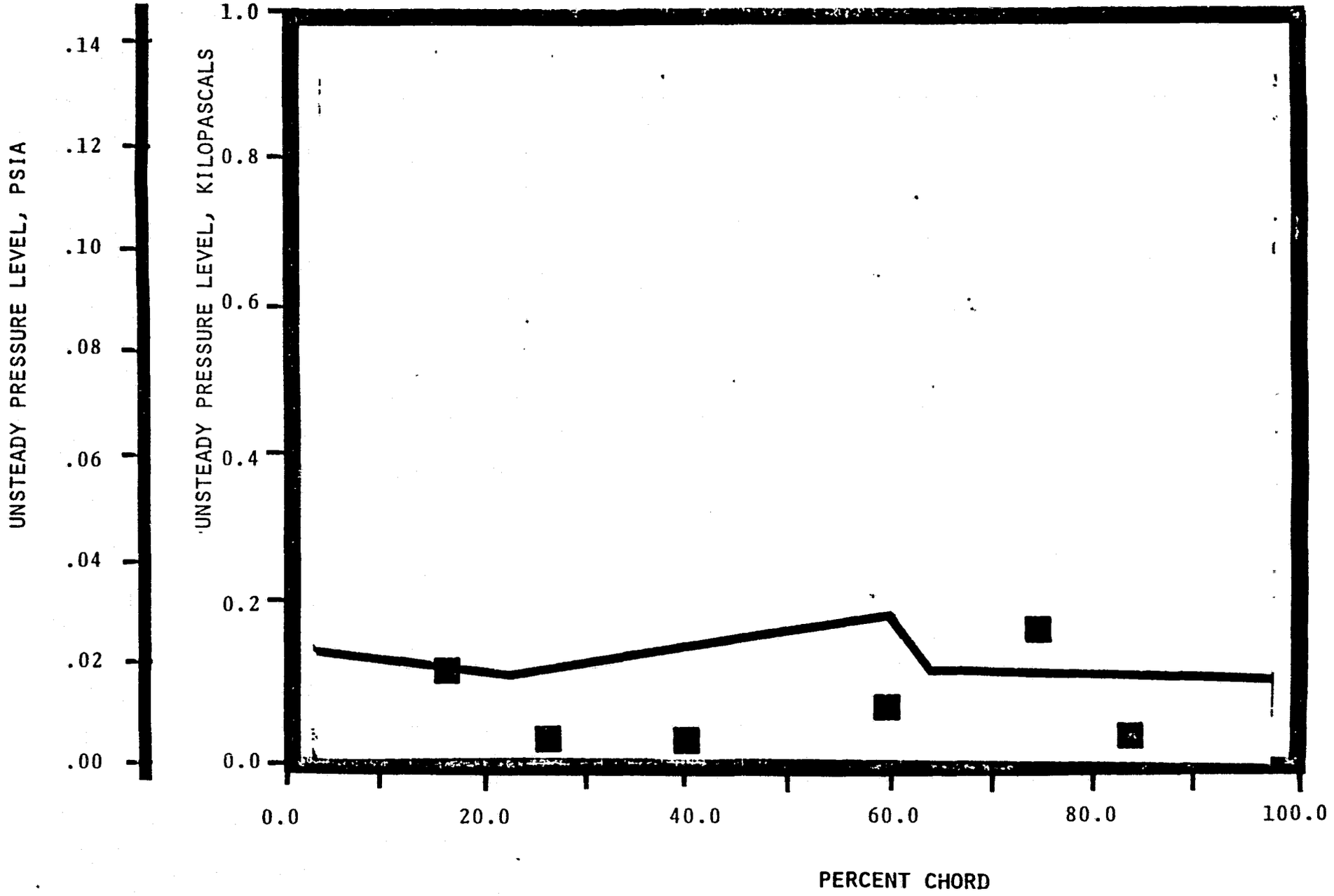

NASA I TORSION CASCADE - REDUCED SOLIDITY - OPEN SETTING

SUCTION SURFACE AERODYNAMIC PHASE LAG DISTRIBUTION

1.315 INLET MACH NUMBER

1.06 STATIC PRESSURE RATIO

0.0 rad (0.°) INTERBLADE PHASE ANGLE

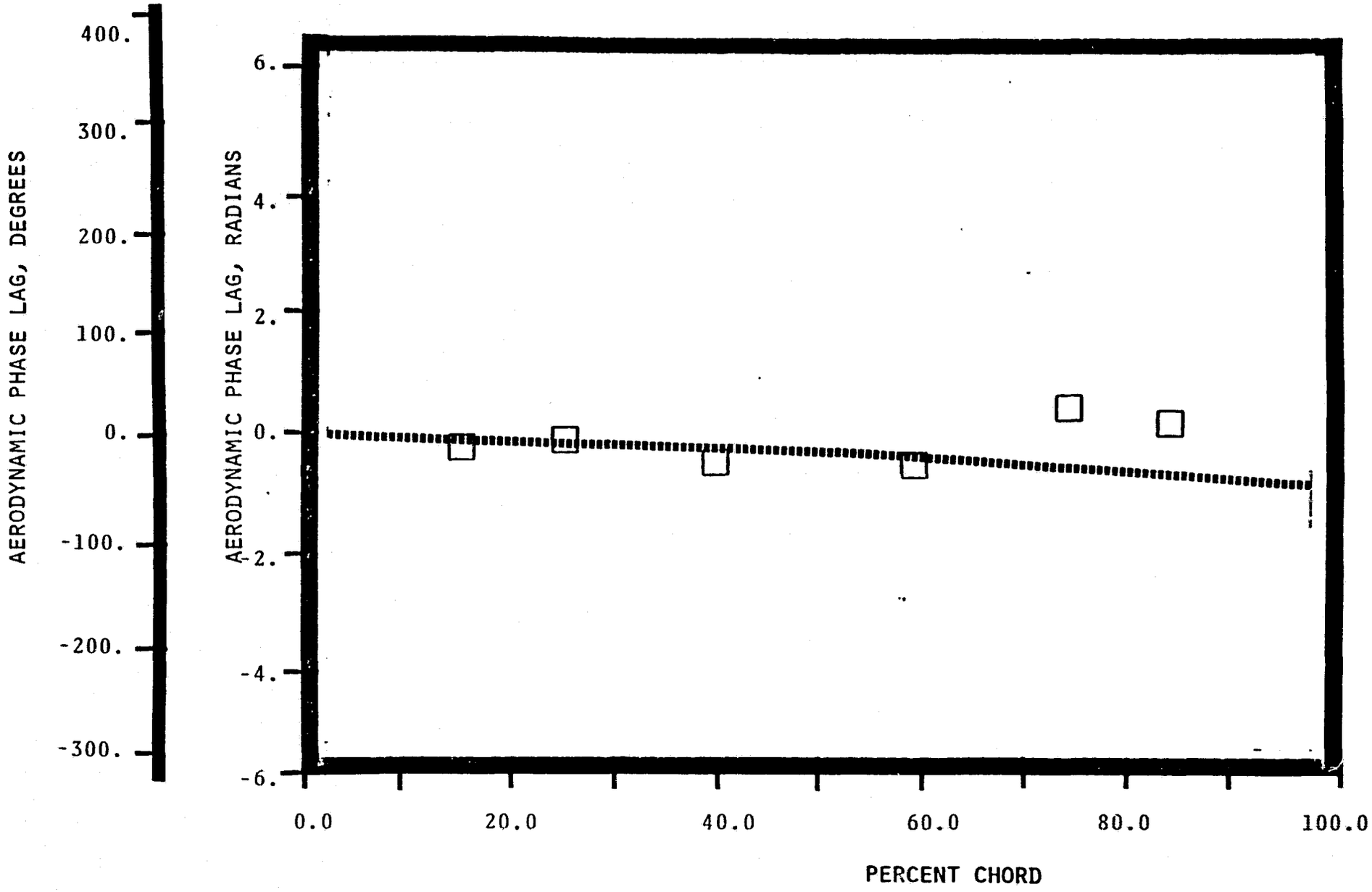

NASA 1 TORSION CASCADE - REDUCED SOLIDITY - OPEN SETTING

SUCTION SURFACE UNSTEADY PRESSURE DISTRIBUTION

1.315 INLET MACH NUMBER.

1.06 STATIC PRESSURE RATIO

0.0 rad (0°) INTERBLADE PHASE ANGLE

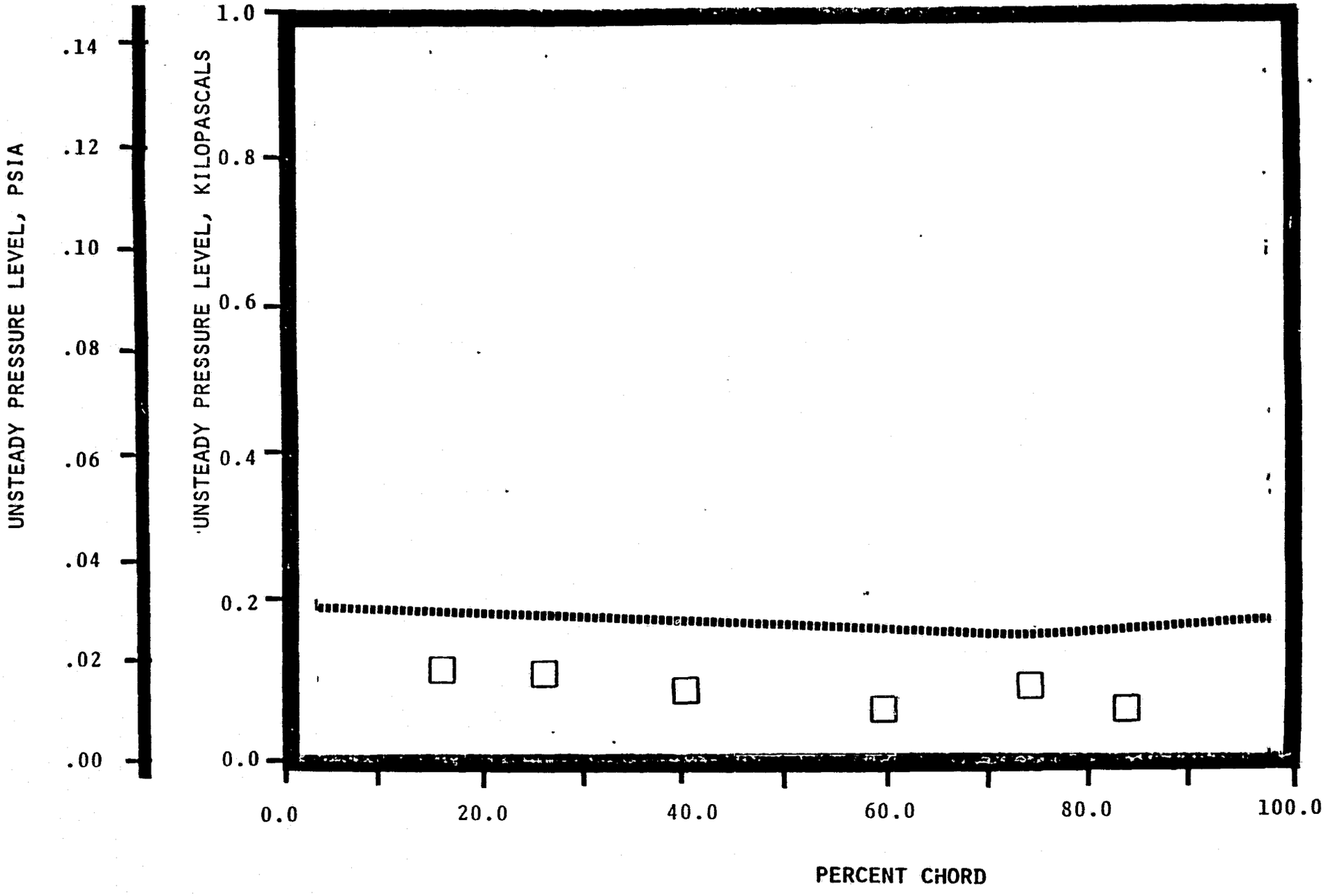

NASA I TORSION CASCADE - REDUCED SOLIDITY - OPEN SETTING

PRESSURE SURFACE AERODYNAMIC PHASE LAG DISTRIBUTION

1.315 INLET MACH NUMBER

1.06 STATIC PRESSURE RATIO

-.52 rad (-30°) INTERBLADE PHASE ANGLE

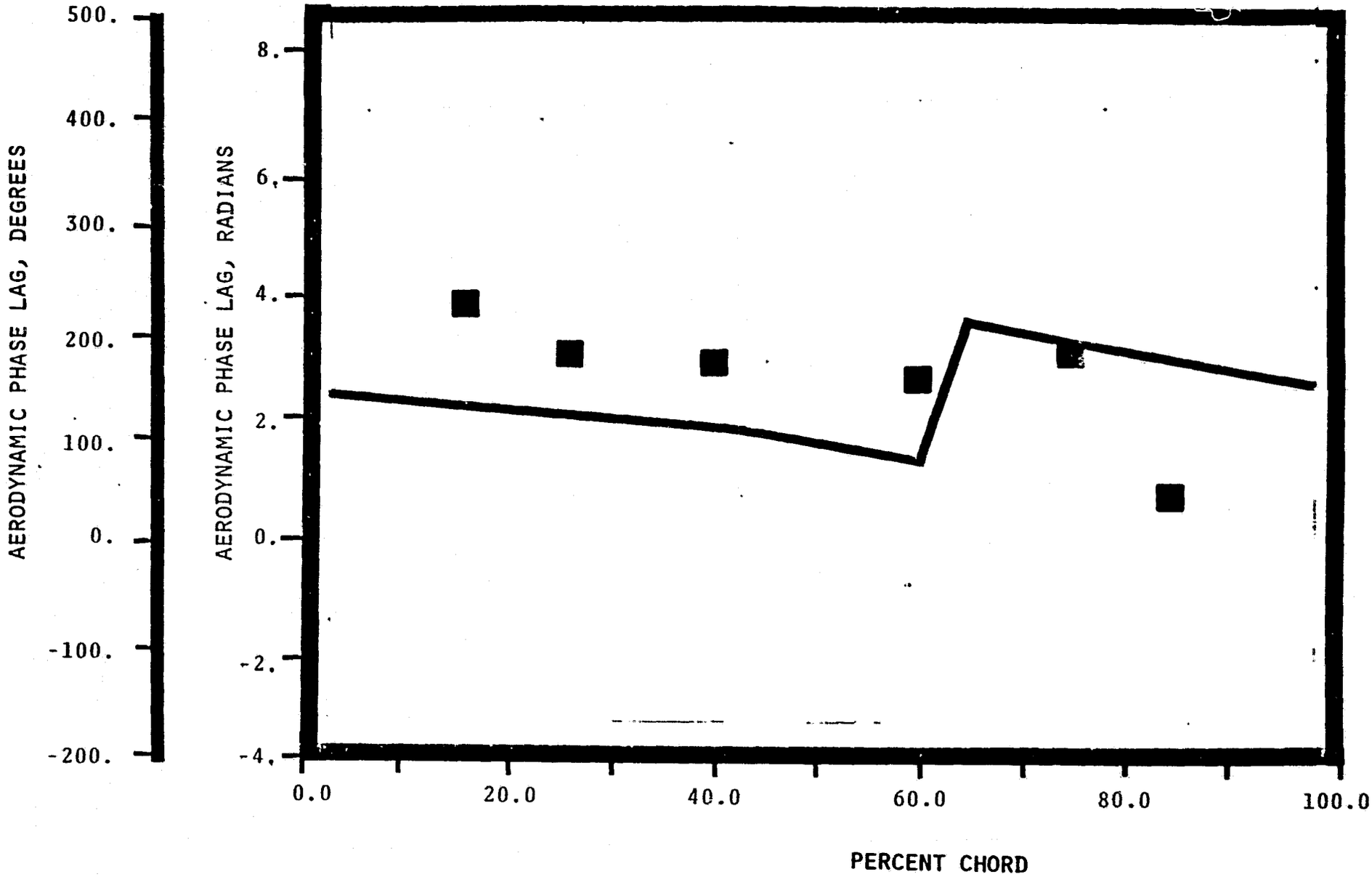

NASA I TORSION CASCADE - REDUCED SOLIDITY - OPEN SETTING

PRESSURE SURFACE UNSTEADY PRESSURE DISTRIBUTION
1.315 INLET MACH NUMBER
1.06 STATIC PRESSURE RATIO
-.52 rad (-30) INTERBLADE PHASE ANGLE

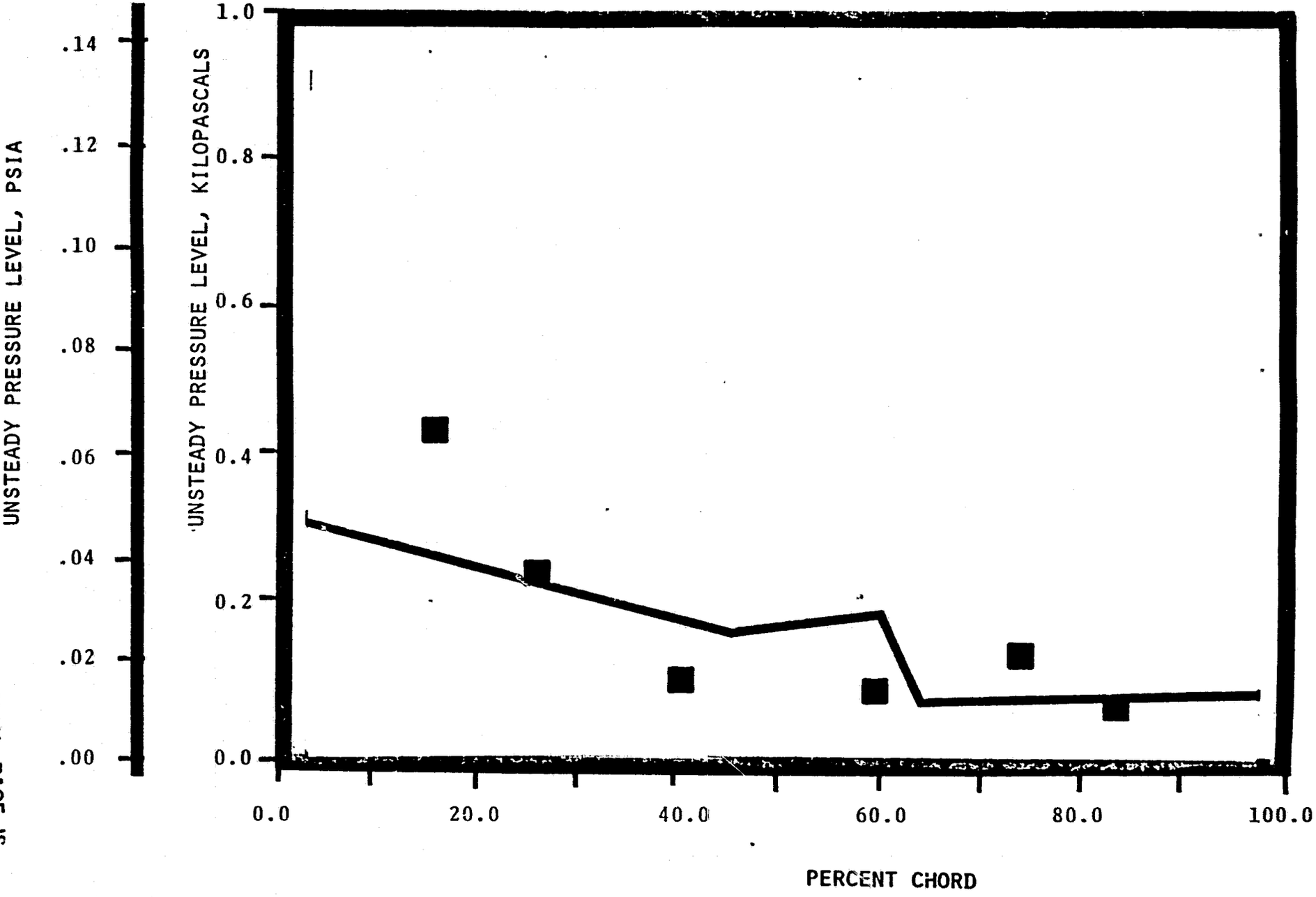

NASA I TORSION CASCADE - REDUCED SOLIDITY - OPEN SETTING

SUCTION SURFACE AERODYNAMIC PHASE LAG DISTRIBUTION

. 1.315 INLET MACH NUMBER

1.06 STATIC PRESSURE RATIO

-.52 rad (-30) INTERBLADE PHASE ANGLE.

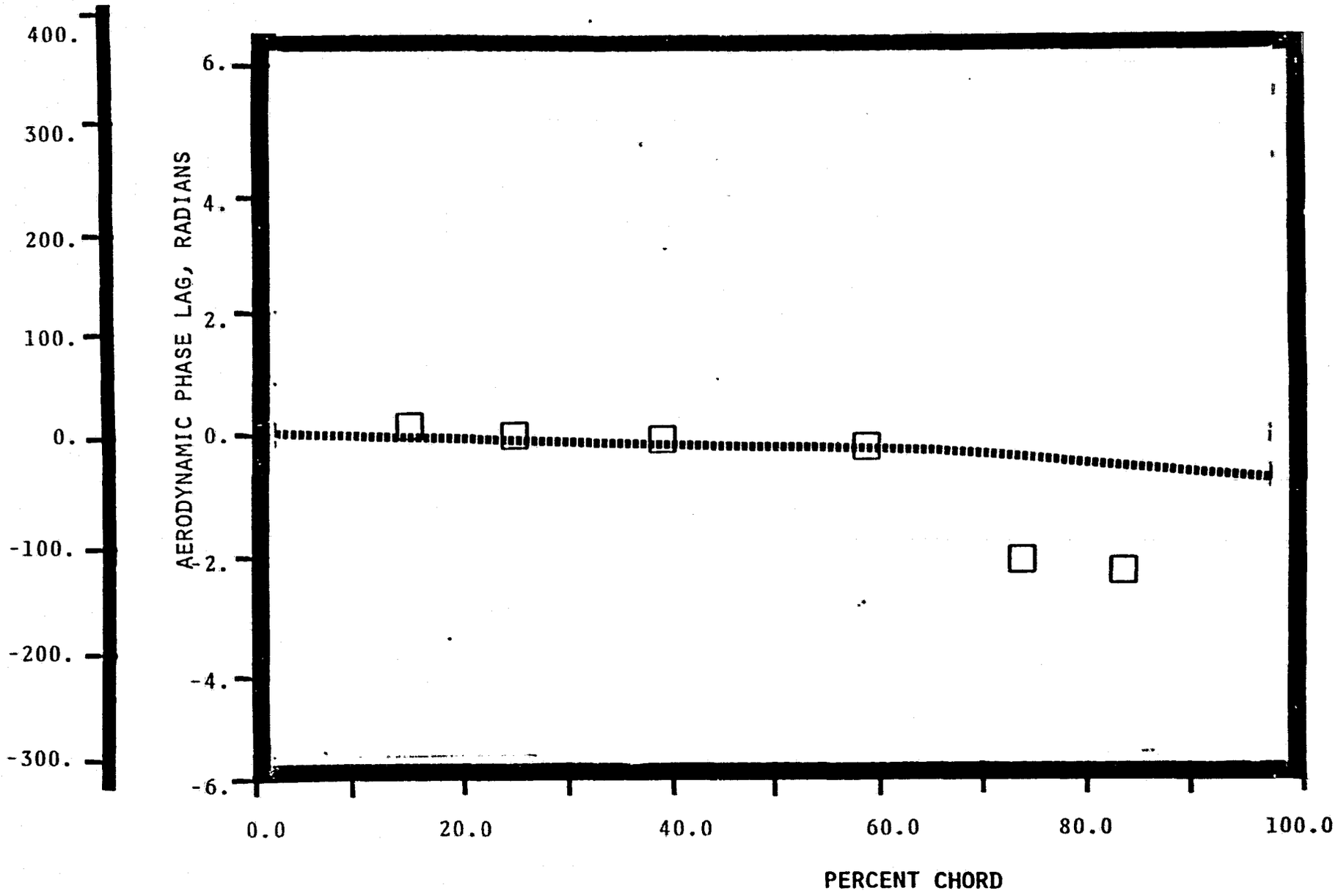

NASA I TORSION CASCADE - REDUCED SOLIDITY - OPEN SETTING

SUCTION SURFACE UNSTEADY PRESSURE DISTRIBUTION

1.315 INLET MACH NUMBER

1.06 STATIC PRESSURE RATIO

-.52 rad (-30) INTERBLADE PHASE ANGLE

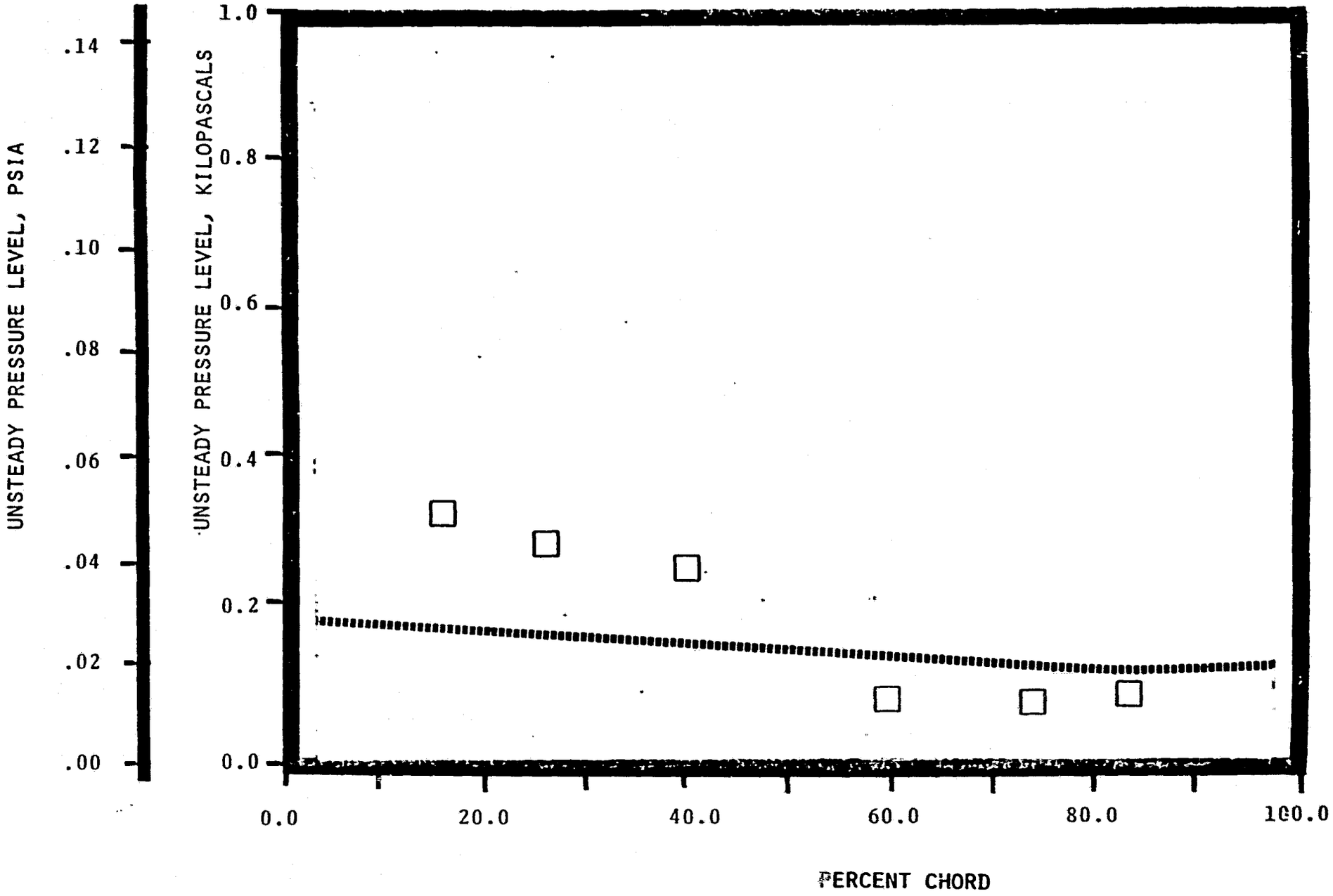

NASA I TORSION CASCADE - REDUCED SOLIDITY - OPEN SETTING

PRESSURE SURFACE AERODYNAMIC PHASE LAG DISTRIBUTION

1.315 INLET MACH NUMBER

1.06 STATIC PRESSURE RATIO

-1.05 rad (-60) INTERBLADE PHASE ANGLE

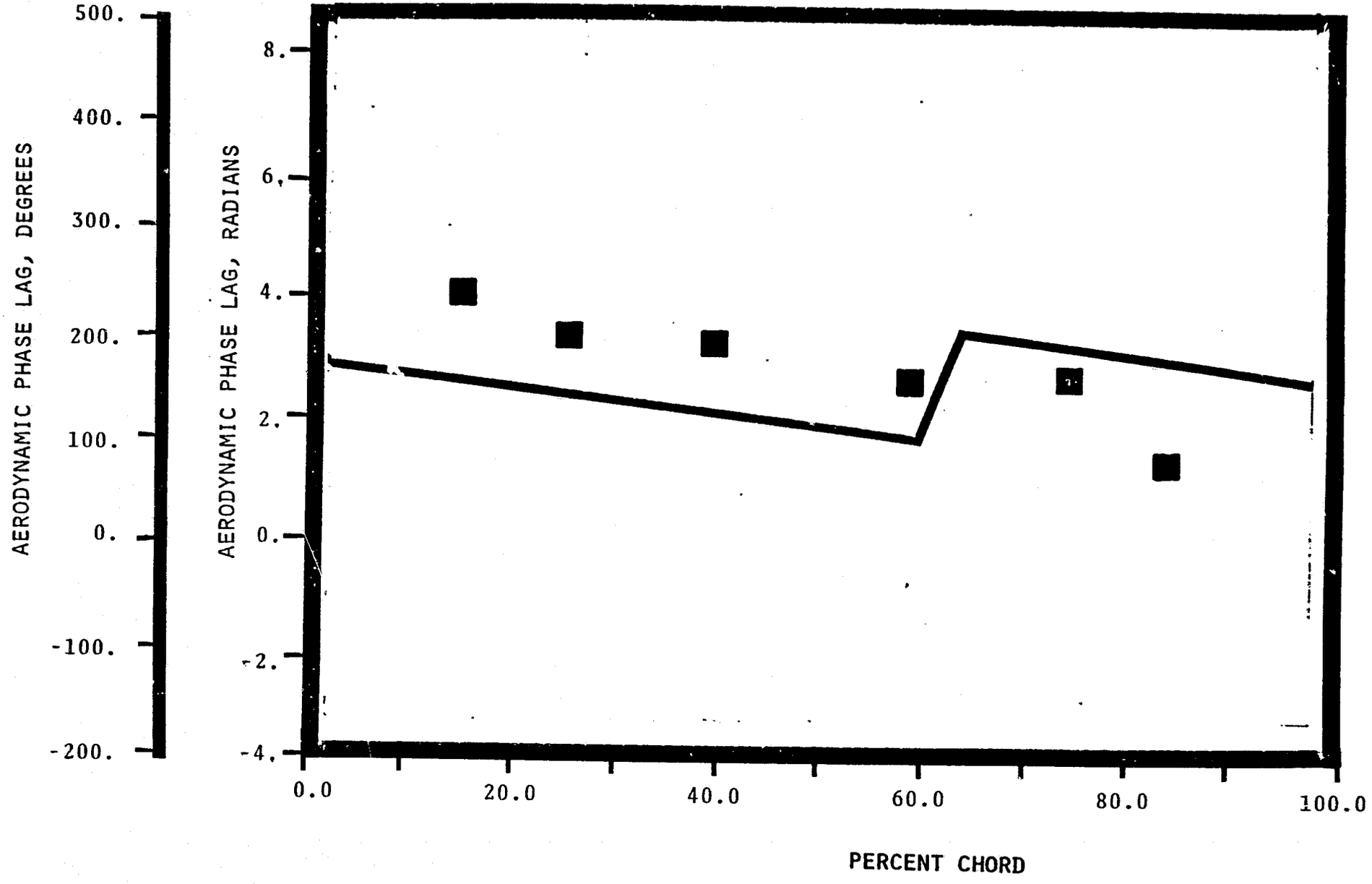

NASA I TORSION CASCADE - REDUCED SOLIDITY - OPEN SETTING

PRESSURE SURFACE UNSTEADY PRESSURE DISTRIBUTION

1.315 INLET MACH NUMBER

1.06 STATIC PRESSURE RATIO

-1.05 rad (-60°) INTERBLADE PHASE ANGLE

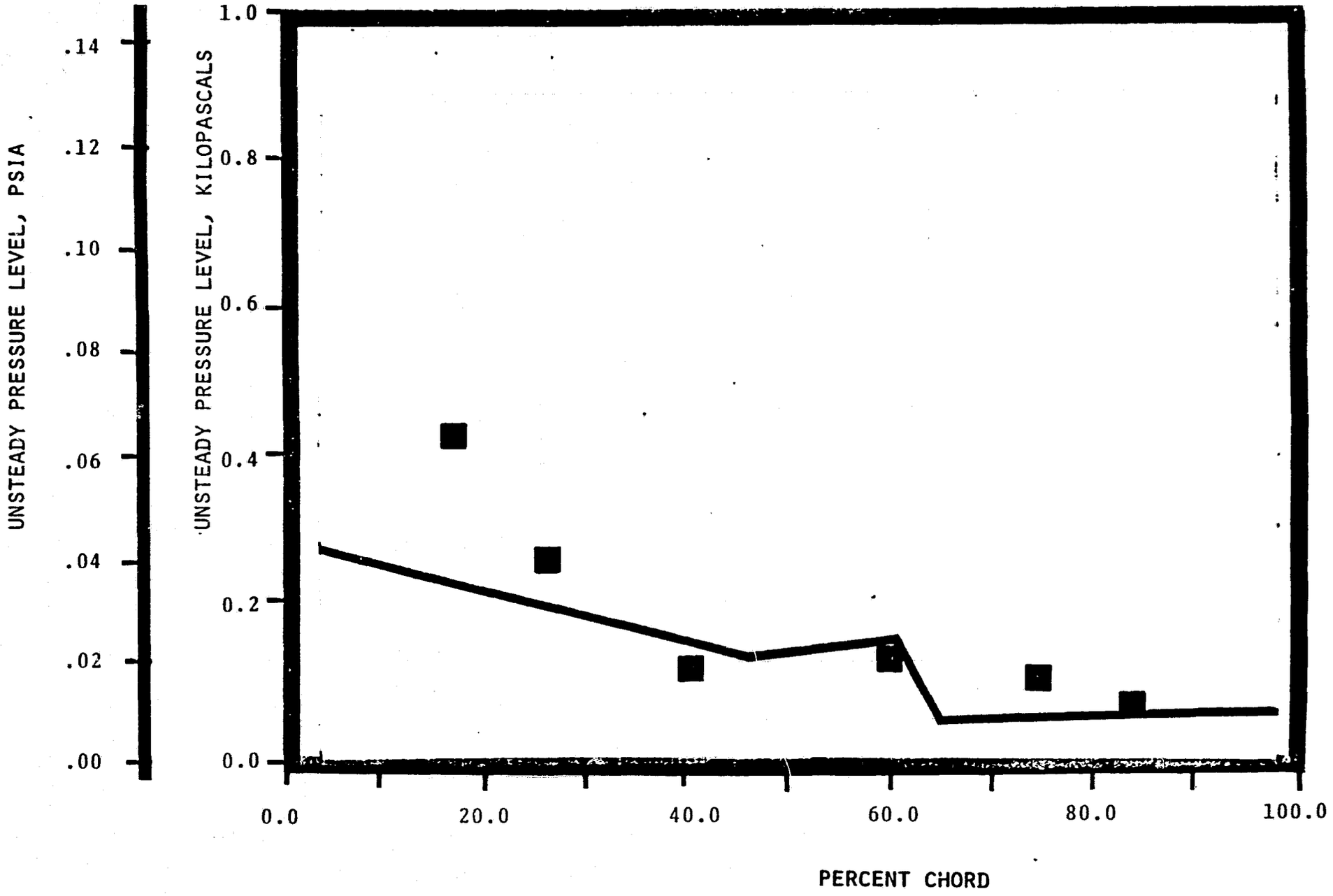

NASA I TORSION CASCADE - REDUCED SOLIDITY - OPEN SETTING

SUCTION SURFACE AERODYNAMIC PHASE LAG DISTRIBUTION

1.315 INLET MACH NUMBER

1.06 STATIC PRESSURE RATIO

-1.05 rad (-60) INTERBLADE PHASE ANGLE

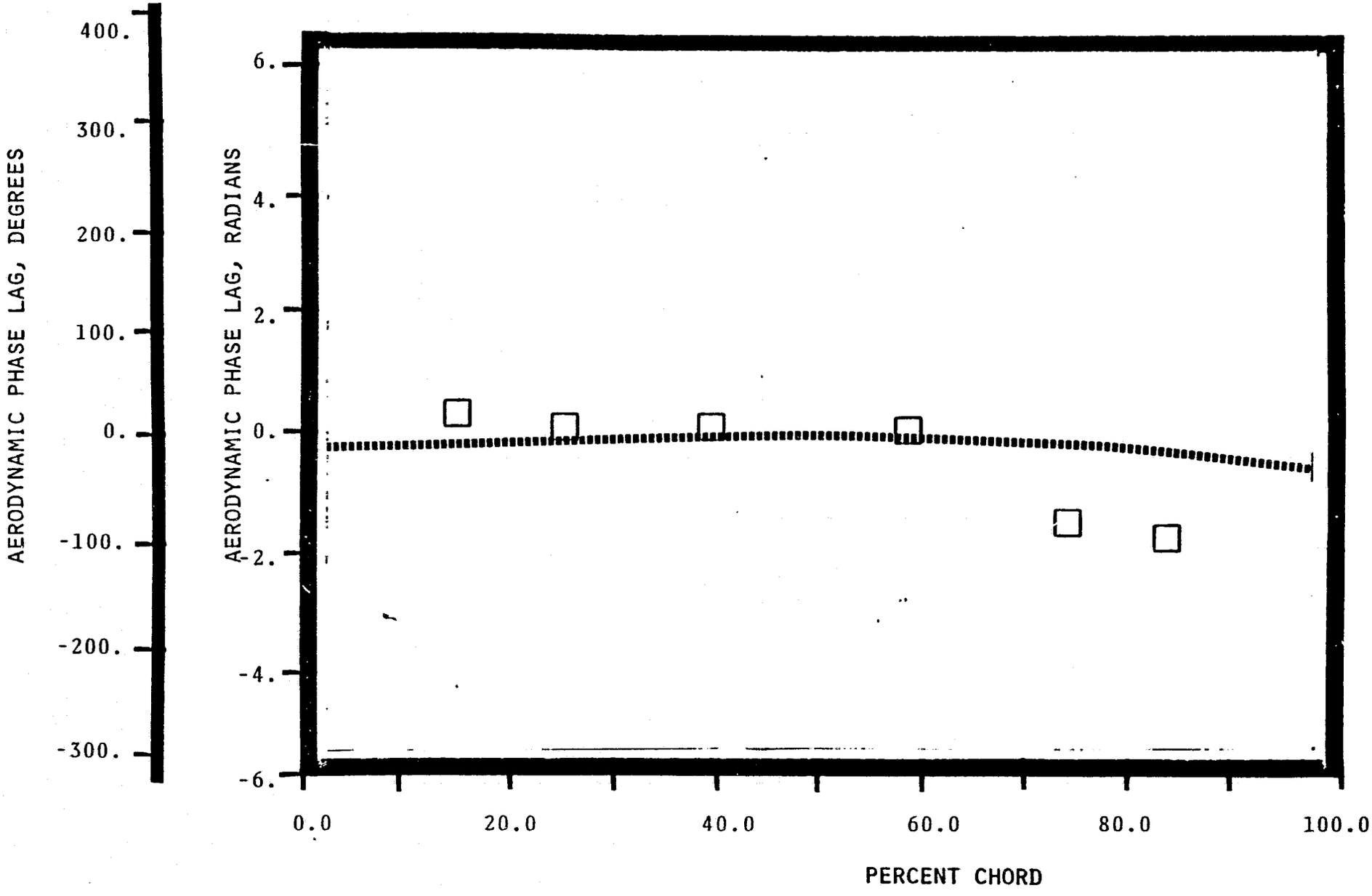

NASA I TORSION CASCADE - REDUCED SOLIDITY - OPEN SETTING

SUCTION SURFACE UNSTEADY PRESSURE DISTRIBUTION

1.315 INLET MACH NUMBER

1.06 STATIC PRESSURE RATIO

-1.05 rad (-60°) INTERBLADE PHASE ANGLE

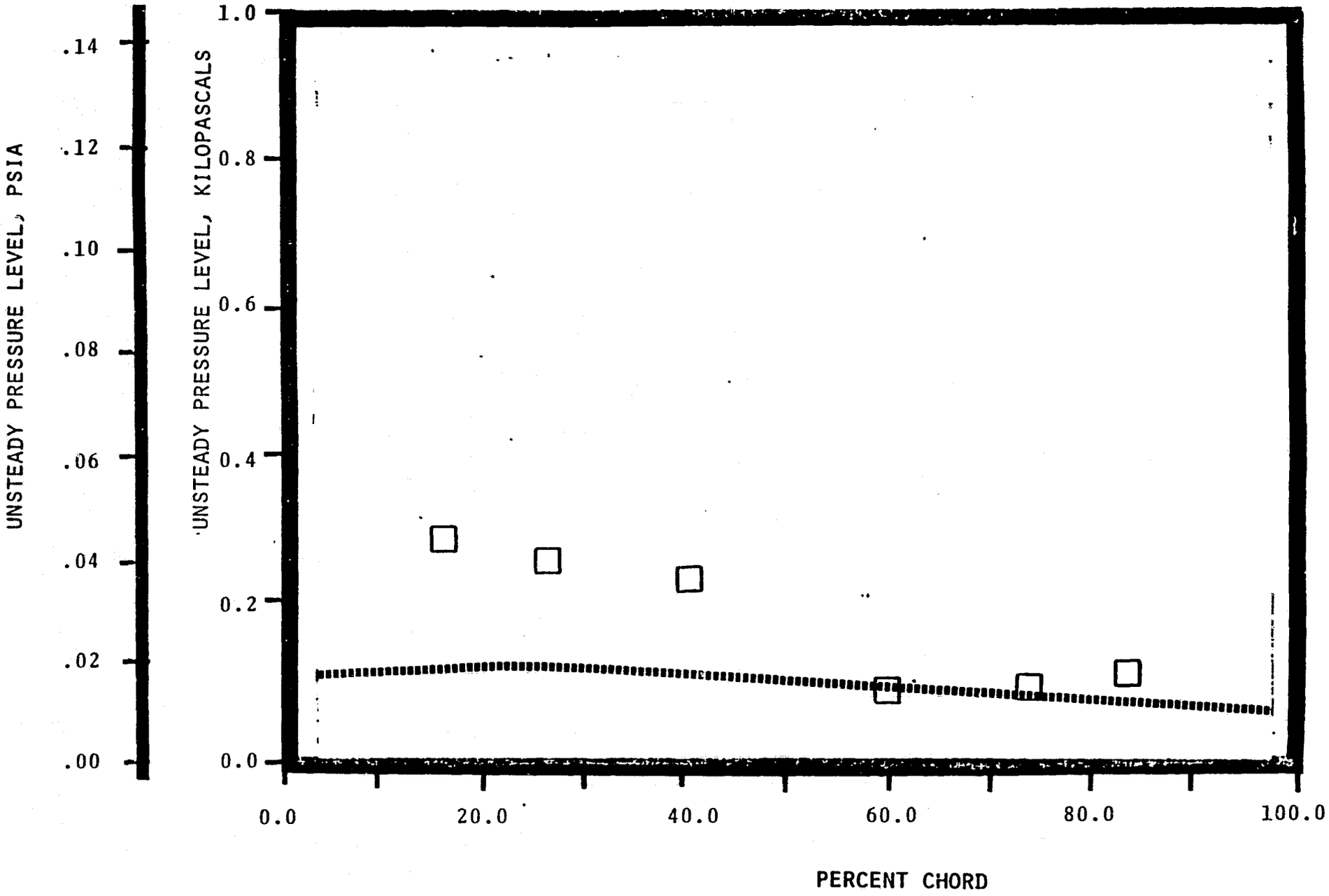

NASA I TORSION CASCADE - REDUCED SOLIDITY - OPEN SETTING

PRESSURE SURFACE AERODYNAMIC PHASE LAG DISTRIBUTION
1.315 INLET MACH NUMBER
1.06 STATIC PRESSURE RATIO
-1.57 rad (-90) INTERBLADE PHASE ANGLE

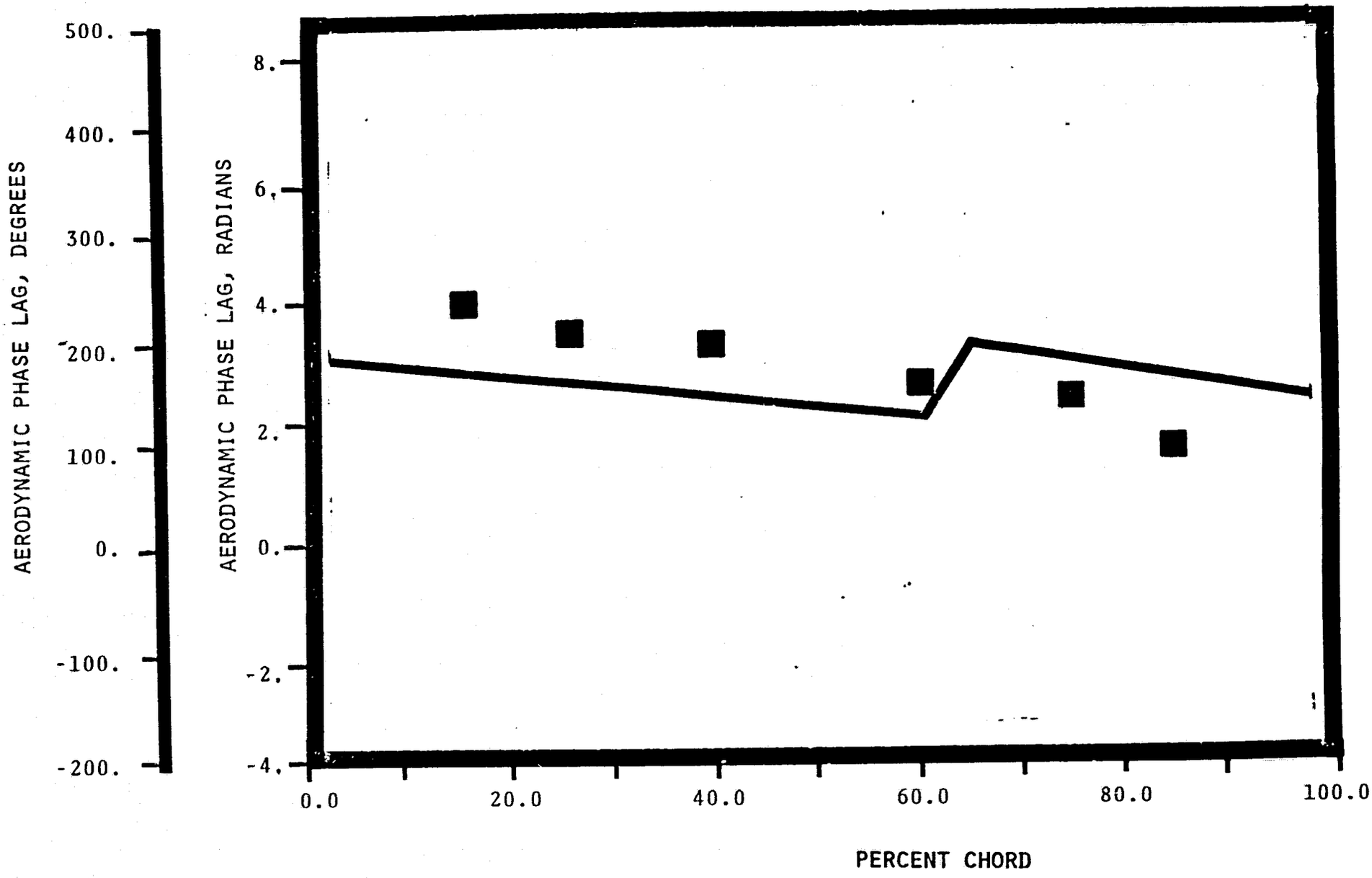

NASA I TORSION CASCADE - REDUCED SOLIDITY - OPEN SETTING

PRESSURE SURFACE UNSTEADY PRESSURE DISTRIBUTION

1.315 INLET MACH NUMBER

1.06 STATIC PRESSURE RATIO

-1.57 rad (-90) INTERBLADE PHASE ANGLE

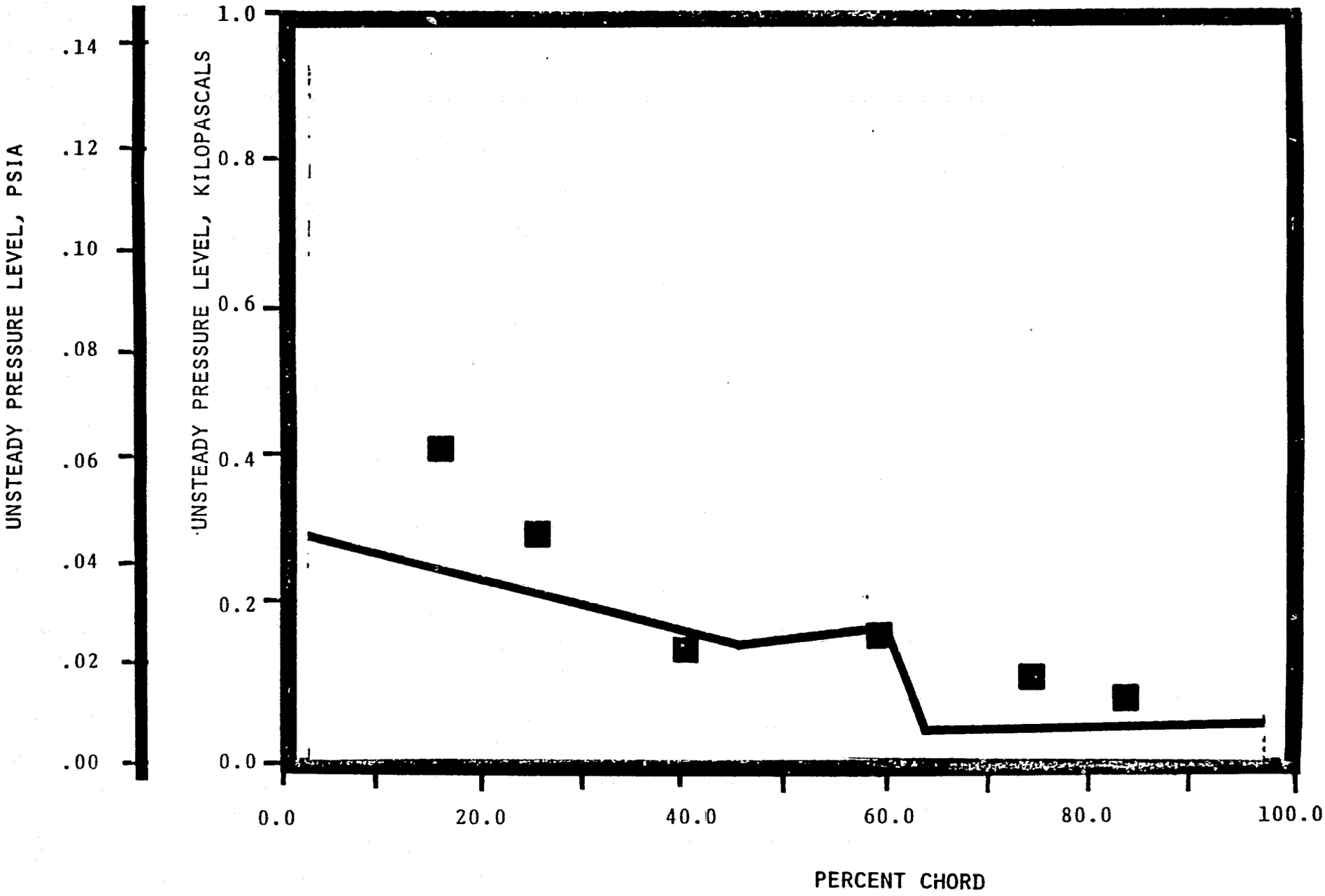

NASA I TORSION CASCADE - REDUCED SOLIDITY - OPEN SETTING

SUCTION SURFACE AERODYNAMIC PHASE LAG DISTRIBUTION

1.315 INLET MACH NUMBER

1.06 STATIC PRESSURE RATIO

-1.57 rad (-90) INTERBLADE PHASE ANGLE

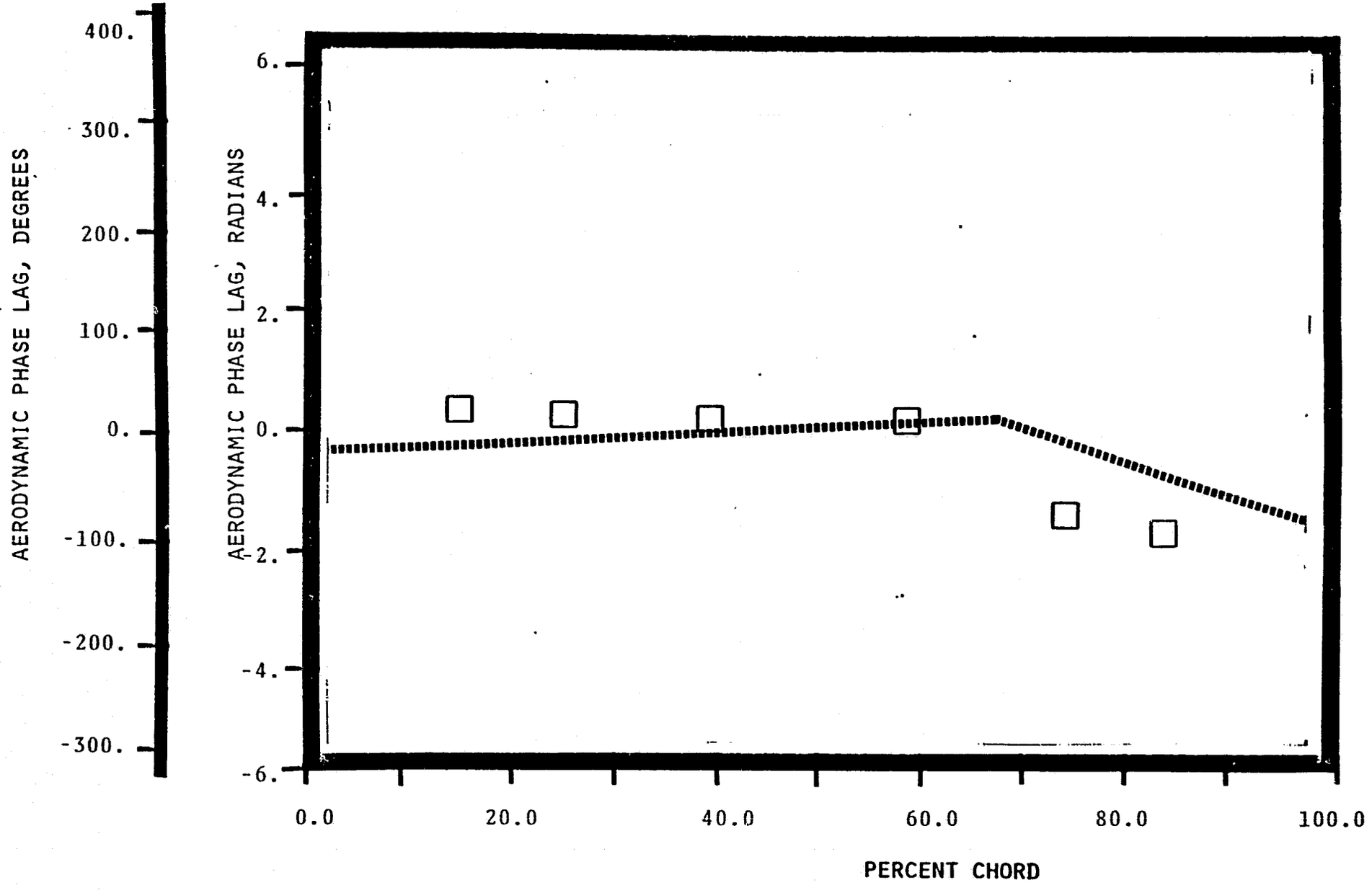

NASA I TORSION CASCADE - REDUCED SOLIDITY - OPEN SETTING

SUCTION SURFACE UNSTEADY PRESSURE DISTRIBUTION

1.315 INLET MACH NUMBER

1.06 STATIC PRESSURE RATIO

-1.57 rad (-90) INTERBLADE PHASE ANGLE

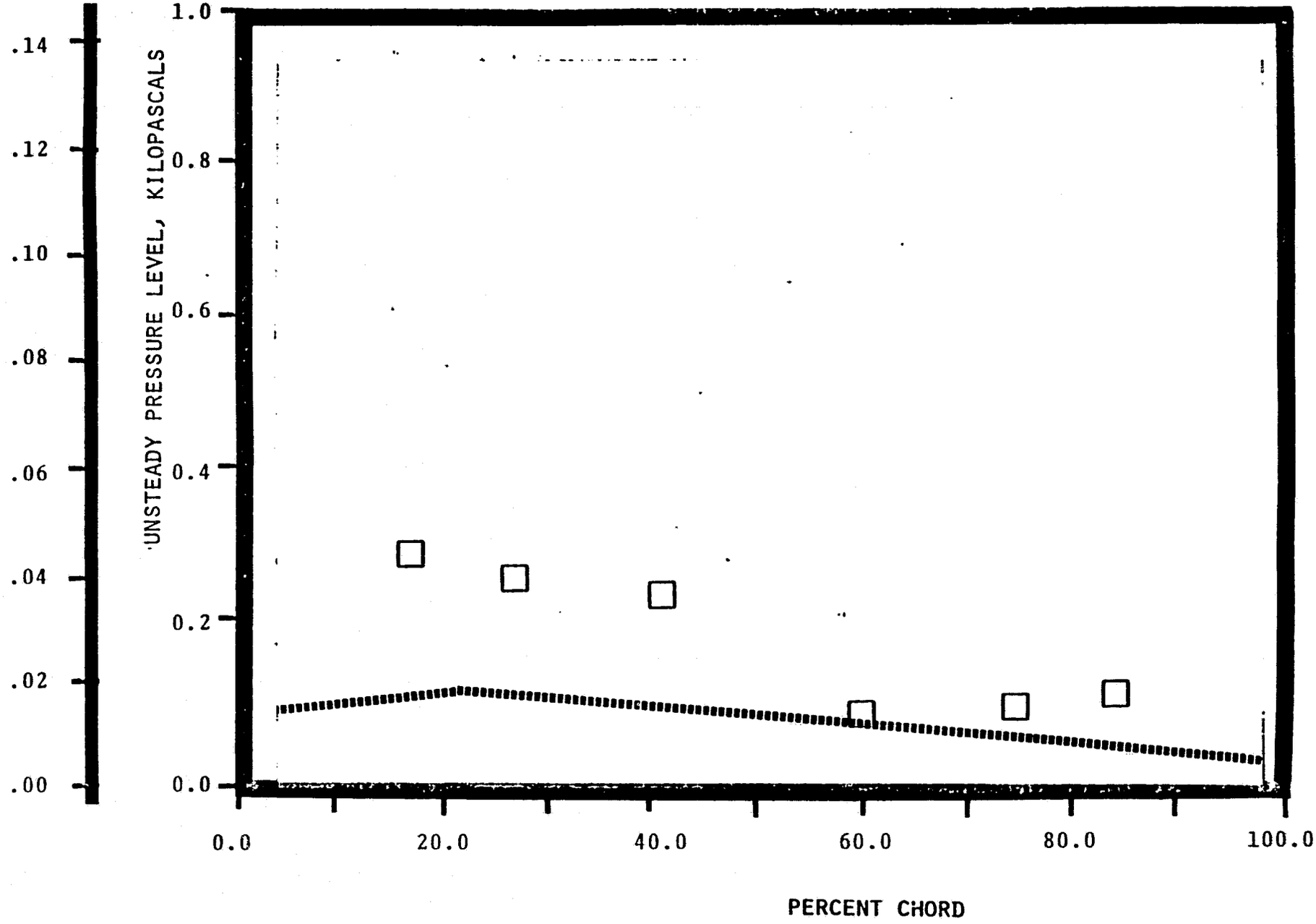

NASA I TORSION CASCADE - REDUCED SOLIDITY - OPEN SETTING

PRESSURE SURFACE AERODYNAMIC PHASE LAG DISTRIBUTION

1.315 INLET MACH NUMBER

1.33 STATIC PRESSURE RATIO

3.14 rad (180°) INTERBLADE PHASE ANGLE

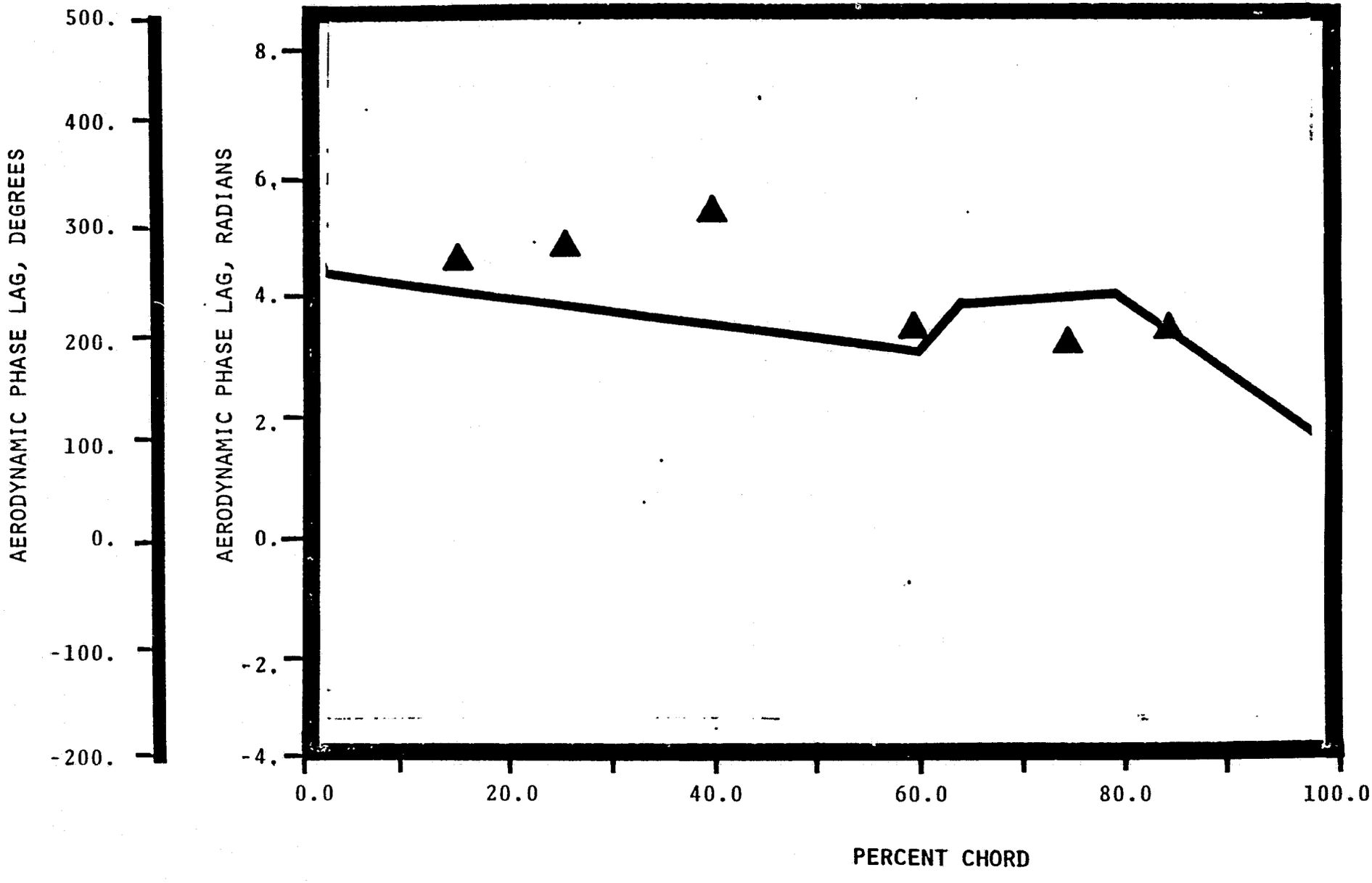

NASA I TORSION CASCADE - REDUCED SOLIDITY - OPEN SETTING

PRESSURE SURFACE UNSTEADY PRESSURE DISTRIBUTION

1.315 INLET MACH NUMBER

1.33 STATIC PRESSURE RATIO

3.14 rad (180°) INTERBLADE PHASE ANGLE

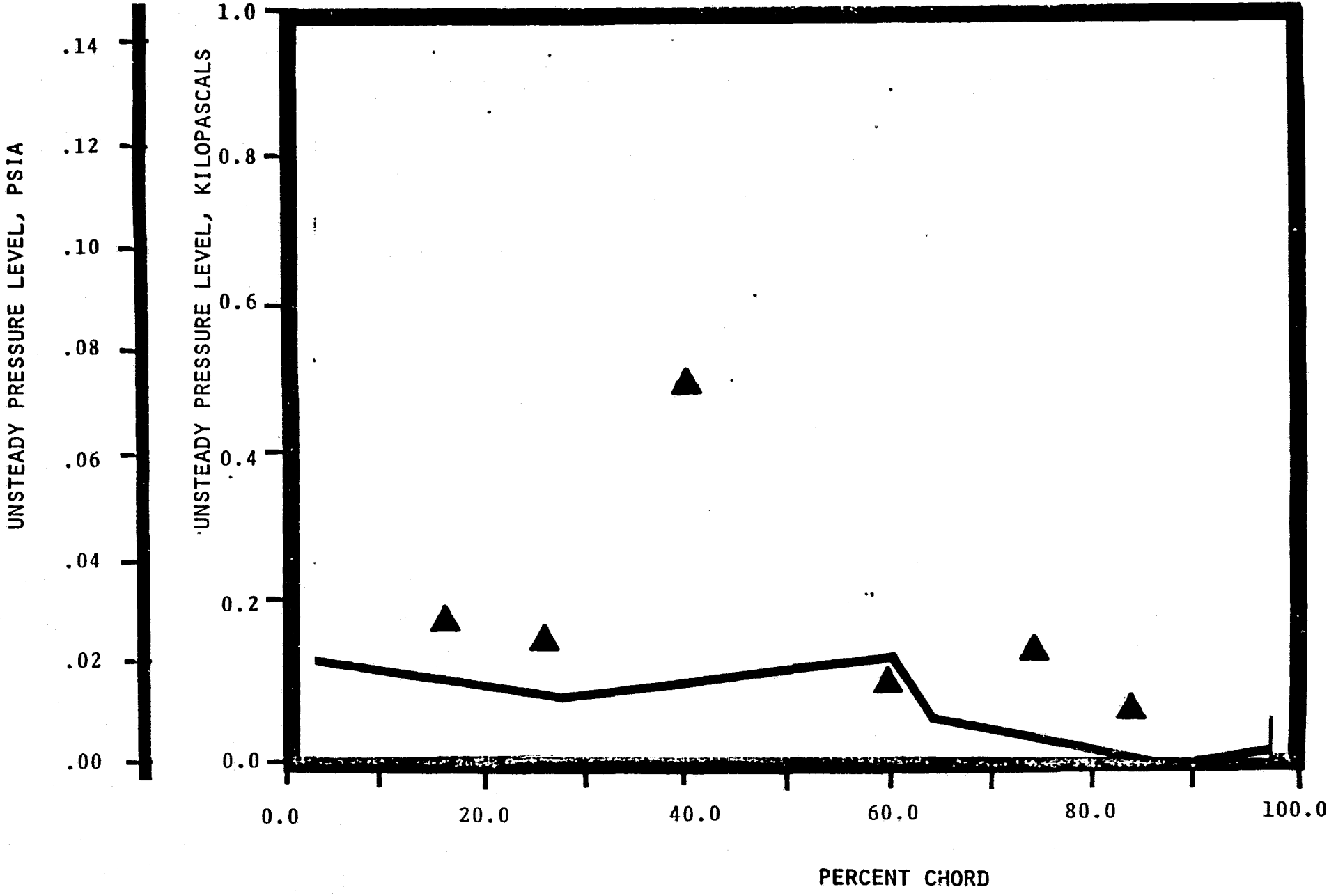

NASA I TORSION CASCADE - REDUCED SOLIDITY - OPEN SETTING

SUCTION SURFACE AERODYNAMIC PHASE LAG DISTRIBUTION

1.315 INLET MACH NUMBER

1.33 STATIC PRESSURE RATIO

3.14 rad(180) INTERBLADE PHASE ANGLE

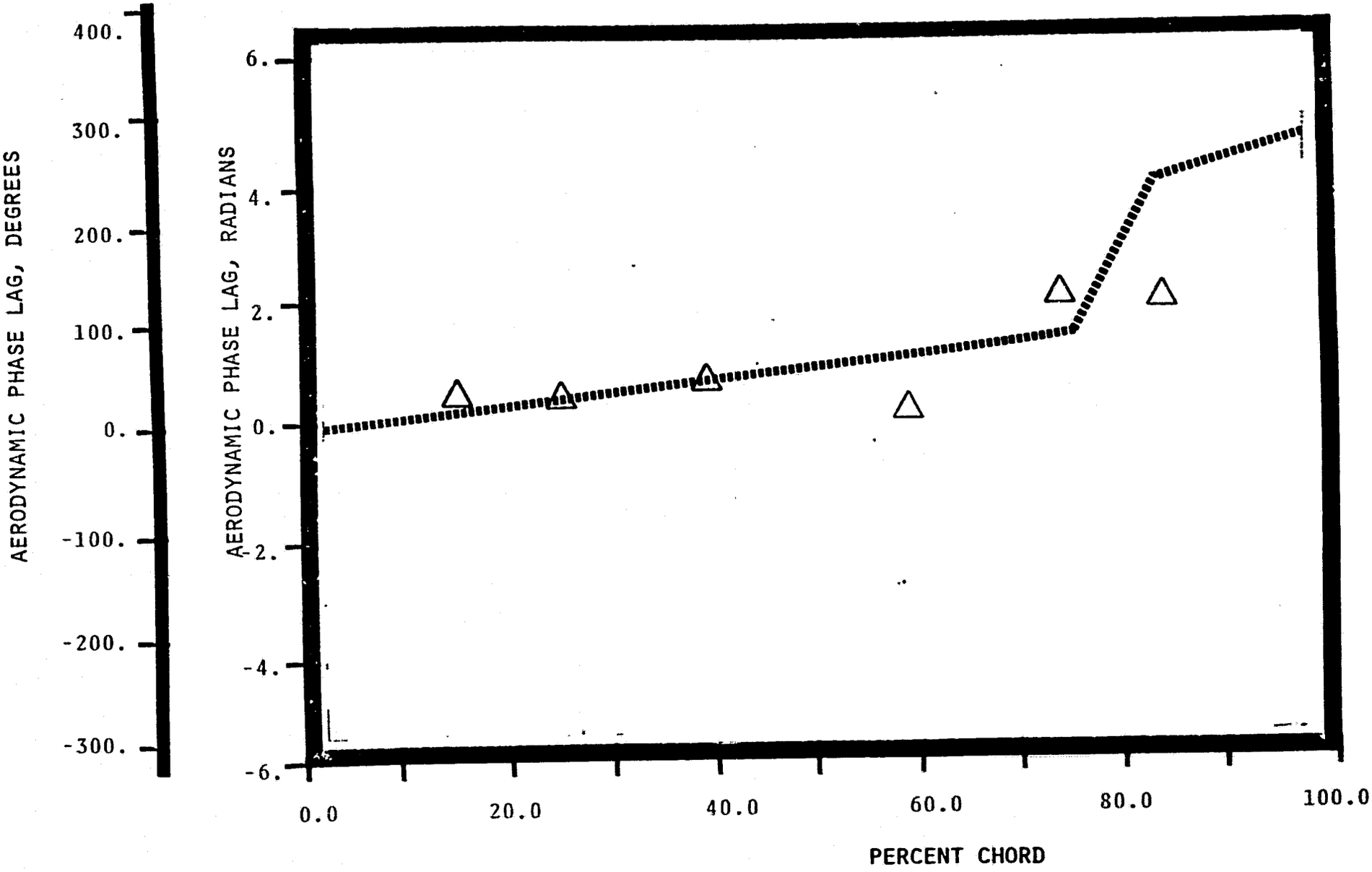

NASA I TORSION CASCADE - REDUCED SOLIDITY - OPEN SETTING

SUCTION SURFACE UNSTEADY PRESSURE DISTRIBUTION

1.315 INLET MACH NUMBER

1.33 STATIC PRESSURE RATIO

3.14 rad (180°) INTERBLADE PHASE ANGLE

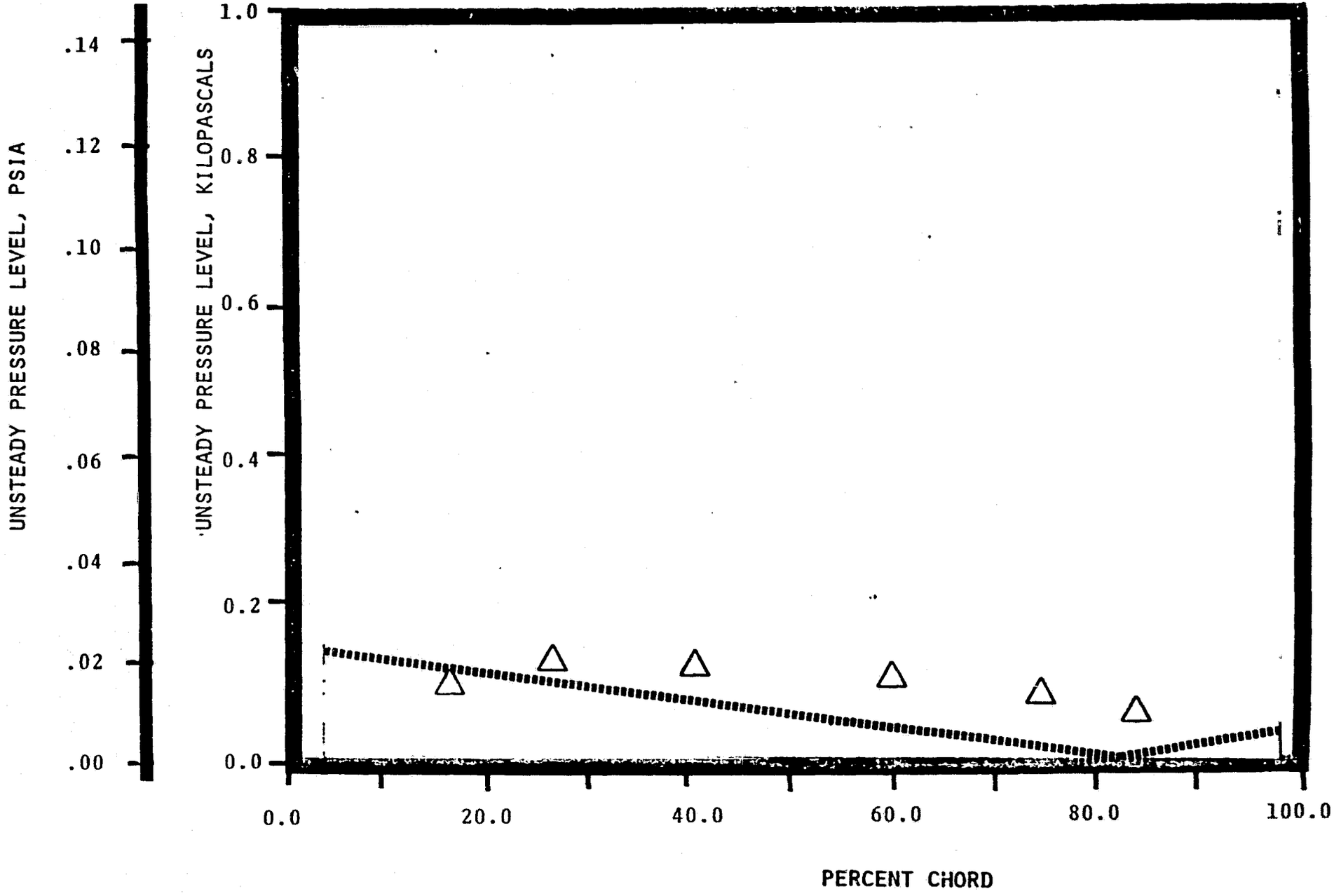

NASA I TORSION CASCADE - REDUCED SOLIDITY - OPEN SETTING

PRESSURE SURFACE AERODYNAMIC PHASE LAG DISTRIBUTION

1.315 INLET MACH NUMBER

1.33 STATIC PRESSURE RATIO

1.57 rad (90°) INTERBLADE PHASE ANGLE

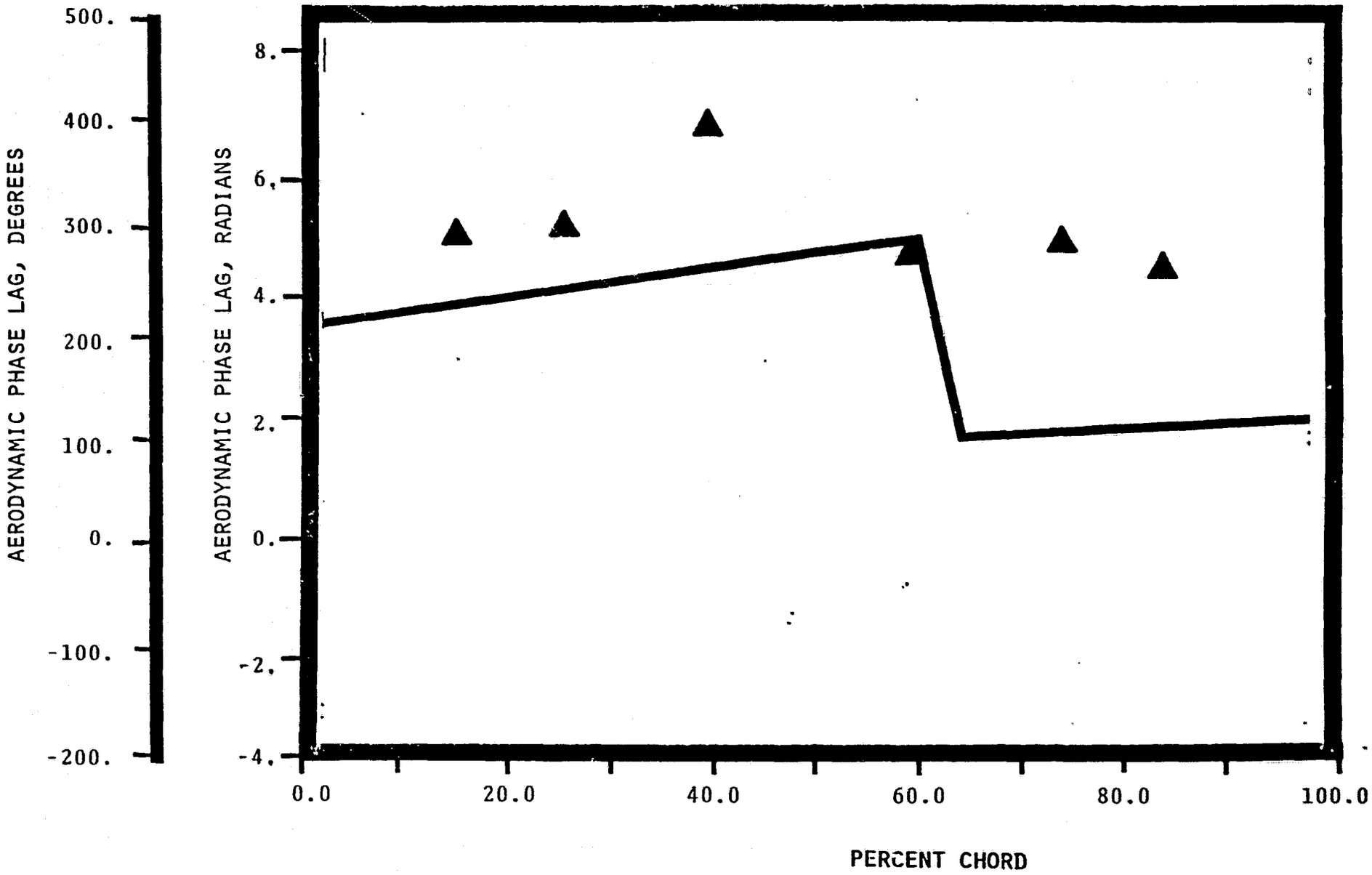

NASA I TORSION CASCADE - REDUCED SOLIDITY - OPEN SETTING

PRESSURE SURFACE UNSTEADY PRESSURE DISTRIBUTION

1.315 INLET MACH NUMBER

1.33 STATIC PRESSURE RATIO

1.57 rad (90°) INTERBLADE PHASE ANGLE

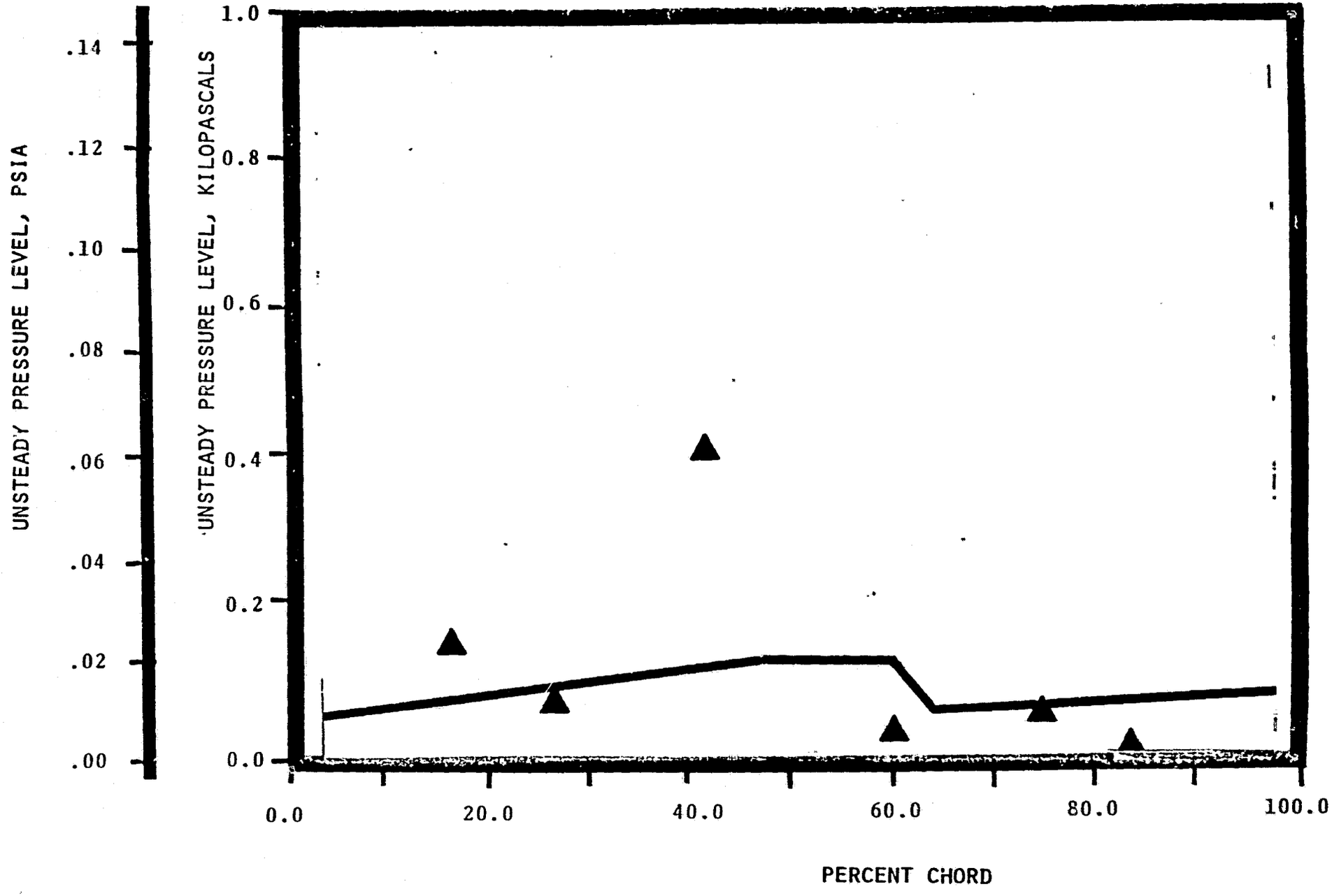

NASA I TORSION CASCADE - REDUCED SOLIDITY - OPEN SETTING

SUCTION SURFACE AERODYNAMIC PHASE LAG DISTRIBUTION

1.315 INLET MACH NUMBER

1.33 STATIC PRESSURE RATIO

1.57 rad (90°) INTERBLADE PHASE ANGLE

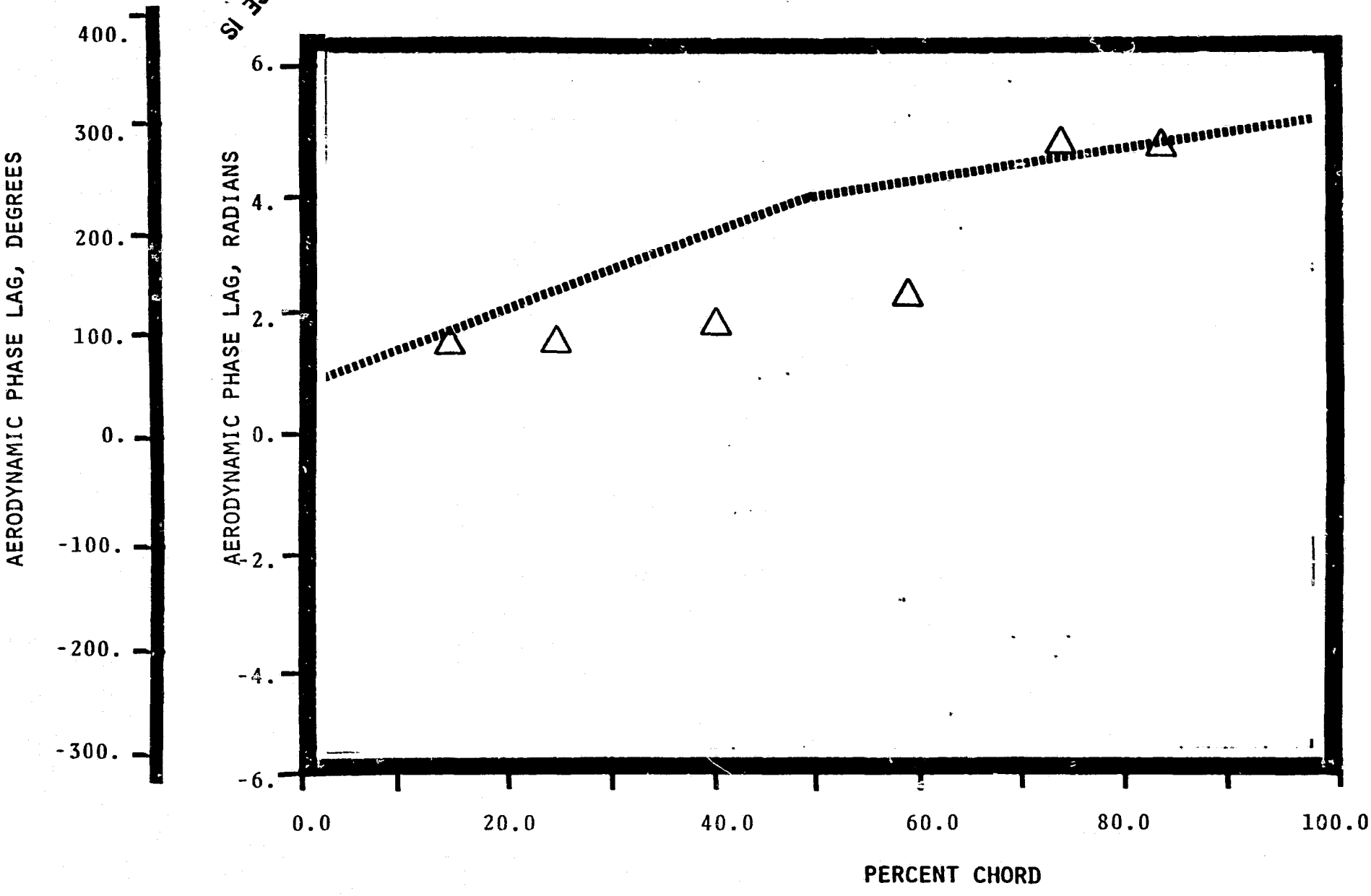

NASA I TORSION CASCADE - REDUCED SOLIDITY - OPEN SETTING

SUCTION SURFACE UNSTEADY PRESSURE DISTRIBUTION

1.315 INLET MACH NUMBER

1.33 STATIC PRESSURE RATIO

1.57 rad (90°) INTERBLADE PHASE ANGLE

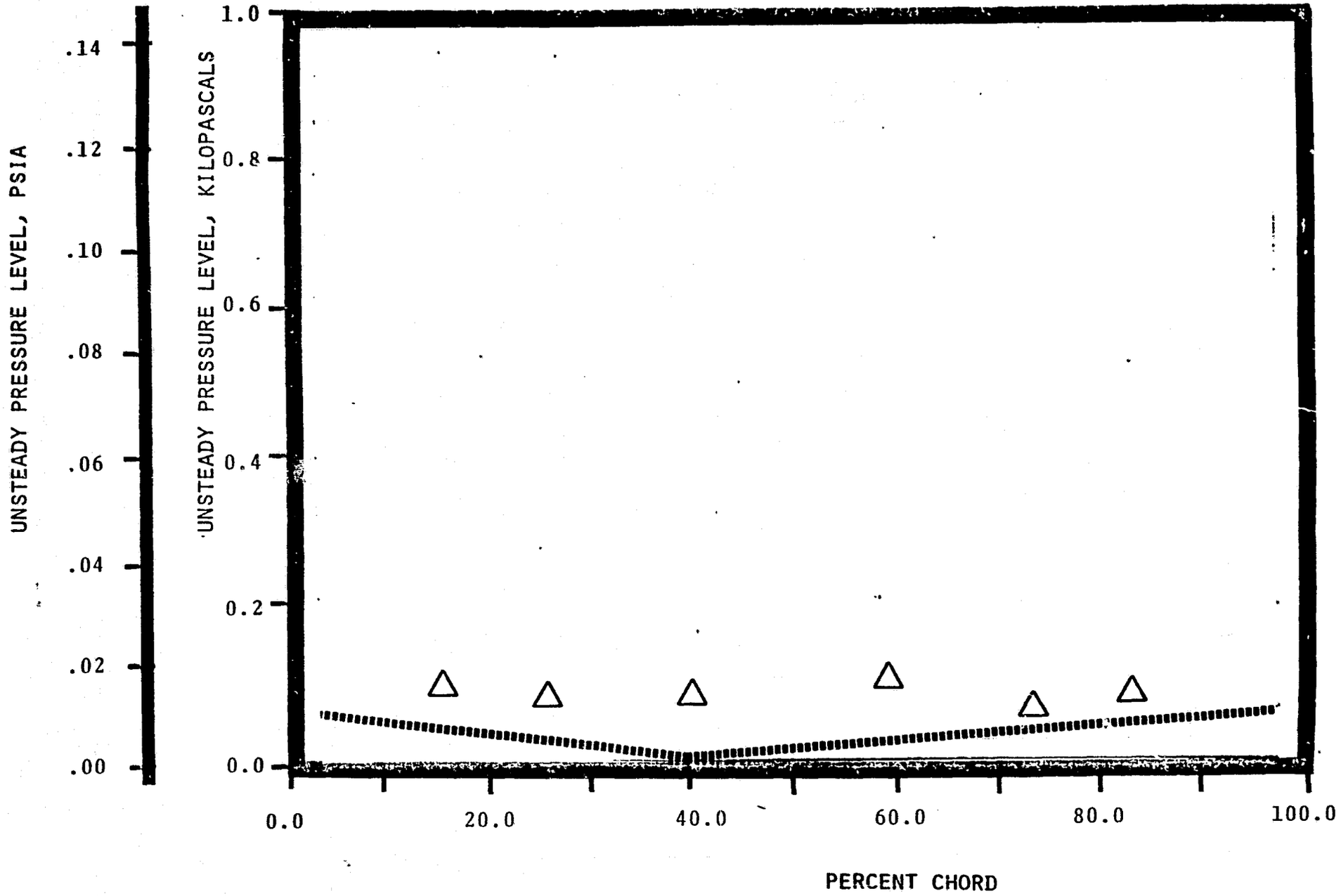

NASA I TORSION CASCADE - REDUCED SOLIDITY - OPEN SETTING

PRESSURE SURFACE AERODYNAMIC PHASE LAG DISTRIBUTION
1.315 INLET MACH NUMBER
1.33 STATIC PRESSURE RATIO
0.0 rad (0°) INTERBLADE PHASE ANGLE

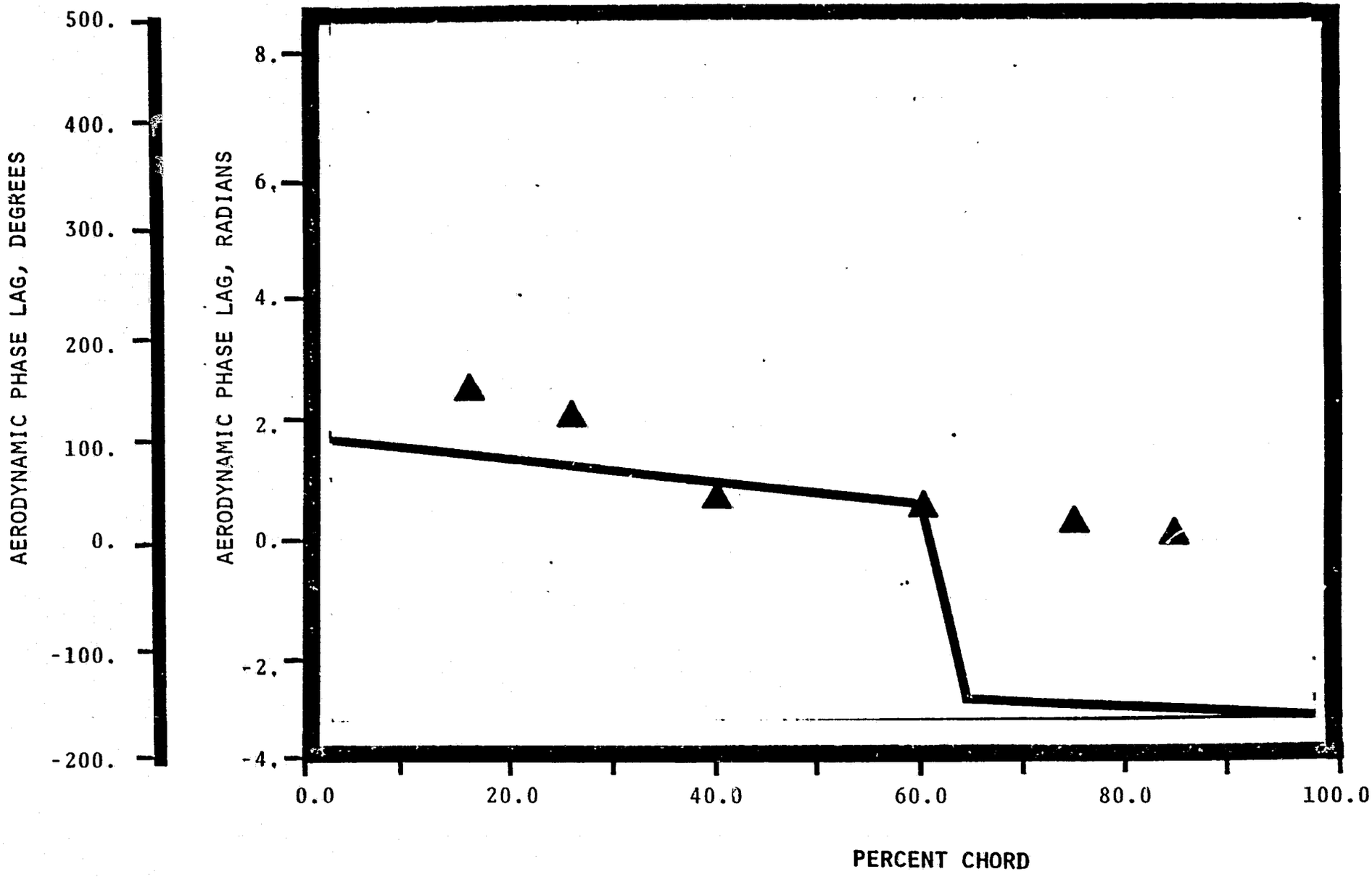

NASA I TORSION CASCADE - REDUCED SOLIDITY - OPEN SETTING

PRESSURE SURFACE UNSTEADY PRESSURE DISTRIBUTION

1.315 INLET MACH NUMBER

1.33 STATIC PRESSURE RATIO

0.0 rad (0°) INTERBLADE PHASE ANGLE

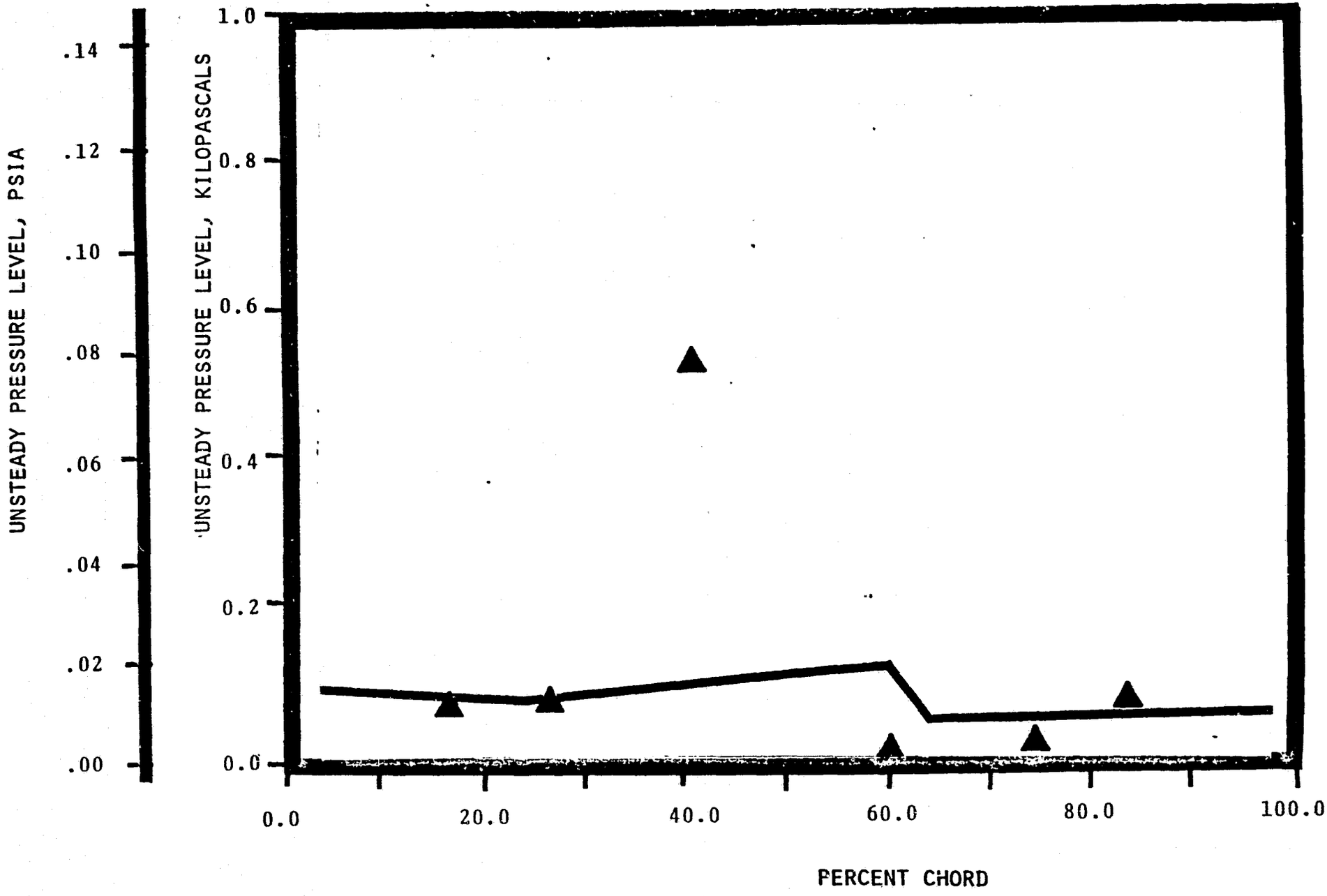

NASA I TORSION CASCADE - REDUCED SOLIDITY - OPEN SETTING

SUCTION SURFACE AERODYNAMIC PHASE LAG DISTRIBUTION

1.315 INLET MACH NUMBER

1.33 STATIC PRESSURE RATIO

0.0 rad (0°) INTERBLADE PHASE ANGLE

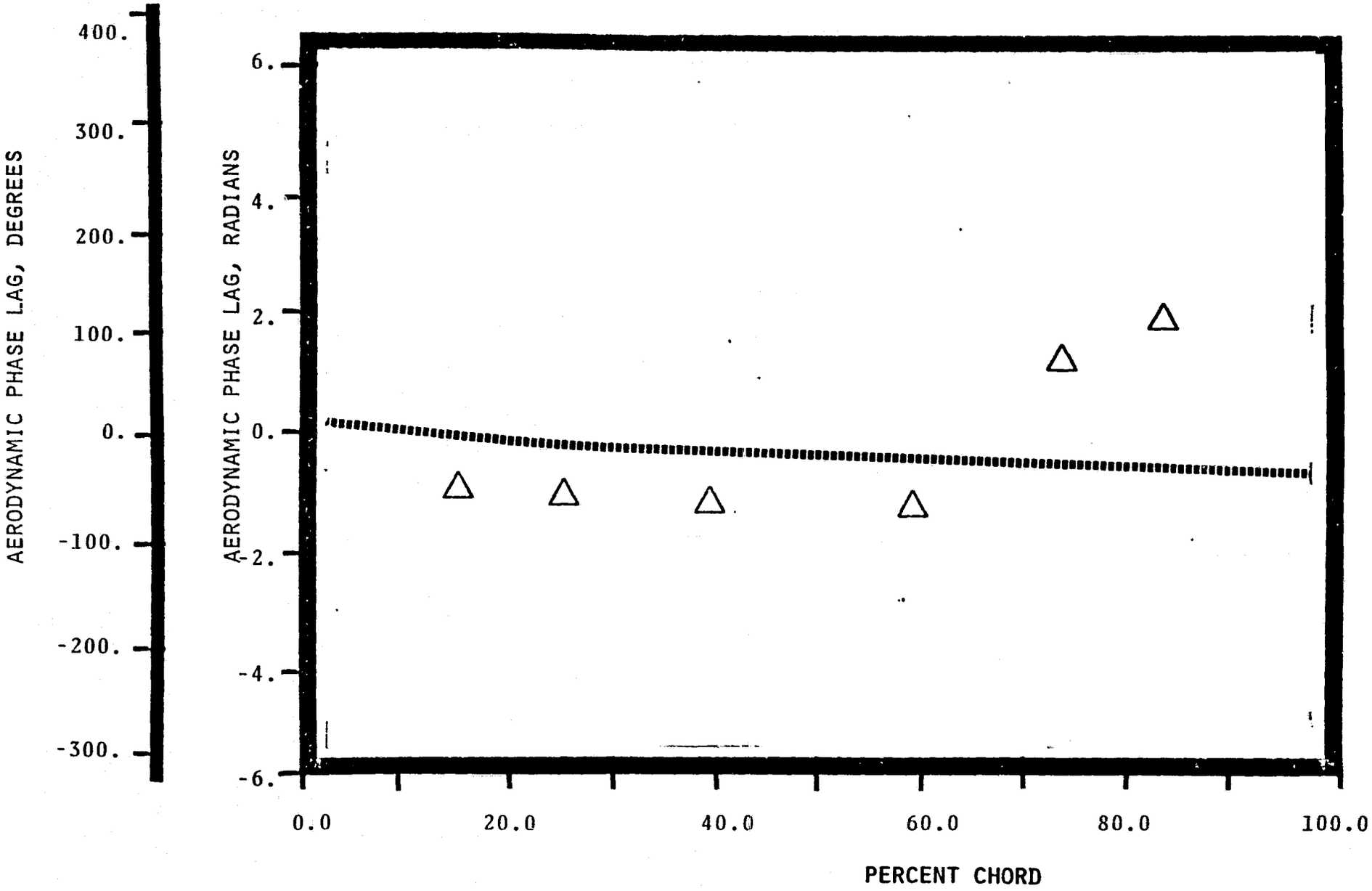

NASA I TORSION CASCADE - REDUCED SOLIDITY - OPEN SETTING

SUCTION SURFACE UNSTEADY PRESSURE DISTRIBUTION

1.315 INLET MACH NUMBER

1.33 STATIC PRESSURE RATIO

0.0 rad (0°) INTERBLADE PHASE ANGLE

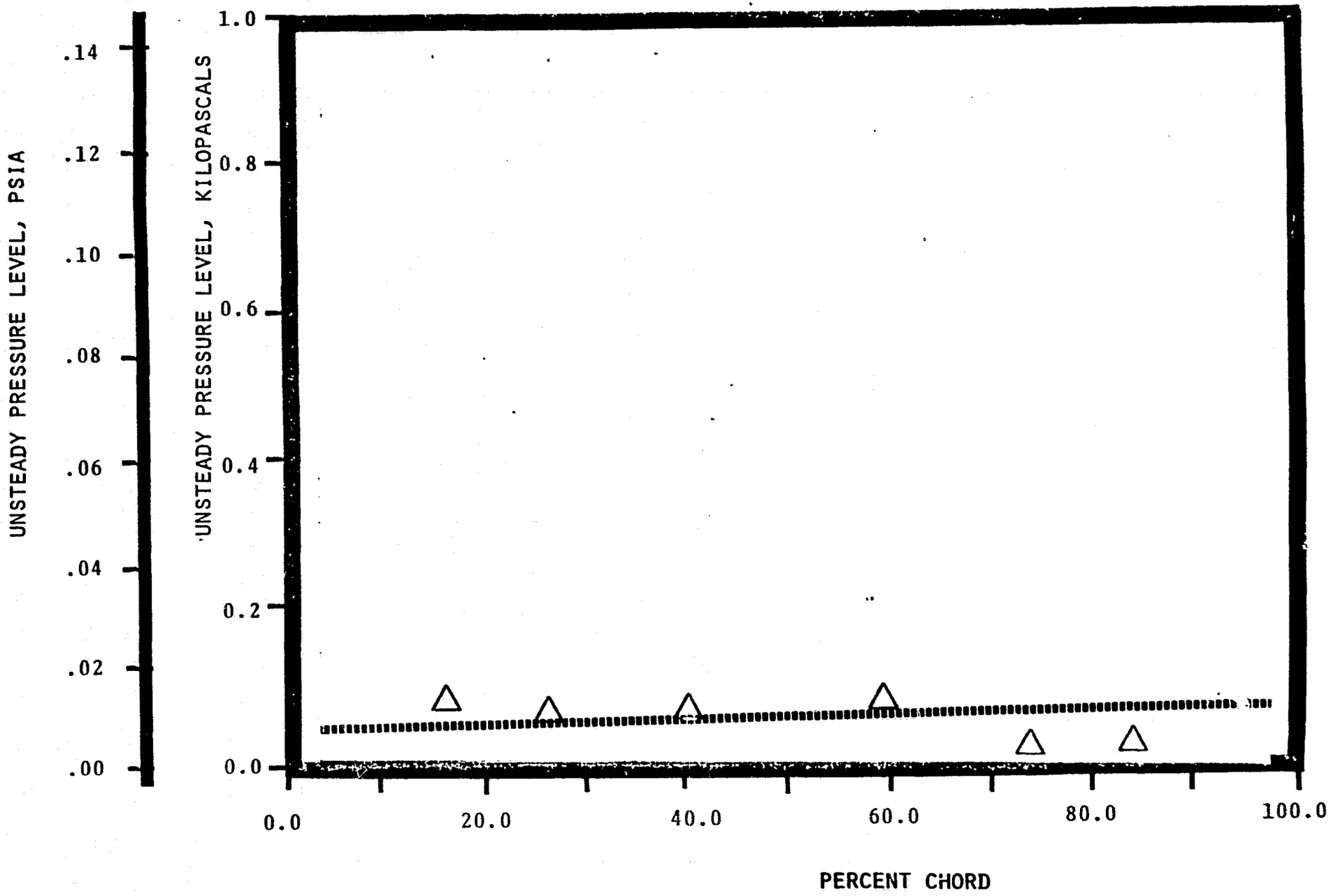

NASA I TORSION CASCADE - REDUCED SOLIDITY - OPEN SETTING

PRESSURE SURFACE AERODYNAMIC PHASE LAG DISTRIBUTION

1.315 INLET MACH NUMBER

1.33 STATIC PRESSURE RATIO

-.52 rad (-30) INTERBLADE PHASE ANGLE

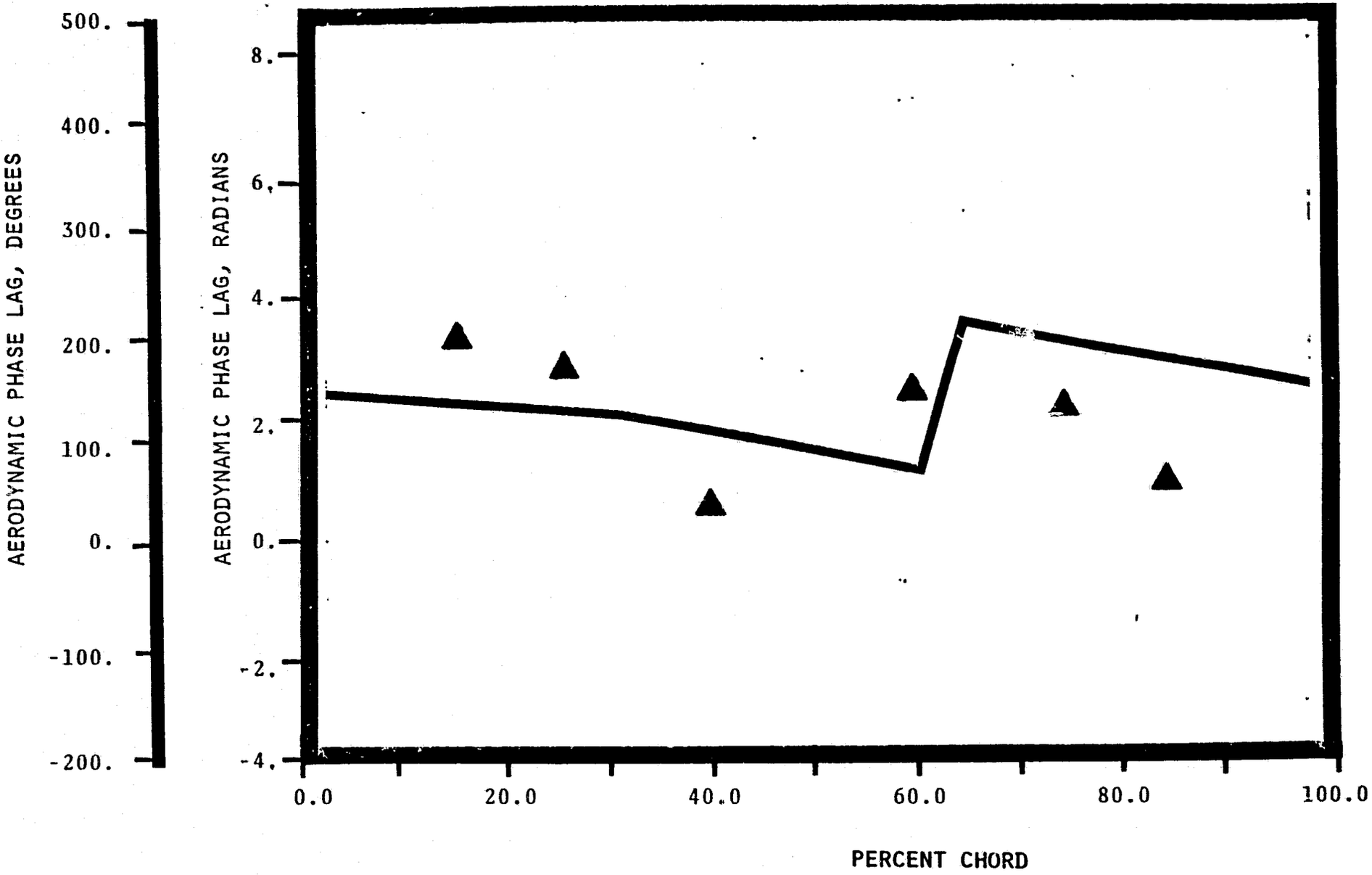

NASA 1 TORSION CASCADE - REDUCED SOLIDITY - OPEN SETTING

PRESSURE SURFACE UNSTEADY PRESSURE DISTRIBUTION

1.315 INLET MACH NUMBER

1.33 STATIC PRESSURE RATIO

-.52 rad (-30°) INTERBLADE PHASE ANGLE

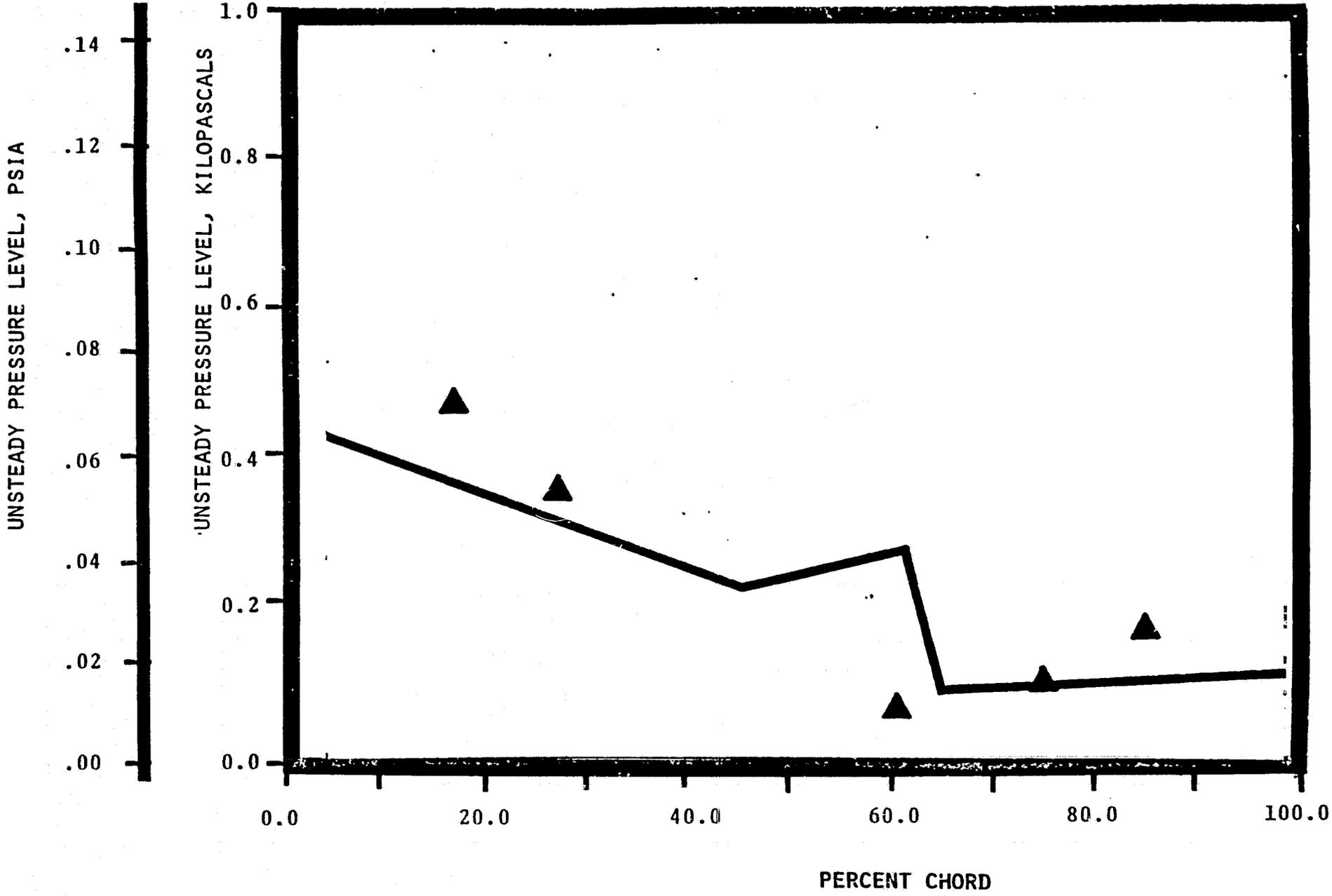

NASA I TORSION CASCADE - REDUCED SOLIDITY - OPEN SETTING

SUCTION SURFACE AERODYNAMIC PHASE LAG DISTRIBUTION

1.315 INLET MACH NUMBER

1.33 STATIC PRESSURE RATIO

-.52 rad (-30) INTERBLADE PHASE ANGLE

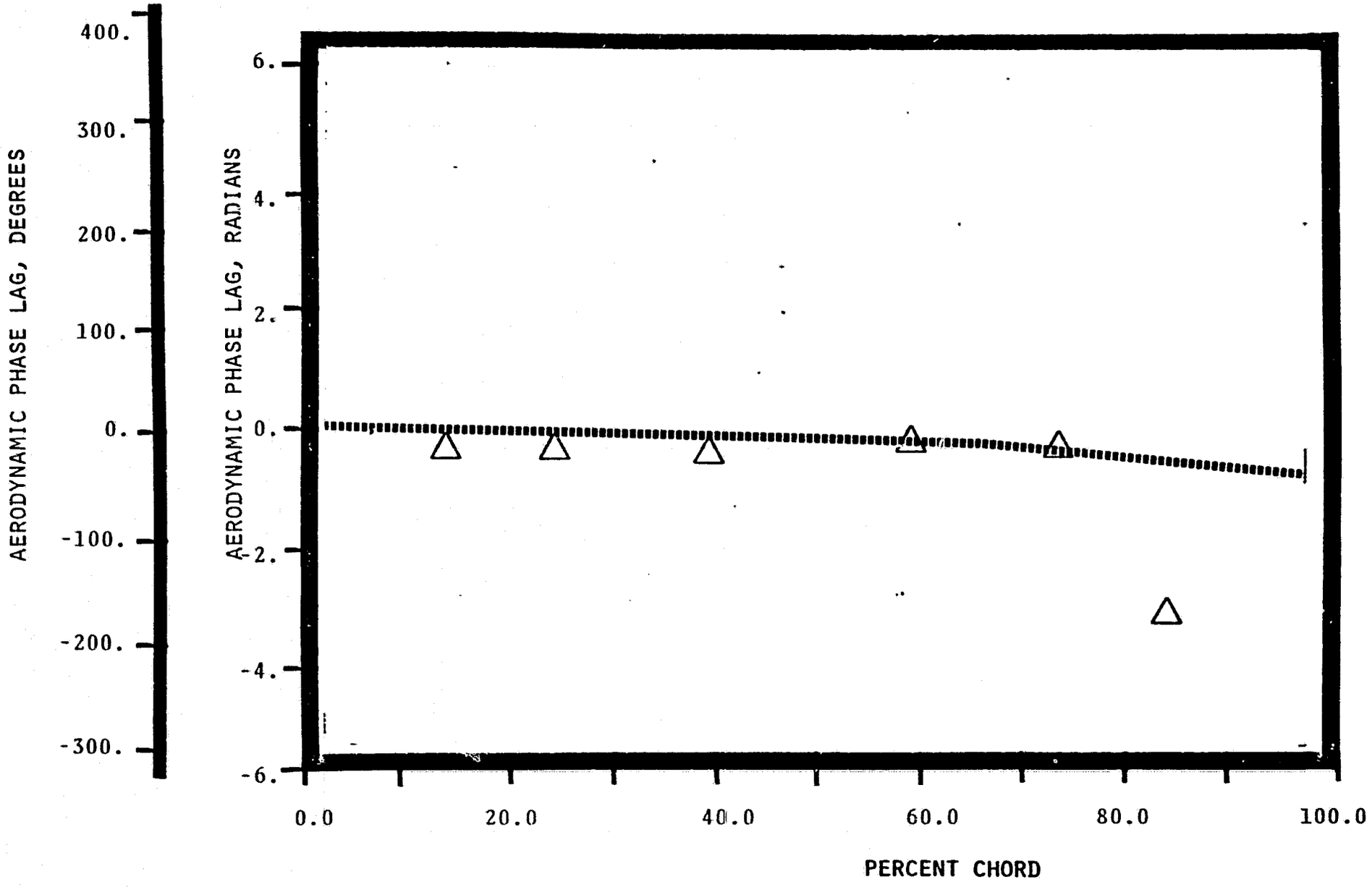

NASA I TORSION CASCADE - REDUCED SOLIDITY - OPEN SETTING

SUCTION SURFACE UNSTEADY PRESSURE DISTRIBUTION

1.315 INLET MACH NUMBER

1.33 STATIC PRESSURE RATIO

-1.52 rad (-30) INTERBLADE PHASE ANGLE

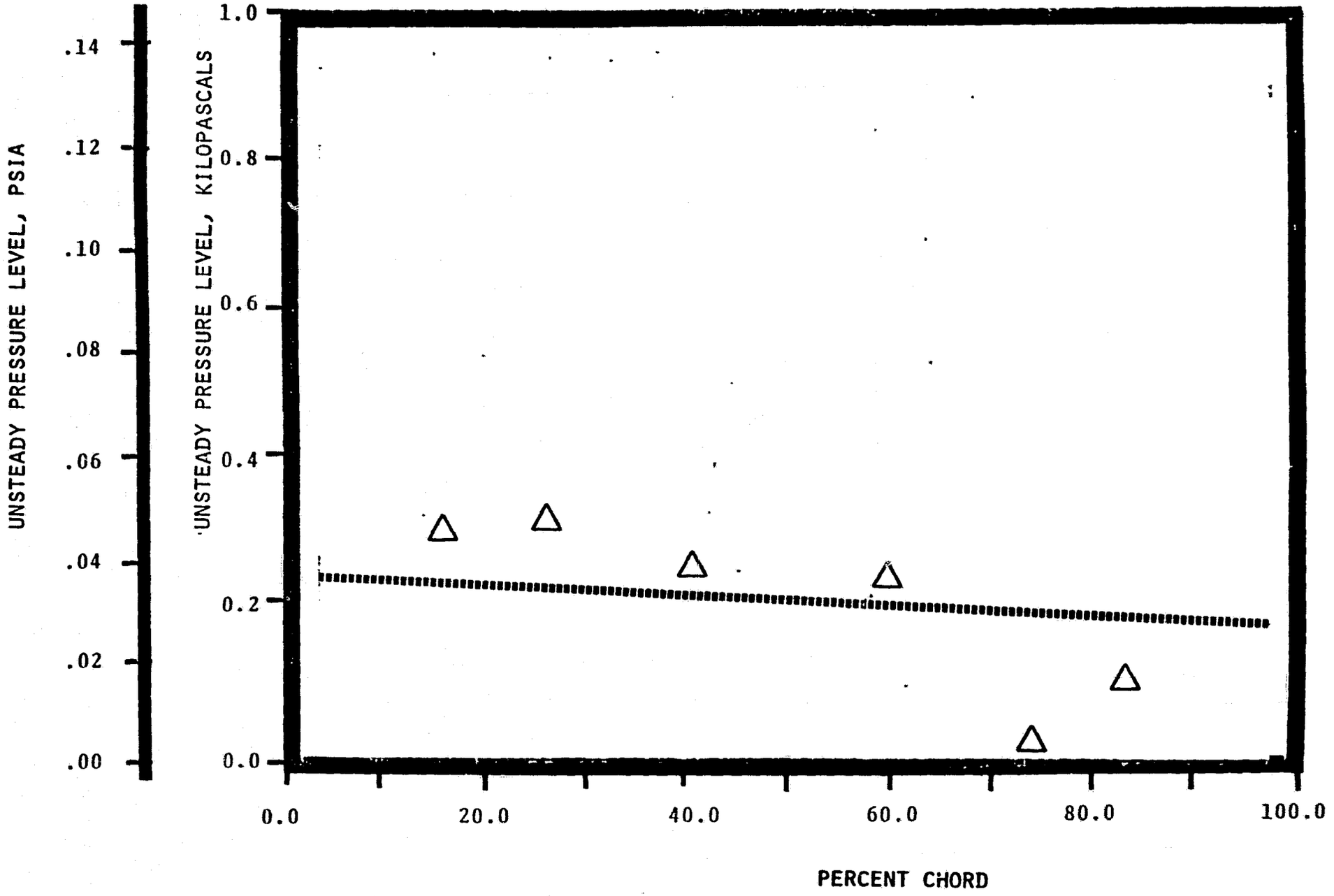

NASA I TORSION CASCADE - REDUCED SOLIDITY - OPEN SETTING

PRESSURE SURFACE AERODYNAMIC PHASE LAG DISTRIBUTION

1.315 INLET MACH NUMBER

1.33 STATIC PRESSURE RATIO

-1.05 rad (-60) INTERBLADE PHASE ANGLE

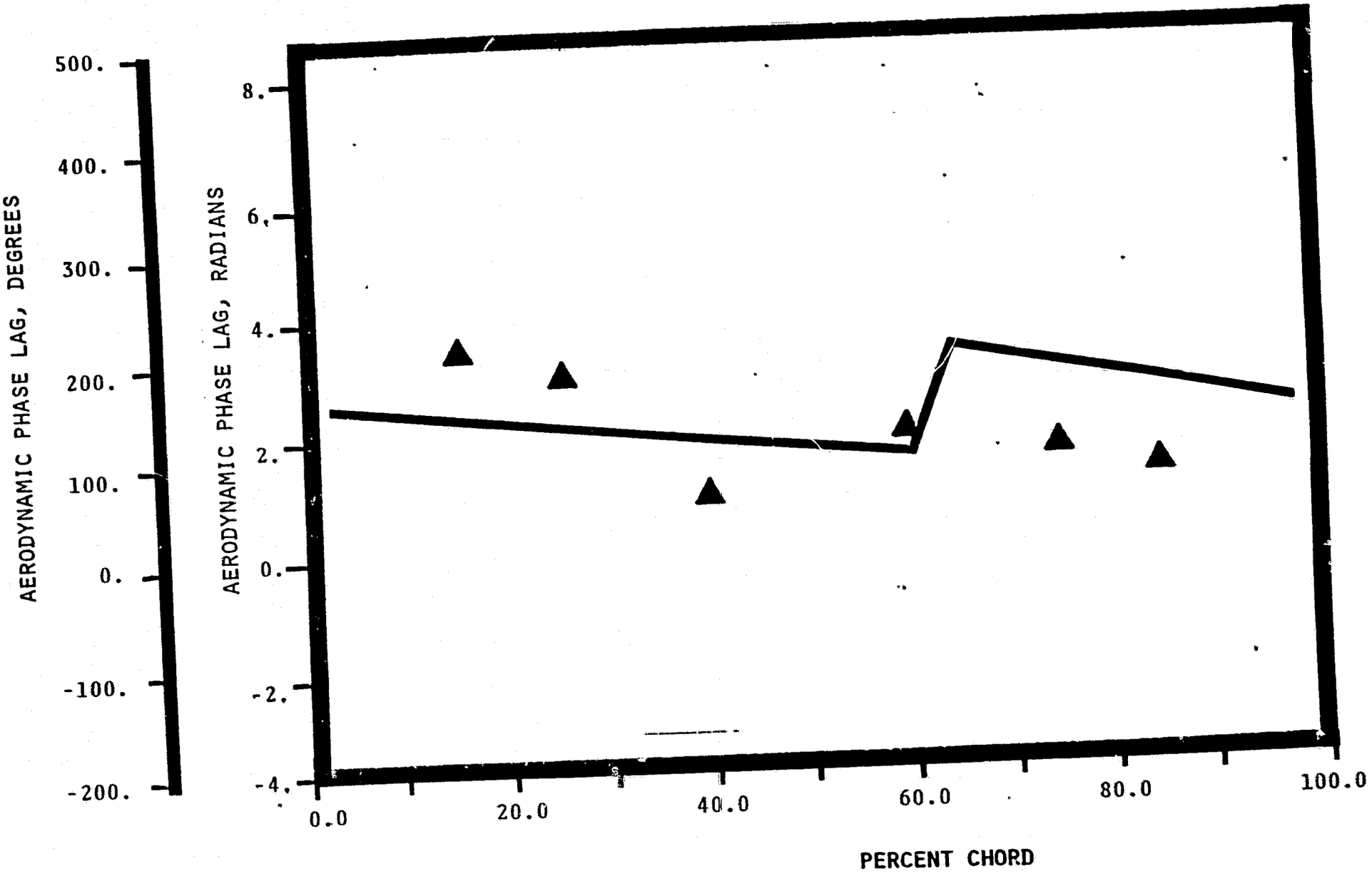

NASA I TORSION CASCADE - REDUCED SOLIDITY - OPEN SETTING

PRESSURE SURFACE UNSTEADY PRESSURE DISTRIBUTION
1.315 INLET MACH NUMBER
1.33 STATIC PRESSURE RATIO
-1.05 rad (-60°) INTERBLADE PHASE ANGLE

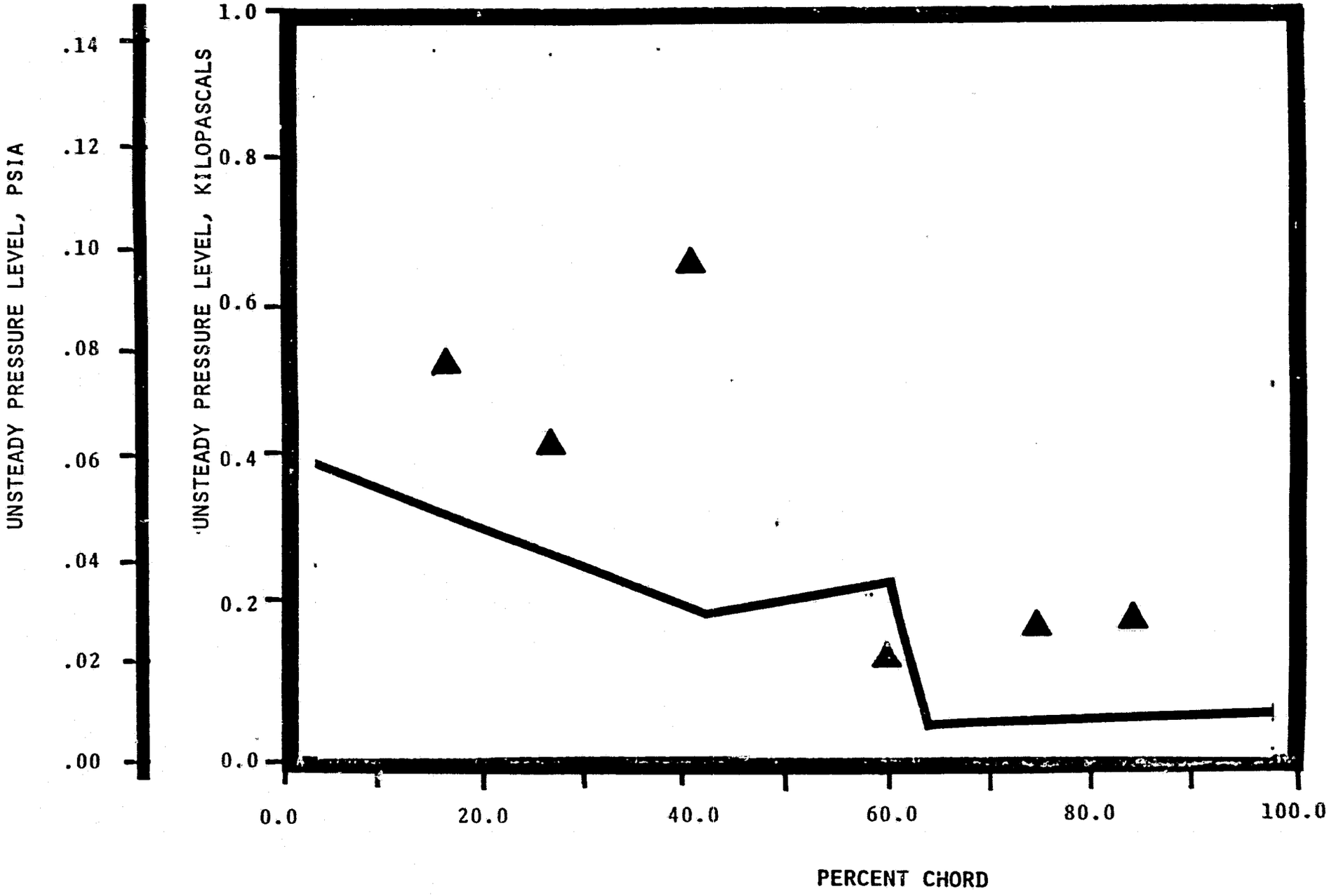

NASA I TORSION CASCADE - REDUCED SOLIDITY - OPEN SETTING

SUCTION SURFACE AERODYNAMIC PHASE LAG DISTRIBUTION

1.315 INLET MACH NUMBER

1.33 STATIC PRESSURE RATIO

-1.05 rad (-60^{0}) INTERBLADE PHASE ANGLE

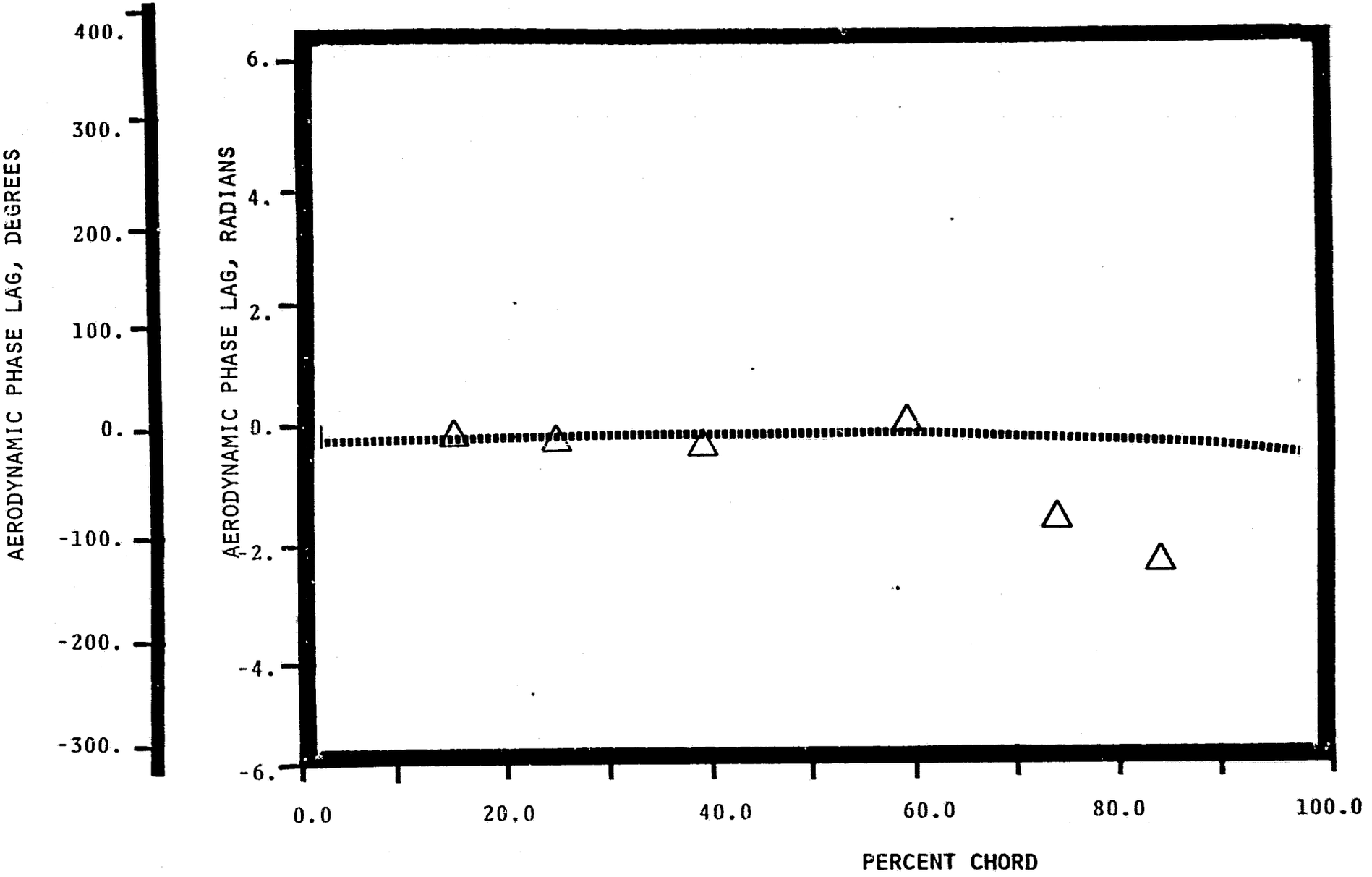

NASA I TORSION CASCADE - REDUCED SOLIDITY - OPEN SETTING

SUCTION SURFACE UNSTEADY PRESSURE DISTRIBUTION

1.315 INLET MACH NUMBER

1.33 STATIC PRESSURE RATIO

-1.05 rad (-60°) INTERBLADE PHASE ANGLE

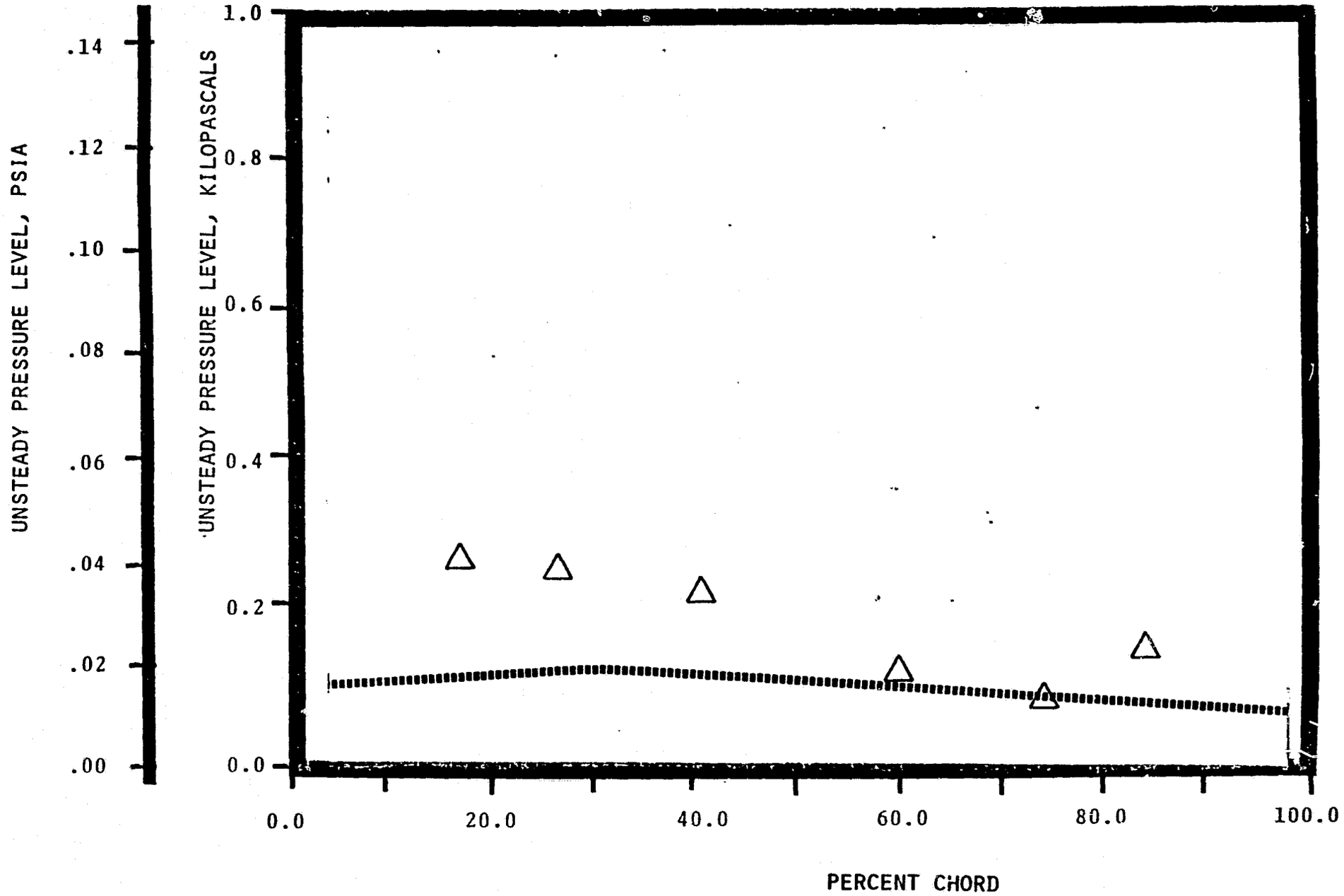

NASA I TORSION CASCADE - REDUCED SOLIDITY - OPEN SETTING

PRESSURE SURFACE AERODYNAMIC PHASE LAG DISTRIBUTION
1.315 INLET MACH NUMBER
1.33 STATIC PRESSURE RATIO
-1.57 rad (-90) INTERBLADE PHASE ANGLE

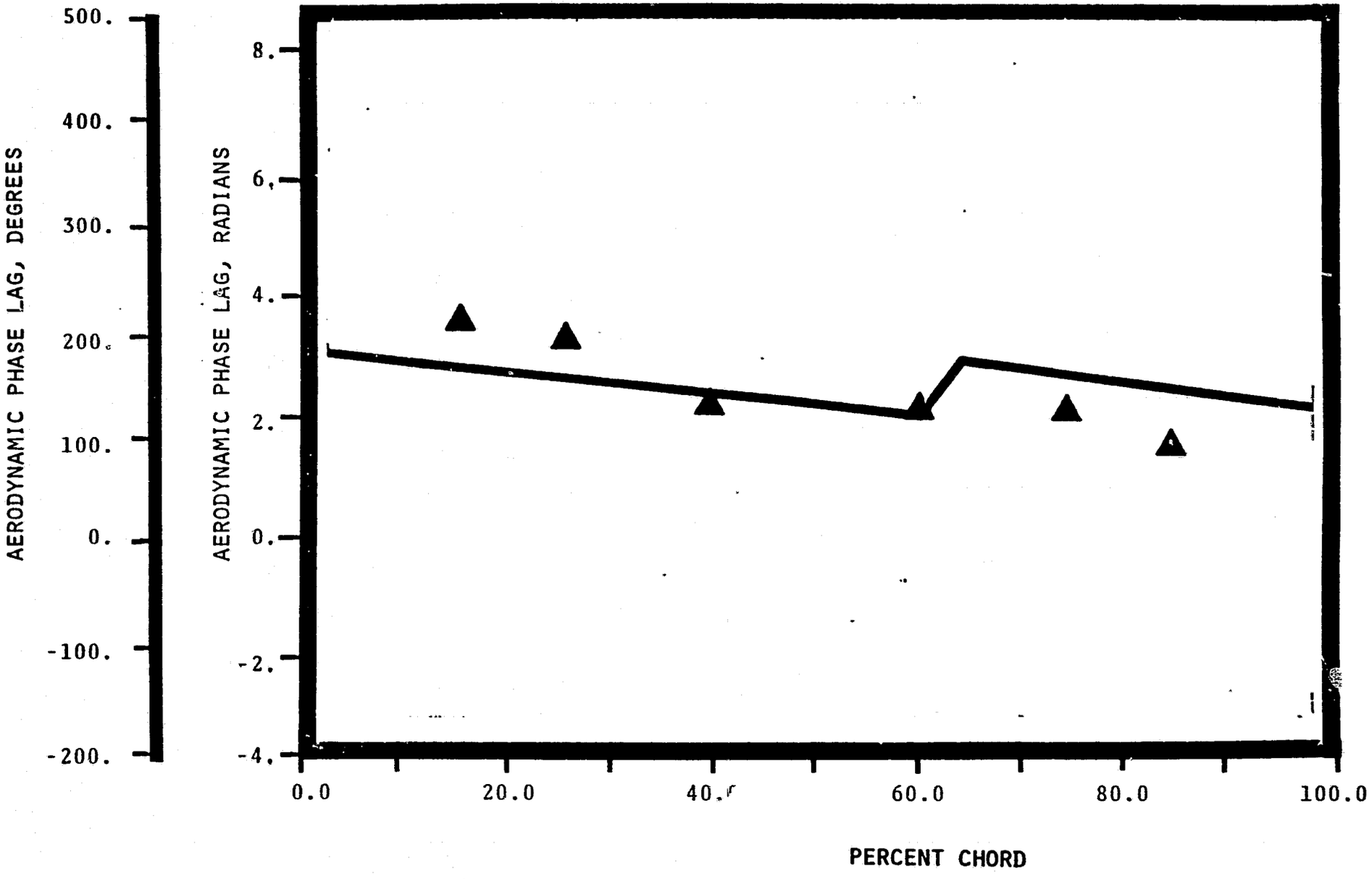

NASA I TORSION CASCADE - REDUCED SOLIDITY - OPEN SETTING

PRESSURE SURFACE UNSTEADY PRESSURE DISTRIBUTION

1.315 INLET MACH NUMBER

1.33 STATIC PRESSURE RATIO

-1.57 rad (-90) INTERBLADE PHASE ANGLE

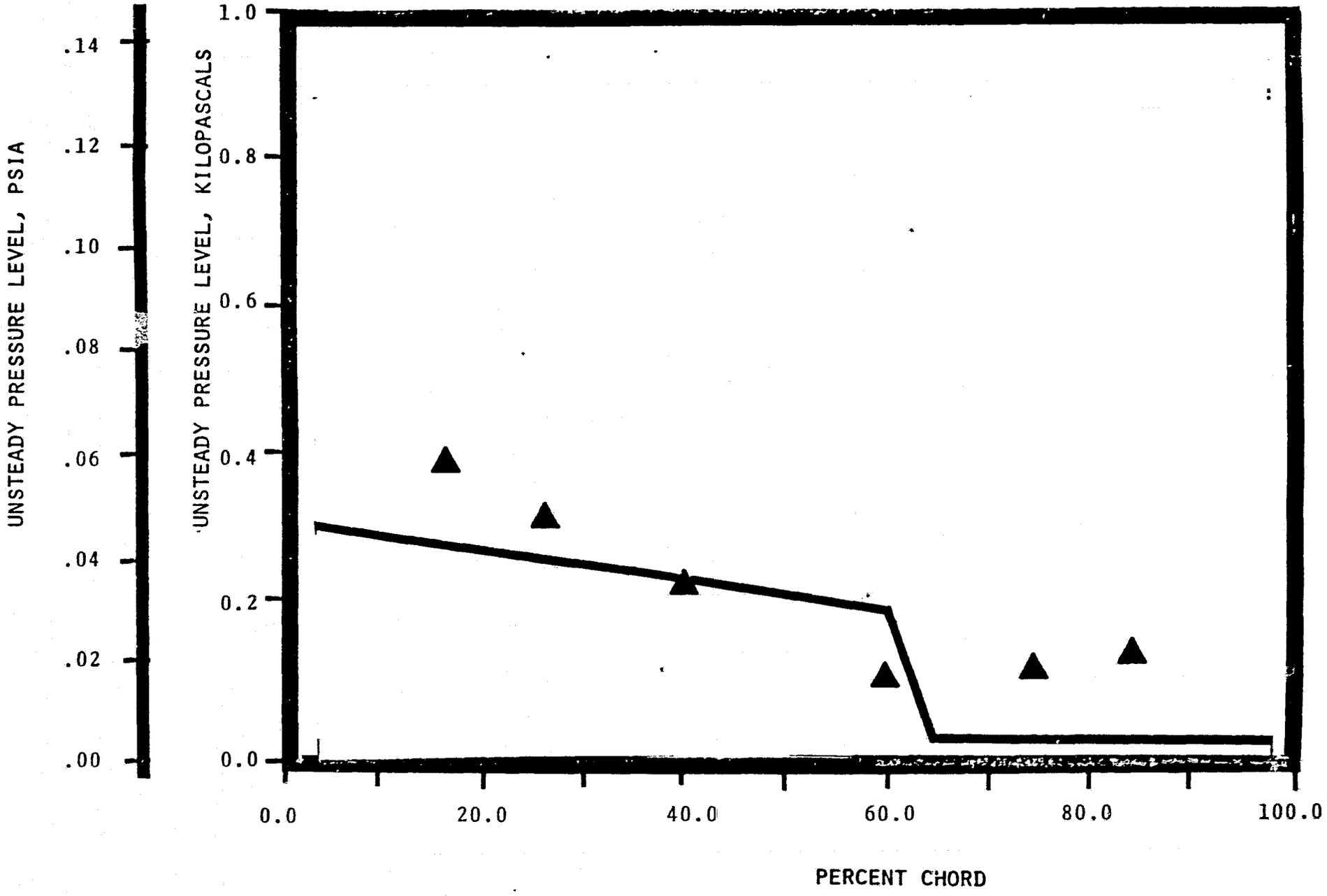

NASA I TORSION CASCADE - REDUCED SOLIDITY - OPEN SETTING

SUCTION SURFACE AERODYNAMIC PHASE LAG DISTRIBUTION

1.315 INLET MACH NUMBER

1.33 STATIC PRESSURE RATIO

-1.57 rad(-90°) INTERBLADE PHASE ANGLE

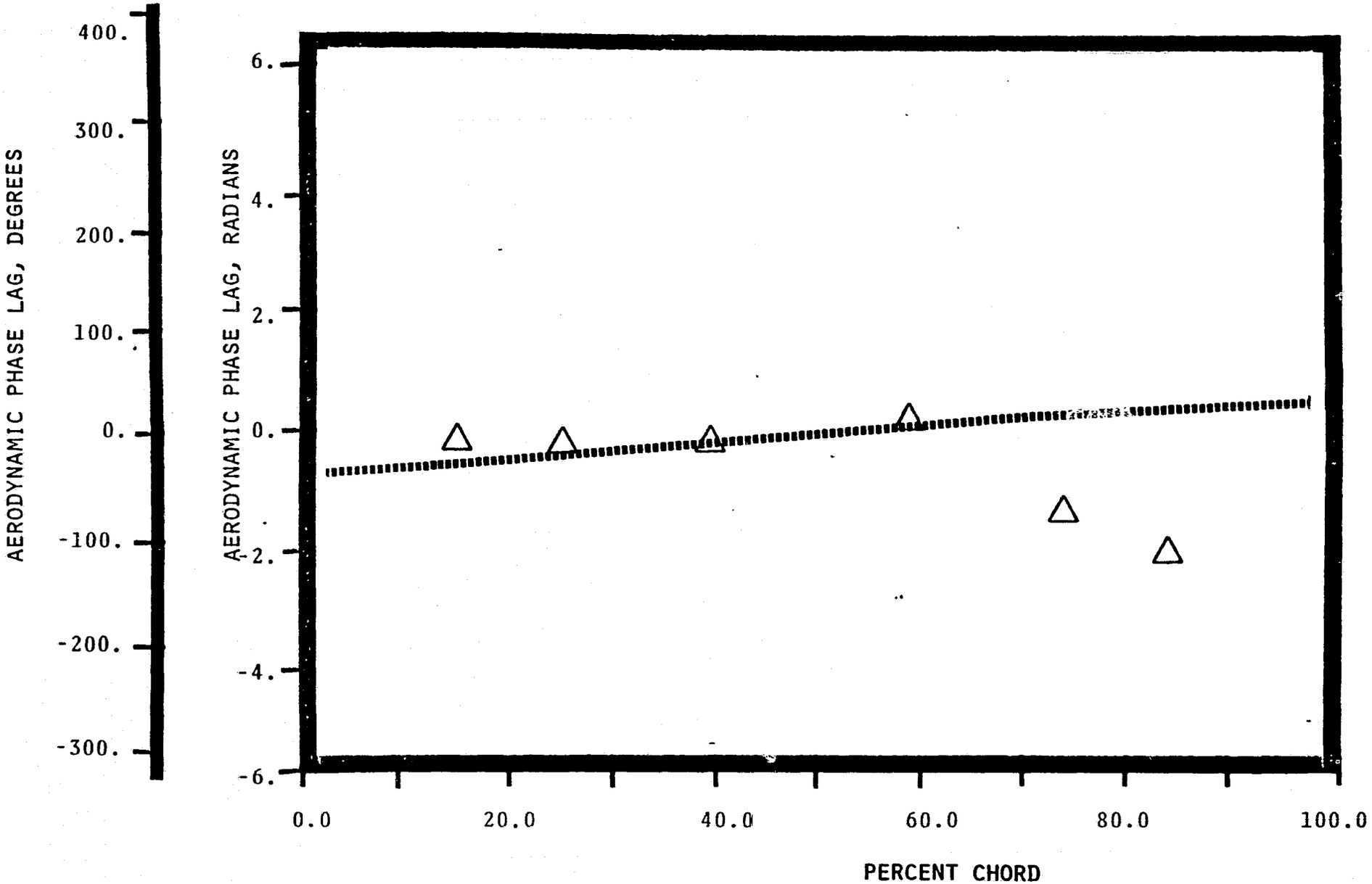

NASA I TORSION CASCADE - REDUCED SOLIDITY - OPEN SETTING

SUCTION SURFACE UNSTEADY PRESSURE DISTRIBUTION

1.315 INLET MACH NUMBER

1.33 STATIC PRESSURE RATIO

-1.57 rad (-90°) INTERBLADE PHASE ANGLE

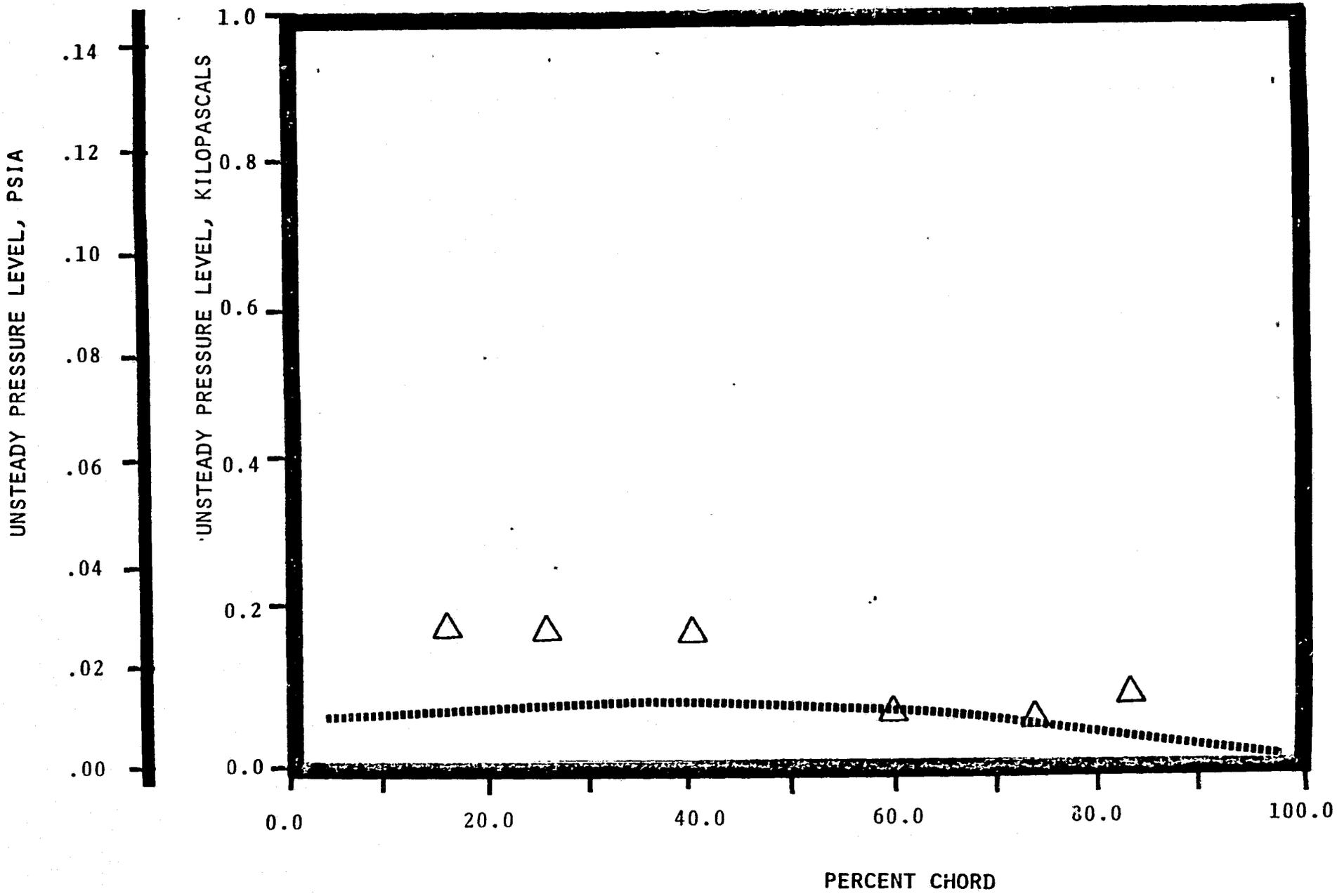

REFERENCES

1. Caruthers, J. E. and Riffel, R. E., "Aerodynamic Analysis of a Supersonic Cascade Vibrating in a Complex Mode." Journal of Sound and Vibration, Vol 71, No. 2, July 22, 1980.

2. Garrick, J. E., and Rubinow, S. J., "Flutter and Oscillating Air Force Calculations for an Airfoil in Two-Dimensional Supersonic Flow." NACA Report 846, 1946.

3. Chalkley, H. G., "A Study of Supersonic Cascade Flutter." Aeronautical Engineers Thesis, Naval Post-graduate School, Monterey, California, June, 1972.

4. Verdon, J. M. and McCune, J. E., "The Unsteady Supersonic Cascade in Subsonic Axial Flow." AIAA Paper No. 75-22, presented at the AIAA 13th Aerospace Sciences Meeting, Pasadena, California, January 20-22, 1975.

5. Brix, C. W. and Platzer, M. F., "Theoretical Investigation of Supersonic Flow Past Oscillating Cascades with Subsonic Leading Edge Locus." AIAA Paper No. 74-14 presented at the AIAA 12th Aerospace Sciences Meeting, Washington, D. C., January 1974.

6. Caruthers, J. E., "Theoretical Analysis of Unsteady Supersonic Flow Through Harmonically Oscillating Turbofan Cascades." PhD thesis, Georgia Institute of Technology, June 1976 (to be published).